

**STIMULI-RESPONSIVE SMALL MOLECULE
PERSULFIDATING AGENTS**

A thesis

submitted in partial fulfilment of the requirements

of the degree of

Doctor of Philosophy

by

PRERONA BORA

20163433



**INDIAN INSTITUTE OF SCIENCE EDUCATION
AND RESEARCH PUNE – 411 008**

2022

Dedicated to

My Parents



भारतीयविज्ञानशिक्षाएवंअनुसंधानसंस्थान, पुणे
INDIAN INSTITUTE OF SCIENCE EDUCATION AND RESEARCH (IISER), PUNE
(An Autonomous Institution, Ministry of Human Resource Development, Govt. of India)
900 NCL Innovation Park Dr Homi Bhabha Road Pune 411008

Harinath Chakrapani, Ph.D.

Professor – Chemistry

www.iiserpune.ac.in/~harinath/

CERTIFICATE

Certified that, the work incorporated in the thesis entitled, “*Stimuli-Responsive Small Molecule Persulfidating Agents*” submitted by *Prerona Bora* was carried out by the candidate, under my supervision. The work presented here or any part of it has not been included in any other thesis submitted previously for the award of any degree or diploma from any other University or institution.

Date:

Pune (MH), India.

C. Harinath

Dr. Harinath Chakrapani

DECLARATION

I declare that this written submission represents my ideas in my own words and where others' ideas have been included; I have adequately cited and referenced the original sources. I also declare that I have adhered to all principles of academic honesty and integrity and have not misrepresented or fabricated or falsified any idea/data/fact/source in my submission. I understand that violation of the above will be cause for disciplinary action by the Institute and can also evoke penal action from the sources which have thus not been properly cited or from whom proper permission has not been taken when needed.

Date: 17th Feb, 2022
Pune (MH), India.



Prerona Bora
20163433

Table of Contents

Table of Contents	I
General Remarks	VI
List of Abbreviations	VIII
Acknowledgements	XIV
Abstract	XVI

CHAPTER 1: Introduction

1.1	Hydrogen sulfide (H ₂ S) signaling	1
1.2	Cellular mechanisms of persulfidation	2
1.3	Physiological relevance of persulfidation	4
1.3.1	Persulfidation of KEAP1	5
1.3.2	Persulfidation protects protein from oxidation	6
1.3.3	Persulfidation of NFκB	6
1.3.4	Persulfidation in neurodegenerative diseases	7
1.3.5	Persulfidation of GAPDH	8
1.4	Low Molecular Weight (LMW) persulfides in biological systems	8
1.5	Biosynthesis of persulfides	9
1.6	Physicochemical properties of persulfides	11
1.7	LMW persulfide generation	14
1.8	Triggerable persulfide donors	15
1.8.1	Chemically activated persulfide prodrugs	15
1.8.2	pH sensitive persulfide donors	16
1.8.3	Thiol activated persulfide donors	19
1.8.4	Light activated persulfide donor	21
1.8.5	Enzyme activated persulfide donors	21
1.9	Motivation and outline of the thesis	23
1.13	References	26

CHAPTER 2: A Vinyl-Boronate Ester Based Persulfide Donor Sensitive to Reactive Oxygen Species (ROS)

2.1	Introduction	38
2.2	Results and Discussion	40
2.2.1	Synthesis of H ₂ O ₂ responsive persulfide donor	40
2.2.2	HPLC analysis for decomposition of 5	41
2.2.3	Detection of persulfides	42
2.2.3.1	Fluorodinitrobenzene (FDNB) method	43
2.2.3.2	Monobromobimane (mBBr) method	44
2.2.4	Decomposition of negative control	46
2.2.5	Selectivity of vinyl boronate esters towards H ₂ O ₂	47
2.2.6	Mechanism	48
2.2.7	MTT assay for cell viability	49
2.2.8	Cytoprotective effect of compound 5	50
2.3	Other reports	52
2.4	Summary	53
2.5	Experimental section	54
2.5.1	Synthesis and characterization of data	54
2.5.2	HPLC based kinetics study	56
2.5.3	HPLC studies for persulfide reactivity with FDNB	56
2.5.4	HPLC studies for persulfide reactivity with mBBr	57
2.5.5	Selectivity of 5 against various analytes	57
2.5.6	Cell viability assay	57
2.5.7	Protection from oxidative stress	58
2.6	NMR spectra of compounds	59
2.7	References	66

CHAPTER 3: Enhancing Intracellular Sulfane Sulfur Through β -glycosidase Activated Prodrugs

3.1	Introduction	70
3.2	Results and discussion	72
3.2.1	Synthesis of β -galactosidase responsive persulfide donors	72
3.2.2	LC/MS analysis for the decomposition of the prodrug 10b	72

Table of Contents

3.2.3	Detection of persulfide/polysulfide from 10b	74
3.2.4	MTT assay for cell viability to determine cytotoxicity of 10b	75
3.2.5	Synthesis of β -glucosidase responsive persulfide donors	76
3.2.6	LC/MS analysis for the decomposition of 11	76
3.2.6.1	Decomposition of 11a by β -glucosidase	76
3.2.6.2	Decomposition of 11b by β -glucosidase	78
3.2.7	Detection of persulfide/polysulfide from 11	79
3.2.7.1	Persulfide/polysulfide generation from 11a	79
3.2.7.2	Persulfide/polysulfide generation from 11b	80
3.2.8	MTT assay for cell viability to determine cytotoxicity of 11	81
3.2.9	Mechanism	82
3.2.9.1	Reactivity of 10b towards <i>N</i> -acetyl cysteine (NAC)	83
3.2.9.2	Reactivity of 10b towards Glutathione (GSH)	84
3.2.10	Intracellular generation of persulfide/polysulfide	85
3.2.11	Cytoprotective effect of compound 11a	86
3.3	Summary	88
3.4	Experimental Section	89
3.4.1	Synthesis and characterization of compounds	89
3.4.2	Persulfide/polysulfide measurement from 10b using LC/MS	93
3.4.3	Persulfide/polysulfide measurement from 11a and 11b using LC/MS	93
3.4.4	Decomposition of 10b in the presence of NAC	94
3.4.5	Decomposition of 10b in the presence of GSH	94
3.4.6	Cell viability assay	94
3.4.7	Detection of persulfides/polysulfides in cells using SSP2	95
3.4.8	Protection from oxidative stress	95
3.5	NMR spectra of compounds	97
3.6	References	102

CHAPTER 4.1: Insights into the therapeutic potential of persulfides using artificial substrates for 3-mercaptopyruvate sulfurtransferase (3-MST)

4.1.1	Introduction	106
4.1.2	Results and discussion	108
4.1.2.1	Synthesis	108
4.1.2.2	Tag Switch technique to detect persulfidation in proteins	109
4.1.2.3	Detection of persulfide/polysulfide using LC/MS	111
4.1.2.4	Mechanism for the formation of persulfide/polysulfide	113
4.1.2.5	Detection of persulfide/polysulfide using the probe SSP2	115
4.1.2.6	Activity of GAPDH	117
4.1.2.7	MTT assay for cell viability	119
4.1.2.8	H ₂ S detection in A549 cells	119
4.1.2.9	Antioxidant effect of compound 25	121
4.1.2.9.1	Hydrogen peroxide (H ₂ O ₂) quenching	121
4.1.2.9.2	Reduction of oxidative stress markers	122
4.1.2.10	Cytoprotective effects of compound 25	123
4.1.2.11	Mitigation of neuroinflammation	126
4.1.3	Summary	128
4.1.4	Experimental Section	130
4.1.4.1	Synthesis and Characterization	130
4.1.4.2	Tag-Switch technique for persulfidation of 3-MST	130
4.1.4.3	Persulfide/polysulfide measurement using SSP2	130
4.1.4.4	Persulfide/polysulfide measurement using LC/MS	131
4.1.4.5	GAPDH activity	132
4.1.4.6	H ₂ S imaging in cells using NBD fluorescein	132
4.1.4.7	Cell viability assay	132
4.1.4.8	ROS quenching	133
4.1.4.9	Measuring intracellular GSSG/GSH and NAD ⁺ /NADH	133
4.1.4.10	Protection from oxidative stress	133
4.1.4.11	Mice studies	134
4.1.4.11.1	Prostaglandin extraction and measurements	134
4.1.4.11.2	Measurement of cytokines	135

4.1.5	References	136
CHAPTER 4.2: β-galactosidase activated prodrug of the artificial substrates for 3-MST		
4.2.1	Introduction	140
4.2.2	Result and discussion	142
4.2.2.1	Synthesis	142
4.2.2.2	Decomposition of 30 in the presence of β -galactosidase	143
4.2.2.3	Decomposition of 30 in the presence of β -galactosidase and 3-MST	144
4.2.2.4	H ₂ S generation from 30 in the presence of β -galactosidase and 3-MST	144
4.2.2.5	Intracellular persulfidation	148
4.2.3	Summary	149
4.2.4	Experimental section	150
4.2.4.1	Synthesis and characterization of compounds	150
4.2.4.2	HPLC based decomposition study of 30	154
4.2.4.3	HPLC based turnover of 26 by 3-MST	155
4.2.4.4	Methylene blue assay for the detection of H ₂ S	155
4.2.5	NMR spectra of compounds	157
4.2.6	References	166
Appendix-I: Synopsis		
		169
Appendix-II: List of Figures		
		199
Appendix-III: List of Schemes		
		211
Appendix IV: Copyright Permits		
		213
Appendix-V: List of Publication		
		214

General remarks

- ¹H NMR spectra were recorded on JEOL ECX 400 MHz or Bruker 400 MHz spectrometer using tetramethylsilane (TMS) as an internal standard ($\delta_{\text{H}} = 0.00$), unless specified otherwise. Chemical shifts are expressed in ppm units downfield to TMS.
- ¹³C NMR spectra were recorded on JEOL ECX 100 MHz or Bruker 100 MHz spectrometer.
- Chemical shifts (δ) are reported in ppm and coupling constant (J) in Hz
- Mass spectra were obtained using HRMS-ESI-Q-Time of Flight LC-MS (Synapt G2, Waters) or MALDI TOF/TOF Analyser (Applied Biosystems 4800 Plus).
- FT-IR spectra were obtained using Bruker Alpha-FT-IR spectrometer and reported in cm^{-1} .
- All reactions were monitored by Thin-Layer Chromatography carried out on precoated Merck silica plates (F254, 0.25 mm thickness); compounds were visualized by UV light.
- All reactions were carried out under nitrogen or argon atmosphere with freshly dried solvents under anhydrous conditions and yields refer to chromatographically homogenous materials unless otherwise stated.
- All evaporations were carried out under reduced pressure on Büchi and Heildoph rotary evaporator below 45 °C unless specified otherwise.
- Silica gel (60-120) and (100-200) mesh were used for column chromatography.
- Materials were obtained from commercial suppliers and were used without further purification.
- Preparative HPLC purification was carried out using high performance liquid chromatography (HPLC) with C-18 preparative column (21.2 mm \times 250 mm, 10 μm ; Kromasil C18).
- HPLC analysis data was obtained using Agilent Technologies 1260 Infinity, C18 reversed phase column (4.6 mm \times 250 mm, 5 μm).
- LC/MS data was obtained using high resolution multiple reaction monitoring (MRM-HR) analysis on a Sciex X500R quadrupole time-of flight (QTOF) mass spectrometer fitted with an Exion UHPLC system using a Kinetex 2.6 mm

General Remarks

hydrophilic interaction liquid chromatography (HILIC) column with 100 Å particle size, 150 mm length and 3 mm internal diameter (Phenomenex)

- Spectrophotometric and fluorometric measurements were performed using Thermo Scientific Varioskan microwell plate reader.

Abbreviations

AA – Arachidonic acid
AAT – Asp aminotransferase
ACN – Acetonitrile
AcOH – Acetic acid
AD – Alzheimer's disease
ARE - Antioxidant response element
ATP – Adenosine triphosphate
au – Arbitrary unit
A549 – human lung cancer cell line
boc –*tert*-butyloxycarbonyl
bs – Broad singlet
BDE – bond dissociation energy
BSA – Bovine serum albumin
BTA – biotin thiol assay
^tBuOH – Tertiary-butanol
CA – Carbonic Anhydrase
CARS – Cysteinyl-tRNA synthetase
Calcd – Calculated
CBS – Cystathionine- β -Synthase
CDCl₃ – Chloroform-D
cGMP – Cyclic guanosine monophosphate
CHCl₃ – Chloroform
CH₂Cl₂ – Dichloromethane
Ctrl – Control
CO – Carbon Monoxide
COS – Carbonyl Sulfide
CSE – Cystathionine- γ -Lyase
CTAB – cetyltrimethylammonium bromide
CysSH – Cysteine
CysS-SH – Cysteine persulfide
CysS-OH – sulfenic acid

CysS-NO – nitrosothiol
DAS - Diallyl sulfide
DADS - Diallyl disulphide
DATS - Diallyl trisulfide
DBU - 1,8-Diazabicyclo[5.4.0]undec-7-ene
dd – Doublet of doublet
DCM – Dichloromethane
DEA/NO – sodium 2-(*N, N*-diethylamino)-diazenolate-2-oxide
DIPEA – diisopropyl ethyl amine
DLD-1 –Human colon carcinoma cells
DMAP – *N, N*-Dimethylaminopyridine
DMEM – Dulbecco's Modified Eagle's Medium
DMF – *N, N'*-Dimethyl formamide
DMSO – Dimethyl sulfoxide
DNA – Deoxyribonucleic acid
D₂O – Deuterium Oxide
DPBS – Dulbecco's Phosphate-Buffered Saline
dt – Doublet of triplet
DTT – dithiothreitol
DTPA – diethylenetriaminepentaacetic acid
δ – Delta (in ppm)
E. coli – *Escherichia coli*
eq. – Equivalentents
ES – Esterase
ESI – Electron spray ionization
Et₃N – Triethylamine
EtOH – Ethanol
EtOAc – Ethyl acetate
Et₂O – Diethyl ether
FBS – Fetal bovine serum
FDNB –Fluorodinitrobenzene
FeCl₃ – Ferric Chloride
g – Gram

G3P – glyceraldehyde-3-phosphate
GAPDH – glyceraldehyde-3-phosphate dehydrogenase
GCL – glutamate-cysteine ligase
GIT – Gastrointestinal tract
GRAS – Generally Recognized As Safe
GSK3 β – glycogen synthase kinase
GSH – Glutathione
GS-T – Glutathione S-Transferase
h – Hours
hCBG – Human cytosolic β -glucosidase
HCl – Hydrochloric acid
HCysS-SH – homocysteine persulfide
HOCl – Hypochlorous acid
HOMO – Highest Occupied Molecular Orbital
HEPES – 2-[4-(2-hydroxyethyl)piperazin-1-yl]ethanesulfonic acid
HEK29 – human embryonic kidney cells
HepG2 –hepatocarcinoma
HPE-IAM – *N*-(4-hydroxyphenethyl)-2-iodoacetamide
HO-1 – heme oxygenase
H₂O – Water
H₂O₂ – Hydrogen peroxide
H₂S – Hydrogen Sulfide
H₂S_n – hydrogen polysulfide
HNO₃ – Nitric acid
HPLC – High performance liquid chromatography
HRMS – High-resolution mass spectrometry
Hz – Hertz
HSNO – Thionitrous acid
HNO – Nitroxyl
IAM – Iodoacetamide
IBD – Inflammatory bowel disease
IC₅₀ – Half maximal inhibitory concentration
I κ B – inhibitor of κ B

IKK – I κ B kinase
IR – Infrared
 J – Coupling constant
KEAP 1 - Kelch-like ECH- associated protein 1
KCl – Potassium Chloride
K₂CO₃ – Potassium carbonate
 λ_{ex} – Excitation wavelength
 λ_{em} – Emission wavelength
LPS – Lipopolysaccharides
LD₅₀ – Median lethal dose
LMW – low molecular weight
 m – Multiplet
MALDI – Matrix-Assisted Laser Desorption Ionization
MEF – mouse embryonic fibroblasts
Me – Methyl
MeOH – Methanol
mg – Milligram
Min. – Minutes
MHz – Megahertz
mL – Millilitre
mM – Millimolar
mmol – Millimoles
mBBr – Monobromobimane
MI/R – myocardial ischemia reperfusion
MS – Mass spectrum
MSBT - Methyl sulfonyl benzothiazole
3-MP – 3-mercaptopyruvate
3-MST – 3-Mercaptopyruvate sulfur transferase
MTT – 3-(4,5-Dimethylthiazol-2-yl)-2,5-diphenyltetrazolium bromide
MW – Molecular weight
 m/z – Mass to Charge ratio
 μM – Micromolar
NaBH₄ – Sodium borohydride

NAC – *N*-acetyl cysteine
NACMe – *N*-acetylcysteine methylester
NAD⁺ – nicotinamide adenine dinucleotide
NADPH – Reduced nicotinamide-adenine-dinucleotide phosphate
NaOMe – sodium methoxide
NFκB – nuclear factor
NaH – Sodium hydride
NaHCO₃ – Sodium bicarbonate
NaI – Sodium iodide
NaSH - Sodium hydrosulfide
Na₂S – Sodium sulfide
Na₂SO₄ – Sodium sulphate
NMR – Nuclear magnetic resonances
NO – Nitric oxide
NQO1 – NAD(P)H quinone oxidoreductase 1
nM – Nanomolar
Nrf2 - nuclear factor erythroid 2-related factor 2
NSAID – Non-Steroidal Anti-inflammatory Drug
NTR – Nitroreductase
N2a – mouse neuroblastoma cell line
•OH – Hydroxyl radical
O₂^{•-} – Superoxide radical
ONOO⁻ – Peroxynitrite
oxPTM – oxidative post translational modification
PBS – Phosphate buffer saline
PD - Parkinson's disease
pH – Potential of hydrogen
Ph – Phenyl
PLA2 – cytosolic phospholipase A2
PPh₃ – Triphenyl phosphine
PSD95 – postsynaptic density 95 protein
Py – Pyridine
ppm – Parts per million

ProPerDP – protein persulfide detection protocol
% – Per cent
ROS – Reactive oxygen species
RPMI – Roswell Park Memorial Institute Medium
RT – Retention Time
rt – Room temperature
s – Singlet
SABG – senescence associated β -galactosidase
S₈ – elemental sulfur
S₂O₃²⁻ – thiosulfate
SH-SY5Y – human neuroblastoma cell line
SQR – sulfide:quinone reductase
t – Triplet
TBSCl - *tert*-butyldimethylsilyl chloride
TEA – Triethylamine
TFA – Trifluoroacetic acid
THF – Tetrahydrofuran
TLC – Thin layer chromatography
TMS – Tetramethylsilane
TLR4 – toll like receptor
tRNA – transfer ribonucleic acid
TSTD – Thiosulfate sulfurtransferase
t_{1/2} – half-life
UV – ultraviolet
 μ g – Microgram
 μ mol – Micromolar
 μ L – Microliter
 μ m – Micrometre
WT- MEF – Wild type mouse embryonic fibroblast cells
Zn(OAc)₂ – Zinc Acetate

Acknowledgement

With great pleasure I would like to take this opportunity to express my sincere gratitude towards my thesis supervisor, Prof. Harinath Chakrapani. Through all the ups and downs of my PhD journey, when I seemed to have lost confidence in myself, he never did. He gave me the intellectual freedom to choose my own research problems and execute them while providing his valuable inputs. I truly appreciate the high standards he has set for each one of us and for maintaining a collaborative environment in the lab, which helped me grow as a researcher. Personally, he has been very approachable and accommodating and I am extremely grateful to have worked under his mentorship.

I would like to thank my RAC committee members, Dr. Amrita Hazra and Dr. C.V Ramana for their valuable suggestions and feedback during the RAC meetings.

I would like to express my gratitude to all the faculty members of IISER Pune for extending a helping hand at various stages of my PhD journey. I thank Dr. Siddhesh Kamat and his group members, particularly Abinaya and Shubham who were kind enough to teach me various chemical biology techniques and for allowing me to use their lab space and facilities. I am also grateful to Dr. Amrita Hazra and her group members for helping me in protein purification. I would like to thank former Director of IISER Pune, Prof. K. N. Ganesh and our current Director, Prof. Jayant. B. Udgoankar for providing some of the top-notch facilities at IISER Pune.

The close-to-6 years that I have spent in IISER Pune have been one of the longest durations I had spent anywhere, apart from home. I have met several people during this journey and each one of them have left a lasting impact on me. I will forever be grateful to my former lab members Dr. Vinayak, Dr. Kundan, Dr. Ravi, Dr. Ajay, Dr. Preeti and Dr. Amogh for helping an amateur person like myself navigate the initial years of my PhD. Specially Preeti, in whom I have found a mentor and a great friend, I thank her for teaching me the basics of research. My current lab members Dr. Kavita, Pooja, Anand, Laxman, Suman, Bharat, Utsav, Pooja, Simran, Minhaj and Dr. Amol who have helped me survive the later years of my PhD, with their jovial nature and incessant banter. I also thank all the MS alumni of the lab, Farhan, Harshit, Gaurav, Sushma, Swetha, Ashwin, Amal, Suraj, Bhakti, Manjima and Jishnu, some of whom I have had the opportunity to mentor. From discussing complex research problems to discussing random topics, from troubleshooting in the lab to our fun escapades, I thank each one of them for making this journey a lot more fun and enduring.

Acknowledgement

I thank the members of the non-teaching staff, instrument operators and administrative staff.

I consider myself extremely lucky to have men in my life who have given me the wings to soar. My late father, for his unwavering belief in me and his support, I miss you everyday Deuta. My husband who has been a constant source of encouragement and fought for me against all odds. Thank you Jugal for all the love and laughter, for never letting me settle, for being ambitious WITH me and for being truly supportive of every decision I make. I am thankful to my mother for being a source of inspiration, my agony aunt, the receiving end of all my outbursts, for all the love and for just being by my side. Thank you, Ma for everything that you do for us. I thank my sisters, Momi ba and Tuki for bringing so much joy and laughter to my life. I also thank my grandparents for their constant love and blessings.

Prerona Bora

Abstract

Hydrogen sulfide (H₂S) plays an integral role in several intracellular signaling processes, modulating an array of physiological functions including vasodilation, neurotransmission, antioxidant response, inflammation, angiogenesis, hypoxia sensing to list a few. One of the widely accepted mechanisms of H₂S signaling is the oxidative post translational modification of cysteine residues in proteins, known as protein persulfidation. While H₂S can persulfidate proteins only under oxidizing conditions, persulfides and polysulfides, collectively termed as sulfane sulfurs can modify proteins directly and are more efficient than H₂S. Additionally, low molecular weight (LMW) persulfides are better reductants and multiple evidences suggest that persulfides are far superior at sequestering oxidants compared to its congeners, thiols and H₂S. Hence, small molecule persulfides have emerged as important intermediates in combating oxidative and electrophilic stress. This has fueled the development of strategies to enhance cellular persulfides and modulate the levels of intracellular protein persulfidation. LMW persulfides are unstable in aqueous solution due to its propensity to undergo disproportionation, therefore, generating these species in cells has been a major challenge. In this regard, we designed two distinct strategies for the generation of persulfides. The first strategy involved design and synthesis of prodrugs of persulfides, wherein the persulfide moiety is masked by a protecting group which can be cleaved in response to an external stimulus. Any diseased condition is often accompanied by an overproduction of free radicals and reactive oxygen species (ROS). So, we synthesized and evaluated a persulfide prodrug responsive to hydrogen peroxide (H₂O₂), a stable ROS. The compound upon activation by H₂O₂ was found to generate persulfides and exhibit cytoprotective effects in cells against oxidative stress induced damage. The next class of prodrugs were designed to be activated by the enzymes β-glycosidase, which are upregulated in cells exposed to stress such as inflammation and cancer. Two series of compounds were synthesized, responsive to β-glucosidase and β-galactosidase respectively. The compounds were found to be cleaved by the aforementioned enzymes to generate sulfane sulfurs along with H₂S. Although these compounds were helpful in providing insights into the physicochemical properties of persulfides and its therapeutic potential, this strategy is limited by the complexity of synthesis and low shelf-stability of the compounds. Our second approach was to leverage the biosynthetic machinery of the cell to generate persulfides. We developed compounds that does not contain the persulfide functional group but can generate persulfides upon entry into cells. Artificial substrates for 3-mercaptopyruvate sulfurtransferase (3-MST), an enzyme involved in sulfur trafficking was synthesized and evaluated. This compound was

found to generate persulfides/polysulfides upon turnover by 3-MST and generate H₂S in cells. Further, antioxidative and anti-inflammatory effects of this compound was demonstrated *in-vitro* and *in-vivo*. Lastly, a prodrug of the artificial substrate for 3-MST, responsive to β -galactosidase, a biomarker for senescent cells was synthesized, as a tool to interrogate the functional consequences of persulfidation in senescence and aging. The compound was selective towards activation by β -galactosidase. Generation of H₂S in the presence of 3-MST and persulfidation of proteins in senescent cells was observed with the compound.

Taken together, we have developed strategies for efficient generation of intracellular persulfides with benign byproducts, that should help us delineate the role of persulfides in cell signaling while harnessing its therapeutic potential.

CHAPTER 1: Introduction

1.1 Hydrogen Sulfide (H₂S) Signaling

Since the emergence of life on earth, sulfur has been an essential element in living organisms, and is used in the construction of biomolecules like amino acids cysteine and methionine, formation of iron sulfur (Fe-S) clusters, coenzymes and co-substrates and a multitude of metabolic pathways. Sulfur containing proteins and peptides (glutathione, GSH for instance) has been a crucial component of the antioxidant machinery of the cell, protecting biomolecules against oxidative damage inflicted under conditions of stress.^{1,2} On the contrary, some sulfur derived entities generated within cells, collectively termed as reactive sulfur species can damage biomolecules at elevated concentrations.^{3,4} This versatile nature of sulfur can be ascribed to its interconvertible oxidation states (Figure 1.1).⁵

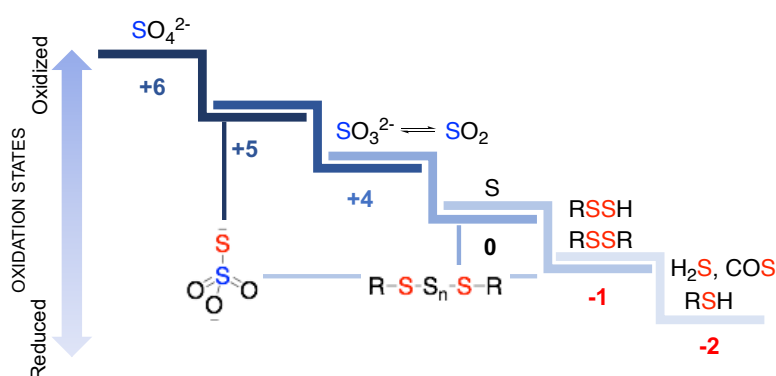


Figure 1.1. Sulfur can exist in different oxidation states. Some of the biologically relevant reactive sulfur species are shown. Red and blue are used to designate negative and positive oxidation states respectively.

Hydrogen sulfide (H₂S) is one of the simplest physiologically relevant thiols. The first report on the physiological relevance of H₂S dates back to 1996, where Kimura and co-workers have reported the role of H₂S as a potential neuromodulator.⁶ Ever since there have been mounting evidence of H₂S mediating several intracellular signaling process, joining the family of gasotransmitters along with nitric oxide (NO) and carbon monoxide (CO). The biosynthesis of H₂S in eukaryotes involves the enzyme 3-mercaptopyruvate sulfurtransferase (3-MST) and other transsulfuration pathway enzymes cystathionine-β-synthase (CBS) and cystathionine-γ-lyase (CSE).⁷⁻¹⁰ H₂S has been reported to play fundamental roles in human physiology, modulating an array of cellular functions including vasodilation,^{11,12} neurotransmission,¹³ angiogenesis,^{14,15} inflammation,^{16,17} hypoxia sensing,¹⁸ myocardial ischemia reperfusion¹⁹ to name a few. Several studies have demonstrated the cytoprotective nature of H₂S, possibly due to its ability to readily react with a variety of reactive species such as oxyradicals,²⁰

hypochlorous acid²¹ and peroxynitrite.²² In fact, H₂S can efficiently scavenge oxidants *in-vitro* at a rate comparable to that of thiols, supported by their similar one electron reduction potentials ($E^{\circ'} (S^{\cdot-}, H^+/HS^-) = 0.92 \text{ V}$; $E^{\circ'} (RS^{\cdot}, H^+/RSH) = 0.96 \text{ V}$).²³ However, in biological systems the possibility of H₂S directly scavenging oxidants is limited by kinetic parameters such as concentration. While thiols such as Glutathione (GSH) is present in millimolar concentrations, the tissue concentration of H₂S is in submicromolar range, several magnitudes lower than thiols, suggesting that H₂S cannot serve as an antioxidant. Nevertheless, multiple studies have demonstrated the antioxidant and protective effects of H₂S in cells exposed to oxidants.

1.2 Cellular mechanisms of persulfidation

One of the widely accepted mechanisms of H₂S signaling is the oxidative post translational modification (oxPTM) of cysteine residues (CysSH), known as protein persulfidation (CysS–SH). Direct reaction of H₂S with CysSH is limited by redox constraints, since the S in both these species exists in the lowest oxidation state (–2). H₂S can only react with oxidized CysSH residues in the protein such as sulfenic acid (CysS–OH), disulfides (CysS–SCys), nitrosothiols (CysS–NO) or glutathionylated (CysS–SG) cysteine (Figure 1.2.a).^{24–26}

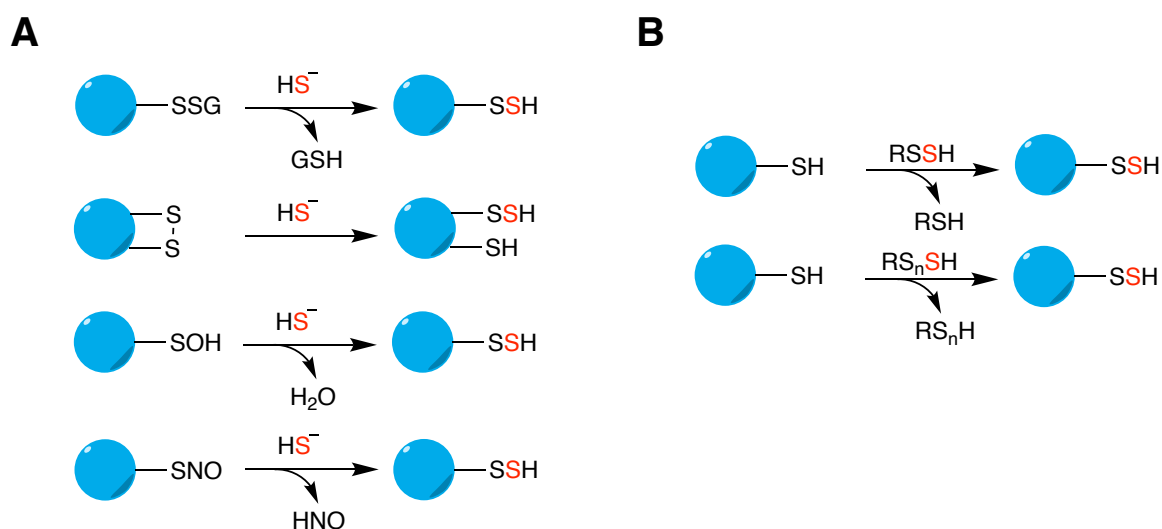


Figure 1.2. a) Persulfidation of proteins by reaction of H₂S with oxidized cysteine residues. b) Protein persulfidation induced by persulfides and polysulfides.

While H₂S can induce persulfidation only under oxidative conditions, sulfane sulfurs can directly modify proteins to form persulfide (Figure 1.2.b).^{27–31} The term ‘sulfane sulfur’ is used for reactive species that has a sulfur bonded to another sulfur atom or an ionizable hydrogen

and is a collective term used to define polysulfides ($\text{RS-S}_n\text{H}$, $\text{RS-S}_n\text{R}$), persulfides (RS-SH), elemental sulfur (S_8) and thiosulfate ($\text{S}_2\text{O}_3^{2-}$).^{32,33}

1. H_2S and disulfides: The reaction between H_2S and a low molecular weight (LMW) disulfide such as cystine and GSSG is slow.^{26,34,35} For instance, the rate constant for reaction with cystine at pH 7.4 at room temperature is 0.6 M^{-1} .³⁶ Although this reaction can be accelerated by the protein microenvironment, as evidenced by the reaction of H_2S with the active site disulfide of sulfide:quinone reductase (SQR).³⁷ Given the cytosolic concentration of disulfides is very low in the reducing milieu of the cell, this mechanism might not be a major contributor to persulfide formation, except under oxidizing conditions.³⁸
2. H_2S and sulfenic acid: Sulfenic acids (RSOH) are produced during oxidation of cysteine residues in the presence of oxidants like hydrogen peroxide (H_2O_2) or hypochlorous acid (HOCl).³⁹ Typically, sulfenic acids being unstable immediately reacts with existing thiols to form disulfides or with H_2S to form persulfides.^{36,40} Consistent with this observation, levels of intracellular persulfidation was found to be elevated under conditions of oxidative stress.³⁶
3. H_2S and nitrosothiols: S-nitrosation (RS-NO) is a post translational modification of cysteine residues mediated by NO .⁴¹ Generally, nitrosothiols (RS-NO) react with H_2S through the N to form thionitrous acid (HSNO).⁴² Alternatively, a nucleophilic attack on the S of RS-NO would yield a persulfide (RS-SH) and nitroxyl (HNO) (Figure 1.3.). The latter is thermodynamically unfavorable; however, a protein microenvironment might facilitate this reaction.^{23,43} RS-NO can be represented by two resonance structures, protein microenvironment stabilizing the resonance form II would make the S more susceptible to nucleophilic attack, thus favoring the formation a persulfide over HSNO .

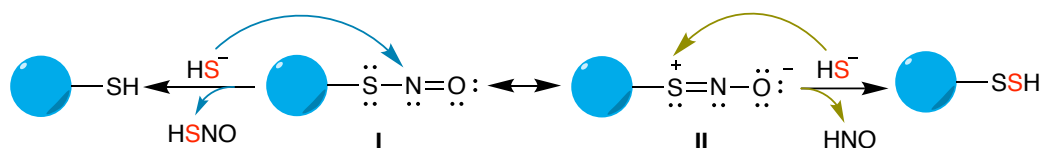


Figure 1.3. Resonance structures of S-nitrosothiol. Nucleophilic attack is favoured on structure II, leading to the formation of a protein persulfide and HNO .

4. H_2S and persulfides: The transfer of the terminal sulfur from persulfides to a thiolate is termed as transpersulfidation and has been documented in several proteins.³¹ A nucleophilic attack of the thiolate on the inner S leads to the generation of H_2S , while

an attack on the terminal S results in a persulfide (Figure 1.4.). The nature of the reaction and the products formed are influenced by a number of factors including steric bulk of the thiolate, protein microenvironment and acidity of the thiolate.⁴⁴ LMW persulfides like CysS–SH and GS–SH are widely prevalent and are major persulfidating agents in biological systems.^{27,44,45} As demonstrated by Akaike and co-workers, a significant upregulation of protein persulfidation was observed in cells overexpressed with CBS and CSE, enzymes involved in the biosynthesis of CysS–SH.²⁷

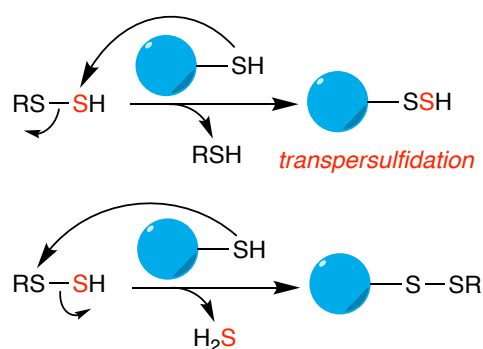


Figure 1.4. Nucleophilic attack of thiol on persulfides, leading to either transpersulfidation or release of H₂S.

- H₂S and polysulfides: Thiols can undergo nucleophilic attack on polysulfides to form persulfides. Polysulfides are common contaminants in commercially available Na₂S or NaSH samples and much of the biological functions mediated by exogenous H₂S have been attributed to polysulfides.^{29,46} Additionally, polysulfide donors have been reported to induce persulfidation of proteins such as glyceraldehyde-3-phosphate dehydrogenase (GAPDH) and kelch like ECH associated protein (KEAP1).^{47,48} However, polysulfides are unstable and prone to reduction, hence their physiological relevance under reducing environment of the cell remains unclear.

1.3. Physiological relevance of persulfidation

In one of the earliest reports, Snyder and co-workers in 2009 have demonstrated that H₂S modifies a large number of proteins by persulfidation and about 10-25% of the proteins, including GAPDH, actin, tubulin was found to be persulfidated under physiological conditions.⁶ Subsequently, using a biotin thiol assay (BTA) >800 proteins in a pancreatic beta cell line were identified to be persulfidated by Banerjee and co-workers.⁴⁹ Detection of protein persulfides has been a major challenge, due to its short half-life and interference from other reactive sulfur species like thiols, sulfenic acids and disulfides. Later, Nagy and co-workers

have developed a specific protein persulfide detection protocol (ProPerDP) to reveal significantly lower levels of protein persulfide (0.1 to 1% of the total protein pool) in human embryonic kidney (HEK293) cells.⁵⁰ Nevertheless, persulfidation of proteins have functional implications in multiple physiological processes, including inflammation,⁵¹ antioxidant response,⁵² neurodegenerative disorders like Parkinson's disease (PD),⁵³ Alzheimer's disease (AD)⁵⁴ and Huntington's disease.⁵⁵

1.3.1. Persulfidation of KEAP1

One of the major antioxidants signaling pathways involves the activation of the transcription factor nuclear factor erythroid 2-related factor 2 (Nrf2).⁵⁶ Under normal conditions, the oxidative stress sensor protein KEAP1 forms a complex with Nrf2 where Nrf2 is ubiquitinated by the Culin3-KEAP1 E3 ubiquitin ligase complex, leading to its proteosomal degradation. Thus, the activity of Nrf2 under homeostatic conditions is tightly regulated.⁵⁷ Under conditions of oxidative stress, H₂S has been reported to modify the Cys151 residue of KEAP1 to form a persulfide, leading to a conformational change and dissociation of the KEAP1-Nrf2 complex. The free Nrf2 then subsequently translocates to the nucleus where it can promote the activation of antioxidant responsive elements (ARE) such as glutathione reductase and glutamate-cysteine ligase (GCL) (Figure 1.5).⁵²

In one report, an onion derived metabolite *S*-1-propenylmercaptocysteine (CySSPe) was demonstrated to exhibit protective effects against oxidative stress. CySSPe mediates persulfidation of KEAP1, facilitating the nuclear translocation of Nrf2 and enhance the expression of antioxidant enzymes such as NQO1, heme oxygenase (HO-1) and GCL.⁵⁸ Another study has reported the antioxidant potential of polysulfides via a similar KEAP1 persulfidation mechanism and regulation of the KEAP1-Nrf2 pathway (Figure 1.5).⁴⁷

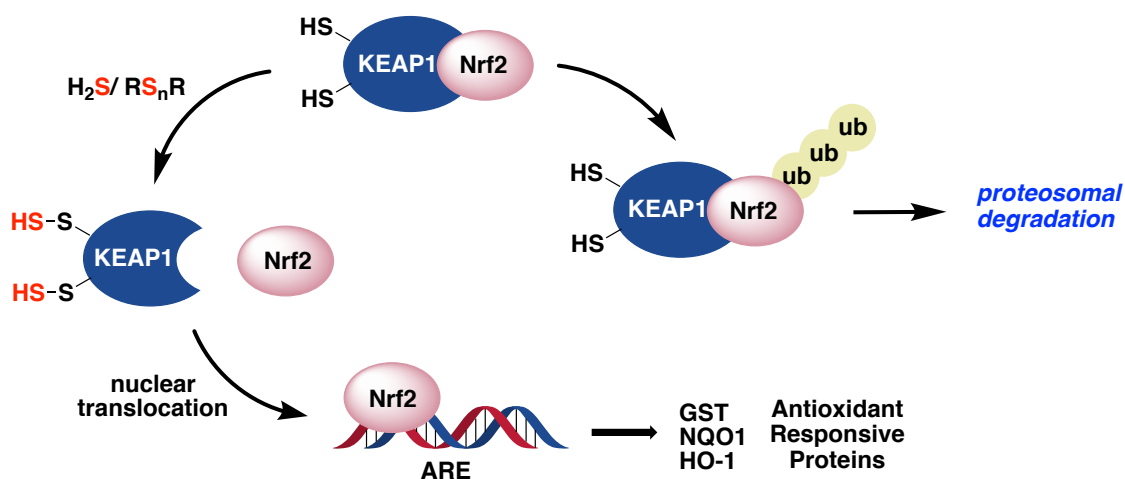


Figure 1.5. Persulfidation regulating the KEAP1-Nrf2 pathway

1.3.2. Persulfidation protects proteins from oxidation

Typically, under conditions of excess H_2O_2 (oxidative stress), cysteine residues in proteins gets oxidized to sulfenic acid (RSOH) which can be further oxidized to the sulfinic (RSO₂H) and sulfonic acid (RSO₃H).⁵⁹ These are considered to be irreversible modifications and can potentially lead to loss of activity of the protein.^{60,61} However, if the cysteine residues are persulfidated, analogous to the reaction of thiols with H_2O_2 , persulfides are likely to form perthiosulfenic acid (RS-SOH). In presence of excess oxidants, RS-SOH can be further oxidized to form the perthiolsulfinic acid (RS-SO₂H) and the perthiosulfonic acid (RS-SO₃H), detected as products of oxidation in papain and glutathione peroxidase.^{36,62} Unlike the sulfinic (RSO₂H) and sulfonic acid (RSO₃H) derived from thiols, the persulfide analogues can be reduced by enzymes such as thioredoxin to restore the native thiol (Figure 1.6).^{63,64} Thus, persulfides can protect proteins from overoxidation under conditions of oxidative stress.

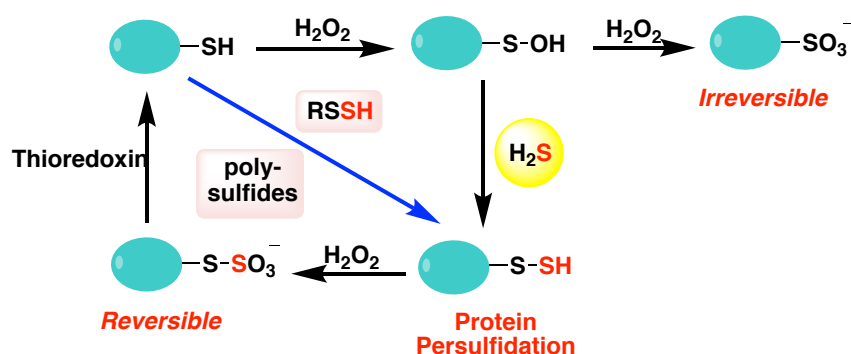


Figure 1.6. Persulfidation protects protein from overoxidation under conditions of oxidative stress.

1.3.3. Persulfidation of NFκB

The innate immune response involves the nuclear factor (NFκB) which is a transcription factor composed of two subunits p65 and p50. In unstimulated cells, the NFκB is sequestered in the cytoplasm by the inhibitor of κB (IκB) which forms a complex with NFκB.⁶⁵ Upon stimulation, the IκB kinase (IKK) phosphorylates the IκB resulting in its ubiquitination and release of NFκB. This is followed by phosphorylation of NFκB which after translocation to the nucleus induces the expression of pro-inflammatory cytokines.⁶⁶ In one of the studies, H₂S was found to elicit an anti-inflammatory response by persulfidation of the Cys38 residue of the p65 subunit of NFκB. Consequently, leading to a decline in its phosphorylation, translocation to the nucleus as well as inhibition of its DNA binding activity (Figure 1.7.).⁵¹ In a separate study, persulfides/polysulfides were found to negatively regulate the toll like receptor (TLR4) mediated inflammatory response.⁶⁷ Persulfides/polysulfides could efficiently suppress the

inflammatory response induced by LPS in macrophages as well as *in vivo*, in a mouse endotoxin shock model, possibly via inhibition of the IKK/NF κ B axis.

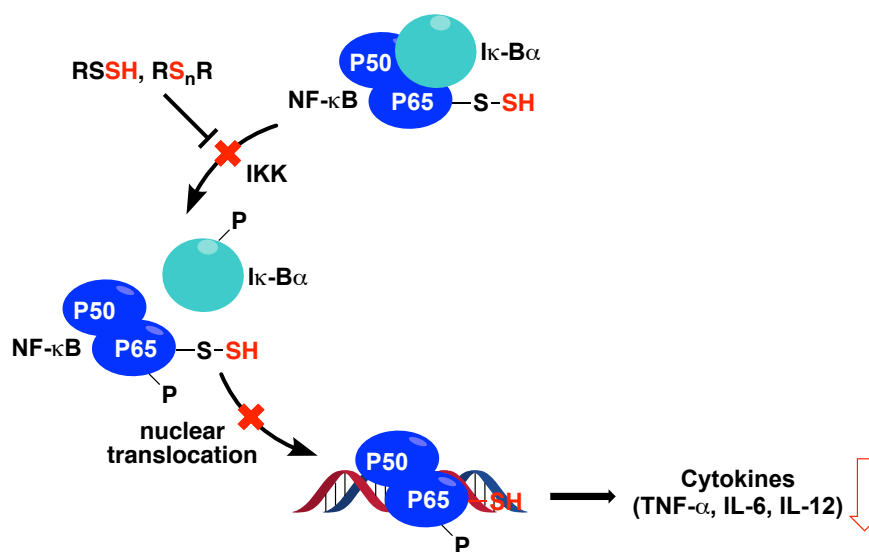


Figure 1.7. Persulfidation of the p65 subunit of NF κ B leads to an inhibition in phosphorylation, nuclear translocation and DNA binding activity of NF κ B, resulting in the downregulation of pro-inflammatory cytokines. Persulfidation of NF κ B elicits an anti-inflammatory effect.

1.3.4. Persulfidation in neurodegenerative diseases

Parkin is a E3 ubiquitin ligase which plays a critical role in degradation of damaged neurons or molecules via ubiquitination in the proteasome. The etiology of Parkinson's disease involves mutation in this protein, leading to an accumulation of toxic soluble proteins in the proteasome.⁶⁸ Persulfidation of parkin reportedly enhances the activity of parkin. However, levels of persulfidation were markedly depleted in patients of Parkinson's disease, resulting in an accumulation of toxic proteins and eventually leading to cell death (Figure 1.8).⁵³

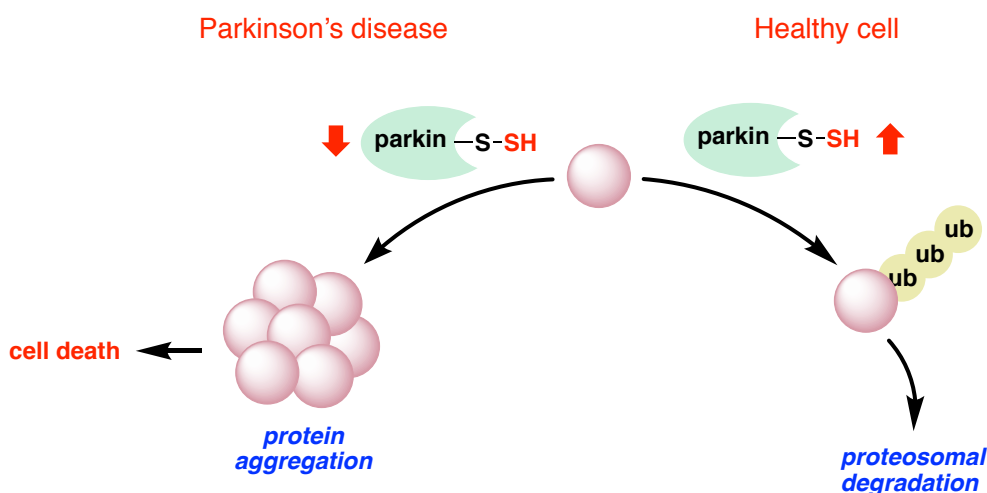


Figure 1.8. Regulatory role of persulfidation on the activity of parkin.

Alzheimer's disease is characterized by an aggregation of microtubule associated proteins such as Tau and β -amyloid peptides. Changes in structural conformations of Tau due to its hyperphosphorylation mediated by the kinase glycogen synthase kinase (GSK3 β), decreases its binding ability to microtubules. This results in aggregation of Tau leading to neurotoxicity. H₂S donors was found to exhibit neuroprotective effects mediated by persulfidation of GSK3 β , inhibiting its activity and preventing hyperphosphorylation of Tau.⁵⁴

1.3.5. Persulfidation of GAPDH

GAPDH is a glycolytic enzyme with a redox active cysteine and is an important regulator of cellular apoptosis. GAPDH being one of the most abundant protein is a commonly identified target in persulfidation screens of proteomes.²⁷ Siah1 is an E3 ubiquitin ligase which consists of a nuclear localization tag. Upon binding to GAPDH, it enables the nuclear translocation of GAPDH, triggering degradation of nuclear proteins and apoptosis.⁶⁹ Persulfidation of GAPDH by H₂S has been proposed to modulate the activity of GAPDH, stabilization of Siah1 leading to the degradation of the postsynaptic density 95 protein (PSD95).⁷⁰ PSD95 promotes synapse maturation and regulates synaptic stability and strength. Loss of PSD95 is implicated in several neurodegenerative diseases such as dementia.

The influence of persulfidation on GAPDH has been previously studied with opposite inferences. Snyder and co-workers reported that GAPDH was found to be endogenously persulfidated at the Cys152 site, which was deficient in CSE knock down cells. Persulfidation reportedly enhanced its activity which was subdued upon treatment with dithiothreitol (DTT), a reducing agent.⁶ On the contrary, persulfidation of GAPDH was shown to inhibit its activity in a study conducted by Jarosz *et al.* However, it was observed that persulfidation in this case occurred at the Cys156 and Cys247 sites and not the Cys152 active site upon treatment with NaSH and polysulfides.⁷¹ A similar effect on persulfidation of GAPDH was reported by Wang and co-workers wherein the activity of GAPDH was inhibited upon treatment with polysulfide donors.⁴⁸

1.4. LMW persulfides in biological systems

With the recent advances in persulfide detection strategies, significant concentrations of LMW persulfides and polysulfides, collectively known as the sulfane sulfur pool have been detected in biological systems. CysS-SH and polysulfides have been detected in a number of cell lines like lung cancer (A549), human neuroblastoma (SH-SY5Y), HeLa and HEK293 cells.^{27,67,72} Akaike and co-workers have detected significantly high concentrations of GS-SH in the brain

tissue of mice (150 μM) along with the heart and lung tissues (50 μM). Additionally, appreciable levels of homocysteine persulfide (HCysS-SH) and CysS-SH along with polysulfides (Cys-SSS-Cys, Cys-SSSS-Cys, GSSSG) were detected in human and mouse plasma.²⁷ Kimura and co-workers have developed an LC/MS based method to detect hydrogen polysulfides (H_2S_n) in the brain tissue of mice models wherein, H_2S_3 was found to be present in similar concentrations as that of H_2S .⁷³

1.5. Biosynthesis of persulfides

Sulfurtransferases are a group of enzymes found in archae, bacteria and eukaryotes that are responsible for transfer of sulfur containing groups.⁷⁴ These are ubiquitously distributed and perform a wide range of functions including sulfur metabolism, cyanide detoxification,^{75,76} iron sulfur cluster formation⁴⁵ and selenium metabolism.⁴⁵ The catalytic cycle of sulfurtransferases proceed via a two-step reaction; the active site cysteine forms a transient persulfide intermediate (S-SH) by accepting a sulfur from a donor compound. The sulfur then subsequently gets transferred to a thiophilic acceptor, regenerating the native enzyme. These thiophilic acceptors can be proteins like thioredoxin or glutaredoxin or small molecule thiols like cysteine or glutathione that can potentially mediate transpersulfidation of proteins (Figure 1.9).⁷⁷⁻⁸⁰ However, persulfidation of two-cysteine containing proteins are reported to be extremely short-lived due to the presence of a resolving cysteine, leading to a competition between transpersulfidation and H_2S release.

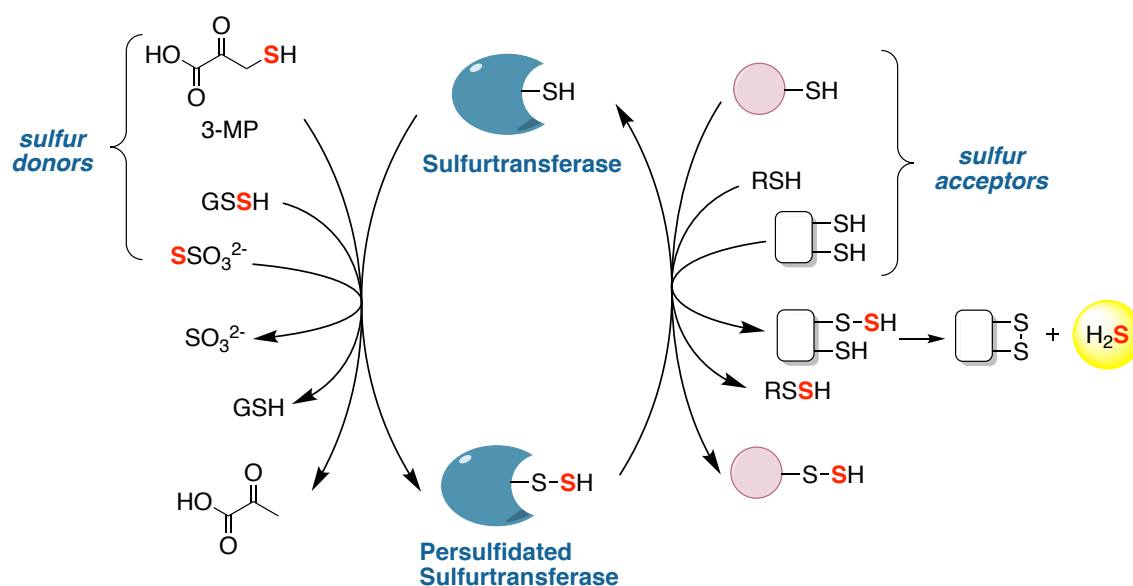


Figure 1.9. Catalytic cycle of sulfurtransferase. First step of the catalytic cycle involves the active site cysteine forming a persulfide intermediate by accepting a sulfur from the sulfur donor. The second step of the catalytic cycle involves sulfur transfer from the persulfidated enzyme to a sulfur acceptor, reinstating the sulfurtransferase to its original state.

owing to the low intracellular concentration of cystine in the cell, substrate level might regulate the production of H_2S over CysS-SH and the latter could be elevated only under conditions that would lead to a higher concentration of intracellular cystine.^{83,84}

Very recently, another enzyme that is involved in the biosynthesis of CysS-SH was discovered.⁸⁵ CysteinyI-tRNA synthetase (CARS) is originally known to catalyze the formation of cysteinyI tRNA via cysteine and aminoacyl tRNA. However, recent biochemical analyses revealed its ability to catalyze the synthesis of CysS-SH using cysteine as the substrate.⁸⁶ It cleaves the carbon-sulfur bond to release the sulfur atom from a donor cysteine and transfers it to another acceptor cysteine molecule, thus forming a persulfide. Subsequent transfer of sulfur atoms to CysS-SH can result in formation of trisulfides (CysS-SSH) and polysulfides (CysS-(S)_nH). Moreover, CARS can catalyze the incorporation of CysS-SH into tRNA which can then lead to the formation of persulfidated proteins via translation (Figure 1.11.).

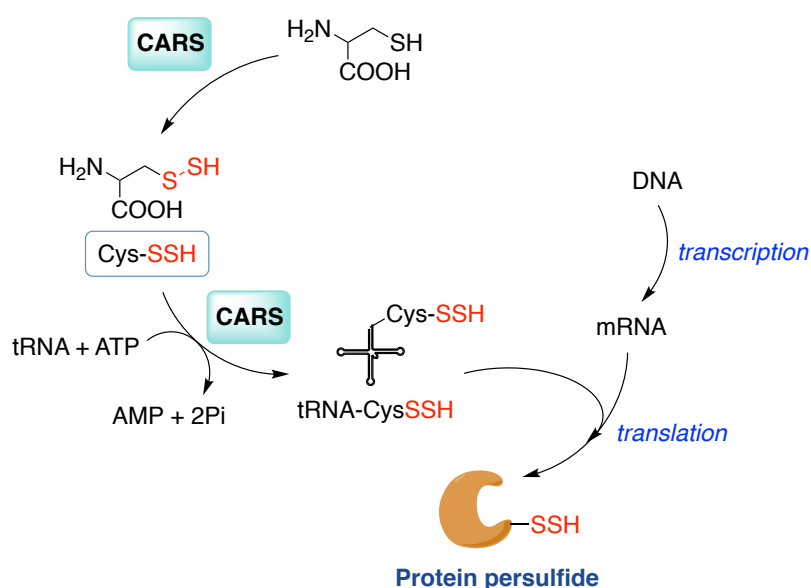


Figure 1.11. CARS catalyzing the synthesis of CysS-SH from cysteine and tRNA of CysS-SH that can ultimately form a persulfidated protein via translation of the mRNA.

1.6. Physicochemical properties of persulfides

Persulfides, although are structurally similar to thiols have properties that are distinct from other physiologically relevant thiols or H_2S . These differences in physicochemical properties have implications in their biological activities as well. In alkaline solutions, persulfides display an absorbance maximum at 335-340 nm with a low absorption coefficient of $\sim 310 \text{ M}^{-1} \text{ cm}^{-1}$.⁸⁷ S-H bond stretching frequency of persulfides in an IR spectra is observed at $\sim 2500 \text{ cm}^{-1}$ whereas for thiols it is $\sim 2570 \text{ cm}^{-1}$, suggesting a stronger S-H bond in thiols.⁸⁷

1. Acidity: In accordance with the weaker S–H bond strength of persulfides as stated above, it is predicted to be more acidic compared to its thiol counterpart. The pK_a of 2-[(3-aminopropyl)amino]ethane persulfide was experimentally determined to be 6.2 ± 0.1 whereas the corresponding thiol has a pK_a value of 7.6 ± 0.1 .⁸⁸ Recently, the pK_a of GS-SH was reported to be 5.45 and a separate computational analysis estimated the pK_a of CysS-SH to be 4.3, both of which are significantly lower than the thiols (>8).^{36,89} These data suggest that under physiological conditions, persulfides will predominantly exist in the ionic form (RSS^-).
2. Spontaneous decay of persulfides: Persulfides are inherently unstable species that decomposes in aqueous solution to produce elemental sulfur among other reactive species. The half-life ($t_{1/2}$) of penicillamine persulfide was found to be 2.7 min at room temperature whereas the $t_{1/2}$ of CysS-SH was estimated to be 35 ± 3 min in buffer at physiological pH of 7.4 and at 37 °C.^{64,83} As evidenced from a real time mass spectrometry analysis, persulfides undergoes a disproportionation reaction in aqueous solutions, involving two molecules of persulfides.⁹⁰ Consistent with the nucleophilic and electrophilic characters possessed by the sulfur atoms in persulfides, the decay products might vary depending on the steric bulk of the alkyl group. For instance, bulky persulfides attack the terminal sulfur leading to the formation of a thiol and elemental sulfur (Figure 1.12.).^{83,87,91} However, smaller substituent persulfides attack the inner sulfur, yielding polysulfides and H_2S . CysS-SH and penicillamine persulfides reportedly undergoes decay through the latter mechanism.^{83,91}

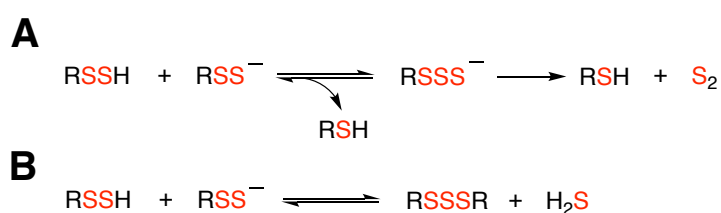


Figure 1.12. Disproportionation of persulfides

3. Nucleophilicity: Persulfides in anionic form display higher nucleophilicity than its corresponding thiol. This is a combined outcome of the α -effect exerted by the vicinal sulfur atom and higher concentration of persulfide anion relative to thiols at physiological pH.^{36,92} Furthermore, computational analysis indicates higher HOMO for persulfides, compared to thiols suggesting better nucleophilicity of persulfides. For instance, methyl persulfide has a HOMO ~ 30 kJ mol⁻¹ higher than that of methyl

thiolate.⁹³ A similar observation was recorded for CysS-SH (~50 kJ mol⁻¹ higher than CysSH) suggesting that persulfides can readily react with electrophilic species.³⁶ Evidently, multiple studies have demonstrated that GS-SH reacts more efficiently with H₂O₂ than GSH.²⁷ Reportedly, GS-SH also reacts with biological electrophiles such as 8-NO₂-cGMP where as GSH and H₂S does not.²⁷

4. Electrophilicity: RS-SH possess mild electrophilic properties as evidenced by its disproportionation reaction (Figure 1.11.) and reaction with various other nucleophiles including cyanide,⁹⁴ thiolate,^{91,94} amines,⁹⁵ phosphines,⁹⁶ sulfite.⁹⁴
5. One electron reductant: Thiols and H₂S are reasonably good antioxidants; the reduction potential for GSH is estimated to be slightly less than 1 V ($E^{\circ}(\text{RS}^{\bullet}, \text{H}^+/\text{RSH}) = 0.96$ V), almost comparable to that of H₂S ($E^{\circ}(\text{S}^{\bullet}, \text{H}^+/\text{HS}^-) = 0.92$ V), suggesting that both thiols and H₂S can easily undergo one electron oxidation.⁹⁷ Persulfides however, have a remarkably lower reduction potential ($E^{\circ}(\text{RSS}^{\bullet}/\text{RSS}^-) = 0.68$ V), indicating that persulfides are far superior reductants than thiols and H₂S.²³ This is in accordance with the lower bond dissociation energy (BDE) of persulfides (~70 kcal mol⁻¹) compared to thiols (~90 kcal mol⁻¹).⁹⁸ The lower BDE of persulfides can be attributed to the increased stability of the RSS[•] owing to the α -effect from the adjacent S atom. Depending on the nature of the radical, persulfides can undergo oxidation through the hydrogen atom or via electron transfer (Scheme 1.1.).⁹⁹ Persulfide reaction with carbon centered radicals, TEMPOL,¹⁰⁰ peroxy radicals^{99,101} have been reported to be much faster than its thiol counterpart.



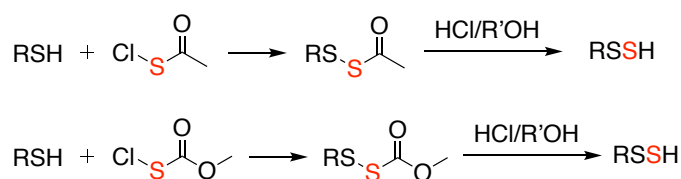
Scheme 1.1. Oxidation of persulfides.

6. Two electron reductant: Persulfides (RS-SH) are reported to have high reactivity with two electron oxidants such as peroxy nitrates and hydrogen peroxides (H₂O₂). As described earlier, persulfides undergo oxidation in presence of H₂O₂ to form perthiosulfenic acid (RS-SOH) and upon further oxidation forms perthiosulfinic acid (RS-SO₂H) and the perthiosulfonic acid (RS-SO₃H), detected as products of oxidation in papain and glutathione peroxidase.^{36,62,102} Unlike their thiol counterparts, the oxidized persulfide residues can be reduced to reinstate the activity of the native thiol back, thus protecting proteins from overoxidation.⁶³

1.7. LMW persulfide generation

The first report of an LMW persulfide or “hydrodisulfide” was by Horst and Gerwalt back in 1954.¹⁰³ It was prepared by hydrolysis of acyl disulfides in acidic conditions. The acyl disulfide intermediates were in turn prepared by reacting sulfenyl chlorides with thiols (Figure 1.13.a). An alternate methodology used for the synthesis of persulfides involves reaction of H₂S with alkyl disulfides (Figure 1.13.b).^{34–36,104} The caveat of this methodology is the reversible nature of the reaction and the collateral consumption of persulfides to form polysulfides and elemental sulfur.

a. Hydrolysis of acyl disulfides



b. Disulfide reaction with H₂S

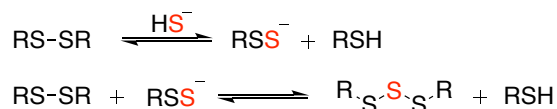
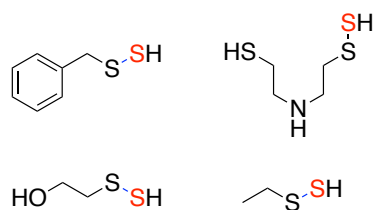


Figure 1.13. a) Synthesis of persulfides from sulfenyl chlorides and thiols, followed by acid mediated hydrolysis of the acyl disulfide intermediate. b) Synthesis of persulfides by reacting alkyl disulfides with H₂S.

Following which there were intermittent reports on the synthesis of few isolated persulfides such as ethyl, benzyl, *tert*-butyl, adamantyl, trityl, diphenylmethyl persulfides etc (Figure 1.14).^{105,106} Out of these trityl persulfides was stable enough, owing to its steric bulk, to be characterized by spectroscopic techniques like NMR, XRD, IR and Raman.¹⁰⁷

a. Unhindered persulfides



b. Hindered persulfides

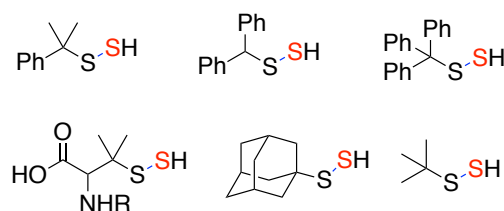


Figure 1.14. Structures of few a) unhindered persulfides b) hindered persulfides

Adamantyl persulfides as well could be stored for extended periods of time under inert conditions and at $-20\text{ }^{\circ}\text{C}$.^{87,108} These LMW persulfides could provide snippets of information regarding the physical and chemical properties of persulfides, along with their reactivity

profiles. However, their chemical biology and their potency in signaling was largely unexplored. It is likely due to the poor aqueous solubility of these compounds or their diminished rate of persulfidation owing to the steric crowding.

1.8. Triggerable persulfide donors

Small molecule persulfides are superior reducing agents and better nucleophiles compared to thiols or H_2S . These reactive species are now recognized as important intermediates in countering oxidative and electrophilic stress.^{27,109,110} Furthermore, persulfidation of proteins is a prominent signaling mechanism mediated by persulfides through which it exerts a wide array of physiological functions. However, persulfides are unstable and undergoes rapid disproportionation in aqueous solution, posing a major challenge in controllable generation of these species *in situ*.⁹⁰ Multiple attempts to isolate persulfides have remained unsuccessful, with the exception of a few sterically hindered persulfides in organic medium, limiting their use in defining their functional implications in biological systems. Hence, to unravel the complex biochemistry of persulfides and delineate its role in sulfur signaling, there is a need to develop precursors or prodrugs. These donors should ideally be shelf stable, cell permeable and generate the active persulfide species upon stimulation by a relevant stimulus (Figure 1.15.). In the recent years, there have been significant advancement in the development of stimuli responsive persulfide prodrugs, as discussed below.

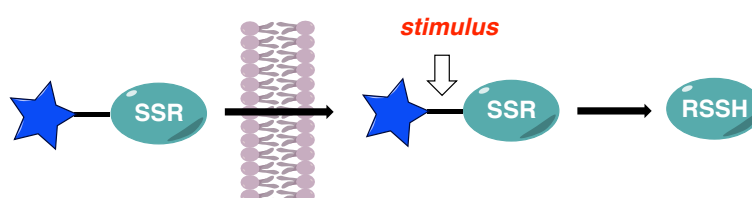


Figure 1.15. Prodrug strategy for intracellular generation of persulfides.

1.8.1. Chemically activated persulfide prodrugs

One of the earliest reports of a persulfide prodrug was from Xian and co-workers wherein the authors have developed a biomimetic persulfidation precursor comprising of 9-fluorenylmethyl disulfide (FmSSPy-A).¹¹¹ This disulfide can undergo thiol exchange with small molecule thiols or protein thiols to form a base sensitive disulfide (RSS-Fm). The adduct can subsequently generate a persulfide upon reaction with a base such as 1,8-diazabicyclo(5.4.0)undec-7-ene (DBU). Using BSA a model protein, the authors have demonstrated the potential of this method to persulfidate proteins (Figure 1.16.). However, the

usage of an organic base such as DBU might pose a limitation for the utility of this system under physiological conditions.

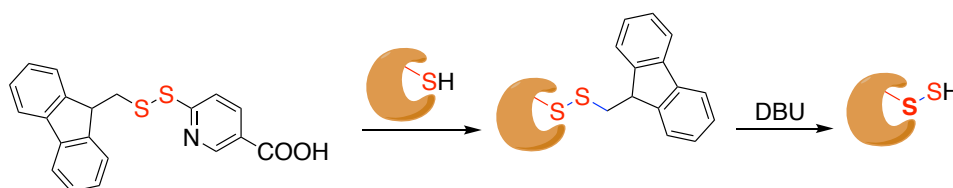


Figure 1.16. 9-Fluorenylmethyl disulfides as biomimetic precursors for persulfides

A class of persulfide prodrugs based on a 1,2-elimination strategy and sensitive to fluoride was reported from the same group (Figure 1.17.).¹¹² Depending on the substituents on Si, the compounds were reported to have varying rates of persulfide release. The compounds were also found to undergo hydrolysis in acidic pH to generate persulfides, although the rate of hydrolysis were extremely slow.

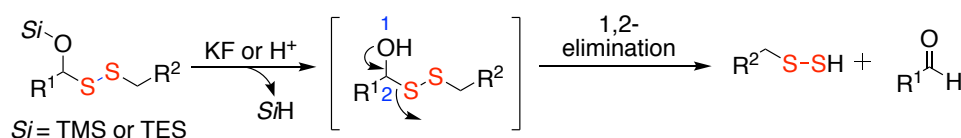


Figure 1.17. Fluoride sensitive prodrugs of persulfides

1.8.2. pH sensitive persulfide donors

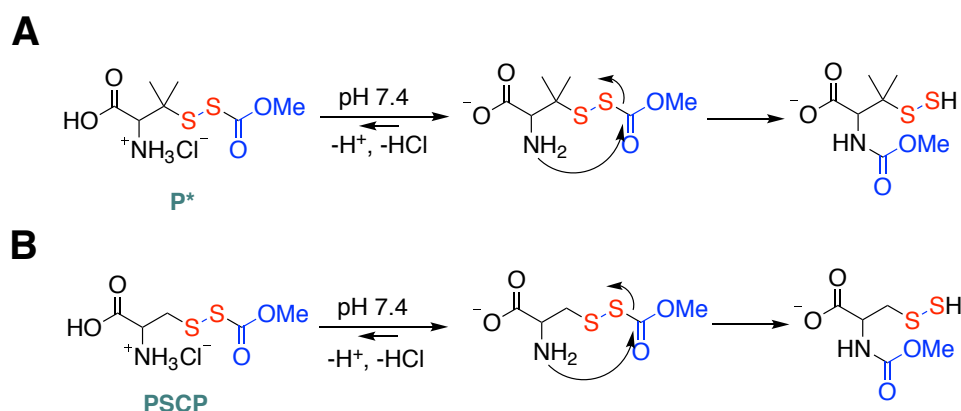


Figure 1.18. pH sensitive persulfide precursors based on -S to -N methoxycarbonyl transfer.

One of the first examples of a persulfide precursor was developed by Galardon and co-workers. The precursor (P*) in aqueous buffer with pH > 6 undergoes spontaneous rearrangement involving an acyl transfer to generate a persulfide *in situ* (Figure 1.18.a).⁹¹ The

prodrug has since been used in several biochemical experiments by various groups to evaluate the biochemistry of persulfides. Yang and co-workers have recently developed a similar strategy to generate cysteine persulfides using a persulfidated cysteine precursor (PSCP) (Figure 1.18.b).¹¹³ PSCP was shown to generate persulfides and polysulfides in liver cancer cell lines and specifically exert anti-cancer effects in the liver cancer cell line SNU 398.

Toscano and group have reported a persulfide prodrug sensitive to pH. In pH 7.4 aqueous buffer, the amine functionality of the *S*-substituted thioisothioureas scaffold is neutralized which then undergoes a 1,2 elimination to generate a persulfide and arylcyanamide as a byproduct (Figure 1.19).¹¹⁴ The rate of persulfide release was tuned by varying the substituents on the aryl ring.

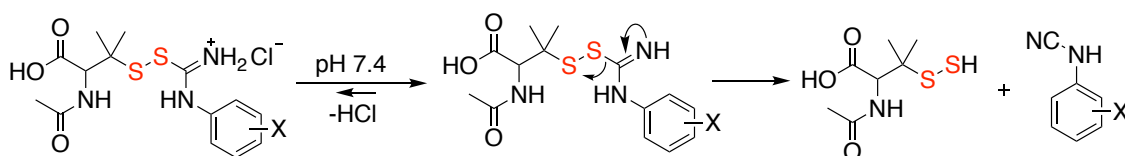


Figure 1.19. pH sensitive thioisothiourea based persulfide precursors

Following this, the group have developed another class of pH sensitive hydrolysis based persulfide prodrugs. The terminal quaternary ammonium salts upon neutralization in pH 7.4 buffer undergoes an intramolecular cyclization to release the persulfide from the perthiocarbamate scaffold.¹¹⁵ These prodrugs in addition to the generation of persulfides undergoes cleavage by thiols to generate COS (COS is known to hydrolyse into H₂S in the presence of the widely prevalent enzyme carbonic anhydrase)¹¹⁶ as well (Figure 1.20.).

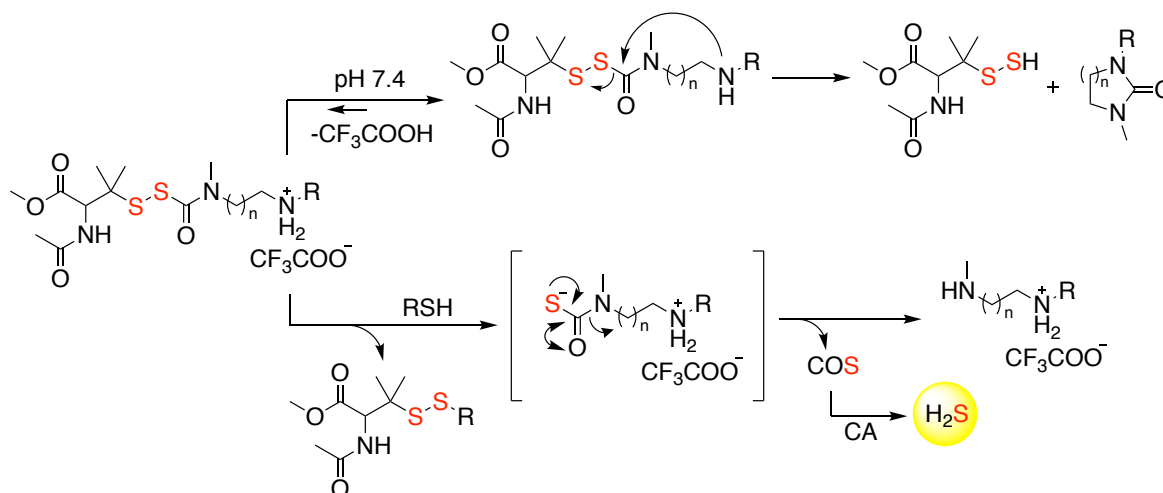


Figure 1.20. Perthiocarbamate based pH sensitive persulfide precursors

As a testament to its therapeutic utility, these compounds were reported to exhibit anti-oxidant properties and protective effects against myocardial ischemia reperfusion (MI/R) injury in mice models.

Another series of hydrolysis based persulfide prodrugs were next developed by the same group, which comprised of alkylsulfenyl thiocarbonate scaffold. The mechanism of RS-SH generation is through hydrolysis of the thiocarbonate scaffold with a phenolate as a leaving group.¹¹⁷ The rate of RS-SH generation can be modulated by varying the substituents on the leaving group. Similar to the perthiocarbamate based donors, these prodrugs were also found to react with thiols to generate COS (Figure 1.21.). The donors were reported to have protective effects against oxidative stress induced cell death.

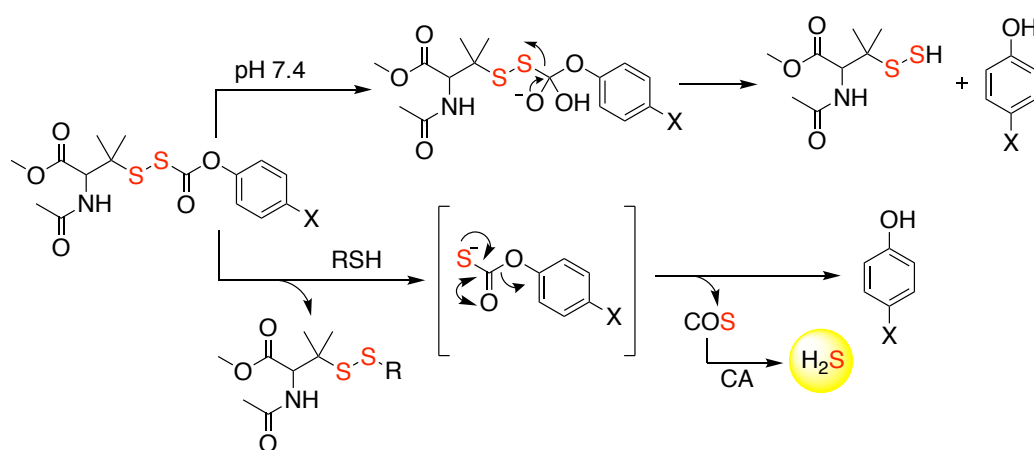


Figure 1.21. Alkylsulfenyl thiocarbonate based pH sensitive persulfide precursors

Xian and co-workers recently have reported diacyl disulfides as precursors for hydrogen persulfide (H₂S₂).¹¹⁸ These precursors undergo hydrolysis by following two pathways, one that generates H₂S₂ and the other that generates H₂S and elemental sulfur (S₈) (Figure 1.22.). The generation of sulfane sulfur from these precursors can be attributed to a combination of both these pathways.

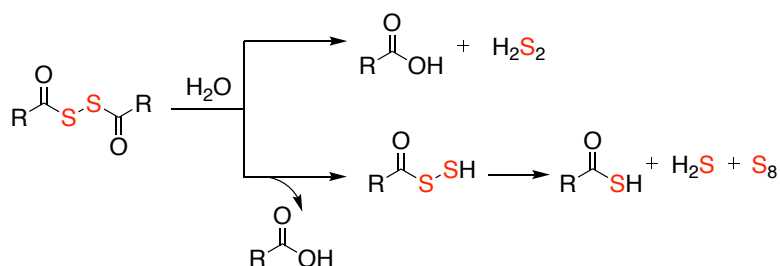


Figure 1.22. Diacyl disulfide based pH sensitive persulfide precursors

1.8.3. Thiol activated persulfide donors

Diallyl disulfide (DADS) and diallyl trisulfide (DATS) are garlic derived organosulfur compounds, produced as decomposition products of allicin that are widely known H₂S donors.^{119–121} Both these compounds have shown promising biological effects such as relaxation of rat aorta rings, attributed to its ability to generate H₂S.¹²² However, Haung and co-workers have demonstrated that DATS rapidly undergoes disulfide exchange with GSH to generate H₂S and other polysulfide species which can be further reduced to H₂S (Figure 1.23a.).¹²³ On the contrary, DADS was found to release only minute amount of H₂S. Reaction of DADS with GSH can follow two distinct pathways, pathway A where DADS can rapidly undergo a disulfide exchange with GSH, which does not result in the formation of H₂S. The alternate pathway (pathway B) observed was its α -carbon nucleophilic substitution on DADS to generate an allyl persulfide intermediate which upon reduction generates H₂S. However, this was a minor pathway and the reaction appeared to be sluggish (Figure 1.23b.).

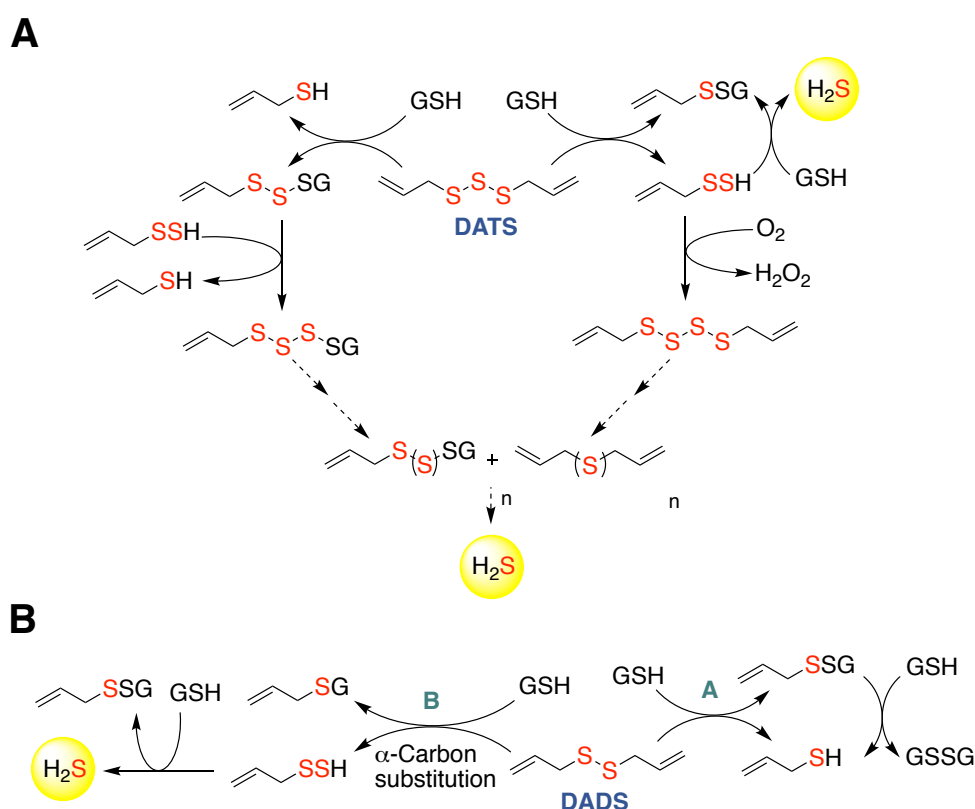


Figure 1.23. a) Reaction of DATS with GSH, generating allyl persulfide, polysulfides and H₂S. b) Reaction of DADS with GSH. Pathway A indicates disulfide exchange with GSH and pathway B indicates α -carbon nucleophilic substitution of GSH

Xian and co-workers have reported a facile method for persulfide/polysulfide generation from cyclic acyl disulfides.¹²⁴ Two series of compounds were developed, dithiolane

and benzodithiolane and reacted with physiologically relevant nucleophiles such as thiols and amines. Dithiolanes on reacting with *n*-BuNH₂ generated a polysulfide species, presumably through the formation of a persulfide intermediate. Whereas its reaction with thiols appeared to have generated multiple intermediates since thiols have the propensity to attack both the carbonyl as well as the disulfide functional group (Figure 1.24a.). On the contrary, reaction of benzodithiolane was found to be more stable with sluggish reactivity towards amine and no reactivity with thiols (Figure 1.24b.).¹²⁴

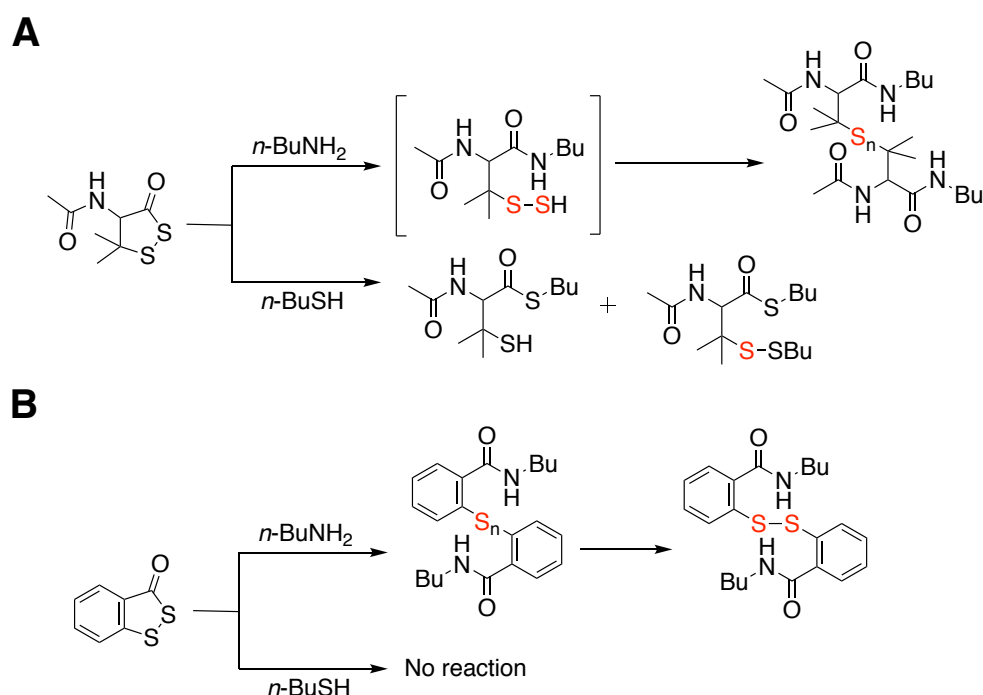


Figure 1.24. Cyclic acyl disulfides as precursors for persulfides.

1.8.4. Light activated persulfide donor

Pradeep Singh and group reported a one and two photon activated persulfide prodrug. The *o*-nitro benzyl moiety upon cleavage by UV light generates a *N*-acetyl cysteine (NAC) persulfide (Figure 1.25.).¹²⁵

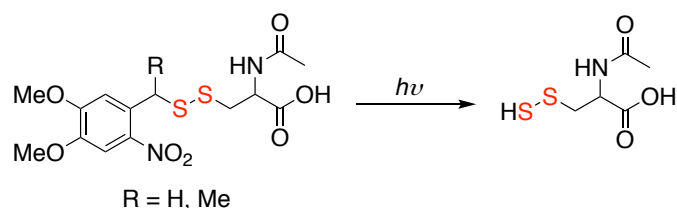


Figure 1.25. UV light activated persulfide donor

1.8.5. Enzyme activated persulfide donors

Wang and co-workers have developed a series of esterase sensitive persulfide donors based on a 1,2 elimination strategy (Figure 1.26). The authors showed tunable release of persulfides by varying the ester functionality, as well as demonstrated their therapeutic potential in a murine model of myocardial infarction reperfusion (MI/R) injury.¹²⁶

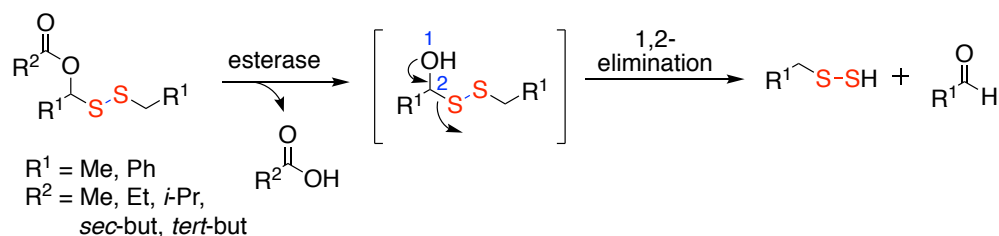


Figure 1.26. Esterase sensitive persulfide prodrugs.

Soon after, another esterase sensitive glutathione persulfide (GS-SH) donor utilizing the trimethyl lock strategy was developed by the same group (Figure 1.27a).¹²⁷ The prodrug was shown to modulate the activity of GAPDH via persulfidation of the protein. It was also reported to have potent cytoprotective effects against oxidative stress induced damage, compared to H₂S and GSH alone. A similar strategy was used to generate hydrogen persulfide (H₂S₂) in the presence of esterase (Figure 1.27b).⁴⁸

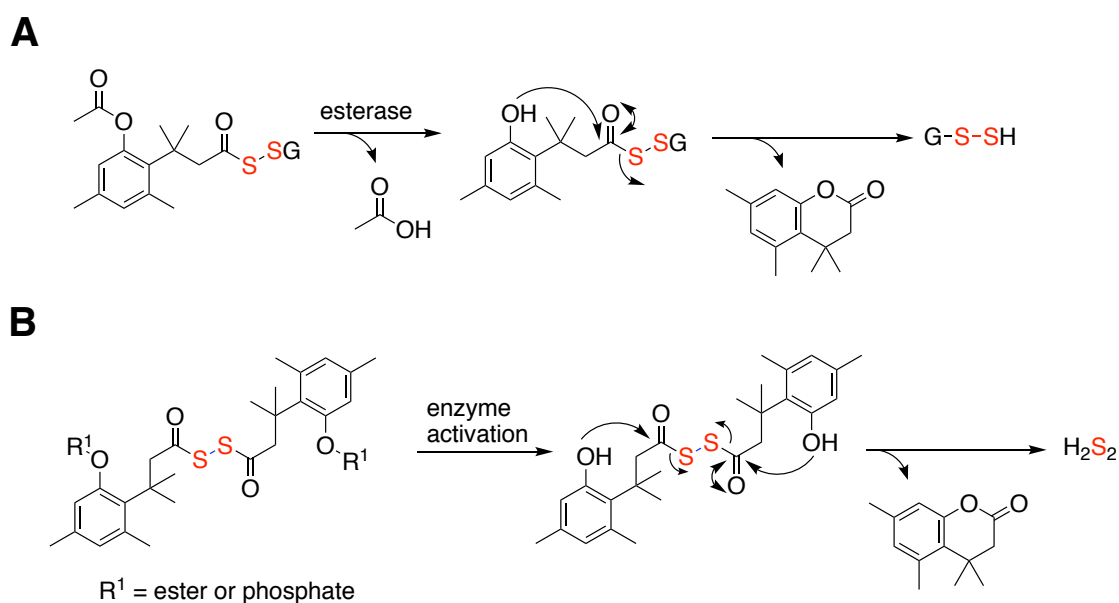


Figure 1.27. a) Esterase sensitive glutathione persulfide prodrug. b) Trimethyl lock based H₂S₂ donor activated by esterase and phosphatase.

Matson and co-workers developed a polymeric persulfide prodrug (poly(EDP-NAC)) triggerable by esterase, based on a 1,6-elimination strategy (Figure 1.28.).¹²⁸ Poly(EDP-NAC) was significantly slow compared to the monomeric counterpart (EDP-NAC) but was reported to be more effective in protecting cardiomyocytes from 5-fluorouracil (5-FU) mediated cytotoxicity.

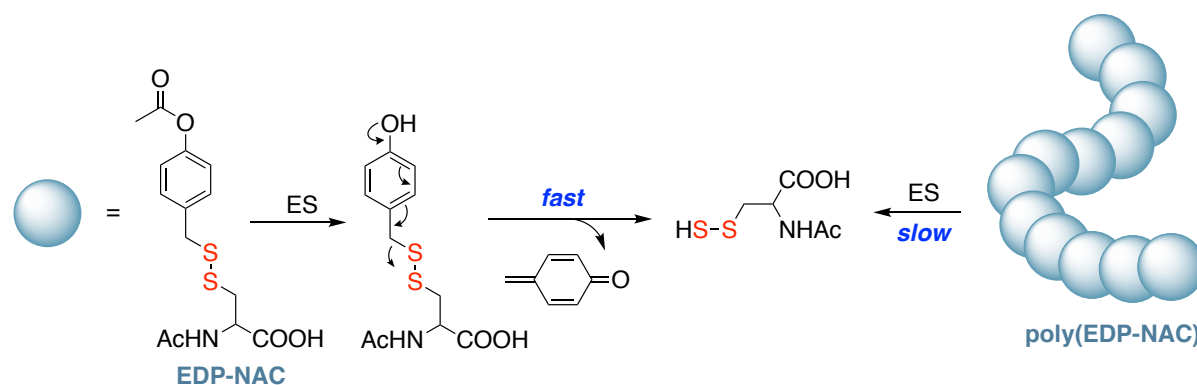


Figure 1.28. Esterase sensitive EDP-NAC and poly(EDP-NAC) based persulfide donors.

Using a similar 1,6-elimination strategy, Matson and group have reported a persulfide prodrug (NDP-NAC) responsive to nitroreductase (NTR) (Figure 1.29.).¹²⁹ NDP-NAC was reported to significantly impact the composition of gut microbiome in mice compared to H₂S or a non-persulfide containing negative control. NDP-NAC facilitated the growth of bacteria in the gut microbiome of the *Turicibacter* genus, particularly *turicibacter sanguinis* which promotes metabolism and overall gastrointestinal health. The compound on the contrary was found to have an inhibitory effect on opportunistic and pathogenic gut bacteria, underlining the importance of these RSS in modulating the gut microbiome under diseased conditions.

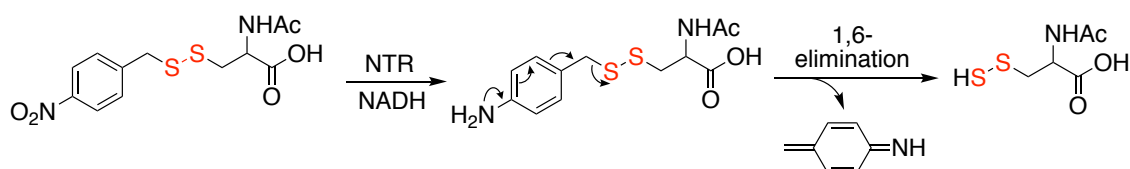


Figure 1.29. Nitroreductase activated persulfide donors.

Recently, Pluth and co-workers have demonstrated the dual release of persulfides and COS in response to esterase and thiols from a perthiocarbonate based scaffold (Figure 1.30.).¹³⁰ The rate of persulfide release was modulated by changing the steric bulk of the alkyl group R².

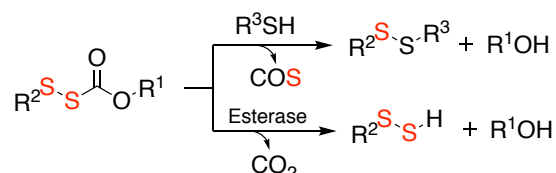


Figure 1.30. Esterase activated perthiocarbonate based persulfide donors.

1.9. Motivation and outline of the thesis

With the advent of reliable persulfide and persulfidation detection techniques, the role of this post translational modification in cellular signaling and its functional implications are beginning to unfold. Small molecule persulfides have gained considerable traction in the recent years as efficient persulfidating agents and as a vital strategy to combat oxidative and electrophilic stress. The propensity of persulfides to undergo disproportionation in aqueous solution have prompted researchers to develop prodrug strategies for the generation of persulfides, *in situ*. The prodrug should ideally be shelf stable, generate persulfides only in the presence of a physiologically relevant stimulus and produce innocuous byproducts. The prodrugs reported thus far are have various limitations including:

- Lack of trigger specificity. While some of these donors spontaneously dissociates in buffer to generate persulfides, others are responsive to stimuli like pH, esterase, thiols which are ubiquitous. Hence, these donors do not offer controlled site directed delivery of persulfides. Some of the prodrugs reported are responsive to chemical stimuli like DBU which limits the use of these donors in biological systems.
- Formation of potentially toxic byproducts. Several of the prodrugs developed undergoes a 1,6-elimination to produce the electrophilic quinone methide as a byproduct which can modify proteins through nucleophilic attack.

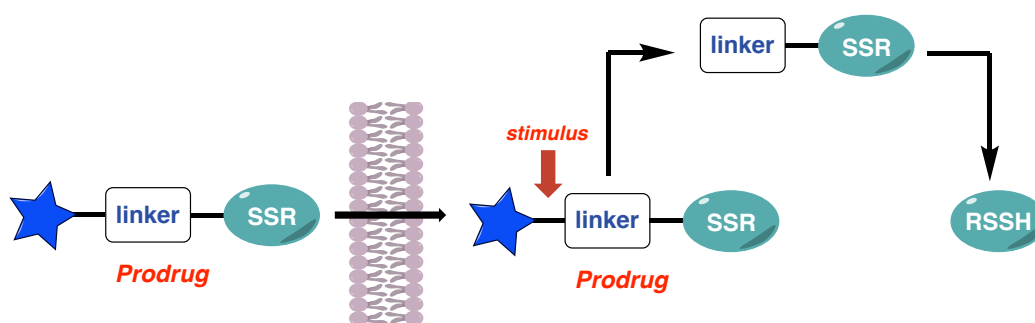


Figure 1.31. General strategy for prodrug activation to generate persulfides.

To address these gaps, our aim was to design cell permeable persulfide prodrugs that are responsive to a disease relevant stimulus (Figure 1.31).

An increased production of reactive oxygen species (ROS) is often associated with several pathological conditions. In **chapter 2**, we propose a persulfide prodrug responsive to elevated ROS, to closely mimic a diseased state. The strategy for persulfide generation is based on a previously unexplored retro-Michael reaction that would yield cinnamaldehyde as the byproduct. The prodrug was tested for cleavage by H₂O₂, a stable ROS and its ability to protect cells against oxidative stress induced cell death. One of the concerns regarding the above strategy is the formation of cinnamaldehyde, which although widely used in the food industry, is a mild electrophile.

In **chapter 3**, we propose a persulfide prodrug activable by the enzyme β -glycosidase. β -glycosidases are a class of enzymes, found to be overexpressed under conditions of stress including inflammation and cancer. The prodrugs upon cleavage by β -glycosidase undergoes an intramolecular cyclization to generate sulfane sulfur intracellularly along with a non-electrophilic, heterocyclic byproduct. The cytoprotective effects of these prodrugs were also studied. Although these prodrugs provided important insights into the physicochemical properties of persulfides along with their therapeutic utility, these classes of prodrugs suffered from certain drawbacks. These include complex synthetic strategies, low shelf stability and the disulfide bond being prone to nucleophilic attack.

In **chapter 4.1**, we designed compounds without the persulfide moiety but upon entry into cells would generate persulfides. We utilized the biochemical machinery of the cell here to develop artificial substrates for the enzyme 3-mercaptopyruvate sulfurtransferase (3-MST). The turnover of the substrates by purified 3-MST to generate sulfane sulfur and their therapeutic effects were studied. In **chapter 4.2**, we designed a β -galactosidase activated prodrug of the artificial substrate for 3-MST. β -galactosidase levels are overexpressed in senescence and it is therefore used as a marker for senescence. The prodrug designed can be used as a tool to study the consequences of persulfidation in senescent cells.

Collectively, we have developed two distinct strategies for the intracellular generation of persulfides. The approaches developed herein will help address important questions regarding the role of persulfides in cellular signaling and understand its therapeutic utility.

1.10. References

- (1) Mishanina, T. V.; Libiad, M.; Banerjee, R., Biogenesis of reactive sulfur species for signaling by hydrogen sulfide oxidation pathways. *Nat. Chem. Biol.* **2015**, *11*, 457.
- (2) Kabil, O.; Vitvitsky, V.; Banerjee, R., Sulfur as a Signaling Nutrient Through Hydrogen Sulfide. *Annu. Rev. Nutr.* **2014**, *34* (1), 171–205.
- (3) Baskar, R.; Li, L.; Moore, P. K., Hydrogen sulfide-induces DNA damage and changes in apoptotic gene expression in human lung fibroblast cells. *FASEB J.* **2007**, *21* (1), 247–255.
- (4) Truong, D. H.; Eghbal, M. A.; Hindmarsh, W.; Roth, S. H.; O'Brien, P. J., Molecular Mechanisms of Hydrogen Sulfide Toxicity. *Drug Metab. Rev.* **2006**, *38* (4), 733–744.
- (5) Bouroushian, M., Electrochemistry of the Chalcogens BT - Electrochemistry of Metal Chalcogenides. *Electrochemistry of Metal Chalcogenides, Monographs in Electrochemistry*; Springer Berlin Heidelberg: Berlin, Heidelberg, 2010; pp 57–75.
- (6) Mustafa, A. K.; Gadalla, M. M.; Sen, N.; Kim, S.; Mu, W.; Gazi, S. K.; Barrow, R. K.; Yang, G.; Wang, R.; Snyder, S. H., H₂S Signals Through Protein S-Sulfhydration. *Sci. Signal.* **2009**, *2* (96), ra72 LP-ra72.
- (7) Bruce King, S., Potential biological chemistry of hydrogen sulfide (H₂S) with the nitrogen oxides. *Free Radic. Biol. Med.* **2013**, *55*, 1–7.
- (8) Kimura, H., Signaling of Hydrogen Sulfide and Polysulfides. *Antioxid. Redox Signal.* **2015**, *22* (5), 347–349.
- (9) Gallyas, F., Involvement of redox-signalling in endogenous hydrogen sulfide production. *Br. J. Pharmacol.* **2012**, *166* (8), 2228–2230.
- (10) Martelli, A.; Testai, L.; Citi, V.; Marino, A.; Pugliesi, I.; Barresi, E.; Nesi, G.; Rapposelli, S.; Taliani, S.; Da Settimo, F.; Breschi, M. C.; Calderone, V., Arylthioamides as H₂S Donors: l-Cysteine-Activated Releasing Properties and Vascular Effects in Vitro and in Vivo. *ACS Med. Chem. Lett.* **2013**, *4* (10), 904–908.
- (11) Yang, G.; Wu, L.; Jiang, B.; Yang, W.; Qi, J.; Cao, K.; Meng, Q.; Mustafa, A. K.; Mu, W.; Zhang, S.; Snyder, S. H.; Wang, R., H₂S as a Physiologic Vasorelaxant: Hypertension in Mice with Deletion of Cystathionine γ -Lyase. *Science* (80-.). **2008**, *322* (5901), 587–590.

-
- (12) Mustafa, A. K.; Sikka, G.; Gazi, S. K.; Stepan, J.; Jung, S. M.; Bhunia, A. K.; Barodka, V. M.; Gazi, F. K.; Barrow, R. K.; Wang, R.; Amzel, L. M.; Berkowitz, D. E.; Snyder, S. H., Hydrogen Sulfide as Endothelial Derived Hyperpolarizing Factor Sulfhydrates Potassium Channels. *Circ. Res.* **2011**, *109* (11), 1259–1268.
- (13) Abe, K.; Kimura, H., The possible role of hydrogen sulfide as an endogenous neuromodulator. *J. Neurosci.* **1996**, *16* (3), 1066 LP – 1071.
- (14) Papapetropoulos, A.; Pyriochou, A.; Altaany, Z.; Yang, G.; Marazioti, A.; Zhou, Z.; Jeschke, M. G.; Branski, L. K.; Herndon, D. N.; Wang, R.; Szabo, C., Hydrogen sulfide is an endogenous stimulator of angiogenesis. *Proc. Natl. Acad. Sci.* **2009**, *106* (51), 21972–21977.
- (15) Szabó, C.; Papapetropoulos, A., Hydrogen sulphide and angiogenesis: mechanisms and applications. *Br. J. Pharmacol.* **2011**, *164* (3), 853–865.
- (16) Whiteman, M.; Winyard, P. G., Hydrogen sulfide and inflammation: the good, the bad, the ugly and the promising. *Expert Rev. Clin. Pharmacol.* **2011**, *4* (1), 13–32.
- (17) Li, L.; Bhatia, M.; Zhu, Y. Z.; Zhu, Y. C.; Ramnath, R. D.; Wang, Z. J.; Anuar, F. B. M.; Whiteman, M.; Salto-Tellez, M.; Moore, P. K., Hydrogen sulfide is a novel mediator of lipopolysaccharide-induced inflammation in the mouse. *FASEB J.* **2005**, *19* (9), 1196–1198.
- (18) Olson, K. R.; Healy, M. J.; Qin, Z.; Skovgaard, N.; Vulesevic, B.; Duff, D. W.; Whitfield, N. L.; Yang, G.; Wang, R.; Perry, S. F., Hydrogen sulfide as an oxygen sensor in trout gill chemoreceptors. *Am. J. Physiol. Integr. Comp. Physiol.* **2008**, *295* (2), R669–R680.
- (19) Zhao, Y.; Bhushan, S.; Yang, C.; Otsuka, H.; Stein, J. D.; Pacheco, A.; Peng, B.; Devarie-Baez, N. O.; Aguilar, H. C.; Lefer, D. J.; Xian, M., Controllable Hydrogen Sulfide Donors and Their Activity against Myocardial Ischemia-Reperfusion Injury. *ACS Chem. Biol.* **2013**, *8* (6), 1283–1290.
- (20) Mills, G.; Schmidt, K. H.; Matheson, M. S.; Meisel, D., Thermal and photochemical reactions of sulfhydryl radicals. Implications for colloid photocorrosion. *J. Phys. Chem.* **1987**, *91* (6), 1590–1596.
- (21) Nagy, P.; Winterbourn, C. C., Rapid Reaction of Hydrogen Sulfide with the Neutrophil Oxidant Hypochlorous Acid to Generate Polysulfides. *Chem. Res. Toxicol.* **2010**, *23*

- (10), 1541–1543.
- (22) Filipovic, M. R.; Miljkovic, J.; Allgäuer, A.; Chaurio, R.; Shubina, T.; Herrmann, M.; Ivanovic-Burmazovic, I., Biochemical insight into physiological effects of H₂S: reaction with peroxyxynitrite and formation of a new nitric oxide donor, sulfinyl nitrite. *Biochem. J.* **2012**, *441* (2), 609–621.
- (23) Koppenol, W. H.; Bounds, P. L., Signaling by sulfur-containing molecules. Quantitative aspects. *Arch. Biochem. Biophys.* **2017**, *617*, 3–8.
- (24) Finkel, T., From Sulfenylation to Sulfhydration: What a Thiolate Needs to Tolerate. *Sci. Signal.* **2012**, *5* (215).
- (25) Kabil, O.; Banerjee, R., Redox Biochemistry of Hydrogen Sulfide. *J. Biol. Chem.* **2010**, *285* (29), 21903–21907.
- (26) Francoleon, N. E.; Carrington, S. J.; Fukuto, J. M., The reaction of H₂S with oxidized thiols: Generation of persulfides and implications to H₂S biology. *Arch. Biochem. Biophys.* **2011**, *516* (2), 146–153.
- (27) Ida, T.; Sawa, T.; Ihara, H.; Tsuchiya, Y.; Watanabe, Y.; Kumagai, Y.; Suematsu, M.; Motohashi, H.; Fujii, S.; Matsunaga, T.; Yamamoto, M.; Ono, K.; Devarie-Baez, N. O.; Xian, M.; Fukuto, J. M.; Akaike, T., Reactive cysteine persulfides and S-polythiolation regulate oxidative stress and redox signaling. *Proc. Natl. Acad. Sci. U.S.A* **2014**, *111* (21), 7606–7611.
- (28) Toohey, J. I., Sulfur signaling: Is the agent sulfide or sulfane? *Anal. Biochem.* **2011**, *413* (1), 1–7.
- (29) Kimura, Y.; Mikami, Y.; Osumi, K.; Tsugane, M.; Oka, J.; Kimura, H., Polysulfides are possible H₂S-derived signaling molecules in rat brain. *FASEB J.* **2013**, *27* (6), 2451–2457.
- (30) Kimura, H., Signaling of Hydrogen Sulfide and Polysulfides. *Antioxid. Redox Signal.* **2014**, *22* (5), 347–349.
- (31) Ono, K.; Akaike, T.; Sawa, T.; Kumagai, Y.; Wink, D. A.; Tantillo, D. J.; Hobbs, A. J.; Nagy, P.; Xian, M.; Lin, J.; Fukuto, J. M., Redox chemistry and chemical biology of H₂S, hydropersulfides, and derived species: Implications of their possible biological activity and utility. *Free. Radic. Biol. Med.* **2014**, *77*, 82–94.
- (32) Wood, J. L., Sulfane sulfur. 1987; pp 25–29.

- (33) Ubuka, T., Assay methods and biological roles of labile sulfur in animal tissues. *J. Chromatogr. B* **2002**, *781* (1–2), 227–249.
- (34) Liu, D. K.; Chang, S. G., Kinetic study of the reaction between cystine and sulfide in alkaline solutions. *Can. J. Chem.* **1987**, *65* (4), 770–774.
- (35) Vasas, A.; Dóka, É.; Fábrián, I.; Nagy, P., Kinetic and thermodynamic studies on the disulfide-bond reducing potential of hydrogen sulfide. *Nitric Oxide* **2015**, *46*, 93–101.
- (36) Cuevasanta, E.; Lange, M.; Bonanata, J.; Coitiño, E. L.; Ferrer-Sueta, G.; Filipovic, M. R.; Alvarez, B., Reaction of Hydrogen Sulfide with Disulfide and Sulfenic Acid to Form the Strongly Nucleophilic Persulfide. *J. Biol. Chem.* **2015**, *290* (45), 26866–26880.
- (37) Mishanina, T. V.; Yadav, P. K.; Ballou, D. P.; Banerjee, R., Transient Kinetic Analysis of Hydrogen Sulfide Oxidation Catalyzed by Human Sulfide Quinone Oxidoreductase. *J. Biol. Chem.* **2015**, *290* (41), 25072–25080.
- (38) Hansen, R. E.; Roth, D.; Winther, J. R., Quantifying the global cellular thiol-disulfide status. *Proc. Natl. Acad. Sci.* **2009**, *106* (2), 422–427.
- (39) Yang, J.; Gupta, V.; Carroll, K. S.; Liebler, D. C., Site-specific mapping and quantification of protein S-sulphenylation in cells. *Nat. Commun.* **2014**, *5* (1), 4776.
- (40) Devarie-Baez, N. O.; Silva Lopez, E. I.; Furdui, C. M., Biological chemistry and functionality of protein sulfenic acids and related thiol modifications. *Free Radic. Res.* **2016**, *50* (2), 172–194.
- (41) Foster, M. W.; Hess, D. T.; Stamler, J. S., Protein S-nitrosylation in health and disease: a current perspective. *Trends Mol. Med.* **2009**, *15* (9), 391–404.
- (42) Filipovic, M. R.; Miljkovic, J. L.; Nauser, T.; Royzen, M.; Klos, K.; Shubina, T.; Koppenol, W. H.; Lippard, S. J.; Ivanović-Burmazović, I., Chemical Characterization of the Smallest S -Nitrosothiol, HSNO; Cellular Cross-talk of H₂S and S -Nitrosothiols. *J. Am. Chem. Soc.* **2012**, *134* (29), 12016–12027.
- (43) Timerghazin, Q. K.; Talipov, M. R., Unprecedented External Electric Field Effects on S -Nitrosothiols: Possible Mechanism of Biological Regulation? *J. Phys. Chem. Lett.* **2013**, *4* (6), 1034–1038.
- (44) Schaedler, T. A.; Thornton, J. D.; Kruse, I.; Schwarzländer, M.; Meyer, A. J.; van Veen, H. W.; Balk, J., A Conserved Mitochondrial ATP-binding Cassette Transporter Exports Glutathione Polysulfide for Cytosolic Metal Cofactor Assembly. *J. Biol. Chem.* **2014**,

- 289 (34), 23264–23274.
- (45) Mueller, E. G., Trafficking in persulfides: delivering sulfur in biosynthetic pathways. *Nat. Chem. Biol.* **2006**, *2*, 185.
- (46) Eberhardt, M.; Dux, M.; Namer, B.; Miljkovic, J.; Cordasic, N.; Will, C.; Kichko, T. I.; de la Roche, J.; Fischer, M.; Suárez, S. A.; Bikiel, D.; Dorsch, K.; Leffler, A.; Babes, A.; Lampert, A.; Lennerz, J. K.; Jacobi, J.; Martí, M. A.; Doctorovich, F.; Högestätt, E. D.; Zygmunt, P. M.; Ivanovic-Burmazovic, I.; Messlinger, K.; Reeh, P.; Filipovic, M. R., H₂S and NO cooperatively regulate vascular tone by activating a neuroendocrine HNO–TRPA1–CGRP signalling pathway. *Nat. Commun.* **2014**, *5* (1), 4381.
- (47) Koike, S.; Ogasawara, Y.; Shibuya, N.; Kimura, H.; Ishii, K., Polysulfide exerts a protective effect against cytotoxicity caused by t -buthylhydroperoxide through Nrf2 signaling in neuroblastoma cells. *FEBS Lett.* **2013**, *587* (21), 3548–3555.
- (48) Yu, B.; Zheng, Y.; Yuan, Z.; Li, S.; Zhu, H.; De La Cruz, L. K.; Zhang, J.; Ji, K.; Wang, S.; Wang, B., Toward Direct Protein S-Persulfidation: A Prodrug Approach That Directly Delivers Hydrogen Persulfide. *J. Am. Chem. Soc.* **2018**, *140* (1), 30–33.
- (49) Gao, X.-H.; Krokowski, D.; Guan, B.-J.; Bederman, I.; Majumder, M.; Parisien, M.; Diatchenko, L.; Kabil, O.; Willard, B.; Banerjee, R.; Wang, B.; Bebek, G.; Evans, C. R.; Fox, P. L.; Gerson, S. L.; Hoppel, C. L.; Liu, M.; Arvan, P.; Hatzoglou, M., Quantitative H₂S-mediated protein sulfhydration reveals metabolic reprogramming during the integrated stress response. *Elife* **2015**, *4*.
- (50) Dóka, É.; Pader, I.; Bíró, A.; Johansson, K.; Cheng, Q.; Ballagó, K.; Prigge, J. R.; Pastor-Flores, D.; Dick, T. P.; Schmidt, E. E.; Arnér, E. S. J.; Nagy, P., A novel persulfide detection method reveals protein persulfide- and polysulfide-reducing functions of thioredoxin and glutathione systems. *Sci. Adv.* **2016**, *2* (1).
- (51) Du, J.; Huang, Y.; Yan, H.; Zhang, Q.; Zhao, M.; Zhu, M.; Liu, J.; Chen, S. X.; Bu, D.; Tang, C.; Jin, H., Hydrogen Sulfide Suppresses Oxidized Low-density Lipoprotein (Ox-LDL)-stimulated Monocyte Chemoattractant Protein 1 generation from Macrophages via the Nuclear Factor κ B (NF- κ B) Pathway. *J. Biol. Chem.* **2014**, *289* (14), 9741–9753.
- (52) Yang, G.; Zhao, K.; Ju, Y.; Mani, S.; Cao, Q.; Puukila, S.; Khaper, N.; Wu, L.; Wang, R., Hydrogen Sulfide Protects Against Cellular Senescence via S-Sulfhydration of Keap1 and Activation of Nrf2. *Antioxid. Redox Signal.* **2013**, *18* (15), 1906–1919.

- (53) Vandiver, M. S.; Paul, B. D.; Xu, R.; Karuppagounder, S.; Rao, F.; Snowman, A. M.; Seok Ko, H.; Il Lee, Y.; Dawson, V. L.; Dawson, T. M.; Sen, N.; Snyder, S. H., Sulfhydration mediates neuroprotective actions of parkin. *Nat. Commun.* **2013**, *4*, 1626.
- (54) Giovinazzo, D.; Bursac, B.; Sbdio, J. I.; Nalluru, S.; Vignane, T.; Snowman, A. M.; Albacarys, L. M.; Sedlak, T. W.; Torregrossa, R.; Whiteman, M.; Filipovic, M. R.; Snyder, S. H.; Paul, B. D., Hydrogen sulfide is neuroprotective in Alzheimer's disease by sulfhydrating GSK3 β and inhibiting Tau hyperphosphorylation. *Proc. Natl. Acad. Sci.* **2021**, *118* (4), e2017225118.
- (55) Paul, B. D.; Sbdio, J. I.; Xu, R.; Vandiver, M. S.; Cha, J. Y.; Snowman, A. M.; Snyder, S. H., Cystathionine γ -lyase deficiency mediates neurodegeneration in Huntington's disease. *Nature* **2014**, *509* (7498), 96–100.
- (56) Wakabayashi, N.; Dinkova-Kostova, A. T.; Holtzclaw, W. D.; Kang, M.-I.; Kobayashi, A.; Yamamoto, M.; Kensler, T. W.; Talalay, P., Protection against electrophile and oxidant stress by induction of the phase 2 response: Fate of cysteines of the Keap1 sensor modified by inducers. *Proc. Natl. Acad. Sci.* **2004**, *101* (7), 2040–2045.
- (57) Kaspar, J. W.; Niture, S. K.; Jaiswal, A. K., Nrf2:INrf2 (Keap1) signaling in oxidative stress. *Free Radic. Biol. Med.* **2009**, *47* (9), 1304–1309.
- (58) Tocmo, R.; Parkin, K., S-1-propenylmercaptocysteine protects murine hepatocytes against oxidative stress via persulfidation of Keap1 and activation of Nrf2. *Free Radic. Biol. Med.* **2019**, *143*, 164–175.
- (59) Paulsen, C. E.; Carroll, K. S., Cysteine-Mediated Redox Signaling: Chemistry, Biology, and Tools for Discovery. *Chem. Rev.* **2013**, *113* (7), 4633–4679.
- (60) Woo, H. A.; Chae, H. Z.; Hwang, S. C.; Yang, K.-S.; Kang, S. W.; Kim, K.; Rhee, S. G., Reversing the Inactivation of Peroxiredoxins Caused by Cysteine Sulfenic Acid Formation. *Science*, **2003**, *300* (5619), 653–656.
- (61) Wood, Z. A.; Poole, L. B.; Karplus, P. A., Peroxiredoxin Evolution and the Regulation of Hydrogen Peroxide Signaling. *Science*, **2003**, *300* (5619), 650–653.
- (62) Zhang, D.; Macinkovic, I.; Devarie-Baez, N. O.; Pan, J.; Park, C.-M.; Carroll, K. S.; Filipovic, M. R.; Xian, M., Detection of Protein S-Sulfhydration by a Tag-Switch Technique. *Angew. Chemie Int. Ed.* **2014**, *53* (2), 575–581.
- (63) Filipovic, M. R., Persulfidation (S-sulfhydration) and H₂S. **2015**; pp 29–59.

- (64) Wedmann, R.; Onderka, C.; Wei, S.; Szijártó, I. A.; Miljkovic, J. L.; Mitrovic, A.; Lange, M.; Savitsky, S.; Yadav, P. K.; Torregrossa, R.; Harrer, E. G.; Harrer, T.; Ishii, I.; Gollasch, M.; Wood, M. E.; Galardon, E.; Xian, M.; Whiteman, M.; Banerjee, R.; Filipovic, M. R., Improved tag-switch method reveals that thioredoxin acts as depersulfidase and controls the intracellular levels of protein persulfidation. *Chem. Sci.* **2016**, *7* (5), 3414–3426.
- (65) Napetschnig, J.; Wu, H., Molecular Basis of NF- κ B Signaling. *Annu. Rev. Biophys.* **2013**, *42* (1), 443–468.
- (66) Aggarwal, B. B.; Gupta, S. C.; Kim, J. H., Historical perspectives on tumor necrosis factor and its superfamily: 25 years later, a golden journey. *Blood* **2012**, *119* (3), 651–665.
- (67) Zhang, T.; Ono, K.; Tsutsuki, H.; Ihara, H.; Islam, W.; Akaike, T.; Sawa, T., Enhanced Cellular Polysulfides Negatively Regulate TLR4 Signaling and Mitigate Lethal Endotoxin Shock. *Cell Chem. Biol.* **2019**, *26* (5), 686-698.e4.
- (68) Shulman, J. M.; De Jager, P. L.; Feany, M. B., Parkinson's Disease: Genetics and Pathogenesis. *Annu. Rev. Pathol. Mech. Dis.* **2011**, *6* (1), 193–222.
- (69) Hara, M. R.; Agrawal, N.; Kim, S. F.; Cascio, M. B.; Fujimuro, M.; Ozeki, Y.; Takahashi, M.; Cheah, J. H.; Tankou, S. K.; Hester, L. D.; Ferris, C. D.; Hayward, S. D.; Snyder, S. H.; Sawa, A., S-nitrosylated GAPDH initiates apoptotic cell death by nuclear translocation following Siah1 binding. *Nat. Cell Biol.* **2005**, *7* (7), 665–674.
- (70) Mir, S.; Sen, T.; Sen, N., Cytokine-Induced GAPDH Sulfhydration Affects PSD95 Degradation and Memory. *Mol. Cell* **2014**, *56* (6), 786–795.
- (71) Jarosz, A. P.; Wei, W.; Gauld, J. W.; Auld, J.; Özcan, F.; Aslan, M.; Mutus, B., Glyceraldehyde 3-phosphate dehydrogenase (GAPDH) is inactivated by S-sulfuration in vitro. *Free Radic. Biol. Med.* **2015**, *89*, 512–521.
- (72) Numakura, T.; Sugiura, H.; Akaike, T.; Ida, T.; Fujii, S.; Koarai, A.; Yamada, M.; Onodera, K.; Hashimoto, Y.; Tanaka, R.; Sato, K.; Shishikura, Y.; Hirano, T.; Yanagisawa, S.; Fujino, N.; Okazaki, T.; Tamada, T.; Hoshikawa, Y.; Okada, Y.; Ichinose, M., Production of reactive persulfide species in chronic obstructive pulmonary disease. *Thorax* **2017**, *72* (12), 1074–1083.
- (73) Kimura, Y.; Koike, S.; Shibuya, N.; Lefer, D.; Ogasawara, Y.; Kimura, H., 3-

- Mercaptopyruvate sulfurtransferase produces potential redox regulators cysteine- and glutathione-persulfide (Cys-SSH and GSSH) together with signaling molecules H_2S_2 , H_2S_3 and H_2S . *Sci. Rep.* **2017**, 7 (1), 10459.
- (74) Bordo, D.; Bork, P., The rhodanese/Cdc25 phosphatase superfamily. *EMBO Rep.* **2002**, 3 (8), 741–746.
- (75) Huang, J.; Niknahad, H.; Khan, S.; O'Brien, P. J., Hepatocyte-Catalysed Detoxification of Cyanide by l- and d-Cysteine. *Biochem. Pharmacol.* **1998**, 55 (12), 1983–1990.
- (76) Nagasawa, H. T.; Goon, D. J. W.; Crankshaw, D. L.; Vince, R.; Patterson, S. E., Novel, Orally Effective Cyanide Antidotes. *J. Med. Chem.* **2007**, 50 (26), 6462–6464.
- (77) Libiad, M.; Yadav, P. K.; Vitvitsky, V.; Martinov, M.; Banerjee, R., Organization of the Human Mitochondrial Hydrogen Sulfide Oxidation Pathway. *J. Biol. Chem.* **2014**, 289 (45), 30901–30910.
- (78) Yadav, P. K.; Yamada, K.; Chiku, T.; Koutmos, M.; Banerjee, R., Structure and kinetic analysis of H_2S production by human mercaptopyruvate sulfurtransferase. *J. Biol. Chem.* **2013**, 288 (27), 20002–20013.
- (79) Nagahara, N.; Yoshii, T.; Abe, Y.; Matsumura, T., Thioredoxin-dependent Enzymatic Activation of Mercaptopyruvate Sulfurtransferase: an intersubunit disulfide bond serves as a redox switch for activation. *J. Biol. Chem.* **2007**, 282 (3), 1561–1569.
- (80) Melideo, S. L.; Jackson, M. R.; Jorns, M. S., Biosynthesis of a Central Intermediate in Hydrogen Sulfide Metabolism by a Novel Human Sulfurtransferase and Its Yeast Ortholog. *Biochemistry* **2014**, 53 (28), 4739–4753.
- (81) Jackson, M. R.; Melideo, S. L.; Jorns, M. S., Human Sulfide:Quinone Oxidoreductase Catalyzes the First Step in Hydrogen Sulfide Metabolism and Produces a Sulfane Sulfur Metabolite. *Biochemistry* **2012**, 51 (34), 6804–6815.
- (82) Yamanishi, T.; Tuboi, S., The Mechanism of the L-Cystine Cleavage Reaction Catalyzed by Rat Liver γ -Cystathionase. *J. Biochem.* **1981**, 89 (6), 1913–1921.
- (83) Yadav, P. K.; Martinov, M.; Vitvitsky, V.; Seravalli, J.; Wedmann, R.; Filipovic, M. R.; Banerjee, R., Biosynthesis and Reactivity of Cysteine Persulfides in Signaling. *J. Am. Chem. Soc.* **2016**, 138 (1), 289–299.
- (84) Vitvitsky, V.; Dayal, S.; Stabler, S.; Zhou, Y.; Wang, H.; Lentz, S. R.; Banerjee, R., Perturbations in homocysteine-linked redox homeostasis in a murine model for

- hyperhomocysteinemia. *Am. J. Physiol. Integr. Comp. Physiol.* **2004**, 287 (1), R39–R46.
- (85) Akaike, T.; Ida, T.; Wei, F.-Y.; Nishida, M.; Kumagai, Y.; Alam, M. M.; Ihara, H.; Sawa, T.; Matsunaga, T.; Kasamatsu, S.; Nishimura, A.; Morita, M.; Tomizawa, K.; Nishimura, A.; Watanabe, S.; Inaba, K.; Shima, H.; Tanuma, N.; Jung, M.; Fujii, S.; Watanabe, Y.; Ohmuraya, M.; Nagy, P.; Feelisch, M.; Fukuto, J. M.; Motohashi, H., Cysteinyl-tRNA synthetase governs cysteine polysulfidation and mitochondrial bioenergetics. *Nat. Commun.* **2017**, 8 (1), 1177.
- (86) Sawa, T.; Motohashi, H.; Ihara, H.; Akaike, T., Enzymatic Regulation and Biological Functions of Reactive Cysteine Persulfides and Polysulfides. *Biomolecules* **2020**, 10 (9), 1245.
- (87) Bailey, T. S.; Pluth, M. D., Reactions of isolated persulfides provide insights into the interplay between H₂S and persulfide reactivity. *Free Radic. Biol. Med.* **2015**, 89, 662–667.
- (88) Everett, S. A.; Folkes, L. K.; Wardman, P.; Asmus, K.-D., Free-Radical Repair by a Novel Perthiol: Reversible Hydrogen Transfer and Perthiyl Radical Formation. *Free Radic. Res.* **1994**, 20 (6), 387–400.
- (89) Benchoam, D.; Semelak, J. A.; Cuevasanta, E.; Mastrogiovanni, M.; Grassano, J. S.; Ferrer-Sueta, G.; Zeida, A.; Trujillo, M.; Möller, M. N.; Estrin, D. A.; Alvarez, B., Acidity and nucleophilic reactivity of glutathione persulfide. *J. Biol. Chem.* **2020**, 295 (46), 15466–15481.
- (90) Kawamura, S.; Kitao, T.; Nakabayashi, T.; Horii, T.; Tsurugi, J., Alkyl hydrodisulfides. VIII. Alkaline decomposition and its competition with nucleophiles. *J. Org. Chem.* **1968**, 33 (3), 1179–1181.
- (91) Isabelle, A.; Erwan, G., A Persulfide Analogue of the Nitrosothiol SNAP: Formation, Characterization and Reactivity. *ChemBioChem* **2014**, 15 (16), 2361–2364.
- (92) Jencks, W. P.; Carriuolo, J., Reactivity of Nucleophilic Reagents toward Esters. *J. Am. Chem. Soc.* **1960**, 82 (7), 1778–1786.
- (93) Saund, S. S.; Sosa, V.; Henriquez, S.; Nguyen, Q. N. N.; Bianco, C. L.; Soeda, S.; Millikin, R.; White, C.; Le, H.; Ono, K.; Tantillo, D. J.; Kumagai, Y.; Akaike, T.; Lin, J.; Fukuto, J. M., The chemical biology of hydropersulfides (RSSH): Chemical stability, reactivity and redox roles. *Arch. Biochem. Biophys.* **2015**, 588, 15–24.

- (94) Kawamura, S.; Otsuji, Y.; Nakabayashi, T.; Kitao, T.; Tsurugi, J., Aralkyl Hydrodisulfides. IV. The Reaction of Benzyl Hydrodisulfide with Several Nucleophiles. *J. Org. Chem.* **1965**, *30* (8), 2711–2714.
- (95) Tsurugi, J.; Abe, Y.; Nakabayashi, T.; Kawamura, S.; Kitao, T.; Niwa, M., Aralkyl hydrodisulfides. XI. Reaction with amines. *J. Org. Chem.* **1970**, *35* (10), 3263–3266.
- (96) Tsurugi, J.; Nakabayashi, T.; Ishihara, T., Aralkyl Hydrodisulfides. 1 III. The Reaction with Tertiary Phosphines. *J. Org. Chem.* **1965**, *30* (8), 2707–2710.
- (97) Madej, E.; Wardman, P., The oxidizing power of the glutathione thiyl radical as measured by its electrode potential at physiological pH. *Arch. Biochem. Biophys.* **2007**, *462* (1), 94–102.
- (98) Benson, S. W., Thermochemistry and kinetics of sulfur-containing molecules and radicals. *Chem. Rev.* **1978**, *78* (1), 23–35.
- (99) Everett, S. A.; Wardman, P., Perthiols as antioxidants: Radical-scavenging and prooxidative mechanisms. 1995; pp 55–69.
- (100) Bianco, C. L.; Chavez, T. A.; Sosa, V.; Saund S., S.; Nguyen, Q. N. N.; Tantillo, D. J.; Ichimura, A. S.; Toscano, J. P.; Fukuto, J. M., The chemical biology of the persulfide (RSSH)/perthiyl (RSS·) redox couple and possible role in biological redox signaling. *Free Radic. Biol. Med.* **2016**, *101*, 20–31.
- (101) Chauvin, J.-P. R.; Haidasz, E. A.; Griesser, M.; Pratt, D. A., Polysulfide-1-oxides react with peroxy radicals as quickly as hindered phenolic antioxidants and do so by a surprising concerted homolytic substitution. *Chem. Sci.* **2016**, *7* (10), 6347–6356.
- (102) Pan, J.; Carroll, K. S., Persulfide Reactivity in the Detection of Protein S-Sulfhydration. *ACS Chem. Biol.* **2013**, *8* (6), 1110–1116.
- (103) Horst, B.; Gerwalt, Z., Über Darstellung und Eigenschaften von Alkyl-hydro-polysulfiden. *Justus Liebigs Ann. Chem.* **2006**, *585* (1), 142–149.
- (104) RAO, G. S.; GORIN, G., Reaction of Cystine with Sodium Sulfide in Sodium Hydroxide Solution. *J. Org. Chem.* **1959**, *24* (6), 749–753.
- (105) Filipovic, M. R.; Zivanovic, J.; Alvarez, B.; Banerjee, R., Chemical Biology of H₂S Signaling through Persulfidation. *Chem. Rev.* **2018**, *118* (3), 1253–1337.
- (106) Park, C.-M.; Weerasinghe, L.; Day, J. J.; Fukuto, J. M.; Xian, M., Persulfides: Current Knowledge and Challenges in Chemistry and Chemical Biology. *Mol. BioSyst.* **2015**, *11*

- (7), 1775–1785.
- (107) Bailey, T. S.; Zakharov, L. N.; Pluth, M. D., Understanding Hydrogen Sulfide Storage: Probing Conditions for Sulfide Release from Hydrodisulfides. *J. Am. Chem. Soc.* **2014**, *136* (30), 10573–10576.
- (108) Heimer, N. E.; Field, L.; Waites, J. A., Organic disulfides and related substances. 44. Preparation and characterization of 1-adamantyl hydrodisulfide as a stable prototype of the series. *J. Org. Chem.* **1985**, *50* (21), 4164–4166.
- (109) Bianco, C. L.; Akaike, T.; Ida, T.; Nagy, P.; Bogdandi, V.; Toscano, J. P.; Kumagai, Y.; Henderson, C. F.; Goddu, R. N.; Lin, J.; Fukuto, J. M., The reaction of hydrogen sulfide with disulfides: formation of a stable trisulfide and implications for biological systems. *Br. J. Pharmacol.* **2019**, *176* (4), 671–683.
- (110) Abiko, Y.; Shinkai, Y.; Unoki, T.; Hirose, R.; Uehara, T.; Kumagai, Y., Polysulfide Na₂S₄ regulates the activation of PTEN/Akt/CREB signaling and cytotoxicity mediated by 1,4-naphthoquinone through formation of sulfur adducts. *Sci. Rep.* **2017**, *7* (1), 4814.
- (111) Park, C.-M.; Johnson, B. A.; Duan, J.; Park, J.-J.; Day, J. J.; Gang, D.; Qian, W.-J.; Xian, M., 9-Fluorenylmethyl (Fm) Disulfides: Biomimetic Precursors for Persulfides. *Org. Lett.* **2016**, *18* (5), 904–907.
- (112) Kang, J.; Xu, S.; Radford, M. N.; Zhang, W.; Kelly, S. S.; Day, J. J.; Xian, M., O→S Relay Deprotection: A General Approach to Controllable Donors of Reactive Sulfur Species. *Angew. Chemie Int. Ed.* **2018**, *57* (20), 5893–5897.
- (113) Zhang, X.; Chen, M.; Ni, X.; Wang, Y.; Zheng, X.; Zhang, H.; Xu, S.; Yang, C., Metabolic Reprogramming of Sulfur in Hepatocellular Carcinoma and Sulfane Sulfur-Triggered Anti-Cancer Strategy. *Front. Pharmacol.* **2020**, *11*.
- (114) Khodade, V. S.; Toscano, J. P., Development of S-Substituted Thioisothioureas as Efficient Hydropersulfide Precursors. *J. Am. Chem. Soc.* **2018**, *140* (50), 17333–17337.
- (115) Khodade, V. S.; Pharoah, B. M.; Paolocci, N.; Toscano, J. P., Alkylamine-Substituted Perthiocarbamates: Dual Precursors to Hydropersulfide and Carbonyl Sulfide with Cardioprotective Actions. *J. Am. Chem. Soc.* **2020**, *142* (9), 4309–4316.
- (116) Haritos, V. S.; Dojchinov, G., Carbonic anhydrase metabolism is a key factor in the toxicity of CO₂ and COS but not CS₂ toward the flour beetle *Tribolium castaneum* [Coleoptera: Tenebrionidae]. *Comp. Biochem. Physiol. Part C Toxicol. Pharmacol.*

- 2005, *140* (1), 139–147.
- (117) Khodade, V. S.; Aggarwal, S. C.; Pharoah, B. M.; Paolocci, N.; Toscano, J. P., Alkylsulfenyl thiocarbonates: precursors to hydroper sulfides potently attenuate oxidative stress. *Chem. Sci.* **2021**, *12* (23), 8252–8259.
- (118) Xu, S.; Wang, Y.; Parent, Z.; Xian, M., Diacyl disulfides as the precursors for hydrogen persulfide (H₂S₂). *Bioorg. Med. Chem. Lett.* **2020**, *30* (4), 126903.
- (119) Munday, R.; Munday, J. S.; Munday, C. M., Comparative effects of mono-, di-, tri-, and tetrasulfides derived from plants of the Allium family: redox cycling in vitro and hemolytic activity and Phase 2 enzyme induction in vivo. *Free Radic. Biol. Med.* **2003**, *34* (9), 1200–1211.
- (120) Yagdi, E.; Cerella, C.; Dicato, M.; Diederich, M., Garlic-derived natural polysulfanes as hydrogen sulfide donors: Friend or foe? *Food Chem. Toxicol.* **2016**, *95*, 219–233.
- (121) Pluth, M.; Bailey, T.; Hammers, M.; Hartle, M.; Henthorn, H.; Steiger, A., Natural Products Containing Hydrogen Sulfide Releasing Moieties. *Synlett* **2015**, *26* (19), 2633–2643.
- (122) Benavides, G. A.; Squadrito, G. L.; Mills, R. W.; Patel, H. D.; Isbell, T. S.; Patel, R. P.; Darley-Usmar, V. M.; Doeller, J. E.; Kraus, D. W., Hydrogen sulfide mediates the vasoactivity of garlic. *Proc. Natl. Acad. Sci.* **2007**, *104* (46), 17977–17982.
- (123) Liang, D.; Wu, H.; Wong, M. W.; Huang, D., Diallyl Trisulfide Is a Fast H₂S Donor, but Diallyl Disulfide Is a Slow One: The Reaction Pathways and Intermediates of Glutathione with Polysulfides. *Org. Lett.* **2015**, *17* (17), 4196–4199.
- (124) Kang, J.; Ferrell, A. J.; Chen, W.; Wang, D.; Xian, M., Cyclic Acyl Disulfides and Acyl Selenylsulfides as the Precursors for Persulfides (RSSH), Selenylsulfides (RSeSH), and Hydrogen Sulfide (H₂S). *Org. Lett.* **2018**, *20* (3), 852–855.
- (125) Chaudhuri, A.; Venkatesh, Y.; Das, J.; Gangopadhyay, M.; Maiti, T. K.; Singh, N. D. P., One- and Two-Photon-Activated Cysteine Persulfide Donors for Biological Targeting. *J. Org. Chem.* **2019**, *84* (18), 11441–11449.
- (126) Zhang, Y.; Yu, B.; Li, Z.; Yuan, Z.; Organ, C. L.; Trivedi, R. L.; Wang, S.; Lefer, D. L.; Wang, B., An Esterase-Sensitive Prodrug Approach for Controllable Delivery of Persulfide Species. *Angew. Chem. Int. Ed.* **2017**, *56* (39), 11749–11753.
- (127) Yuan, Z.; Zheng, Y.; Yu, B.; Wang, S.; Yang, X.; Wang, B., Esterase-Sensitive

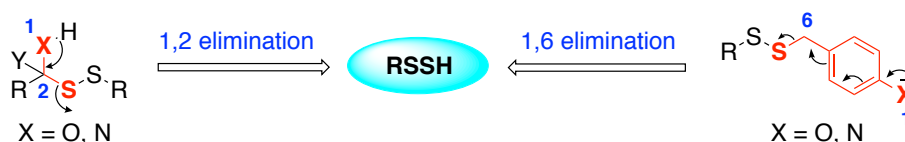
- Glutathione Persulfide Donor. *Org. Lett.* **2018**, *20* (20), 6364–6367.
- (128) Dillon, K. M.; Carrazzone, R. J.; Wang, Y.; Powell, C. R.; Matson, J. B., Polymeric Persulfide Prodrugs: Mitigating Oxidative Stress through Controlled Delivery of Reactive Sulfur Species. *ACS Macro Lett.* **2020**, *9* (4), 606–612.
- (129) Dillon, K. M.; Morrison, H. A.; Powell, C. R.; Carrazzone, R. J.; Ringel-Scaia, V. M.; Winckler, E. W.; Council-Troche, R. M.; Allen, I. C.; Matson, J. B., Targeted Delivery of Persulfides to the Gut: Effects on the Microbiome. *Angew. Chemie Int. Ed.* **2021**, *60* (11), 6061–6067.
- (130) Fosnacht, K. G.; Cerda, M. M.; Mullen, E. J.; Pigg, H. C.; Pluth, M. D., Esterase-Activated Perthiocarbonate Persulfide Donors Provide Insights into Persulfide Persistence and Stability. *ACS Chem. Biol.* **2022**, acschembio.1c00805.

CHAPTER 2: A Vinyl-Boronate Ester Based Persulfide Donor Sensitive to Reactive Oxygen Species (ROS)

2.1. Introduction

Persulfides have been reported to have lower pK_a values,¹ are more nucleophilic² and have lower reduction potentials compared to their corresponding thiols.³ As a result, persulfides are prone to disproportionation with very short half-lives in aqueous medium.⁴ Under oxidative stress, persulfides can prevent overoxidation of proteins by (i) directly scavenging the oxidants⁵ (ii) persulfidating cysteine residues in proteins, the oxidized forms of which can be reduced to regenerate the native cysteine⁶ or (iii) upregulation of antioxidant genes mediated by persulfidation of the KEAP1-Nrf2 axis.⁷ Therefore, enhancing persulfides has emerged as an important therapeutic strategy in countering oxidative or electrophilic stress. Given the unstable nature of persulfides in biological milieu, generating persulfides in situ in a controlled manner can be challenging. Small molecule stimuli responsive precursors or prodrugs of persulfides can aid in overcoming these challenges and can be used as tools to study the intricate redox biology of these reactive sulfur species.

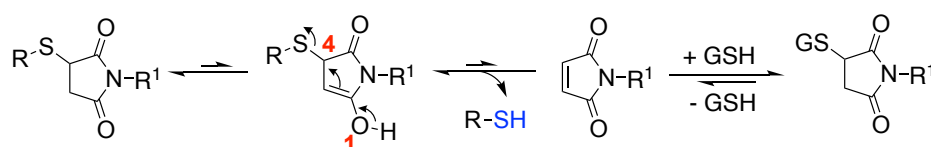
A general strategy to generate a persulfide involves stimuli responsive deprotection followed by self-immolation to generate a persulfide. The classes of persulfide prodrugs reported to date can be broadly classified into two categories based on the self-immolation strategy (Scheme 2.1). The first class of donors involve a 1,2-elimination mechanism that would respond to various chemical or enzymatic stimuli such as fluoride, pH or esterase.^{8–10} The second class of donors involve a 1,6-elimination mechanism that generates a relatively toxic quinone methide byproduct.¹¹ Additionally, the lack of selectivity in these donors might limit their utility in biological systems.



Scheme 2.1. Classes of persulfide prodrugs based on the self-immolation strategy.

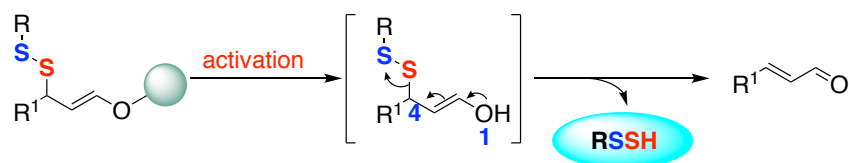
To address these limitations, we designed a prodrug based on a previously unexplored 1,4-O,S-relay or a retro-Michael reaction with a persulfide as a leaving group. Formerly, these types of retro-Michael reactions were used for the release of a thiol group, where the keto form tautomerizes to the enol form that subsequently undergoes a 1,4-elimination. Thioether-

succinimide linkages that undergo retro-Michael reaction and a thiol exchange in thiol-rich medium, is a well-defined strategy used in drug delivery. However, the half-lives for these retro-Michael reactions ranged from 19 h to 337 h (Scheme 2.2).^{12,13} The kinetics of this retro-Michael reaction is a function of the pK_a of the thiol and the nature of *N*-substituents in the succinimide. Electron withdrawing *N*-substituents coupled with a low pK_a thiol enhances the rate of retro-Michael and thiol exchange reaction.¹⁴



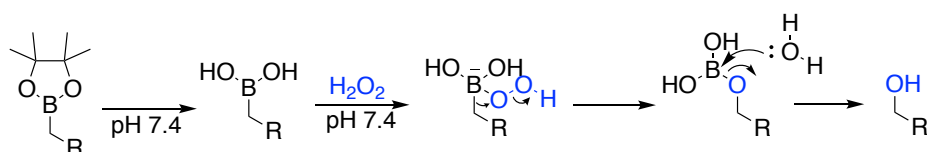
Scheme 2.2. Retro-Michael reaction of thiol-succinimide adducts.

Bypassing the tautomerization step by directly masking the enol in the form of a prodrug, activated by a specific stimulus might accelerate the rate of the retro-Michael reaction. Additionally, since the pK_a of a persulfide ranges a few units lower than their corresponding thiol, we envisaged that persulfides would serve as better leaving groups (Scheme 2.3).



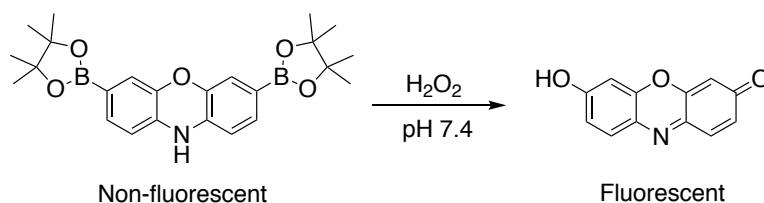
Scheme 2.3. Design of persulfide prodrugs based on 1,4-O,S relay mechanism or retro-Michael reaction.

Elevated levels of reactive oxygen species (ROS) can be associated with several diseased conditions like neurodegeneration, tumor progression, aging, inflammation and diabetes.^{7,15-17} Therefore, to interrogate the role of persulfides in diseased conditions, an ideal prodrug should be responsive to high levels of ROS. Boronate esters are known to react selectively with ROS such as hydrogen peroxide (H_2O_2).¹⁸ The boronate ester undergoes spontaneous hydrolysis in buffer to the corresponding boronic acid, followed by a subsequent nucleophilic attack by peroxide. Oxidation of the boronic acid results in the formation of the free alcohol (Scheme 2.4.).



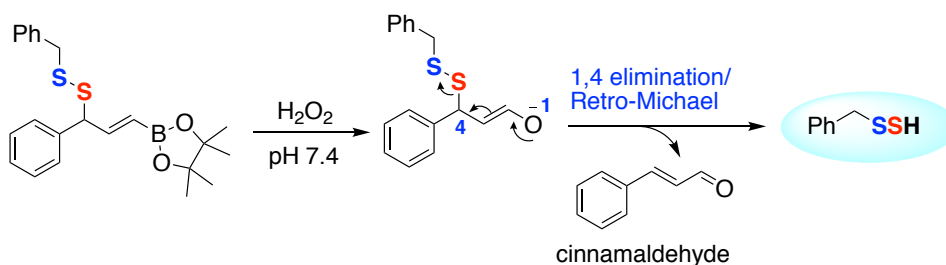
Scheme 2.4. Mechanism of boronate ester cleavage by H_2O_2 .

Aryl boronate esters have been extensively used in prodrug chemistry to mask phenols and deliver drugs, latent fluorophores and reactive species.^{19,20} For instance, Chang and co-workers have reported a fluorescent probe for intracellular detection of H₂O₂ (Scheme 2.5).



Scheme 2.5. Boronate ester based fluorescent probes for detection of H₂O₂.

The proposed design of the ROS sensitive persulfide donor involves masking the enol as a vinyl boronate ester. It was hypothesized that the vinyl boronate ester would be oxidized in the presence of H₂O₂ to generate the free enolate that can undergo a retro-Michael or 1,4 elimination to release the persulfide and form cinnamaldehyde as a byproduct (Scheme 2.6). Cinnamaldehyde is a constituent of cinnamon oil, is widely used in the food industry and has been classified as Generally Recognized As Safe (GRAS).



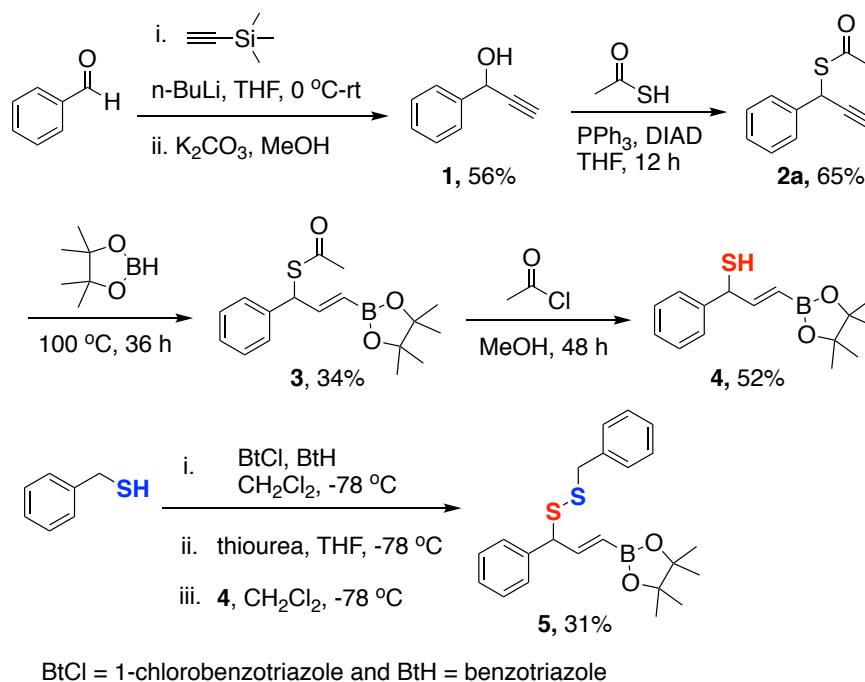
Scheme 2.6. Design of ROS sensitive persulfide donor.

2.2. Results and Discussion

2.2.1. Synthesis of H₂O₂ responsive persulfide donor

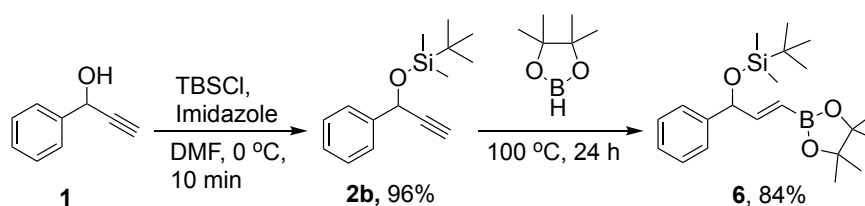
To test our hypothesis, the persulfide donor was synthesized in 6 steps. Trimethylsilyl (TMS) acetylene was activated using *n*-BuLi and reacted with benzaldehyde followed by deprotection of the trimethylsilyl group to give compound **1** in 56% yield.²¹ Compound **1** was then coupled with thioacetic acid under Mitsunobu reaction conditions to form **2a** in 65% yield.²² This was followed by a hydroboration reaction with pinacolborane to afford compound **3** as a trans isomer, evident from the NMR coupling constant ($J = 17.2$ Hz) in 34% yield. Deprotection of the thioacetate by acid hydrolysis in the presence of acetyl chloride and methanol gave the thiol **4** as an intermediate. Finally, the thiol **4** was coupled with benzyl

mercaptan using a previously reported protocol,²³ in the presence of 1-chlorobenzotriazole, benzotriazole and thiourea to give the persulfide prodrug **5** in 31% yield (Scheme 2.7.).



Scheme 2.7. Synthesis of H₂O₂ responsive persulfide prodrug **5**.

Compound **6** which would cleave in the presence of H₂O₂ but not generate a persulfide was synthesized as the negative control. It was synthesized from **1** in two steps. The secondary alcohol was protected by *tert*-butyldimethylsilyl chloride (TBSCl) in the presence of imidazole to give **2b** in 96% yield followed by hydroboration in presence of pinacolborane to afford compound **6** in 84% yield (Scheme 2.8.).



Scheme 2.8. Synthesis of negative control **6**.

2.2.2. HPLC analysis for decomposition of **5**

First, in order to ascertain the reactivity of the prodrug towards H₂O₂ an HPLC based assay was performed to monitor the decomposition of compound **5**. A solution of compound **5** in acetonitrile (ACN) when injected into the HPLC eluted at retention time (RT) 16.3 min. (Figure 2.1). When a solution of **5** in pH 7.4 phosphate buffer was injected, the peak at RT 16.3

min attributable to **5** was not observed. Instead, a new peak at RT 13.7 min was recorded which presumably is the boronic acid, formed upon hydrolysis of the boronate ester functionality in accordance with previous reports.¹⁸ Compound **5** was next incubated with H₂O₂ (10 eq) in pH 7.4 buffer, and the HPLC profiles were recorded at different time points. A peak for the boronic acid (RT 13.7 min) was observed within 5 min which was gradually consumed over 90 min (Figure 2.1).

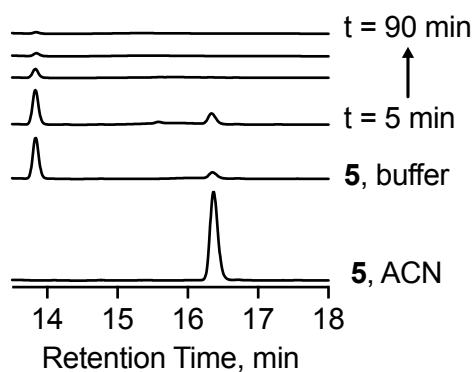


Figure 2.1. HPLC traces for the decomposition of **5** in the presence of H₂O₂ (10 eq) in pH 7.4 buffer.

A time course of decomposition was obtained and the curve fitting to first order gave a pseudo first order rate constant k_1 $5.3 \times 10^{-2} \text{ min}^{-1}$ (Figure 2.2).

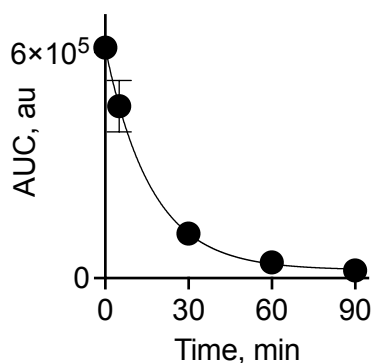
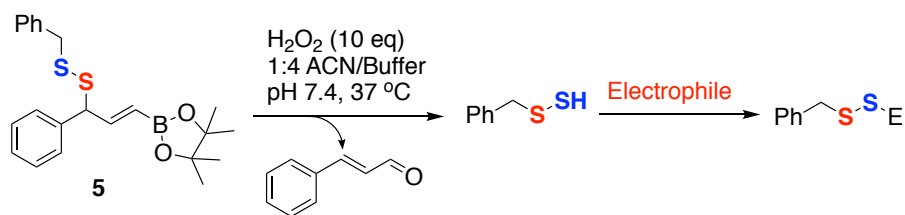


Figure 2.2. Decomposition of the boronic acid of compound **5** as monitored by HPLC. Curve fitting to first order gave a pseudo first order rate constant k_1 $5.3 \times 10^{-2} \text{ min}^{-1}$.

2.2.3. Detection of persulfides

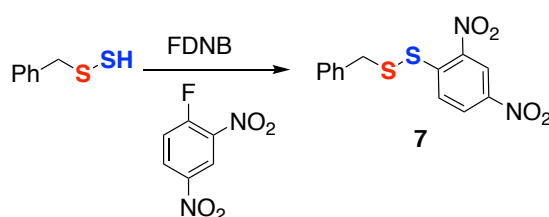
Once it was established that compound **5** can be cleaved by H₂O₂ under physiological conditions, we next attempted to detect the release of the persulfide. Persulfides are highly reactive metastable species which makes its detection and quantification quite challenging. The most commonly used method is to leverage its nucleophilicity and trap it as an adduct by reacting it with suitable electrophiles (Scheme 2.9.).



Scheme 2.9. Detection of persulfide by trapping it with an electrophile.

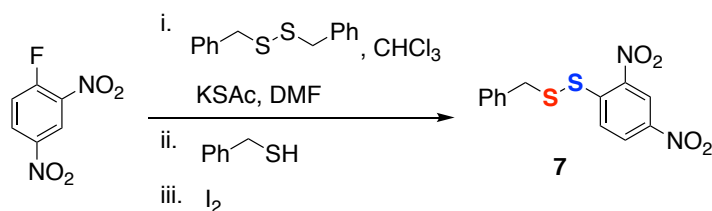
2.2.3.1. Fluorodinitrobenzene (FDNB) method

FDNB was used as an electrophile that would trap the persulfide in the form of the adduct **7**. The formation of **7** can be monitored by HPLC (Scheme 2.10).



Scheme 2.10. Detection of benzyl persulfide by trapping it with FDNB.

Compound **7** was synthesized using a previously reported protocol⁸ (Scheme 2.11.) and upon injecting into the HPLC yielded a distinct peak at RT 11.3 min (Figure 2.3).



Scheme 2.11. Synthesis of FDNB-persulfide adduct **7**.

Compound **5** was incubated with FDNB in the presence of H₂O₂ in pH 7.4 buffer at room temperature and injected into the HPLC at pre-determined time points. The reaction was performed at room temperature due to the propensity of persulfides to undergo decomposition at elevated temperature. A complete consumption of the prodrug **5** (RT 16.3 min) along with the peak for the corresponding boronic acid (RT 13.7 min) was observed within 90 mins. A concomitant formation of the adduct **7** was detected within 5 min, that gradually increased in intensity over 90 min (Figure 2.3). The rate constant (k_3) for the formation of **7** was calculated to be 0.15 min⁻¹. Upon incubation of compound **5** with FDNB in the absence of H₂O₂, as expected, no indication for the formation of the adduct **7** was observed (Figure 2.4).

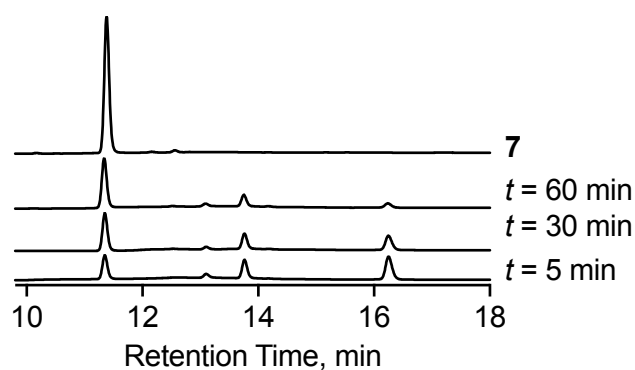


Figure 2.3. HPLC analysis to monitor the formation of adduct **7** upon reaction of **5** with H_2O_2 in the presence of FDNB in pH 7.4 buffer (containing 20% ACN) (Absorbance at 250 nm).

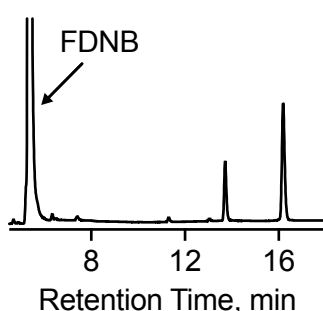
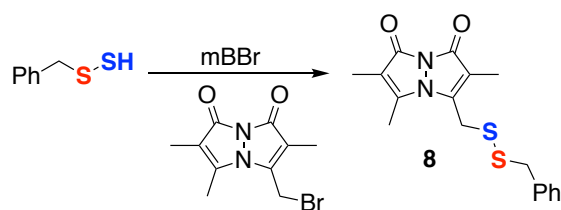


Figure 2.4. Reaction of **5** without H_2O_2 in the presence of FDNB after 30 min.

2.2.3.2. Monobromobimane (mBBr) method

To further confirm the results, another independent assay was performed where monobromobimane (mBBr) was used as the electrophile. Reaction of the persulfide with mBBr is expected to generate the adduct **8** (Scheme 2.12.).



Scheme 2.12. Detection of benzyl persulfide by trapping it with mBBr.

When compound **5** was incubated with H_2O_2 and mBBr in pH 7.4 buffer at 37 °C (Figure 2.5), a distinct peak was observed at retention time 6.5 min which was confirmed to be the adduct **8** by mass spectrometry ($m/z = 369.0707$; observed, 369.2551) (Figure 2.6). The intensity of the peak increased over a period of 90 min along with the peak for cinnamaldehyde at retention time 5.3 mins, following complete consumption of the starting compound (Figure 2.5). The time course for the rate of formation of **8** was monitored and its rate constant (k_4) was calculated

to be 0.12 min^{-1} . The rate of formation of cinnamaldehyde was monitored under these conditions and the rate constant (k_{cinn}) was calculated to be $12.8 \times 10^{-2} \text{ min}^{-1}$ (Figure 2.7). These data collectively suggest the generation of benzyl persulfide from compound **5**, when treated with H_2O_2 .

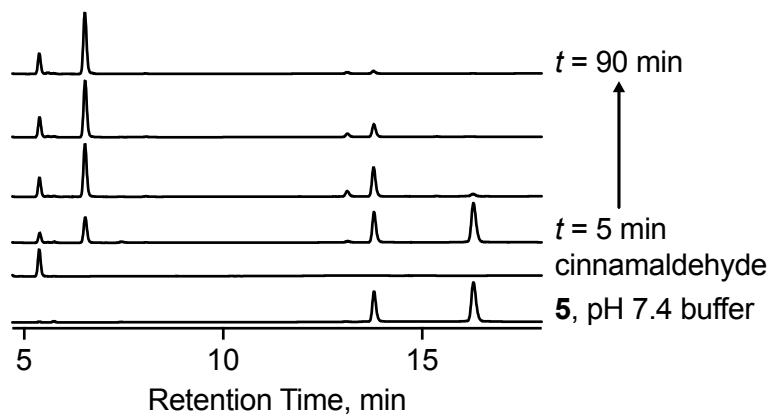


Figure 2.5. HPLC analysis to monitor the formation of adduct **8** upon reaction of **5** with H_2O_2 in the presence of mBBR in pH 7.4 buffer (containing 20% ACN) (Absorbance at 250 nm).

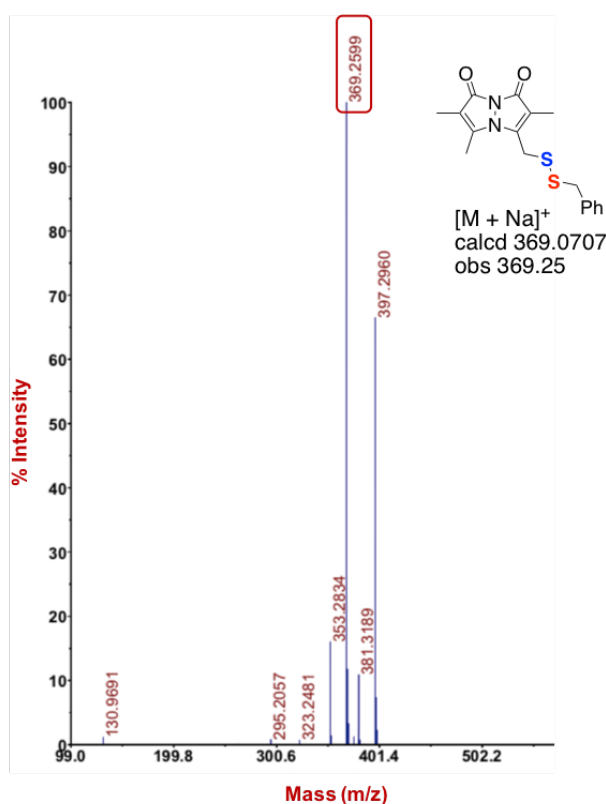


Figure 2.6. MALDI-TOF of the peak eluted at RT 6.5 min which is attributable to **8** $[\text{M} + \text{Na}]^+$ Calculated: 369.0707, Found: 369.2551.

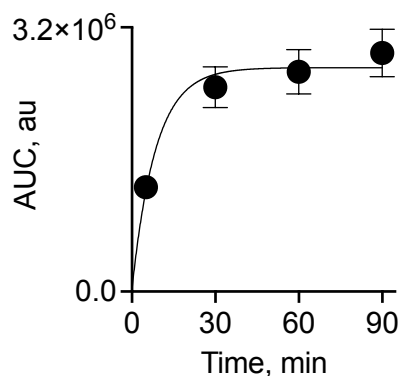
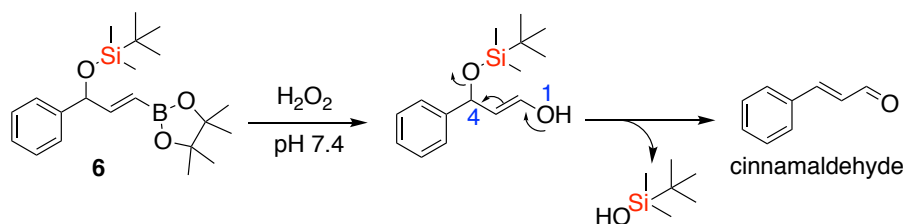


Figure 2.7. Formation of cinnamaldehyde from **5** upon treatment with H_2O_2 in the presence of mBBR, as monitored by HPLC. Curve fitting to first order gave a pseudo first order rate constant $k_{\text{cinn}} 12.8 \times 10^{-2} \text{ min}^{-1}$.

2.2.4. Decomposition of negative control

Using a similar protocol, the release of cinnamaldehyde from the negative control **6** in the presence of H_2O_2 (10 eq) was monitored. Compound **6** should undergo decomposition to generate a cinnamaldehyde but not the persulfide (Scheme 2.13.).



Scheme 2.13. Decomposition of **6** in the presence of H_2O_2 to generate cinnamaldehyde.

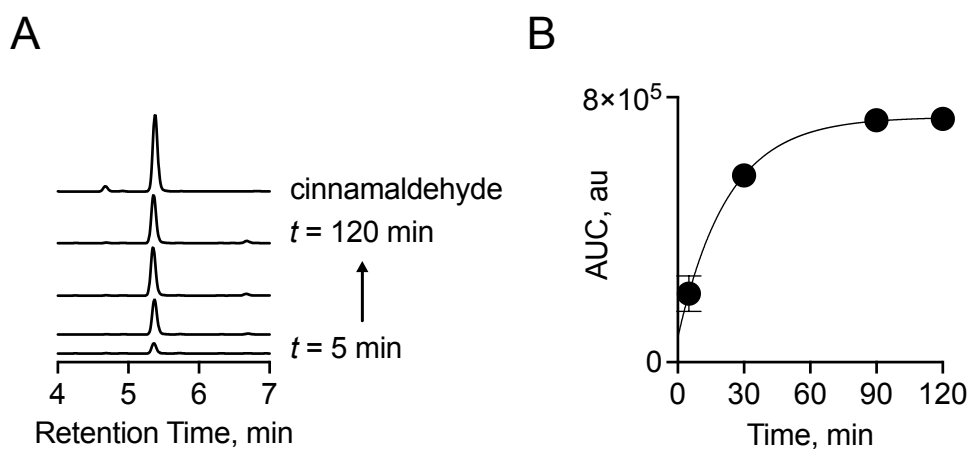


Figure 2.8. a) HPLC traces showing the formation of cinnamaldehyde from **6** upon treatment with H_2O_2 . b) Area under the curve for the peak corresponding to cinnamaldehyde.

The decomposition of **6** could not be monitored due to its low UV absorbance. However, the formation of cinnamaldehyde was observed under these conditions (Figure 2.8.a) and curve fitting to first order gave a pseudo first order rate constant (k_2) of $4.8 \times 10^{-2} \text{ min}^{-1}$ (Figure 2.8.b), which was found to be similar to the rate of decomposition (k_1) of **5** (Figure 2.3). The yield of cinnamaldehyde formed under these conditions was calculated to be 73%. The $\text{p}K_a$ of *tert*-butyldimethylsilanol is estimated to be 15, suggesting that this strategy can be used for delivery of poorly acidic alcohols as well. Previously, a similar vinyl-boronate ester scaffold was used to deprotect alcohols with $\text{p}K_a > 11$.²⁴

2.2.5. Selectivity of vinyl boronate esters towards H_2O_2

To test the selectivity of **5** towards activation by H_2O_2 , a series of experiments were performed. First, a TLC based experiment was carried out to monitor the formation of adduct **7**. Compound **5** was incubated with various oxidants in the presence of FDNB in pH 7.4 buffer at room temperature for 1 h. The reaction mixture was then extracted with ethyl acetate and the organic layer was spotted on a TLC plate. The formation of the adduct was visualized under a UV lamp. Adduct **7** was observed only when compound **5** was treated with H_2O_2 and not in the presence of any other oxidants (Figure 2.9).

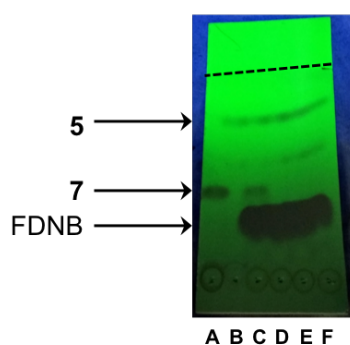


Figure 2.9. TLC analysis to monitor the formation of **7** upon reaction of **5** with various analytes. (A) authentic **7** (R_f 0.37) (B) **5** alone (R_f 0.66) (C) **5** + H_2O_2 (D) **5** + HOCl (E) **5** + TBHP (F) **5** + GSH.

Next, in another independent TLC based experiment the formation of cinnamaldehyde from compound **6** under the aforementioned conditions was tested. No evidence for the formation of cinnamaldehyde was observed except when **6** was treated with H_2O_2 (Figure 2.10.a). Separately, in another experiment the formation of cinnamaldehyde from compound **6** was estimated by monitoring its absorbance at 290 nm (Figure 2.10.b). The results obtained

were in accordance with the TLC experiment. It can therefore be concluded that the vinyl boronate ester scaffold is significantly selective towards H_2O_2 compared to other reactive oxygen and sulfur species.

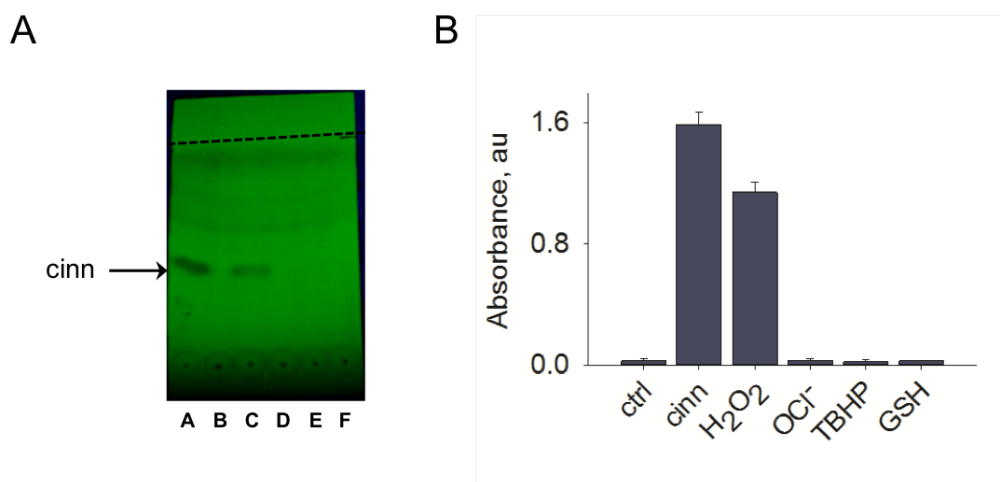


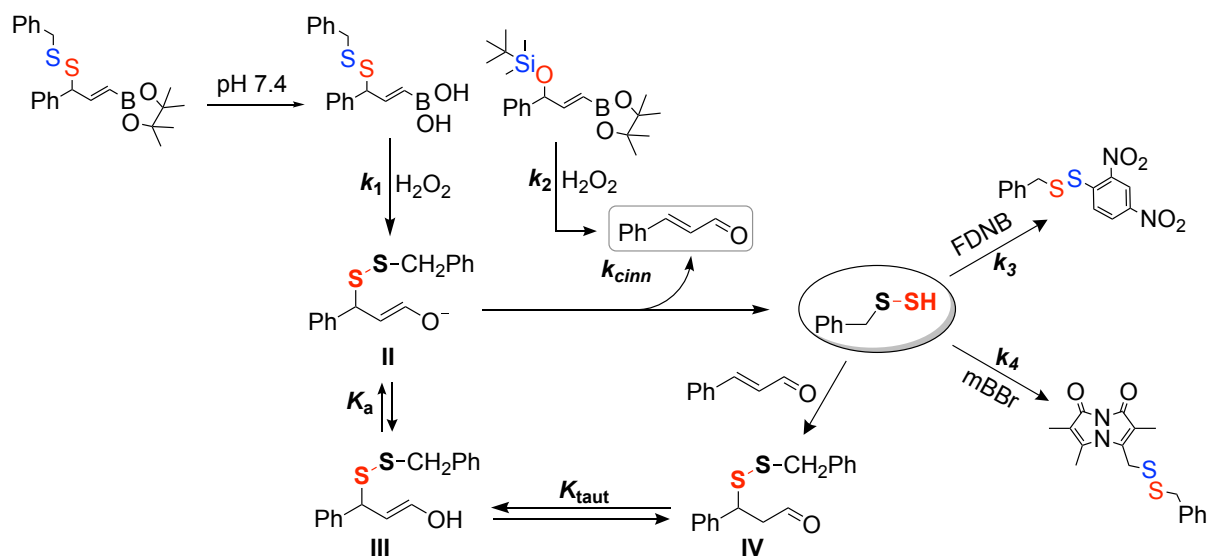
Figure 2.10. a) Formation of cinnamaldehyde from **6** was monitored using TLC. (A) authentic cinnamaldehyde (R_f 0.4) (B) **6** alone (C) **6** + H_2O_2 (D) **6** + HOCl (E) **6** + TBHP (F) **6** + GSH. b) Formation of cinnamaldehyde from **6** in the presence of various reactive oxygen and sulfur species (Abs = 290 nm).

2.2.6. Mechanism

Based on these observations, a mechanism for the generation of persulfides from the vinyl boronate ester scaffold was proposed. The boronate ester moiety hydrolyses in pH 7.4 buffer to form the boronic acid, as observed by the HPLC analysis. The boronic acid functional group reacts with H_2O_2 (10 eq) to form the enolate intermediate (**II**) which then undergoes 1,4-elimination to generate the persulfide and form cinnamaldehyde as a byproduct. The rate of formation of cinnamaldehyde (k_{cinn}) is comparable to the rates of formation of the persulfide adducts (**7** and **8**), suggesting that the formation of persulfide and the cinnamaldehyde is a concerted process. Therefore, the oxidation of the boronate ester by H_2O_2 is most likely the rate determining step.

As discussed above, retro-Michael reactions involving thioethers of *N*-ethylmaleimide have been previously reported, with half-lives ranging from hours to days.^{12,13} However, as envisaged, the present strategy provides distinct advantages over the existing ones, due to the direct generation of an enolate (**II**) that accelerates the rate of retro-Michael reaction. The enolate (**II**) can accept a proton to form the enol (**III**) which can tautomerize to the keto form (**IV**). The equilibrium constant for tautomerism (K_{taut}) which is defined as $[\text{enol}]/[\text{keto}]$ has

been reported to be in the range of $10^{-3} - 10^{-4}$ for aliphatic aldehydes. Therefore, once the enol forms it will rapidly tautomerize to the aldehyde **IV** and the generation of persulfide from **IV** might be extremely slow. Since we have observed the yields of cinnamaldehyde and the FDNB-persulfide adduct **7** in excess of 70%, this might not be a major competitive pathway. Thus, enolate **II** once formed will rapidly undergo a 1,4 elimination to generate the persulfide (Scheme 2.14.).



Scheme 2.14. Mechanism of persulfide generation from **5** in the presence of H_2O_2 . The rate constant for decomposition of **5**, $k_1 = 5.3 \times 10^{-2} \text{ min}^{-1}$, the rate constant for formation of cinnamaldehyde from **6**, $k_2 = 4.8 \times 10^{-2} \text{ min}^{-1}$, the rate constant for formation of cinnamaldehyde from **5** in the presence of mBBBr, $k_{\text{cinn}} = 12.8 \times 10^{-2} \text{ min}^{-1}$. The rate constants for formation of **7** ($k_3 = 0.15 \text{ min}^{-1}$) and **8** ($k_4 = 0.12 \text{ min}^{-1}$).

2.2.7. MTT assay for cell viability

The cytotoxicity of compound **5** and **6** were evaluated using a standard MTT assay to estimate the cell viability. Human colon carcinoma cells (DLD-1) were treated with varying concentrations of **5** and **6** and incubated for 2 h following which cell viability was measured. The compounds were found to be well tolerated by the cells for 2 h with no significant cytotoxicity even at 100 μM (Figure 2.11).

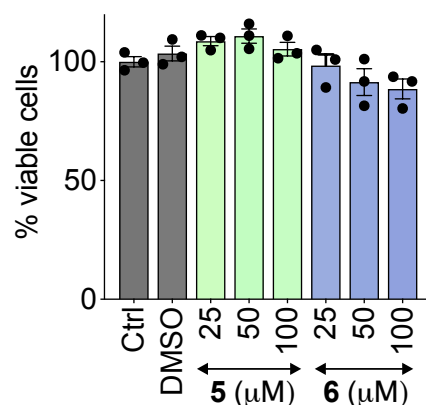


Figure 2.11. Cell viability assay with compound **5** and **6** on colon carcinoma cell line (DLD-1) for 2 h.

2.2.8. Cytoprotective effect of compound **5**

Menadione is a polycyclic aromatic ketone that generates ROS by redox cycling, carried out by one electron reductive enzymes such as NADPH (Figure 2.12.a).²⁵ Menadione at higher concentrations can induce oxidative stress associated with mitochondrial DNA damage and cell death.²⁶ JCHD is a juglone derivative that produces superoxides (Figure 2.12.b).²⁷ Menadione and JCHD were used to induce oxidative stress within cells. Colon cells are being constantly exposed to xenobiotic and pathogen induced stress. Hence, DLD-1 cells were treated with varying concentrations of JCHD and menadione for 2 h to evaluate their toxicity profile. At 50 μM concentration of both menadione and JCHD, greater than 50% cell death was observed (Figure 2.13.).

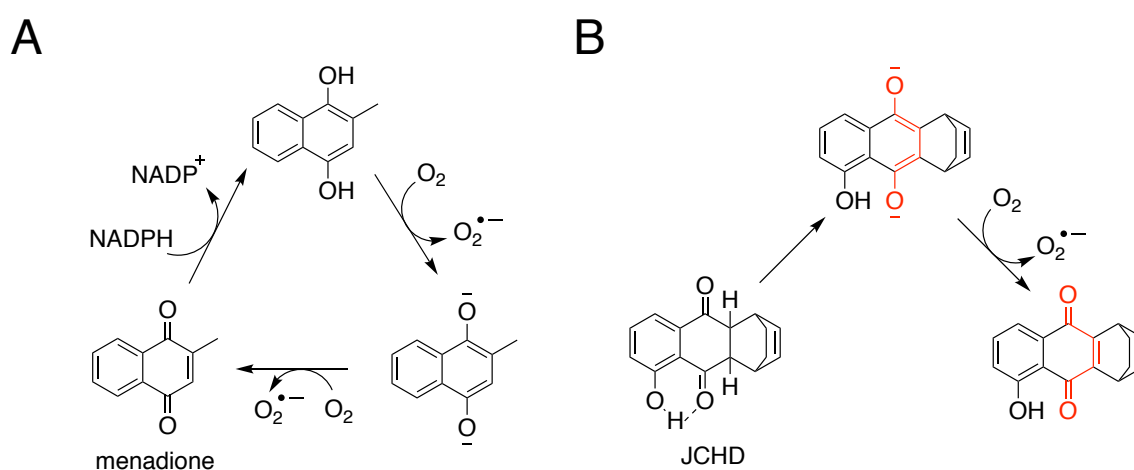


Figure 2.12. (a) Generation of ROS from menadione. (b) Generation of ROS from JCHD.

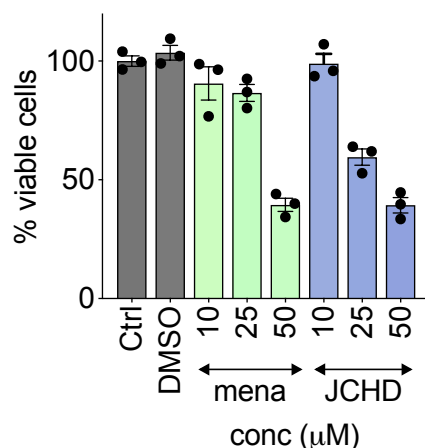


Figure 2.13. Induction of cell death in colon carcinoma cell line (DLD-1) upon incubation with menadione and JCHD for 2 h.

Next, the ability of the persulfide prodrug **5** to protect cells from cytotoxicity induced by oxidative stress was evaluated. DLD-1 cells were co-incubated with menadione (50 μM) and varying concentrations of **5** for 2 h, post which cell viability was measured using MTT assay. A dose dependent increase in cell viability was observed (Figure 2.14.a). Next, when DLD-1 cells were co-incubated with JCHD (50 μM) and varying concentrations of **5** for 2h, the results obtained were in accordance with the previous experiment (Figure 2.14.b). Compound **6** which is the negative control showed no significant enhancement in cell viability under similar conditions (Figure 2.14).

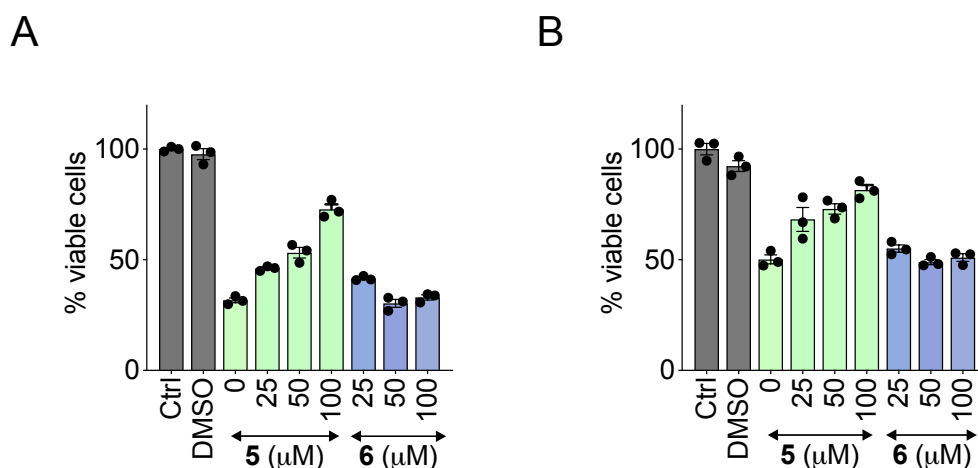
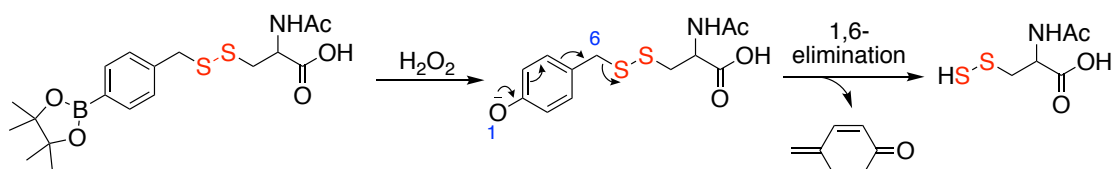


Figure 2.14. a) Cytoprotective effects of compound **5** against menadione (50 μM). Results are expressed as mean ± SEM (n = 3). [****] p < 0.0001 vs menadione] A similar assay was conducted with **6**. No significant effect on the percentage of viable cells during incubation of **6** with menadione was observed. (b) Cytoprotective effects of compound **5** against JCHD (50 μM). Results are expressed as mean ± SEM (n = 3). [***] p < 0.001, vs JCHD] A similar assay was conducted with **6**, and no significant effect was observed.

This suggests that the H_2O_2 consumption during oxidation of the boronate ester group did not play a significant role in the observed cytoprotective effects and were rather mediated by persulfides. Therefore, it can be concluded that the persulfide donor **5** was able to rescue cells from the oxidative stress induced cell death by menadione and JCHD.

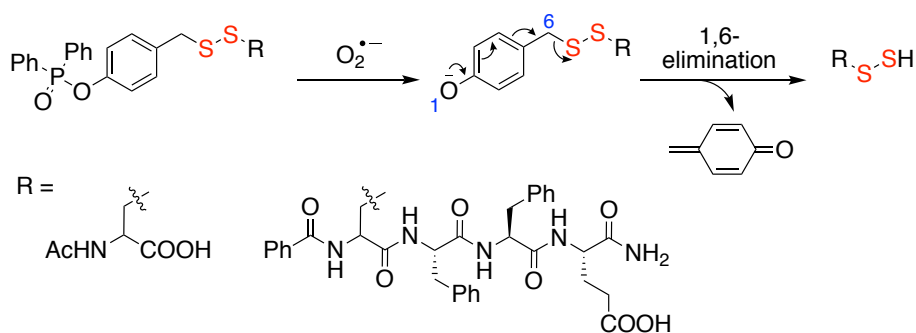
2.3. Other reports

While this work was in progress, Matson and co-workers reported a ROS responsive persulfide donor based on the 1,6-O,S relay mechanism with aryl boronate ester as the cleavable group (Scheme 2.15). The prodrug was shown to protect cells from oxidative stress induced cell death of H9c2 cardiomyocytes as a testament to its therapeutic utility. However, the formation of quinone methide byproduct might limit its further utility.¹¹



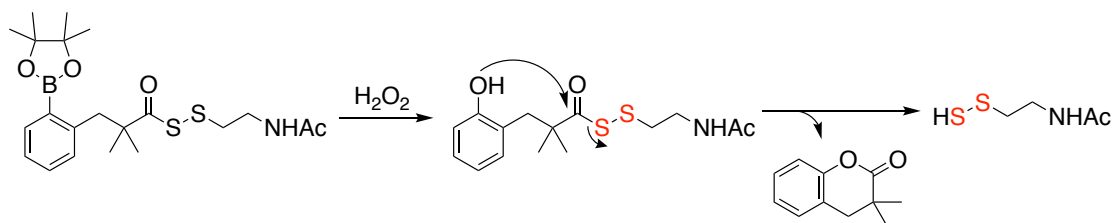
Scheme 2.15. Boronate ester based persulfide donors responsive to H_2O_2 .

Another example of ROS stimulated persulfide prodrug was reported from the same group using a similar strategy. The prodrugs (SOPD-Pep) consists of a diphenylphosphonate moiety as the cleavable group that is sensitive to superoxides ($\text{O}_2^{\bullet-}$), a ROS. Following cleavage of the diphenylphosphonate moiety, the phenolate undergoes 1,6-elimination to generate the persulfide of a short self-assembling tetrapeptide (Scheme 2.16). SOPD-Pep was shown to exhibit potent anti-inflammatory effects in RAW macrophages.²⁸



Scheme 2.16. Persulfide donors responsive to superoxide.

Lukesh and co-workers, very recently have further leveraged the boronate ester scaffold to develop a H_2O_2 responsive persulfide prodrug. Once cleaved by H_2O_2 , the phenolate undergoes intramolecular cyclization to release a *N*-acetylcysteamine persulfide and a lactone as an innocuous byproduct (Scheme 2.17).²⁹



Scheme 2.17. Boronate ester based persulfide donors responsive to H_2O_2 .

2.4. Summary

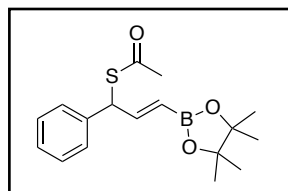
In conclusion, a new class of persulfide donors based on a retro-Michael reaction as the key step has been reported. The generation of persulfides from the vinyl boronate ester scaffold was independently validated using two different assays and a mechanism that is consistent with the experimental data was proposed. The major byproduct generated from this strategy is cinnamaldehyde that is innocuous and FDA approved as a GRAS compound. The compound was found to be well tolerated by the cells. As a testament to its therapeutic utility, the compound was found to protect cells from xenobiotic induced oxidative stress.

2.5. Experimental Section

2.5.1. Synthesis and characterization of data

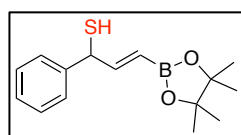
Compounds **1**²¹, **2a**²² and **7**⁸ were synthesized using a previously reported procedure and the analytical data collected was consistent with the reported values.

(E)-S-(1-phenyl-3-(4,4,5,5-tetramethyl-1,3,2-dioxaborolan-2-yl)allyl) ethanethioate (3):



Pinacolborane (860 μ L, 5.91 mmol) was added to *S*-(1-phenylprop-2-yn-1-yl) ethanethioate (**2a**) (750 mg, 3.94 mmol) and heated to 110 $^{\circ}$ C in a sealed tube for 24 h. Upon completion, the reaction mixture was quenched with H₂O and extracted with EtOAc (3 \times 50 mL). The combined organic layers were washed with brine, dried over anhydrous Na₂SO₄, filtered and the filtrate was concentrated under reduced pressure to afford the crude product. The crude obtained was purified by silica gel column chromatography to give the desired product **3** (650 mg, 52 % yield) as a colourless oil: FT-IR (ν_{\max} , cm⁻¹) 2923, 2855, 1696, 1633, 1453; ¹H NMR (400MHz, CDCl₃): δ 7.38-7.24 (m, 5H), 6.80 (dd, J = 17.2, 6.2 Hz, 1H), 5.60 (dd, J = 17.2, 1.6 Hz, 1H), 5.34 (dd, J = 6.2, 1.6 Hz, 1H), 2.32 (s, 3H) 1.25 (s, 12H); ¹³C NMR (100 MHz, CDCl₃) δ 193.7 150.2, 139.2, 128.6, 128.4, 127.5, 83.4, 51.6, 30.4, 24.8, 24.7.; HRMS for C₁₇H₂₃BO₃S [M+Na]⁺: Calculated: 341.1358, Found: 341.1359.

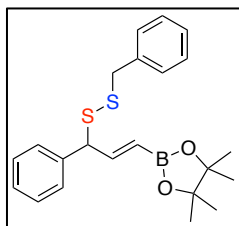
(E)-1-phenyl-3-(4,4,5,5-tetramethyl-1,3,2-dioxaborolan-2-yl)prop-2-ene-1-thiol (4):



To a solution of compound **3** (650 mg, 2.04 mmol) in methanol was added acetyl chloride (1.0 mL, 14.3 mmol) at 0 $^{\circ}$ C and the reaction mixture was stirred at room temperature for 24 h. After completion of the reaction, the solvent was evaporated and the crude was purified by silica gel column chromatography to obtain the thiol **4** as a smelly, brown liquid: FT-IR (ν_{\max} , cm⁻¹) 2926, 2861, 1631, 1453; ¹H NMR (400 MHz, CDCl₃): δ 7.39-7.30 (m, 5H), 6.88 (dd, J = 17.2, 6.2 Hz, 1H), 5.57 (dd, J = 17.2, 1.6 Hz, 1H), 4.76 (m, 1H), 2.07 (d, J = 4 Hz, 1H), 1.26 (s, 12H); ¹³C NMR (100 MHz, CDCl₃): δ 150.5, 138.5, 125.8, 124.6, 124.5, 80.5, 45.1, 21.9.

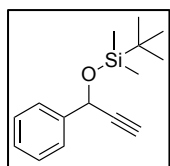
(E)-2-(3-(benzylthio)prop-1-en-1-yl)-4,4,5,5-tetramethyl-1,3,2-dioxaborolane (5):

To a stirred solution of 1-chlorobenzotriazole (75 mg, 0.48 mmol) and benzotriazole (30 mg, 0.24 mmol) in DCM (5 mL) was added a solution of benzylmercaptan (30 μ L, 0.24 mmol) in DCM (2 mL) at -78 $^{\circ}$ C under N₂ atmosphere. After 10 min, a solution of thiourea (56 mg,



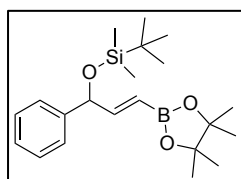
0.724 mmol) in THF (5 mL) was added and left to stir for 10 min followed by addition of the thiol **4** (100 mg, 0.362 mmol) in DCM (2 mL). The reaction mixture was stirred overnight with gradual warming to room temperature. Upon completion, as monitored by TLC the solvent was evaporated, the product was diluted with H₂O and extracted with EtOAc (3 × 50 mL). the combined organic layers were washed with brine, dried over anhydrous Na₂SO₄, filtered and the filtrate was evaporated under reduced pressure to afford the crude product. The crude was then purified by reverse phase HPLC using ACN-H₂O as the eluent to afford the desired product **5** (30 mg, 31% yield) as a sticky liquid: FT-IR (ν_{\max} , cm⁻¹) 2983, 2928, 1629, 1453; ¹H NMR (400 MHz, CDCl₃): δ 7.33-7.22 (m, 10H), 6.78 (dd, J = 17.6, 8.8 Hz, 1H), 5.50 (dd, J = 17.6, 0.9 Hz, 1H), 4.06 (d, J = 8.8 Hz, 1H), 3.76 (m, 2H), 1.26 (s, 12H); ¹³C NMR (100 MHz, CDCl₃): δ 142.5, 138.7, 137.3, 129.6, 128.6, 128.5, 128.4, 127.8, 127.5, 83.4, 60.3, 43.4, 24.8, 24.7; HRMS (ESI) for C₂₂H₂₇BO₂S₂ [M+H]⁺ Calculated: 399.1624, Found: 399.1627.

***tert*-butyldimethyl((1-phenylprop-2-yn-1-yl)oxy)silane (**2b**):**



To a solution of compound **1** (550 mg, 4.16 mmol) in DMF was added imidazole (850 mg, 12.5 mmol) followed by TBSCl (1.25 g, 8.3 mmol) at 0 °C. After 10 min, following complete consumption of the starting material by TLC, the reaction was quenched by adding saturated NH₄Cl solution and the resulting solution was extracted with EtOAc (3 × 50 mL). The combined organic phase was washed with brine, dried over anhydrous Na₂SO₄, filtered and the filtrate was evaporated under reduced pressure. The crude product was purified by silica gel column chromatography using EtOAc/hexane as the mobile phase to afford the desired compound **2b** (980 mg, 96%) as a yellow oil: ¹H NMR (400 MHz, CDCl₃): δ 7.51-7.29 (m, 5H), 5.49 (d, J = 2.3 Hz, 1H), 2.56 (d, J = 2.3 Hz, 1H), 0.94 (s, 9H) 0.18 (s, 3H), 0.14 (s, 3H).

***(E)*-tert-butyl dimethyl((1-phenyl-3-(4,4,5,5-tetramethyl-1,3,2-dioxaborolan-2-yl)allyl)oxy)silane (**6**):**



Compound **6** was synthesized according to the procedure outlined for **3**. Compound **2b** (500 mg, 2 mmol), pinacolborane (440 μ L, 3 mmol) were used to afford **6** (645 mg, 84%) as a white solid: FT-IR (ν_{\max} , cm⁻¹): 2937, 2859, 1639, 1462, 1257; ¹H NMR (400 MHz, CDCl₃): δ 7.31 (m, 5H), 6.67 (dd, J = 17.2, 6.2 Hz, 1H), 5.75 (dd, J = 17.2, 1.6 Hz, 1H), 5.20 (dd, J = 6.2, 1.6 Hz, 1H), 1.24

(s, 12H), 0.90 (s, 9H), 0.05 (s, 3H), -0.07 (s, 3H)); ^{13}C NMR (100 MHz, CDCl_3): δ 155.3, 143.1, 128.2, 127.1, 126.2, 83.2, 77.3, 25.9, 24.8, 24.8, 18.3, -4.8, -4.9; HRMS(ESI) for $\text{C}_{21}\text{H}_{35}\text{BO}_3\text{Si}$ $[\text{M}+\text{Na}]^+$ Calculated: 397.2346, Found :397.2348.

2.5.2. HPLC based kinetics study: A stock solution of **5** (10 mM), **6** (10 mM) and cinnamaldehyde (10 mM) was prepared in DMSO. The reaction mixture consisted of reaction buffer (980 μL of 50 mM phosphate buffer containing 20% ACN and 10 μM diethylenetriaminepentaacetic acid (DTPA), **5** (10 μL , 10 mM) and H_2O_2 (10 μL , 100 mM). The reaction mixture was stirred at 37 $^\circ\text{C}$, 100 μL aliquots were taken out at reported time intervals, filtered (0.22 micron filter) and injected (25 μL) in a High Performance Liquid Chromatography (HPLC Agilent Technologies 1260 Infinity). The stationary phase was C-18 reverse phase column (Phenomenex, 5 μm , 4.6 \times 250 mm) while the mobile phase used was $\text{H}_2\text{O}/\text{ACN}$, a gradient starting with 40: 60 \rightarrow 0 min, 40: 60 to 25: 75 \rightarrow 0 – 5 min, 25: 75 to 10: 90 \rightarrow 5 – 10 min, 10: 90 to 0: 100 \rightarrow 10 – 15 min, 0: 100 to 0: 100 \rightarrow 15 – 17 min, 0: 100 to 40: 60 \rightarrow 17 – 20 min, 40: 60 to 40: 60 \rightarrow 20 – 22 min was used with flow of 1 mL/min. Under these conditions, **5** in ACN eluted at 16.3 min and cinnamaldehyde at 5.3 min. Upon incubation in the reaction buffer for 5 min, a new peak at 13.7 min was observed which presumably is the boronic acid formed by hydrolysis of the boronate ester moiety. A similar protocol was followed to monitor the release of cinnamaldehyde from **6**, although the decomposition of **6** could not be monitored due to its low UV absorbance.

2.5.3. HPLC studies for persulfide reactivity with FDNB: Stock solutions of **5** (10 mM), **7** (10 mM) and 1-Fluoro-2,4-dinitrobenzene (FDNB, 400 mM) were prepared in DMSO and stored at 0 $^\circ\text{C}$ under dark condition. The reaction mixture was prepared by adding 100 μM of **5** (10 μL , 10 mM) to the reaction buffer (970 μL of 50 mM phosphate buffer containing 20% ACN and 10 μM DTPA) followed by addition of 1 mM of H_2O_2 (10 μL , 100 mM) and 4 mM of FDNB (10 μL , 400 mM). The resulting mixture was incubated at 25 $^\circ\text{C}$. 100 μL aliquots were taken out at pre-determined time intervals, filtered (0.22 micron filter) and injected (25 μL) in a High Performance Liquid Chromatography (HPLC Agilent Technologies 1260 Infinity). The stationary phase was C-18 reverse phase column (Phenomenex, 5 μm , 4.6 \times 250 mm) while the mobile phase used was $\text{H}_2\text{O}/\text{ACN}$, a gradient starting with 40: 60 \rightarrow 0 min, 40: 60 to 25: 75 \rightarrow 0 – 5 min, 25: 75 to 10: 90 \rightarrow 5 – 10 min, 10: 90 to 0: 100 \rightarrow 10 – 15 min, 0: 100 to 0: 100 \rightarrow 15 – 17 min, 0: 100 to 40: 60 \rightarrow 17 – 20 min, 40: 60 to 40: 60 \rightarrow 20 – 22 min

was used with flow of 1 mL/min. Under these conditions, the FDNB-persulfide adduct (**7**) elutes at 11.3 min. Each independent experiment was carried out in triplicate.

2.5.4. HPLC studies for persulfide reactivity with mBBr: Stock solutions of **5** (10 mM) and monobromobimane (mBBr, 100 mM) were prepared in DMSO and stored at 0 °C under dark condition. The reaction mixture was prepared by adding 100 μM of **5** (10 μL, 10 mM) to the reaction buffer (970 μL of 50 mM phosphate buffer containing 20% ACN and 10 μM DTPA) followed by addition of 1 mM of H₂O₂ (10 μL, 100 mM) and 1mM of mBBr (10 μL, 100 mM). The resulting mixture was incubated at 37 °C for mBBr. 100 μL aliquots were taken out at pre-determined time intervals, filtered (0.22 micron filter) and injected (25 μL) in a High Performance Liquid Chromatography (HPLC Agilent Technologies 1260 Infinity). The stationary phase was C-18 reverse phase column (Phenomenex, 5 μm, 4.6 × 250 mm) while the mobile phase used was H₂O/ACN, a gradient starting with 40: 60 → 0 min, 40: 60 to 25: 75 → 0 – 5 min, 25: 75 to 10: 90 → 5 - 10 min, 10: 90 to 0: 100 → 10 – 15 min, 0: 100 to 0: 100 → 15 – 17 min, 0: 100 to 40: 60 → 17 – 20 min, 40: 60 to 40: 60 → 20 – 22 min was used with flow of 1 mL/min. Under these conditions, the mBBr-persulfide adduct (**8**) elutes at 6.5 min. Each independent experiment was carried out in triplicate.

2.5.5. Selectivity of **5 against various analytes:** Stock solutions of H₂O₂ (100 mM), HOCl (100 mM) and GSH (100 mM) was prepared in DI water, tert-butyl hydroperoxide (TBHP, 100 mM) was prepared in DMSO. A TLC experiment was conducted to test the selectivity of the vinyl boronate scaffold towards H₂O₂. Compound **5** (2 μL, 10 mM) was treated with the analyte (2 μL, 100 mM) followed by addition of FDNB (2 μL, 400 mM) in phosphate buffer (pH 7.4, 50 mM, 10 mM DTPA) containing 20% ACN. The formation of the persulfide FDNB adduct (**7**) was monitored by TLC. Similarly, compound **6** (2 μL, 10 mM) was treated with various analytes (2 μL, 100 mM) in phosphate buffer (pH 7.4, 50 mM, 10 mM DTPA) containing 20% ACN. The formation of cinnamaldehyde from **6** was monitored by TLC.

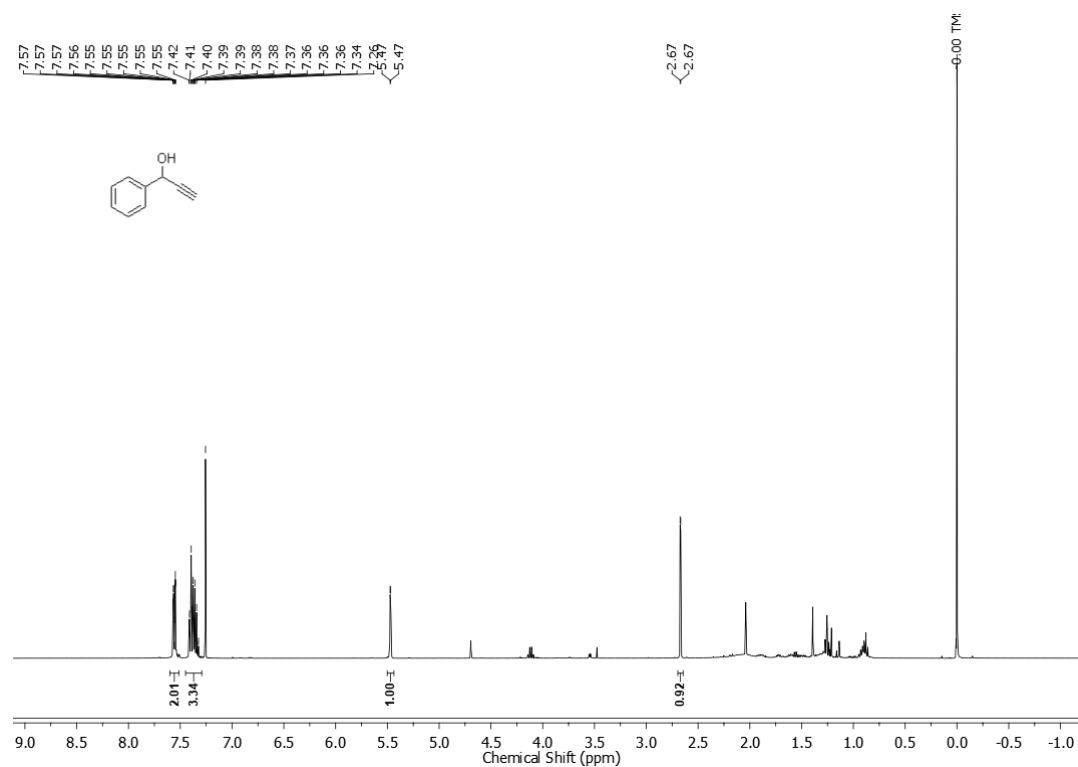
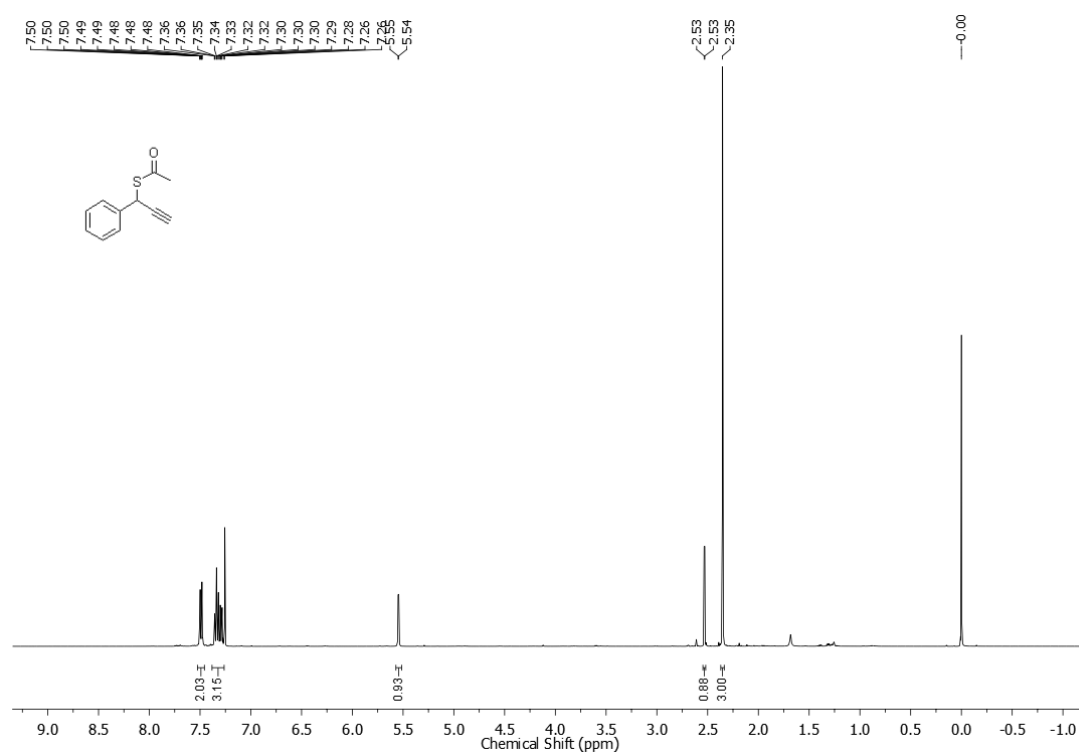
In another independent experiment, compound **6** (3 mL, 10 mM) was incubated with various analytes (3 mL, 100 mM) in 294 mL 1:4 ACN-phosphate buffer (pH 7.4, 50 mM, 10 mM DTPA) at 37 °C for 1 h. Each assay was done in triplicate in vials with closed lids. An aliquot of 200 mL was transferred to a 96 well plate and the absorbance at 290 nm, corresponding to formation of cinnamaldehyde was recorded using a microtiter plate reader.

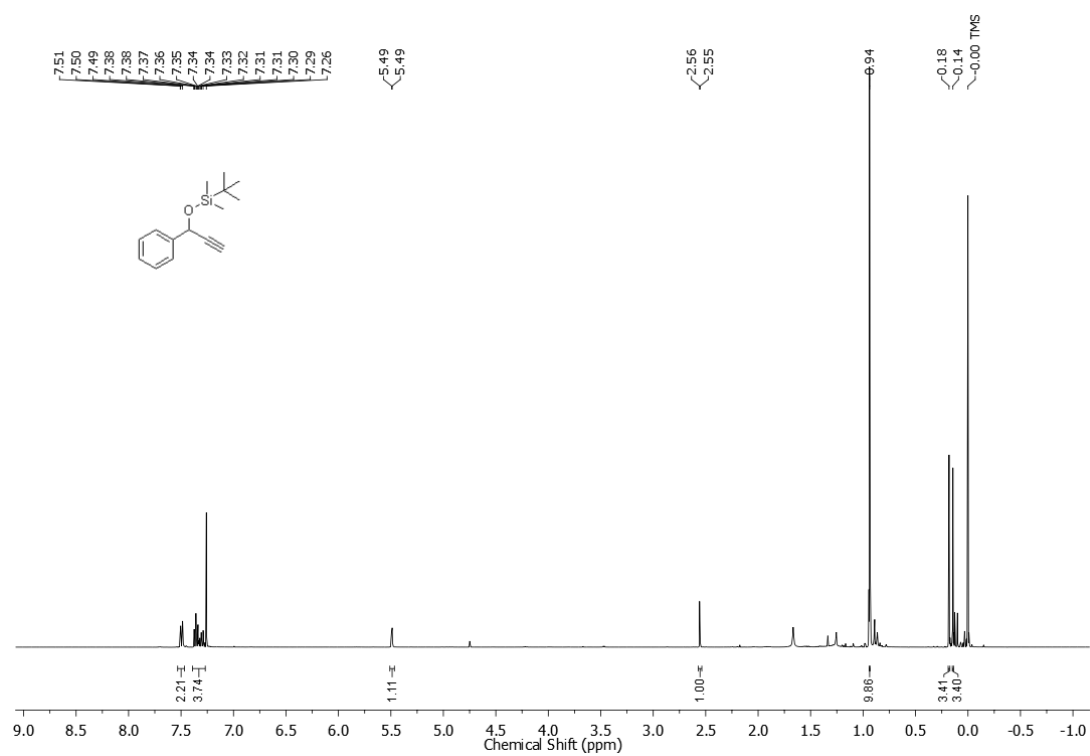
2.5.6. Cell viability assay: DLD-1 cells were seeded at a concentration of 1×10^4 cells/well overnight in a 96-well plate in complete RPMI media supplemented with 10% FBS (fetal

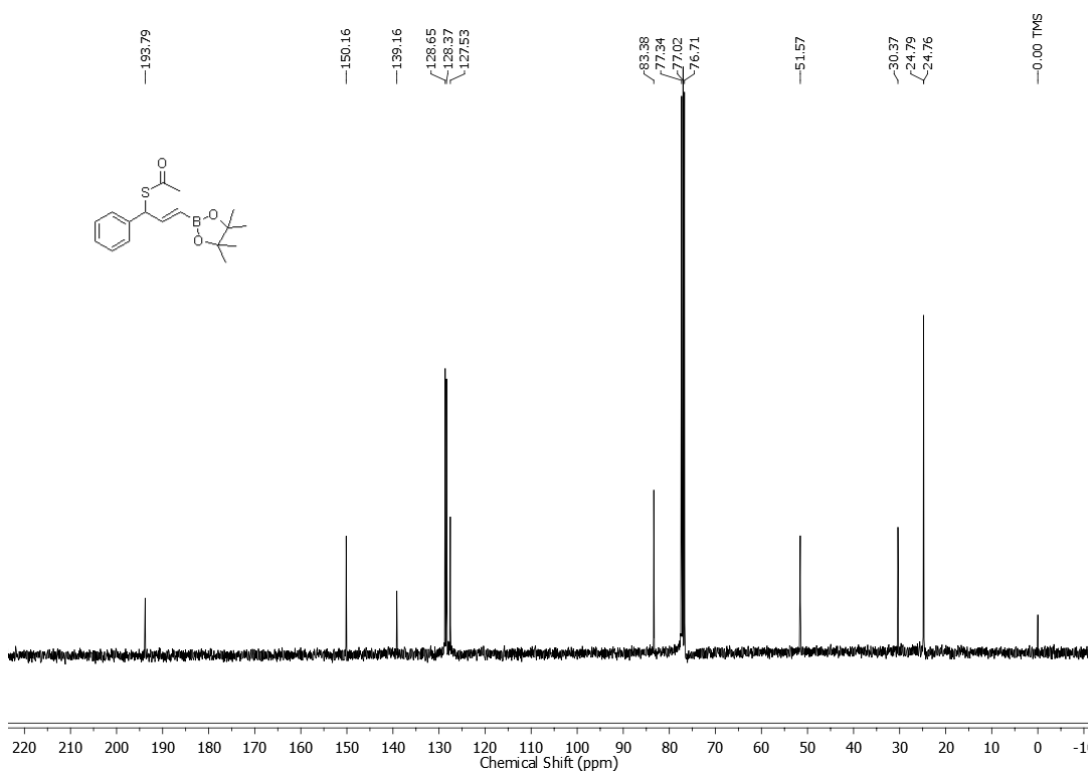
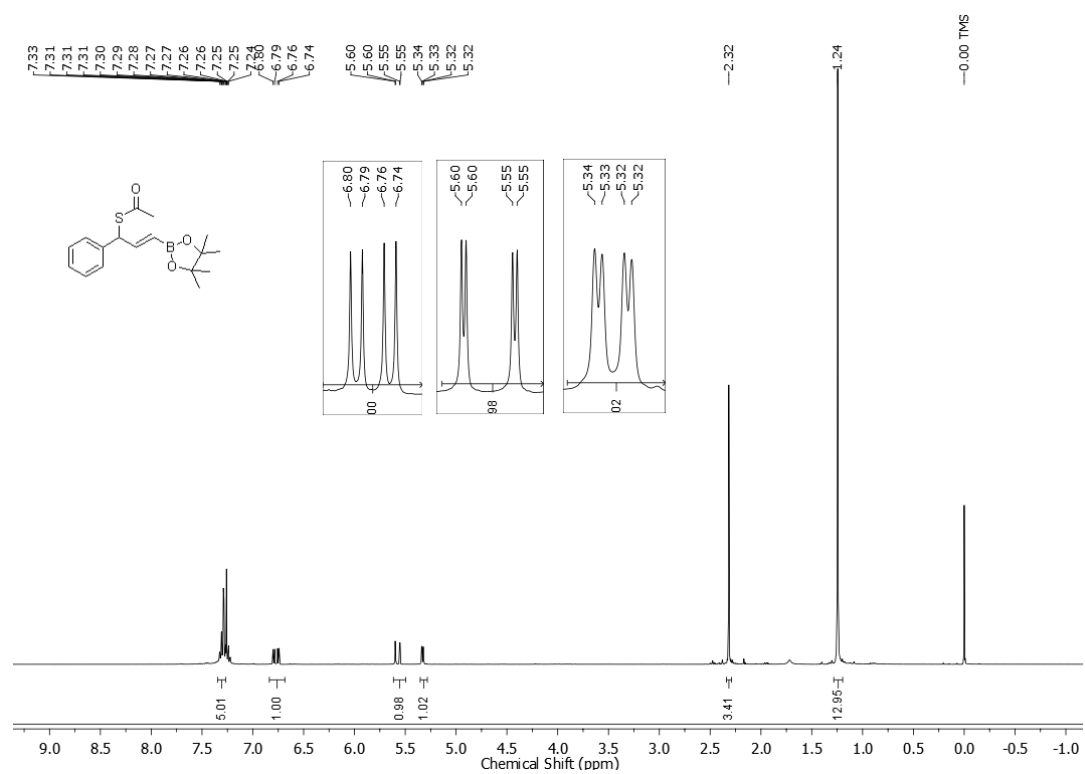
bovine serum) and 1% antibiotic solution and incubated in an atmosphere of 5% CO₂ at 37 °C for 16 h. Following this, the cells were exposed to varying concentrations of the compounds. Stocks were prepared in DMSO and the final concentrations of DMSO did not exceed 0.5%. The cells were incubated for 2 h at 37 °C. The media was removed and a stock solution of 3-(4, 5-dimethylthiazol-2-yl)-2, 5-diphenyl tetrazolium bromide (MTT) was prepared 3.5 mg in 700 µL RPMI. This stock was diluted with 6.3 mL RPMI and 100 µL of the resulting solution was added to each well. After 4 h incubation, the media was removed carefully and 100 µL of DMSO was added. Spectrophotometric analysis of each well using a microplate reader (Thermo Scientific Varioskan) at 570 nm was carried out to estimate cell viability.

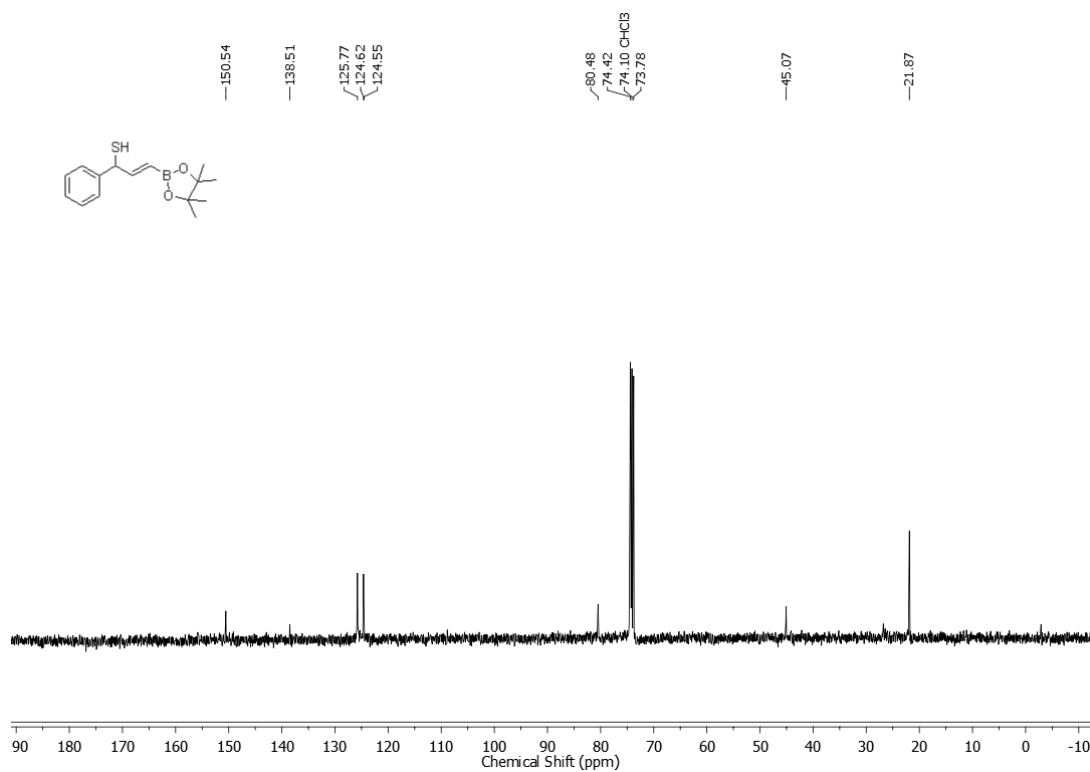
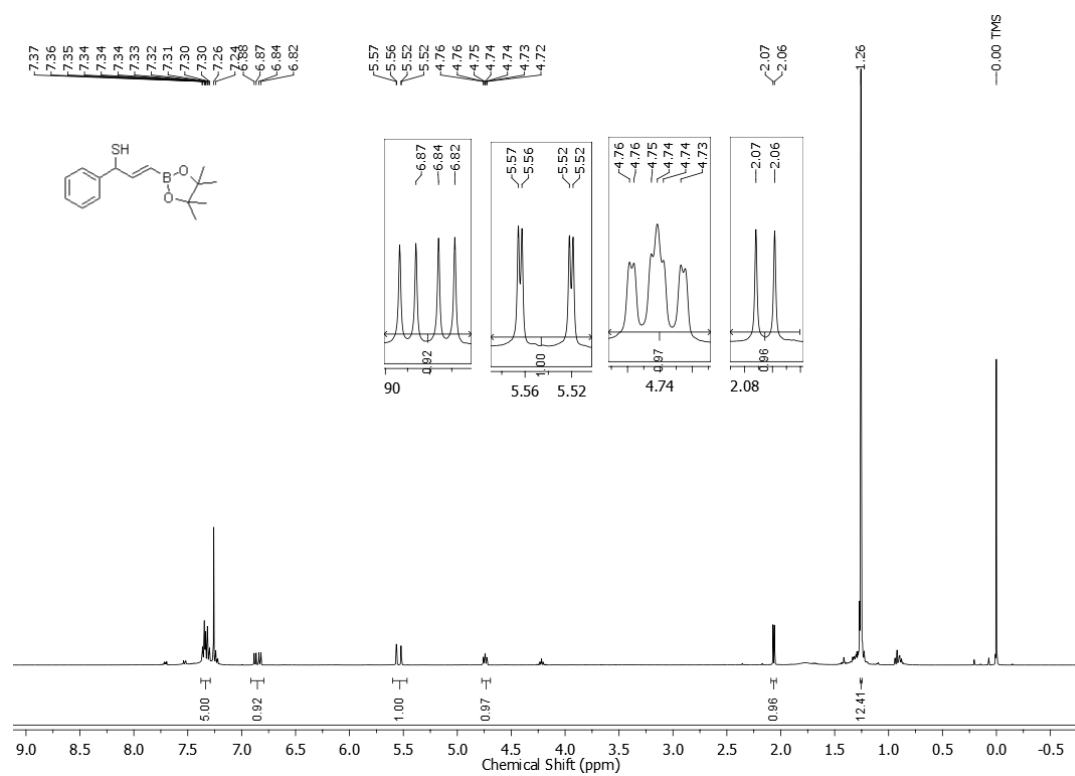
2.5.7. Protection from oxidative stress: Human colon adenocarcinoma cells DLD-1 were seeded in a 96-well plate with 10⁴ cells/well in RPMI media supplemented with 10% FBS (fetal bovine serum) and 1% antibiotic solution and incubated in an atmosphere of 5% CO₂ at 37 °C for 16 h. Stock solutions of compounds were prepared in RPMI with final concentration of DMSO not exceeding 0.5%. After 16 h, the cells were co-treated with different concentrations of the compound and menadione (50 µM) or JCHD (50 µM). The cells were incubated for 2 h at 37 °C following which it was treated with MTT. A stock solution of MTT was prepared by dissolving 3.5 mg in 7 mL RPMI media and 100 mL of this stock was added to each well. After incubating at 37 °C for 4 h, the media was carefully removed and 100 mL of DMSO was added to each well. Absorbance at 570 nm was recorded using a microplate reader (Thermo Scientific Varioskan) to estimate the cell viability.

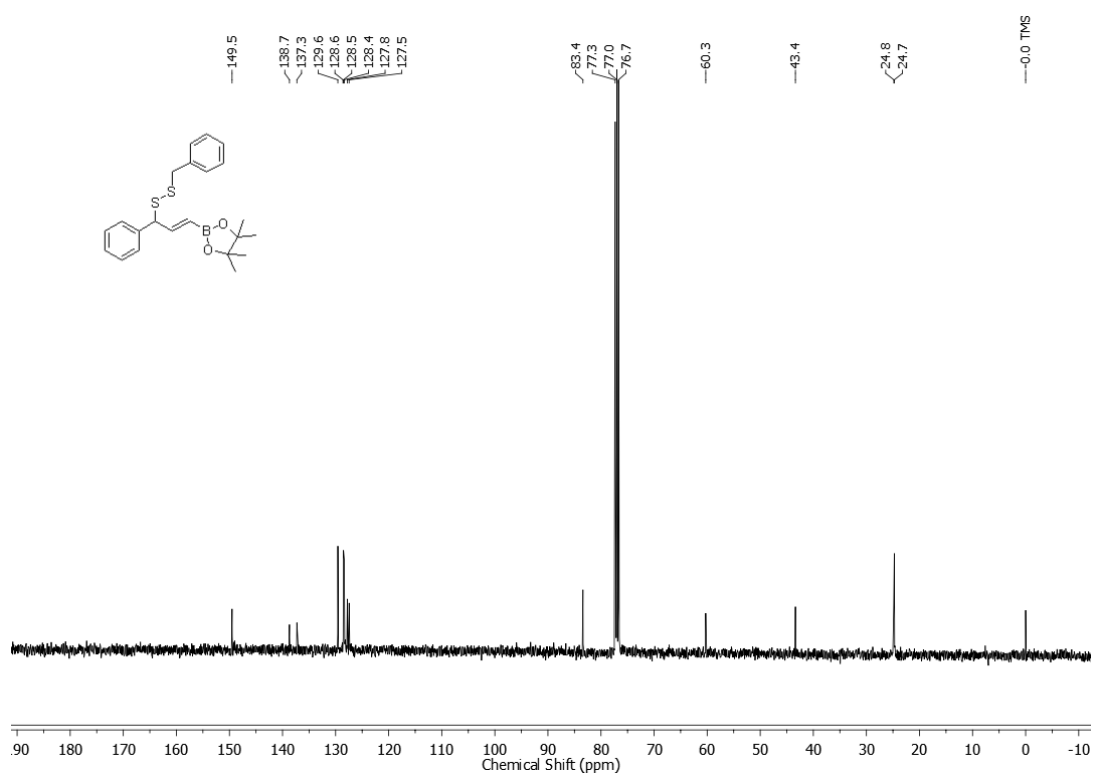
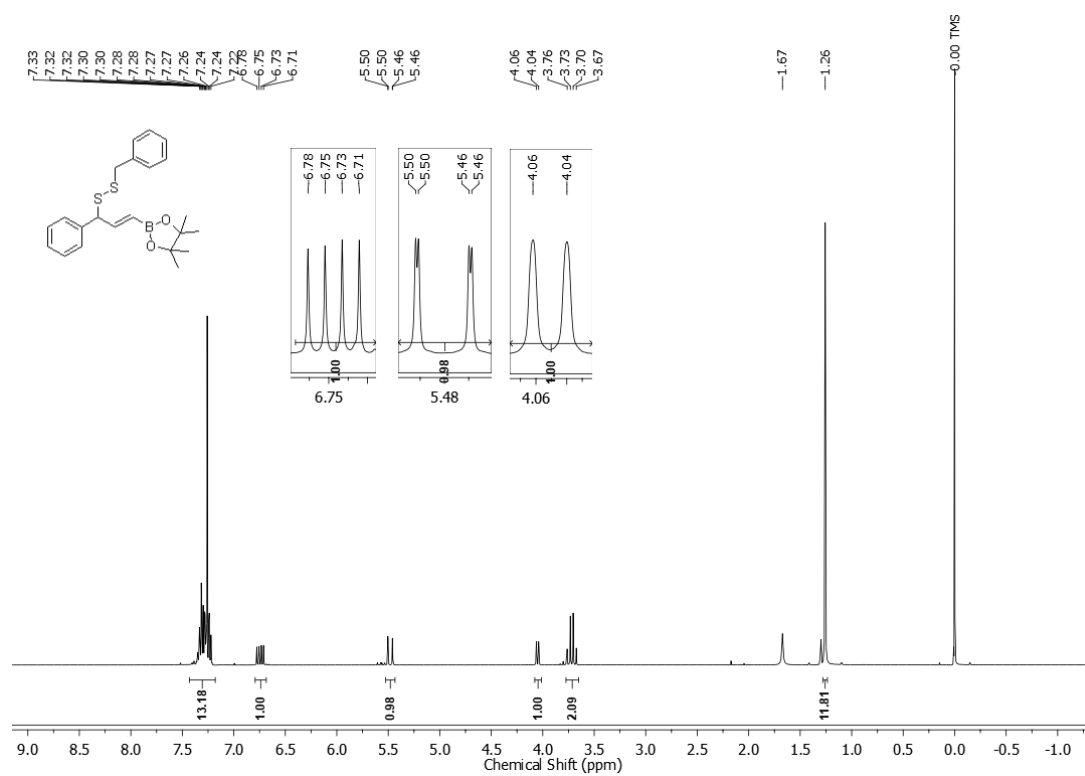
2.6. NMR spectra of compounds

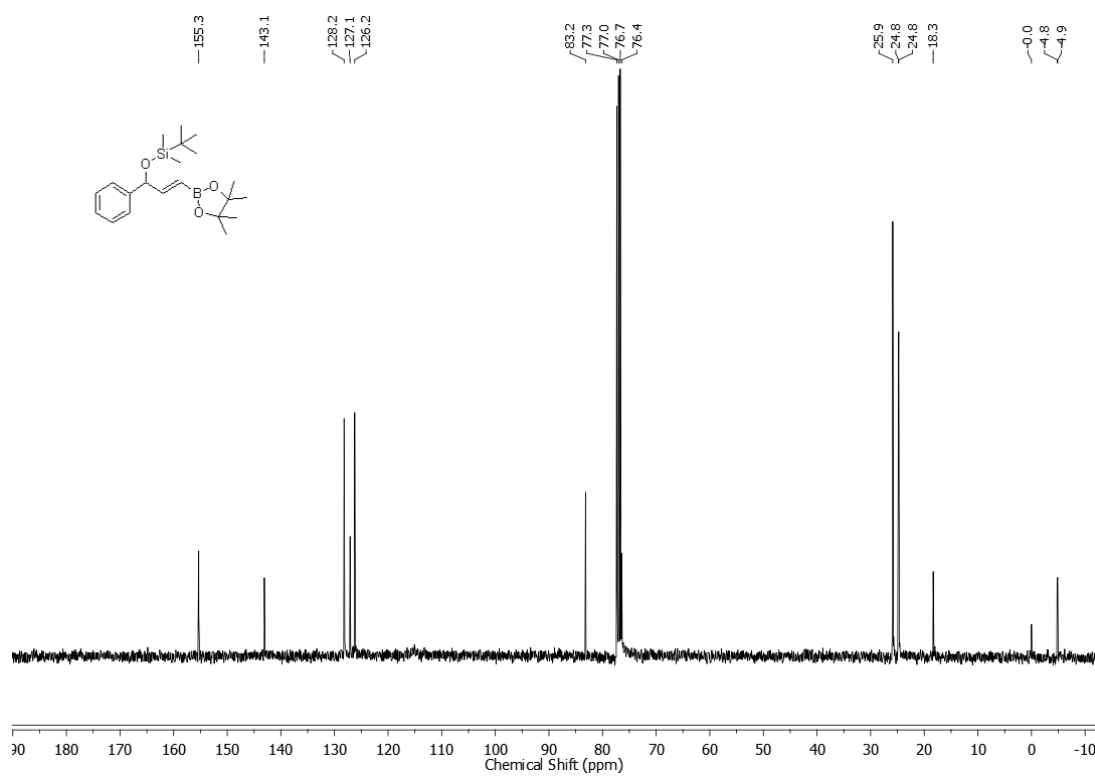
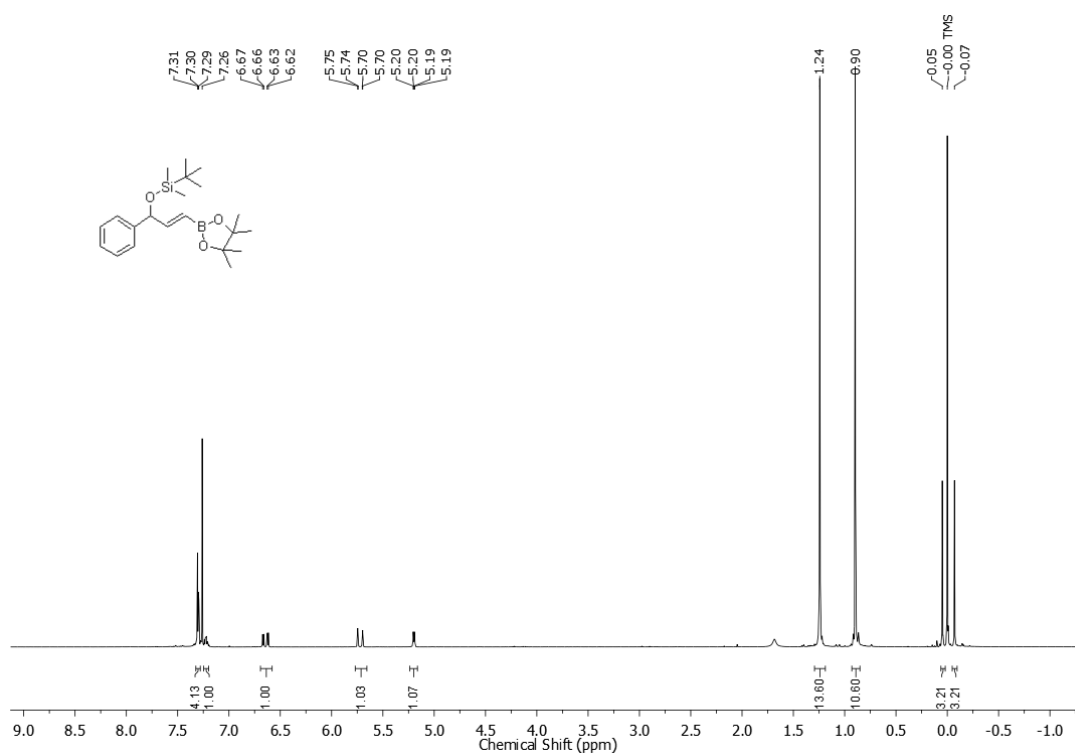
 ^1H NMR spectra of 1 ^1H NMR spectra of 2a

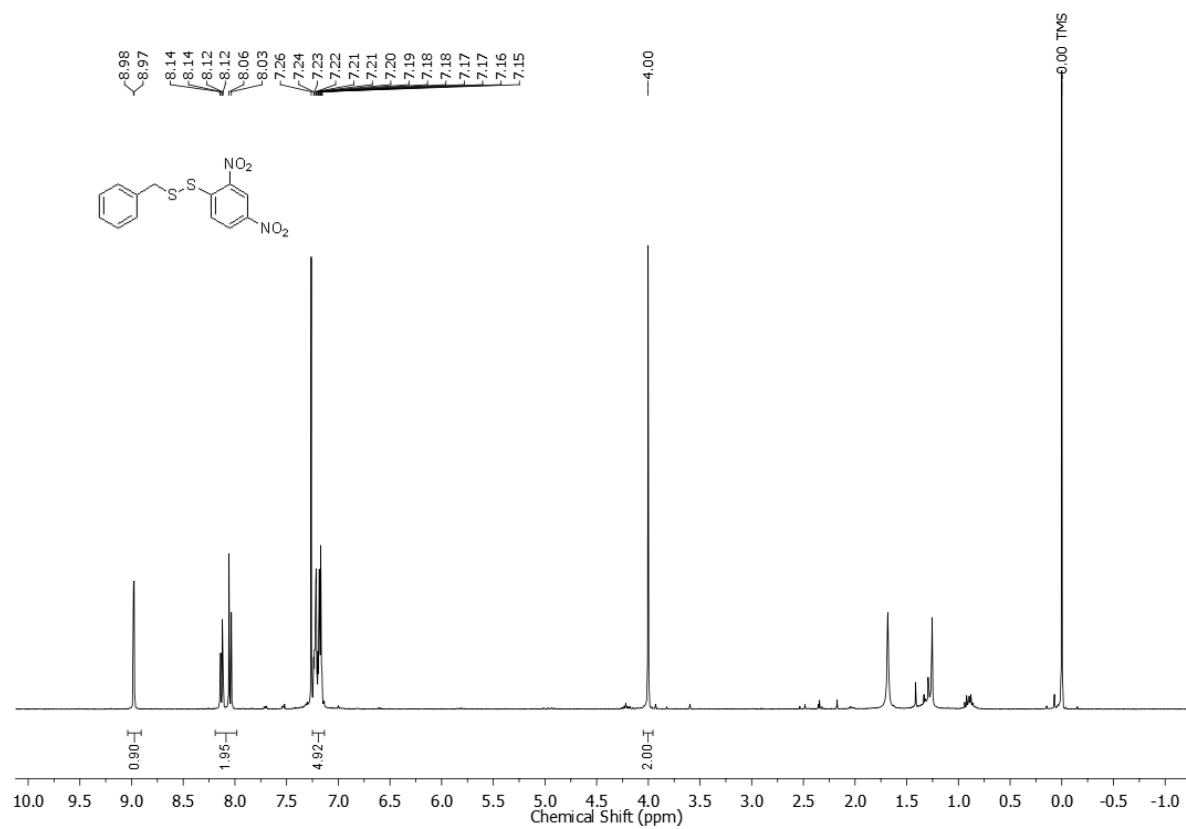
^1H NMR spectra of **2b**

^1H and ^{13}C NMR spectra of **3**

^1H and ^{13}C NMR spectra of **4**

^1H and ^{13}C NMR spectra of **5**

^1H and ^{13}C NMR spectra of **6**

^1H NMR spectra of 7

2.7. References

- (1) Everett, S. A.; Folkes, L. K.; Wardman, P.; Asmus, K.-D., Free-Radical Repair by a Novel Perthiol: Reversible Hydrogen Transfer and Perthiyl Radical Formation. *Free Radic. Res.* **1994**, *20* (6), 387–400.
- (2) Saund, S. S.; Sosa, V.; Henriquez, S.; Nguyen, Q. N. N.; Bianco, C. L.; Soeda, S.; Millikin, R.; White, C.; Le, H.; Ono, K.; Tantillo, D. J.; Kumagai, Y.; Akaike, T.; Lin, J.; Fukuto, J. M., The chemical biology of hydropersulfides (RSSH): Chemical stability, reactivity and redox roles *Arch. Biochem. Biophys.* **2015**, *588*, 15–24.
- (3) Koppenol, W. H.; Bounds, P. L., Signaling by sulfur-containing molecules. Quantitative aspects. *Arch. Biochem. Biophys.* **2017**, *617*, 3–8.
- (4) Yadav, P. K.; Martinov, M.; Vitvitsky, V.; Seravalli, J.; Wedmann, R.; Filipovic, M. R.; Banerjee, R., Biosynthesis and Reactivity of Cysteine Persulfides in Signaling. *J. Am. Chem. Soc.* **2016**, *138* (1), 289–299.
- (5) Ida, T.; Sawa, T.; Ihara, H.; Tsuchiya, Y.; Watanabe, Y.; Kumagai, Y.; Suematsu, M.; Motohashi, H.; Fujii, S.; Matsunaga, T.; Yamamoto, M.; Ono, K.; Devarie-Baez, N. O.; Xian, M.; Fukuto, J. M.; Akaike, T., Reactive cysteine persulfides and S-polythiolation regulate oxidative stress and redox signaling. *Proc. Natl. Acad. Sci. U.S.A* **2014**, *111* (21), 7606–7611.
- (6) Wedmann, R.; Onderka, C.; Wei, S.; Szijártó, I. A.; Miljkovic, J. L.; Mitrovic, A.; Lange, M.; Savitsky, S.; Yadav, P. K.; Torregrossa, R.; Harrer, E. G.; Harrer, T.; Ishii, I.; Gollasch, M.; Wood, M. E.; Galardon, E.; Xian, M.; Whiteman, M.; Banerjee, R.; Filipovic, M. R., Improved tag-switch method reveals that thioredoxin acts as depersulfidase and controls the intracellular levels of protein persulfidation. *Chem. Sci.* **2016**, *7* (5), 3414–3426.
- (7) Yang, G.; Zhao, K.; Ju, Y.; Mani, S.; Cao, Q.; Puukila, S.; Khaper, N.; Wu, L.; Wang, R., Hydrogen Sulfide Protects Against Cellular Senescence via S-Sulfhydration of Keap1 and Activation of Nrf2. *Antioxid. Redox Signal.* **2013**, *18* (15), 1906–1919.
- (8) Zheng, Y.; Yu, B.; Li, Z.; Yuan, Z.; Organ, C. L.; Trivedi, R. K.; Wang, S.; Lefer, D. J.; Wang, B., An Esterase-Sensitive Prodrug Approach for Controllable Delivery of Persulfide Species. *Angew. Chem. Int. Ed.* **2017**, *56* (39), 11749–11753.
- (9) Kang, J.; Xu, S.; Radford, M. N.; Zhang, W.; Kelly, S. S.; Day, J. J.; Xian, M., O→S

- Relay Deprotection: A General Approach to Controllable Donors of Reactive Sulfur Species. *Angew. Chemie Int. Ed.* **2018**, *57* (20), 5893–5897.
- (10) Khodade, V. S.; Toscano, J. P., Development of S-Substituted Thioisothioureas as Efficient Hydropersulfide Precursors. *J. Am. Chem. Soc.* **2018**, *140* (50), 17333–17337.
- (11) Powell, C. R.; Dillon, K. M.; Wang, Y.; Carrazzone, R. J.; Matson, J. B., A Persulfide Donor Responsive to Reactive Oxygen Species: Insights into Reactivity and Therapeutic Potential. *Angew. Chemie. Int. Ed.* **2018**, *57* (21), 6324–6328
- (12) Baldwin, A. D.; Kiick, K. L., Tunable Degradation of Maleimide–Thiol Adducts in Reducing Environments. *Bioconjug. Chem.* **2011**, *22* (10), 1946–1953.
- (13) Weissman, M. R.; Winger, K. T.; Ghiassian, S.; Gobbo, P.; Workentin, M. S., Insights on the Application of the Retro Michael-Type Addition on Maleimide-Functionalized Gold Nanoparticles in Biology and Nanomedicine. *Bioconjug. Chem.* **2016**, *27* (3), 586–593.
- (14) Wu, H.; LeValley, P. J.; Luo, T.; Kloxin, A. M.; Kiick, K. L., Manipulation of Glutathione-Mediated Degradation of Thiol–Maleimide Conjugates. *Bioconjug. Chem.* **2018**, *29* (11), 3595–3605.
- (15) Mustafa, A. K.; Gadalla, M. M.; Sen, N.; Kim, S.; Mu, W.; Gazi, S. K.; Barrow, R. K.; Yang, G.; Wang, R.; Snyder, S. H., H₂S Signals Through Protein S-Sulfhydration. *Sci. Signal.* **2009**, *2* (96), ra72 LP-ra72.
- (16) Zhao, W.; Zhang, J.; Lu, Y.; Wang, R., The vasorelaxant effect of H₂S as a novel endogenous gaseous K(ATP) channel opener. *EMBO J.* **2001**, *20* (21), 6008–6016.
- (17) Mustafa, A. K.; Sikka, G.; Gazi, S. K.; Steppan, J.; Jung, S. M.; Bhunia, A. K.; Barodka, V. M.; Gazi, F. K.; Barrow, R. K.; Wang, R.; Amzel, L. M.; Berkowitz, D. E.; Snyder, S. H., Hydrogen Sulfide as Endothelial Derived Hyperpolarizing Factor Sulfhydrates Potassium Channels. *Circ. Res.* **2011**, *109* (11), 1259–1268.
- (18) Sikora, A.; Zielonka, J.; Lopez, M.; Joseph, J.; Kalyanaraman, B., Direct oxidation of boronates by peroxynitrite: Mechanism and implications in fluorescence imaging of peroxynitrite. *Free Radic. Biol. Med.* **2009**, *47* (10), 1401–1407.
- (19) Miller, E. W.; Albers, A. E.; Pralle, A.; Isacoff, E. Y.; Chang, C. J., Boronate-Based Fluorescent Probes for Imaging Cellular Hydrogen Peroxide. *J. Am. Chem. Soc.* **2005**, *127* (47), 16652–16659.

- (20) Dharmaraja, A. T.; Ravikumar, G.; Chakrapani, H., A Small Molecule for Controlled Generation of Reactive Oxygen Species (ROS). *Org. Lett.* **2014**, *16* (10), 2610–2613.
- (21) Zheng, M.; Wu, F.; Chen, K.; Zhu, S., Styrene as 4 π -Component in Zn(II)-Catalyzed Intermolecular Diels–Alder/Ene Tandem Reaction. *Org. Lett.* **2016**, *18* (15), 3554–3557.
- (22) Yang, F.; Jin, T.; Bao, M.; Yamamoto, Y., Facile synthesis of 3,4-diiiododihydrothiophenes via electrophilic iodocyclization. *Tetrahedron Lett.* **2011**, *52* (8), 936–938.
- (23) Hunter, R.; Caira, M.; Stellenboom, N., Inexpensive, One-Pot Synthesis of Unsymmetrical Disulfides Using 1-Chlorobenzotriazole. *J. Org. Chem.* **2006**, *71* (21), 8268–8271.
- (24) Brooks, A. D.; Yeung, K.; Lewis, G. G.; Phillips, S. T., A strategy for minimizing background signal in autoinductive signal amplification reactions for point-of-need assays. *Anal. Methods* **2015**, *7* (17), 7186–7192.
- (25) Criddle, D. N.; Gillies, S.; Baumgartner-Wilson, H. K.; Jaffar, M.; Chinje, E. C.; Passmore, S.; Chvanov, M.; Barrow, S.; Gerasimenko, O. V; Tepikin, A. V; Sutton, R.; Petersen, O. H., Menadione-induced Reactive Oxygen Species Generation via Redox Cycling Promotes Apoptosis of Murine Pancreatic Acinar Cells. *J. Biol. Chem.* **2006**, *281* (52), 40485–40492.
- (26) Loor, G.; Kondapalli, J.; Schriewer, J. M.; Chandel, N. S.; Vanden Hoek, T. L.; Schumacker, P. T., Menadione triggers cell death through ROS-dependent mechanisms involving PARP activation without requiring apoptosis. *Free Radic. Biol. Med.* **2010**, *49* (12), 1925–1936.
- (27) Dharmaraja, A. T.; Alvala, M.; Sriram, D.; Yogeewari, P.; Chakrapani, H., Design, synthesis and evaluation of small molecule reactive oxygen species generators as selective Mycobacterium tuberculosis inhibitors. *Chem. Commun.* **2012**, *48* (83), 10325–10327.
- (28) Wang, Y.; Dillon, K. M.; Li, Z.; Winckler, E. W.; Matson, J. B., Alleviating Cellular Oxidative Stress through Treatment with Superoxide-Triggered Persulfide Prodrugs. *Angew. Chemie Int. Ed.* **2020**, *59* (38), 16698–16704.
- (29) Hankins, R. A.; Suarez, S. I.; Kalk, M. A.; Green, N. M.; Harty, M. N.; Lukesh, J. C.,

An Innovative Hydrogen Peroxide-Sensing Scaffold and Insight Towards its Potential as an ROS-Activated Persulfide Donor. *Angew. Chemie Int. Ed.* **2020**, *59* (49), 22238–22245.

CHAPTER 3: Enhancing Intracellular Sulfane Sulfur Through β -glycosidase Activated Prodrugs

3.1. Introduction

β -glycosidases are enzymes that typically catalyzes the hydrolysis of β -glycosidic bonds in carbohydrates, glycoproteins and glycolipids. These enzymes are primarily present in the upper gastrointestinal (GI) tract, produced by the colonic microflora. The major glycosidases produced by the gut microbiota include enzymes such as β -D-galactosidase, β -D-glucosidase, β -D-xylopyranosidase and α -L-arabinofuranosidase.¹ Elevated levels of β -glycosidase have been observed in several inflammatory disorders including inflammatory bowel disorder (IBD), ulcerative colitis, Crohn's disease and cancer.^{2,3} Drug delivery to the colon is often complicated due to absorption and degradation of the drug in the upper GI tract resulting in systemic side effects and poor bioavailability.⁴ Therefore, prodrug strategies employing β -glycosidase as the trigger have been widely used for delivery of drugs to the colon.

Chang and co-workers have developed a β -glycosidase based prodrug of the steroid dexamethasone, for the delivery of the drug to the colon (Figure 3.1.).² The prodrug was found to be better absorbed with better bioavailability and reduced side effects in an IBD model of colitis, without compromising on the efficacy. Similarly, β -glycosidase activated prodrugs of the non-steroidal anti-inflammatory drug (NSAID), 4-aminosalicylic acid was developed for the treatment of ulcerative colitis.⁵ Prodrugs of the gasotransmitter nitric oxide (NO), responsive to β -glycosidase was previously reported as tools to be used in biomedical research (Figure 3.1.).^{6,7}

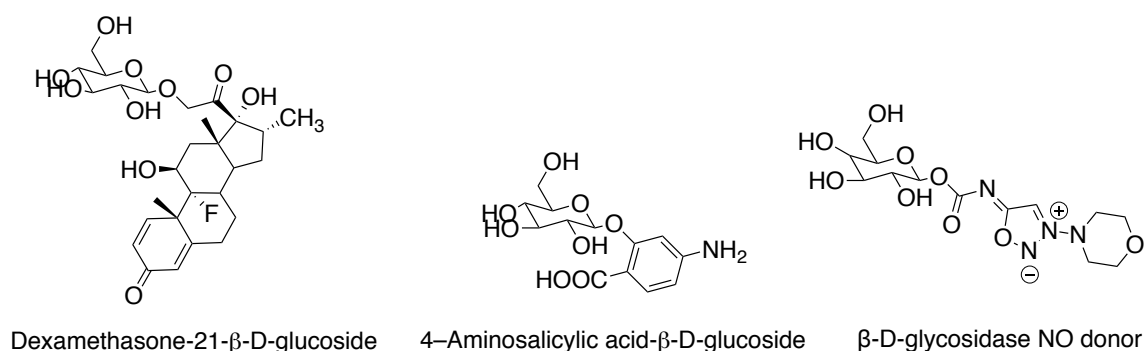


Figure 3.1. β -glycosidase activated prodrugs

The underlying etiology of these inflammatory disorders are multifactorial and is often associated with an excessive production of ROS, leading to collateral tissue damage.⁸ Under these conditions, modulating the levels of ROS by an exogenous supply of antioxidants or upregulating the cellular antioxidant machinery is a possible therapeutic approach. Multiple H₂S-NSAID hybrids are in preclinical and clinical trials, the clinical indications being attributed to H₂S.⁹ Wallace and co-workers had developed a H₂S hybrid of mesalamine, ATB-429 and demonstrated its efficacy in reducing the severity of colitis in mouse model, compared to the parent NSAID alone.¹⁰ Thus, implying that H₂S might be acting in synergy with the NSAID to enhance its anti-inflammatory properties. Glcare Pharma's drug GIC-1001 which is a salt comprising of an H₂S donor and the anti-spasmodic drug trimebutine is in phase II clinical trials for the treatment of IBD.¹¹ Additionally, our group has recently developed a class of COS/H₂S-NSAID donors that exhibits cytoprotective effects against xenobiotic induced stress in colon cells.¹²

Sulfane sulfurs comprising of persulfides and polysulfides have been established as potent antioxidants. These reactive species are more efficient at sequestering oxidants compared to H₂S and are known to upregulate the antioxidant machinery of the cell via persulfidation, in response to oxidative stress.¹³⁻¹⁶ We therefore, proposed the design of β -glycosidase activated persulfide donors comprising of two series (**10-11**), responsive to β -galactosidase and β -glucosidase respectively (Figure 3.2). As per our hypothesis, upon cleavage by β -glycosidase the phenolate would undergo an intramolecular cyclization, resulting in the formation of a heterocyclic byproduct (**12**) with simultaneous release of the persulfide. This strategy offers distinct advantages over the existing prodrug strategies, including the enhanced aqueous solubility of the prodrugs and the formation of a potentially non-toxic, non-electrophilic byproduct. The LD₅₀ of *N*-methylbenzoxazolone (**12**) has been reported to be 890 mg/kg in mice, suggesting that **12** has a very low toxicity profile.¹⁷

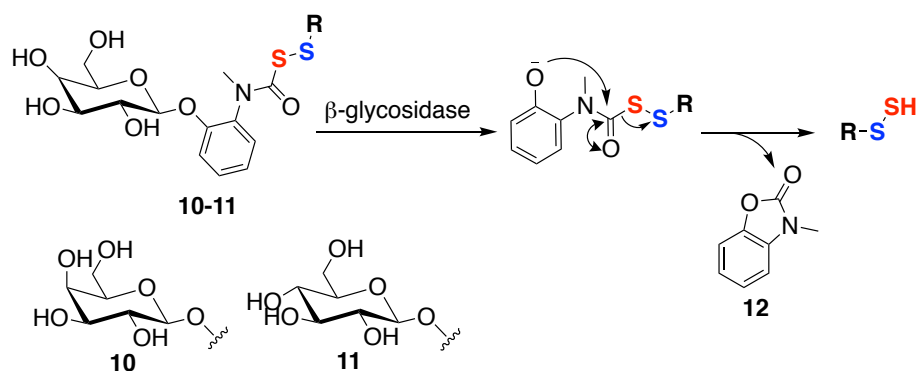
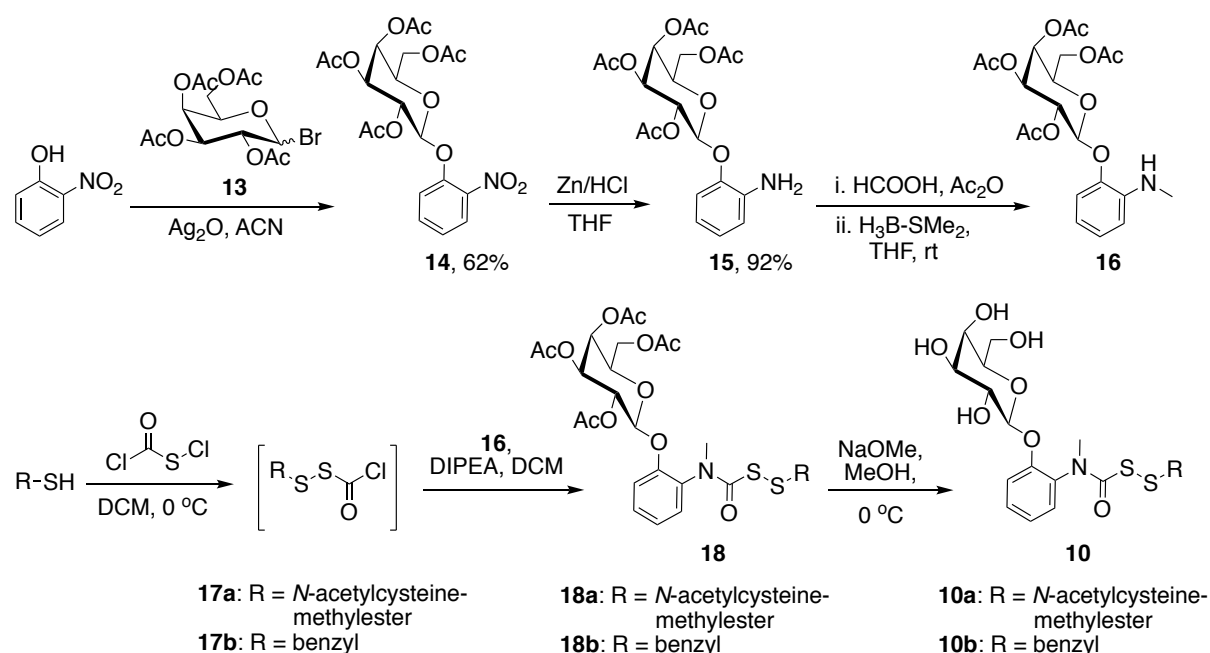


Figure 3.2. Design of β -glycosidase activated persulfide donor.

3.2. Results and Discussion

3.2.1. Synthesis of β -galactosidase responsive persulfide donors

For the β -galactosidase series (**10**), we designed two compounds **10a** and **10b** where the R groups are *N*-acetylcysteine methylester (NACMe) and benzyl respectively (Scheme 3.1.). The synthesis of the persulfide donors **10** was started by reacting 2-nitrophenol with the β -galactopyranosyl bromide **13** and silver oxide (Ag_2O), using a reported protocol¹⁸ to afford compound **14** in 62% yield. Reduction of the nitro group was carried out by zinc and 6N hydrochloric acid to give the aniline derivative **15** in 92% yield. This was followed by formylation of the aniline and its subsequent reduction using borane dimethyl sulfide to obtain **16**, which was taken forward without further purification.¹⁹ In a separate reaction, the thiols were reacted with chlorocarbonylsulfonyl chloride to give **17** as an unstable intermediate.²⁰ Despite several attempts, the NACMe derivative **18a** could not be synthesized. However, the benzyl persulfide derivative **18b** was successfully synthesized by reacting the *S*-perthiocarbonyl chloride **17b** with **16**. Final deacetylation of the galactoside in **18b** using sodium methoxide (NaOMe) in methanol gave compound **10b** in 31% yield (Scheme 3.1).



Scheme 3.1. Synthesis of β -galactopyranosyl derivatives (**10**).

3.2.2. LC/MS analysis for the decomposition of the prodrug **10b**

With the compound in hand, an LC/MS based assay was performed to ascertain the reactivity of **10b** towards β -galactosidase. The decomposition of **10b** in the presence of β -

galactosidase was monitored. **10b** was incubated at 37 °C with β -galactosidase (2 U/mL) in pH 7.4 phosphate buffer and aliquots from the reaction mixture were injected into an LC/MS at pre-determined time points. The peak corresponding to **10b** with $m/z = 468.1146$ ($[M + H]^+$ expected $m/z = 468.1151$) gradually disappeared over 60 mins. A time course of decomposition was obtained and the curve fitting to first order gave a pseudo first order rate constant k_1 $6.8 \times 10^{-2} \text{ min}^{-1}$ (Figure 3.3.).

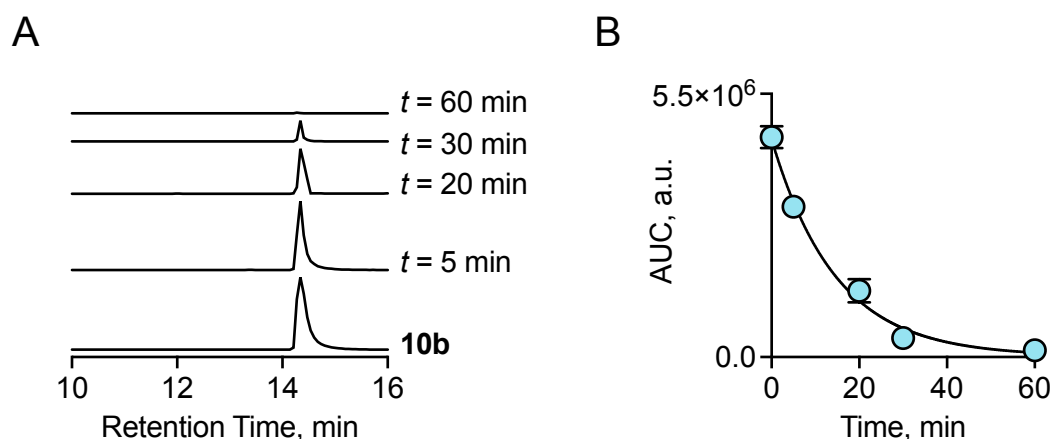


Figure 3.3. a) Extracted ion chromatograms for **10b** ($m/z = 468.1146$; expected $m/z = 468.1151$) at different time points. Decomposition of **10b** over 60 min in the presence of β -galactosidase was observed. b) Curve fitting to first order gave a rate constant of 0.0684 min^{-1} ($R^2 = 0.9929$).

Along with the decomposition of **10b**, a peak for the formation of the *N*-methylbenzoxazolone byproduct (**12**) was observed with $m/z = 150.0545$ $[M + H]^+$ (expected $m/z = 150.0555$), which gradually increased in intensity over a period of 60 min. Curve fitting to first order gave a pseudo first order rate constant of $8.6 \times 10^{-2} \text{ min}^{-1}$ (Figure 3.4.).

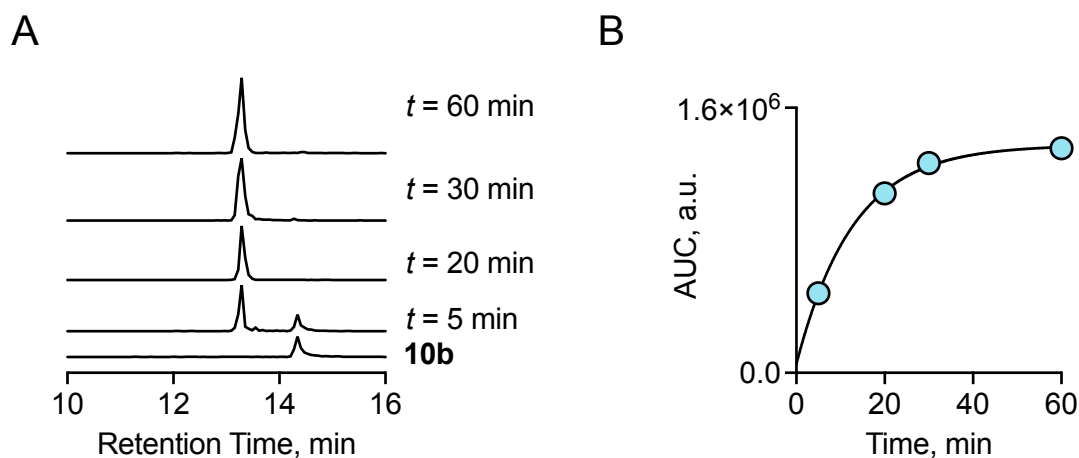
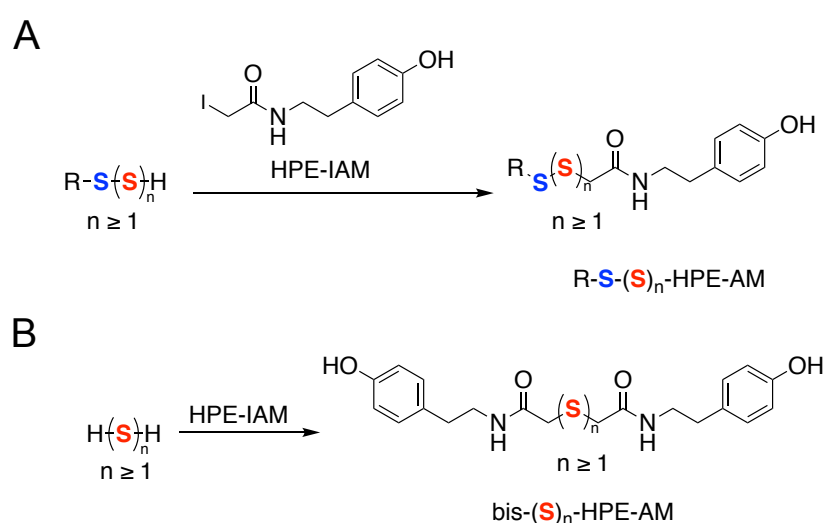


Figure 3.4. a) Extracted ion chromatograms for the formation of byproduct (**12**) ($m/z = 150.0545$; expected $m/z = 150.0555$) at given time points. Formation of **12** from **10b** over 60 min in the presence of β -galactosidase was observed. b) Curve fitting to first order gave a rate constant of 0.0858 min^{-1} ($R^2 = 0.999$).

3.2.3. Detection of persulfide/polysulfide from **10b**

After establishing that **10b** can be efficiently cleaved by β -galactosidase to release the byproduct **12**, the generation of persulfides from **10b** was next assessed. Persulfides can be detected by reacting it with a suitable electrophile. *N*-(4-hydroxyphenethyl)-2-iodoacetamide (HPE-IAM) has been previously reported as an effective persulfide alkylating agent due to its mild electrophilic nature.²¹ Additionally, it can prevent substantial decay of persulfides or polysulfides from alkaline hydrolysis.^{22,23} Persulfides being unstable can undergo disproportionation to form polysulfides ($\text{RS}(\text{S})_n\text{H}$) and hydrogen polysulfides (H_2S_n) which can react with HPE-IAM and hence be detected as HPE-IAM adducts as well (Scheme 3.2.).



Scheme 3.2. a) Reaction scheme showing detection of persulfides/polysulfides as their HPE-AM adducts. b) Hydrogen sulfide/ polysulfides as their bis-S-HPE-AM adducts.

Compound **10b** was incubated with 2 U/mL of β -galactosidase and HPE-IAM (20 eq) in pH 7.4 phosphate buffer and incubated at 37 °C. After incubating for 60 min, an aliquot of the reaction mixture was injected in to the LC/MS. A peak at RT 15.8 min was observed and attributed to benzyl persulfide (BnS-SH) with $m/z = 334.0915$ ($[\text{M}+\text{H}]^+$; expected, 334.0935) (Figure 3.5.a.). Interestingly, a peak for benzyl trisulfide (BnS-SSH) and a peak for benzyl tetrasulfide (BnS-SSSH) was detected as well (Figure 3.5.a.). Hydrogen sulfide (H_2S) and hydrogen polysulfides (H_2S_n) upon reaction with HPE-IAM will form bis- S_n -HPE-AM adducts. H_2S was detected as the bis-S-HPE-AM adduct at RT 12.9 min with $m/z = 389.1540$ ($[\text{M}+\text{H}]^+$; expected, 389.1535). Similarly, H_2S_2 was detected as the bis- S_2 -HPE-AM adduct and H_2S_3 as the bis- S_3 -HPE-AM (Figure 3.5.b.). From the above data, it can be concluded that compound **10b** reacts with β -galactosidase to generate persulfides as well as polysulfides.

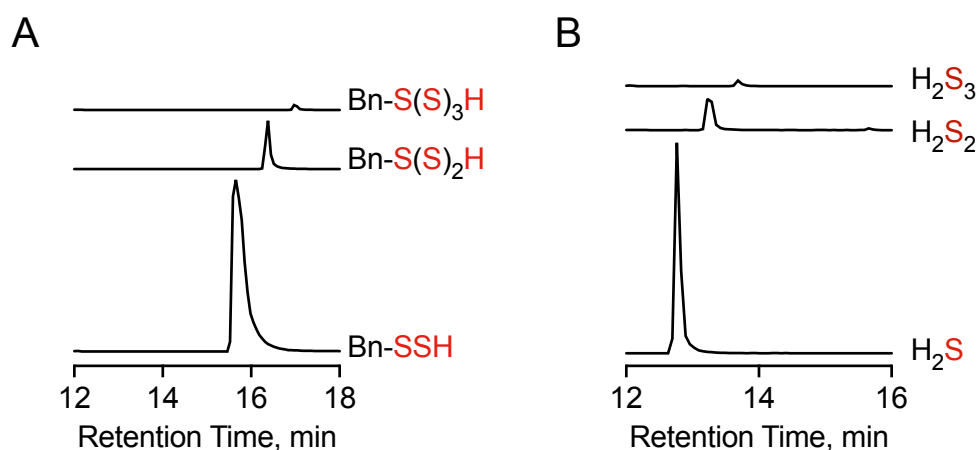


Figure 3.5. a) Extracted ion chromatogram of benzyl persulfides and polysulfides generated from compound **10b**, detected as their HPE-AM adducts using LC/MS. Bn-SS-HPE-AM ($m/z = 334.0915$ $[M+H]^+$; expected, 334.0935); Bn-S(S)₂-HPE-AM ($m/z = 366.0659$ $[M+H]^+$; expected, 366.0656); Bn-S(S)₃-HPE-AM ($m/z = 398.0379$ $[M+H]^+$; expected, 398.0377). b) Extracted ion chromatogram of hydrogen sulfide and hydrogen polysulfides detected as their bis-HPE-AM adducts. Bis-S-HPE-AM ($m/z = 389.1540$ $[M+H]^+$; expected, 389.1535); bis-S₂-HPE-AM ($m/z = 421.1258$ $[M+H]^+$; expected, 421.1256); bis-S₃-HPE-AM ($m/z = 453.0980$ $[M+H]^+$; expected, 453.0976).

3.2.4. MTT assay for cell viability to determine cytotoxicity of **10b**

Human cytosolic β -glycosidase is present in significant concentrations in the liver, kidney, spleen and colon.^{24,25} Human colon carcinoma (DLD-1) and hepatocarcinoma (HepG2) cell line were therefore used as model systems.

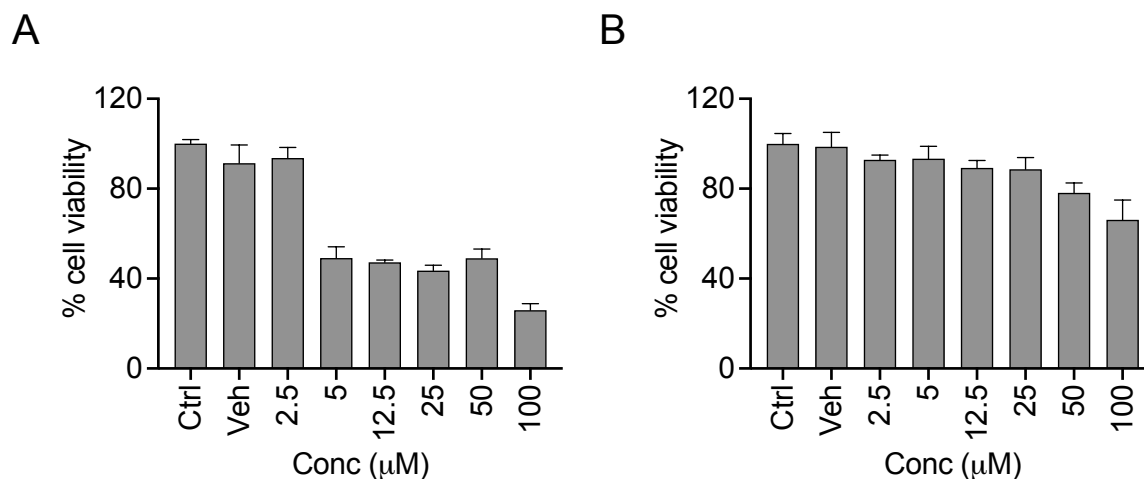


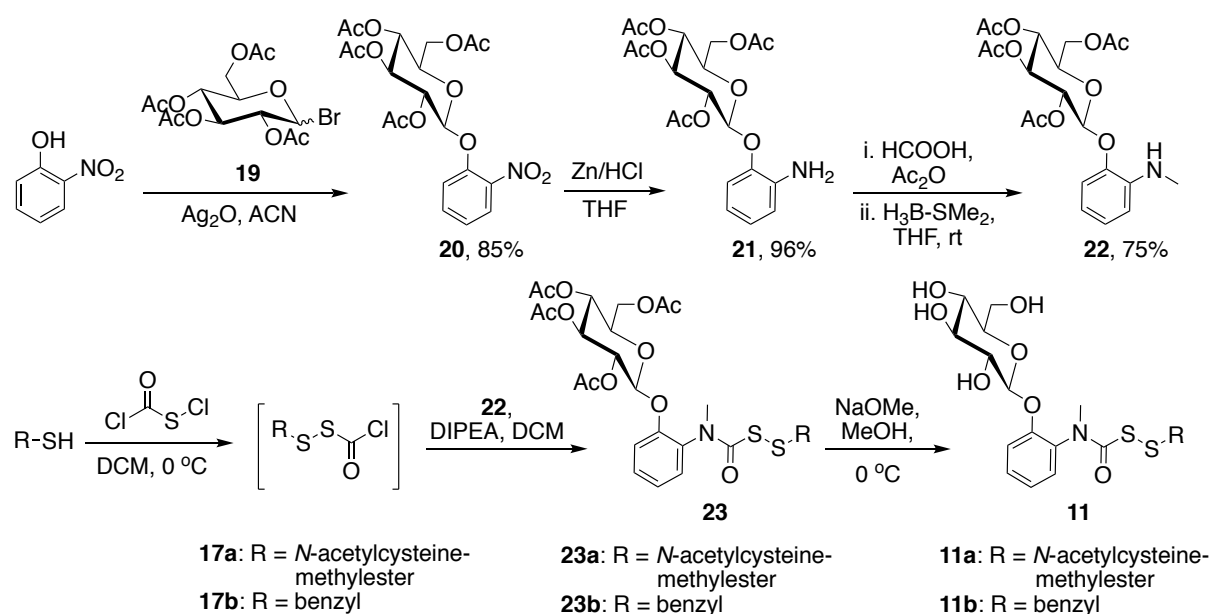
Figure 3.6. Cell viability assay carried out with the compound **10b** for 24 h on a) DLD-1 cells b) HepG2 cells. All data are presented as mean \pm SD ($n = 3$ /group).

The cytotoxicity of compound **10b** was evaluated using a standard MTT assay to estimate the cell viability. DLD-1 and HepG2 cells were treated with varying concentrations of **10b** and incubated for 24 h following which cell viability was measured. The compound was found to

be cytotoxic in DLD-1 cell line (Figure 3.6.a) and exhibit moderate toxicity in HepG2 cell line (Figure 3.6.b).

3.2.5. Synthesis of β -glucosidase responsive persulfide donors

The next series of compounds, **11a** and **11b** were designed to be responsive to β -glucosidase. Using a similar protocol as outlined above, the glucopyranosyl derivative of *N*-methylaniline, **22** was prepared (Scheme 3.3). It was reacted with the *S*-perthiocarbonyl chloride **17a**, derived from NACMe to obtain compound **23a** and final deacetylation was carried out to obtain compound **11a**. **11b** was similarly synthesized by reacting compound **22** with the *S*-perthiocarbonyl chloride **17b**, derived from benzylmercaptan followed by final deacetylation. Compounds **11a** and **11b** were prepared by MS student Ms. Manjima B. Sathian.



Scheme 3.3. Synthesis of β -glucopyranosyl derivatives (**11**).

3.2.6. LC/MS analysis for the decomposition of **11**

3.2.6.1. Decomposition of **11a** by β -glucosidase

The reactivity of the prodrugs towards β -glucosidase was next analyzed. **11a** was incubated with β -glucosidase (10 U/mL) at 37°C in pH 7.4 phosphate buffer. Aliquots from the reaction mixture were injected into the LC/MS at pre-determined time points. A peak with $m/z = 521.1250$ ($[\text{M} + \text{H}]^+$ expected $m/z = 521.1264$) corresponding to **11a** was observed, which was gradually consumed over a period of 10 h (Figure 3.7.a). Curve fitting to first order gave a pseudo first order rate constant k_1 $5.4 \times 10^{-3} \text{ min}^{-1}$ (Figure 3.7.b).

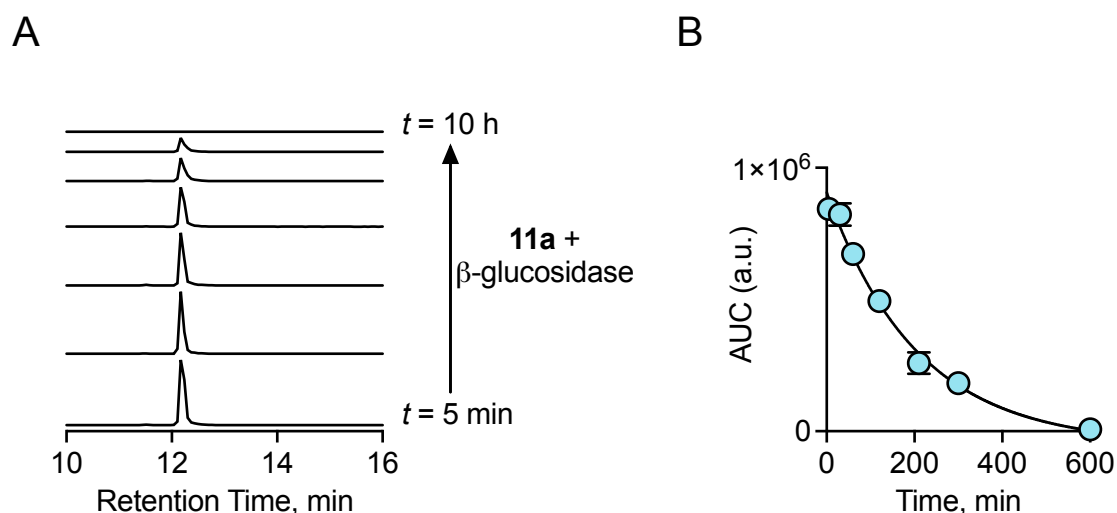


Figure 3.7. a) Extracted ion chromatograms for **11a** ($m/z = 521.1250$; expected $m/z = 521.1264$) at different time points (5, 30, 60, 120, 210, 300, 600 min). Decomposition of **11a** over 10 h in the presence of β -glucosidase was observed, as monitored by LC/MS. b) Curve fitting to first order gave a rate constant of $5.4 \times 10^{-3} \text{ min}^{-1}$.

Concomitant formation of the byproduct **12** at RT 13.3. min was observed with $m/z = 150.0551$ [$M + H$] $^+$ (expected $m/z = 150.0555$) under the given conditions (Figure 3.8.a). A time course for the rate of formation of **12** was obtained and curve fitting to first order gave a rate constant of $7.1 \times 10^{-3} \text{ min}^{-1}$, which is similar to the rate of decomposition of **11a** (Figure 3.8.b).

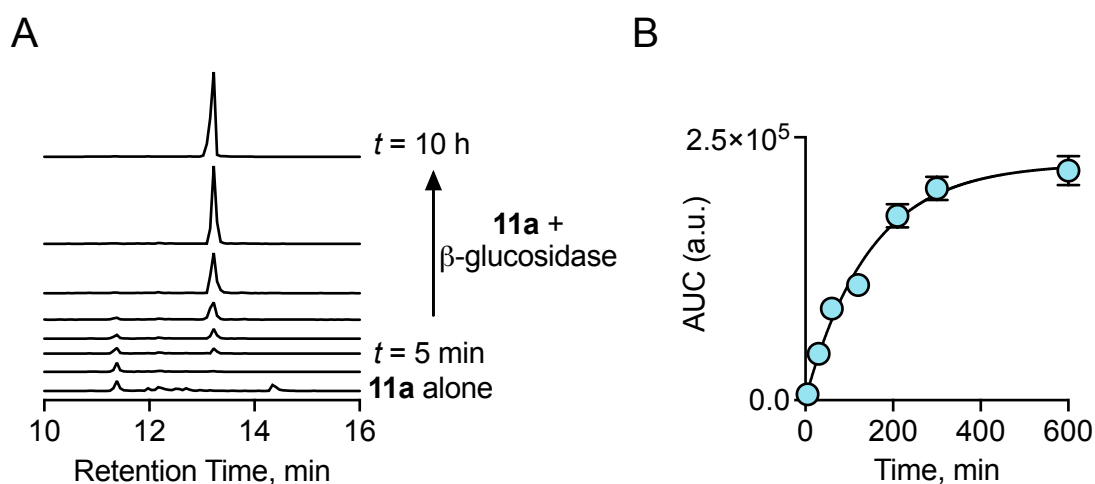


Figure 3.8. a) Extracted ion chromatograms for the formation of byproduct (**12**) ($m/z = 150.0551$; expected $m/z = 150.0555$) at given time points (5, 30, 60, 120, 210, 300, 600 min). Formation of **12** over 10 h in the presence of β -glucosidase was observed. b) Curve fitting to first order gave a rate constant of $7.1 \times 10^{-3} \text{ min}^{-1}$.

3.2.6.2. Decomposition of **11b** by β -glucosidase

A similar experiment was carried out with the benzyl persulfide derivative **11b**. **11b** was incubated with β -glucosidase (10 U/mL) at 37 °C in pH 7.4 phosphate buffer. LC/MS analysis revealed a complete decomposition of **11b** with $m/z = 468.1153$ $[M + H]^+$ (expected $m/z = 468.1151$) over a period of 10 h (Figure 3.9.a). A first order rate constant for the decomposition of **11b** was calculated to be $4.4 \times 10^{-3} \text{ min}^{-1}$ (Figure 3.9.b).

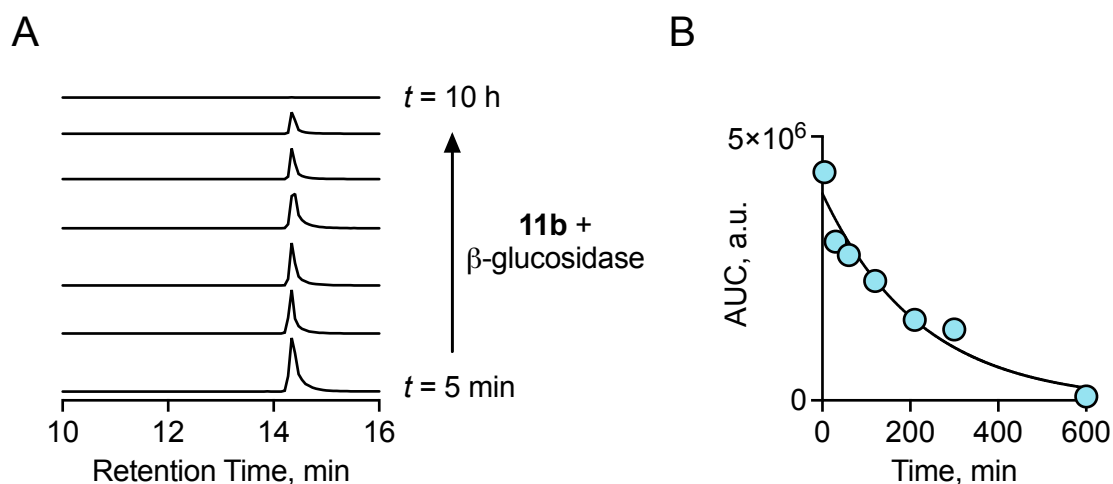


Figure 3.9. a) Extracted ion chromatograms for **11b** ($m/z = 468.1153$; expected $m/z = 468.1151$) at different time points (5, 30, 60, 120, 210, 300, 600 min). Decomposition of **11b** over 10 h in the presence of β -glucosidase was observed. b) Curve fitting to first order gave a rate constant of $4.4 \times 10^{-3} \text{ min}^{-1}$, ($R^2 = 0.958$).

A concomitant formation of the byproduct **12** at RT 13.3 min was observed under the above conditions, over a period of 10 h. The rate constant for the formation of **12** was calculated to be $7.4 \times 10^{-3} \text{ min}^{-1}$ (Figure 3.10.).

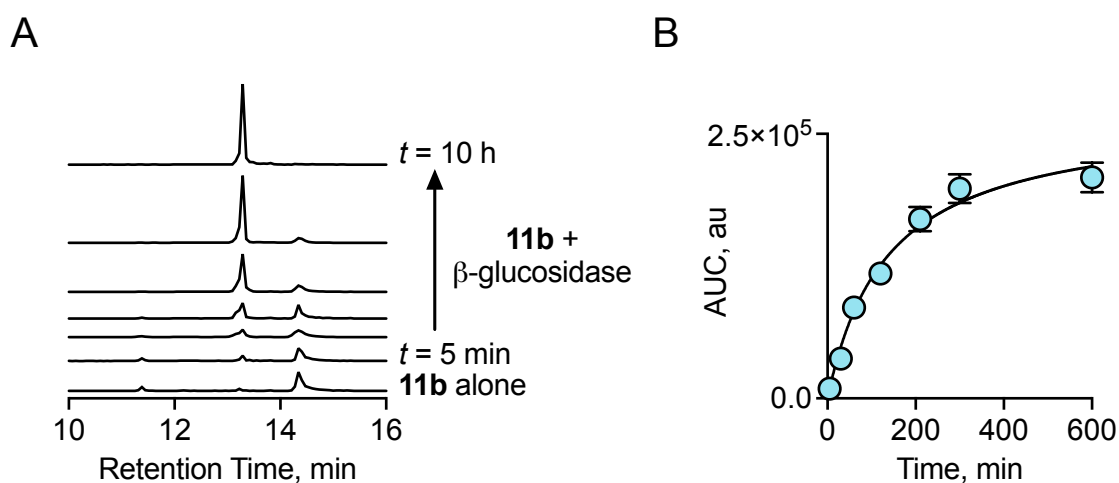


Figure 3.10. a) Extracted ion chromatograms for the formation of byproduct (**12**) ($m/z = 150.0545$; expected $m/z = 150.0555$) at given time points (5, 30, 60, 120, 210, 300, 600 min). Formation of **12**

from **11b** over 10 h in the presence of β -glucosidase was observed. b) Curve fitting to first order gave a rate constant of $7.4 \times 10^{-3} \text{ min}^{-1}$ ($R^2 = 0.9936$).

3.2.7. Detection of persulfide/polysulfide from **11**

3.2.7.1. Persulfide/polysulfide generation from **11a**

Next, persulfide/polysulfide generation from the NACMe derivative **11a** was assessed. **11a** was incubated with 10 U/mL of β -glucosidase and HPE-IAM (20 eq) in pH 7.4 phosphate buffer and incubated at 37 °C. Aliquots from this reaction mixture was injected in to the LC/MS at pre-determined intervals. A peak RT 12.4 min was observed which can be attributable to the HPE-AM persulfide adduct of NACMe with $m/z = 387.1042$ ($[M+H]^+$ expected $m/z = 387.1048$). The peak for HPE-IAM adduct of NACMe persulfide (NACMeS-SH) appeared within 5 min of incubation and gradually increased in intensity over a period of 10 h (Figure 3.11.).

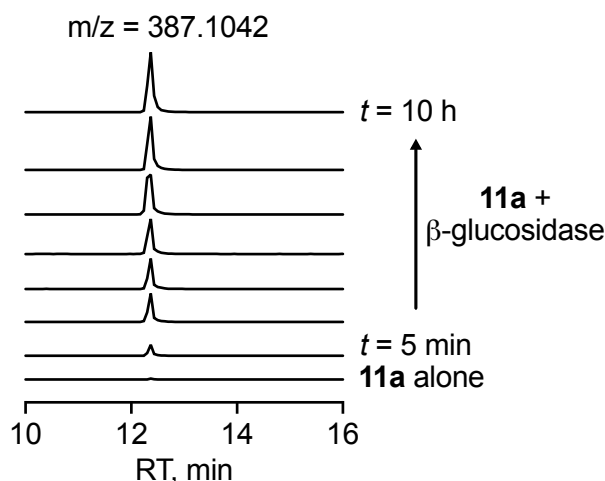


Figure 3.11. Extracted ion chromatograms for the formation of the persulfide adduct of HPE-IAM (NACMeS-SH) ($m/z = 387.1042$; expected $m/z = 387.1048$) at the given time points (5, 30, 60, 120, 210, 300, 600 min). Formation of NACMeS-SH over 10 h in the presence of β -glucosidase was observed.

In addition, peaks for HPE-AM polysulfide adducts NACMeS-SSH and NACMeS-SSSH were detected as well (Figure 3.12.a). Appreciable amounts of H_2S , H_2S_2 and H_2S_3 were also detected along with the persulfide/polysulfide adducts of NACMe (Figure 3.12.b). Generation of disulfides and trisulfides of NACMe were observed as well under the aforementioned condition (Figure 3.13.). A peak for disulfide was obtained at RT 11.4 min with $m/z = 353.0849$ $[M + H]^+$ (expected $m/z = 353.0841$) whereas a peak for the trisulfide was obtained at RT 12.3 min with $m/z = 385.0560$ $[M + H]^+$ (expected $m/z = 385.0562$).

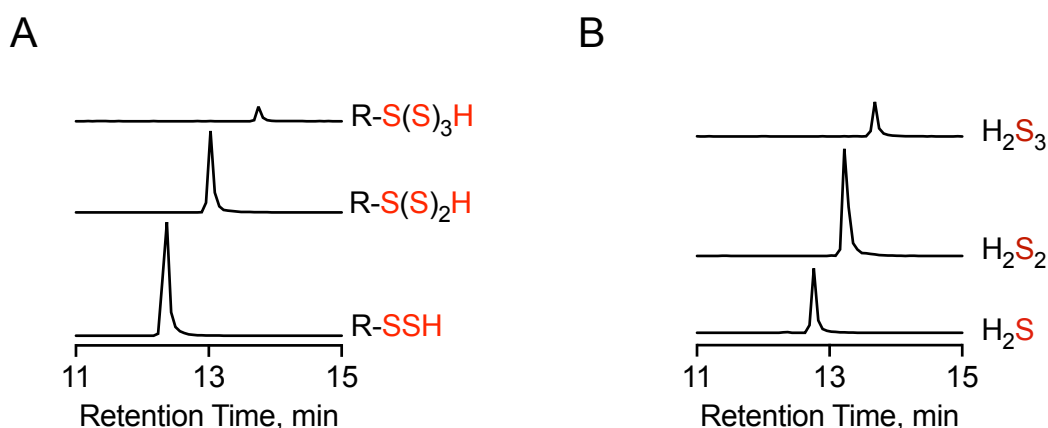


Figure 3.12. a) Extracted ion chromatogram of persulfides and polysulfides of *N*-acetylcysteine methyl ester (NACMe-S(S)_nH) generated from compound **11a**, detected as their HPE-AM adducts using LC/MS (R = *N*-acetylcysteine methyl ester, NACMe). NACMe-SS-HPE-AM ($m/z = 387.1042$ [M+H]⁺; expected, 387.1048); NACMe-S(S)₂-HPE-AM ($m/z = 419.0781$ [M+H]⁺; expected, 419.0769); NACMe-S(S)₃-HPE-AM ($m/z = 451.0500$ [M+H]⁺; expected, 451.0490). b) Extracted ion chromatogram of hydrogen sulfide and hydrogen polysulfides detected as their bis-HPE-AM adducts. Bis-S-HPE-AM ($m/z = 389.1545$ [M+H]⁺; expected, 389.1535); bis-S₂-HPE-AM ($m/z = 421.1272$ [M+H]⁺; expected, 421.1256); bis-S₃-HPE-AM ($m/z = 453.0991$ [M+H]⁺; expected, 453.0976)

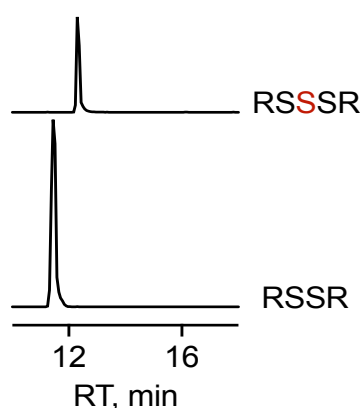


Figure 3.13. Disulfide and trisulfide (R = *N*-acetylcysteine methylester, NACMe) formed upon incubation of **11a** in the presence of β -glucosidase. A peak for disulfide was obtained at RT 11.4 min with an observed $m/z = 353.0849$ [M + H]⁺ (expected $m/z = 353.0841$). A peak for the trisulfide was obtained at RT 12.3 min with an observed $m/z = 385.0560$ [M + H]⁺ (expected $m/z = 385.0562$).

3.2.7.2. Persulfide/polysulfide generation from **11b**

A similar experiment was carried out for the benzyl derivative **11b**. **11b** was incubated with 10 U/mL of β -glucosidase and HPE-IAM (20 eq) in pH 7.4 phosphate buffer at 37 °C. LC/MS analysis revealed the generation of benzyl persulfide (BnS-SH) as the HPE-AM adduct with $m/z = 334.0922$ ([M + H]⁺ expected $m/z = 334.0935$), over a time period of 10 h (Figure 3.14.). Additionally, as expected polysulfides adducts of benzyl (BnS-SSH) and hydrogen polysulfides (H₂S_n, n = 1, 2, 3) were detected along with the persulfide (Figure 3.15.).

These experiments collectively suggest that the prodrugs can be cleaved by β -glucosidase to generate persulfides and polysulfides which were detected as adducts of HPE-IAM.

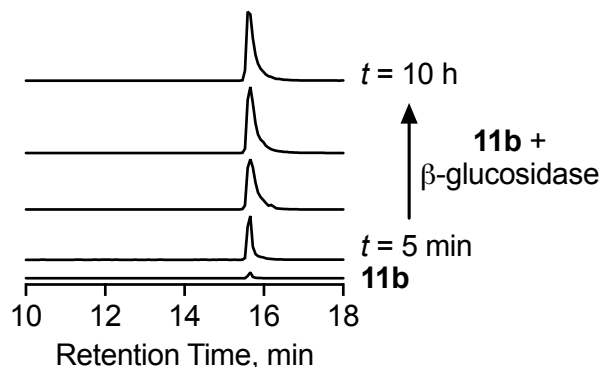


Figure 3.14. Extracted ion chromatograms for the formation of the benzyl persulfide adduct of HPE-IAM (BnSS-HPE-AM) ($m/z = 334.0922$; expected $m/z = 334.0935$) from **11b** upon incubation with β -glucosidase at the given time points (5, 30, 60, 120, 210, 300, 600 min). Formation of BnS-SH over 10 h in the presence of β -glucosidase was observed.

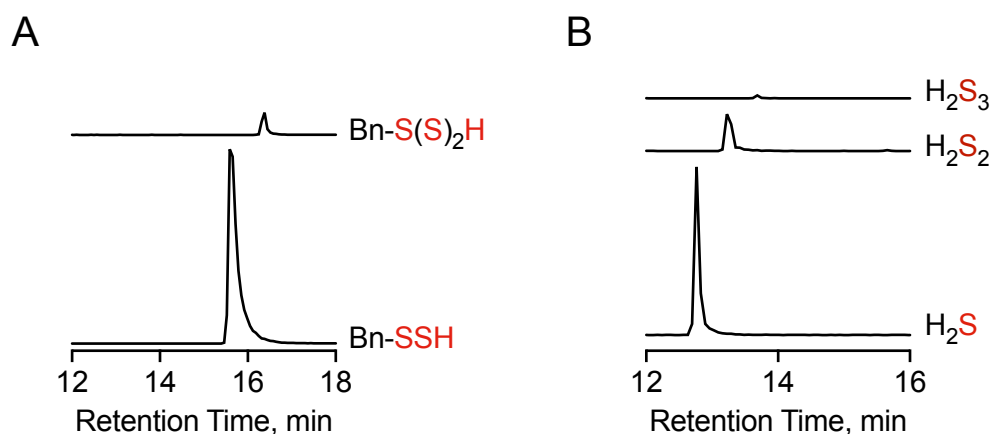


Figure 3.15. a) Extracted ion chromatogram of benzyl persulfides and polysulfides generated from compound **11b**, detected as their HPE-AM adducts using LC-MS. Bn-SS-HPE-AM ($m/z = 334.0922$ $[M+H]^+$; expected, 334.0935); Bn-S(S)₂-HPE-AM ($m/z = 366.0654$ $[M+H]^+$; expected, 366.0656). b) Extracted ion chromatogram of hydrogen sulfide and hydrogen polysulfides detected as their bis-HPE-AM adducts. Bis-S-HPE-AM ($m/z = 389.1539$ $[M+H]^+$; expected, 389.1535); bis-S₂-HPE-AM ($m/z = 421.1264$ $[M+H]^+$; expected, 421.1256); bis-S₃-HPE-AM ($m/z = 453.0988$ $[M+H]^+$; expected, 453.0976).

3.2.8. MTT assay for cell viability to determine cytotoxicity of **11**

The cytotoxicity of compounds **11a** and **11b** were evaluated using a standard MTT assay to estimate the cell viability. DLD-1 and HepG2 were treated with varying concentrations of **11a** and **11b** and incubated for 24 h following which cell viability was measured. **11a** was found to be well tolerated by both the cell lines and no significant cytotoxicity was observed

up to 100 μM (Figure 3.16.). However, **11b** was found to be significantly cytotoxic in DLD-1 cell line and exhibit moderate toxicity in HepG2 cell line. (Figure 3.17.).

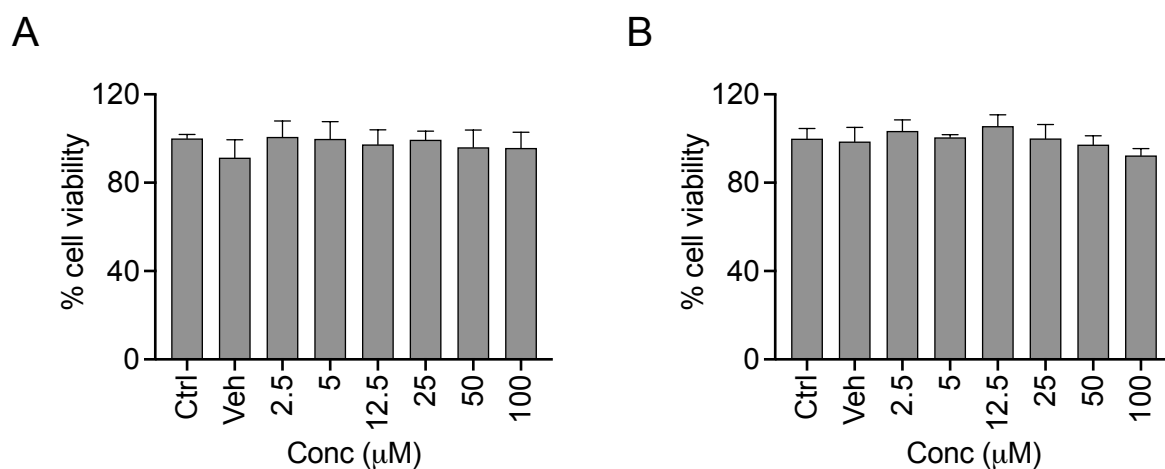


Figure 3.16. a) Cell viability assay carried out with the compound **11a** for 24 h on a) DLD-1 cells b) HepG2 cells. No significant change in viable cells upon treatment with the compound compared with the control was observed. All data are presented as mean \pm SD ($n=3/\text{group}$).

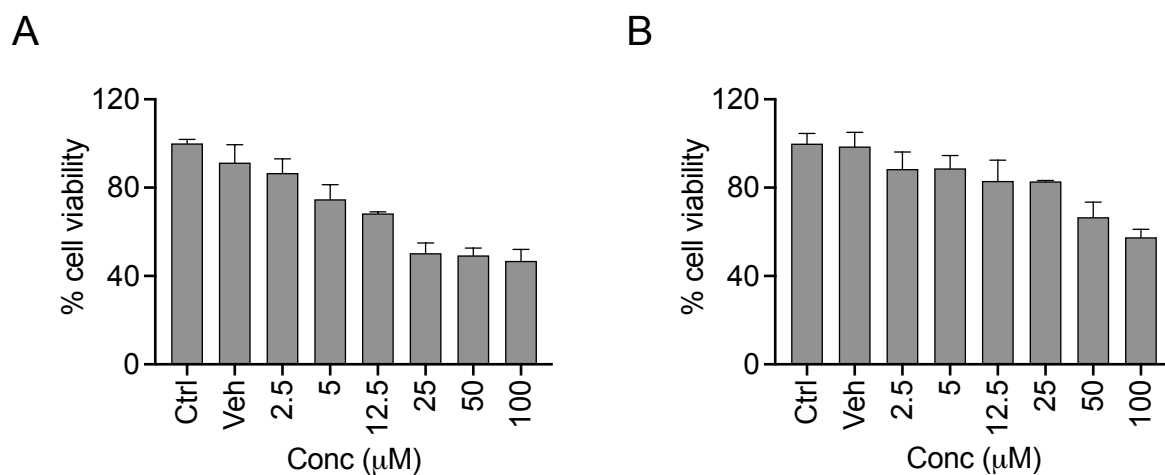
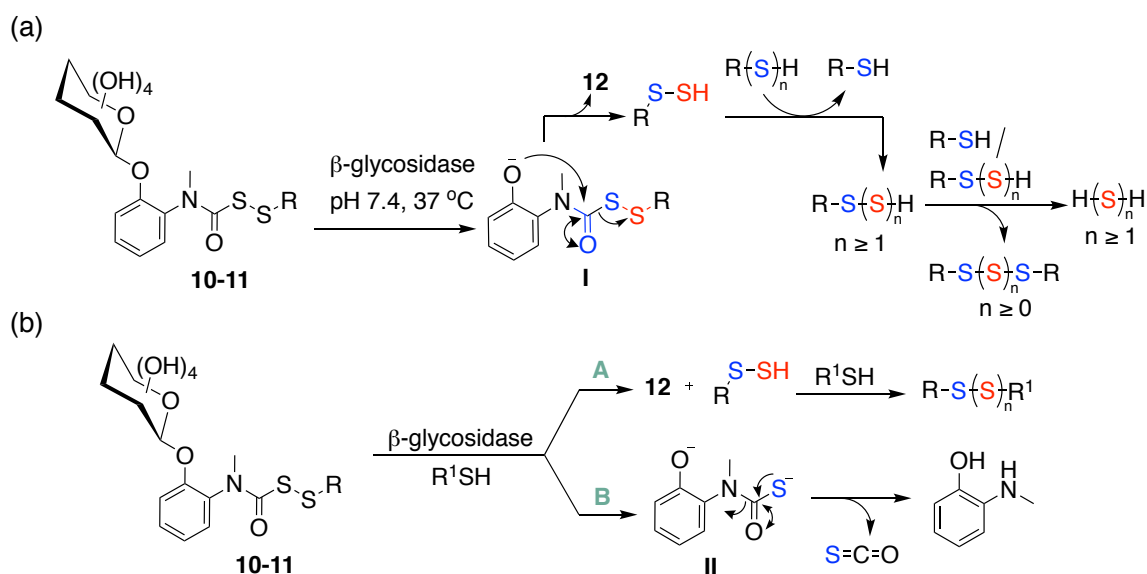


Figure 3.17. Cell viability assay carried out with the compound **11b** for 24 h on a) DLD-1 cells b) HepG2 cells. All data are presented as mean \pm SD ($n=3/\text{group}$).

3.2.9. Mechanism

Based on the above observations, a mechanism for the generation of persulfides/polysulfides from the glycopersulfide prodrugs were formulated (Scheme 3.4). The glycoside in prodrugs **10-11** is cleaved by the enzyme β -glycosidase to form the intermediate I. The phenolate in I undergoes an intramolecular cyclization to release the persulfide and form the heterocyclic byproduct **12**. The persulfide once released can further react with itself to form

the hydropolysulfide ($\text{RS-S}_n\text{H}$) species. These species being unstable in nature can ultimately be reduced by thiols or persulfides to generate hydrogen sulfide (H_2S) or polysulfide (H_2S_n).



Scheme 3.4. a) Proposed mechanism for the generation of persulfides and polysulfides from compounds **10-11**. b) Probable pathways for decomposition in the presence of a thiol.

The persulfide scaffold has been previously reported to be susceptible to thiols, generating COS as a by-product.²⁰ COS is known to hydrolyze into H_2S catalyzed by the widely prevalent enzyme carbonic anhydrase.²⁶ Therefore, in the presence of both β -glycosidase and thiols, there are two possible competing pathways, A and B as shown in Scheme 3.4.b. Pathway A is indicative of persulfide generation as a result of β -glycosidase activation while pathway B indicates COS release upon cleavage of the disulfide bond by thiols.

3.2.9.1. Reactivity of **10b** towards *N*-acetyl cysteine (NAC)

To ascertain the reactivity of the prodrugs towards thiols, compound **10b** was reacted with *N*-acetylcysteine (NAC) in the presence of β -galactosidase. **10b** was co-incubated with 2 U/mL of β -galactosidase and 0.5 mM NAC in pH 7.4 phosphate buffer and incubated at 37 °C. The formation of the byproduct **12** was monitored. A 25% reduction in the yield of **12** was observed within 30 min of incubation, suggesting that thiol reactivity is a minor competing pathway (Figure 3.18.). The reaction was carried out in the absence of HPE-IAM due to its propensity to react with NAC, thus making it inaccessible. However, formation of mixed disulfides (NAC-SS-Bn) and trisulfides (NAC-SSS-Bn) of NAC with benzyl were observed, indicative of β -galactosidase cleavage through pathway A (Figure 3.19.).

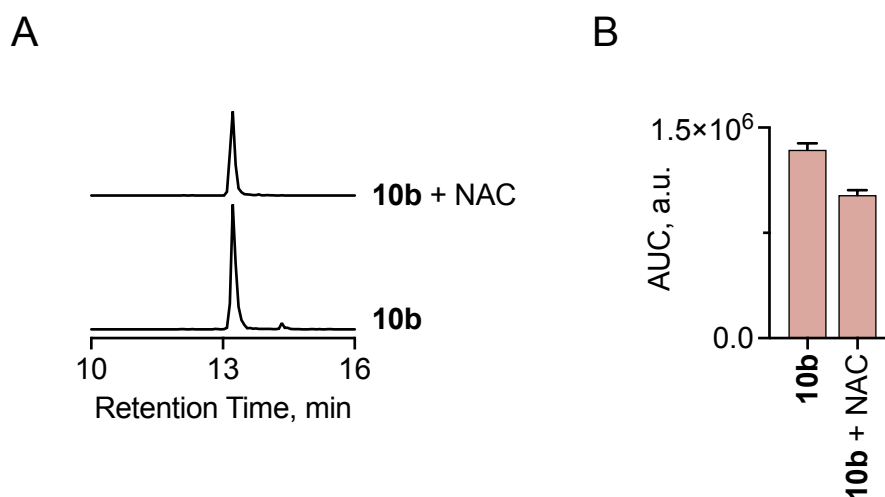


Figure 3.18. a) Extracted ion chromatograms for the formation of byproduct (**12**) ($m/z = 150.0545$; expected $m/z = 150.0555$) upon incubation of **10b** with β -galactosidase in the presence or absence of NAC. b) Quantification of the area under the curve (AUC) for the peak corresponding to **12**. 25% reduction in the yield of **12** was observed upon incubation with NAC.

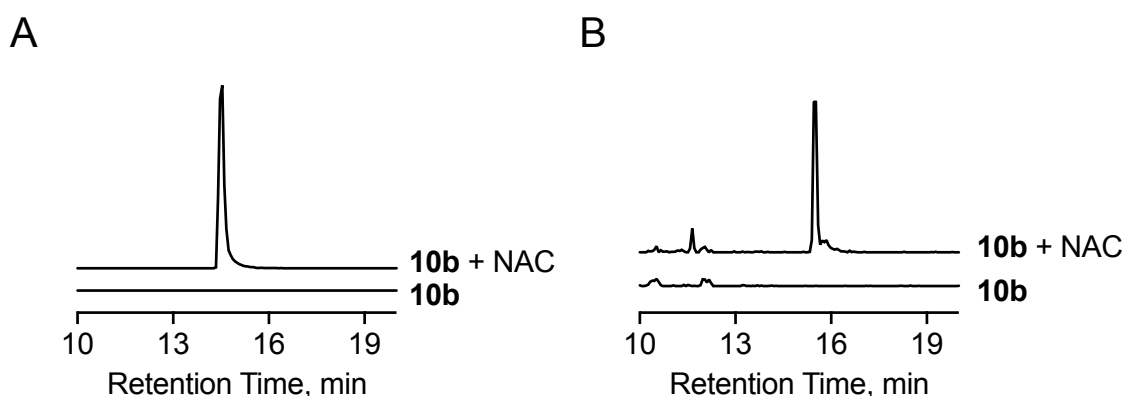


Figure 3.19. a) Extracted ion chromatograms for the formation of mixed disulfide NAC-SS-Bn ($m/z = 150.0545$; expected $m/z = 286.0572$) upon incubation of **10b** with β -galactosidase in the presence of NAC. b) Extracted ion chromatograms for the formation of mixed trisulfide NAC-SSS-Bn ($m/z = 318.0309$; expected $m/z = 318.0292$) upon incubation of **10b** with β -galactosidase in the presence of NAC.

3.2.9.2. Reactivity of **10b** towards Glutathione (GSH)

A similar experiment was carried out using glutathione (GSH) as the thiol. **10b** was co-incubated with 2 U/mL of β -galactosidase and 1 mM GSH in pH 7.4 phosphate buffer and incubated at 37 °C. In contrast to NAC, a 65% reduction in the formation of the byproduct **12** was observed within 30 min of incubation, suggesting that pathway B is predominant in case of GSH (Figure 3.20.). This might be an outcome of the elevated concentration of GSH used, as a close mimic of the physiological system.

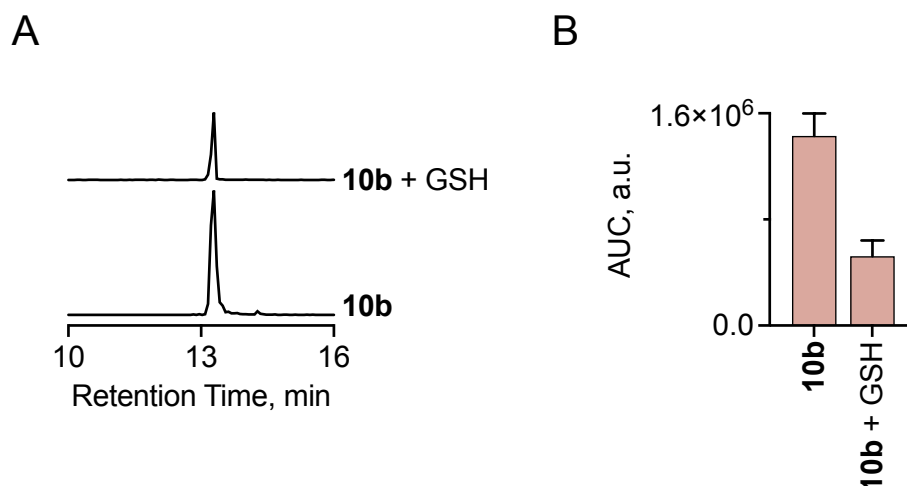
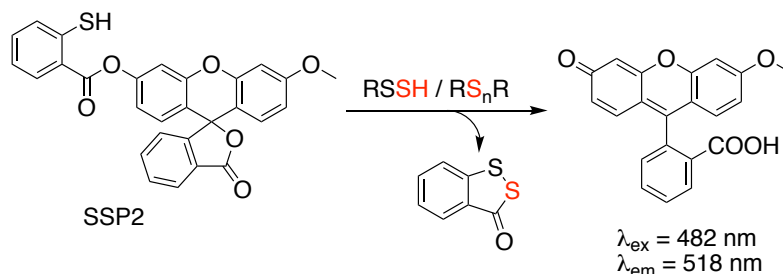


Figure 3.20. a) Extracted ion chromatograms for the formation of byproduct (**12**) ($m/z = 150.0558$; expected $m/z = 150.0555$) upon incubation of **10b** with β -galactosidase in the presence or absence of GSH. b) Quantification of the area under the curve (AUC) for the peak corresponding to **12**. 65% reduction in the yield of **12** was observed upon incubation with GSH.

3.2.10. Intracellular generation of persulfide/polysulfide

The glucoside derivatives **11** have a slower rate of decomposition by β -glucosidase derived from almonds, with half-lives greater than 120 min. Given the potential reactivity of the prodrugs towards thiols, it was envisaged that the major pathway for intracellular decomposition would be pathway B (Scheme 3.4.b). However, previous reports suggest structural variations between human and other eukaryotic β -glucosidases.²⁷ Human cytosolic β -glucosidase (hCBG) is reportedly more efficient at hydrolysis of β -glucosidic bonds than the ones derived from plants. This suggests that intracellular β -glucosidase present in mammalian cells might accelerate the cleavage of **11** to generate persulfide/polysulfide via pathway A (Scheme 3.4.).



Scheme 3.5. Release of fluorescein from SSP2 upon reaction with persulfides/polysulfides.

To assess the intracellular generation of persulfide/polysulfide from these prodrugs, **11a** was chosen due to its low toxicity profile compared to the benzyl derivatives. To detect intracellular persulfide/polysulfide, the previously reported probe SSP2 was used.²⁸ The probe

reacts with sulfane sulfur to release fluorescein that produces a distinct fluorescent signal at 518 nm with excitation at 482 nm (Scheme 3.5.).

DLD-1 cells were pre-treated with 50 μM SSP2 in the presence of cetyltrimethylammonium bromide (CTAB) followed by incubation with varying doses of **11a** for 1 h. Fluorescence was measured in the GFP channel of a fluorescence microscope. A significant increment in fluorescence, corresponding to the generation of persulfide/polysulfide was observed at a concentration of 0.5 mM of **11a** (Figure 3.21). An elevated dose of the compound is required to observe an enhanced signal perhaps due to the relatively lower stability of persulfide/polysulfides in the reducing environment of the cell. Nevertheless, this data indicates that **11a** is cell permeable and is able to enhance the levels persulfide/polysulfides in cells.

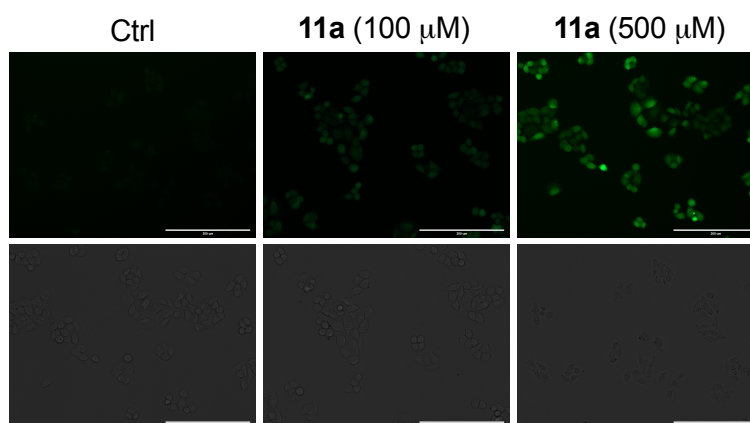
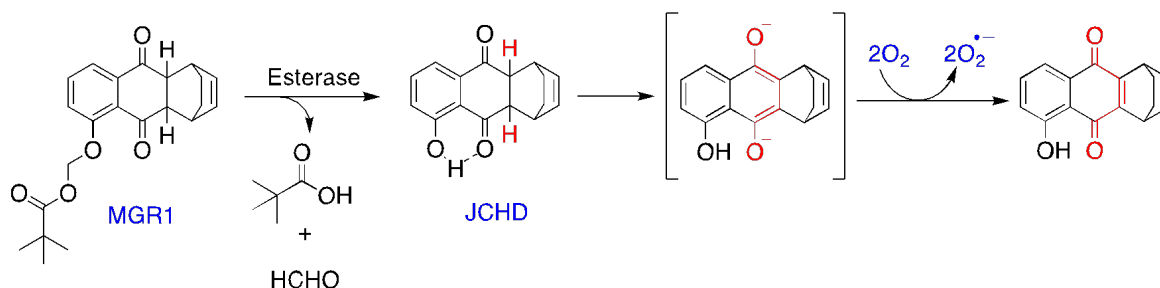


Figure 3.21. Detection of persulfide/polysulfide generated by compound **11a** in DLD-1 cells, using the dye SSP2. The cells were imaged in the 20x GFP filter. Scale bar is 200 μm .

3.2.11. Cytoprotective effect of compound **11a**

MGR-1 is a prodrug of the ROS generator JCHD, which upon cleavage by the widely prevalent enzyme esterase would generate JCHD in cells (Scheme 3.6.).²⁹ JCHD is a juglone derivative that produces superoxide which spontaneously dismutates to generate hydrogen peroxide (H_2O_2) in cells, thus inducing oxidative stress mediated cell death.³⁰ DLD-1 and HepG2 cells were treated with varying concentrations of MGR-1 for 4 h to evaluate their toxicity profile. The IC_{50} of MGR-1 on both these cell lines were determined. The IC_{50} of MGR-1 in DLD-1 was found to be 27 μM whereas in HepG2 it was found to be 12 μM (Figure 3.22). Therefore, a concentration of 35 μM was used on DLD-1 cell line and 20 μM on HepG2 cell line to induce greater than 50% cell death.



Scheme 3.6. ROS generation from MGR-1

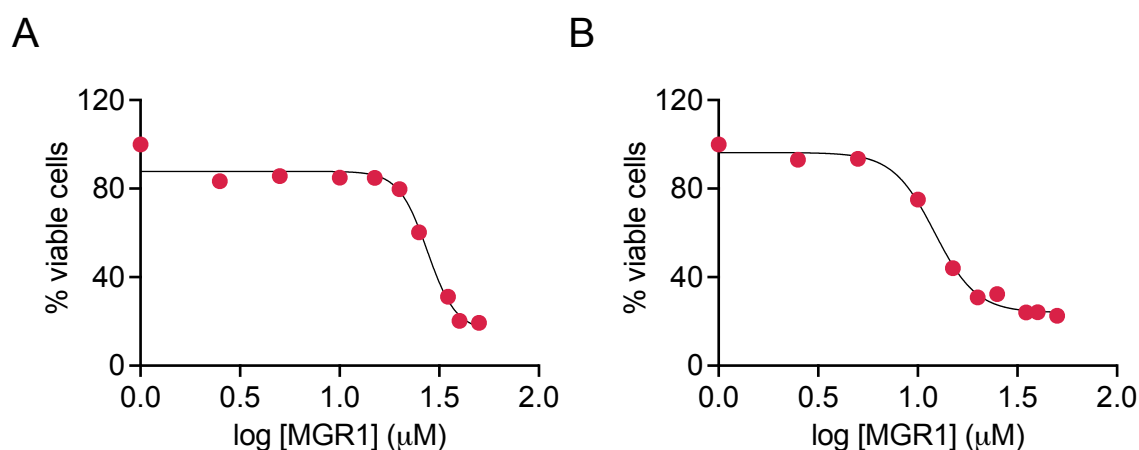


Figure 3.22. a) Cell viability assay carried out with the MGR-1 for 4 h on DLD-1 cells to determine its IC_{50} . IC_{50} was calculated to be $27 \mu\text{M}$. All data are presented as mean \pm SD ($n = 3/\text{group}$). b) Cell viability assay carried out with the MGR-1 for 4 h on HepG2 cells. IC_{50} was calculated to be $12 \mu\text{M}$.

Next, the ability of the persulfide prodrug **11a** to protect cells from the oxidative stress induced cell death was evaluated. DLD-1 cells were pre-incubated with varying concentrations of **11a** for 12 h followed by treatment with MGR-1 ($35 \mu\text{M}$) for 4 h. Cell viability was then measured using a standard MTT assay. A dose dependent increase in cell viability was observed (Figure 3.23.a). To further corroborate our results, a similar experiment was conducted on another cell line HepG2 and a similar result was obtained (Figure 3.23.b). Under the above conditions, NAC failed to exhibit protective effects, suggesting that the cytoprotective effects were mediated by persulfides and not the NAC scaffold.

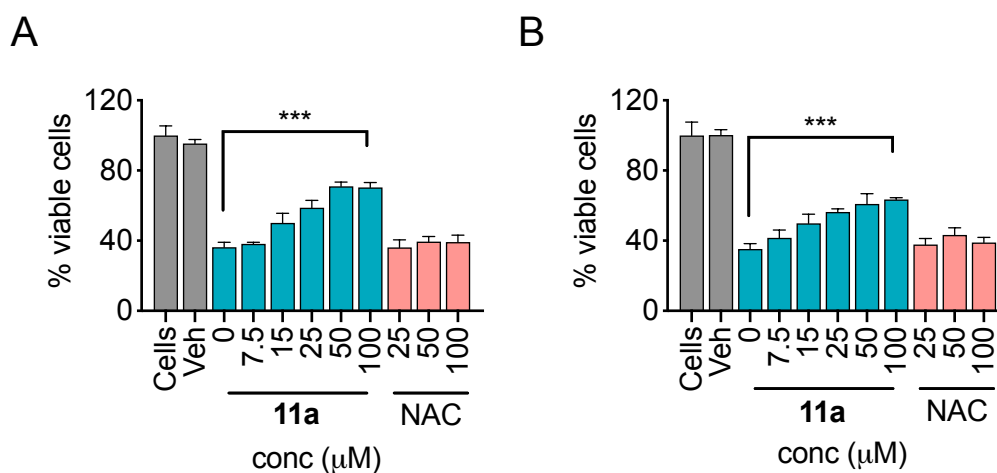


Figure 3.23. a) Cytoprotective effects of **11a** against ROS induced cell death. DLD-1 cells were pre-treated with varying doses of **11a** for 12 h followed by treatment with the cell permeable ROS generator MGR-1 (20 mM) for 4h. A similar experiment was carried out with *N*-acetylcysteine (NAC). No significant effects on cell viability was observed with NAC. Results are presented as mean \pm SD (n = 3). (***) p < 0.001 vs MGR-1. b) A similar experiment carried out on the liver cell line (HepG2). A dose dependant increment in cell viability was observed upon pre-treatment with **11a**, against cell death induced by MGR-1. No significant effects on cell viability was obtained with NAC. Results are presented as mean \pm SD (n = 3). (***) p < 0.001 vs MGR-1.

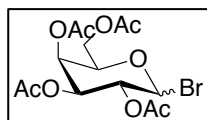
3.3. Summary

In conclusion, a new class of enzyme activated persulfide donors with relatively benign byproducts have been reported. Two series of prodrugs were developed, one responsive to β -galactosidase (**10**) and the other series were responsive to β -glucosidase (**11**). The generation of persulfides from these prodrugs were demonstrated by an LC/MS based technique after trapping it with the electrophile HPE-IAM. The β -glucosidase prodrug **11a** with NACMe persulfide as the leaving group was found to be well tolerated by cells. **11a** was found to be cell permeable and enhance intracellular persulfide/polysulfides, detected using the probe SSP2. Finally, as a testament to its therapeutic potential, **11a** was demonstrated to be protective in cells against oxidative stress induced cell death in two different cells lines.

3.4. Experimental Section

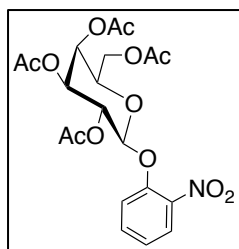
3.4.1. Synthesis and characterization of compounds

(2*R*,3*S*,4*S*,5*R*,6*S*)-2-(acetoxymethyl)-6-bromotetrahydro-2*H*-pyran-3,4,5-triyl triacetate (13):



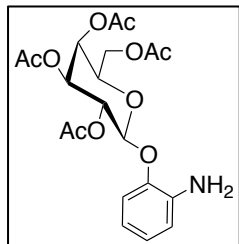
To a solution of β -D-galactose pentaacetate (1.4 g, 3.6 mmol) in anhydrous DCM (10 mL), HBr in acetic acid (5.8 mL, 71.7 mmol) was added dropwise at 0 °C under N₂ atmosphere and stirred at room temperature for 2 h. After completion of the reaction (TLC analysis), the reaction mixture was quenched with NaHCO₃ followed by extraction with DCM (3 × 20 mL). The combined organic layers were washed with brine, dried over anhydrous Na₂SO₄, filtered and the filtrate was concentrated under reduced pressure to afford the crude product. The product was immediately used in the next step without further purification.

(2*R*,3*S*,4*S*,5*R*,6*S*)-2-(acetoxymethyl)-6-(2-nitrophenoxy)tetrahydro-2*H*-pyran-3,4,5-triyl triacetate (14)¹⁸:



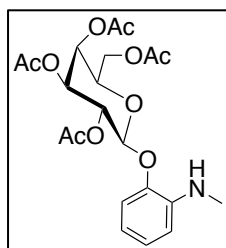
To a solution of 2-nitrophenol (500 mg, 3.65 mmol) in anhydrous ACN (8 mL), Ag₂O (845 mg, 3.65 mmol) was added. To this heterogenous reaction mixture, a solution of compound **13** (1.5 g, 3.65 mmol) in ACN was added dropwise under N₂ atmosphere at 0 °C. The reaction mixture was gradually warmed up to room temperature and left to stir for 12 h. After completion of the reaction as determined by TLC, the reaction mixture was filtered through celite and washed with CHCl₃. The filtrate was evaporated, the crude product obtained was diluted with H₂O and extracted with CHCl₃ (3 × 50 mL). The crude product obtained after evaporation of the filtrate was purified by column chromatography using 60-120 silica gel as the stationary phase. A gradient starting from 2% ethylacetate in hexane was used as the mobile phase and the compound was eluted at 50%. The product was obtained as an off-white solid (1.05 g, 62 %). FT-IR (ν_{max} ; cm⁻¹): 1535, 1219; ¹H NMR (400 MHz, CDCl₃): δ 7.8 (dd, J = 8.0, 1.6 Hz, 1H), 7.55 – 7.51 (m, 1H), 7.38 (dd, J = 8.0, 1.2 Hz, 1H), 7.23 – 7.19 (m, 1H), 5.58 (dd, J = 12.0, 8.0 Hz, 1H), 5.48 (d, J = 4.0 Hz, 1H), 5.13 – 5.08 (m, 2H), 4.29 (dd, J = 12.0, 7.0 Hz, 1H), 4.19 (dd, J = 12.0, 7.0 Hz, 1H), 4.10 – 4.06 (m, 1H), 2.19 (s, 3H), 2.14 (s, 3H), 2.07 (s, 3H), 2.02 (s, 3H). ¹³C NMR (100 MHz, CDCl₃): δ 170.6, 170.4, 169.5, 149.4, 141.7, 133.8, 125.3, 124.0, 120.1, 100.3, 72.4, 70.6, 68.3, 61.9, 20.8, 20.7, 20.6; HRMS (ESI) for C₂₀H₂₃NO₁₂ [M+Na]⁺ Calculated: 492.1117, Found: 492.1112.

(2*R*,3*S*,4*S*,5*R*,6*S*)-2-(acetoxymethyl)-6-(2-aminophenoxy)tetrahydro-2*H*-pyran-3,4,5-triyl triacetate (15):



Compound **14** (300 mg, 0.64 mmol) was dissolved in dry THF (5 mL) and degassed for 10 min. To this solution was added Zinc dust (418 mg, 6.4 mmol) following which 6*N* HCl (530 μ L, 3.2 mmol) was added dropwise at 0 °C and the reaction was stirred at room temperature for 36 h. Upon completion of the reaction (TLC analysis), the reaction mixture was passed through celite and washed with ethyl acetate. The filtrate was treated with 1*N* NaHCO₃ until the pH of the solution turned neutral. The mixture was then extracted with EtOAc (3 \times 20 mL). The combined organic layers were washed with brine, dried over Na₂SO₄, filtered and the filtrate was concentrated under reduced pressure. The crude product obtained was washed with diethyl ether (3 \times 2 mL) to obtain compound **15** as a light brown solid (260 mg, 92%). FT-IR (ν_{max} , cm⁻¹): 2926, 1618, 1371; ¹H NMR (400 MHz, CDCl₃): δ 6.98-6.88 (m, 2H), 6.72-6.65 (m, 2H), 5.53-5.46 (m, 2H), 5.14 (dd, *J* = 12.0, 4.0 Hz, 1H), 4.98 (d, *J* = 8.0 Hz, 1H), 4.28 (m, 2H), 4.06 (t, *J* = 8.0 Hz, 1H), 3.8 (s, 2H), 2.19 (s, 3H), 2.10 (s, 3H), 2.07 (s, 3H), 2.02 (s, 3H); ¹³C NMR (100 MHz, CDCl₃): δ 170.8, 170.3, 169.9, 169.6, 144.5, 137.7, 124.4, 118.2, 116.2, 115.9, 100.6, 72.6, 72.1, 71.3, 68.5, 62.0, 20.9, 20.8, 20.8, 20.7; HRMS for C₂₀H₂₅NO₁₀ [M+K]⁺ Calculated: 478.1116, Found: 478.1110

(2*R*,3*S*,4*S*,5*R*,6*S*)-2-(acetoxymethyl)-6-(2-(methylamino)phenoxy)tetrahydro-2*H*-pyran-3,4,5-triyl triacetate (16)¹⁹:

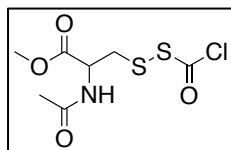


Formic acid (215 μ L, 5.7 mmol) and acetic anhydride (540 μ L, 5.7 mmol) was heated at 70 °C for 2 h. The reaction mixture was cooled to room temperature and to that a solution of compound **15** (250 mg, 0.57 mmol) in THF (5 mL) was added. The reaction was stirred for 3 h at room temperature. Following complete consumption of starting material (TLC analysis), the reaction mixture was poured into hexane (20 mL) and the mixture was stirred for 30 min. The precipitate obtained was filtered, washed with hexane and dried to obtain the formyl product.

To a solution of the above formyl compound in dry THF (5 mL), 2*M* borane dimethylsulfide (850 μ L) was added dropwise at 0 °C under N₂ atmosphere. The reaction was stirred for 4 h at room temperature. Upon completion as monitored by TLC, the reaction was quenched using methanol and the solvent was evaporated to obtain the crude product. The product was then

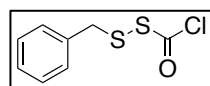
suspended in water and extracted using EtOAc (3 × 20 mL), washed with brine, dried over Na₂SO₄, filtered and the filtrate was concentrated to obtain compound **16**. The product **16** being unstable was immediately used in the next step without further purification. ¹H NMR (400 MHz, CDCl₃) δ 7.02 – 6.98 (td, *J* = 7.6, 1.2 Hz, 1H), 6.90 (dd, *J* = 8.4, 1.6 Hz, 1H), 6.62 – 6.59 (m, 2H), 5.51 – 5.46 (m, 2H), 5.13 (dd, *J* = 10.0, 4.0 Hz, 1H), 4.97 (d, *J* = 8.0 Hz, 1H), 4.26 – 4.14 (m, 3H), 4.07 (m, 1H), 2.83 (s, 3H), 2.19 (s, 3H), 2.08 (s, 3H), 2.06 (s, 3H), 2.02 (s, 3H).

methyl *N*-acetyl-*S*-((chlorocarbonyl)thio)cysteinate (17a):



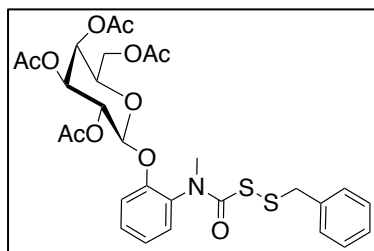
To a solution of *N*-acetylcysteine methylester (65 mg, 0.35 mmol) in anhydrous CHCl₃ (4 mL), chlorocarbonyl sulfenyl chloride (62 μL, 0.7 mmol) was added dropwise at 0 °C. The reaction was complete in 30 min as indicated by TLC. The intermediate was immediately taken forward without further purification.

***SS*-benzyl carbonochlorido(dithioperoxoate) (17b):**



To a solution of benzyl mercaptan (50 mg, 0.4 mmol) in anhydrous CHCl₃ (4 mL), chlorocarbonyl sulfenyl chloride (68 μL, 0.8 mmol) was added dropwise at 0 °C. The reaction was complete within 45 min as indicated by TLC. This intermediate was immediately taken forward without further purification.

(2*R*,3*S*,4*S*,5*R*,6*S*)-2-(acetoxymethyl)-6-(2-((benzyl)disulfannecarbonyl)(methyl) amino) phenoxy tetrahydro-2*H*-pyran-3,4,5-triyl triacetate (18b)²⁰:

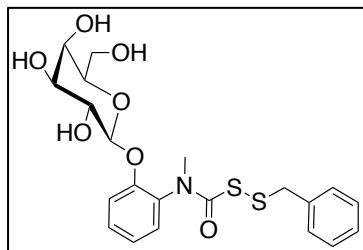


Compound **16** (90 mg, 0.2 mmol) was dissolved in anhydrous CHCl₃ and DIPEA (165 μL, 1 mmol) was added dropwise at 0 °C. This was followed by the addition of compound **17b** to the reaction mixture and the reaction was stirred at room temperature. Upon completion (TLC analysis), the reaction was

quenched by adding water and the product was extracted using CHCl₃ (3 × 20 mL). The combined organic phase was washed with brine, dried over Na₂SO₄, filtered and the filtrate was concentrated. The crude obtained was purified by reverse phase HPLC using ACN-H₂O as the eluent. Compound **18b** was obtained as a white solid after purification (43 mg, 34%). FT-IR (ν_{max}; cm⁻¹): 1680, 1495; ¹H NMR (400 MHz, CDCl₃) δ 7.38 – 7.31 (m, 7H), 7.22 (dd, *J* = 12.0, 1.7 Hz, 1H), 7.14 (td, *J* = 8.0, 1.5 Hz, 1H), 5.54 – 5.45 (m, 2H), 5.09 (dd, *J* = 10.0, 4.0 Hz, 1H), 5.00 (d, *J* = 8.0 Hz, 1H), 4.29 – 4.25 (m, 1H), 4.19 – 4.15 (m, 1H), 4.05 – 3.90 (m, 4H), 3.27 (s, 3H), 2.19 (s, 3H), 2.09 (s, 6H), 2.00 (s, 3H); ¹³C NMR (100 MHz, CDCl₃) δ 170.3, 170.2, 170.0,

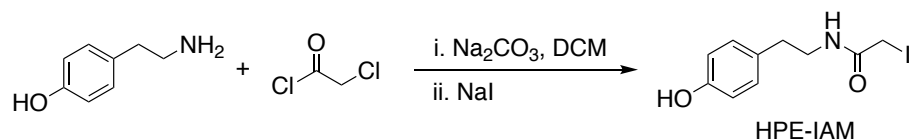
169.7, 165.9, 153.9, 136.3, 131.4, 131.0, 130.5, 129.6, 129.5, 128.5, 127.6, 124.1, 118.0, 100.2, 71.3, 70.6, 67.9, 66.9, 61.5, 43.5, 37.9, 20.8, 20.7, 20.5; HRMS (ESI) for $C_{29}H_{33}NO_{11}S_2$ $[M+Na]^+$ Calculated: 658.1393. Found: 658.1389.

***SS*-benzyl methyl(2-(((2*S*,3*S*,4*S*,5*R*,6*R*)-3,4,5-trihydroxy-6-(hydroxymethyl)tetrahydro-2*H*-pyran-2-yl)oxy)phenyl)carbamo(dithioperoxoate) (10b):**



18b (100 mg, 157 μ mol) was dissolved in anhydrous methanol (3 mL). Sodium methoxide (8.5 mg, 157 μ mol) was added to the solution at 0 °C and stirred at room temperature for 1h. Upon completion (TLC analysis), the reaction was quenched by addition of amberlite resin. The reaction mixture was filtered through a cotton plug and the filtrate was evaporated under reduced pressure. The crude obtained was purified by reverse phase HPLC using ACN- H_2O as the eluent to obtain **10b** (23 mg, 31%). FT-IR (ν_{max} ; cm^{-1}): 3367, 1665; 1H NMR (400 MHz, $CDCl_3$) δ 7.41 – 7.24 (m, 7H), 7.09 – 7.05 (m, 1H), 4.95 (dd, $J = 25.0, 8.0$ Hz, 1H), 3.98 – 3.81 (m, 10H), 3.65 – 3.62 (m, 1H), 3.31 (d, $J = 9.0$ Hz, 3H); ^{13}C NMR (100 MHz, $CDCl_3$) δ 166.2, 156.0, 137.7, 131.8, 130.4, 129.3, 128.2, 123.5, 117.8, 102.7, 78.2, 78.0, 74.5, 71.3, 62.6, 43.9, 38.3; HRMS (ESI) for $C_{21}H_{25}NO_7S_2$ $[M+H]^+$ Calculated: 468.1150, Found: 468.1141.

***N*-(4-hydroxyphenethyl)-2-iodoacetamide (HPE-IAM):**



To a solution of tyramine (500 mg, 3.64 mmol) in a saturated Na_2CO_3 and DCM (1:1) was added 2-chloroacetyl chloride (300 μ L, 3.64 mmol). The reaction mixture was stirred at room temperature for 2 h, Upon completion (TLC analysis), the reaction was quenched by addition of water and the product was extracted using DCM (3 \times 20 mL). The solvent passed through anhydrous Na_2SO_4 , filtered and the filtrate was evaporated under reduced pressure.

The crude obtained was dissolved in anhydrous dimethyl formamide (DMF) and sodium iodide (3.3 g, 22 mmol) was added. The reaction mixture was stirred at room temperature for 24 h. Upon completion (TLC analysis), the reaction was quenched by adding water and the product was extracted using ethyl acetate (3 \times 20 mL). The combined organic phase was washed with brine, dried over Na_2SO_4 , filtered and the filtrate was concentrated. The crude obtained was purified by reverse phase HPLC using ACN- H_2O as the eluent. Compound HPE-IAM was

obtained as a white solid after purification. ^1H NMR (400 MHz, CDCl_3) δ 9.16 (s, 1H), 8.27 (t, $J=4.0$ Hz, 1H), 7.01–6.98 (m, 2H), 6.69–6.65 (m, 2H), 3.61 (s, 1H), 3.19 (q, $J=8.0$ Hz, 2H), 2.57 (t, $J=8.0$ Hz, 2H).

3.4.2. Persulfide/polysulfide measurement from 10b using LC/MS: Stock solutions of **10b** (20 mM) and HPE-IAM (125 mM) were prepared in DMSO. Stock solution of β -galactosidase (100 U/mL) was prepared in DI water. The reaction mixture for **10b** was prepared by adding 100 μM of **10b** (2.5 μL , 20 mM stock), 2 mM HPE-IAM (8 μL , 125 mM), 2 U/mL β -galactosidase (10 μL , 100 U/mL stock) and the volume was adjusted to 500 μL using 20 mM phosphate buffer, pH 7.4. The reaction mixture was incubated at 37 $^\circ\text{C}$. 100 μL aliquots of the reaction mixture was taken at pre-determined time points and the reaction was quenched by adding 100 μL of methanol. The samples were centrifuged at 10000g for 10 min at 4 $^\circ\text{C}$, the supernatant was collected and assessed thereafter by LC/MS. All measurements were done using a previously established LC/MS method³¹ with slight modification. Measurements were carried out in the positive ion mode using high resolution multiple reaction monitoring (MRM-HR) analysis on a Sciex X500R quadrupole time-of flight (QTOF) mass spectrometer fitted with an Exion UHPLC system using a Kinetex 2.6 mm hydrophilic interaction liquid chromatography (HILIC) column with 100 \AA particle size, 150 mm length and 3 mm internal diameter (Phenomenex). Acetonitrile (A) and 0.1% formic acid in water (B) was used as the mobile phase. Nitrogen was the nebulizer gas, with the nebulizer pressure set at 50 psi. The MRM-HR mass spectrometry parameters for measuring polysulfides are: m/z precursor ion mass (Q1, $M + \text{H}^+$)/ product ion mass (Q3, $M + \text{H}^+$) 468.12/105.05 (**10b**), 150.06/76.00 (**12**), 334.10/121.10 (BnSS-HPE-AM), 366.06/121.10 (BnSSS-HPE-AM), 398.04/121.10 (BnSSSS-HPE-AM), 389.16/121.10 (bis-S-HPE-AM), 421.13/121.10 (bis-SS-HPE-AM), 453.09/121.1 (bis-SSS-HPE-AM), declustering potential =80 V, entrance potential = 10 V, collision energy = 20 V, and collision exit potential = 5 V.

3.4.3. Persulfide/polysulfide measurement from 11a and 11b using LC/MS: Stock solutions of **11a** (20 mM), **11b** (20 mM) and HPE-IAM (125 mM) were prepared in DMSO. Stock solution of β -glucosidase (90 U/mL) was prepared in DI water. The reaction mixture for **11a** and **11b** was prepared by adding 100 μM of the compounds **11a** or **11b** (5 μL , 20 mM stock) along with 2 mM HPE-IAM (16 μL , 125 mM) and 10 U/mL β -glucosidase (111 μL , 90 U/mL stock). The volume was adjusted to 1 mL using 20 mM phosphate buffer, pH 7.4 and the reaction mixture was incubated at 37 $^\circ\text{C}$. 100 μL aliquots of the reaction mixture was taken

at pre-determined time points and the reaction was quenched by adding 100 μ L of methanol. The samples were centrifuged at 10000g for 10 min at 4 $^{\circ}$ C, the supernatant was collected and assessed thereafter by LC/MS using the method described above. The MRM-HR mass spectrometry parameters for measuring polysulfides are: m/z precursor ion mass (Q1, M + H⁺)/product ion mass (Q3, M + H⁺) 521.13/105.05 (**11a**), 150.06/76.00 (**12**), 387.11/121.10 (NACMeSS-HPE-AM), 419.08/121.10 (NACMeSSS-HPE-AM), 451.05/121.10 (NACMeSSSS-HPE-AM), 468.12/105.05 (**11b**), 334.10/121.10 (BnSS-HPE-AM), 366.06/121.10 (BnSSS-HPE-AM), 398.04/121.10 (BnSSSS-HPE-AM), 389.16/121.10 (bis-S-HPE-AM), 421.13/121.10 (bis-SS-HPE-AM), 453.09/121.1 (bis-SSS-HPE-AM), declustering potential = 80 V, entrance potential = 10 V, collision energy = 20 V, and collision exit potential = 5 V.

3.4.4. Decomposition of 10b in the presence of NAC: Stock solution of **10b** (20 mM) was prepared in DMSO. β -galactosidase (100 U/mL) and *N*-acetyl cysteine (NAC, 100 mM) were prepared in DI water. The reaction mixture was prepared by adding 100 μ M of **10b** (2.5 μ L, 20 mM stock), 2 U/mL β -galactosidase (10 μ L, 100 U/mL stock) and 0.5 mM NAC (2.5 μ L, 100 mM stock). The volume was adjusted to 0.5 mL using 20 mM phosphate buffer, pH 7.4 and the reaction was incubated at 37 $^{\circ}$ C. After 30 min, 100 μ L aliquots of the reaction mixture was taken and was quenched by adding 100 μ L of methanol. The samples were centrifuged at 10000g for 10 min at 4 $^{\circ}$ C and the supernatants were collected and assessed thereafter by LC/MS using the method described above.

3.4.5. Decomposition of 10b in the presence of GSH: Stock solution of **10b** (20 mM) was prepared in DMSO. β -galactosidase (100 U/mL) and glutathione (GSH, 100 mM) were prepared in DI water. The reaction mixture was prepared by adding 100 μ M of **10b** (2.5 μ L, 20 mM stock), 2 U/mL β -galactosidase (10 μ L, 100 U/mL stock) and 1 mM GSH (5 μ L, 100 mM stock). The volume was adjusted to 0.5 mL using 20 mM phosphate buffer, pH 7.4 and the reaction was incubated at 37 $^{\circ}$ C. After 30 min, 100 μ L aliquots of the reaction mixture was taken and was quenched by adding 100 μ L of methanol. The samples were centrifuged at 10000g for 10 min at 4 $^{\circ}$ C and the supernatants were collected and assessed thereafter by LC/MS using the method described above.

3.4.6. Cell viability assay: Human colon adenocarcinoma cells (DLD-1) and hepatocarcinoma cells (HepG2) were seeded at a concentration of 1×10^4 cells/well in a 96-well plate in Roswell Park Memorial Institute (RPMI) media supplemented with 10% FBS (fetal bovine serum) and

1% antibiotic solution and incubated in an atmosphere of 5% CO₂ at 37 °C for 16 h. Following this, the cells were exposed to varying concentrations of the compounds. Stock solutions of compounds were prepared in DMSO and the final concentration of DMSO did not exceed 0.5%. The cells were then incubated for 24 h at 37 °C. A 0.5 mg/mL stock solution of 3-(4, 5-dimethylthiazol-2-yl)-2, 5-diphenyl tetrazolium bromide (MTT) was prepared in RPMI. The old media from the cells were removed, 100 µL of the MTT stock was added to each well and incubated for 4 h at 37 °C. After 4 h incubation, the media was carefully removed and 100 µL of DMSO was added. Spectrophotometric analysis of each well at 570 nm using a microplate reader (Thermo Scientific Varioskan) was carried out to estimate cell viability.

3.4.7. Detection of persulfides/polysulfides in cells using SSP2:^{13,28} DLD-1 cells were seeded in a 12 well plate with 10⁵ cells/well in RPMI media supplemented with 10% FBS (fetal bovine serum) and 1% antibiotic solution and incubated in an atmosphere of 5% CO₂ at 37 °C for 48 h. After incubation, the old media was removed and the cells were washed with 500 µL PBS. This was followed by addition of 1 mL fresh serum free RPMI media containing SSP2 (50 µM) along with cetyltrimethylammonium bromide (CTAB, 500 µM) and the cells were incubated at 37 °C for 20 mins. The media was removed and cells were washed with serum free media to remove the excess probe. This was followed by incubation with **11a** (100 µM, 500 µM) in serum free media for 1 h at 37 °C. Cells were finally washed twice with PBS were imaged on EVOS fluorescence microscope using GFP (green fluorescence protein) filter.

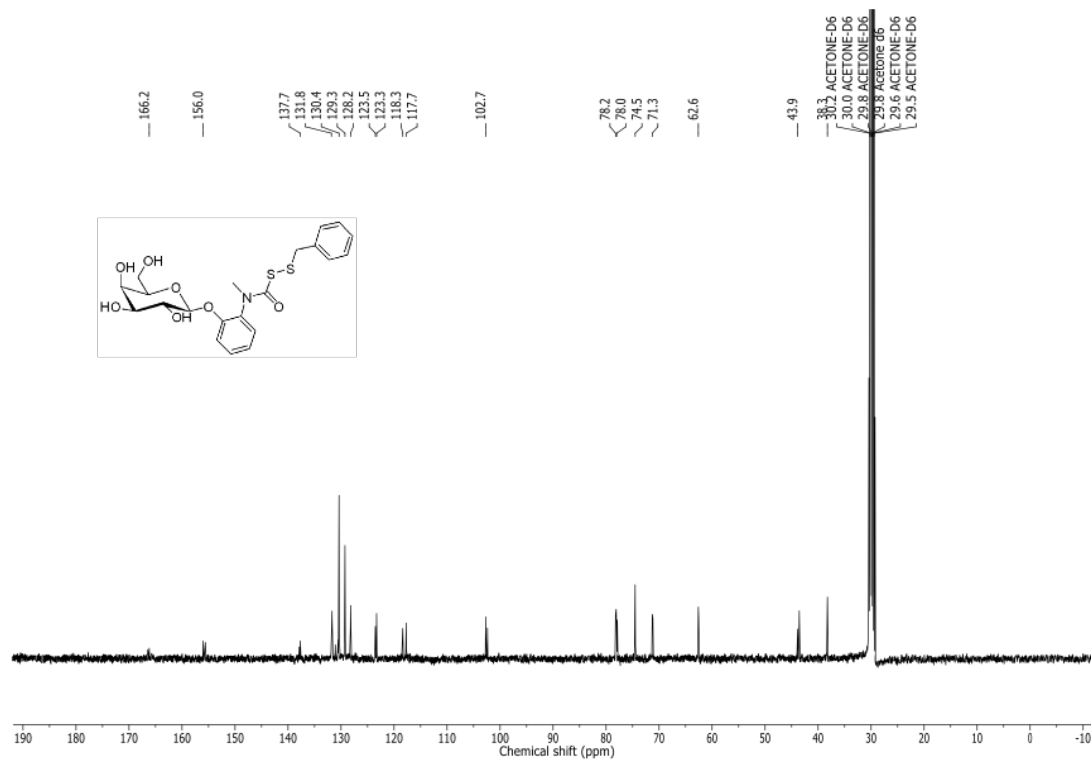
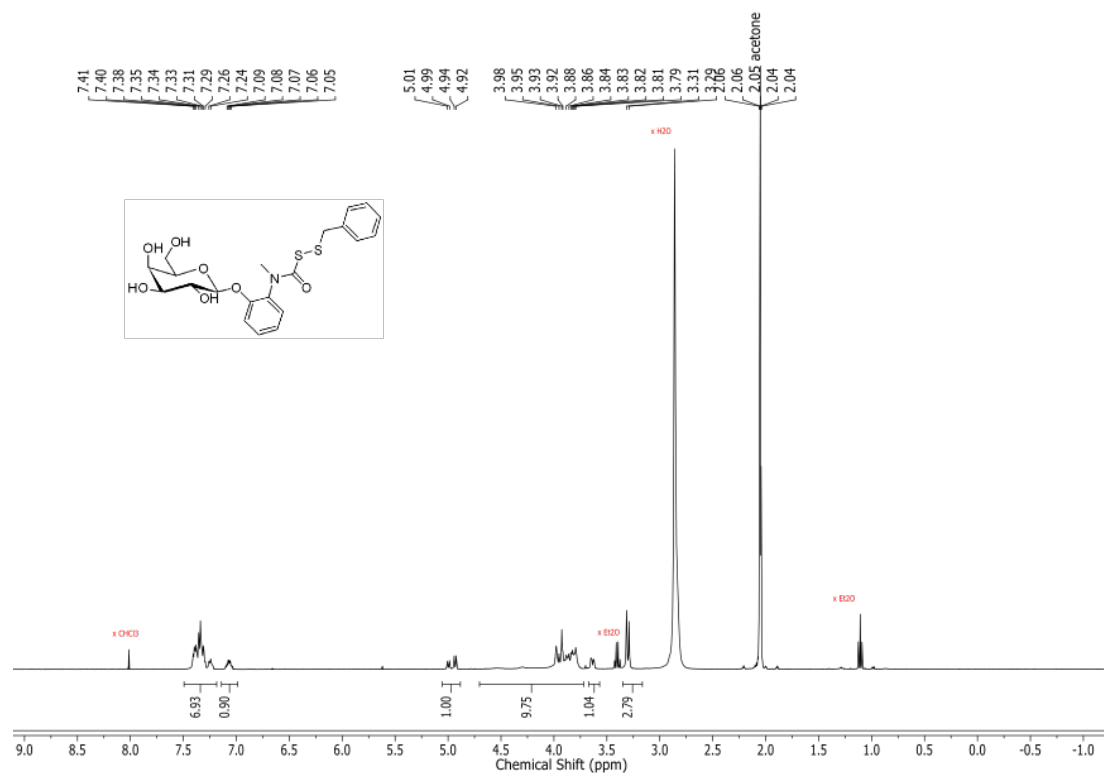
3.4.8. Protection from oxidative stress:

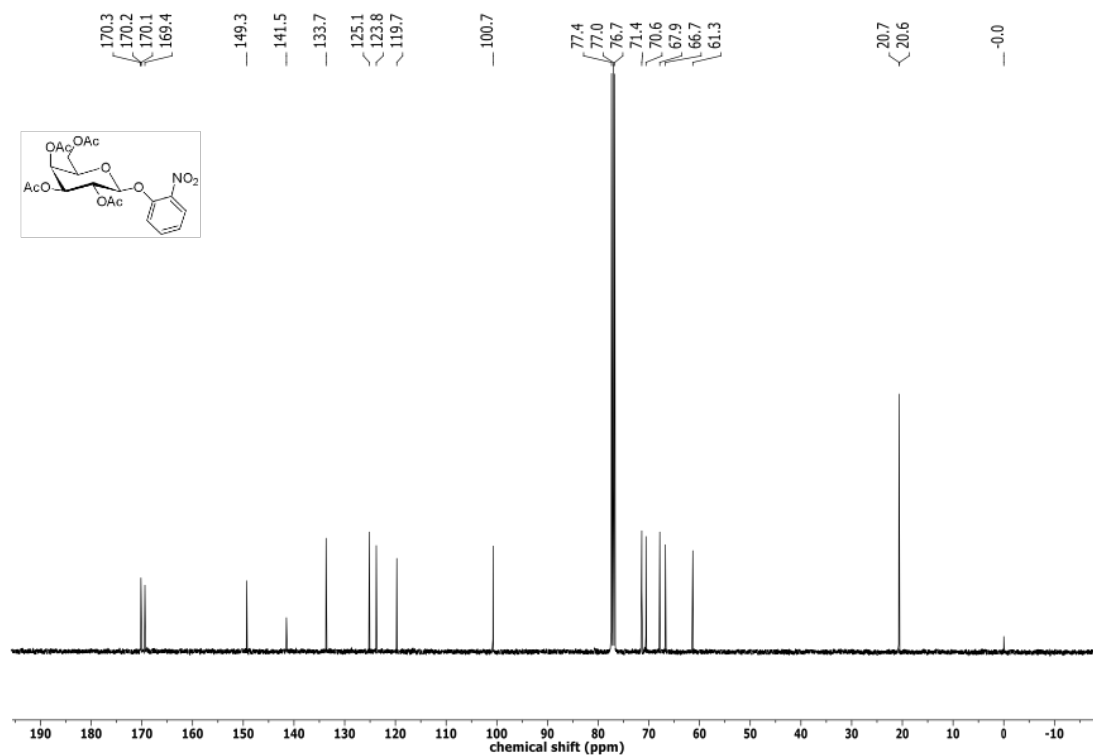
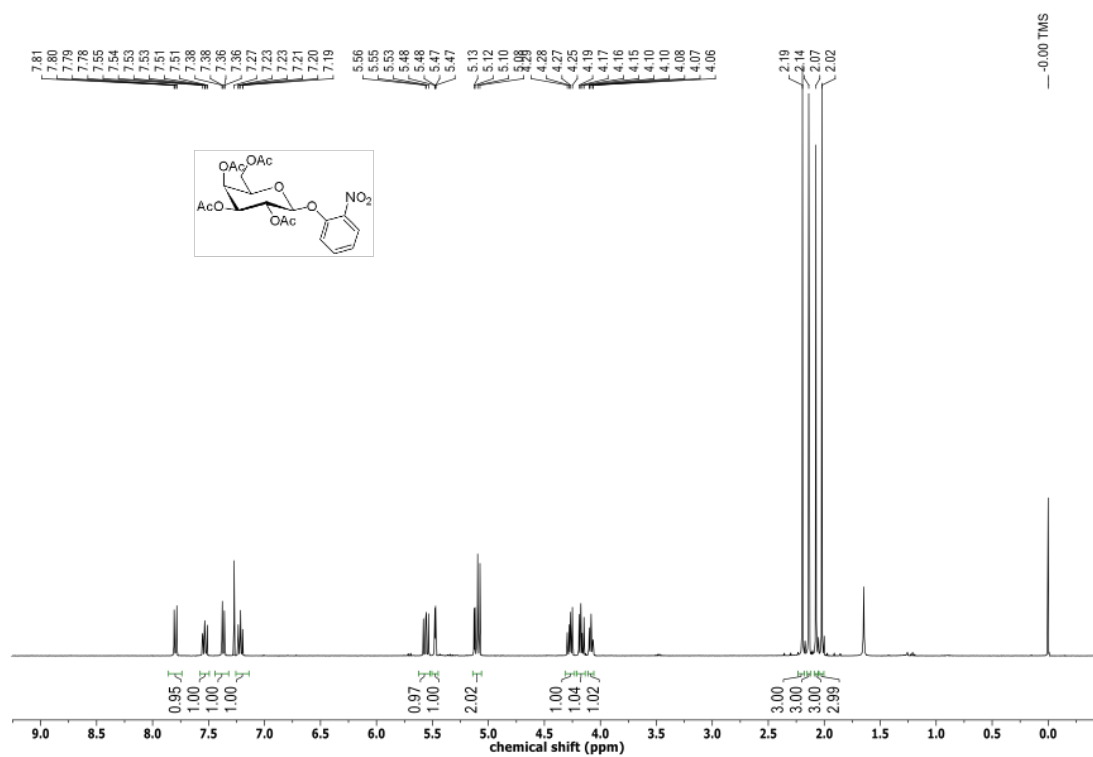
DLD-1 cells: DLD-1 were seeded in a 96-well plate with 10⁴ cells/well in RPMI media supplemented with 10% FBS (fetal bovine serum) and 1% antibiotic solution and incubated in an atmosphere of 5% CO₂ at 37 °C for 16 h. Stock solutions of compounds were prepared in DMSO with final concentration of DMSO not exceeding 0.5%. After 16 h, the cells were pre-treated with different concentrations of the compounds for 12 h followed by treatment with MGR-1 (35 µM) for 4 h at 37 °C. The media was removed and MTT assay was carried out as described above to determine cell viability.

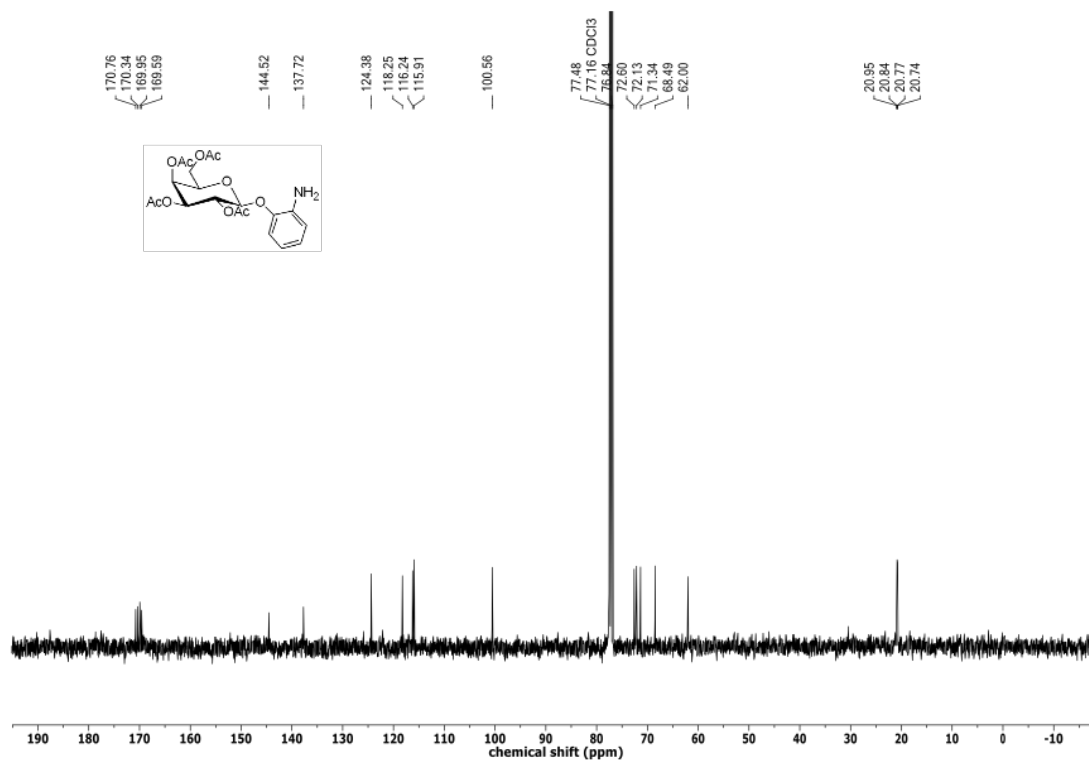
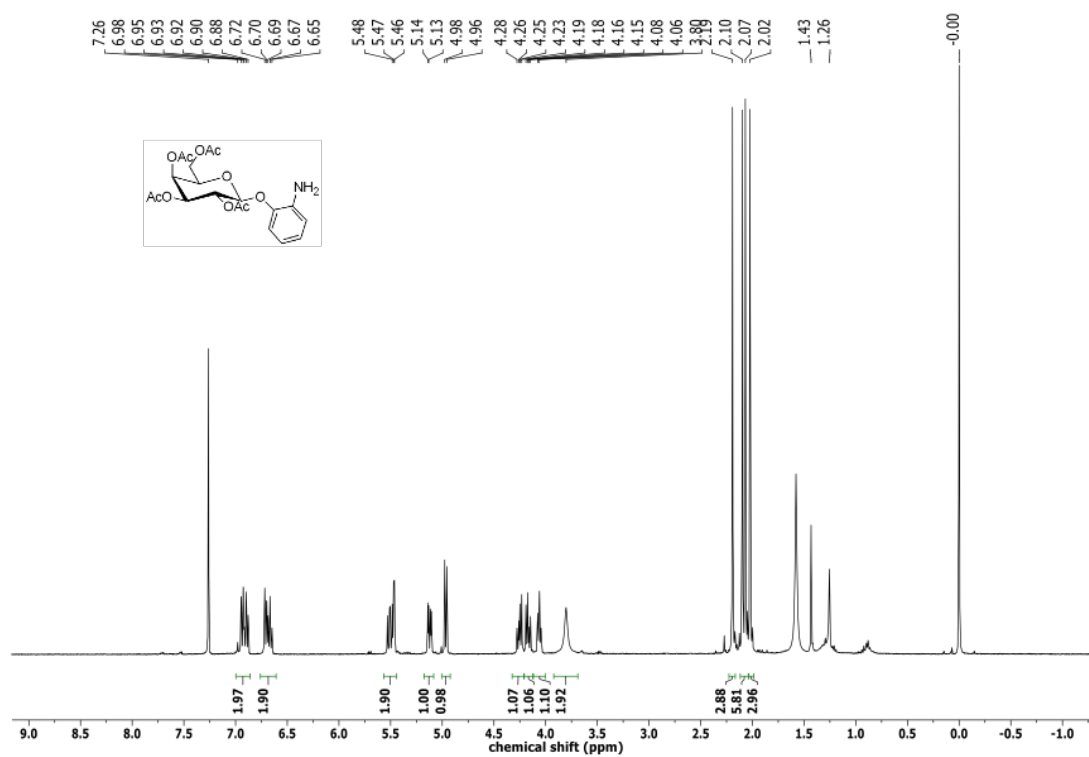
HepG2 cells: HepG2 were seeded in a 96-well plate with 2.5 × 10⁴ cells/well in RPMI media supplemented with 10% FBS (fetal bovine serum) and 1% antibiotic solution and incubated in an atmosphere of 5% CO₂ at 37 °C for 16 h. Stock solutions of compounds were prepared in DMSO with final concentration of DMSO not exceeding 0.5%. After 16 h, the cells were pre-

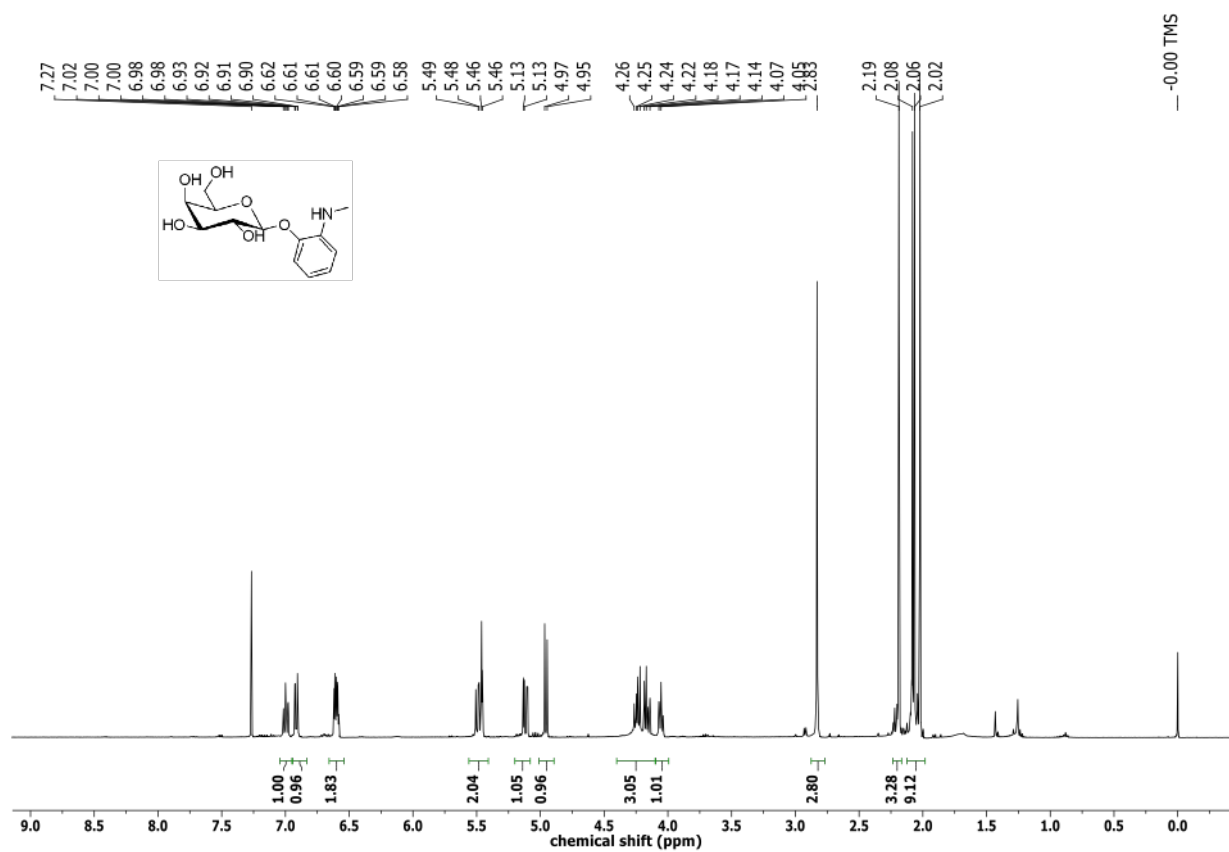
treated with different concentrations of the compounds for 12 h followed by treatment with MGR1 (20 μ M) for 4 h at 37 °C. The media was removed and MTT assay was performed as described above to determine cell viability.

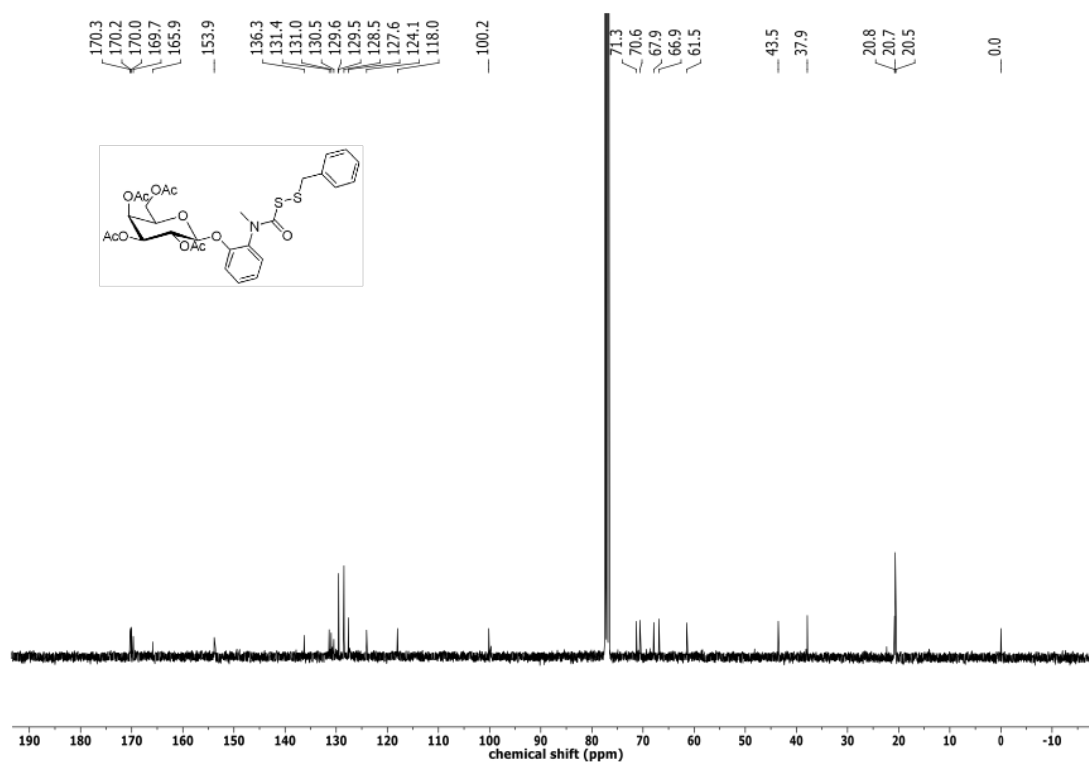
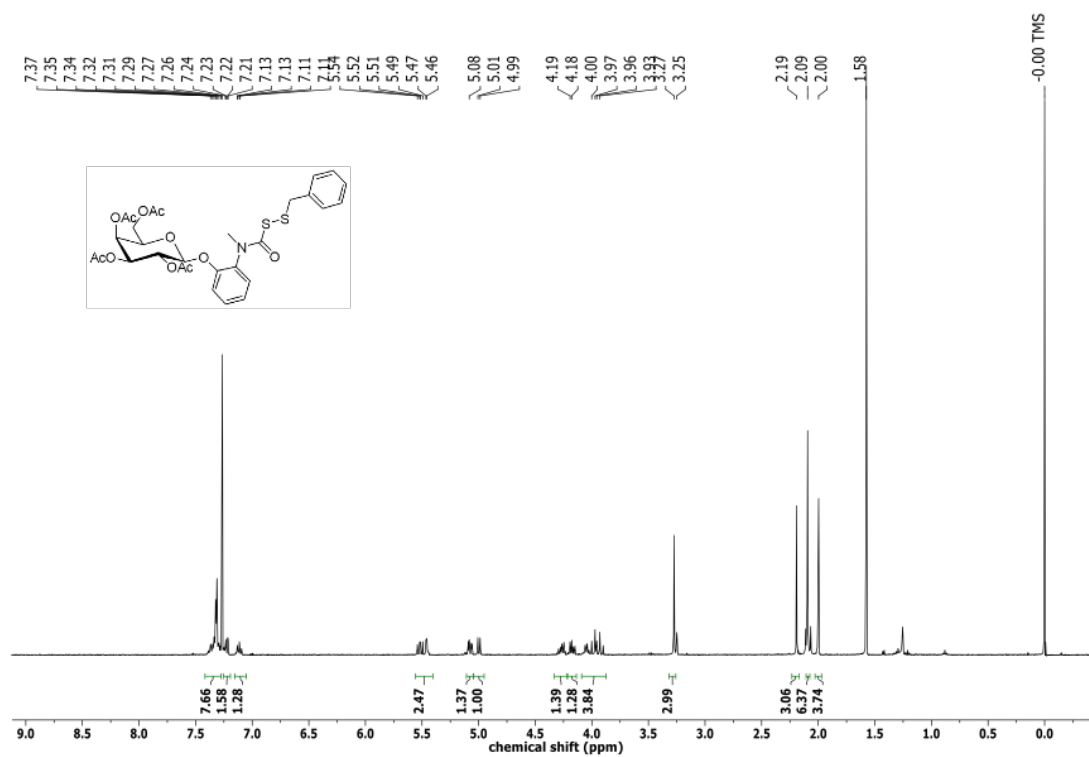
3.5. NMR spectra of compounds

 ^1H and ^{13}C NMR spectra of **10b**

^1H and ^{13}C NMR spectra of **14**

^1H and ^{13}C NMR spectra of **15**

^1H NMR spectra of 16

^1H and ^{13}C NMR spectra of **18b**

3.6. References

- (1) Rubinstein, A., Approaches and Opportunities in Colon-Specific Drug Delivery. *Crit. Rev. Ther. Drug Carr. Syst.* **1995**, *12* (2–3), 101–149.
- (2) Friend, D. R.; Chang, G. W., A colon-specific drug-delivery system based on drug glycosides and the glycosidases of colonic bacteria. *J. Med. Chem.* **1984**, *27* (3), 261–266.
- (3) Englyst, H., Polysaccharide breakdown by mixed populations of human faecal bacteria. *FEMS Microbiol. Lett.* **1987**, *45* (3), 163–171.
- (4) Friend, D. R., New oral delivery systems for treatment of inflammatory bowel disease, *Adv. Drug Deliv. Rev.* **2005**, *57* (2), 247–265.
- (5) Li, F.; Wu, G.; Zheng, H.; Wang, L.; Zhao, Z., Synthesis, colon-targeted studies and pharmacological evaluation of an anti-ulcerative colitis drug 4-Aminosalicylic acid- β -O-glucoside. *Eur. J. Med. Chem.* **2016**, *108*, 486–494.
- (6) Cai, T. B.; Lu, D.; Tang, X.; Zhang, Y.; Landerholm, M.; Wang, P. G., New Glycosidase Activated Nitric Oxide Donors: Glycose and 3-Morphorlinosydnonimine Conjugates. *J. Org. Chem.* **2005**, *70* (9), 3518–3524.
- (7) Valdez, C. A.; Saavedra, J. E.; Showalter, B. M.; Davies, K. M.; Wilde, T. C.; Citro, M. L.; Barchi, J. J.; Deschamps, J. R.; Parrish, D.; El-Gayar, S.; Schleicher, U.; Bogdan, C.; Keefer, L. K., Hydrolytic Reactivity Trends among Potential Prodrugs of the O² -Glycosylated Diazeniumdiolate Family. Targeting Nitric Oxide to Macrophages for Antileishmanial Activity. *J. Med. Chem.* **2008**, *51* (13), 3961–3970.
- (8) Zhu, H.; Li, Y. R., Oxidative stress and redox signaling mechanisms of inflammatory bowel disease: updated experimental and clinical evidence. *Exp. Biol. Med.* **2012**, *237* (5), 474–480.
- (9) Wallace, J. L.; Wang, R., Hydrogen sulfide-based therapeutics: exploiting a unique but ubiquitous gasotransmitter. *Nat. Rev. Drug Discov.* **2015**, *14*, 329.
- (10) Fiorucci, S.; Orlandi, S.; Mencarelli, A.; Caliendo, G.; Santagada, V.; Distrutti, E.; Santucci, L.; Cirino, G.; Wallace, J. L., Enhanced activity of a hydrogen sulphide-releasing derivative of mesalamine (ATB-429) in a mouse model of colitis. *Br. J. Pharmacol.* **2009**, *150* (8), 996–1002.

-
- (11) Cenac, N.; Castro, M.; Desormeaux, C.; Colin, P.; Sie, M.; Ranger, M.; Vergnolle, N., A novel orally administered trimebutine compound (GIC-1001) is anti-nociceptive and features peripheral opioid agonistic activity and Hydrogen Sulphide-releasing capacity in mice. *Eur. J. Pain* **2016**, *20* (5), 723–730.
- (12) Chauhan, P.; Gupta, K.; Ravikumar, G.; Saini, D. K.; Chakrapani, H., Carbonyl Sulfide (COS) Donor Induced Protein Persulfidation Protects against Oxidative Stress. *Chem. – An Asian J.* **2019**, *14* (24), 4717–4724.
- (13) Ida, T.; Sawa, T.; Ihara, H.; Tsuchiya, Y.; Watanabe, Y.; Kumagai, Y.; Suematsu, M.; Motohashi, H.; Fujii, S.; Matsunaga, T.; Yamamoto, M.; Ono, K.; Devarie-Baez, N. O.; Xian, M.; Fukuto, J. M.; Akaike, T., Reactive cysteine persulfides and S-polythiolation regulate oxidative stress and redox signaling. *Proc. Natl. Acad. Sci. U.S.A* **2014**, *111* (21), 7606–7611.
- (14) Yang, G.; Zhao, K.; Ju, Y.; Mani, S.; Cao, Q.; Puukila, S.; Khaper, N.; Wu, L.; Wang, R., Hydrogen Sulfide Protects Against Cellular Senescence via S-Sulphydration of Keap1 and Activation of Nrf2. *Antioxid. Redox Signal.* **2013**, *18* (15), 1906–1919.
- (15) Tocmo, R.; Parkin, K., S-1-propenylmercaptocysteine protects murine hepatocytes against oxidative stress via persulfidation of Keap1 and activation of Nrf2. *Free Radic. Biol. Med.* **2019**, *143*, 164–175.
- (16) Wedmann, R.; Onderka, C.; Wei, S.; Sziđártó, I. A.; Miljkovic, J. L.; Mitrovic, A.; Lange, M.; Savitsky, S.; Yadav, P. K.; Torregrossa, R.; Harrer, E. G.; Harrer, T.; Ishii, I.; Gollasch, M.; Wood, M. E.; Galardon, E.; Xian, M.; Whiteman, M.; Banerjee, R.; Filipovic, M. R., Improved tag-switch method reveals that thioredoxin acts as depersulfidase and controls the intracellular levels of protein persulfidation. *Chem. Sci.* **2016**, *7* (5), 3414–3426.
- (17) *Registry of Toxic Effects of Chemical Substances*, 1985th–1986th ed.; Sweet, D. V., Ed.; US Department of Health and Human Services CDC, 1987.
- (18) Chen, X.; Ma, X.; Zhang, Y.; Gao, G.; Liu, J.; Zhang, X.; Wang, M.; Hou, S., Ratiometric fluorescent probes with a self-immolative spacer for real-time detection of β -galactosidase and imaging in living cells. *Anal. Chim. Acta* **2018**, *1033*, 193–198.
- (19) Okamoto, I.; Terashima, M.; Masu, H.; Nabeta, M.; Ono, K.; Morita, N.; Katagiri, K.; Azumaya, I.; Tamura, O., Acid-induced conformational alteration of cis-preferential

- aromatic amides bearing N-methyl-N-(2-pyridyl) moiety. *Tetrahedron* **2011**, *67* (44), 8536–8543.
- (20) Khodade, V. S.; Pharoah, B. M.; Paolocci, N.; Toscano, J. P., Alkylamine-Substituted Perthiocarbamates: Dual Precursors to Hydropersulfide and Carbonyl Sulfide with Cardioprotective Actions. *J. Am. Chem. Soc.* **2020**, *142* (9), 4309–4316.
- (21) Hamid, H. A.; Tanaka, A.; Ida, T.; Nishimura, A.; Matsunaga, T.; Fujii, S.; Morita, M.; Sawa, T.; Fukuto, J. M.; Nagy, P.; Tsutsumi, R.; Motohashi, H.; Ihara, H.; Akaike, T., Polysulfide stabilization by tyrosine and hydroxyphenyl-containing derivatives that is important for a reactive sulfur metabolomics analysis. *Redox Biol.* **2019**, *21*, 101096.
- (22) Numakura, T.; Sugiura, H.; Akaike, T.; Ida, T.; Fujii, S.; Koarai, A.; Yamada, M.; Onodera, K.; Hashimoto, Y.; Tanaka, R.; Sato, K.; Shishikura, Y.; Hirano, T.; Yanagisawa, S.; Fujino, N.; Okazaki, T.; Tamada, T.; Hoshikawa, Y.; Okada, Y.; Ichinose, M., Production of reactive persulfide species in chronic obstructive pulmonary disease. *Thorax* **2017**, *72* (12), 1074–1083.
- (23) Akaike, T.; Ida, T.; Wei, F.-Y.; Nishida, M.; Kumagai, Y.; Alam, M. M.; Ihara, H.; Sawa, T.; Matsunaga, T.; Kasamatsu, S.; Nishimura, A.; Morita, M.; Tomizawa, K.; Nishimura, A.; Watanabe, S.; Inaba, K.; Shima, H.; Tanuma, N.; Jung, M.; Fujii, S.; Watanabe, Y.; Ohmuraya, M.; Nagy, P.; Feelisch, M.; Fukuto, J. M.; Motohashi, H., Cysteinyl-tRNA synthetase governs cysteine polysulfidation and mitochondrial bioenergetics. *Nat. Commun.* **2017**, *8* (1), 1177.
- (24) Hultberg, B.; Öckerman, P. A., β -Glucosidase activities in human tissues findings in Gaucher's disease. *Clin. Chim. Acta* **1970**, *28* (1), 169–174.
- (25) Arafa, H. M. M., Possible contribution of β -glucosidase and caspases in the cytotoxicity of glufosfamide in colon cancer cells. *Eur. J. Pharmacol.* **2009**, *616* (1–3), 58–63.
- (26) Chengelis, C. P.; Neal, R. A., Studies of carbonyl sulfide toxicity: Metabolism by carbonic anhydrase. *Toxicol. Appl. Pharmacol.* **1980**, *55* (1), 198–202.
- (27) Tribolo, S.; Berrin, J.-G.; Kroon, P. A.; Czjzek, M.; Juge, N., The Crystal Structure of Human Cytosolic β -Glucosidase Unravels the Substrate Aglycone Specificity of a Family 1 Glycoside Hydrolase. *J. Mol. Biol.* **2007**, *370* (5), 964–975.
- (28) Chen, W.; Liu, C.; Peng, B.; Zhao, Y.; Pacheco, A.; Xian, M., New fluorescent probes for sulfane sulfurs and the application in bioimaging. *Chem. Sci.* **2013**, *4* (7), 2892.

-
- (29) Kelkar, D. S.; Ravikumar, G.; Mehendale, N.; Singh, S.; Joshi, A.; Sharma, A. K.; Mhetre, A.; Rajendran, A.; Chakrapani, H.; Kamat, S. S., A chemical–genetic screen identifies ABHD12 as an oxidized-phosphatidylserine lipase. *Nat. Chem. Biol.* **2019**, *15* (2), 169–178.
- (30) Dharmaraja, A. T.; Alvala, M.; Sriram, D.; Yogeeswari, P.; Chakrapani, H., Design, synthesis and evaluation of small molecule reactive oxygen species generators as selective *Mycobacterium tuberculosis* inhibitors. *Chem. Commun.* **2012**, *48* (83), 10325–10327.
- (31) Zhang, T.; Ono, K.; Tsutsuki, H.; Ihara, H.; Islam, W.; Akaike, T.; Sawa, T., Enhanced Cellular Polysulfides Negatively Regulate TLR4 Signaling and Mitigate Lethal Endotoxin Shock. *Cell Chem. Biol.* **2019**, *26* (5), 686-698.e4.

CHAPTER 4.1: Insights into the therapeutic potential of persulfides using artificial substrates for 3-mercaptopyruvate sulfurtransferase (3-MST)

4.1.1. Introduction

One of the important enzymes involved in the biogenesis of persulfides is the H₂S producing enzyme, 3-mercaptopyruvate sulfurtransferase (3-MST) a member of the sulfurtransferase family. 3-MST is ubiquitously present across all mammalian tissues, with an over-expression in the kidney, cardiac cells, brain, liver and endocrine organs.¹ It is a 33 kDa protein with a redox active cysteine at its catalytic site. 3-mercaptopyruvate (3-MP) is formed from L-cysteine by the action of L-cysteine aminotransferase (CAT) using α -ketoglutarate as a co-substrate. 3-MST utilizes 3-MP as the sulfur acceptor to form a transient persulfide intermediate in its active site cysteine and an enolate of pyruvate as the byproduct.^{2,3} The enolate subsequently tautomerizes to the keto form (Figure 4.1.1.a).

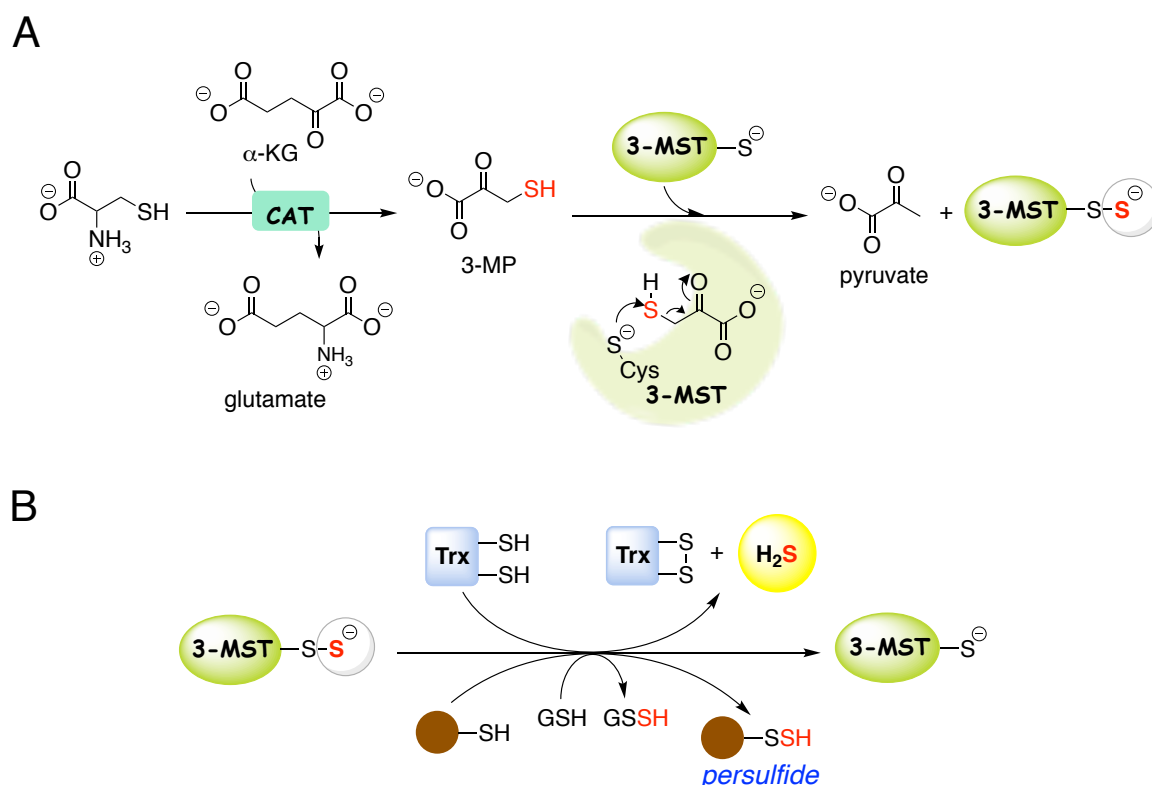


Figure 4.1.1. a) Reaction mechanism for turnover of 3-mercaptopyruvate (3-MP) by 3-mercaptopyruvate sulfurtransferase (3-MST) to form a transient 3-MST persulfide intermediate and pyruvate as the byproduct. b) The 3-MST persulfide can undergo reduction to generate H₂S or transfer the sulfur to other acceptor proteins leading to total cellular persulfidation.

Analysis of the crystal structure of human 3-MST-3-MP revealed that Arg¹⁸⁸ and Arg¹⁹⁷ stabilizes the incoming 3-MP via electrostatic interactions with the carboxyl and carbonyl

group of 3-MP.³ Whereas the catalytic triad comprising of His⁷⁴, Ser²⁵⁰ and Asp⁶³ are involved in activating the catalytic site Cys²⁴⁸. The sulfur can be further transferred to target proteins or be reduced by thioredoxin to generate H₂S. Subsequent turnover of 3-MP by the 3-MST persulfide, leading to the formation of polysulfides have also been reported (Figure 4.1.1.b).⁴

This redox sensitive cysteine residue is prone to oxidation in an oxidative environment, inhibiting its activity. Since L-cysteine is a precursor to 3-MP, inhibition of 3-MST conserves cysteine, upregulating the production of cellular reductants under conditions of oxidative stress.⁵ It is also involved in cyanide detoxification,⁶ synthesis of thiouridine in tRNA,⁷ regulation of sulfane sulfur in the brain⁴ and iron sulfur clusters.⁸ 3-MST has therefore been characterized as a detoxification enzyme and as an intracellular antioxidant. Deficiency of 3-MST results in a rare genetic disorder known as mercaptolactate-cysteine disulfiduria (MCDU).⁹ Its deficiency in animal models has also been reported to be associated with anxiety like behavior, underlining the importance of 3-MST in normal metabolism and functioning.^{1,10}

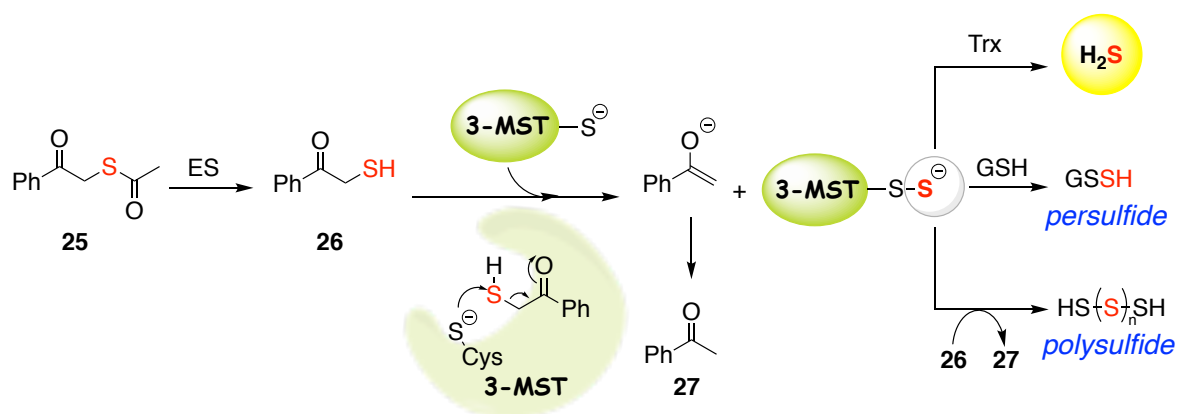


Figure 4.1.2. An artificial substrate having a similar enolizable ketone and a sulfur donor was designed, which upon turnover by 3-MST feeds into the biosynthetic machinery of the cell to induce persulfidation and generate H₂S. Acetophenone would be generated as a byproduct.

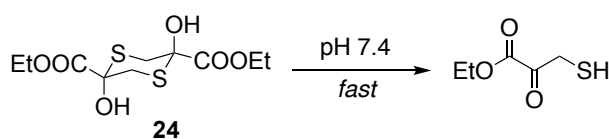
The natural substrate for 3-MST which is 3-MP can reportedly generate H₂S spontaneously, through non-enzymatic mechanisms, which can be a potential limitation.¹¹ Therefore, we considered developing an artificial substrate with structural features similar to 3-MP, that would be essential for the formation of 3-MST persulfide. We hypothesized that the 3-MST persulfide once formed would feed into the biosynthetic machinery for total cellular persulfidation and H₂S generation. Therefore, we designed compound **26** that has a sulfur donor and an enolizable ketone, similar to 3-MP and would form acetophenone (**27**) as the byproduct after tautomerization (Figure 4.1.2.). Due to the propensity of thiols to undergo

aerial oxidation, **26** was protected as the thioacetate (**25**) to impart stability and longer shelf-life. The thioacetate in **25** can be easily deprotected by the widely prevalent enzyme esterase.

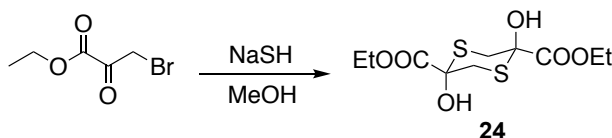
4.1.2. Results and Discussion

4.1.2.1. Synthesis

24 is a dimer of 3-MP ethyl ester that rapidly dissociates in buffer to generate two moles of 3-MP ethyl ester (Scheme 4.1.1.). It was synthesized by reacting ethyl bromopyruvate with sodium hydrogen sulfide (NaSH) in methanol (Scheme 4.1.2.).⁶ **24** was used as a positive control in all the experiments.

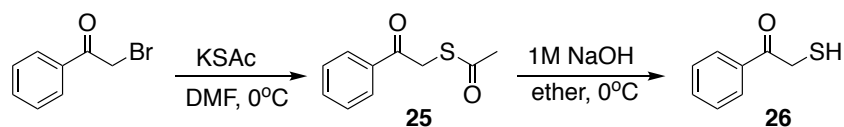


Scheme 4.1.1. 3-MP ethyl ester exists as a dimer which rapidly dissociates in buffer to give the monomer.



Scheme 4.1.2. Synthesis of the dimer of 3-MP ethyl ester, **24**.

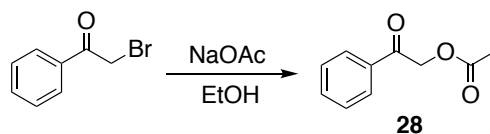
The synthesis of the thiol **26** was carried out in 2 steps using previously reported protocols.^{12,13} Phenacyl bromide was reacted with potassium thioacetate to give the thioacetate **25** in 78% yield. This was followed by deprotection of the thioacetate in 1M aq NaOH in diethyl ether to afford the thiol **26** (Scheme 4.1.3.).



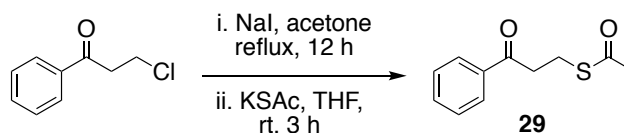
Scheme 4.1.3. Synthesis of phenacyl thiol **26**.

Compound **28** where the sulfur was replaced with oxygen, would not generate the 3-MST persulfide and therefore was used as a negative control. It was synthesized from phenacyl bromide by reacting it with sodium acetate (Scheme 4.1.4).¹⁴ The synthesis of compound **28** was carried out by Mr. Mrutyunjay Nair. An extra methylene group would prevent the formation of an enolate and hence the 3-MST persulfide would not be formed. **29** with an extra methylene group was synthesized as the second negative control. It was synthesized from 3-

chloropropiophenone by reacting it with sodium iodide followed by potassium thioacetate (Scheme 4.1.5). The synthesis of compound **29** was performed by Mr. Suman Manna.



Scheme 4.1.4. Synthesis of negative control **28**.



Scheme 4.1.5. Synthesis of negative control **29**.

4.1.2.2. Tag Switch technique to detect persulfidation in proteins

First, we evaluated the formation of 3-MST persulfide in its active site cysteine as 3-MST accepts the sulfur from the artificial substrate **26**. A previously reported tag-switch technique was used to detect the protein persulfide.^{15,16} The first step in this technique involves blocking of the persulfide and the residual thiol groups in the protein by the thiol blocking reagent methyl sulfonyl benzothiazole (MSBT-A) (Figure 4.1.3).

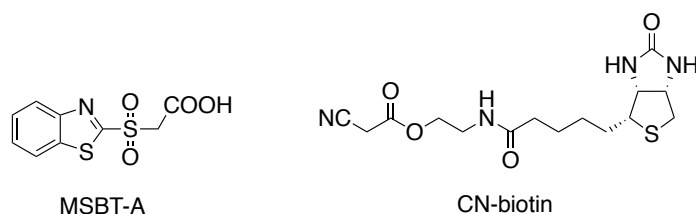


Figure 4.1.3. Structures of reagents used in the tag-switch technique

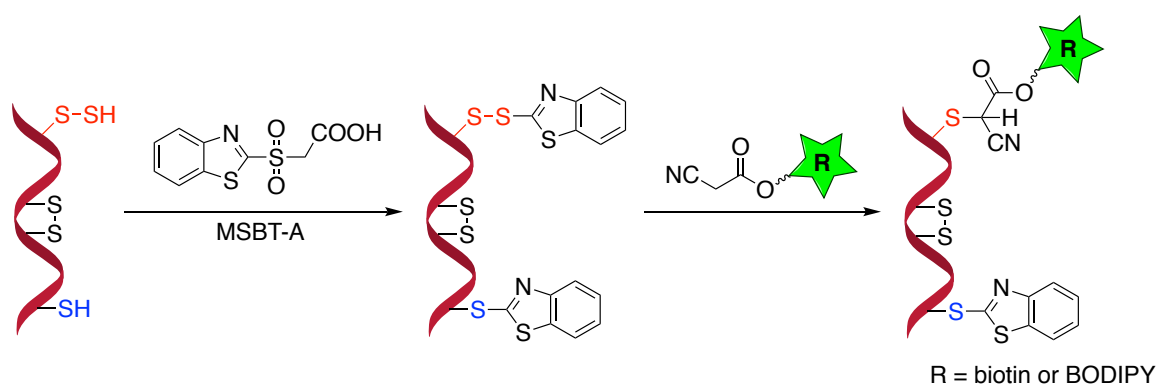


Figure 4.1.4. Tag-switch technique for detection of protein persulfides.

Upon reacting with MSBT-A, thiols form a thioether bond while persulfides form a reactive mixed disulfide bond. This mixed disulfide bond has enhanced reactivity towards nucleophiles compared to a thioether bond or an intramolecular disulfide bond in the protein. Therefore, introducing a tag-switching reagent, comprising of a nucleophile along with a reporting group which can either be biotin or a fluorophore such as BODIPY, can selectively label persulfides (Figure 4.1.4). The nucleophile used here is a methyl cyanoacetate that is coupled to biotin (Figure 4.1.3). The biotinylated protein can be subsequently detected using Western blot analysis.

To test the formation of the 3-MST persulfide, 3-MST was treated with compound **25** in the presence of esterase in pH 7.4 buffer and incubated at 37 °C for 1 h. The reaction samples were then reacted with MSBT-A followed by CN-biotin. A similar experiment was carried out with the positive control **24**, which dissociates in buffer to produce the ethylester of 3-MP (E3-MP) and the negative controls **28** and **29**. The samples were subsequently analyzed using the Western blot technique. A strong band was observed when 3-MST was treated with the positive control **24** suggesting the formation of a 3-MST persulfide. A similar result was obtained with the substrate **25**. Whereas, the negative controls **28** and **29** produced a significantly diminished signal under similar conditions (Figure 4.1.5.a). The bands were quantified using ImageJ (Figure 4.1.5.b).

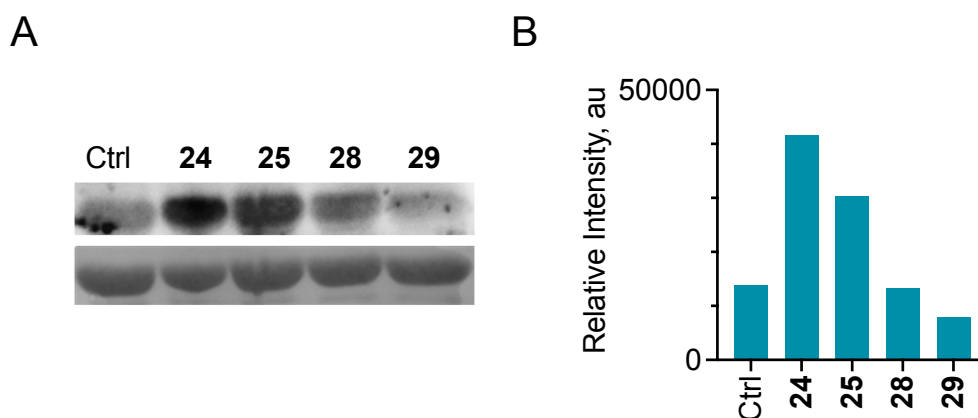


Figure 4.1.5. (a) Persulfidation of 3-MST by the ethyl ester of 3-MP (**24**) and the artificial substrate (**25**) in presence of ES, detected using the modified tag-switch technique. Compounds **28** and **29** were used as negative controls. PonceauS staining was used as a loading control. (b) Relative quantification of the bands using ImageJ.

To further corroborate our results, the active site cysteine residue in 3-MST was replaced with alanine (C238A 3-MST). The C238A mutant was generated by Ms. Rupali Sathe from Dr. Amrita Hazra's lab in IISER Pune. A similar tag-switch assay was carried out using

the C238A 3-MST mutant. Under the reaction conditions described above, significantly weaker bands were observed when the C238A 3-MST mutant was treated with compounds **24** and **25** compared to the wildtype 3-MST (Figure 4.1.6.a). The bands were quantified using ImageJ (Figure 4.1.6.b). Collectively, these data suggest the formation of a 3-MST persulfide as an intermediate when treated with the artificial substrate **25**.

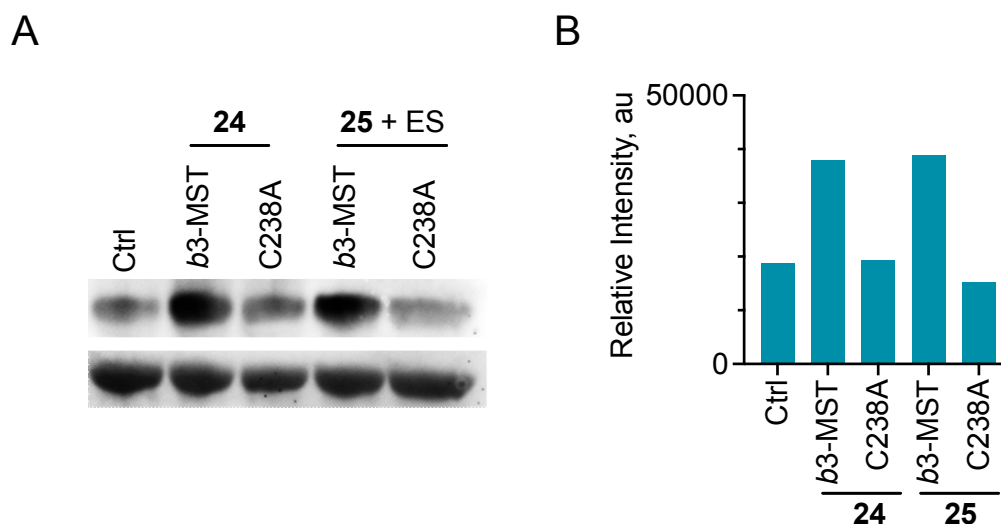


Figure 4.1.6. (a) Persulfidation of wt 3-MST and 3-MST C238A mutant by compounds **24** and **25** in the presence of esterase (ES) were studied using the modified tag-switch technique. PonceauS staining was used as a loading control. (b) Relative quantification of the bands was done using ImageJ.

4.1.2.3. Detection of persulfide/polysulfide using LC/MS

Upon establishing that **25** is turned over by 3-MST to form the 3-MST persulfide as an intermediate, the formation of persulfide/polysulfide was next evaluated by leveraging the ability of 3-MST-SS⁻ to transfer the sulfane sulfur to a small molecule acceptor thiol. GSH being the most abundant and biologically relevant thiol was used as a thiol acceptor. GSH upon reacting with 3-MST-SS⁻ will form GSH persulfide (GS-SH). These reactive sulfur species being unstable in nature was trapped with an electrophile, monobromobimane (mBBr) and detected as their bimane adducts.¹⁷

Compound **25** was incubated with 3-MST in the presence of esterase in pH 7.4 tris-HCl buffer for 30 min followed by treatment with GSH and finally mBBr. LC/MS analysis of the above reaction mixture showed the formation of GSS-bimane adduct (expected m/z = 530.1379; observed m/z = 530.1357) (Figure 4.1.7.).

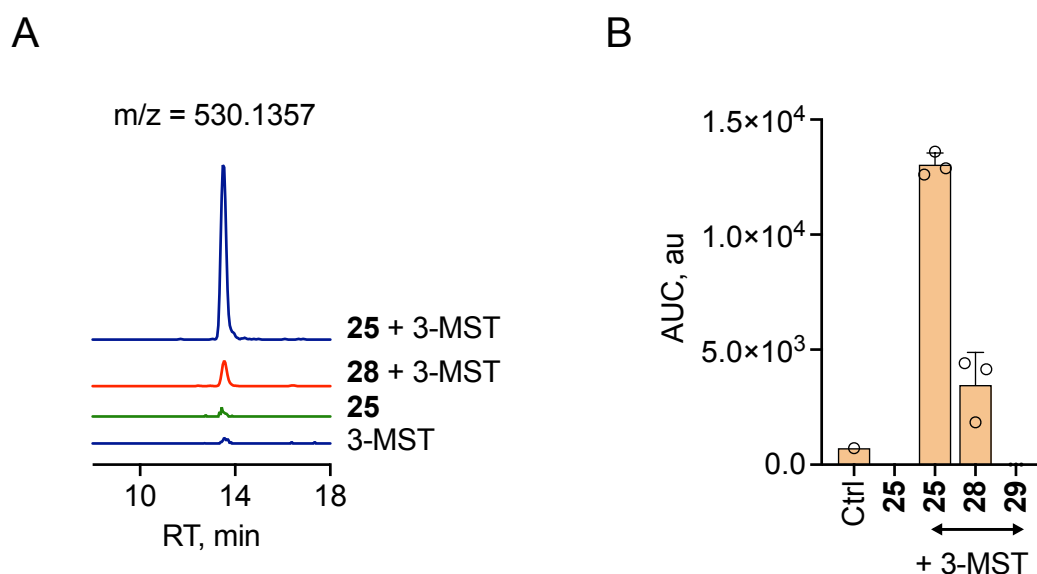


Figure 4.1.7. (a) Extracted ion chromatograms from an LC/MS analysis of GSS-bimane ($[M+H]^+$ expected = 530.1379; observed = 530.1357) showing the formation of GSSH upon reacting **25** with 3-MST in the presence of esterase followed by treatment with GSH. b) Area under the curve (AUC) for the peak corresponding to GSS-bimane. Ctrl refers to enzyme alone.

Interestingly, the formation of bis-S-bimane adduct (expected, $[M+H]^+ = 415.144$; observed $[M+H]^+ = 415.1433$) (Figure 4.1.8.), suggesting the generation of H_2S and GSSSG (expected $[M+H]^+ = 645.1319$; $[M+H]^+ = 645.1315$) (Figure 4.1.9.) were also observed along with the GSS-bimane adduct.

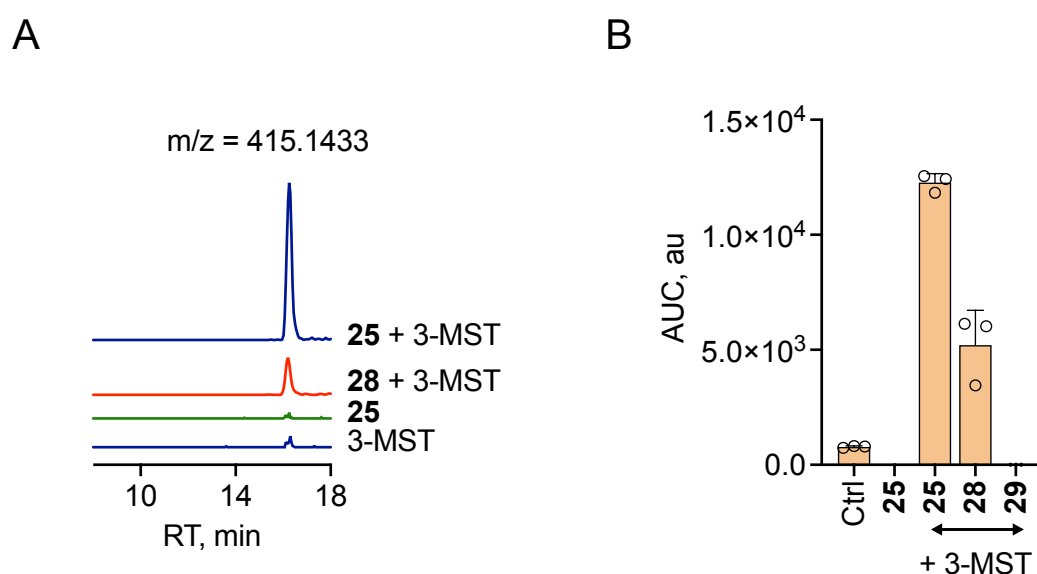


Figure 4.1.8. a) Extracted ion chromatograms from an LC/MS analysis of bis-S-bimane ($[M+H]^+$ expected = 415.144; observed = 415.1433) indicating the formation of H_2S upon reacting **25** with 3-MST in the presence of esterase followed by treatment with GSH. b) Area under the curve (AUC) for the peak corresponding to bis-S-bimane. Ctrl refers to enzyme alone.

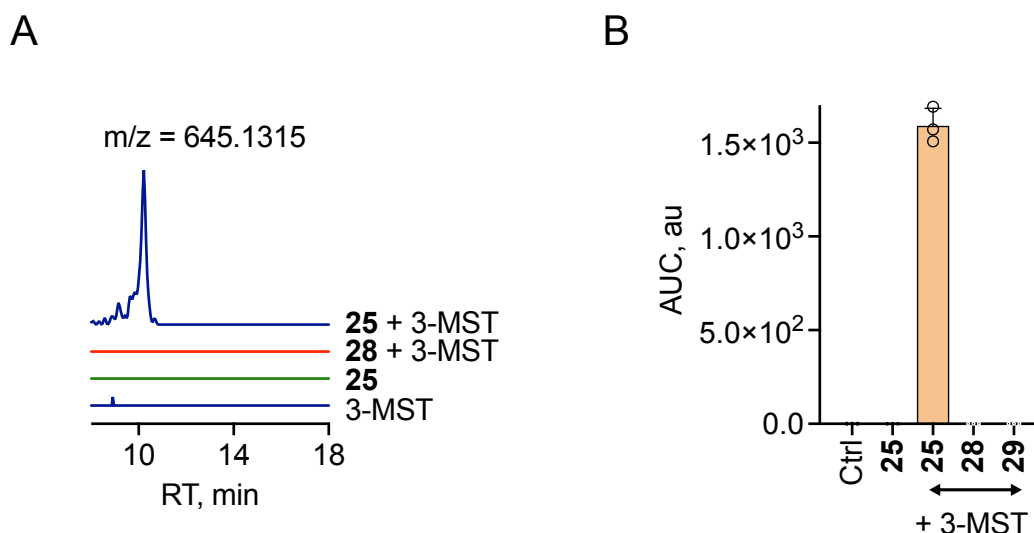


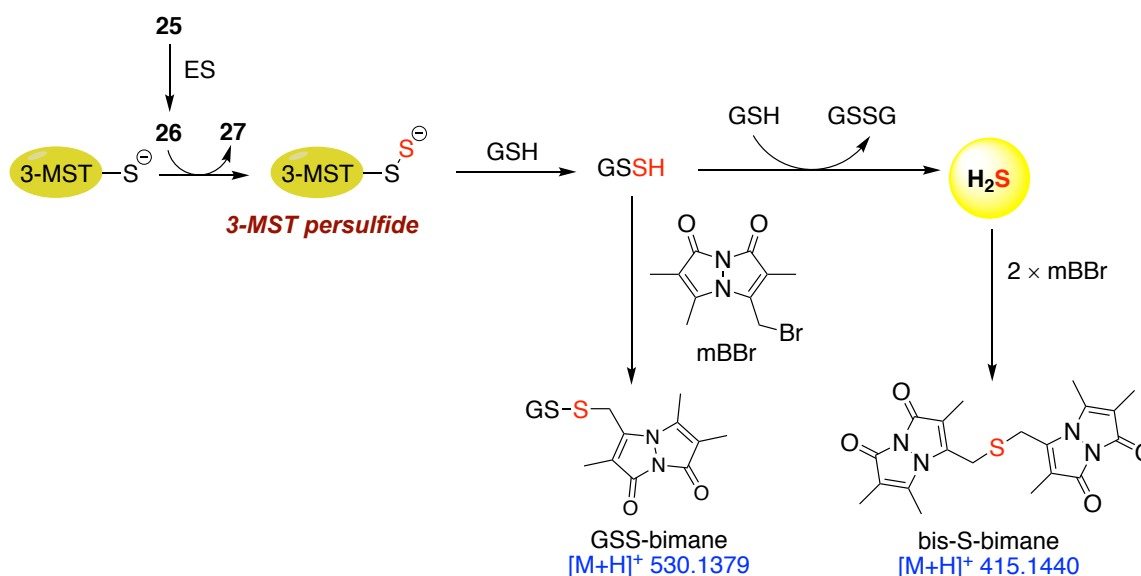
Figure 4.1.9. a) Extracted ion chromatograms from an LC/MS analysis of GSSSG ($[M+H]^+$ expected = 645.1319; observed = 645.1315) indicating the formation of GSSSG upon reacting **25** with 3-MST in the presence of ES followed by treatment with GSH. b) Area under the curve (AUC) for the peak corresponding to GSSSG. Ctrl refers to enzyme alone.

Compound **25** in the absence of 3-MST however, did not generate any of these sulfur species. Thus, indicating that GS-SH, H₂S and GSSSG are formed only in the reaction sample containing **25**, esterase and 3-MST. However, during the incubation of **29** with 3-MST, the formation of GSS-bimane and bis-S-bimane adducts were observed at diminished levels when compared with a similar experiment conducted with **25** + ES + 3-MST. While the origin of this result is yet to be characterized, it appears that **29** undergoes decomposition to produce a persulfide or H₂S as a minor pathway.

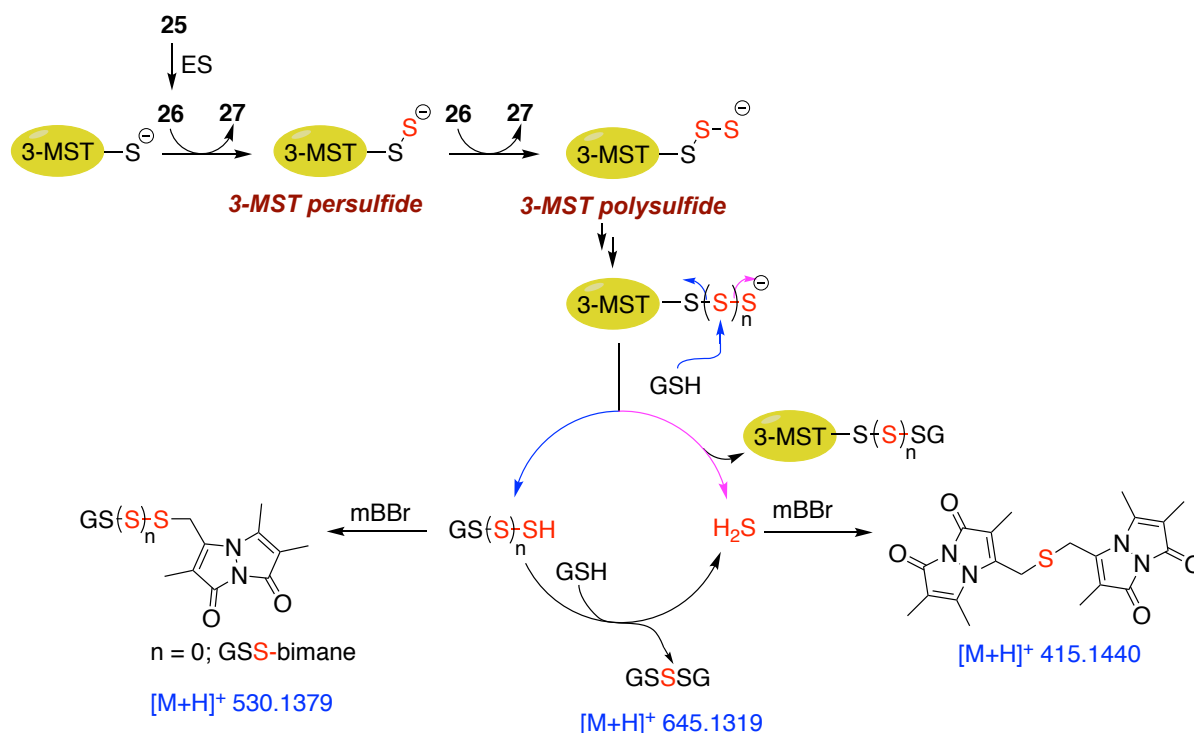
4.1.2.4. Mechanism for the formation of persulfide/polysulfide

A mechanism for the generation of GSH persulfide/polysulfide was formulated based on the above observations. **25** is cleaved in the presence of esterase to form the active substrate **26**, which upon turnover by 3-MST would generate the 3-MST-SS⁻ as an intermediate and acetophenone **27** as the byproduct. In the presence of a thiol acceptor such as GSH, 3-MST-SS⁻ can transfer its persulfide, forming GS-SH which was detected as the GSS-bimane adduct. GS-SH can be reduced by another mole of GSH to generate H₂S which was detected as the bis-S-bimane adduct (Scheme 4.1.6.).

In the absence of a reducing agent such as dithiothreitol (DTT), the 3-MST-SS⁻ can further turnover another mole of **26** to form the 3-MST-SSS⁻ and subsequently a 3-MST-S_nS⁻ intermediate. 3-MST polysulfide upon treatment with GSH generates GS-S_nH and ultimately form GSSSG along with H₂S (Scheme 4.1.7.).



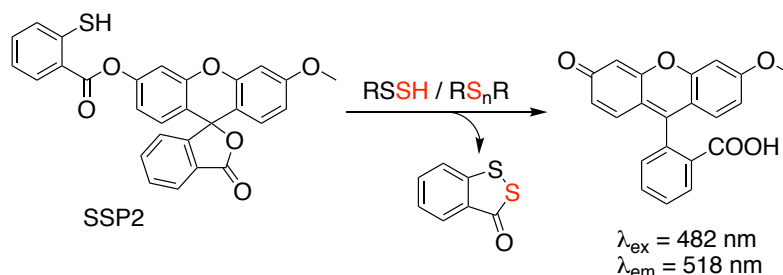
Scheme 4.1.6. A schematic diagram of the various reactive sulfur species formed when 3-MST-SS⁻, generated by reacting 3-MST and **25** is treated with GSH. Due to the short half-life of GS-SH under the reaction conditions, this species was detected as its bimane adduct by reacting it with monobromobimane (mBBr) (GSS-bimane [M+H]⁺ = 530.1379). H₂S was detected as its bis-S-bimane adduct ([M+H]⁺ = 415.144).



Scheme 4.1.7. A schematic for the generation of 3-MST polysulfide and its degradation products. GSSSG formed by the reaction of GSH with glutathione polysulfide (GS-S_nH) was also observed ([M+H]⁺ = 645.1319). In the presence of mBBr, formation of adducts GSS-bimane and bis-S-bimane as depicted above is also possible.

4.1.2.5. Detection of persulfide/polysulfide using the probe SSP2

The formation of persulfide/polysulfide was next studied using a fluorescent probe, SSP2.¹⁸ The probe reacts with sulfane sulfur to release fluorescein that produces a distinct fluorescent signal at 518 nm with excitation at 482 nm (Scheme 4.1.8).



Scheme 4.1.8. Release of fluorescein from SSP2 upon reaction with persulfides/polysulfides.

The probe was first validated by using GS-S_nH that was prepared as per a reported protocol.¹⁹ Briefly, 1 equivalent each of GSH, DEA/NO (sodium 2-(*N,N*-diethylamino)-diazene-2-oxide) and NaSH was reacted at room temperature for 20 min. Varying concentrations of GS-S_nH were subjected to SSP2 and incubated in the dark for 10 mins. Thereafter, the fluorescence signal corresponding to the release of fluorescein was measured using a microtiter plate reader (excitation 482 nm; emission 518 nm). A concentration dependent increase in fluorescence was observed (Figure 4.1.10). While the thiols GSH and *N*-acetyl cysteine did not produce any fluorescence signal, suggesting that fluorescein is released from SSP2 only when it reacts with persulfides/polysulfides.

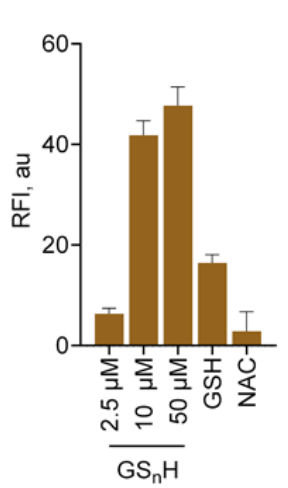


Figure 4.1.10. Validation of the probe SSP2 using varying concentrations of GS-S_nH. ($\lambda_{\text{ex}} = 482 \text{ nm}$; $\lambda_{\text{em}} = 518 \text{ nm}$)

Next, the ability of compound **25** to generate persulfides/polysulfides upon turnover by 3-MST was assessed. In the absence of a reducing agent such as DTT, 3-MST-SS⁻ can further

catalyze the turnover of **26** to **27**, likely forming a 3-MST polysulfide. Compound **25** was incubated with 3-MST in the presence of esterase at 37 °C in pH 7.4 tris-HCl buffer followed by incubation with SSP2 in the dark. A fluorescence emission spectrum was recorded using a fluorescence spectrophotometer (excitation 482 nm; emission 500 to 650 nm). A signal corresponding to the generation of fluorescein was observed under these conditions (Figure 4.1.11.a). A similar reaction was carried out in the presence of DTT, which would reduce the persulfide/polysulfide to H₂S, hence a diminished signal for fluorescence is expected. In the presence of DTT, a considerable quenching of the fluorescence signal was observed (Figure 4.1.11.b).

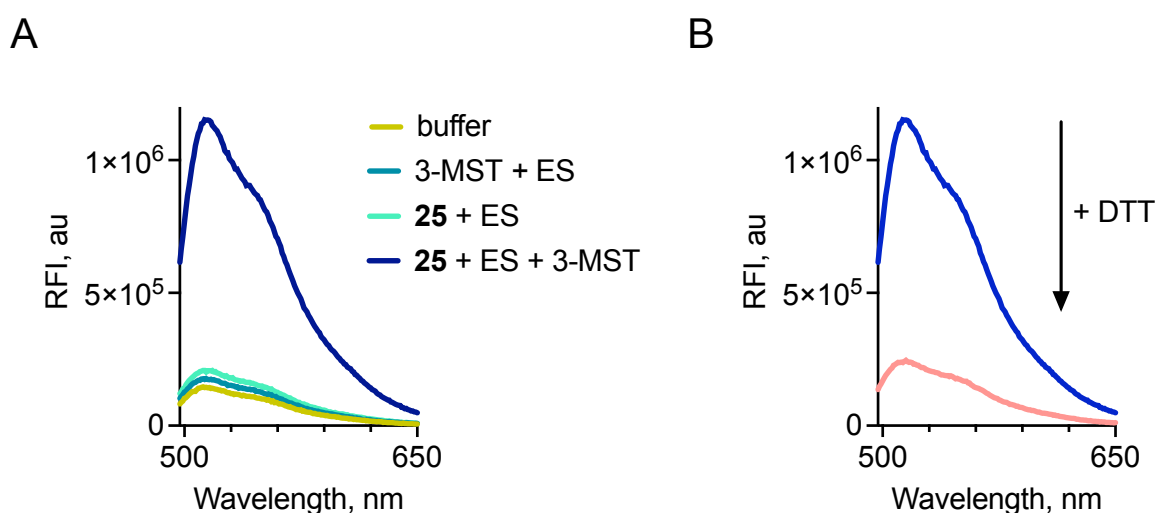


Figure 4.1.11. a) Persulfide/polysulfide detection using probe SSP2. Fluorescence emission spectra of SSP2 ($\lambda_{\text{ex}} = 482$ nm) upon treatment with 3-MST and **25** in the presence of esterase. b) Fluorescence quenching of SSP2 upon addition of DTT to the reaction sample containing 3-MST, **25** and esterase. A significant decrease in signal was observed likely due to the reduction of persulfide/polysulfide to the native thiol.

To further corroborate our results, varying concentrations of **25** was reacted with 3-MST in the presence of esterase followed by incubation with SSP2. The release of fluorescein was measured using a microtiter plate reader (excitation 482 nm; emission 518 nm). A dose dependent increase in fluorescence corresponding to the formation of persulfide/polysulfide was observed (Figure 4.1.12.). Treatment of the above reaction mixture with DTT, resulted in a diminished signal. Iodoacetamide (IAM) is widely used as a thiol blocking agent because of its propensity to react with thiols. The active site cysteine of 3-MST was blocked by pre-treatment with IAM followed by treatment with **25** + ES. A significantly diminished signal was recorded when **25** + ES was reacted with the IAM pre-treated 3-MST. This result was in accordance with the tag-switch assay where the cysteine mutant failed to generate the 3-MST-

SS⁻. Similar results were obtained with the positive control **24**. No significant fluorescence signal was observed from the negative controls **28** and **29** (Figure 4.1.12.).

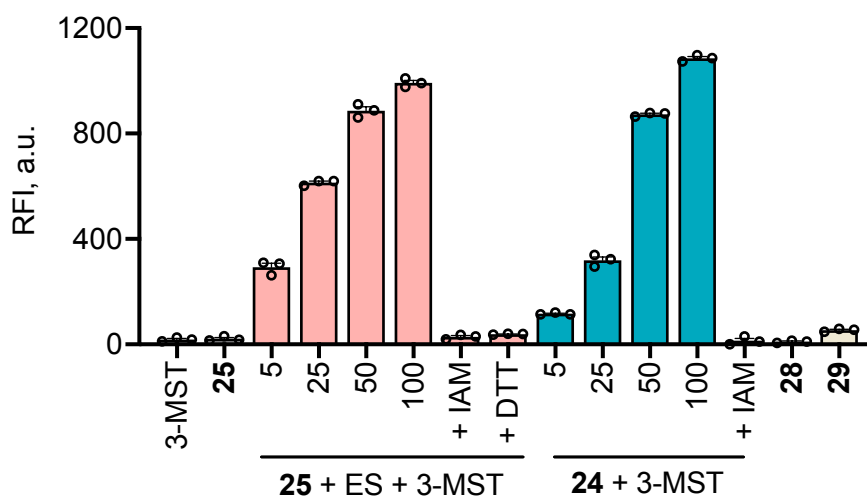
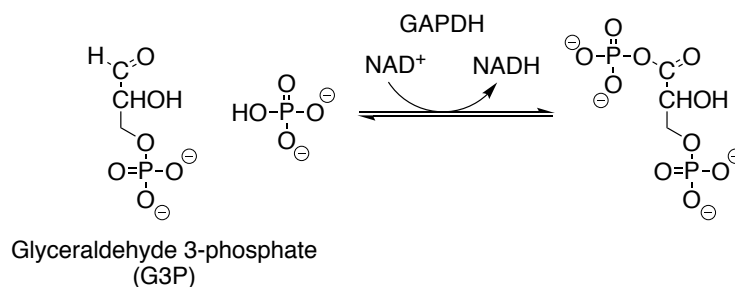


Figure 4.1.12. Persulfide/polysulfide detection using SSP2: 3-MST ctrl refers to 3-MST alone and **25** ctrl refers to **25** + ES only; **25** refers to co-incubation of varying concentrations of **25**, ES and 3-MST; +DTT: addition of DTT; +IAM: addition of iodoacetamide, an electrophile that reacts with thiols; **24** refers to incubation **24** with 3-MST; **28** and **29** refers to the incubation of the compounds with ES followed by treatment with 3-MST.

4.1.2.6. Activity of GAPDH

GAPDH is a redox sensitive protein involved in the glycolytic cycle, wherein the active site cysteine residue is susceptible to redox fluctuations. GAPDH was one of the first proteins to be detected in the persulfidated form,²⁰ however its influence on the activity of GAPDH have been subject to much debate. The activity of GAPDH is measured as a function of NADH formation while catalyzing the conversion of glyceraldehyde-3-phosphate (G3P) (Scheme 4.1.9.).²¹



Scheme 4.1.9. Reaction catalyzed by GAPDH.

The effect of persulfidation on the activity of GAPDH was next evaluated by utilizing the artificial substrate-3-MST system. 3-MST-SS⁻ once formed from treatment with **25** in the

presence of esterase should transfer the sulfane sulfur to the active site cysteine of GAPDH, thus persulfidating GAPDH.

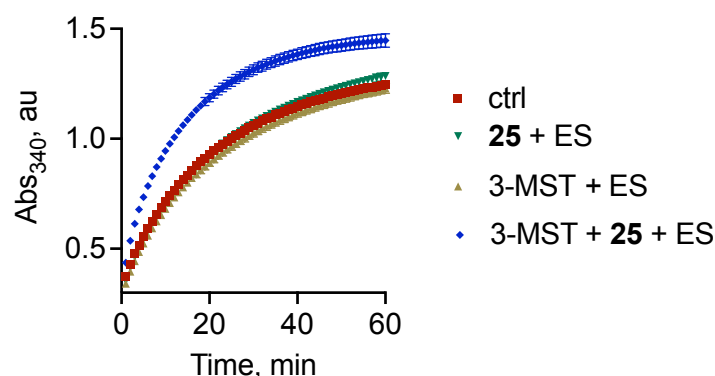


Figure 4.1.13. Activity of GAPDH was measured by monitoring the formation of NADH, real-time at 340 nm. A significant increment in the activity of GAPDH was observed when treated with 3-MST persulfide generated by reacting **25** with 3-MST in the presence of esterase (blue) compared to GAPDH alone (ctrl, red). GAPDH and ES were present across all groups.

To address this point, 3-MST-SS⁻ was prepared by incubating 3-MST with **25** for 1 h in the presence of esterase (1 U/mL). This was followed by addition of GAPDH and incubation for another 1 h. An aliquot of this reaction sample was then added to the GAPDH assay buffer consisting of G3P, sodium pyrophosphate and nicotinamide adenine dinucleotide (NAD⁺). The formation of NADH was spectrophotometrically monitored in real time by following its absorbance at 340 nm. Under these experimental conditions, the activity of GAPDH was found to be significantly enhanced upon treatment with 3-MST-SS⁻, when compared to untreated GAPDH (Figure 4.1.13.).

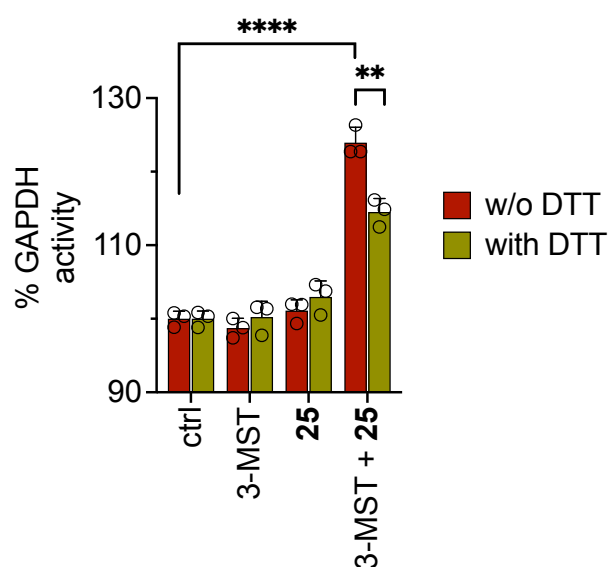


Figure 4.1.14. Each group was treated with 2 mM DTT following which the GAPDH activity was measured after 1 h. Addition of DTT to the reaction sample containing **25** and 3-MST led to a decrease

in the % activity of GAPDH. Ctrl represents GAPDH alone. GAPDH and ES were present across all groups. All data are presented as mean \pm SD (n =3/group). **p < 0.01 vs the sample w/o DTT, ****p < 0.0001 versus ctrl, by Student's two-tailed unpaired parametric *t*-test.

Further, upon treatment of the above reaction samples with 2 mM dithiothreitol (DTT), which would reduce the persulfide to the parent thiol, a reversal in the activity of GAPDH was observed (Figure 4.1.14.). Thus, persulfidation of the redox active cysteine thiol regulates the activity of the enzyme.

4.1.2.7. MTT assay for cell viability

After establishing the formation of 3-MST-SS⁻ when reacted with the artificial substrate **25** and the subsequent generation of persulfide/polysulfide, the cytotoxicity of **25** was evaluated using a standard MTT assay. Human lung carcinoma cell line (A549) was treated with varying concentrations of **25** and incubated for 24 h following which the MTT assay was performed to measure cell viability. The compound was found to be well tolerated by the cells for 24 h with no significant cytotoxicity even at 50 μ M (Figure 4.1.15.).

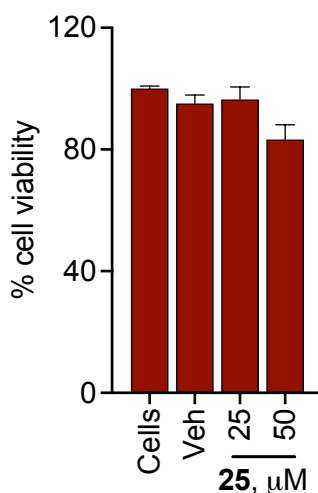


Figure 4.1.15. Compound **25** was tested for its cytotoxicity in A549 cell line using the MTT assay.

4.1.2.8. H₂S detection in A549 cells

Next, the ability of the artificial substrate **25** to permeate cells and feed in as a substrate for cellular 3-MST was assessed. The 3-MST-SS⁻ formed as an intermediate can transfer the sulfur to thiophilic acceptors such as thioredoxin or cysteine, subsequently undergoing reduction to eliminate H₂S (Figure 4.1.1.).³ Intracellular H₂S was detected in A549 cell line using a previously reported fluorescent probe for H₂S, NBD Fluorescein.²² H₂S upon reacting with the dye will release fluorescein which can be visualized using a fluorescence microscope.

An esterase sensitive COS/H₂S donor developed in our lab was used as a positive control (Figure 4.1.16.a).²³ When the cells were co-treated with COS/H₂S donor (50 μM) along with the probe (10 μM) for 1 h, an enhanced fluorescence signal was observed. Under similar conditions, compound **25** (100 μM) generated a strong fluorescence signal as well. The signal observed with the negative control **28** (100 μM) was significantly diminished, as expected (Figure 4.1.16.b). This suggests that compound **25** is cell permeable and can generate H₂S within cells.

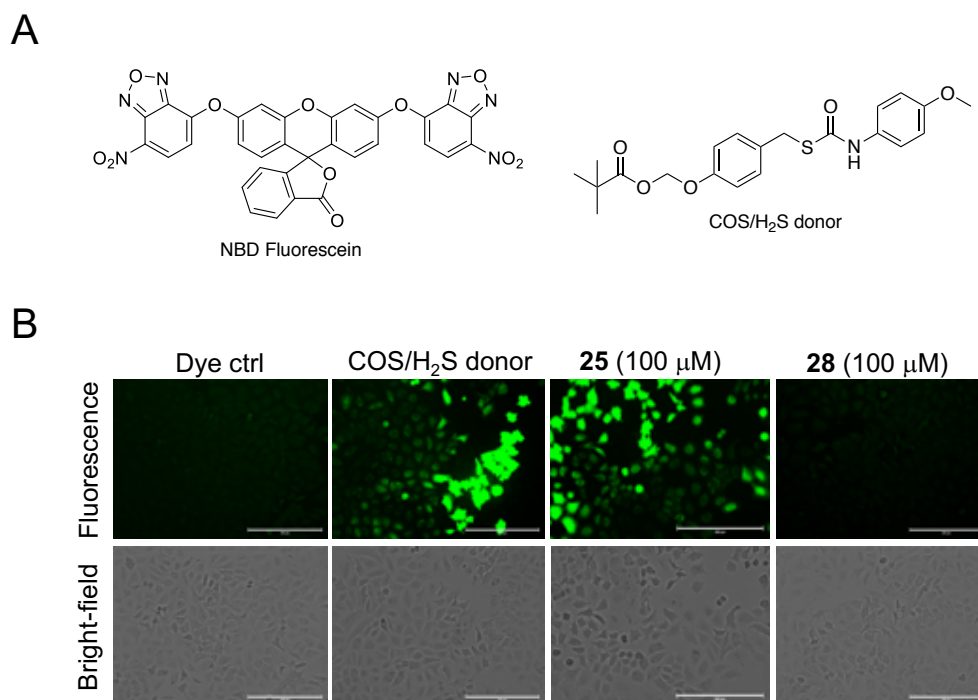


Figure 4.1.16. a) Structures of the reagents used. b) H₂S detection using the NBD-Fluorescein dye in A549 cells. The cells were imaged in the 20× GFP filter. Scale bar is 200 μm.

To further assess the selectivity of the compound towards 3-MST, a 3-MST knock down cell line was generated (3-MST KD) by introducing 3-MST shRNA in A549 cell line. The corresponding scrambled cell line with a non-targeting shRNA was used, wherein the levels of 3-MST has not been perturbed. The cell lines were provided by Ms. Kavya Gupta from Dr. Deepak Saini's lab in IISc Bangalore. When the cells were co-incubated with the COS/H₂S donor and NBD-fluorescein, an enhanced fluorescence signal was observed both in the scrambled as well as 3-MST KD cell line. However, a significantly diminished signal was observed when the 3-MST KD cell line was treated with compound **25**, compared to the scrambled cell line. Negative control **28** failed to produce a signal in either of the cell lines (Figure 4.1.17.). Collectively, the data suggests that H₂S generation from **25** was mediated by the enzyme 3-MST.

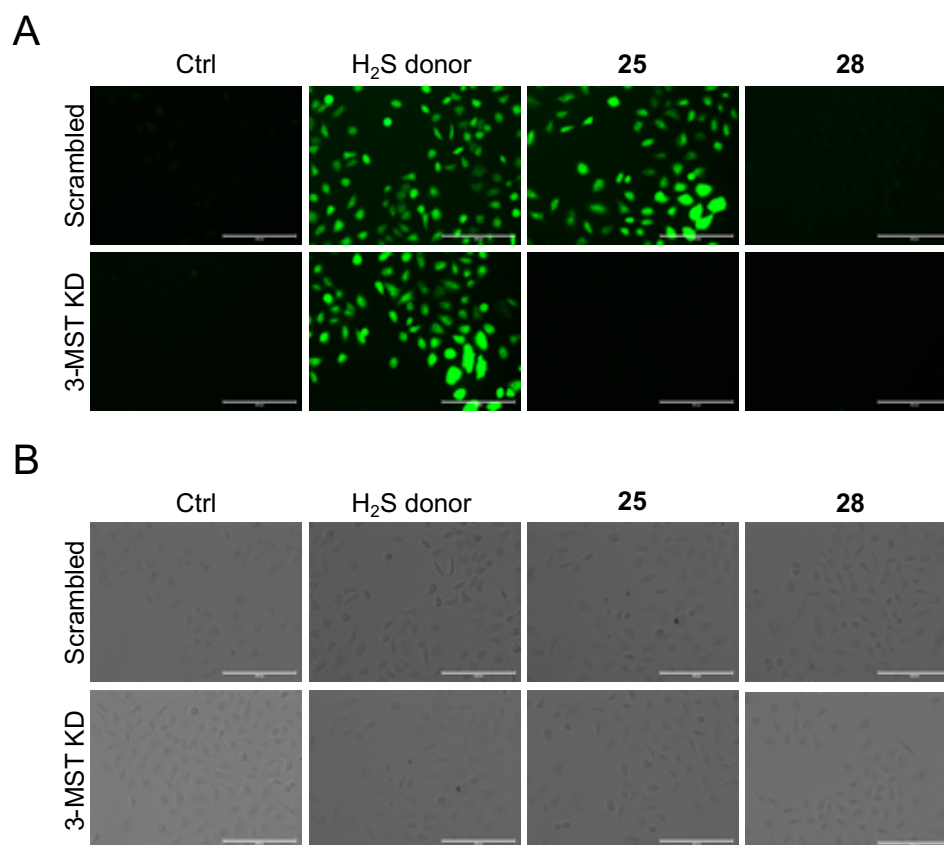


Figure 4.1.17. a) Detection of H₂S in 3-MST KD A549 cell line and the corresponding scrambled cell line using NBD fluorescein. Ctrl refers to untreated cells. Scale bar represents 200 μ m. b) Representative bright field images of H₂S detection using the NDB Fluorescein assay in scrambled and 3-MST KD A549 cells. Scale bar is 200 μ m.

4.1.2.9. Antioxidant effect of compound 25

4.1.2.9.1. Hydrogen peroxide (H₂O₂) quenching

Persulfides and polysulfides have been reported to have antioxidant properties and are more efficient in countering oxidative stress compared to its congeners.¹⁹ To test this, a reported ROS generator MGR-1 was used to induce oxidative stress in cells.²⁴ MGR-1 is an esterase activated prodrug of JCHD, that produces superoxide (Figure 4.1.18.a). Intracellular hydrogen peroxide (H₂O₂) levels were measured using a previously reported fluorescent probe TCF-B (Figure 4.1.18.a).²⁵ The boronate ester moiety in TCF-B is oxidized by H₂O₂ to release tricyanofuran (TCF) fluorophore that can be visualized using fluorescence microscopy. A549 cells were pre-treated with varying concentrations of **25** for 12 h followed by co-treatment with MGR-1 (25 μ M) and TCF-B (25 μ M) for 1 h. A similar experiment was carried out with the negative control **28**. A dose dependent quenching in fluorescence was observed, that was unperturbed in case of the negative control **28**. (Figure 4.1.18.b).

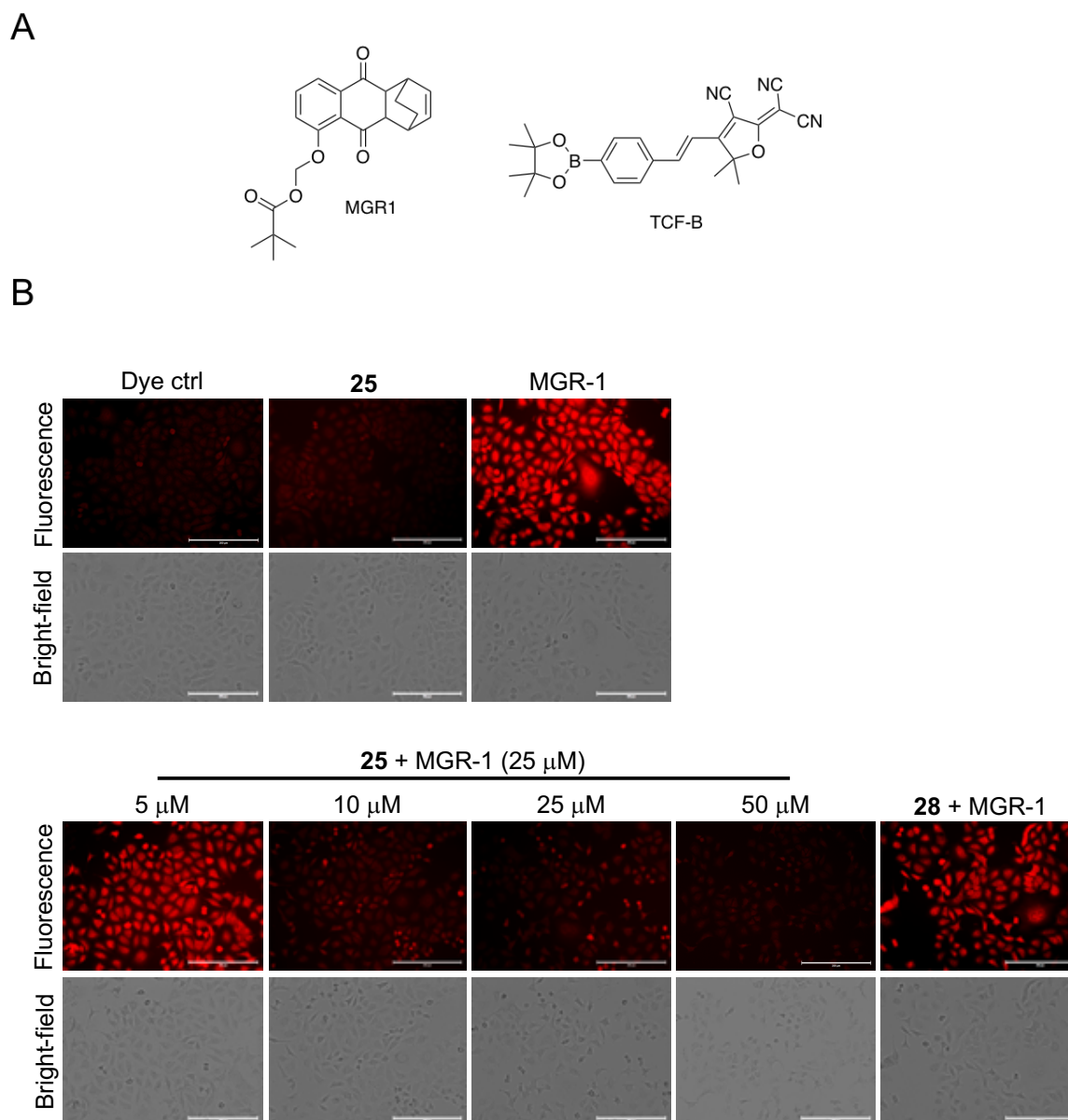


Figure 4.1.18. a) Structures of reagents used in the assay.

b) (TOP) A549 cells were treated with veh control (DMSO), **25** (50 μM) and MGR-1 (25 μM)

(BOTTOM) A549 cells treated with varying concentrations of **25** (5 μM , 10 μM , 25 μM and 50 μM) or **28** (50 μM) for 12 h followed by treatment with MGR-1 (25 μM). Intracellular H_2O_2 was detected using the H_2O_2 -sensitive turn-on fluorescence sensor TCF-B. Cells were imaged using a 20 \times TxRed filter. Scale bar is 200 μm .

4.1.2.9.2. Reduction of oxidative stress markers

NAD^+/NADH and GSSG/GSH ratio are important biomarkers of redox homeostasis in cells and are consequently used to measure cellular oxidative stress. Under oxidative stress conditions, the oxidized forms like GSSG and NAD^+ will be predominant and hence the ratios will be elevated. NAD^+/NADH and GSSG/GSH ratio were tested across three cell lines, lung

cancer cell line (A549), mouse embryonic fibroblasts (MEF) and mouse neuroblastoma cells (N2a) in the presence of the ROS generator MGR-1. Elevated levels of both NAD^+/NADH and GSSG/GSH ratio were observed. Upon pre-treatment of the cells with compound **25** for 12 h followed by treatment with MGR-1 for 1 h, a significant reduction in the levels of both these markers were recorded. A similar experiment conducted with compound **28** did not show any effect (Figure 4.1.19.).

Together, from both these experiments it can be concluded that mitigation of oxidative stress was mediated by persulfides generated from compound **25** upon turnover by cellular 3-MST.

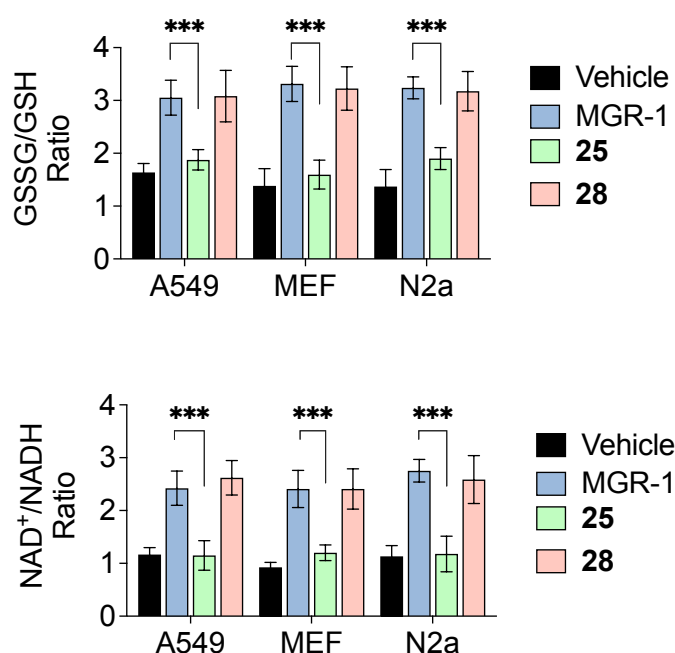


Figure 4.1.19. Biomarkers for oxidative stress: Three cell lines (A549, mouse embryonic fibroblasts (MEF) and N2a) were pretreated with vehicle, **25** or **28** and exposed to MGR-1 following which NAD^+/NADH ratio and GSSG/GSH ratio were determined using an ELISA assay. All data are presented as mean \pm SD (n = 5 per group). ***p < 0.001 vs MGR-1.

4.1.2.10. Cytoprotective effects of compound **25**

Upon determining the antioxidant properties of **25**, its ability to rescue cells from ROS induced cell death was next studied. **25** and **28** were first tested for its cytotoxicity profile in Mouse Embryonic Fibroblasts (MEFs) using a standard MTT assay. Both these compounds were observed to be well tolerated for a period of 24 h and no toxicity was observed up to a concentration of 50 μM (Figure 4.1.20.).

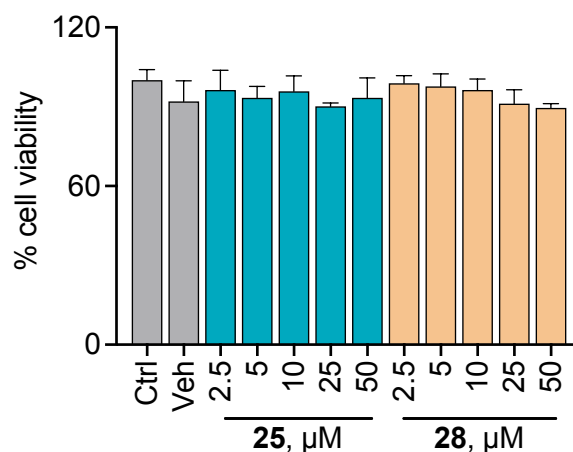


Figure 4.1.20. Cell viability assay conducted on mouse embryonic fibroblast (MEF) cells: Cells were treated with **25** or **28** and a standard cell viability assay was used to assess the number of viable cells after 24 h. No significant effect of **25** or **28** on MEF cell viability was observed. All data are presented as mean \pm SD (n=3/group).

MEF cells were then pre-treated with varying concentrations of **25** for 24 h following which the cells were treated with MGR-1 for 4 h. A dose dependent increase in cell viability was observed in cells pretreated with **25** against oxidative stress induced cytotoxicity. However, the negative control **28** had no effect against MGR-1 (Figure 4.1.21.). The above data implies the therapeutic potential of the artificial substrate **25**.

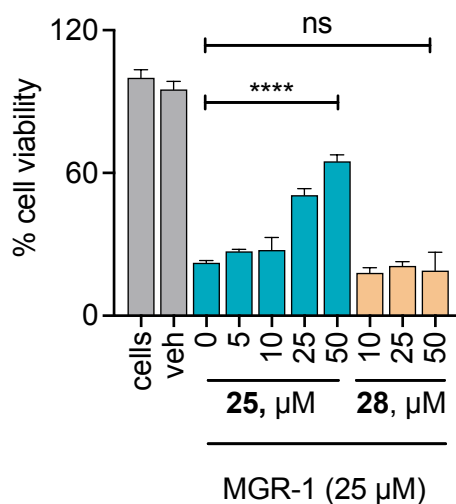


Figure 4.1.21. MEF cells were first treated with **25** or **28** followed by treatment with MGR-1, a known inducer of oxidative stress in cells. Dose-dependent protection of cells from MGR-1-induced cell death by **25** was observed. Negative control **6** did not show any significant cytoprotective effect under similar conditions. Student's two-tailed unpaired parametric *t*-test was carried out to determine significance: All data are presented as mean \pm SD (n=3/group). ****p < 0.0001 vs MGR-1; ns = non-significant versus MGR-1 only.

Persulfidation of key proteins such as parkin and GSK-3 β , involved in neurodegenerative diseases like Parkinsons disease and Alzheimers disease has been reported

to have protective effects via modulation of their catalytic activity. Additionally, 3-MST is the major enzyme contributing to the formation of H₂S and sulfane sulfur in the brain. Therefore, the potential of the artificial substrate **25** to exhibit neuroprotective effects were next tested. Neuro2A (N2a), a neuroblastoma cell line was used for this purpose. A cell viability assay conducted on N2a showed no potential toxicity of the compounds for a period of 12 h (Figure 4.1.22.).

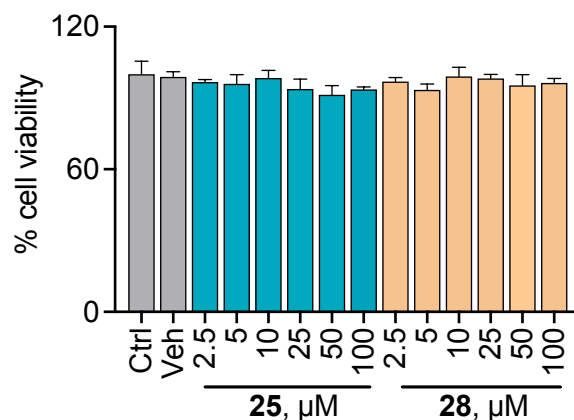


Figure 4.1.22. Cell viability assay carried out with substrate **25** as well as negative control **28** on N2a cells for 12 h. All data are presented as mean \pm SD (n=3/group).

Cells were then pre-treated with varying concentrations of **25** and the negative controls **27** and **28** for 12 h, followed by the ROS generator MGR-1 for 4 h. A dose dependent increase in cell viability was observed only with **25** and not the negative controls (Figure 4.1.23.).

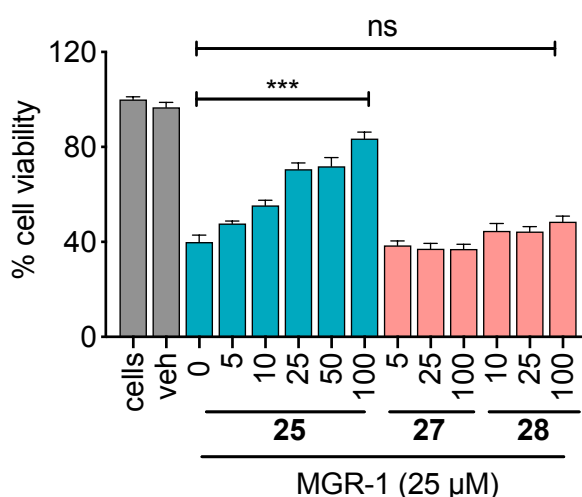


Figure 4.1.23. Cell viability assay conducted on N2a cells. A dose-dependent protection of cells from MGR-1 induced cell death by **25** was observed. The byproduct ketone **27** or the negative control **28** did not show any protection against the cytotoxic effects of MGR-1. All data are presented as mean \pm SEM (n = 3 per group). ***p < 0.001 vs MGR-1.

To further corroborate our results, an independent experiment with another ROS generator menadione was conducted. Similar results were obtained, thus demonstrating the neuroprotective effects of **25** (Figure 4.1.24.).

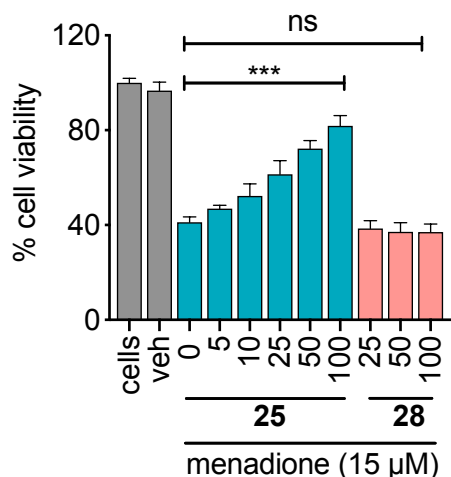


Figure 4.1.24. Cell viability assay conducted on N2a cells. Dose-dependent protection of cells from menadione-induced cell death by **25** was observed. Negative control **28** did not show any protective effect in this assay. All data are presented as mean \pm SD (n=3/group). ***p < 0.001 vs menadione; ns = non-significant compared to menadione only.

3.1.2.11. Mitigation of neuroinflammation

Persulfides/polysulfides have been reported to have anti-inflammatory effects.^{26,27} To evaluate the same, a mouse endotoxin shock model was used. First, C57BL/6J mice were intraperitoneally injected once daily with compound **25** for a period of 7 days and it was found to be well tolerated. Next, the mice were pre-treated with **25** for 4 h, followed by lipopolysaccharide (LPS) treatment and another dose of **25**. *in vivo* studies were conducted by Dr. Shubham Singh from Dr. Siddhesh Kamat's group in Dept. of Biology, IISER Pune. Proinflammatory cytokines and prostaglandins were measured in the brain tissue of these mice. In the control group treated with LPS alone, significantly elevated levels of cytokines TNF- α and IL-6 were found, compared to the vehicle-treated mice. In the group pre-treated with **25**, a marked decrease in the levels of cytokines were observed, whereas NaSH failed to exhibit similar effects (Figure 4.1.25.a).

LPS is known to induce the production of pro-inflammatory prostaglandins (PG). PGE₂ is one of the most abundant PG produced during inflammation and is an important mediator of several biological functions.²⁸ PGD₂ on the other hand is an isomer of PGE₂ and is synthesized

primarily in the brain where it is involved in the regulation of various activities of the central nervous system.²⁹ Hence, PGE₂/PGD₂ levels can be used as a reliable marker for inflammation. LC/MS analysis of brain tissue homogenates were carried out to measure the levels of PGE₂/PGD₂. A similar result was obtained wherein, the levels were significantly lower in groups pre-treated with **25** compared to LPS only treatment (Figure 4.1.25.b). These results collectively demonstrate the potential of **25** to mitigate neuroinflammation.

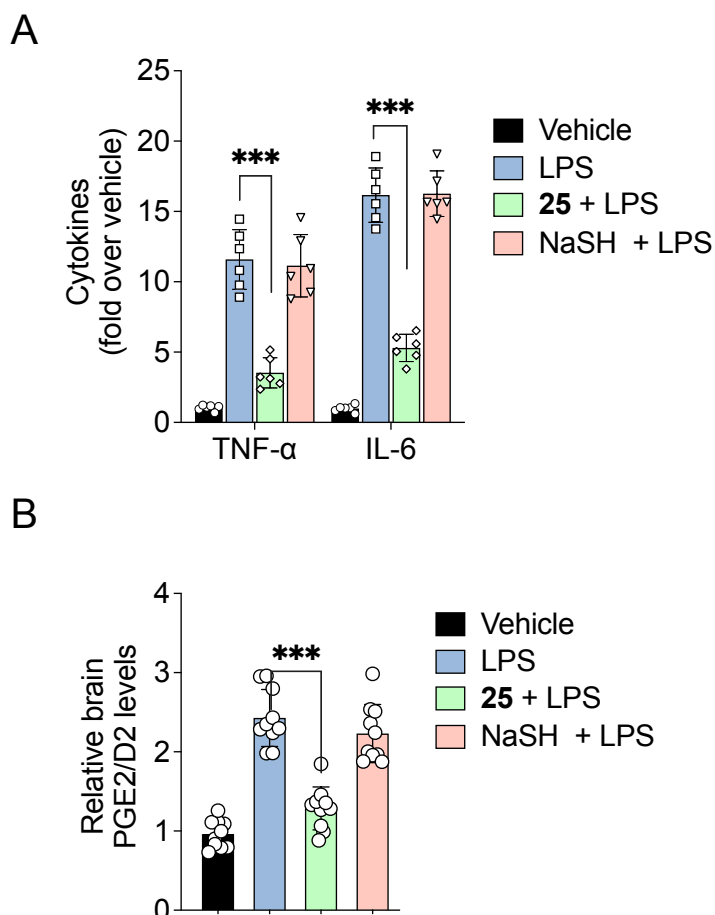


Figure 4.1.25. Mouse endotoxin shock model: Animals were treated with **25** (20 mg/kg) or NaSH (20 mg/kg) 4 h prior to treatment with lipopolysaccharide (LPS, 5 mg/kg). 30 min post-administration of LPS, another dose of **25** or NaSH was given. The brain tissue samples were harvested followed by measurement of: (A) Pro-inflammatory cytokines, TNF- α and IL-6 using a standard ELISA assay. All data are presented as mean \pm SD (n = 6 per group). ***p < 0.001 vs LPS; and (B) Prostaglandins PGE₂/D₂ using LC/MS. All data are presented as mean \pm SD (n = 10 per group). ***p < 0.001 vs LPS.

PGs generation is significantly elevated during inflammation and contributes to the development of the signs of inflammation. LPS, a component of the gram-negative bacteria induces the expression of cytosolic phospholipase A₂ (PLA₂). Arachidonic acid (AA) is then released from the cell membrane, catalyzed by PLA₂ which can then be converted to cyclic

endoperoxides PGH_2 by COX enzymes, leading to the downstream production of pro-inflammatory prostaglandins.²⁸ While COX-1 is a housekeeping enzyme, COX-2 is an inducible enzyme, induced by inflammatory stimuli. Several reports suggest that H_2S -NSAID hybrids can exhibit potent anti-inflammatory effects by inhibiting the expression of COX-2, leading to the inhibition of PG production (Figure 4.1.26).³⁰

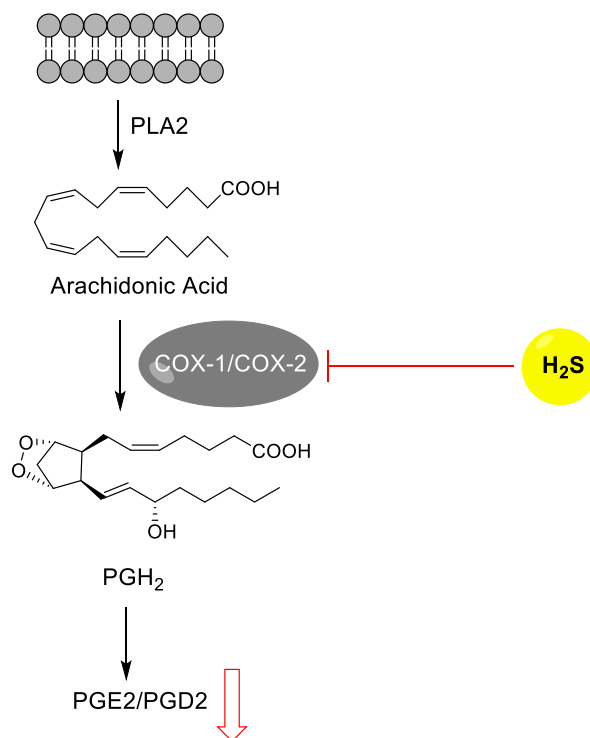


Figure 4.1.26. Mechanistic insights into pro-inflammatory prostaglandins formation.

4.1.3. Summary

In conclusion, 3-MST is a key enzyme that regulates the sulfane sulfur pool, especially in the brain. Herein, we have developed an artificial substrate, **25** which upon deprotection by esterase will generate the active compound **26**. The sulfur from **26** will be accepted by the active site cysteine of 3-MST, forming a 3-MST persulfide intermediate and acetophenone (**27**) as the byproduct. A reported tag-switch technique was used to detect the formation of the 3-MST-SS⁻, which was not observed upon mutation of the active site cysteine, a C238A mutant of 3-MST. Persulfidation of target proteins or thiols can be induced by sulfur transfer from **25** via 3-MST and under these conditions, GSH was found to be persulfidated as detected by an LC/MS based technique. Change in the activity of GAPDH mediated by persulfidation was next evaluated wherein, the activity of GAPDH was found to be significantly enhanced. A

reversal in activity was noted upon subsequent incubation with DTT, a reducing agent. The substrate **25** was found to be well tolerated by cells and was capable of producing H₂S in human lung carcinoma, A549 cells. The selectivity of the artificial substrate **25** towards 3-MST was further validated by using a 3-MST KD cell line, where **25** failed to produce H₂S. Mitigation of oxidative stress by **25** was demonstrated in multiple cell lines. Additionally, **25** was able to rescue cells from ROS induced lethality as demonstrated in two different cell lines. Finally, **25** was shown to alleviate inflammation in a mouse endotoxin shock model.

4.1.4. Experimental Section

4.1.4.1. Synthesis and characterization of data

Compounds **24**⁶ and **28**¹⁴ were synthesized as per previously reported protocol.

4.1.4.2. Tag-Switch technique for persulfidation of 3-MST

Stock solutions of compounds, MSBT-A and CN-biotin were prepared in DMSO. To 100 μ L of 3-MST (0.4 mg/mL; wt or C238A mutant) were added compounds (2 μ L of 10 mM stock) followed by addition of 1 U/mL esterase (10 μ L of 100 U/mL stock) and incubated for 1 h. This was followed by addition of 10 μ L of 25% SDS (sodium dodecyl sulfate) and MSBT-A (6 μ L of 200 mM stock) and further incubated for 30 min at 37 °C. The reaction mixtures were desalted using Amicon centrifugal filters. The residues were collected and treated with CN-biotin (4 μ L of 50 mM stock) and incubated for 1 h at 37 °C. The reaction mixtures were desalted again using Amicon centrifugal filters.

The residues were collected, mixed with 4 \times Laemmli Buffer and resolved on a 12% polyacrylamide gel. Proteins were then transferred onto a PVDF membrane, blocked using 3% BSA for 1 h and incubated overnight at 4 °C with anti-biotin antibody produced in goat followed by HRP-conjugated anti-goat secondary antibody. The signal was visualized using Advansta WestBright ECL chemiluminescent HRP substrate.

4.1.4.3. Persulfide/polysulfide measurement using SSP2:^{18,19}

GS_nH was prepared by reacting 10 mM GSH, 10 mM DEA/NO (sodium 2-(*N*, *N*-diethylamino)-diazene-2-oxide) and 10 mM NaSH at room temperature for 20 min.

Stock solutions of **25** (10 mM), **24** (10 mM), **28** (10 mM), **29** (10 mM) and SSP2 (5 mM) were prepared in DMSO. DTT (100 mM), iodoacetamide (IAA, 100 mM) and esterase (100 U/mL) were prepared in DI water. The reaction mixture was prepared by adding 10 μ M 3-MST (30 μ L, 106 μ M stock), **24** or **25**, **28**, **29** along with 1 U/mL esterase (3 μ L, 100 U/mL stock) and the volume was adjusted to 300 μ L using 20 mM tris-HCl pH 7.4 buffer. The reaction was incubated for 30 min at 37 °C.

A similar reaction was set up wherein the above reaction mixture was treated with 10 mM DTT (30 μ L of 100 mM stock) after 30 min and further incubated at 37 °C for 30 min.

In a separate group, 3-MST was pre-incubated with 1 mM IAA (3 μ L, 100 mM stock) for 30 min followed by addition of 100 μ M **25** or 100 μ M **24** and 1U/mL esterase. The reaction was incubated for 30 min at 37 °C.

The above treatment groups were finally incubated with 50 μ M SSP2 (3 μ L, 5 mM) at 37 °C for 10 min in the dark. 200 μ L aliquot of each sample were transferred to a 96 well plate and the fluorescence was recorded ($\lambda_{\text{ex}} = 482$ nm, $\lambda_{\text{em}} = 518$ nm) using a microplate reader (Thermo Scientific VarioskanFlash).

4.1.4.4. Persulfide/polysulfide measurement using LC/MS:¹⁹ Stock solutions of **25** (10 mM), **28** (10 mM) and **29** (10 mM) were prepared in DMSO. GSH (10 mM) and esterase (100 U/mL) were prepared in DI water. The reaction mixture was prepared by adding 10 μ M 3-MST (10 μ L, 106 μ M stock), **25**, **28** or **29** along with 1U/mL esterase (1 μ L, 100 U/mL) and the volume was adjusted to 100 μ L using 20 mM tris-HCl pH 7.4 buffer. The reaction mixture was incubated for 30 min at 37 °C. 1 mM GSH (10 μ L of 10 mM) was then added and incubated at 37 °C for 30 min. 50 μ L aliquot of the above reaction samples were added to a 50 μ L methanol solution of 20 mM monobromobimane (mBBBr, final concentration 10 mM) and incubated in the dark at 37 °C for 15 min. The samples were centrifuged at 10000g for 10 min at 4 °C and the supernatants were collected and assessed thereafter by LC/MS. All measurements were done using a previously established LC/MS method¹⁹ in the positive ion mode using high resolution multiple reaction monitoring (MRM-HR) analysis on a Sciex X500R quadrupole time-of flight (QTOF) mass spectrometer fitted with an Exion UHPLC system using a Kinetex 2.6 mm hydrophilic interaction liquid chromatography (HILIC) column with 100 Å particle size, 150 mm length and 3 mm internal diameter (Phenomenex). Nitrogen was the nebulizer gas, with the nebulizer pressure set at 50 psi. The MRM-HR mass spectrometry parameters for measuring polysulfides are: GSS-bimane precursor ion mass (Q1, M + H⁺) = 530, product ion mass (Q3, M + H⁺) = 192, declustering potential = 130 V, entrance potential = 10 V, collision energy = 33 V, and collision exit potential = 10 V; GSSSG precursor ion mass (Q1, M + H⁺) = 645, product ion mass (Q3, M + H⁺) = 387, declustering potential = 170 V, entrance potential = 10 V, collision energy = 21 V, and collision exit potential = 10 V; bis-S-bimane precursor ion mass (Q1, M + H⁺) = 415, product ion mass (Q3, M + H⁺) = 193, declustering potential = 130 V, entrance potential = 10 V, collision energy = 13 V, and collision exit potential = 10 V.

4.1.4.5. GAPDH activity:^{20,31} 1 mg/mL stock of GAPDH was prepared in pH 7.4 phosphate buffer (50 mM). The GAPDH was reduced by incubating it with 10 mM DTT for 1 h at room temperature. The DTT was removed by desalting using Amico Ultracel 10K tube and washing with phosphate buffer. Finally, the concentration of GAPDH was adjusted to 1 mg/mL.

The reaction mixture was prepared by adding 2 μ M 3-MST (20 μ L, 32 μ M stock), 200 μ M **25** (6 μ L, 10 mM), 1U/mL esterase (3 μ L, 100 U/mL) and the final volume was adjusted to 300 μ L using pH 7.4 phosphate buffer (50 mM). After 30 min of incubation at 37 °C, 20 μ g/mL GAPDH (5.6 μ L, 1 mg/mL) was added and further incubated at 37 °C for 30 min. GAPDH activity was studied as described below. GAPDH activity was tested using a previously reported protocol.²³ Briefly, 100 μ L aliquot of each treatment group was mixed with equal volume of GAPDH assay buffer. GAPDH assay buffer is constituted of 20 mM tris-HCl buffer (pH 7.8), 100 mM NaCl, 0.1 mg/mL bovine serum albumin (BSA), 20 mM sodium arsenate, 10 mM sodium pyrophosphate, 6 mM glyceraldehyde-3-phosphate and 1 mM NAD⁺ (nicotinamide adenine dinucleotide). The formation of NADH was monitored spectrophotometrically in real time at 340 nm and 37 °C using a microplate reader (Thermo Scientific VarioskanFlash).

For the experiment carried out with DTT, all reaction conditions were similar, except that 150 μ L aliquot from the standard reaction mixture was taken and treated with 2 mM DTT (3 μ L, 100 mM) and incubated at 37 °C for 1 h. 100 μ L of this reaction mixture was used for further analysis.

4.1.4.6. H₂S imaging in cells using NBD fluorescein:²² A549 scrambled and 3-MST KD cells were seeded in a 12-well plate with 10⁴ cells/well in DMEM media supplemented with 10% FBS and 1% antibiotic solution and incubated in an atmosphere of 5% CO₂ at 37 °C for 48 h. After incubation, the old media was removed and the cells were washed with 1 mL of sterile 1 \times PBS. This was followed by the addition of 1 mL fresh DMEM media. The cells were co-treated with a COS/H₂S donor (50 μ M) or the artificial substrate **25** (100 μ M) and NBD-fluorescein dye (10 μ M) in both the cell lines and were incubated at 37 °C for 1 h. After 1 h, cells were washed twice with 1 \times PBS and then imaged on an EVOS fluorescence microscope using 20x GFP (green fluorescence protein) filter.

4.1.4.7. Cell viability assay: A549 cells, mouse embryonic fibroblasts (MEFs) and mouse neuroblastoma cells (N2a) were seeded at a concentration of 1 \times 10⁴ cells/well overnight in a

96-well plate in complete DMEM media. Following this, the cells were exposed to varying concentrations of the compounds. Stock solutions of compounds were prepared in DMSO and the final concentration of DMSO did not exceed 0.5%. The cells were incubated for 12 h or 24 h at 37 °C. A 0.5 mg/mL stock solution of 3-(4, 5-dimethylthiazol-2-yl)-2, 5-diphenyl tetrazolium bromide (MTT) was prepared in DMEM. After incubation, the old media from the cells were removed, 100 µL of the MTT stock was added to each well and incubated for 4 h at 37 °C. After 4 h incubation, the media was carefully removed and 100 µL of DMSO was added. Spectrophotometric analysis of each well at 570 nm using a microplate reader (Thermo Scientific Varioskan) was carried out to estimate cell viability.

4.1.4.8. ROS quenching: A549 cells were seeded in a 12-well plate with 10^5 cells/well in Roswell Park Memorial Institute (RPMI) medium supplemented with 10% FBS and 1% antibiotic solution and incubated in an atmosphere of 5% CO₂ at 37 °C for 48 h. The cells were treated with **25** (0, 10, 25 and 50 µM) or **28** (50 µM) and incubated for 12 h at 37 °C after which MGR-1 (25 µM) and TCF-B (25 µM) were co-incubated for 1 h. After 1 h, the media was removed, cells were washed twice with 1× PBS and the cells were imaged on an EVOS fluorescence microscope using a 20x TxRed filter.

4.1.4.9. Measuring intracellular GSSG/GSH and NAD⁺/NADH: A549, MEF and N2a cells were grown in 100 mm petri plates in an atmosphere of 5% CO₂ at 37 °C. The cells were pre-treated with compounds **25** (50 µM) or **28** (50 µM) for 12 h followed by treatment with MGR-1 (25 µM) for 1 h. Each group had 5 replicates. The cells from each treatment groups were harvested and the ratio of GSSG/GSH and NAD⁺/NADH was measured using ELISA kits from Abcam (ab239709 for GSSG/GSH and ab65348 for NAD⁺/NADH) as per manufacturer's protocol.

4.1.4.10. Protection from oxidative stress:

MEF cells: MEF were seeded in a 96-well plate with 10^4 cells/well in DMEM media supplemented with 10% FBS (fetal bovine serum) and 1% antibiotic solution and incubated in an atmosphere of 5% CO₂ at 37 °C for 16 h. Stock solutions of compounds were prepared in DMSO with final concentration of DMSO not exceeding 0.5%. After 16 h, the cells were pre-treated with different concentrations of the compound for 24 h followed by treatment with MGR-1 (25 µM). The cells were incubated for 4 h at 37 °C following which the media was removed and MTT assay was carried out as described above to determine cell viability.

N2a cells: N2a were seeded in a 96-well plate with 2.5×10^4 cells/well in DMEM media supplemented with 10% FBS (fetal bovine serum) and 1% antibiotic solution and incubated in an atmosphere of 5% CO₂ at 37 °C for 24 h. Stock solutions of compounds were prepared in DMSO with final concentration of DMSO not exceeding 0.5%. After 24 h, the cells were pre-treated with different concentrations of the compound for 12 h followed by treatment with menadione (15 μM) or MGR-1 (25 μM). The cells were incubated for 4 h at 37 °C following which the media was removed MTT assay was performed as described above to determine cell viability.

4.1.4.11. Mice studies: This experiment was conducted by Dr. Shubham Singh from Dr. Siddhesh Kamat's lab in IISER Pune. All mouse studies described in the manuscript received formal approval from the Indian Institute of Science Education and Research, Pune-Institutional Animal Ethics Committee (protocol no: IISER_Pune IAEC/2019_2/07), constituted as per the guidelines outlined by the Committee for the Purpose of Control and Supervision of Experiments on Animals (CPCSEA), Government of India. All mice were maintained at National Facility for Gene Function in Health and Disease (NFGFHD) at IISER Pune, supported by a grant from the Department of Biotechnology, Govt. of India (BT/INF/22/SP17358/2016). All mice used in the study were generated by breeding wild type C57BL/6J mice and had *ad libitum* access to water and food. All mice used for experiment were age and gender matched. For compound toxicity studies in mice, the test compound was intraperitoneally injected at 20 mg/kg body weight (o.d.) for 7 days and the mice were monitored for any changes in their routine cage behavior. After 7 days, all mice were euthanized, their tissues were harvested, and examined for any signs of inflammation and/or toxicity. For the experiments where neuroinflammation was studied, an intraperitoneal injection of lipopolysaccharide (LPS) in 1× PBS (vehicle) at a dose of 5 mg/kg body weight was used to generate systemic inflammation. The test compounds (NaSH or **25**) were also injected intraperitoneally in two doses – the first at 20 mg/kg body weight 4 h before the LPS administration and second dose of 20 mg/kg body weight 30 min after the LPS administration, following which, the mice were kept overnight.

4.1.4.11.1 Prostaglandin extraction and measurements: Mice were deeply anesthetized with isoflurane and euthanized by cervical dislocation. The brains of the mice were dissected within 15 s post decapitation, divided into two sagittal equal halves, weighed, washed with cold phosphate buffered saline (PBS) and flash frozen in liquid nitrogen. The prostaglandins were extracted and measured using protocols described previously.^{24,32} Briefly, half brains

were re-suspended in 2 mL cold 1× PBS and the lipids from them were extracted using 6 mL of 1:1 (vol/vol) ethyl acetate: hexane containing 1 nmol of 17:1 free fatty acid (FFA) (internal standard) per sample by dounce homogenization. The resulting mixture was vortexed vigorously and centrifuged at 2,500 g for 15 min to separate the aqueous and organic layers. Thereafter, the top (organic) layer containing the lipids (prostaglandins) was collected in a glass vial and dried under an inert N₂ stream at room temperature. Dried extracts were re-solubilized in 200 µL of 2:1 (v/v) chloroform: methanol (MeOH), and 20 µL was injected into liquid chromatography coupled mass spectrometry (LC/MS) instrument for prostaglandin measurements. All the prostaglandin measurements were done as per as previously established multiple reaction monitoring high resolution (MRM-HR) methods⁷ set on Sciex X500R QTOF mass spectrometer coupled to an Exion-series UHPLC with a quaternary pump. Briefly, the lipids were separated using a Gemini 5U C18 Phenomenex column (5 µm, 50 × 4.6 mm) using LC solvents as follows: Solvent A: 95:5 (v/v) water: MeOH + 0.1% (vol/vol) ammonium hydroxide and Solvent B: 60:35:5 (v/v/v) isopropanol: MeOH: water + 0.1 % (vol/vol) ammonium hydroxide. The LC runs were for 30 min with gradient of 0% solvent B for 5 min, linear gradient of solvent B (0% to 100%) for 20 min followed by 100% solvent B for 5 min all at a flow rate of 0.3 mL per min. MS was calibrated in negative mode and samples were analyzed with the following parameters: Mode: Electrospray ionization (ESI), curtain gas 1 = 60 psi, curtain gas 2 = 40 psi, ion spray voltage = - 4.5 kV, and temperature = 500 °C. All quantifications were done by normalizing the metabolite area under the curve to the area under the curve for the internal standard, followed by normalization to weight of the tissue.

4.1.4.11.2. Measurement of cytokines: One half of the brains were re-suspended in 2 mL cold 1× PBS and homogenized using dounce homogenization. The protein in each sample was estimated using Bradford assay and was finally adjusted to 1 mg/mL in each sample. The cytokines in each samples were measured using an ELISA kit.

4.1.5. References

- (1) Nagahara, N., Multiple role of 3-mercaptopyruvate sulfurtransferase: antioxidative function, H₂S and polysulfide production and possible SO_x production. *Br. J. Pharmacol.* **2018**, *175* (4), 577–589.
- (2) Nagahara, N.; Yoshii, T.; Abe, Y.; Matsumura, T., Thioredoxin-dependent Enzymatic Activation of Mercaptopyruvate Sulfurtransferase: an intersubunit disulfide bond serves as a redox switch for activation. *J. Biol. Chem.* **2007**, *282* (3), 1561–1569.
- (3) Yadav, P. K.; Yamada, K.; Chiku, T.; Koutmos, M.; Banerjee, R., Structure and kinetic analysis of H₂S production by human mercaptopyruvate sulfurtransferase. *J. Biol. Chem.* **2013**, *288* (27), 20002–20013.
- (4) Kimura, Y.; Koike, S.; Shibuya, N.; Lefer, D.; Ogasawara, Y.; Kimura, H., 3-Mercaptopyruvate sulfurtransferase produces potential redox regulators cysteine- and glutathione-persulfide (Cys-SSH and GSSH) together with signaling molecules H₂S₂, H₂S₃ and H₂S. *Sci. Rep.* **2017**, *7* (1), 10459.
- (5) Nagahara, N.; Katayama, A., Post-translational Regulation of Mercaptopyruvate Sulfurtransferase via a Low Redox Potential Cysteine-sulfenate in the Maintenance of Redox Homeostasis. *J. Biol. Chem.* **2005**, *280* (41), 34569–34576.
- (6) Nagasawa, H. T.; Goon, D. J. W.; Crankshaw, D. L.; Vince, R.; Patterson, S. E., Novel, Orally Effective Cyanide Antidotes. *J. Med. Chem.* **2007**, *50* (26), 6462–6464.
- (7) Ikeuchi, Y.; Shigi, N.; Kato, J.-I.; Nishimura, A.; Suzuki, T., Mechanistic insights into sulfur relay by multiple sulfur mediators involved in thiouridine biosynthesis at tRNA wobble positions. *Mol. Cell* **2006**, *21* (1), 97–108.
- (8) Mueller, E. G., Trafficking in persulfides: delivering sulfur in biosynthetic pathways. *Nat. Chem. Biol.* **2006**, *2*, 185.
- (9) Crawhall, J. C.; Parker, R.; Sneddon, W.; Young, E. P.; Ampola, M. G.; Efron, M. L.; Bixby, E. M., Beta Mercaptolactate-Cysteine Disulfide: Analog of Cystine in the Urine of a Mentally Retarded Patient. *Science* **1968**, *160* (3826), 419–420.
- (10) Nagahara, N.; Nagano, M.; Ito, T.; Shimamura, K.; Akimoto, T.; Suzuki, H., Antioxidant enzyme, 3-mercaptopyruvate sulfurtransferase-knockout mice exhibit increased anxiety-like behaviors: a model for human mercaptolactate-cysteine disulfiduria. *Sci. Rep.* **2013**, *3*, 1986.
- (11) Coletta, C.; Módis, K.; Szczesny, B.; Brunyánszki, A.; Oláh, G.; Rios, E. C. S.; Yanagi, K.; Ahmad, A.; Papapetropoulos, A.; Szabo, C., Regulation of Vascular Tone,

- Angiogenesis and Cellular Bioenergetics by the 3-Mercaptopyruvate Sulfurtransferase/H₂S Pathway: Functional Impairment by Hyperglycemia and Restoration by dl- α -Lipoic Acid. *Mol. Med.* **2015**, *21* (1), 1–14.
- (12) Liénard, B. M. R.; Garau, G.; Horsfall, L.; Karsisiotis, A. I.; Damblon, C.; Lassaux, P.; Papamicael, C.; Roberts, G. C. K.; Galleni, M.; Dideberg, O.; Frère, J.-M.; Schofield, C. J., Structural basis for the broad-spectrum inhibition of metallo- β -lactamases by thiols. *Org. Biomol. Chem.* **2008**, *6* (13), 2282–2294.
- (13) Hatanaka, T.; Yuki, R.; Saito, R.; Sasaki, K., α -Methylphenacyl thioesters as convenient thioacid precursors. *Org. Biomol. Chem.* **2016**, *14* (45), 10589–10592.
- (14) Crank, G.; Khan, H. R. *Formation of Thioamide Derivatives from Reactions of Isothiocyanates with Oxazol-2-amines*; 1985; Vol. 38.
- (15) Zhang, D.; Macinkovic, I.; Devarie-Baez, N. O.; Pan, J.; Park, C.-M.; Carroll, K. S.; Filipovic, M. R.; Xian, M., Detection of Protein S-Sulfhydration by a Tag-Switch Technique. *Angew. Chemie Int. Ed.* **2014**, *53* (2), 575–581.
- (16) Wedmann, R.; Onderka, C.; Wei, S.; Szijártó, I. A.; Miljkovic, J. L.; Mitrovic, A.; Lange, M.; Savitsky, S.; Yadav, P. K.; Torregrossa, R.; Harrer, E. G.; Harrer, T.; Ishii, I.; Gollasch, M.; Wood, M. E.; Galardon, E.; Xian, M.; Whiteman, M.; Banerjee, R.; Filipovic, M. R., Improved tag-switch method reveals that thioredoxin acts as depersulfidase and controls the intracellular levels of protein persulfidation. *Chem. Sci.* **2016**, *7* (5), 3414–3426.
- (17) Shibuya, N.; Tanaka, M.; Yoshida, M.; Ogasawara, Y.; Togawa, T.; Ishii, K.; Kimura, H., 3-Mercaptopyruvate Sulfurtransferase Produces Hydrogen Sulfide and Bound Sulfane Sulfur in the Brain. *Antioxid. Redox Signal.* **2009**, *11* (4), 703–714.
- (18) Chen, W.; Liu, C.; Peng, B.; Zhao, Y.; Pacheco, A.; Xian, M., New fluorescent probes for sulfane sulfurs and the application in bioimaging. *Chem. Sci.* **2013**, *4* (7), 2892.
- (19) Ida, T.; Sawa, T.; Ihara, H.; Tsuchiya, Y.; Watanabe, Y.; Kumagai, Y.; Suematsu, M.; Motohashi, H.; Fujii, S.; Matsunaga, T.; Yamamoto, M.; Ono, K.; Devarie-Baez, N. O.; Xian, M.; Fukuto, J. M.; Akaike, T., Reactive cysteine persulfides and S-polythiolation regulate oxidative stress and redox signaling. *Proc. Natl. Acad. Sci. U.S.A* **2014**, *111* (21), 7606–7611.
- (20) Mustafa, A. K.; Gadalla, M. M.; Sen, N.; Kim, S.; Mu, W.; Gazi, S. K.; Barrow, R. K.; Yang, G.; Wang, R.; Snyder, S. H., H₂S Signals Through Protein S-Sulfhydration. *Sci. Signal.* **2009**, *2* (96), ra72 LP-ra72.
- (21) Mustafa, A. K.; Gadalla, M. M.; Sen, N.; Kim, S.; Mu, W.; Gazi, S. K.; Barrow, R. K.;

- Yang, G.; Wang, R.; Snyder, S. H., H₂S Signals Through Protein S-Sulfhydration. *Sci. Signal.* **2009**, *2* (96), ra72 LP-ra72.
- (22) Wei, C.; Zhu, Q.; Liu, W.; Chen, W.; Xi, Z.; Yi, L., NBD-based colorimetric and fluorescent turn-on probes for hydrogen sulfide. *Org. Biomol. Chem.* **2014**, *12* (3), 479–485.
- (23) Chauhan, P.; Bora, P.; Ravikumar, G.; Jos, S.; Chakrapani, H., Esterase Activated Carbonyl Sulfide/Hydrogen Sulfide (H₂S) Donors. *Org. Lett.* **2017**, *19* (1), 62–65.
- (24) Kelkar, D. S.; Ravikumar, G.; Mehendale, N.; Singh, S.; Joshi, A.; Sharma, A. K.; Mhetre, A.; Rajendran, A.; Chakrapani, H.; Kamat, S. S., A chemical–genetic screen identifies ABHD12 as an oxidized-phosphatidylserine lipase. *Nat. Chem. Biol.* **2019**, *15* (2), 169–178.
- (25) Xu, F.; Tang, W.; Kang, S.; Song, J.; Duan, X., A highly sensitive and photo-stable fluorescent probe for endogenous intracellular H₂O₂ imaging in live cancer cells. *Dye. Pigment.* **2018**, *153*, 61–66.
- (26) Du, J.; Huang, Y.; Yan, H.; Zhang, Q.; Zhao, M.; Zhu, M.; Liu, J.; Chen, S. X.; Bu, D.; Tang, C.; Jin, H., Hydrogen Sulfide Suppresses Oxidized Low-density Lipoprotein (Ox-LDL)-stimulated Monocyte Chemoattractant Protein 1 generation from Macrophages via the Nuclear Factor κ B (NF- κ B) Pathway. *J. Biol. Chem.* **2014**, *289* (14), 9741–9753.
- (27) Zhang, T.; Ono, K.; Tsutsuki, H.; Ihara, H.; Islam, W.; Akaike, T.; Sawa, T., Enhanced Cellular Polysulfides Negatively Regulate TLR4 Signaling and Mitigate Lethal Endotoxin Shock. *Cell Chem. Biol.* **2019**, *26* (5), 686-698.e4.
- (28) Legler, D. F.; Bruckner, M.; Uetz-von Allmen, E.; Krause, P., Prostaglandin E2 at new glance: Novel insights in functional diversity offer therapeutic chances. *Int. J. Biochem. Cell Biol.* **2010**, *42* (2), 198–201.
- (29) Eguchi, N.; Minami, T.; Shirafuji, N.; Kanaoka, Y.; Tanaka, T.; Nagata, A.; Yoshida, N.; Urade, Y.; Ito, S.; Hayaishi, O., Lack of tactile pain (allodynia) in lipocalin-type prostaglandin D synthase-deficient mice. *Proc. Natl. Acad. Sci.* **1999**, *96* (2), 726–730.
- (30) Van Dingenen, J.; Pieters, L.; Vral, A.; Lefebvre, R. A., The H₂S-Releasing Naproxen Derivative ATB-346 and the Slow-Release H₂S Donor GYY4137 Reduce Intestinal Inflammation and Restore Transit in Postoperative Ileus. *Front. Pharmacol.* **2019**, *10*.
- (31) Yu, B.; Zheng, Y.; Yuan, Z.; Li, S.; Zhu, H.; De La Cruz, L. K.; Zhang, J.; Ji, K.; Wang, S.; Wang, B., Toward Direct Protein S-Persulfidation: A Prodrug Approach That Directly Delivers Hydrogen Persulfide. *J. Am. Chem. Soc.* **2018**, *140* (1), 30–33.
- (32) Nomura, D. K.; Morrison, B. E.; Blankman, J. L.; Long, J. Z.; Kinsey, S. G.; Marcondes,

M. C. G.; Ward, A. M.; Hahn, Y. K.; Lichtman, A. H.; Conti, B.; Cravatt, B. F., Endocannabinoid Hydrolysis Generates Brain Prostaglandins That Promote Neuroinflammation. *Science*. **2011**, *334* (6057), 809–813.

CHAPTER 4.2. β -galactosidase activated prodrug of the artificial substrates for 3-MST**4.2.1. Introduction**

Aging is a biological phenomenon characterized by a progressive decline in physiological functioning of the body, accompanied by an increase in age-associated disorders. A significant accumulation of senescent cells is an important hallmark of aging.¹ Biomarkers of senescent cells include cell cycle arrest, metabolic and morphological changes, altered gene expressions and upregulated pro-inflammatory markers.²⁻⁴ Multiple theories have been proposed to understand the process of aging and a prominent one amongst these is the one proposed by Denham Herman. They proposed that deleterious free radicals and oxidants damaging biomolecules is a major contributor to the process of aging.⁵ Therefore, countering these species or inhibiting their production might aid in reducing the rate of aging or prevent incidences of age associated disorders. This theory is now widely accepted with several studies demonstrating the effects of antioxidants such as vitamin C, vitamin E, resveratrol, glutathione and antioxidant enzymes in boosting health and longevity of life.^{6,7}

H₂S with its documented antioxidant properties have shown promising results in preventing oxidative damage and impairment of age associated disorders. A marked decline in plasma H₂S levels was observed in individuals aged above 50.⁸ However, the underlying mechanisms implying the role of H₂S in aging were unclear. Wang and co-workers in 2013 have demonstrated that H₂S was able to attenuate oxidative stress while delaying cellular senescence, mediated by persulfidation of the KEAP1-Nrf2 axis.⁹ H₂S induces persulfidation of KEAP1, facilitating the translocation of Nrf2 to the nucleus and upregulate the expression of antioxidant enzymes glutamate-cysteine ligase and glutathione reductase. As per a recent report from Filipovic and co-workers, a considerable decline in the levels of persulfidation was observed in aged animals.¹⁰ Alternatively, an increase in persulfidation achieved through dietary or pharmacological intervention not only extended the life span of the animals but improved their ability to cope with stress. Thus, persulfidation plays a crucial role in the process of aging and inducing this modification might have pharmacological implications.

As discussed previously, artificial substrates for 3-MST is an effective strategy to alter the levels of intracellular persulfides and alleviate oxidative damage. Furthermore, the artificial substrate confers structural stability with longer shelf life compared to the generic persulfide functional group. Therefore, we proposed the design of a prodrug of the artificial substrate of 3-MST that can be selectively cleaved in senescent cells. β -galactosidase is overexpressed in

senescent cells, an outcome of increased lysosomal biogenesis and senescence associated β -galactosidase (SABG) is used as a biomarker for detection of senescent cells.¹¹ SABG activated probes are extensively used for imaging senescent cells (Figure 4.2.1).^{12–14}

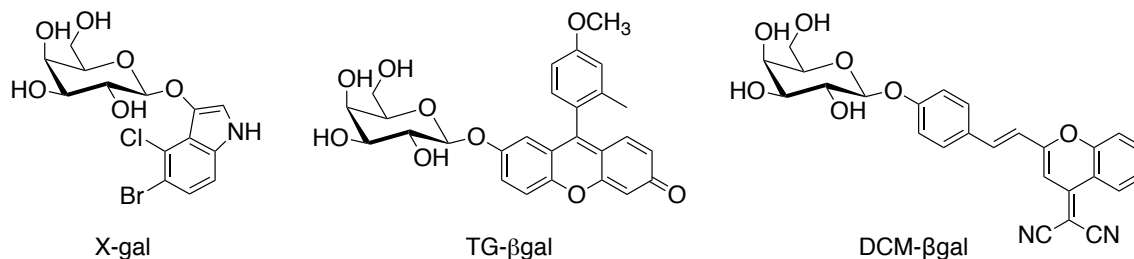


Figure 4.2.1. Probes for β -galactosidase for imaging senescence

We designed prodrug **30** that can be cleaved by the enzyme β -galactosidase. Subsequent intramolecular cyclization of the phenolate will release the artificial substrate **26** along with the heterocyclic byproduct **31** (Figure 4.2.2.a). **26**, as demonstrated in chapter 4.1 can generate a range of reactive sulfur species including H_2S , persulfides/polysulfides, catalyzed by the enzyme 3-MST (Figure 4.2.2.b).

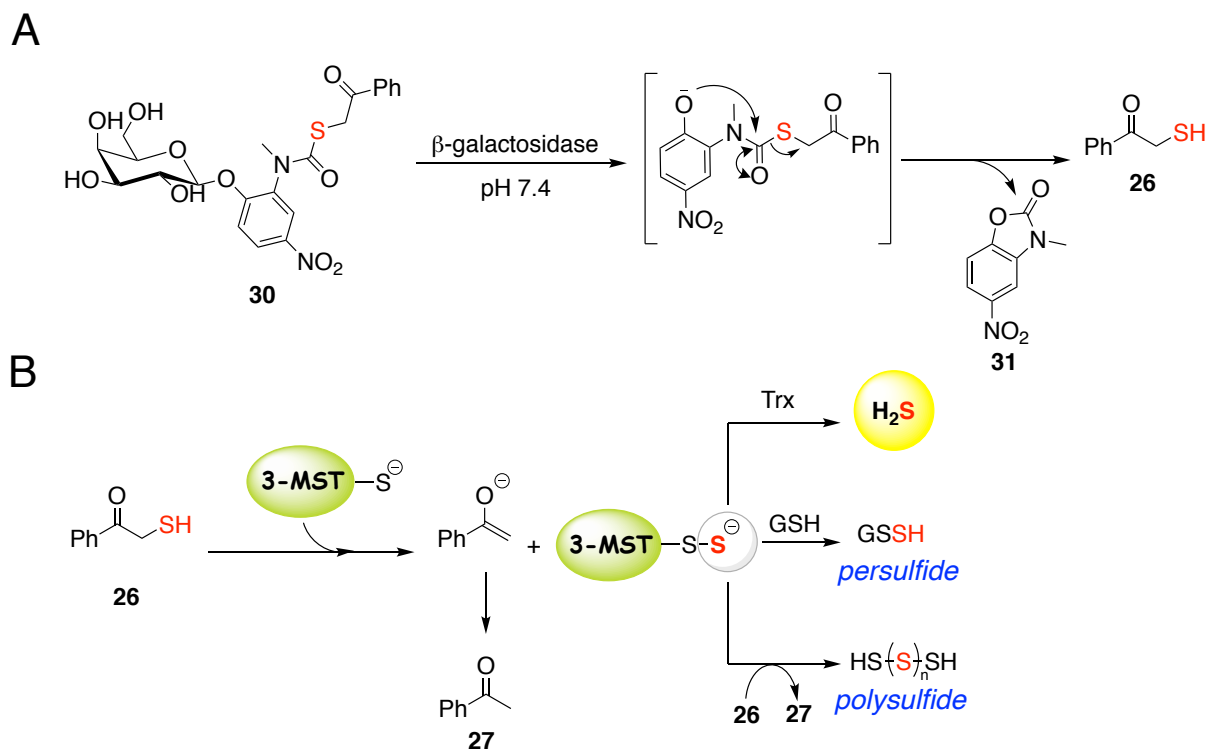
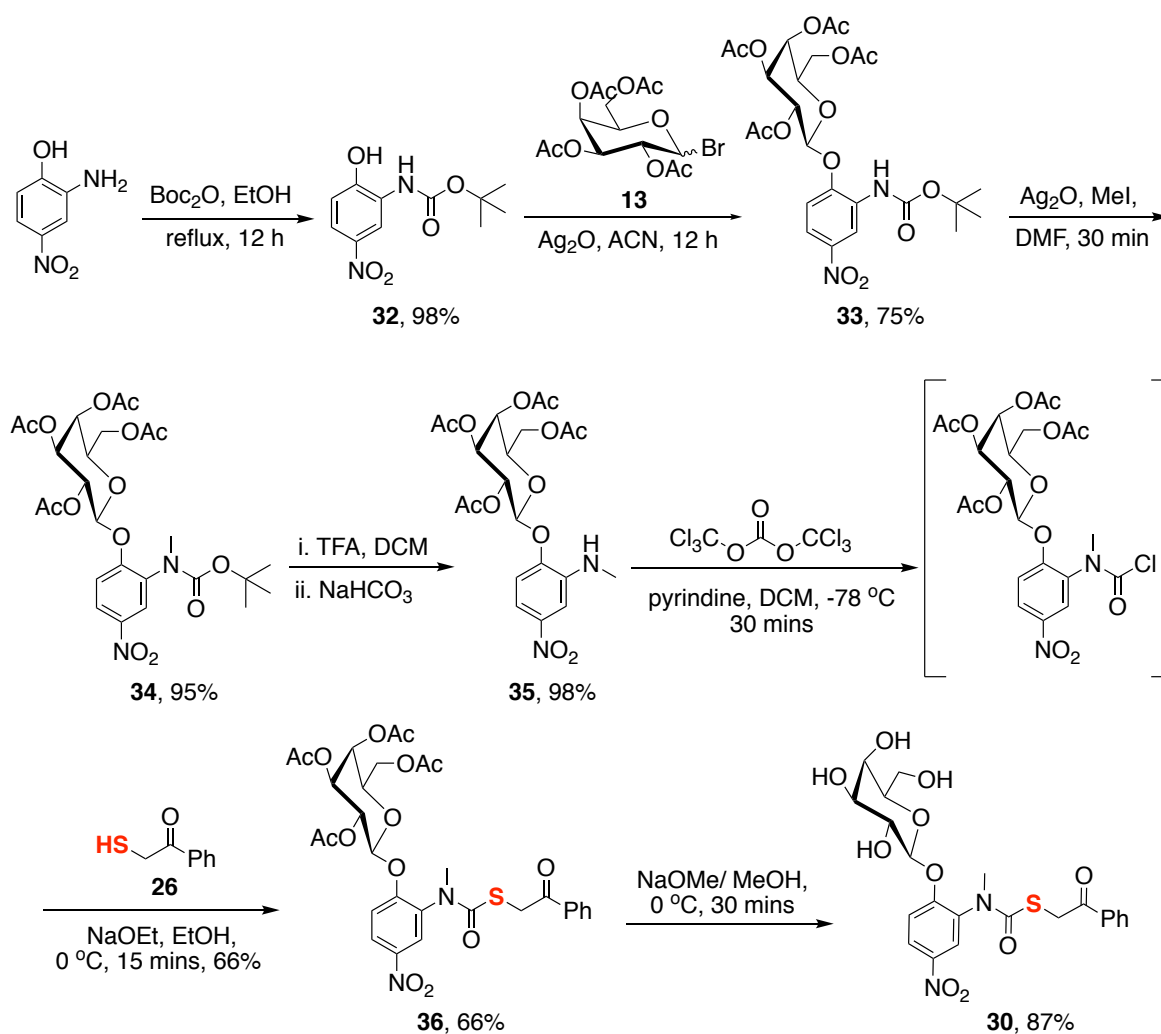


Figure 4.2.2. a) Design of β -galactosidase activated prodrug (**30**) of the artificial substrate (**26**). b) Catalytic turnover of **26** by 3-MST to generate H_2S and persulfides/polysulfides.

4.2.2. Results and Discussion

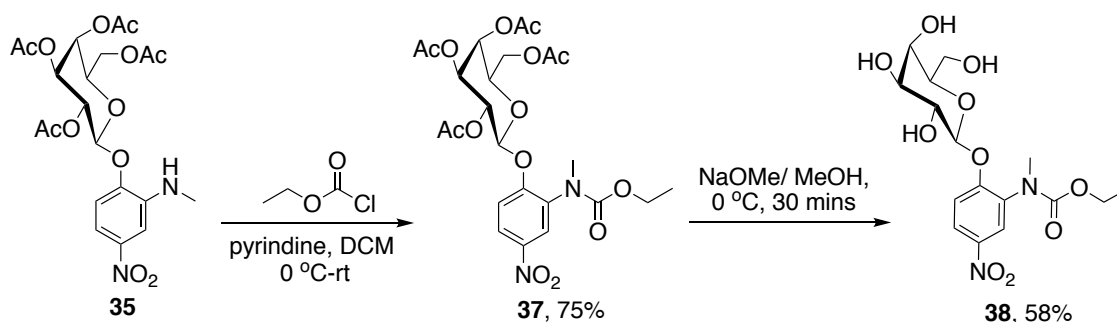
4.2.2.1. Synthesis

Compound **30** was synthesized starting from 2-amino-4-nitrophenol in 7 steps (scheme 4.2.1.). The amine in 2-amino-4-nitrophenol was protected with *tert*-butyloxycarbonyl (boc) to give **32** in 98% yield.¹⁵ **32** was then reacted with β -galactopyranosyl bromide and silver oxide (Ag_2O) to afford compound **33** in 75% yield.¹⁶ **33** was *N*-methylated by using methyl iodide in the presence of Ag_2O to form **34**, followed by deprotection of the boc to obtain **35**.¹⁷ For coupling **26** to the *N*-methyl derivative **35**, **35** was activated to form a formyl intermediate by reacting it with triphosgene.¹⁸ The formyl intermediate was then immediately reacted with **26** in the presence of freshly prepared sodium ethoxide to yield the coupled thiocarbamate **36**.¹⁹ Final deacetylation of the galactoside was carried out to obtain the final prodrug **30** in 87% yield.



Scheme 4.2.1. Synthesis of β -galactosidase activated prodrug of 3-MST artificial substrate **30**.

Compound **38**, which would undergo a similar intramolecular cyclization upon cleavage by β -galactosidase but would generate ethanol, was designed as the negative control. **38** was prepared starting from **35** in two steps (scheme 4.2.2.). **35** was reacted with ethylchloroformate to form **37**, followed by deacetylation to obtain **38** in 58% yield.



Scheme 4.2.2. Synthesis of negative control **38**.

4.2.2.2. Decomposition of **30** in the presence of β -galactosidase

With compound **30** in hand, its ability to generate the artificial substrate **26** in the presence of β -galactosidase was tested. **30** was incubated with β -galactosidase (2 U/mL) in pH 7.4 phosphate buffer at 37 °C. As monitored by HPLC, within 5 min of incubation appearance of two new peaks at retention time (RT) 10.2 min and 11.6 min were observed, along with the peak for **30** (Figure 4.2.3.). The peak for **30** was completely consumed within 30 min. The peak at RT 10.2 min was attributed to the byproduct **31** and the one at RT 11.6 min to the artificial substrate **26** respectively, by comparing it with the RT of the authentic compounds. The yield of the byproduct formed under these conditions was calculated to be 92%.

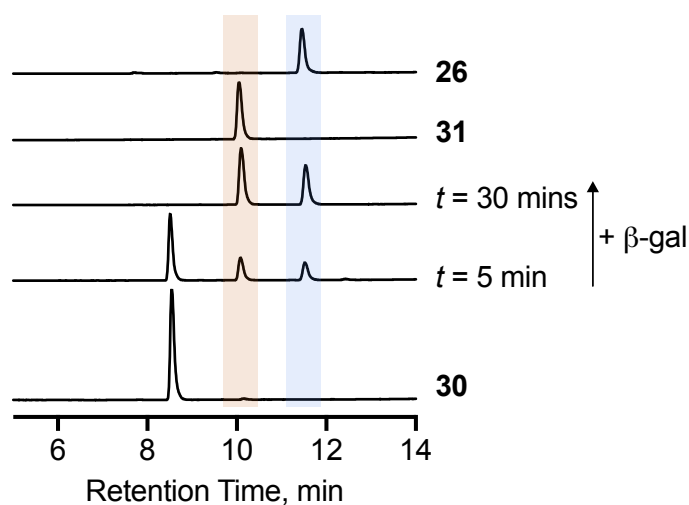


Figure 4.2.3. HPLC decomposition profile of **30** in the presence of β -galactosidase.

4.2.2.3. Decomposition of **30** in the presence of β -galactosidase and 3-MST

Next, the turnover of **26** generated from **30** in the presence of β -galactosidase, by 3-MST was evaluated. **30** was incubated with β -galactosidase (2 U/mL), *E. coli* 3-MST (*b3*-MST, 1 μ M) and dithiothreitol (DTT, 10 mM) in pH 7.4 phosphate buffer at 37 °C. DTT is a reducing agent used to mimic the functions of thioredoxin due to its structural similarities. As monitored by HPLC, **30** was consumed within 60 min with the appearance of two new peaks attributable to the byproduct **31** and acetophenone **27** was observed (Figure 4.2.4.). From the above observation, it can be concluded that **30** undergoes cleavage by β -galactosidase to release the artificial substrate **26** which is then turned over by 3-MST in the presence of DTT, forming acetophenone **27** and **31** as the byproducts.

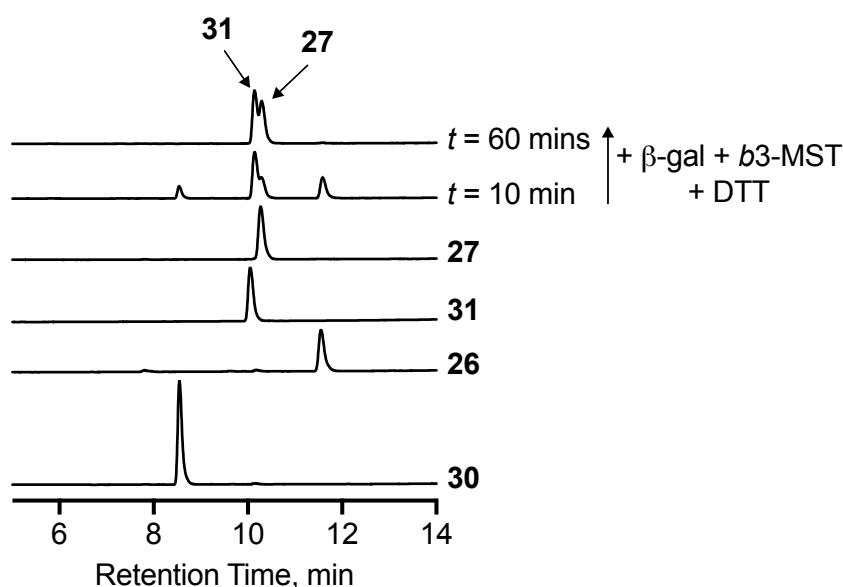
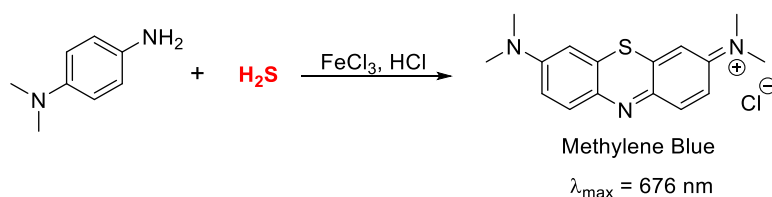


Figure 4.2.4. HPLC profile for catalytic turnover of **26**, generated from **30** upon treatment with β -galactosidase (2 U/mL), by *b3*-MST.

4.2.2.4. H₂S generation from **30** in the presence of β -galactosidase and 3-MST

In the previous experiments the release of **26** from the prodrug **30** upon treatment with β -galactosidase and its subsequent turnover by 3-MST to form **27** as the byproduct was demonstrated. We next attempted to detect H₂S under these conditions using a standard methylene blue assay.²⁰ In this assay, H₂S is first trapped by Zn(OAc)₂ as ZnS which is then reacted with *N,N*-dimethyl-*p*-phenylene diamine and FeCl₃ under acidic conditions to form the methylene blue complex. Methylene blue is a colored dye with a characteristic absorbance at 676 nm (Scheme 4.2.3).



Scheme 4.2.3. Formation of methylene blue dye by H_2S .

30 was incubated with β -galactosidase (2 U/mL), *b3*-MST (1 μM) and DTT (10 mM) in phosphate buffer at 37 $^\circ\text{C}$ for 60 min. An aliquot of this reaction mixture was treated with the methylene blue reagents (*N,N*-dimethyl-*p*-phenylene diamine and FeCl_3) and further incubated for 30 min. The samples were then transferred to a well plate and the absorbance profile was recorded from 550 nm to 800 nm (Figure 4.2.5.). It was observed that **30** only in the presence of β -galactosidase, *b3*-MST and DTT produced a signal for methylene blue, suggesting the generation of H_2S (purple, Figure 4.2.5.a). DTT enhances the catalytic efficiency of *b3*-MST, however, even in the absence of DTT a minor amount of H_2S generation was observed (green). **25** was used as a positive control, which gives a distinct signal for H_2S generation (red). **30** in the absence of β -galactosidase or *b3*-MST failed to produce H_2S , so did the negative control **38** under similar conditions. (Figure 4.2.5.b).

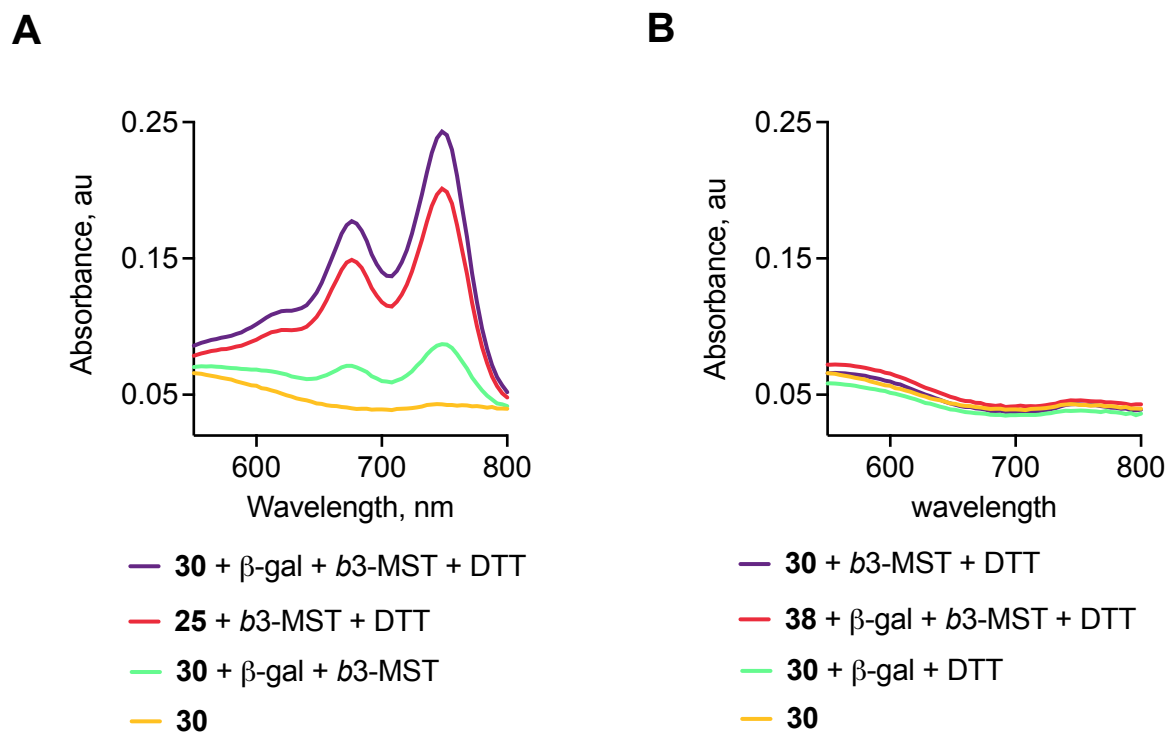


Figure 4.2.5. a) Methylene blue absorbance profile obtained for catalytic turnover of **30** in the presence of β -galactosidase (2 U/mL), *b3*-MST and DTT. **25** was used as the positive control. b) **30** in the absence of β -galactosidase (2 U/mL) and *b3*-MST does not produce H_2S . **38** was used as the negative control.

Further, the absorbance maximum of methylene blue at 676 nm was measured as a function of H₂S formation. A similar observation was recorded (Figure 4.2.6).

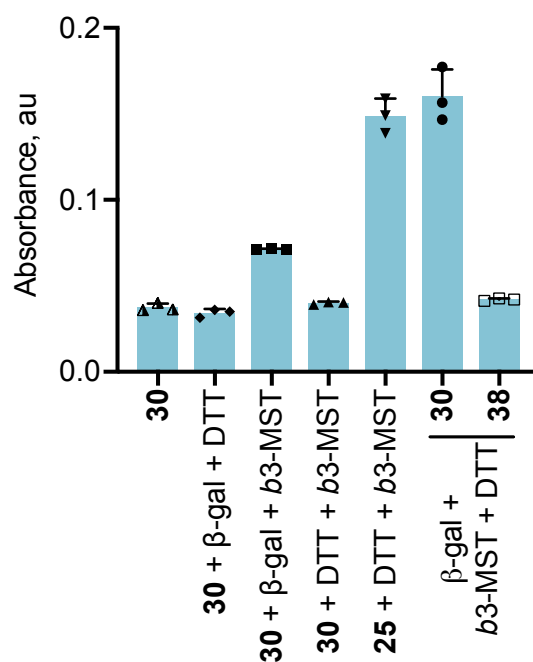


Figure 4.2.6. Absorbance of methylene blue recorded at 676 nm as a function of H₂S formation. Significant generation of H₂S was observed from **30** upon incubation with β -galactosidase, b3-MST and DTT.

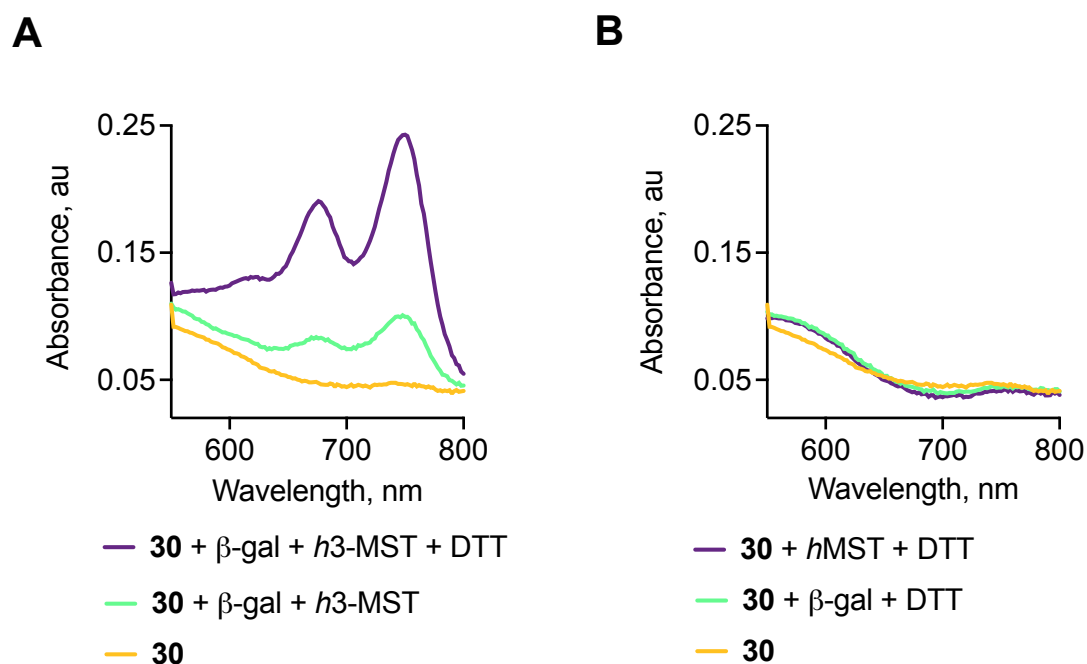


Figure 4.2.7. a) Methylene blue absorbance profile obtained for catalytic turnover of **30** in the presence of β -galactosidase (2 U/mL), h3-MST and DTT. b) **30** in the absence of β -galactosidase (2 U/mL) and h3-MST does not produce H₂S.

A similar experiment as described above was carried out using the human homolog of 3-MST (*h3-MST*). A signal for the generation of H₂S was observed upon incubation of **30** with β -galactosidase (2 U/mL), *h3-MST* (1 μ M) and DTT (10 mM) in pH 7.4 phosphate buffer at 37 °C for 60 min (purple) (Figure 4.2.7.a). Slight amount of H₂S was detected even in the absence of DTT, suggesting a sluggish turnover of the substrate (green). No signal for H₂S was detected in the absence of either β -galactosidase or *h3-MST* (Figure 4.2.7.b).

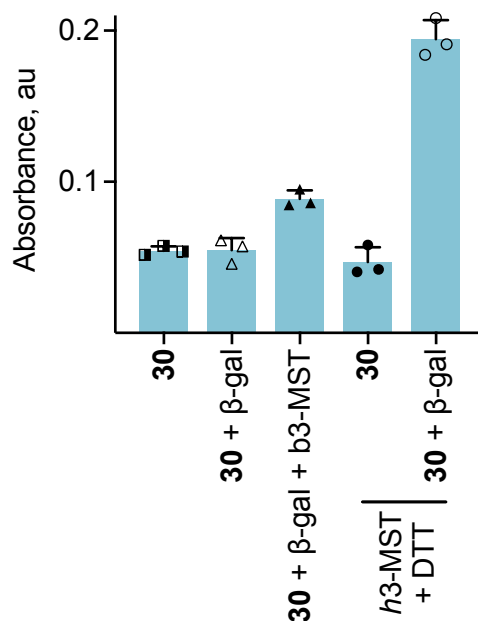


Figure 4.2.8. Absorbance of methylene blue recorded at 676 nm as a function of H₂S formation. Significant generation of H₂S was observed from **30** upon incubation with β -galactosidase, *h3-MST* and DTT.

Thus, from the above experiments it can be concluded that prodrug **30** can be efficiently cleaved by β -galactosidase to release the free artificial substrate (**26**) for 3-MST and the byproduct **31** in excellent yield. Subsequent catalysis of **26** by 3-MST under reducing conditions (DTT) results in the formation of H₂S and acetophenone (**27**) as the byproduct.

4.2.2.5. Intracellular persulfidation

The ability of prodrug **30** to permeate cells and mediate intracellular persulfidation was next investigated. Tag-switch assay described in chapter 4.1 was used for the detection of persulfides in cells. Briefly, cellular proteins are first treated with the thiol blocking reagent MSBT-A which reacts with both thiols and persulfides forming the MSBT-A adduct. This is followed by treatment with the tag-switching nucleophile, cyanoacetic acid tagged with the

fluorescent dye BODIPY (CN-BOT) which will selectively label the persulfide groups.²¹ This technique allows for the detection of protein persulfidation in cells.

The data for intracellular protein persulfidation was provided by Ms. Kavya Gupta from Dr. Deepak K. Saini's group in IISc Bangalore. A549 cells were irradiated with 7Gy IR to induce senescence. Both senescent and non-senescent cells were incubated with **30** (100 μ M) and Na₂S (100 μ M) for 1 h. The cells were then fixed with ice cold methanol and the cell membrane was permeabilized by using ice cold acetone. The cells were then incubated with MSBT-A overnight followed by treatment with CN-BOT for 1 h to tag the protein persulfides with BODIPY, which can be visualized under the microscope. Senescent cells treated with **30** produced a significantly enhanced signal compared to a similar treatment on non-senescent cells (Figure 4.2.9). This data implies that **30** is selectively activated and is able to induce persulfidation in senescent cells, possibly due to an overexpression of β -galactosidase.

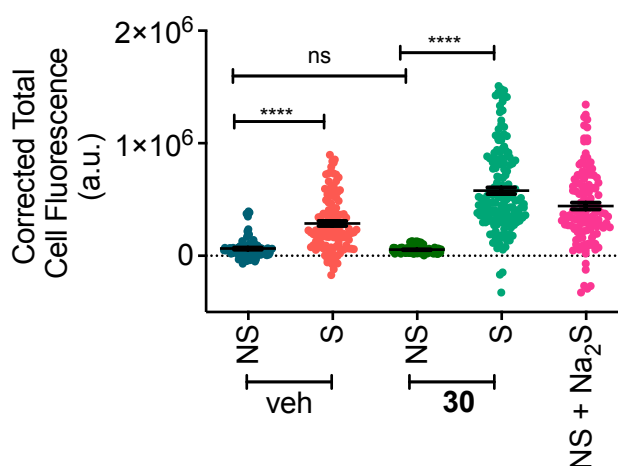


Figure 4.2.9. Quantification of the fluorescence signal induced by **30** and Na₂S in A549 senescent and non-senescent cell lines using the tag-switch technique. All data are presented as mean \pm SD (n = 3/group). Significance was determined with respect to control in each cell line by Student's two-tailed unpaired parametric t test: ****p < 0.0001 versus ctrl group while ns = non-significant.

4.2.3. Summary

To summarize, a prodrug (**30**) of the artificial substrate for 3-MST (**26**) that is sensitive to cleavage by β -galactosidase was developed as a tool to investigate the role of persulfidation in senescence. **30** was shown to be efficiently cleaved upon exposure to β -galactosidase to release the free substrate and the byproduct **31** in excellent yield. Further, the turnover of the substrate **26** by both bacterial (*b3*-MST) and human (*h3*-MST) to generate H₂S under reducing conditions (DTT) was demonstrated. Finally, we provide evidence for the ability of **30** to selectively induce intracellular protein persulfidation in senescent cells over non-senescent

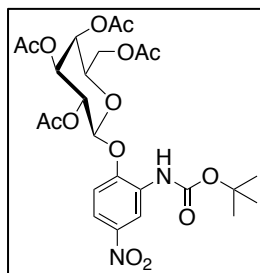
cells. Collectively, our data suggests that **30** is a cell permeable persulfidating agent which can be used as a tool to interrogate the implications of persulfidation in senescence and aging.

4.2.4. Experimental Section

4.2.4.1. Synthesis and characterization of compounds

32 was prepared using a previously reported protocol.¹⁵ **13** was synthesized as per protocol outlined in chapter 3.

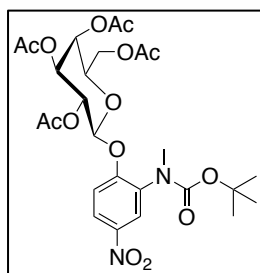
(2R,3S,4S,5R,6S)-2-(acetoxymethyl)-6-(2-((tert-butoxycarbonyl)amino)-4-nitrophenoxy)tetrahydro-2H-pyran-3,4,5-triyl triacetate (33**):**



To an ice cold solution of *tert*-butyl (2-hydroxy-5-nitrophenyl)carbamate (**32**) (2 g, 7.8 mmol) and Ag₂O (1.8 g, 7.8 mmol) in anhydrous acetonitrile (ACN) was added a solution of **13** (3.2 g, 7.8 mmol). The resulting mixture was stirred at room temperature (rt) for 12 h. After completion as determined by TLC, the reaction mixture was filtered

through celite and washed with EtOAc. The filtrate was evaporated, the crude product obtained was diluted with H₂O and extracted with EtOAc (3 × 50 mL). The combined organic layers were passed through anhydrous Na₂SO₄, filtered and the filtrate was evaporated to obtain the crude compound. The compound was further purified by silica gel column chromatography to give the desired product as a white solid (3.5 g, 75 %). FT-IR (ν_{\max} , cm⁻¹) 3323, 2855, 1696, 1633, 1543; ¹H NMR (400MHz, CDCl₃): δ 9.08 (s, 1H), 7.87 (dd, J = 9.0, 2.7 Hz, 1H), 7.19 (s, 1H), 7.10 (d, J = 9.0 Hz, 1H), 5.57–5.5 (m, 2H) 5.19 (dd, J = 11.0, 3 Hz, 1H), 5.08 (d, J = 8.0 Hz, 1H), 4.25–4.12 (m, 3H), 2.2 (s, 3H), 2.12 (s, 3H), 2.09 (s, 3H), 2.03 (s, 3H), 1.56 (s, 9H); ¹³C NMR (100 MHz, CDCl₃) δ 170.3, 170.2, 170.0, 169.9, 152.2, 148.8, 143.8, 130.0, 117.8, 113.9, 113.7, 100.0, 81.4, 71.6, 70.0, 68.6, 66.6, 61.3, 28.2, 20.8, 20.7, 20.6, 20.5; HRMS for C₂₅H₃₂N₂O₁₄ [M+Na]⁺: Calculated: 607.1751, Found: 607.1750.

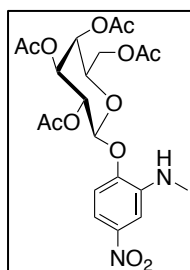
(2R,3S,4S,5R,6S)-2-(acetoxymethyl)-6-(2-((tert-butoxycarbonyl)(methyl)amino)-4-nitrophenoxy)tetrahydro-2H-pyran-3,4,5-triyl triacetate (34**):**



To a solution of compound **33** (3 g, 5.1 mmol) in anhydrous ACN at 0 °C was added Ag₂O (8.3 g, 36 mmol) and methyl iodide (1.6 mL, 25.6 mmol). The reaction was stirred at rt for 30 mins. After completion as determined by TLC, the reaction mixture was filtered through celite and washed with EtOAc. The filtrate was evaporated, the crude product obtained was diluted with H₂O and extracted with EtOAc (3 × 50 mL). The combined organic layers were passed through anhydrous Na₂SO₄, filtered and the filtrate was evaporated to obtain

the crude compound. The compound was further purified by silica gel column chromatography to give the desired product as a white solid (2.9 g, 95%). FT-IR (ν_{\max} , cm^{-1}) 3315, 2852, 1692, 1633; ^1H NMR (400MHz, CDCl_3): δ 8.13–8.10 (m, 2H), 7.23–7.21 (m, 1H), 5.55–5.48 (m, 2H), 5.14–5.10 (m, 2H), 4.24–4.11 (m, 3H), 3.12 (s, 3H), 2.19 (s, 3H), 2.08 (s, 3H), 2.06 (s, 3H), 2.02 (s, 3H), 1.26 (s, 9H); ^{13}C NMR (100 MHz, CDCl_3) δ 170.2, 170.0, 168.9, 157.0, 142.9, 123.4, 115.8, 80.8, 71.5, 70.5, 68.1, 66.7, 61.3, 29.7, 28.2, 20.7, 20.6, 20.5; HRMS for $\text{C}_{26}\text{H}_{34}\text{N}_2\text{O}_{14}$ $[\text{M}+\text{Na}]^+$: Calculated: 621.1907, Found: 621.1899.

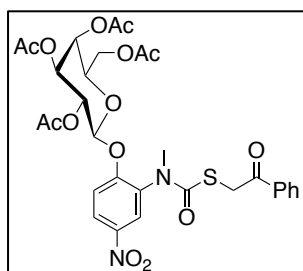
(2*R*,3*S*,4*S*,5*R*,6*S*)-2-(acetoxymethyl)-6-(2-(methylamino)-4-nitrophenoxy)tetrahydro-2*H*-pyran-3,4,5-triyl triacetate (35):



To a solution of **34** (1 g, 1.7 mmol) in dichloromethane (6.4 mL) at 0 °C was added trifluoroacetic acid (TFA) (6.4 mL, 83.5 mmol) and stirred for 10 mins. After completion as determined by TLC analysis, the reaction was quenched by adding sodium bicarbonate solution and extracted with CH_2Cl_2 (3 × 25 mL). The combined organic layers were passed through anhydrous Na_2SO_4 ,

filtered and the filtrate was evaporated to obtain the crude compound. The crude was further purified using silica gel column chromatography to obtain **35** as a yellow solid (810 mg, 98%). FT-IR (ν_{\max} , cm^{-1}) 3038, 1696, 1633; ^1H NMR (400MHz, CDCl_3): δ 7.54 (dd, $J = 8.8, 2.7$ Hz, 1H), 7.38 (d, $J = 2.6$ Hz, 1H), 6.92 (d, $J = 8.8$ Hz, 1H), 5.52–5.48 (m, 2H), 5.18 (dd, $J = 11.0, 3$ Hz, 1H), 5.08 (d, $J = 8.0$ Hz, 1H), 4.52 (s, 1H), 4.27–4.11 (m, 3H), 2.91 (s, 3H), 2.19 (s, 3H), 2.09 (s, 3H), 2.03 (s, 3H), 2.04 (s, 3H); ^{13}C NMR (100 MHz, CDCl_3) δ 170.4, 170.2, 170.0, 148.1, 144.5, 140.3, 112.3, 111.9, 104.1, 99.7, 71.5, 70.2, 68.7, 66.7, 61.4, 30.0, 21.0, 20.7, 20.7, 20.6; HRMS for $\text{C}_{21}\text{H}_{26}\text{N}_2\text{O}_{12}$ $[\text{M}+\text{Na}]^+$: Calculated: 499.1564, Found: 499.1565.

(2*R*,3*S*,4*S*,5*R*,6*S*)-2-(acetoxymethyl)-6-(2-(methyl((2-oxo-2-phenylethyl)thio)carbonyl)amino)-4-nitrophenoxy)tetrahydro-2*H*-pyran-3,4,5-triyl triacetate (36):



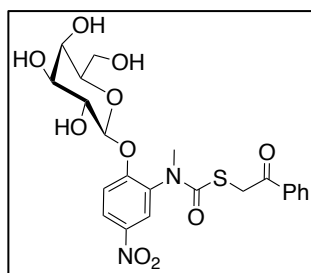
A solution of **35** (300 mg, 0.6 mmol) in anhydrous CH_2Cl_2 was cooled to 0 °C. Pyridine (97 μL , 1.2 mmol) was added to the reaction mixture followed by addition of triphosgene (268 mg, 0.9 mmol). The reaction was allowed to warm up to rt and stirred at rt for 2 h. Upon completion as evidenced by TLC analysis, the reaction was quenched

by adding 1N HCl and extracted with CH_2Cl_2 (3 × 25 mL). The combined organic layers were passed through anhydrous Na_2SO_4 , filtered and the filtrate was evaporated to obtain the crude

compound. The carbamoyl chloride intermediate obtained was immediately carried forward for the next reaction without further purification.

A suspension of the carbamoyl chloride in ethanol was cooled to 0 °C. The thiol **26** (203 mg, 1.3 mmol) was dissolved in ethanol separately and a freshly prepared solution of sodium ethoxide (NaOEt) was added to it. This solution of the mercaptide was then added to the suspension of the carbamoyl chloride in ethanol, dropwise. The reaction was stirred at 0 °C for 10 mins. Upon complete consumption of the carbamoyl chloride, the reaction was quenched by adding water and extracted with CH₂Cl₂ (3 × 25 mL). The combined organic layers were passed through anhydrous Na₂SO₄, filtered and the filtrate was evaporated to obtain the crude compound. The crude obtained was purified by reverse phase HPLC using ACN-H₂O as the eluent to afford the desired product as a white solid (200 mg, 66%). FT-IR (ν_{max} , cm⁻¹) 3349, 2864, 1696, 1623, 1514; ¹H NMR (400MHz, CDCl₃): δ 8.28 (m, 2H), 8.02 (d, J = 7.5 Hz, 2H), 7.26–7.58 (m, 1H), 7.51–7.45 (m, 3H), 5.55–5.51 (m, 2H), 5.33 (dd, J = 30.0, 7 Hz, 2H), 4.5–4.18 (m, 5H), 3.25 (s, 3H), 2.2 (s, 3H), 2.09 (s, 3H), 2.01 (s, 3H), 1.98 (s, 3H); ¹³C NMR (100 MHz, CDCl₃): δ 193.5, 170.3, 170.1, 169.9, 169.5, 166.8, 158.5, 143.4, 133.8, 133.7, 128.8, 128.7, 128.5, 126.0, 119.0, 99.7, 71.7, 70.4, 67.9, 66.8, 61.4, 45.4, 38.8, 37.0, 29.7, 20.7, 20.7, 20.6, 20.5; HRMS for C₃₀H₃₂N₂O₁₄S [M+Na]⁺: Calculated: 676.1574, Found: 676.1572.

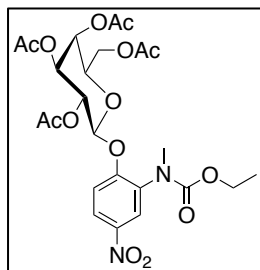
S-(2-oxo-2-phenylethyl) methyl(5-nitro-2-(((2S,3R,4S,5R,6R)-3,4,5-trihydroxy-6-(hydroxymethyl)tetrahydro-2H-pyran-2-yl)oxy)phenyl)carbamothioate (30):



To an ice cooled solution of **36** (200 mg, 0.3 mmol) in anhydrous methanol was added sodium methoxide (NaOMe) (16 mg, 0.3 mmol). The reaction was warmed up to rt and stirred at rt for 60 min. After completion, the reaction was quenched by adding amberlyst catalyst and subsequently filtered. The methanol was evaporated and

purified using reverse phase HPLC using ACN-H₂O as the eluent to afford the desired product as a sticky solid which was triturated in CHCl₃ to obtain a white solid (130 mg, 86%). FT-IR (ν_{max} , cm⁻¹) 3328, 1696, 1663, 1553; ¹H NMR (400MHz, CD₆CO): δ 8.34 (s, 2H), 8.08 (d, J = 7.5 Hz, 2H), 7.69–7.54 (m, 4H), 5.29–5.15 (m, 1H), 4.52–4.03 (m, 3H), 3.92–3.89 (m, 1H), 3.84–3.71 (m, 7H), 3.32–3.27 (m, 3H); ¹³C NMR (100 MHz, CD₆CO): δ 194.1, 166.9, 160.3, 159.9, 141.9, 133.5, 130.8, 128.8, 128.4, 127.1, 126.9, 126.2, 116.5, 102.1, 76.2, 74.1, 73.6, 71.0, 68.9, 61.4, 38.3, 36.4; HRMS for C₂₂H₂₄N₂O₁₀S [M+Na]⁺: Calculated: 531.1049, Found: 531.1052.

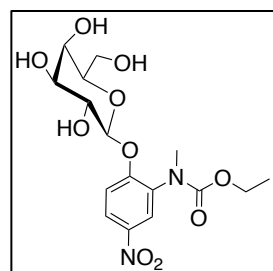
(2*R*,3*S*,4*S*,5*R*,6*S*)-2-(acetoxymethyl)-6-(2-((ethoxycarbonyl)(methyl)amino)-4-nitrophenoxy)tetrahydro-2*H*-pyran-3,4,5-triyl triacetate (37):



To an ice cooled solution of **35** (200 mg, 0.4 mmol) was added pyridine (65 μ L, 0.8 mmol) followed by addition of ethyl chloroformate (76 μ L, 0.8 mmol). The reaction was left to warm up to rt and stirred at rt for 12 h. After completion, the reaction was quenched by adding 1N HCl and extracted with CH_2Cl_2 (3×25 mL). The combined organic layers were

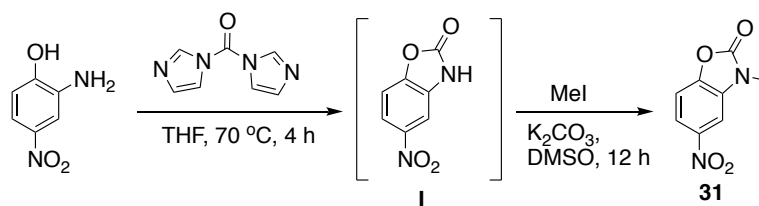
passed through anhydrous Na_2SO_4 , filtered and the filtrate was evaporated to obtain the crude compound. The crude obtained was purified by reverse phase HPLC using ACN- H_2O as the eluent to afford the desired product as a pale-yellow solid (175 mg, 75%). FT-IR (ν_{max} , cm^{-1}) 2923, 2855, 1696, 1633, 1453; ^1H NMR (400MHz, CD_3Cl): δ 8.17 (dd, $J = 8.8, 2.7$ Hz, 2H), 7.27 (m, 1H), 5.55–5.48 (m, 2H), 5.13 (dd, $J = 11.0, 3$ Hz, 2H), 4.26–4.10 (m, 5H), 3.18 (s, 3H), 2.20 (s, 3H), 2.09 (s, 3H), 2.06 (s, 3H), 2.02 (s, 3H), 1.36–1.26 (m, 3H); ^{13}C NMR (100 MHz, CDCl_3) δ 170.3, 170.1, 170.0, 157.3, 155.1, 143.0, 133.5, 125.6, 124.0, 115.2, 98.9, 71.6, 70.5, 68.0, 66.7, 62.0, 61.4, 29.7, 20.7, 20.6, 20.5, 14.5; HRMS for $\text{C}_{24}\text{H}_{30}\text{N}_2\text{O}_{14}$ [$\text{M}+\text{Na}$] $^+$: Calculated: 593.1595, Found: 593.1599.

ethylmethyl(5-nitro-2-(((2*S*,3*R*,4*S*,5*R*,6*R*)-3,4,5-trihydroxy-6-(hydroxymethyl)tetrahydro-2*H*-pyran-2-yl)oxy)phenyl)carbamate (38):



Compound **37** was synthesized according to the procedure outlined for **30**. Compound **37** (100 mg, 0.18 mmol) and NaOMe (10 mg, 0.18 mmol) were used to afford **38** as a colorless liquid (42 mg, 58%). FT-IR (ν_{max} , cm^{-1}) 2923, 2855, 1696, 1633, 1453; ^1H NMR (400MHz, CD_3OD): δ 8.21 (dd, $J = 9, 2.8$ Hz, 1H), 8.14 (s, 1H), 7.45 (d, $J = 9$ Hz, 1H), 5.07 (d, $J = 7.7$ Hz, 1H), 4.2–4.08 (m, 2H), 3.91 (d, $J = 3.3$ Hz, 1H), 3.84–3.72 (m, 4H), 3.60 (dd, $J = 9.6, 3.3$ Hz, 1H), 3.31–3.29 (m, 1H), 3.23 (s, 3H), 1.34–1.11 (m, 3H); ^{13}C NMR (100 MHz, CD_3OD) δ 158.3, 156.4, 142.0, 132.4, 124.6, 124.0, 115.7, 100.9, 76.0, 73.6, 70.5, 68.7, 62.0, 61.0, 36.1, 13.4; HRMS for $\text{C}_{16}\text{H}_{22}\text{N}_2\text{O}_{10}$ [$\text{M}+\text{Na}$] $^+$: Calculated: 425.1172, Found: 425.1170.

3-methyl-5-nitrobenzo[*d*]oxazol-2(3*H*)-one (31):



Scheme 4.2.4. Synthesis of **31**

To a stirred solution of 2-amino-4-nitrophenol (100 mg, 0.65 mmol) in dry THF was added carbonyldiimidazole (136 mg, 0.844 mmol) and the reaction was stirred at 70 °C for 4 h. Upon completion of the reaction, the reaction solvent was evaporated under reduced pressure, the crude was dissolved in water and extracted with CH₂Cl₂. The combined organic layer was washed with brine, passed through Na₂SO₄, filtered and the filtrate was evaporated to obtain intermediate I, which was carried forward to the next reaction without purification

The intermediate I was dissolved in DMSO (2 mL) and K₂CO₃ (84 mg, 0.61 mmol) was added to the solution, followed by addition of methyl iodide (110 μL, 1.66 mmol). The reaction mixture was left to stir overnight. The reaction mixture was quenched by addition of water and extracted with CH₂Cl₂. The combined organic layer was washed with brine, passed through Na₂SO₄, filtered and the filtrate was evaporated to obtain the crude product. The crude was further purified by silica gel column chromatography. FT-IR (ν_{\max} , cm⁻¹) 2845, 1624, 1593, 1553; ¹H NMR (400MHz, CD₃Cl): δ 8.15 (dd, $J = 8.8, 2.7$ Hz, 1H), 7.89 (d, $J = 4$ Hz, 1H), 7.34–7.32 (d, $J = 8$ Hz, 1H), 3.5 (s, 3H); ¹³C NMR (100 MHz, CDCl₃) δ 154.1, 146.7, 144.6, 132.3, 119.3, 109.9, 104.0, 28.6; HRMS for C₈H₆N₂O₄ [M+Na]⁺: Calculated: 217.0225, Found: 217.0229.

4.2.4.2. HPLC based decomposition study of 30

A stock solution of **30** (10 mM), **26** (10 mM) and **31** (10 mM) was prepared in DMSO. Stock solution of β -galactosidase (100 U/mL) was prepared in deionised (DI) water. The reaction mixture was prepared by adding 100 μM of **30** (5 μL, 10 mM stock) and 2 U/mL β -galactosidase (10 μL, 100 U/mL stock) and the volume was adjusted to 500 μL using 20 mM phosphate buffer, pH 7.4. The reaction mixture was stirred at 37 °C, 100 μL aliquots were taken out at set time points, filtered (0.22-micron filter) and injected (25 μL) in a High Performance Liquid Chromatography (HPLC Agilent Technologies 1260 Infinity). The stationary phase was C-18 reverse phased column (Phenomenex, 5 μm, 4.6 × 250 mm). Acetonitrile (A) and 0.01% trifluoroacetic acid in water (B) was used as the mobile phase. A

gradient starting with 30: 70 → 0 min, 40: 60 to 30: 70 → 0 – 5 min, 30: 70 to 10: 90 → 5 – 17 min, 10: 90 to 30: 70 → 17 – 20 min, 30: 70 to 30: 70 → 20 – 22 min was used with flow of 1 mL/min. Under these conditions, **30** in buffer eluted at 8.5 min, **26** at 11.6 min and **31** at 10.2 min.

4.2.4.3. HPLC based turnover of **26** by **3-MST**

A stock solution of **30** (10 mM), **27** (10 mM) and **31** (10 mM) were prepared in DMSO. Stock solutions of β -galactosidase (100 U/mL) and DTT (100 mM) were prepared in DI water. The reaction mixture was prepared by adding 100 μ M of **30** (3 μ L, 10 mM stock), 2 U/mL β -galactosidase (6 μ L, 100 U/mL stock), 2 μ M 3-MST (22 μ L, 27 μ M stock) and 1 mM DTT (3 μ L, 100 mM stock). The volume was adjusted to 300 μ L using 20 mM phosphate buffer, pH 7.4. The reaction mixture was stirred at 37 °C, 100 μ L aliquots were taken out at set time points, filtered (0.22-micron filter) and injected (25 μ L) in a High Performance Liquid Chromatography (HPLC Agilent Technologies 1260 Infinity). The stationary phase was C-18 reverse-phase column (Phenomenex, 5 μ m, 4.6 \times 250 mm). Acetonitrile (A) and 0.01% trifluoroacetic acid in water (B) was used as the mobile phase. A gradient starting with 30: 70 → 0 min, 40: 60 to 30: 70 → 0 – 5 min, 30: 70 to 10: 90 → 5 – 17 min, 10: 90 to 30: 70 → 17 – 20 min, 30: 70 to 30: 70 → 20 – 22 min was used with flow of 1 mL/min. Under these conditions, **30** in buffer eluted at 8.5 min, **27** at 10.3 min and **31** at 10.2 min.

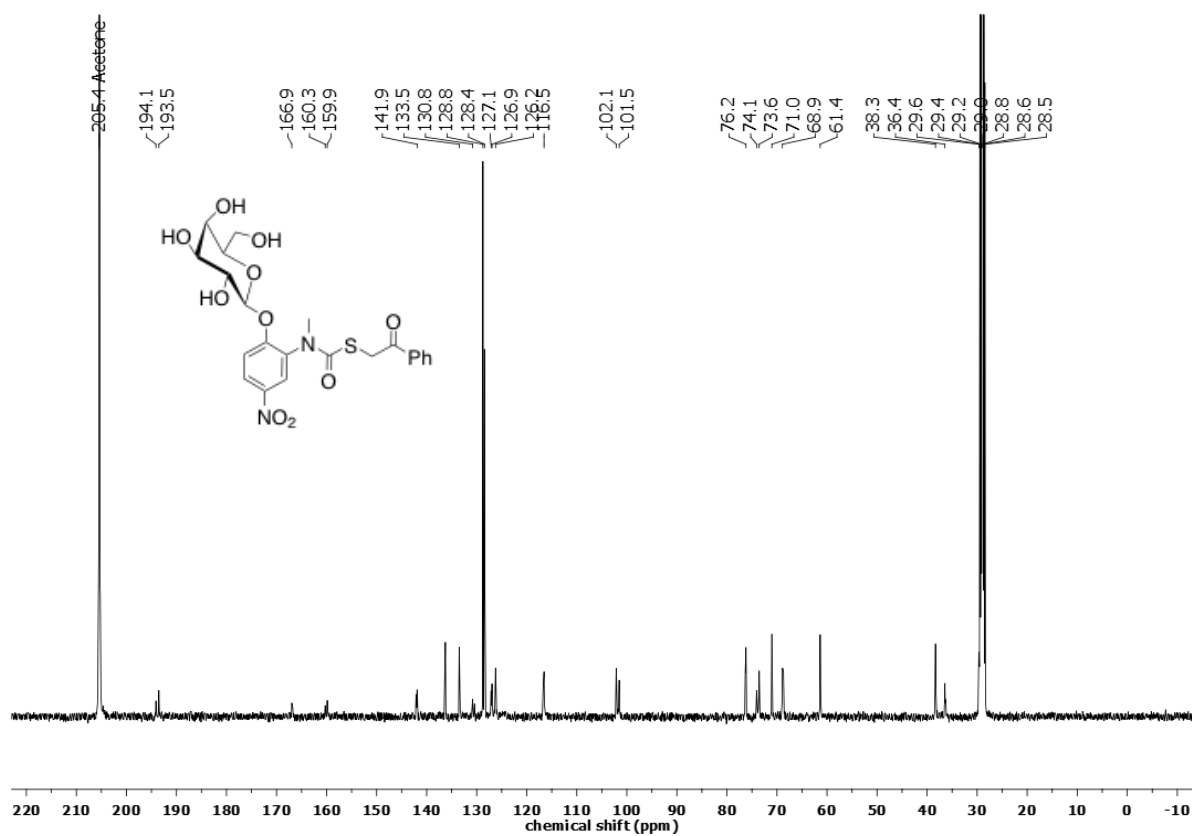
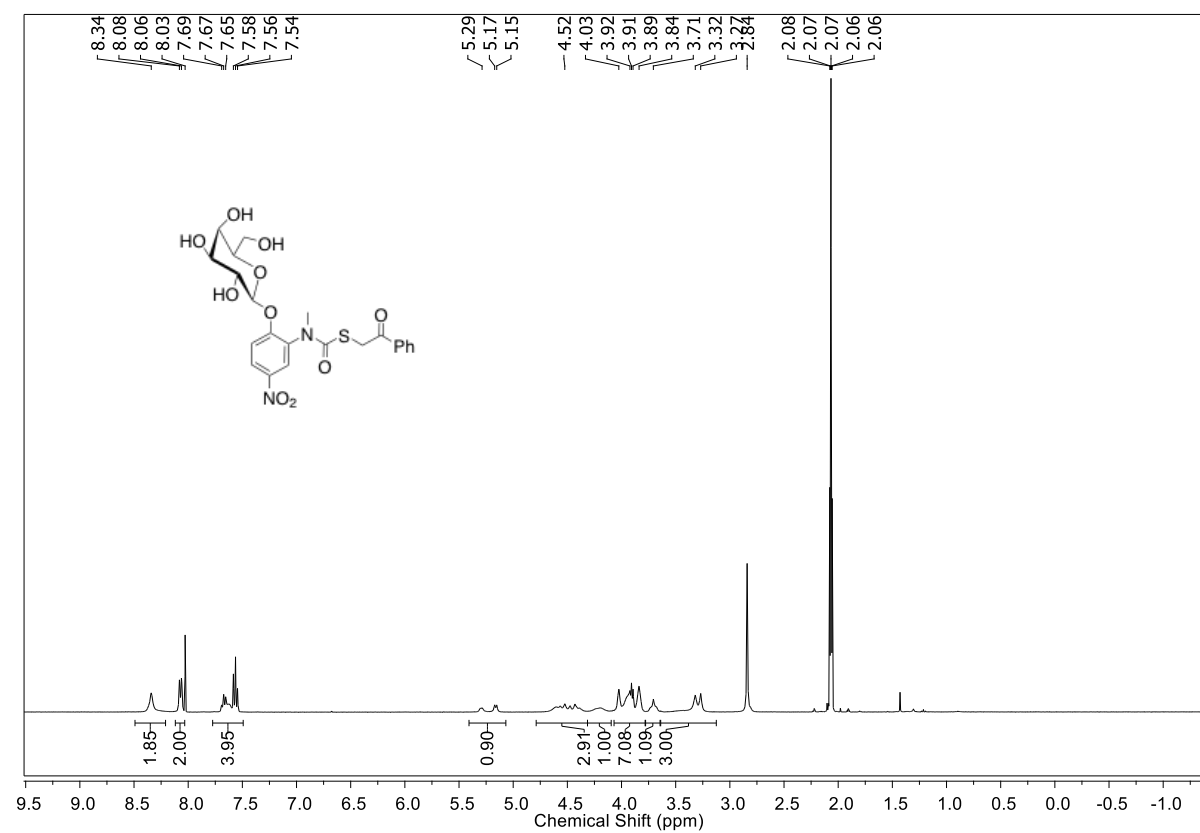
4.2.4.4. Methylene blue assay for the detection of H₂S

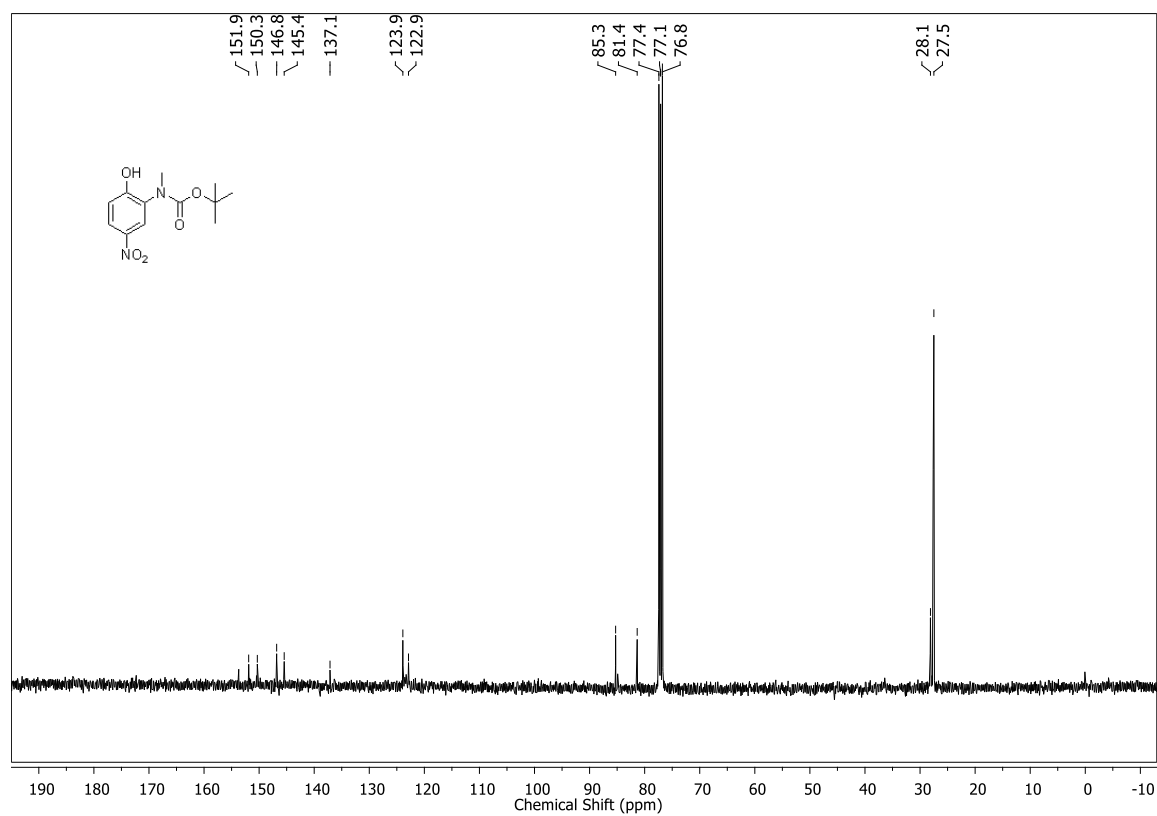
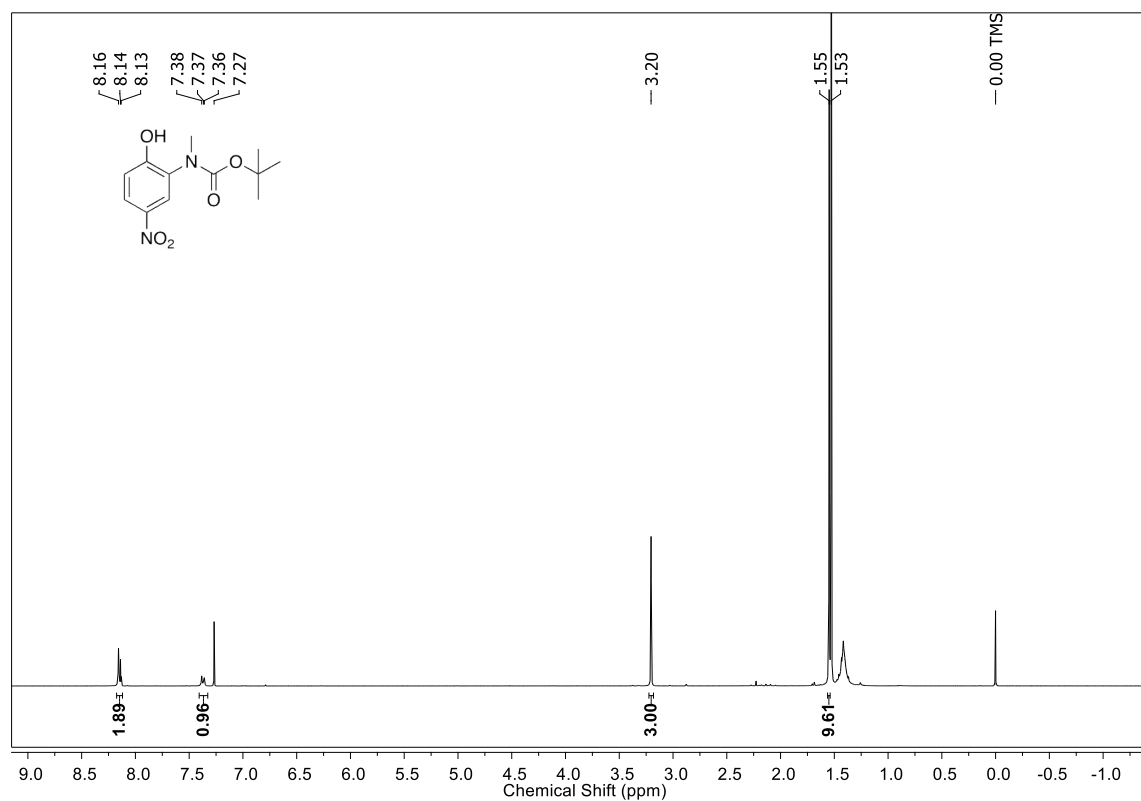
A stock solution of **25** (10 mM), **30** (10 mM) and **38** (10 mM) were prepared in DMSO. β -galactosidase (100 U/mL), DTT (100 mM) and Zn(OAc)₂·2H₂O (40 mM) were prepared in DI water. Stock solution of FeCl₃ (30 mM) was prepared in 1.2 M HCl and *N,N*-dimethyl-*p*-phenylenediamine sulfate (DMPPDA) (20 mM) was prepared in 7.2 M HCl.

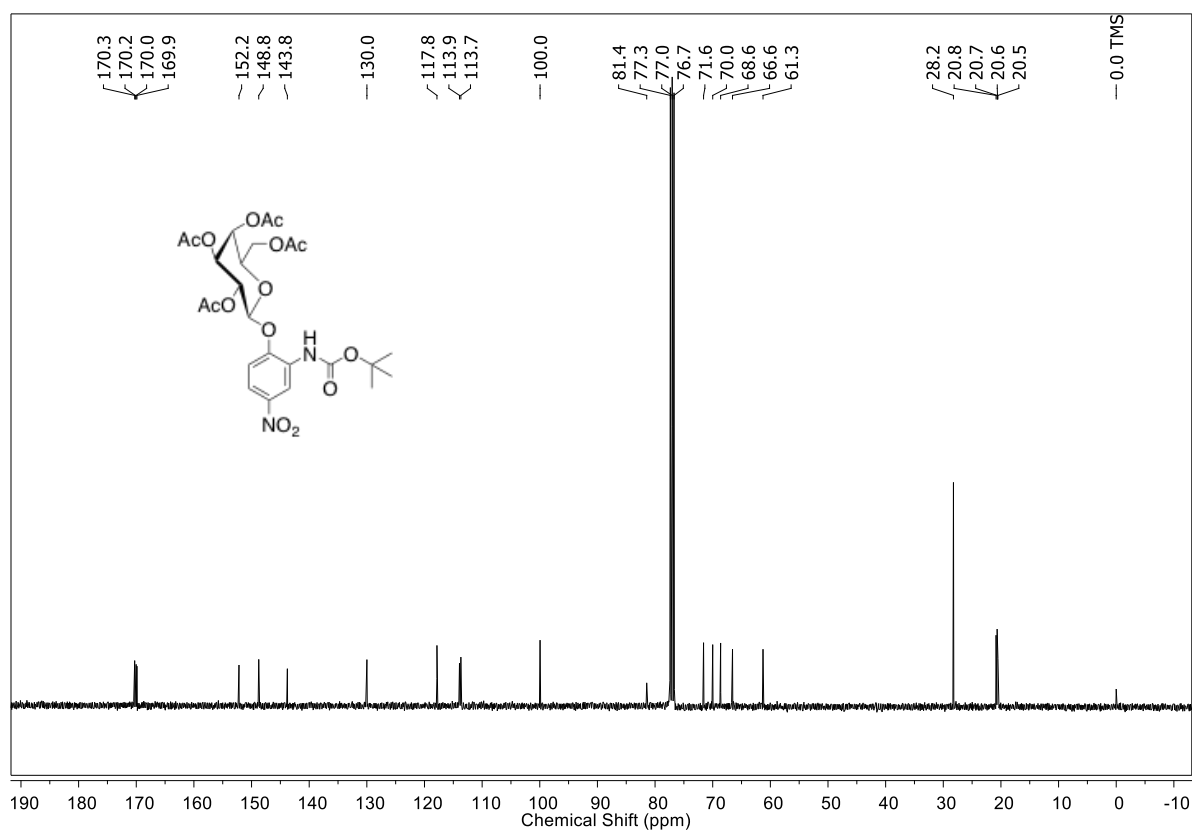
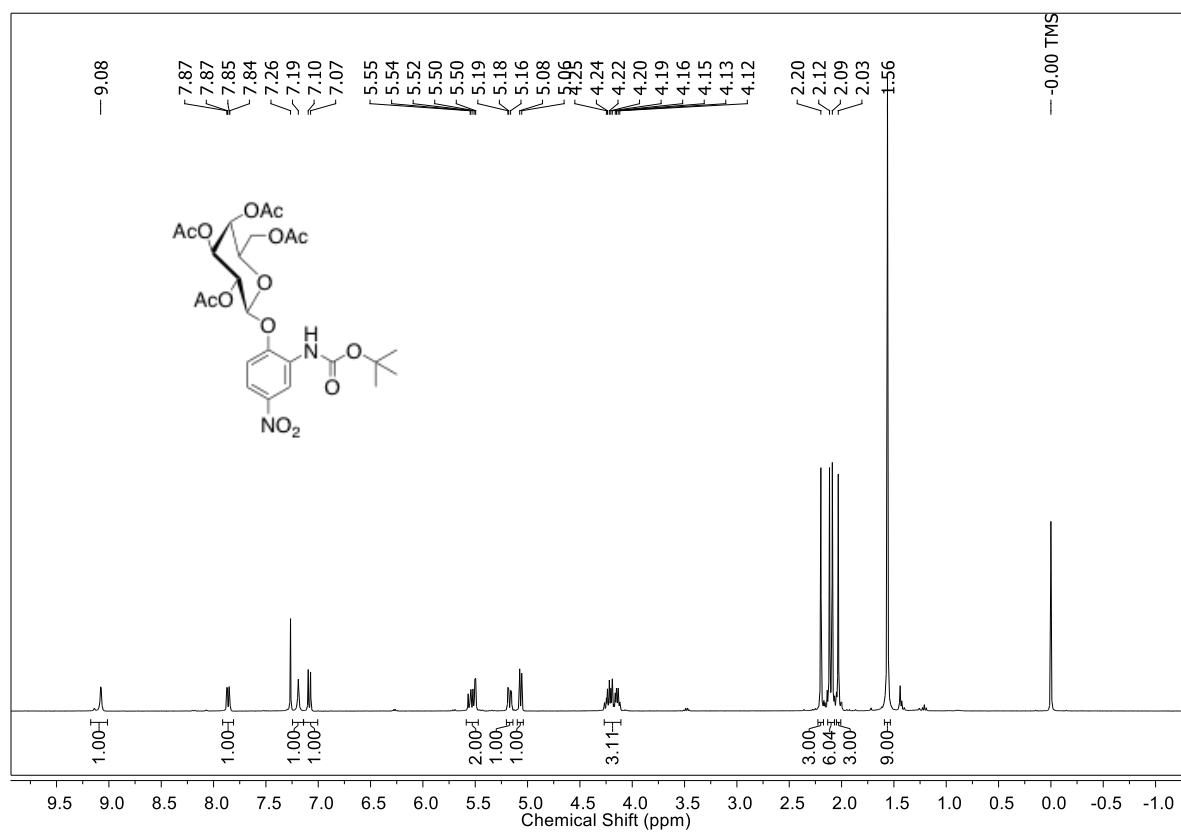
The compounds (100 μ M) were treated with 2 U/mL β -galactosidase (4 μ L, 100 U/mL) in pH 7.4 phosphate buffer (20 mM). The volume was adjusted to 200 μ L using 20 mM phosphate buffer, pH 7.4 and incubated at 37 °C for 30 mins. This was followed by addition of 1 μ M *b3*-MST (3 μ L, 66 μ M stock) or 1 μ M wt *h3*-MST (5 μ L, 40 μ M stock), 1 mM DTT (2 μ L, 100 mM stock) and 400 μ M Zn(OAc)₂ (2 μ L, 40 mM stock) and further incubated for 2 h. 100 μ L aliquot was taken from each reaction set and diluted with 100 μ L of FeCl₃ (30 mM stock in 1.2 M HCl) and 100 μ L of DMPPDA (20 mM in 7.2 M HCl). The mixture was further incubated at 37 °C for 30 mins. The aliquots were transferred to a 96 well plate (200 μ L/well)

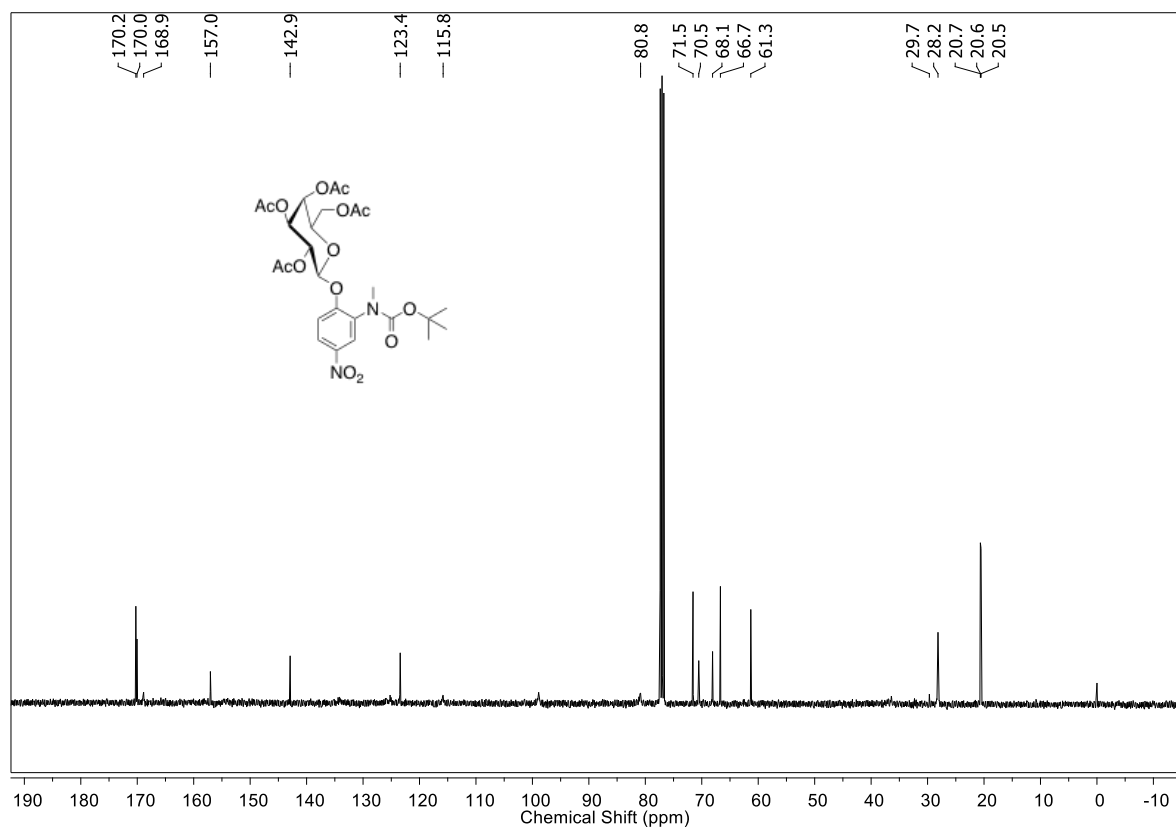
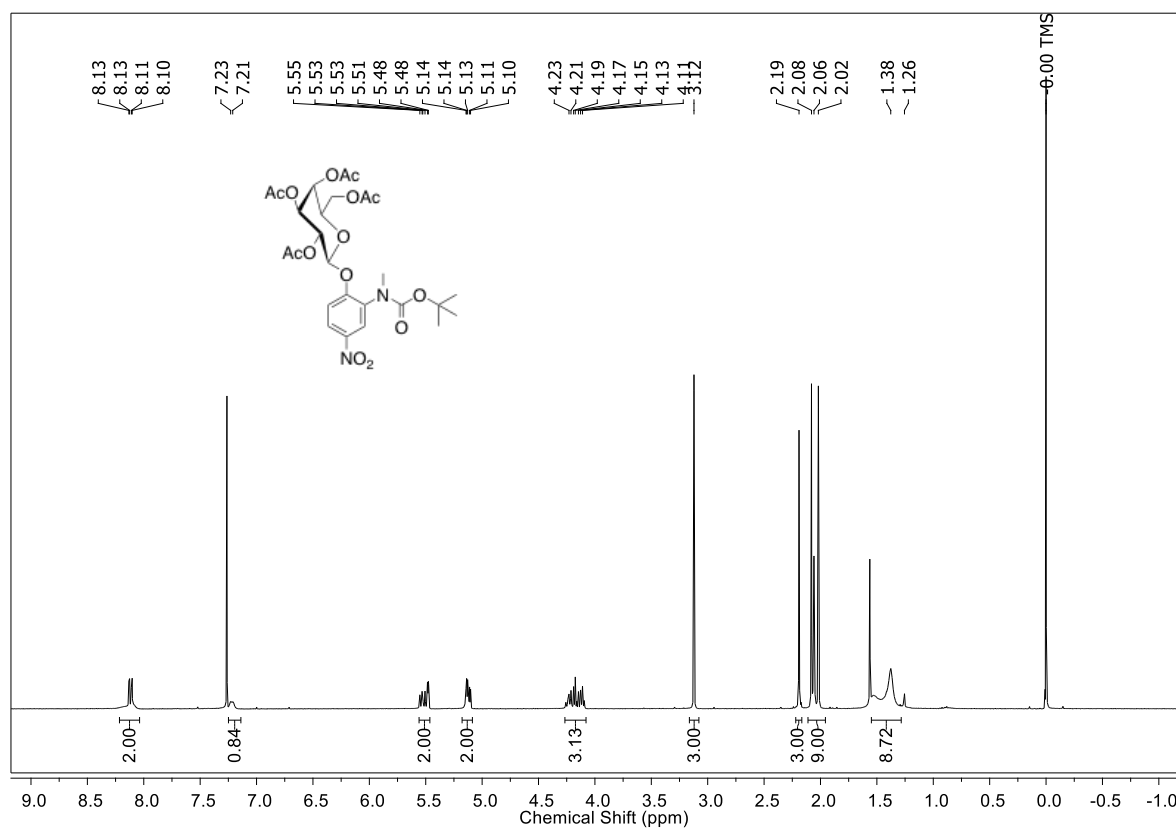
and the absorbance spectra were recorded from 550 nm to 800 nm range using a microtiter plate reader. Absorbance value for methylene blue was recorded at 676 nm.

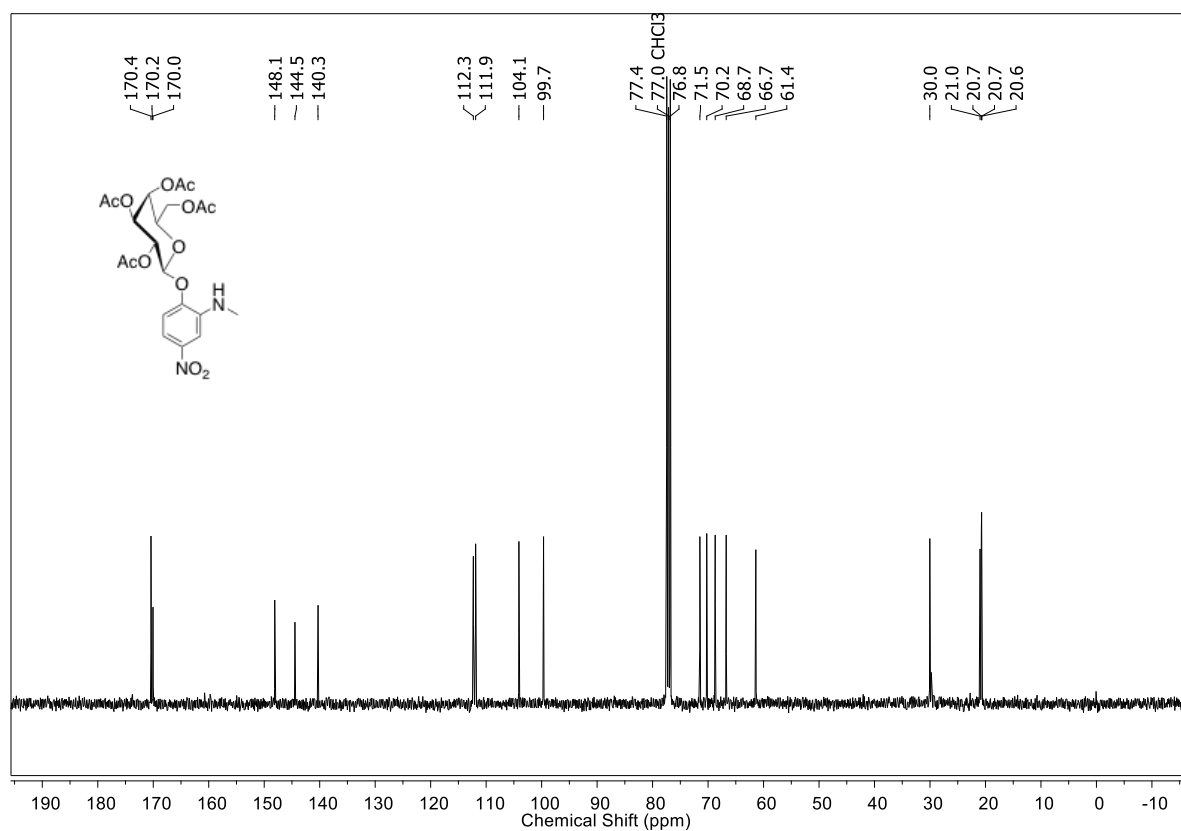
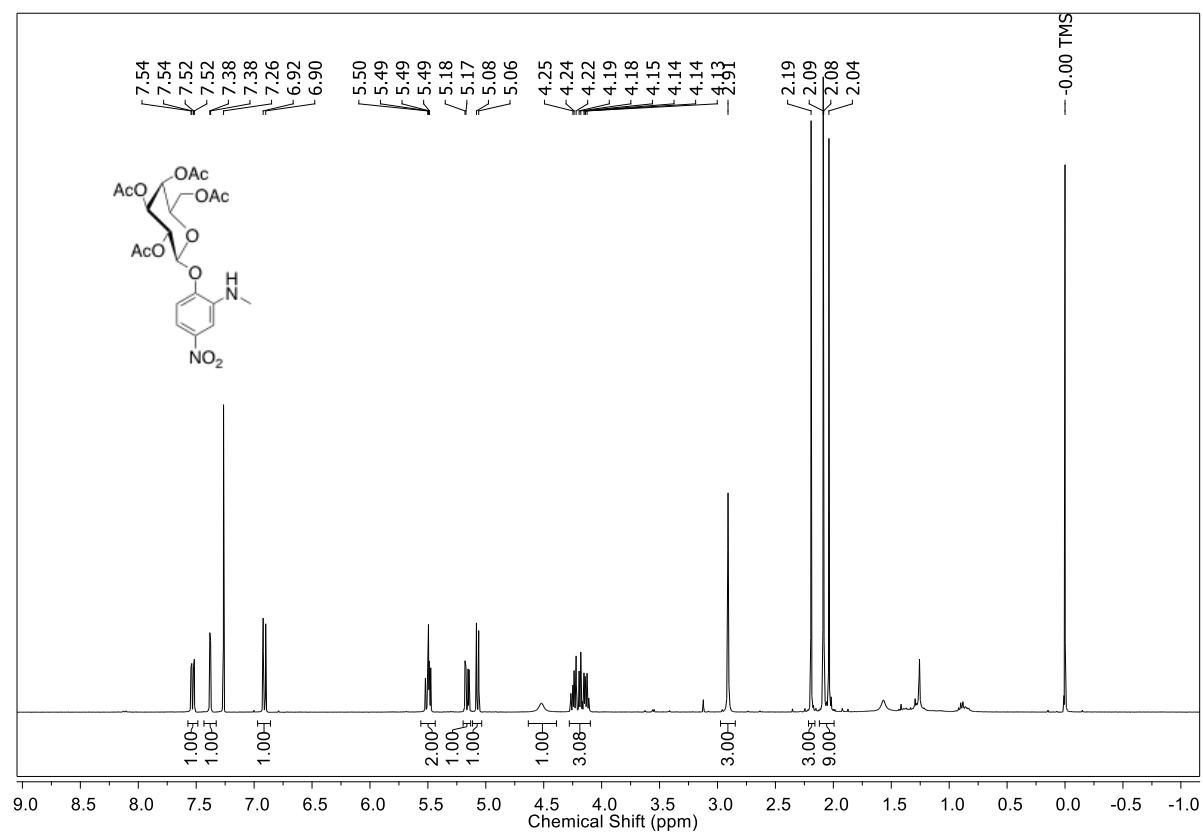
4.2.5. NMR spectra of compounds

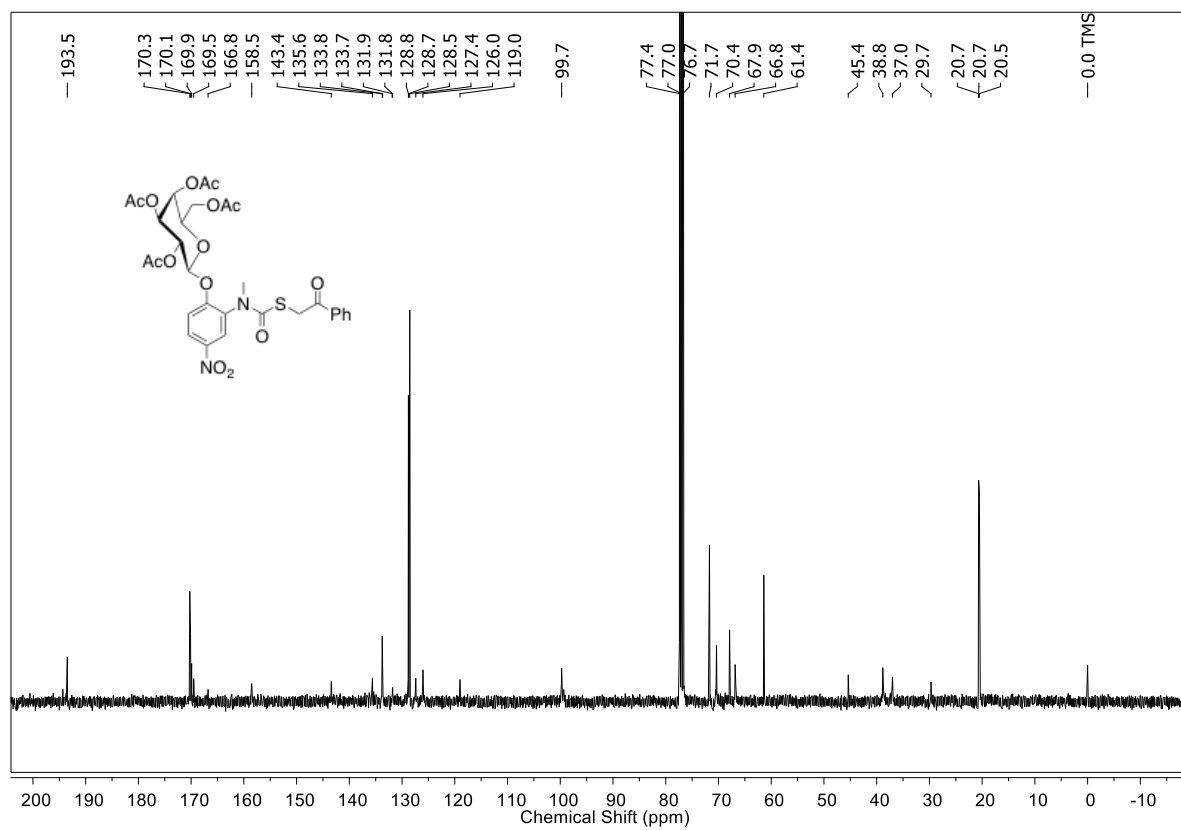
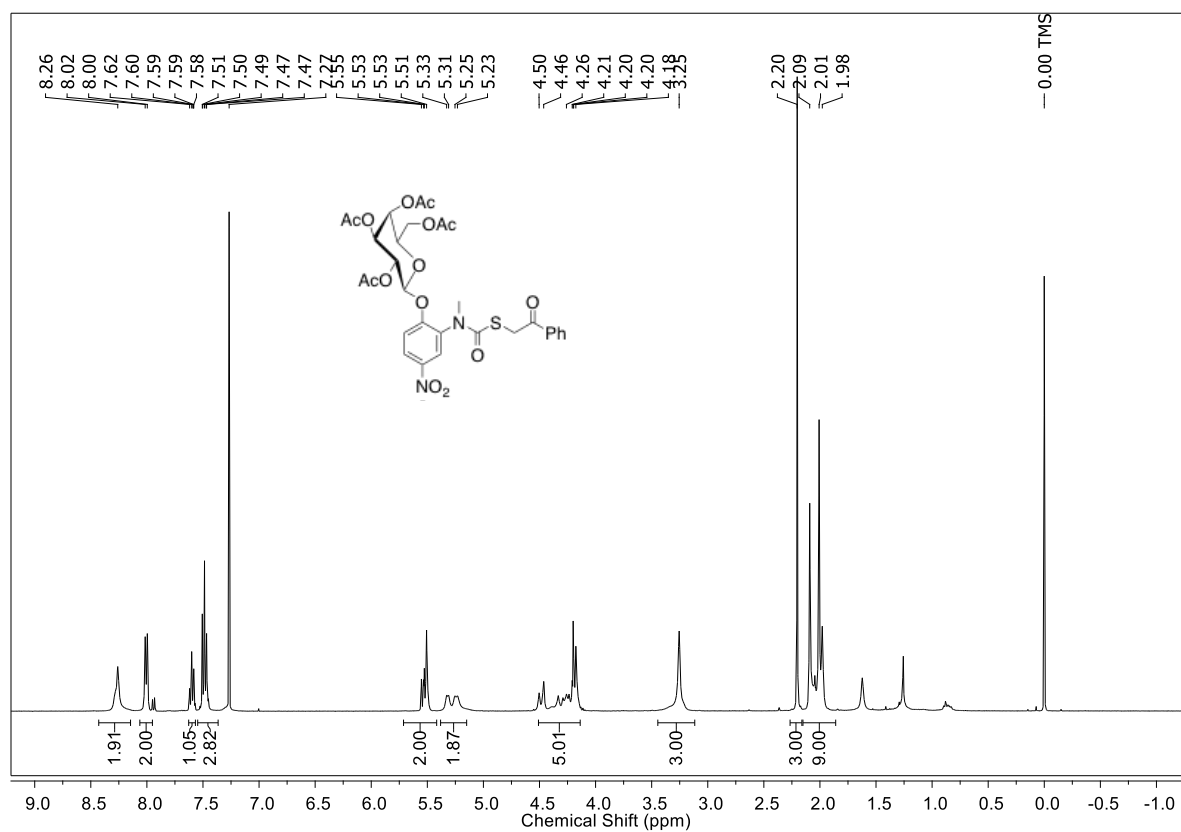
 ^1H and ^{13}C NMR spectra of **30**

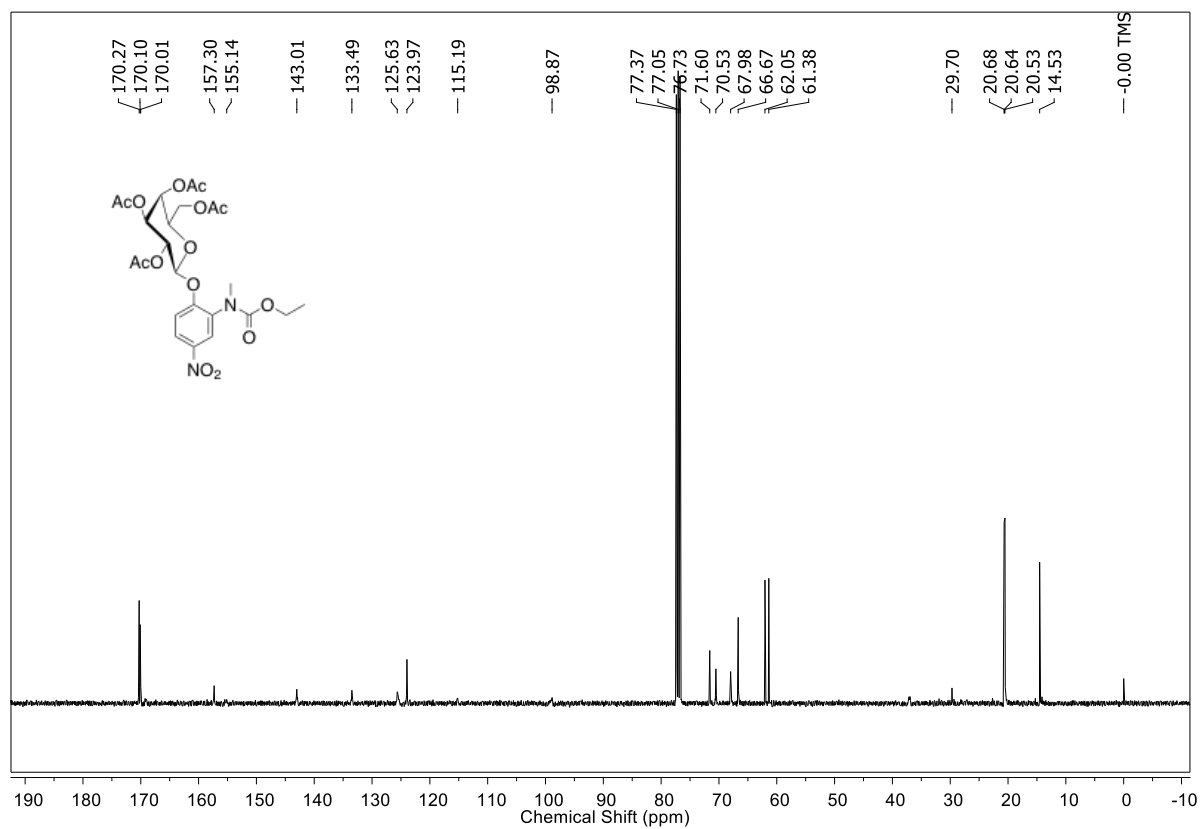
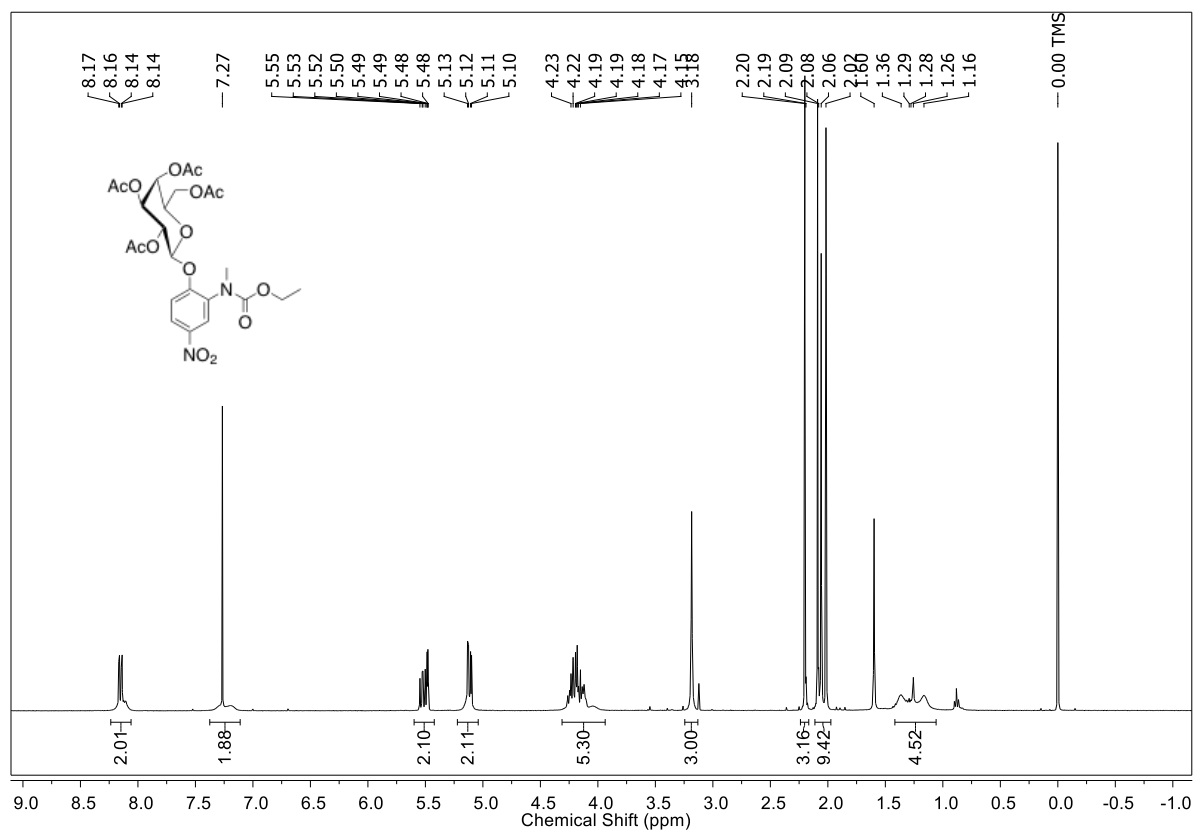
^1H and ^{13}C NMR spectra of **32**

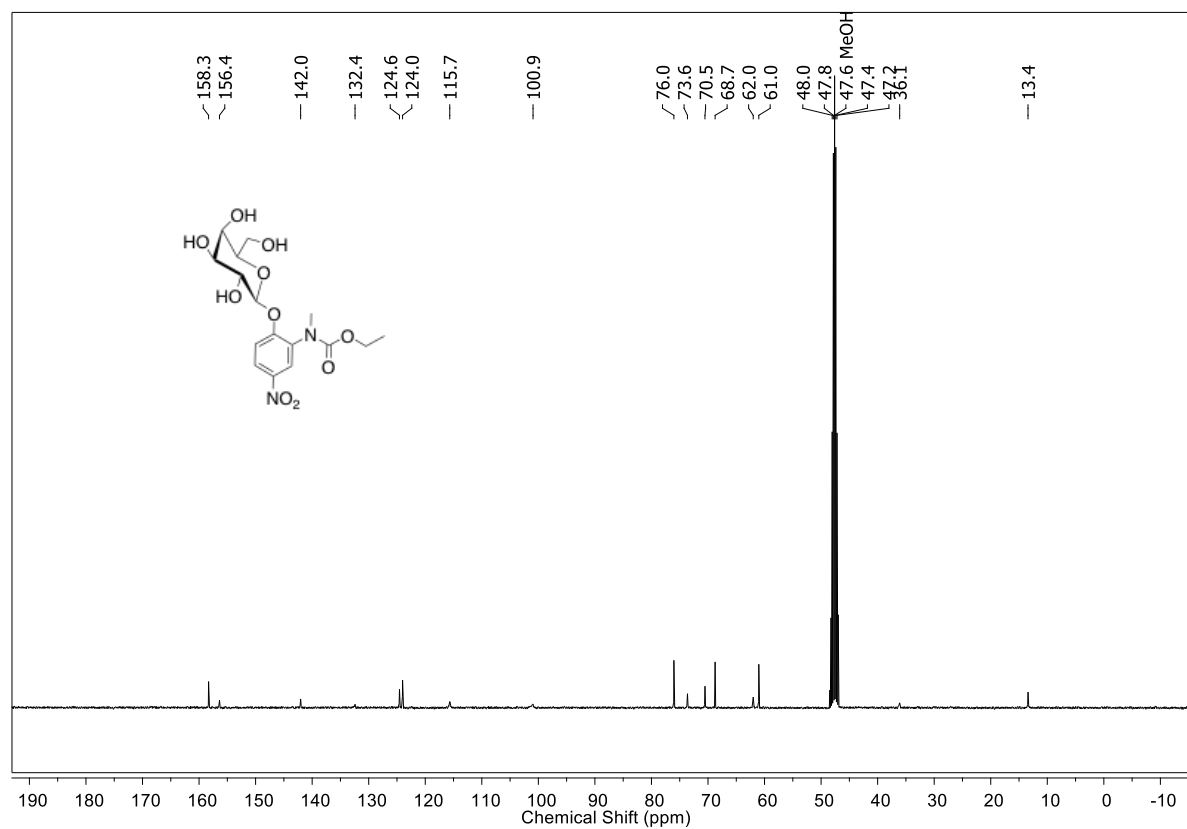
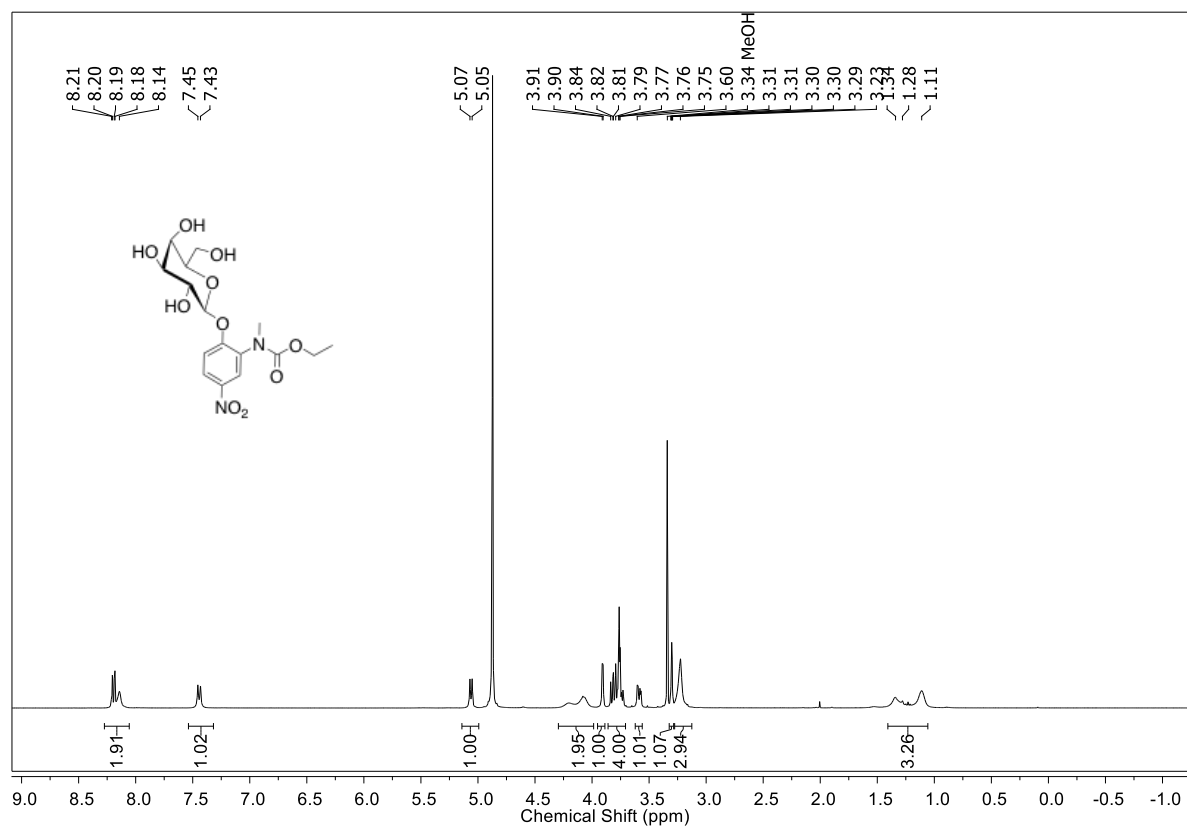
^1H and ^{13}C NMR spectra of **33**

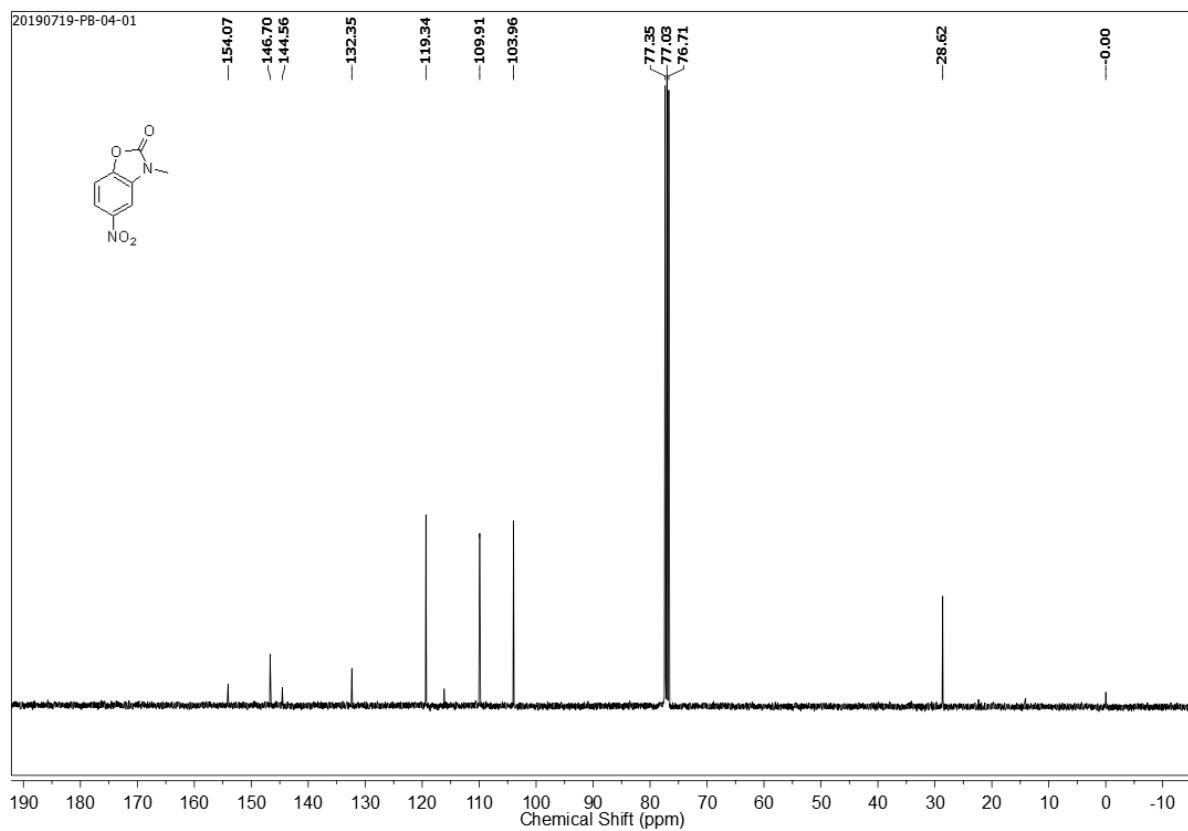
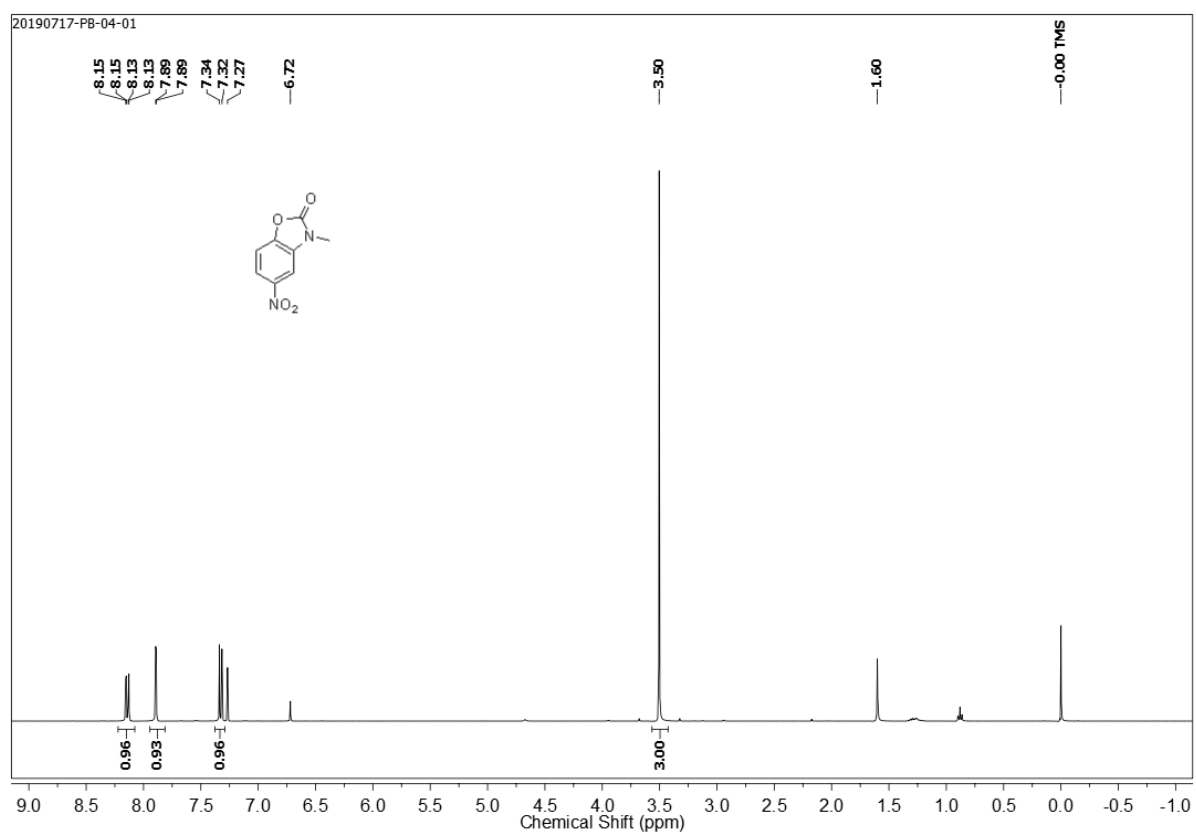
^1H and ^{13}C NMR spectra of **34**

^1H and ^{13}C NMR spectra of **35**

^1H and ^{13}C NMR spectra of **36**

^1H and ^{13}C NMR spectra of **37**

^1H and ^{13}C NMR spectra of **38**

^1H and ^{13}C NMR spectra of **31**

4.2.6. References

- (1) White, R. R.; Vijg, J., Do DNA Double-Strand Breaks Drive Aging? *Mol. Cell* **2016**, *63* (5), 729–738.
- (2) Dou, Z.; Ghosh, K.; Vizioli, M. G.; Zhu, J.; Sen, P.; Wangensteen, K. J.; Simithy, J.; Lan, Y.; Lin, Y.; Zhou, Z.; Capell, B. C.; Xu, C.; Xu, M.; Kieckhaefer, J. E.; Jiang, T.; Shoshkes-Carmel, M.; Tanim, K. M. A. Al; Barber, G. N.; Seykora, J. T.; Millar, S. E.; Kaestner, K. H.; Garcia, B. A.; Adams, P. D.; Berger, S. L., Cytoplasmic chromatin triggers inflammation in senescence and cancer. *Nature* **2017**, *550* (7676), 402–406.
- (3) Neurohr, G. E.; Terry, R. L.; Lengfeld, J.; Bonney, M.; Brittingham, G. P.; Moretto, F.; Miettinen, T. P.; Vaites, L. P.; Soares, L. M.; Paulo, J. A.; Harper, J. W.; Buratowski, S.; Manalis, S.; van Werven, F. J.; Holt, L. J.; Amon, A., Excessive Cell Growth Causes Cytoplasm Dilution And Contributes to Senescence. *Cell* **2019**, *176* (5), 1083-1097.e18.
- (4) Sapienza, P.; Mallette, F. A., Cellular Senescence in Postmitotic Cells: Beyond Growth Arrest. *Trends Cell Biol.* **2018**, *28* (8), 595–607.
- (5) Harman, D., Aging: A Theory Based on Free Radical and Radiation Chemistry. *J. Gerontol.* **1956**, *11* (3), 298–300.
- (6) Fusco, D.; Colloca, G.; Lo Monaco, M. R.; Cesari, M., Effects of antioxidant supplementation on the aging process. *Clin. Interv. Aging* **2007**, *2* (3), 377–387.
- (7) Bonnefoy, M.; Draï, J.; Kostka, T., Antioxidants to slow aging, facts and perspectives. *Presse Med.* **2002**, *31* (25), 1174–1184.
- (8) Chen, Y.-H.; Yao, W.-Z.; Geng, B.; Ding, Y.-L.; Lu, M.; Zhao, M.-W.; Tang, C.-S., Endogenous Hydrogen Sulfide in Patients With COPD. *Chest* **2005**, *128* (5), 3205–3211.
- (9) Yang, G.; Zhao, K.; Ju, Y.; Mani, S.; Cao, Q.; Puukila, S.; Khaper, N.; Wu, L.; Wang, R., Hydrogen Sulfide Protects Against Cellular Senescence via S-Sulfhydration of Keap1 and Activation of Nrf2. *Antioxid. Redox Signal.* **2013**, *18* (15), 1906–1919.
- (10) Zivanovic, J.; Kouroussis, E.; Kohl, J. B.; Adhikari, B.; Bursac, B.; Schott-Roux, S.; Petrovic, D.; Miljkovic, J. L.; Thomas-Lopez, D.; Jung, Y.; Miler, M.; Mitchell, S.;

- Milosevic, V.; Gomes, J. E.; Benhar, M.; Gonzales-Zorn, B.; Ivanovic-Burmazovic, I.; Torregrossa, R.; Mitchell, J. R.; Whiteman, M.; Schwarz, G.; Snyder, S. H.; Paul, B. D.; Carroll, K. S.; Filipovic, M. R., Selective Persulfide Detection Reveals Evolutionarily Conserved Antiaging Effects of S-Sulphydration. *Cell Metab.* **2019**, *30* (6), 1152-1170.e13.
- (11) Dimri, G. P.; Lee, X.; Basile, G.; Acosta, M.; Scott, G.; Roskelley, C.; Medrano, E. E.; Linskens, M.; Rubelj, I.; Pereira-Smith, O., A biomarker that identifies senescent human cells in culture and in aging skin in vivo. *Proc. Natl. Acad. Sci.* **1995**, *92* (20), 9363–9367.
- (12) Horwitz, J. P.; Chua, J.; Curby, R. J.; Tomson, A. J.; Da Rooge, M. A.; Fisher, B. E.; Mauricio, J.; Klundt, I., Substrates for Cytochemical Demonstration of Enzyme Activity. I. Some Substituted 3-Indolyl- β -D-glycopyranosides 1a. *J. Med. Chem.* **1964**, *7* (4), 574–575.
- (13) Urano, Y.; Kamiya, M.; Kanda, K.; Ueno, T.; Hirose, K.; Nagano, T., Evolution of Fluorescein as a Platform for Finely Tunable Fluorescence Probes. *J. Am. Chem. Soc.* **2005**, *127* (13), 4888–4894.
- (14) Gu, K.; Xu, Y.; Li, H.; Guo, Z.; Zhu, S.; Zhu, S.; Shi, P.; James, T. D.; Tian, H.; Zhu, W.-H., Real-Time Tracking and In Vivo Visualization of β -Galactosidase Activity in Colorectal Tumor with a Ratiometric Near-Infrared Fluorescent Probe. *J. Am. Chem. Soc.* **2016**, *138* (16), 5334–5340.
- (15) Huvelle, S.; Alouane, A.; Le Saux, T.; Jullien, L.; Schmidt, F., Syntheses and kinetic studies of cyclisation-based self-immolative spacers. *Org. Biomol. Chem.* **2017**, *15* (16), 3435–3443.
- (16) Chen, X.; Ma, X.; Zhang, Y.; Gao, G.; Liu, J.; Zhang, X.; Wang, M.; Hou, S., Ratiometric fluorescent probes with a self-immolative spacer for real-time detection of β -galactosidase and imaging in living cells. *Anal. Chim. Acta* **2018**, *1033*, 193–198.
- (17) Youn, S. W.; Kim, Y. H., Pd(II)/Ag(I)-Promoted One-Pot Synthesis of Cyclic Ureas from (Hetero)Aromatic Amines and Isocyanates. *Org. Lett.* **2016**, *18* (23), 6140–6143.
- (18) Patel, J. Z.; Nevalainen, T. J.; Savinainen, J. R.; Adams, Y.; Laitinen, T.; Runyon, R. S.;

- Vaara, M.; Ahenkorah, S.; Kaczor, A. A.; Navia-Paldanius, D.; Gynther, M.; Aaltonen, N.; Joharapurkar, A. A.; Jain, M. R.; Haka, A. S.; Maxfield, F. R.; Laitinen, J. T.; Parkkari, T., Optimization of 1,2,5-Thiadiazole Carbamates as Potent and Selective ABHD6 Inhibitors. *ChemMedChem* **2015**, *10* (2), 253–265.
- (19) Hiskey, R. G.; Carroll, F. I.; Smith, R. F.; Corbett, R. T., N,N-Diphenylthiocarbamates as Derivatives of Mercaptans 1. *J. Org. Chem.* **1961**, *26* (11), 4756–4757.
- (20) Chauhan, P.; Bora, P.; Ravikumar, G.; Jos, S.; Chakrapani, H., Esterase Activated Carbonyl Sulfide/Hydrogen Sulfide (H₂S) Donors. *Org. Lett.* **2017**, *19* (1), 62–65.
- (21) Wedmann, R.; Onderka, C.; Wei, S.; Szijártó, I. A.; Miljkovic, J. L.; Mitrovic, A.; Lange, M.; Savitsky, S.; Yadav, P. K.; Torregrossa, R.; Harrer, E. G.; Harrer, T.; Ishii, I.; Gollasch, M.; Wood, M. E.; Galardon, E.; Xian, M.; Whiteman, M.; Banerjee, R.; Filipovic, M. R., Improved tag-switch method reveals that thioredoxin acts as depersulfidase and controls the intracellular levels of protein persulfidation. *Chem. Sci.* **2016**, *7* (5), 3414–3426.

Synopsis

Stimuli-Responsive Small Molecule Persulfidating Agents

CHAPTER 1: Introduction

Hydrogen sulfide (H_2S) is one of the simplest physiologically relevant thiols. The first report on the physiological relevance of H_2S dates back to 1996, where Kimura and co-workers have reported the role of H_2S as a potential neuromodulator.¹ Ever since there have been mounting evidence of H_2S mediating several intracellular signaling process, joining the family of gasotransmitters along with nitric oxide (NO) and carbon monoxide (CO). H_2S has been reported to play fundamental roles in human physiology, modulating an array of cellular functions including vasodilation,^{2,3} neurotransmission,⁴ angiogenesis,^{5,6} inflammation,^{7,8} hypoxia sensing,⁹ myocardial ischemia reperfusion¹⁰ to name a few. Several studies have demonstrated the cytoprotective nature of H_2S , possibly due to its ability to readily react with a variety of reactive species such as oxyradicals,¹¹ hypochlorous acid¹² and peroxynitrite.¹³

One of the widely accepted mechanisms of H_2S signaling is the oxidative post translational modification (oxPTM) of cysteine residues (CysSH), known as protein persulfidation (CysS–SH). Direct reaction of H_2S with CysSH is limited by redox constraints, since the S in both these species exists in the lowest oxidation state (–2). H_2S can only react with oxidized CysSH residues in the protein such as sulfenic acid (CysS–OH), disulfides (CysS–SCys), nitrosothiols (CysS–NO) or glutathionylated (CysS–SG) cysteine (Figure 1a).^{14–16}

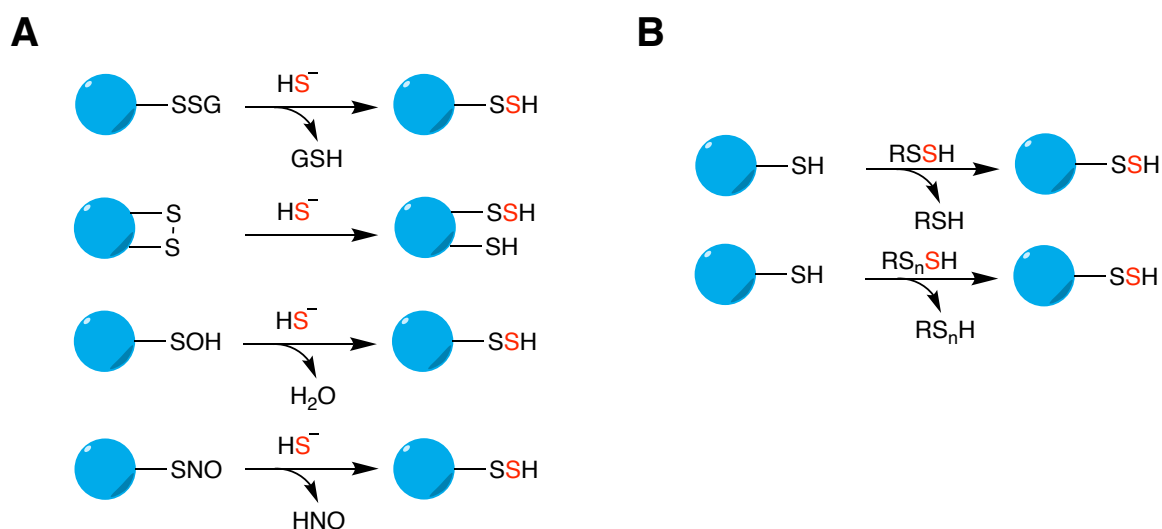


Figure 1. a) Persulfidation of proteins by reaction of H_2S with oxidized cysteine residues. b) Protein persulfidation induced by persulfides and polysulfides.

While H_2S can induce persulfidation only under oxidative conditions, persulfides (RS-SH) and polysulfides ($\text{RS-S}_n\text{H}$, $\text{RS-S}_n\text{R}$) can directly modify proteins to form persulfide (Figure 1b).¹⁷⁻²¹ Persulfidation of proteins have functional implications in multiple physiological processes, including inflammation,²² antioxidant response,²³ neurodegenerative disorders like Parkinson's disease (PD),²⁴ Alzheimer's disease (AD)²⁵ and Huntington's disease.²⁶ Typically, under conditions of excess H_2O_2 (oxidative stress), cysteine residues in proteins gets oxidized to sulfenic acid (RSOH) which can be further oxidized to the sulfinic (RSO_2H) and sulfonic acid (RSO_3H).²⁷ These are considered to be irreversible modifications and can potentially lead to loss of activity of the protein.^{28,29} However, if the cysteine residues are persulfidated, analogous to the reaction of thiols with H_2O_2 , persulfides are likely to form perthiosulfenic acid (RS-SOH). In presence of excess oxidants, RS-SOH can be further oxidized to form the perthiosulfinic acid ($\text{RS-SO}_2\text{H}$) and the perthiosulfonic acid ($\text{RS-SO}_3\text{H}$), detected as products of oxidation in papain and glutathione peroxidase.^{30,31} Unlike the sulfinic (RSO_2H) and sulfonic acid (RSO_3H) derived from thiols, the persulfide analogues can be reduced by enzymes such as thioredoxin to restore the native thiol (Figure 2).^{32,33} Thus, persulfides can protect proteins from overoxidation under conditions of oxidative stress.

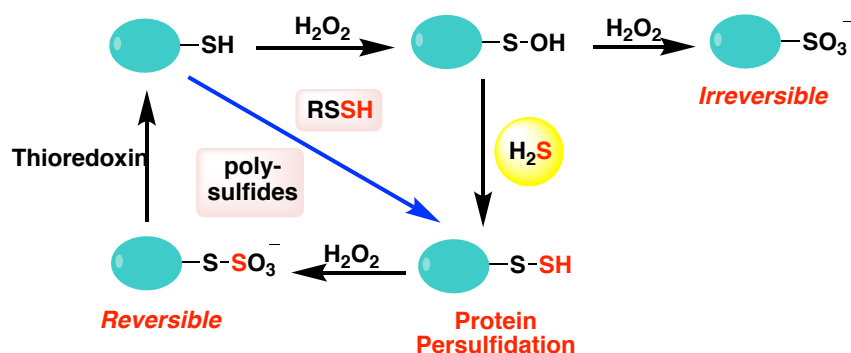


Figure 2. Persulfidation protects protein from overoxidation under conditions of oxidative stress.

With the recent advances in persulfide detection strategies, significant concentrations of LMW persulfides and polysulfides, collectively known as the sulfane sulfur pool have been detected in biological systems. CysS-SH and polysulfides have been detected in a number of cell lines like lung cancer (A549), human neuroblastoma (SH-SY5Y), HeLa and HEK293 cells.^{17,34,35} Akaike and co-workers have detected significantly high concentrations of GS-SH in the brain tissue of mice ($150 \mu\text{M}$) along with the heart and lung tissues ($50 \mu\text{M}$).

One of the major pathways for the biosynthesis of persulfides involves the enzyme, sulfurtransferase. The catalytic cycle of sulfurtransferases proceeds via a two-step reaction; the

active site cysteine forms a transient persulfide intermediate (S-SH) by accepting a sulfur from a donor compound. The sulfur then subsequently gets transferred to a thiophilic acceptor, regenerating the native enzyme. These thiophilic acceptors can be proteins like thioredoxin or glutaredoxin or small molecule thiols like cysteine or glutathione that can potentially mediate transpersulfidation of proteins (Figure 3).^{36–39} However, persulfidation of two-cysteine containing proteins are reported to be extremely short-lived due to the presence of a resolving cysteine, leading to a competition between transpersulfidation and H₂S release.

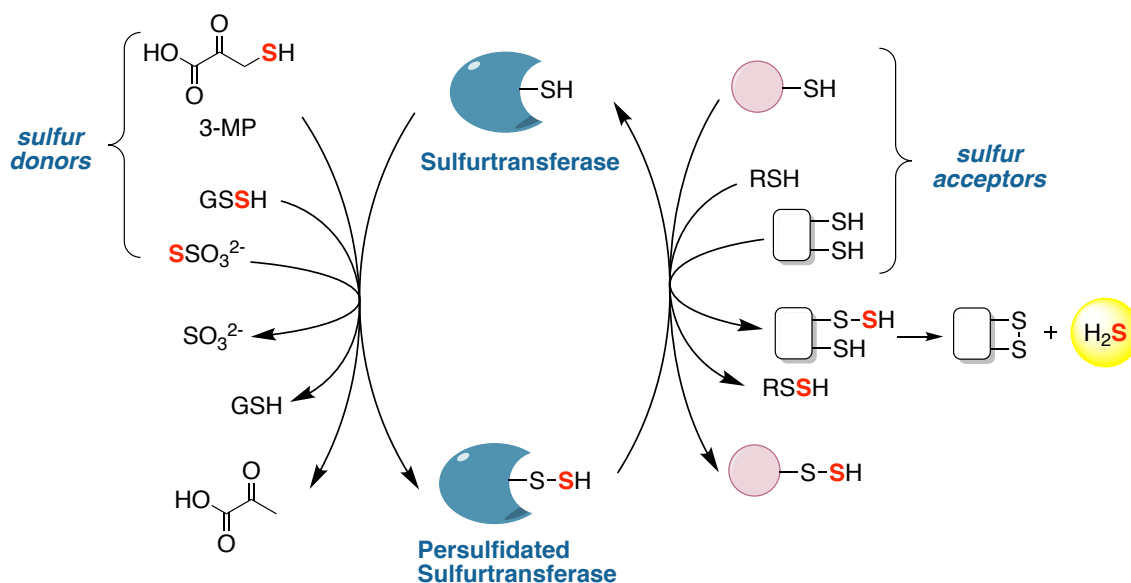


Figure 3. Catalytic cycle of sulfurtransferase. First step of the catalytic cycle involves the active site cysteine forming a persulfide intermediate by accepting a sulfur from the sulfur donor. The second step of the catalytic cycle involves sulfur transfer from the persulfidated enzyme to a sulfur acceptor, reinstating the sulfurtransferase to its original state.

Apart from sulfurtransferase, CBS and CSE, the H₂S producing transsulfuration pathway enzymes are also involved in the biogenesis of LMW persulfides in mammals. The formation of CysS-SH from cystine by CSE was initially reported in 1981.⁴⁰ Only recently, CBS was found to undergo a similar reaction as well (Figure 4).¹⁷

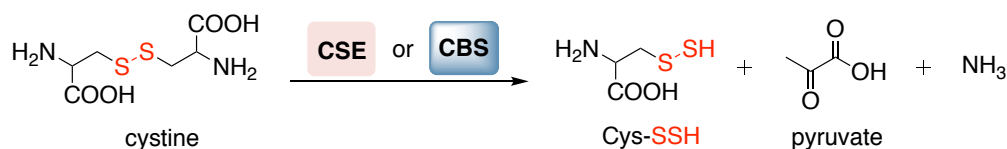


Figure 4. CBS and CSE catalyzing the synthesis of CysS-SH using cystine as the substrate.

Very recently, another enzyme that is involved in the biosynthesis of CysS-SH was discovered.⁴¹ CysteinyI-tRNA synthetase (CARS) is originally known to catalyze the

formation of cysteinyl tRNA via cysteine and aminoacyl tRNA. However, recent biochemical analyses revealed its ability to catalyze the synthesis of CysS-SH using cysteine as the substrate.⁴²

Small molecule persulfides are superior reducing agents and better nucleophiles compared to thiols or H₂S. These reactive species are now recognized as important intermediates in countering oxidative and electrophilic stress.^{17,43,44} Furthermore, persulfidation of proteins is a prominent signaling mechanism mediated by persulfides through which it exerts a wide array of physiological functions. However, persulfides are unstable and undergoes rapid disproportionation in aqueous solution, posing a major challenge in controllable generation of these species *in situ*.⁴⁵ Multiple attempts to isolate persulfides have remained unsuccessful, with the exception of a few sterically hindered persulfides in organic medium, limiting their use in defining their functional implications in biological systems. Hence, to unravel the complex biochemistry of persulfides and delineate its role in sulfur signaling, there is a need to develop precursors or prodrugs of persulfides. These donors should ideally be shelf stable, cell permeable and generate the active persulfide species upon stimulation by a relevant stimulus (Figure 5.). In the recent years, there have been significant advancement in the development of stimuli responsive persulfide prodrugs. The prodrugs reported thus far are have various limitations including lack of trigger specificity and formation of potentially toxic byproducts.

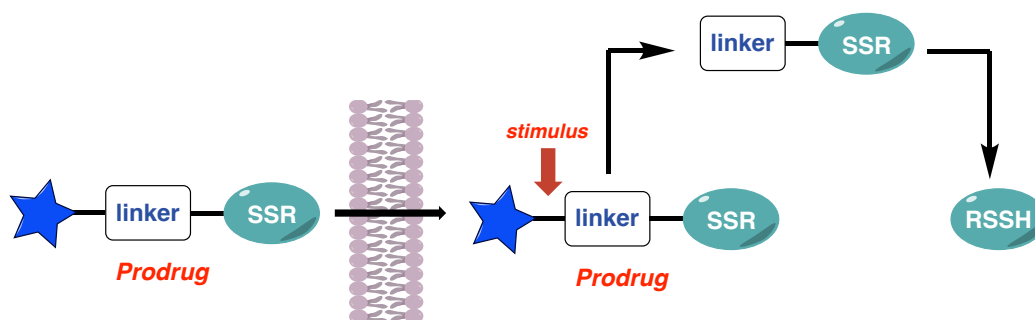


Figure 5. General strategy for prodrug activation to generate persulfides.

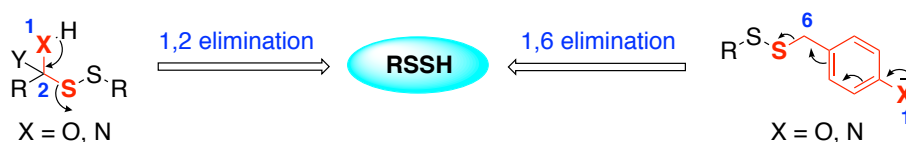
To address these gaps, our aim was to design cell permeable persulfide prodrugs that are responsive to a disease relevant stimulus. In **chapter 2**, we propose a persulfide prodrug responsive to elevated ROS, to closely mimic a diseased state. The strategy for persulfide generation is based on a previously unexplored retro-Michael reaction that would yield cinnamaldehyde as the byproduct. The prodrug was tested for its ability to protect cells against

oxidative stress induced cell death. One of the concerns regarding the above strategy is the formation of cinnamaldehyde, which although widely used in the food industry, is a mild electrophile. In **chapter 3**, we propose a persulfide prodrug activable by the enzyme β -glycosidase, found to be overexpressed under conditions of stress including inflammation and cancer. The prodrugs upon cleavage by β -glycosidase undergoes an intramolecular cyclization to generate sulfane sulfur intracellularly along with a non-electrophilic, heterocyclic byproduct. Although these prodrugs provided important insights into the physicochemical properties of persulfides along with their therapeutic utility, these classes of prodrugs suffered from certain drawbacks. These include complex synthetic strategies, low shelf stability and the disulfide bond being prone to nucleophilic attack. In **chapter 4.1**, we designed compounds without the persulfide moiety but upon entry into cells would generate persulfides. We utilized the biochemical machinery of the cell here to develop artificial substrates for the enzyme 3-mercaptopyruvate sulfurtransferase (3-MST). In **chapter 4.2**, we designed a β -galactosidase activated prodrug of the artificial substrate for 3-MST. β -galactosidase levels are overexpressed in senescence and it is therefore used as a marker for senescence. The prodrug designed can be used as a tool to study the consequences of persulfidation in senescent cells.

Collectively, we have developed two distinct strategies for the intracellular generation of persulfides. The approaches developed herein will help address important questions regarding the role of persulfides in cellular signaling and understand its therapeutic utility.

CHAPTER 2: A Vinyl-Boronate Ester Based Persulfide Donor Sensitive to Reactive Oxygen Species (ROS)

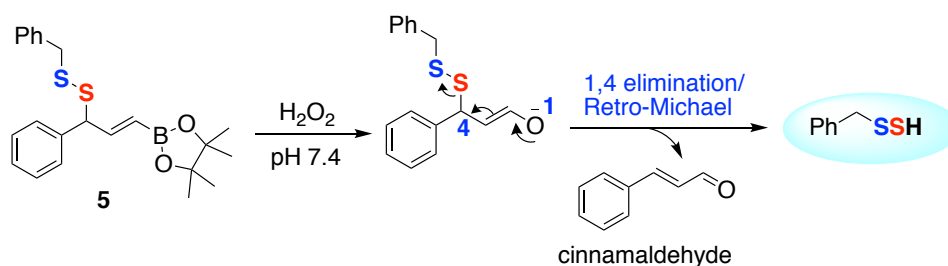
The classes of persulfide prodrugs reported to date can be broadly classified into two categories based on the self-immolation strategy; 1,2-elimination mechanism and 1,6-elimination mechanism that generates a relatively toxic quinone methide byproduct (Scheme 1).⁴⁶



Scheme 1. Classes of persulfide prodrugs based on the self-immolation strategy.

The lack of selectivity in these donors might limit their utility in biological systems. To address these limitations, we designed a prodrug based on a previously unexplored 1,4-O,S-relay or a retro-Michael reaction with a persulfide as a leaving group. Elevated levels of

reactive oxygen species (ROS) can be associated with several diseased conditions.^{3,23,47,48} Therefore, to interrogate the role of persulfides in diseased conditions, we proposed the design of a ROS sensitive persulfide donor. It involves masking the enol as a vinyl boronate ester. It was hypothesized that the vinyl boronate ester would be oxidized in the presence of H₂O₂ to generate the free enolate that can undergo a retro-Michael or 1,4 elimination to release the persulfide and form cinnamaldehyde as a byproduct (Scheme 2).



Scheme 2. Design of ROS sensitive persulfide donor.

Compound **5** was synthesized as the ROS sensitive persulfide donor in 31% yield. **5** in pH 7.4 buffer hydrolyses to the boronic acid which upon incubation with H₂O₂ (10 eq) gradually decomposes over a period of 90 min (Figure 6). A time course of decomposition was obtained and the curve fitting to first order gave a pseudo first order rate constant k_1 $5.3 \times 10^{-2} \text{ min}^{-1}$.

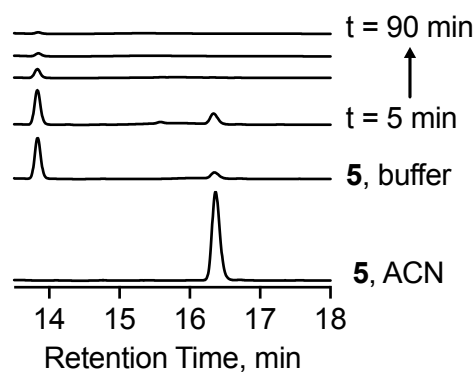
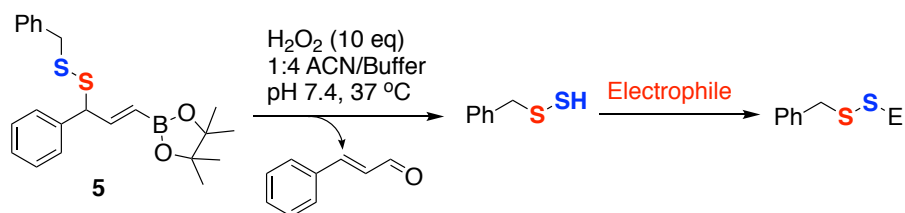


Figure 6. HPLC traces for the decomposition of **5** in the presence of H₂O₂ (10 eq) in pH 7.4 buffer.

Once it was established that compound **5** can be cleaved by H₂O₂ under physiological conditions, we next attempted to detect the release of the persulfide. Persulfides can be detected by trapping it as an adduct of a suitable electrophile (Scheme 3). The adduct formed with electrophile fluorodinitrobenzene (FDNB) was **7** and with monobromobimane (mBBBr) was **8**. The adducts formed were monitored by HPLC.



Scheme 3. Detection of persulfide by trapping it with an electrophile.

Compound **5** upon incubation with FDNB in the presence of H_2O_2 showed a gradual decomposition of the peak corresponding to boronic acid of **5** with a concomitant formation of the adduct **7**, over 60 min (Figure 7). The rate constant (k_3) for the formation of **7** was calculated to be 0.15 min^{-1} .

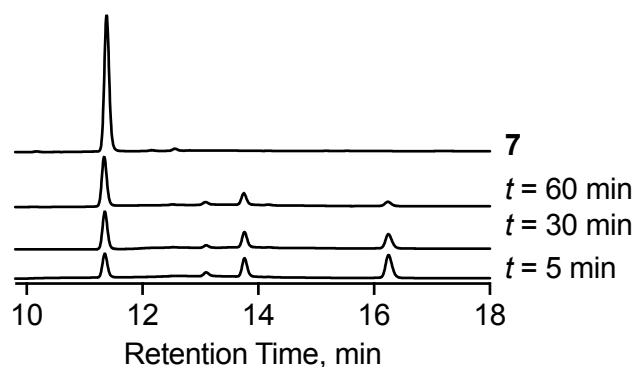


Figure 7. HPLC analysis to monitor the formation of adduct **7** upon reaction of **5** with H_2O_2 in the presence of FDNB in pH 7.4 buffer (containing 20% ACN).

5 was incubated with mBBBr in the presence of H_2O_2 , the boronic acid of **5** decomposed to form the adduct **8** and cinnamaldehyde over a period of 90 min (Figure 8). The formation of adduct **8** was confirmed by mass spectrometry ($m/z = 369.0707$; observed, 369.2551).

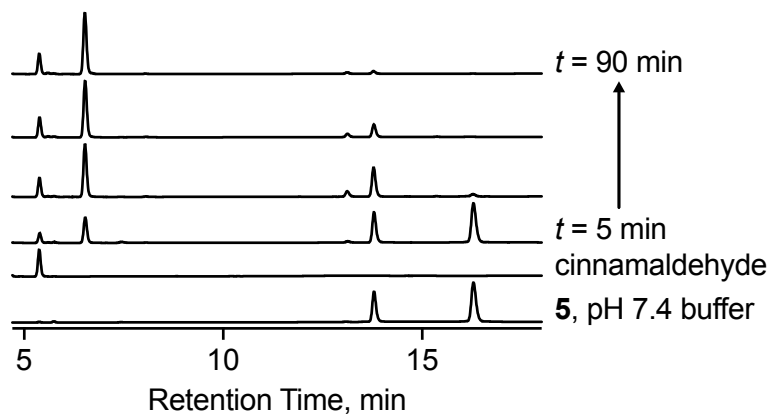


Figure 8. HPLC analysis to monitor the formation of adduct **8** upon reaction of **5** with H_2O_2 in the presence of mBBBr in pH 7.4 buffer (containing 20% ACN).

The time course for the rate of formation of **8** was monitored and its rate constant (k_4) was calculated to be 0.12 min^{-1} . The rate of formation of cinnamaldehyde was monitored under these conditions and the rate constant (k_{cinn}) was calculated to be $12.8 \times 10^{-2} \text{ min}^{-1}$.

To test the selectivity of **5** towards activation by H_2O_2 , a TLC based experiment was carried out to monitor the formation of adduct **7** in the presence of FDNB. Adduct **7** was observed only when compound **5** was treated with H_2O_2 and not in the presence of any other oxidants (Figure 9).

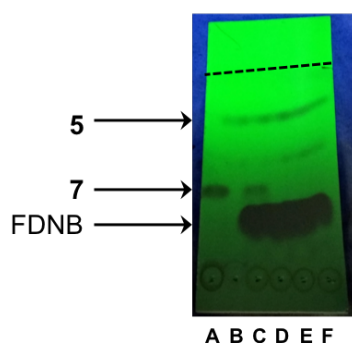
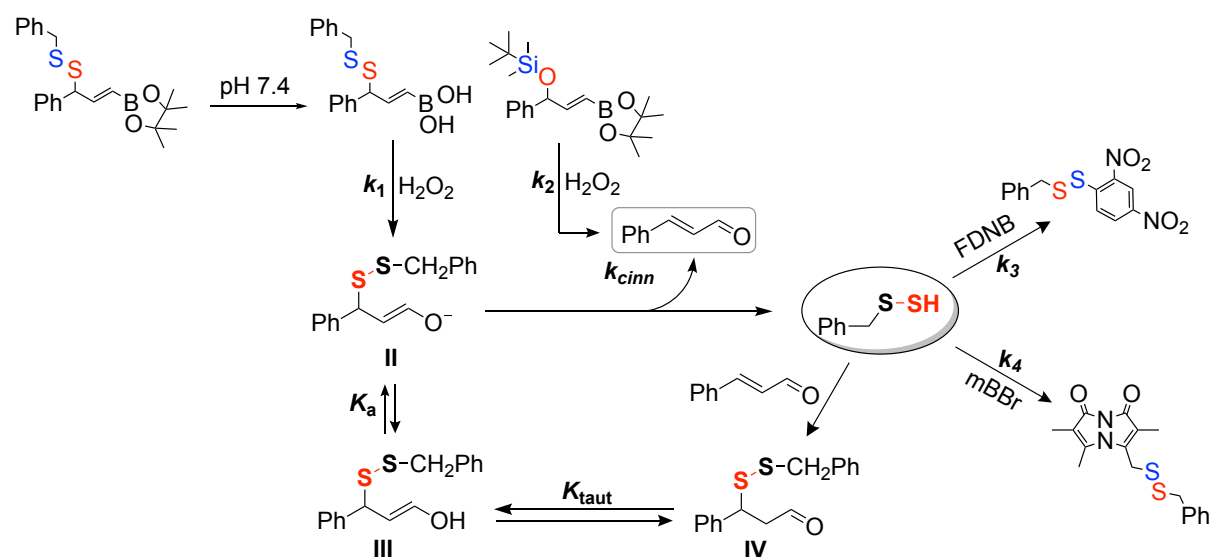


Figure 9. TLC analysis to monitor the formation of **7** upon reaction of **5** with various analytes. (A) authentic **7** (R_f 0.37) (B) **5** alone (R_f 0.66) (C) **5** + H_2O_2 (D) **5** + HOCl (E) **5** + TBHP (F) **5** + GSH.



Scheme 4. Mechanism of persulfide generation from **5** in the presence of H_2O_2 .

Based on these observations, a mechanism for the generation of persulfides from the vinyl boronate ester scaffold was proposed (Scheme 4). The boronate ester moiety hydrolyses in pH 7.4 buffer to form the boronic acid, as observed by the HPLC analysis. The boronic acid functional group reacts with H_2O_2 (10 eq) to form the enolate intermediate (**II**) which then

undergoes 1,4-elimination to generate the persulfide and form cinnamaldehyde as a byproduct. The rate of formation of cinnamaldehyde (k_{cinn}) is comparable to the rates of formation of the persulfide adducts (**7** and **8**), suggesting that the formation of persulfide and the cinnamaldehyde is a concerted process. Therefore, the oxidation of the boronate ester by H_2O_2 is most likely the rate determining step.

Next, the ability of the persulfide prodrug **5** to protect cells from cytotoxicity induced by oxidative stress was evaluated. Menadione and JCHD were used as ROS generators to induce oxidative stress in cells. Co-treatment of DLD-1 cells with **5** and oxidants showed a dose dependent increase in cell viability, compared to the negative control **6**. Thus, suggesting that the persulfide donor **5** was able to rescue cells from the oxidative stress induced cell death by menadione and JCHD (Figure 10).

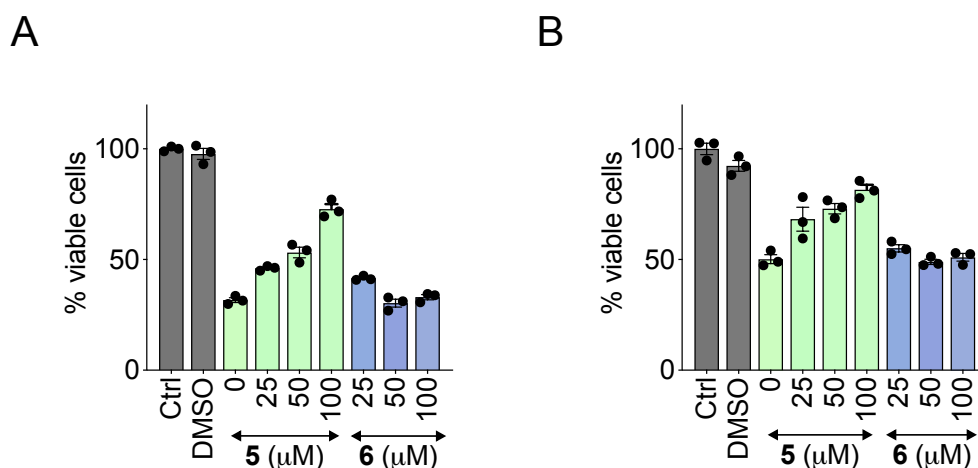


Figure 10. a) Cytoprotective effects of compound **5** against menadione (50 μM). (b) Cytoprotective effects of compound **5** against JCHD (50 μM). Results are expressed as mean ± SEM (n = 3).

CHAPTER 3: Enhancing Intracellular Sulfane Sulfur Through β-glycosidase Activated Prodrugs

Elevated levels of β-glycosidase have been observed in several inflammatory disorders including inflammatory bowel disorder (IBD), ulcerative colitis, Crohn's disease and cancer.^{49,50} The underlying etiology of these inflammatory disorders are multifactorial and is often associated with an excessive production of ROS, leading to collateral tissue damage.⁵¹ Under these conditions, modulating the levels of ROS by an exogenous supply of antioxidants or upregulating the cellular antioxidant machinery is a possible therapeutic approach. Sulfane sulfurs comprising of persulfides and polysulfides have been established as potent antioxidants.^{17,23,33,52} We therefore, proposed the design of β-glycosidase activated persulfide

donors comprising of two series (**10-11**), responsive to β -galactosidase and β -glucosidase respectively (Figure 11). As per our hypothesis, upon cleavage by β -glycosidase the phenolate would undergo an intramolecular cyclization, resulting in the formation of a heterocyclic byproduct (**12**) with the simultaneous release of the persulfide.

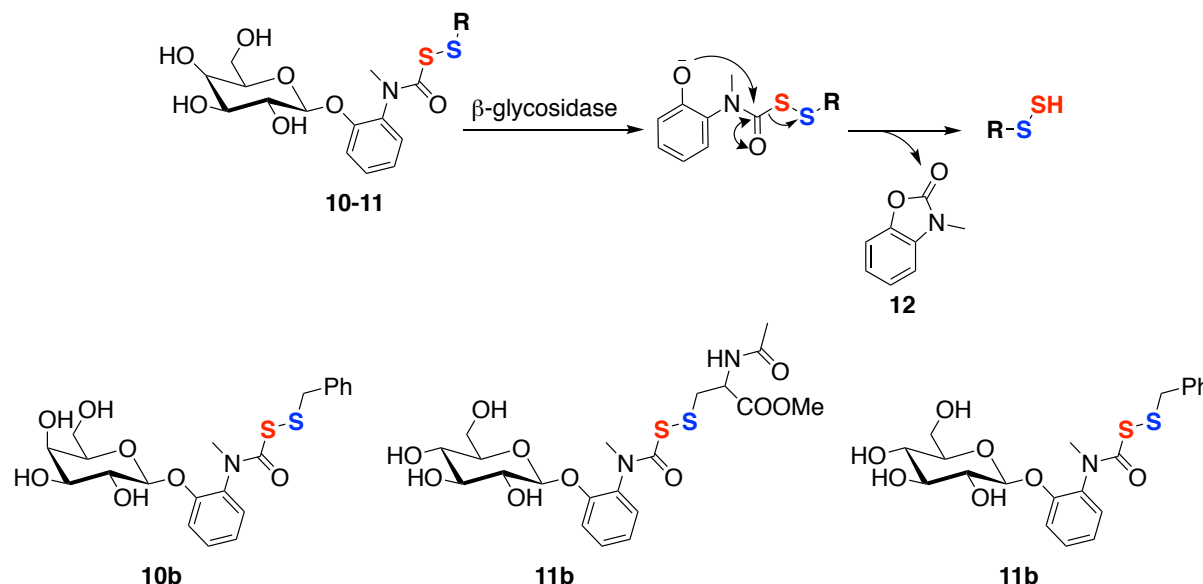


Figure 11. Design of β -glycosidase activated persulfide donor.

Compound **10b** was synthesized as the β -galactosidase activated prodrug and **11a** and **11b** were synthesized as the prodrug activable by β -glucosidase. **11a** upon incubation with β -glucosidase (10 U/mL) decomposed over a period of 10 h with a pseudo first order rate constant k_1 $5.4 \times 10^{-3} \text{ min}^{-1}$ (Figure 12a). LC/MS analysis showed a concomitant formation of the byproduct **12** with a rate constant of $7.1 \times 10^{-3} \text{ min}^{-1}$, which is similar to the rate of decomposition of **11a** (Figure 12b).

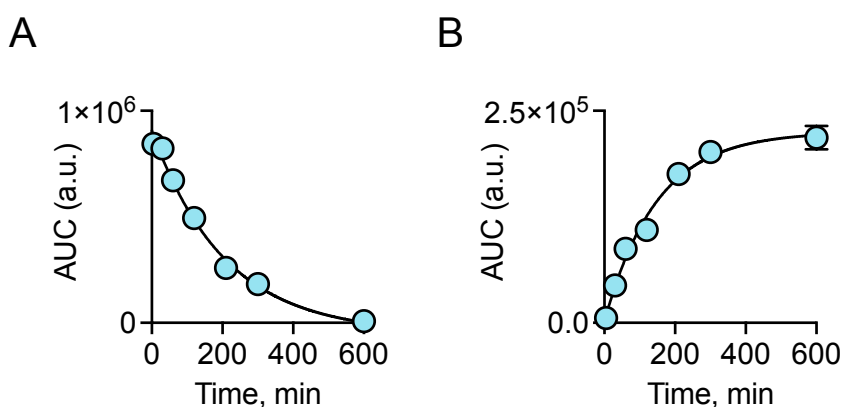


Figure 12. a) Decomposition of **11a** over 10 h in the presence of β -glucosidase was observed, as monitored by LC/MS. Curve fitting to first order gave a rate constant of $5.4 \times 10^{-3} \text{ min}^{-1}$. b) Formation of **12** over 10 h in the presence of β -glucosidase was observed. Curve fitting to first order gave a rate constant of $7.1 \times 10^{-3} \text{ min}^{-1}$.

Next, persulfide/polysulfide generation from the NACMe derivative **11a** was assessed. Persulfides can be detected by reacting it with a suitable electrophile. *N*-(4-hydroxyphenethyl)-2-iodoacetamide (HPE-IAM) has been previously reported as an effective persulfide alkylating agent due to its mild electrophilic nature.⁵³ **11a** was incubated with 10 U/mL of β -glucosidase and HPE-IAM (20 eq) in pH 7.4 phosphate buffer and incubated at 37 °C. The peak for the formation of the HPE-IAM adduct of NACMe persulfide (NACMeS-SH) was observed, which gradually increased over 10 h. In addition, peaks for HPE-AM polysulfide adducts NACMeS-SSH and NACMeS-SSSH were detected as well (Figure 13a). Appreciable amounts of H₂S, H₂S₂ and H₂S₃ were also detected along with the persulfide/polysulfide adducts of NACMe (Figure 13b). Generation of disulfides and trisulfides of NACMe were observed as well under the aforementioned condition.

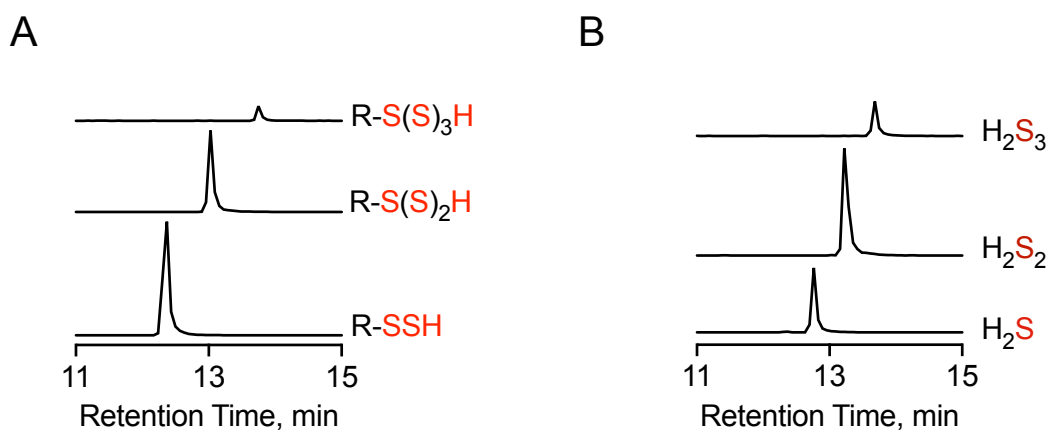
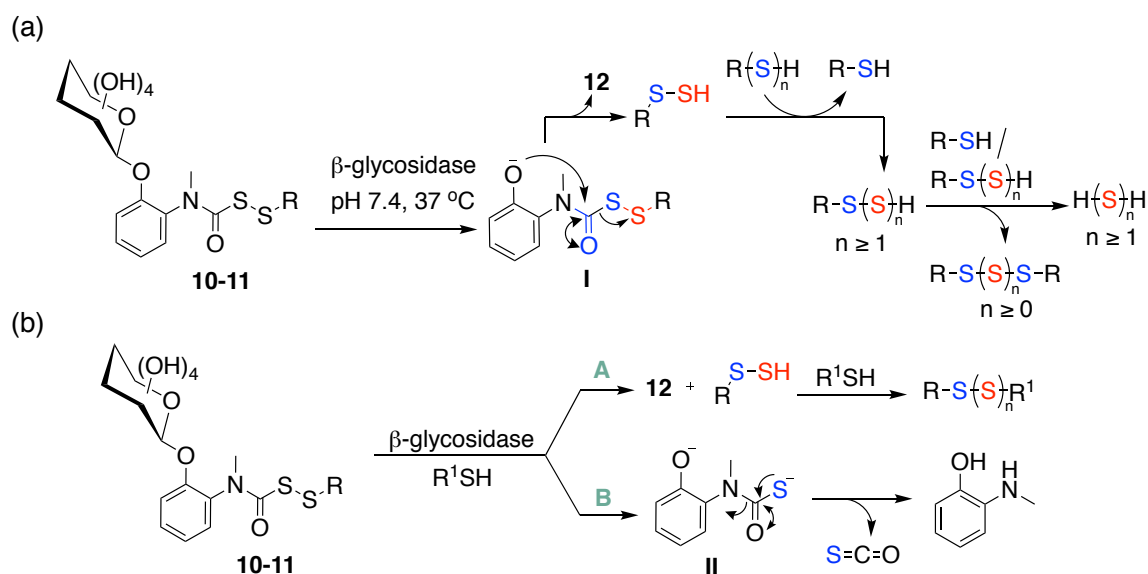


Figure 13. a) Extracted ion chromatogram of persulfides and polysulfides of *N*-acetylcysteine methyl ester (NACMe-S(S)_nH) generated from compound **11a**, detected as their HPE-AM adducts using LC/MS (R = *N*-acetylcysteine methyl ester, NACMe. b) Extracted ion chromatogram of hydrogen sulfide and hydrogen polysulfides detected as their bis-HPE-AM adducts.

Based on the above observations, a mechanism for the generation of persulfides/polysulfides from the glycopersulfide prodrugs was formulated (Scheme 5). The glycoside in prodrugs **10-11** is cleaved by the enzyme β -glycosidase to form the intermediate I. The phenolate in I undergoes an intramolecular cyclization to release the persulfide and form the heterocyclic byproduct **12**. The persulfide once released can further react with itself to form the hydropolysulfide (RSS_nH) species. These species being unstable in nature can ultimately be reduced by thiols or persulfides to generate hydrogen sulfide (H₂S) or polysulfide (H₂S_n).



Scheme 5. a) Proposed mechanism for the generation of persulfides and polysulfides from compounds **10-11**. b) Probable pathways for decomposition in the presence of a thiol.

The persulfide scaffold has been previously reported to be susceptible to thiols, generating COS as a by-product.⁵⁴ COS is known to hydrolyse into H₂S catalysed by the widely prevalent enzyme carbonic anhydrase.⁵⁵ Therefore, in the presence of both β -glycosidase and thiols, there are two possible competing pathways, A and B as shown in Scheme 5b. Pathway A is indicative of persulfide generation as a result of β -glycosidase activation while pathway B indicates COS release upon cleavage of the disulfide bond by thiols.

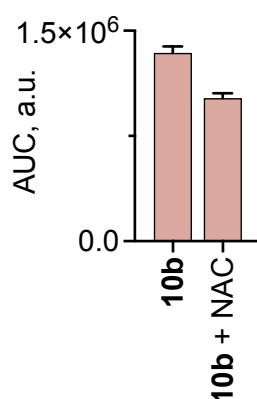


Figure 14. Quantification of the area under the curve (AUC) for the peak corresponding to **12**.

To ascertain the reactivity of the prodrugs towards thiols, compound **10b** was reacted with *N*-acetylcysteine (NAC) in the presence of β -galactosidase. The formation of the byproduct **12** was monitored. A 25% reduction in the yield of **12** was observed within 30 min of incubation, suggesting that thiol reactivity is a minor competing pathway (Figure 14). In

contrast to NAC, a 65% reduction in the formation of the byproduct **12** was observed within 30 min of incubation, suggesting that pathway B is predominant in case of GSH.

Cytotoxicity of compounds **10-11** were tested in two different cell lines, DLD-1 and HepG2. The benzyl persulfide derivatives **10b** and **11b** appeared to be mildly cytotoxic, presumably due to the benzyl moiety, whereas the NACMe persulfide derivative **11a** was well tolerated up to a concentration of 100 μM . To assess the intracellular generation of persulfide/polysulfide from these prodrugs, **11a** was chosen due to its low toxicity profile. To detect intracellular persulfide/polysulfide, the previously reported probe SSP2 was used.⁵⁶ DLD-1 cells were pre-treated with 50 μM SSP2 in the presence of cetyltrimethylammonium bromide (CTAB) followed by incubation with varying doses of **11a** for 1 h. A significant increment in fluorescence, corresponding to the generation of persulfide/polysulfide was observed at a concentration of 0.5 mM of **11a** (Figure 15).

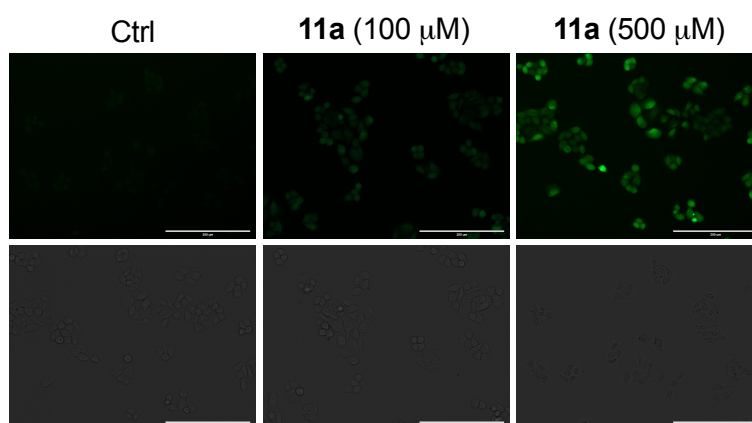


Figure 15. Detection of persulfide/polysulfide generated by compound **11a** in DLD-1 cells, using the dye SSP2. The cells were imaged in the 20x GFP filter. Scale bar is 200 μm .

Next, the ability of the persulfide prodrug **11a** to protect cells from the oxidative stress induced cell death was evaluated. MGR-1 a prodrug of the ROS generator JCHD, which upon cleavage by the widely prevalent enzyme esterase would generate JCHD in cells, was used as the ROS generator. DLD-1 cells were pre-incubated with varying concentrations of **11a** for 12 h followed by treatment with MGR-1 (35 μM) for 4 h. A dose dependent increase in cell viability was observed (Figure 16a). To further corroborate our results, a similar experiment was conducted on another cell line HepG2 and a similar result was obtained (Figure 16b). Collectively, these results suggest that **11a** is a cell permeable persulfide generator that has the potential to protect cells against oxidative damage.

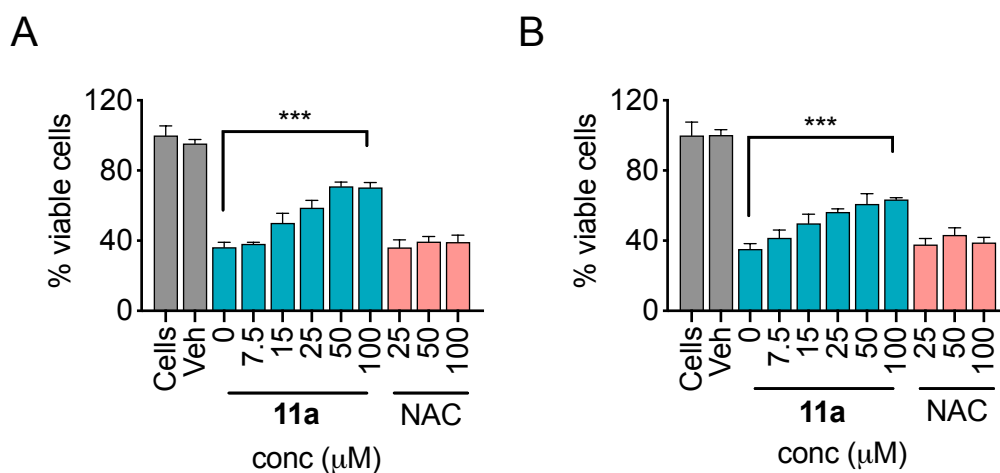


Figure 16. a) Cytoprotective effects of **11a** against ROS induced cell death on DLD-1 cells b) A similar experiment carried out on the liver cell line (HepG2). Results are presented as mean \pm SD (n = 3). (***) p < 0.001 vs MGR-1.

CHAPTER 4.1: Insights into the therapeutic potential of persulfides using artificial substrates for 3-mercaptopyruvate sulfurtransferase (3-MST)

One of the important enzymes involved in the biogenesis of persulfides is the H₂S producing enzyme, 3-mercaptopyruvate sulfurtransferase (3-MST) a member of the sulfurtransferase family. 3-MST utilizes 3-MP as the sulfur acceptor to form a transient persulfide intermediate in its active site cysteine and an enolate of pyruvate as the byproduct.^{37,38} The enolate subsequently tautomerizes to the keto form. The natural substrate for 3-MST which is 3-MP can reportedly generate H₂S spontaneously, through non-enzymatic mechanisms, which can be a potential limitation.⁵⁷ Therefore, we considered developing an artificial substrate with structural features similar to 3-MP, that would be essential for the formation of 3-MST persulfide. We hypothesized that the 3-MST persulfide once formed would feed into the biosynthetic machinery for total cellular persulfidation and H₂S generation. Therefore, we designed compound **26** that has a sulfur donor and an enolizable ketone, similar to 3-MP and would form acetophenone (**27**) as the byproduct after tautomerization (Figure 17). Due to the propensity of thiols to undergo aerial oxidation, **26** was protected as the thioacetate (**25**) to impart stability and longer shelf-life. The thioacetate in **25** can be easily deprotected by the widely prevalent enzyme esterase. **24**, the dimer of ethyl ester of 3-MP was used as the positive control in all the experiments. **28** with an O instead of the S and **29** with an extra methylene group were used as the negative controls.

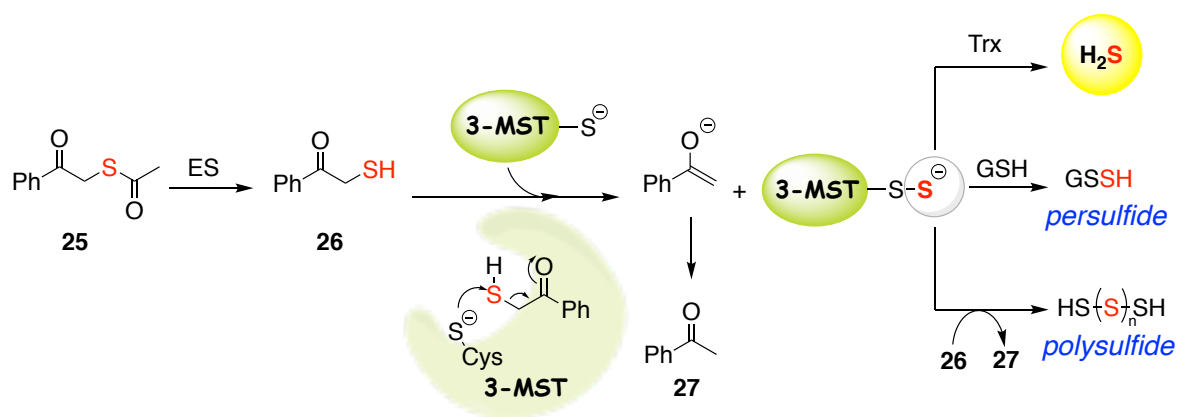


Figure 17. An artificial substrate having a similar enolizable ketone and a sulfur donor was designed, which upon turnover by 3-MST feeds into the biosynthetic machinery of the cell to induce persulfidation and generate H₂S. Acetophenone would be generated as a byproduct.

First, we evaluated the formation of 3-MST persulfide in its active site cysteine as 3-MST accepts the sulfur from the artificial substrate **26**. A previously reported tag-switch technique was used to detect the protein persulfide.^{31,33} To test the formation of the 3-MST persulfide, 3-MST was treated with compound **25** in the presence of esterase in pH 7.4 buffer and incubated at 37 °C for 1 h, followed by tag switching reagents, MSBT-A and CN-biotin. A strong band was observed when 3-MST was treated with the positive control **24** suggesting the formation of a 3-MST persulfide. A similar result was obtained with the substrate **25**. Whereas, the negative controls **28** and **29** produced a significantly diminished signal under similar conditions (Figure 18a). The bands were quantified using ImageJ (Figure 18b).

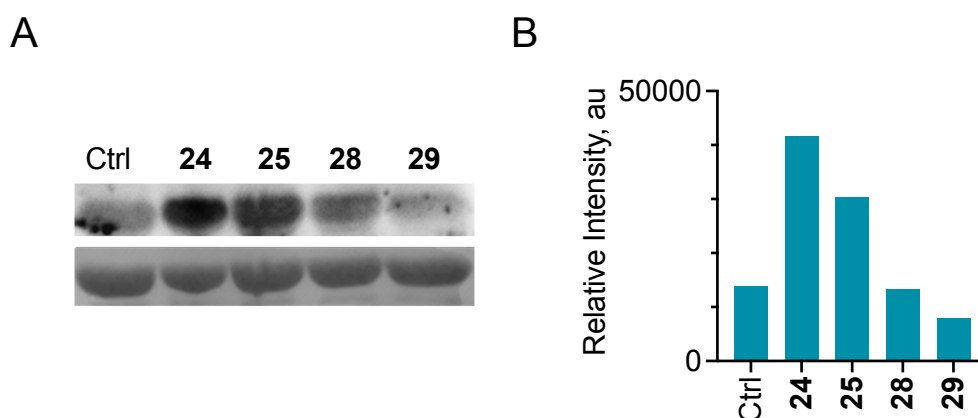


Figure 18. (a) Persulfidation of 3-MST by the ethyl ester of 3-MP (**24**) and the artificial substrate (**25**) in presence of ES, detected using the modified tag-switch technique. Compounds **28** and **29** were used as negative controls. PonceauS staining was used as a loading control. (b) Relative quantification of the bands using ImageJ.

The formation of persulfide/polysulfide was next studied using a fluorescent probe, SSP2.⁵⁶ The ability of compound **25** to generate persulfides/polysulfides upon turnover by 3-MST was

assessed. In the absence of a reducing agent such as DTT, 3-MST-SS⁻ can further catalyse the turnover of **26** to **27**, likely forming a 3-MST polysulfide. Varying concentrations of **25** was reacted with 3-MST in the presence of esterase followed by incubation with SSP2. The release of fluorescein was measured using a microtiter plate reader (excitation 482 nm; emission 518 nm). A dose dependent increase in fluorescence corresponding to the formation of persulfide/polysulfide was observed (Figure 19). Treatment of the above reaction mixture with DTT, resulted in a diminished signal. The active site cysteine of 3-MST was blocked by pre-treatment with IAM followed by treatment with **25** + ES. A significantly diminished signal was recorded when **25** + ES was reacted with the IAM pre-treated 3-MST. Similar results were obtained with the positive control **24**. No significant fluorescence signal was observed from the negative controls **28** and **29** (Figure 19).

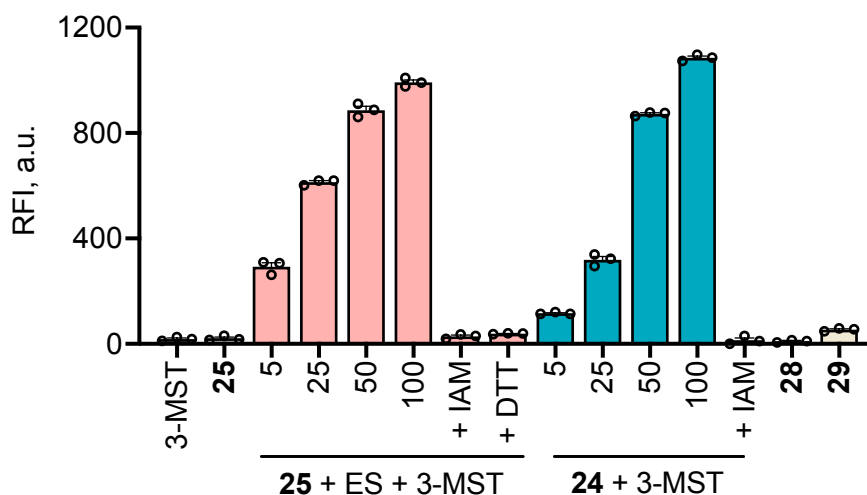


Figure 19. Persulfide/polysulfide detection using SSP2: 3-MST ctrl refers to 3-MST alone and **25** ctrl refers to **25** + ES only; **25** refers to co-incubation of varying concentrations of **25**, ES and 3-MST; +DTT: addition of DTT; +IAM: addition of iodoacetamide, an electrophile that reacts with thiols; **24** refers to incubation **24** with 3-MST; **28** and **29** refers to the incubation of the compounds with ES followed by treatment with 3-MST.

The effect of persulfidation on the activity of GAPDH was next evaluated by utilizing the artificial substrate-3-MST system. 3-MST-SS⁻ was prepared by incubating 3-MST with **25** for 1 h in the presence of esterase (1 U/mL). This was followed by addition of GAPDH and incubation for another 1 h. Under these experimental conditions, the activity of GAPDH was found to be significantly enhanced upon treatment with 3-MST-SS⁻, when compared to untreated GAPDH (Figure 20).

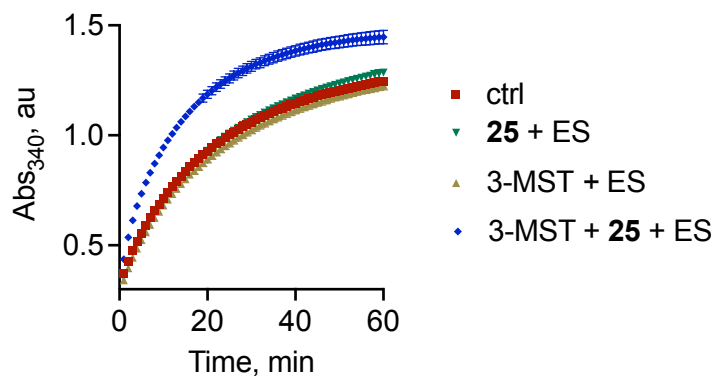


Figure 20. Activity of GAPDH was measured by monitoring the formation of NADH, real-time at 340 nm.

Next, the ability of the artificial substrate **25** to permeate cells and feed in as a substrate for cellular 3-MST was assessed. The 3-MST-SS⁻ formed as an intermediate can transfer the sulfur to thiophilic acceptors such as thioredoxin or cysteine, subsequently undergoing reduction to eliminate H₂S.³⁷ Intracellular H₂S was detected in A549 cell line using a previously reported fluorescent probe for H₂S, NBD Fluorescein.⁵⁸ A 3-MST knock down cell line was generated (3-MST KD) by introducing 3-MST shRNA in A549 cell line. When the cells were co-incubated with the COS/H₂S donor and NBD-fluorescein, an enhanced fluorescence signal was observed both in the scrambled as well as 3-MST KD cell line. However, a significantly diminished signal was observed when the 3-MST KD cell line was treated with compound **25**, compared to the scrambled cell line. Negative control **28** failed to produce a signal in either of the cell lines (Figure 21). Thus, implying that the H₂S generated by **25** is mediated by 3-MST.

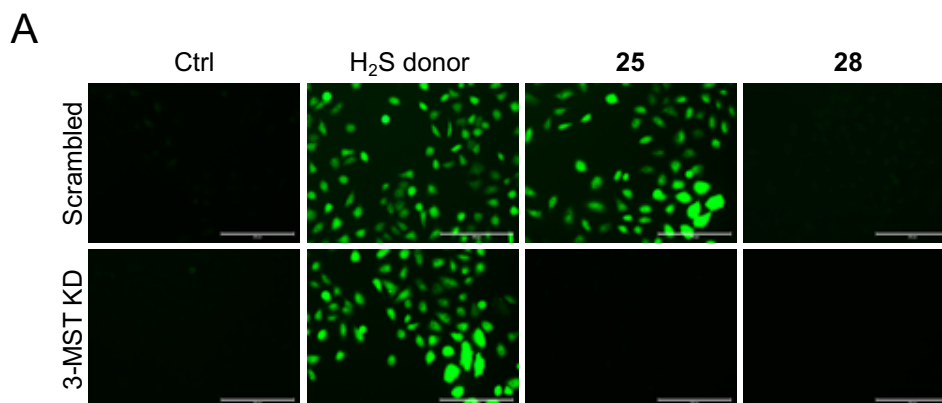


Figure 21. a) Detection of H₂S in 3-MST KD A549 cell line and the corresponding scrambled cell line using NBD fluorescein. Ctrl refers to untreated cells. Scale bar represents 200 μ m.

Next, antioxidant effect of **25** was tested. To test this, a reported ROS generator MGR-1 was used to induce oxidative stress in cells.⁵⁹ Intracellular hydrogen peroxide (H_2O_2) levels were measured using a previously reported fluorescent probe TCF-B.⁶⁰ A549 cells were pre-treated with varying concentrations of **25** for 12 h followed by co-treatment with MGR-1 (25 μ M) and TCF-B (25 μ M) for 1 h. A similar experiment was carried out with the negative control **28**. A dose dependent quenching in fluorescence was observed, that was unperturbed in case of the negative control **28** (Figure 22).

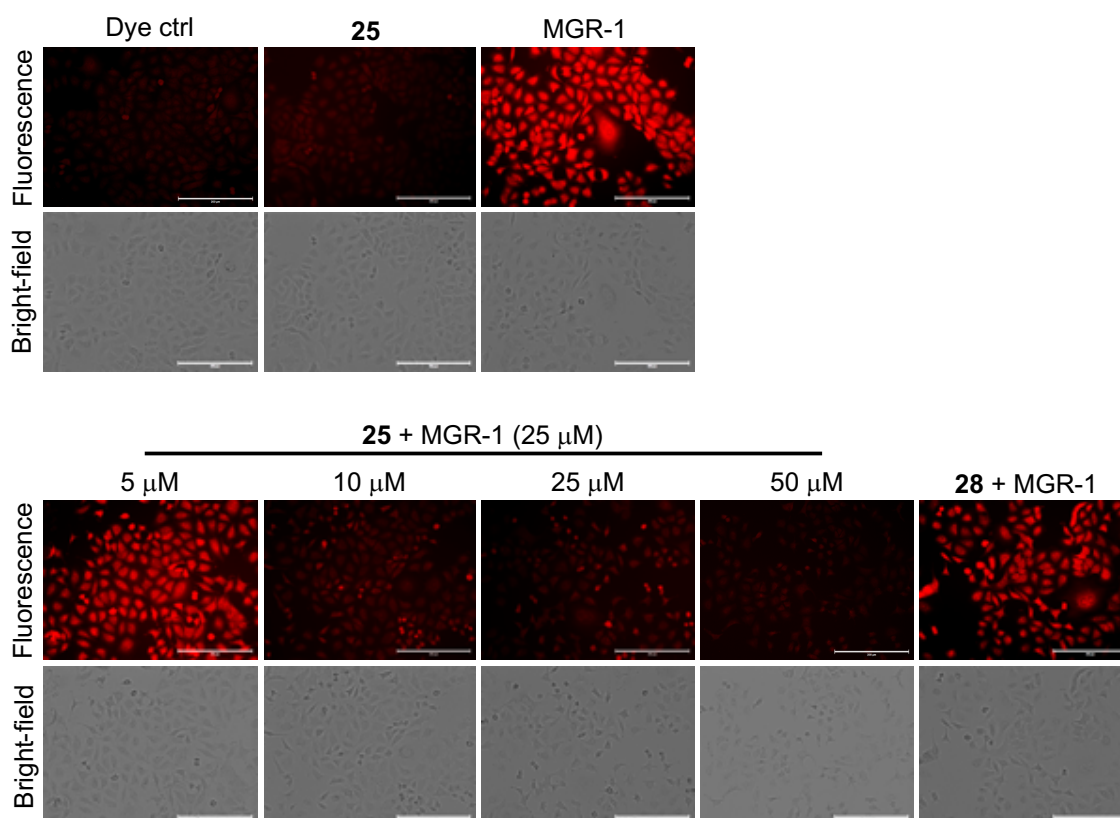


Figure 22. (TOP) A549 cells were treated with veh control (DMSO), **25** (50 μ M) and MGR-1 (25 μ M) (BOTTOM) A549 cells treated with varying concentrations of **25** (5 μ M, 10 μ M, 25 μ M and 50 μ M) or **28** (50 μ M) for 12 h followed by treatment with MGR-1 (25 μ M). Intracellular H_2O_2 was detected using the H_2O_2 -sensitive turn-on fluorescence sensor TCF-B. Cells were imaged using a 20 \times TxRed filter. Scale bar is 200 μ m.

A cell viability assay conducted on N2a showed no potential toxicity of the compounds for a period of 12 h. Upon determining the antioxidant properties of **25**, its ability to rescue cells from ROS induced cell death was next studied. Cells were then pre-treated with varying concentrations of **25** and the negative controls **27** and **28** for 12 h, followed by the ROS generator MGR-1 for 4 h. A dose dependent increase in cell viability was observed only with **25** and not the negative controls (Figure 23.).

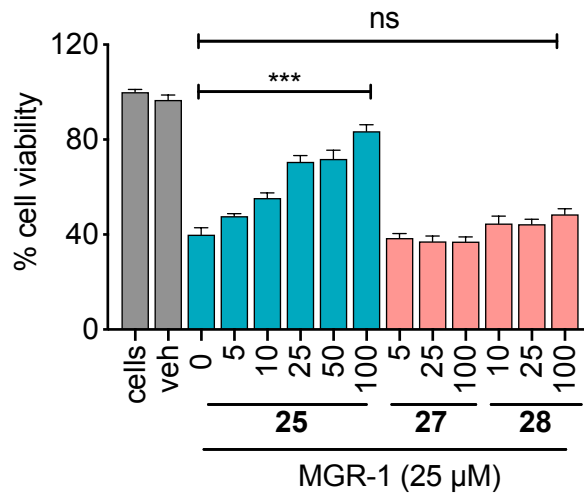


Figure 23. Cell viability assay conducted on N2a cells. A dose-dependent protection of cells from MGR-1 induced cell death by **25** was observed. The byproduct ketone **27** or the negative control **28** did not show any protection against the cytotoxic effects of MGR-1. All data are presented as mean \pm SEM (n = 3 per group). ***p < 0.001 vs MGR-1.

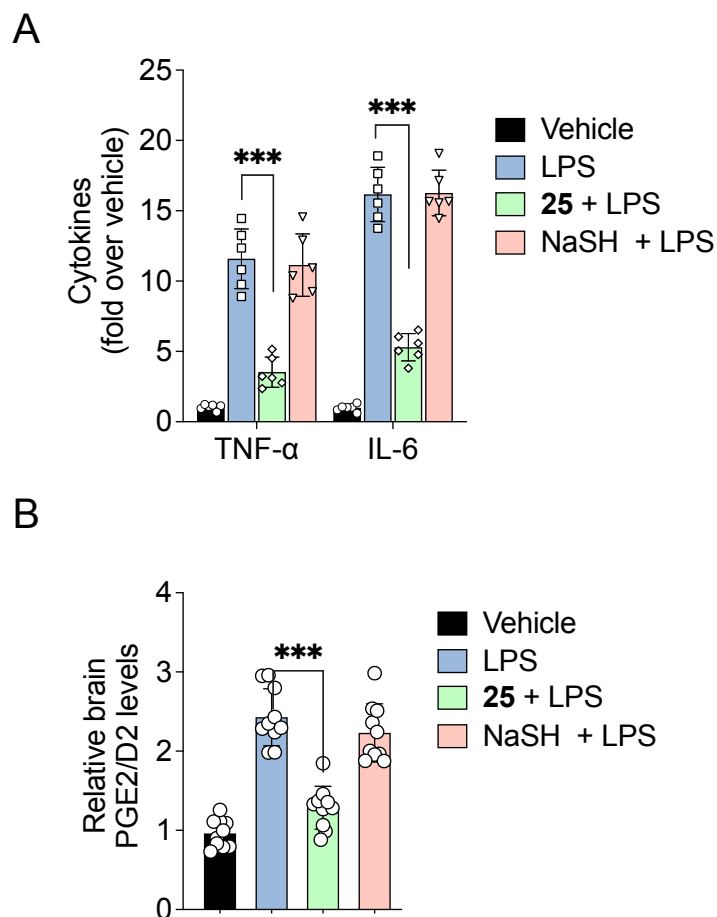


Figure 24. Mouse endotoxin shock model: Animals were treated with **25** (20 mg/kg) or NaSH (20 mg/kg) 4 h prior to treatment with lipopolysaccharide (LPS, 5 mg/kg). 30 min post-administration of LPS, another dose of **25** or NaSH was given. The brain tissue samples were harvested followed by measurement of: (A) Pro-inflammatory cytokines, TNF- α and IL-6 using a standard ELISA assay. All

data are presented as mean \pm SD (n = 6 per group). ***p < 0.001 vs LPS; and (B) Prostaglandins PGE₂/D₂ using LC/MS. All data are presented as mean \pm SD (n = 10 per group). ***p < 0.001 vs LPS.

Finally, anti-inflammatory effects of **25** was studied in mice model. The mice were pre-treated with **25** for 4 h, followed by lipopolysaccharide (LPS) treatment and another dose of **25**. Proinflammatory cytokines and prostaglandins were measured in the brain tissue of these mice. In the control group treated with LPS alone, significantly elevated levels of cytokines TNF- α and IL-6 were found, compared to the vehicle-treated mice. In the group pre-treated with **25**, a marked decrease in the levels of cytokines were observed, whereas NaSH failed to exhibit similar effects (Figure 24a). PGE₂/PGD₂ levels are used as a reliable marker for inflammation. LC/MS analysis of brain tissue homogenates were carried out to measure the levels of PGE₂/PGD₂. A similar result was obtained wherein, the levels were significantly lower in groups pre-treated with **25** compared to LPS only treatment (Figure 24b). These results collectively demonstrate the potential of **25** to mitigate neuroinflammation.

CHAPTER 4.2. β -galactosidase activated prodrug of the artificial substrates for 3-MST

In chapter 4.2, we propose the design of β -galactosidase activated 3-MST artificial substrate. It has been proposed that deleterious free radicals and oxidants damaging biomolecules is a major contributor to the process of aging.⁶¹ Therefore, countering these species or inhibiting their production might aid in reducing the rate of aging or prevent incidences of age associated disorders. This theory is now widely accepted with several studies demonstrating the effects of antioxidants such as vitamin C, vitamin E, resveratrol, glutathione and antioxidant enzymes in boosting health and longevity of life.^{62,63}

We designed prodrug **30** that can be cleaved by the enzyme β -galactosidase. Subsequent intramolecular cyclization of the phenolate will release the artificial substrate **26** along with the heterocyclic byproduct **31** (Figure 25a). **26**, as demonstrated in chapter 4.1 can generate a range of reactive sulfur species including H₂S, persulfides/polysulfides, catalysed by the enzyme 3-MST (Figure 25b).

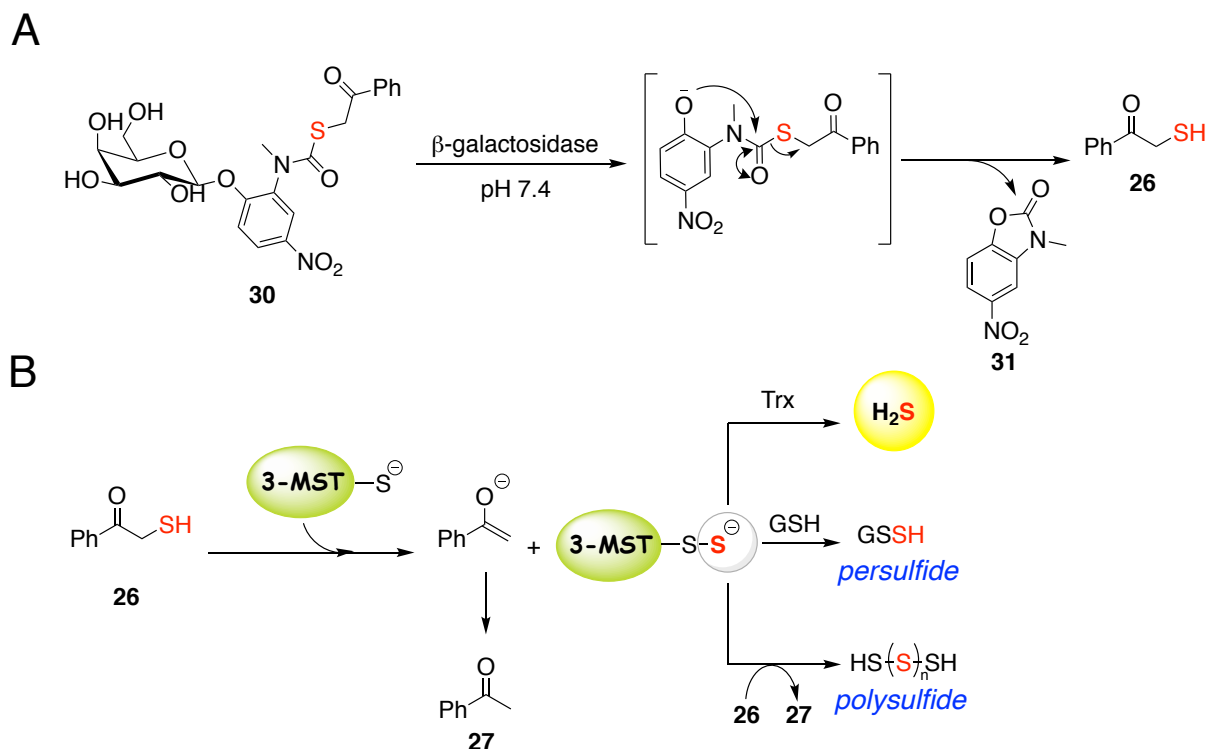


Figure 25. a) Design of β -galactosidase activated prodrug (**30**) of the artificial substrate (**26**). b) Catalytic turnover of **26** by 3-MST to generate H_2S and persulfides/polysulfides.

With compound **30** in hand, its ability to generate the artificial substrate **26** in the presence of β -galactosidase was tested. **30** upon incubation with β -galactosidase decomposed within 30 min with the concomitant formation of the byproduct **31** in 92% yield (Figure 26).

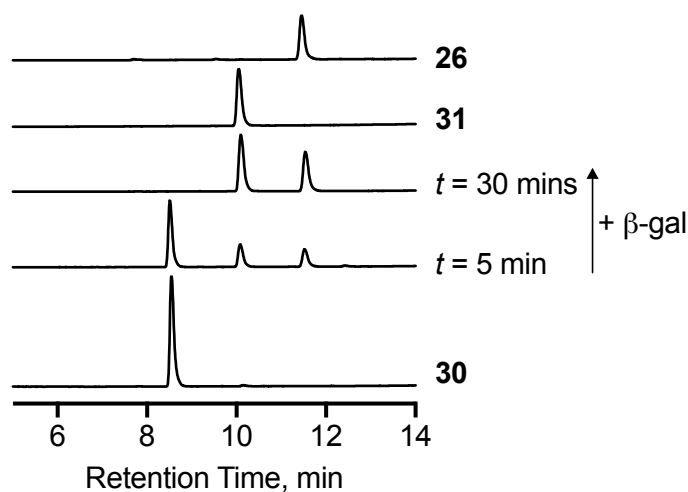


Figure 26. HPLC decomposition profile of **30** in the presence of β -galactosidase.

Next, the turnover of **26** generated from **30** in the presence of β -galactosidase, by 3-MST was evaluated. **30** was incubated with β -galactosidase (2 U/mL), *E. coli* 3-MST (*b3*-MST, 1 μM) and dithiothreitol (DTT, 10 mM) in pH 7.4 phosphate buffer at 37 $^\circ\text{C}$. As monitored by HPLC,

30 was consumed within 60 min with the appearance of two new peaks attributable to the byproduct **31** and acetophenone **27** was observed (figure 27).

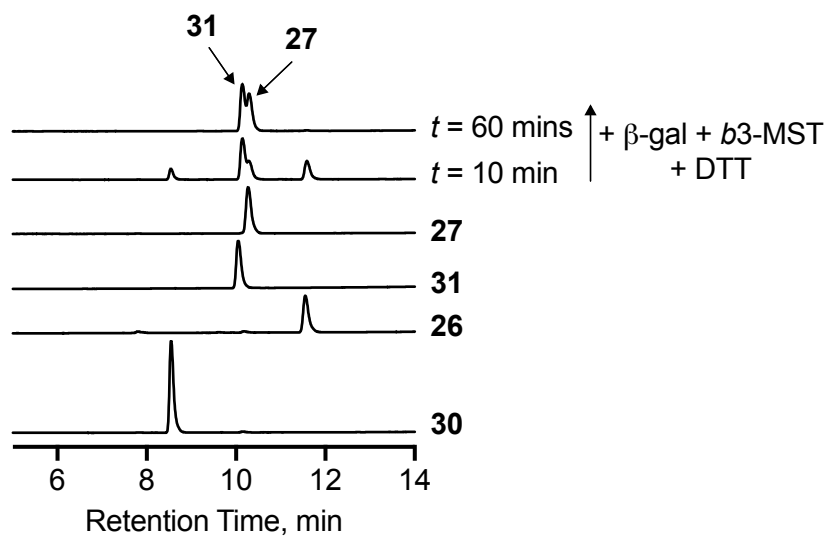


Figure 27. HPLC profile for catalytic turnover of **26**, generated from **30** upon treatment with β -galactosidase (2 U/mL), by *b3*-MST.

From the above observation, it can be concluded that **30** undergoes cleavage by β -galactosidase to release the artificial substrate **26** which is then turned over by 3-MST in the presence of DTT, forming acetophenone **27** and **31** as the byproducts. We next attempted to detect H_2S under these conditions using a standard methylene blue assay.⁶⁴ **30** was incubated with β -galactosidase (2 U/mL), *b3*-MST (1 μM) and DTT (10 mM) in phosphate buffer at 37 $^\circ\text{C}$ for 60 min. An aliquot of this reaction mixture was treated with the methylene blue reagents (*N,N*-dimethyl-*p*-phenylene diamine and FeCl_3) and further incubated for 30 min. The samples were then transferred to a well plate and the absorbance profile was recorded from 550 nm to 800 nm. It was observed that **30** only in the presence of β -galactosidase, *b3*-MST and DTT produced a signal for methylene blue, suggesting the generation of H_2S (purple, Figure 28a). DTT enhances the catalytic efficiency of 3-MST, however, even in the absence of DTT a minor amount of H_2S generation was observed (green). **25** was used as a positive control, which gives a distinct signal for H_2S generation (red). **30** in the absence of β -galactosidase or *b3*-MST failed to produce H_2S , so did the negative control **38** under similar conditions. (Figure 28b).

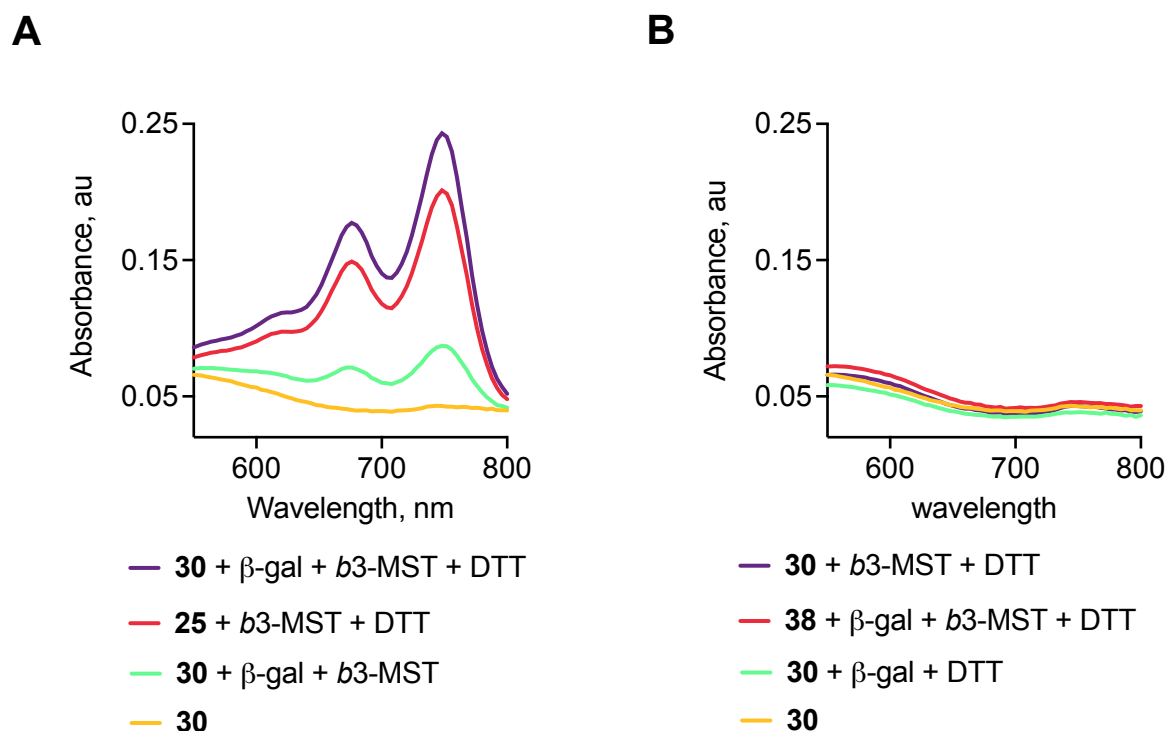


Figure 28. a) Methylene blue absorbance profile obtained for catalytic turnover of **30** in the presence of β -galactosidase (2 U/mL), *b3*-MST and DTT. **25** was used as the positive control. b) **30** in the absence of β -galactosidase (2 U/mL) and *b3*-MST does not produce H_2S . **38** was used as the negative control.

The ability of prodrug **30** to permeate cells and mediate intracellular persulfidation was next investigated. Tag-switch assay described in chapter 4.1 was used for the detection of persulfides in cells. A549 cells were irradiated with 7Gy IR to induce senescence. Both senescent and non-senescent cells were incubated with **30** (100 μ M) and Na_2S (100 μ M) for 1 h. The cells were then incubated with MSBT-A overnight followed by treatment with CN-BOT for 1 h to tag the protein persulfides with BODIPY, which can be visualized under the microscope

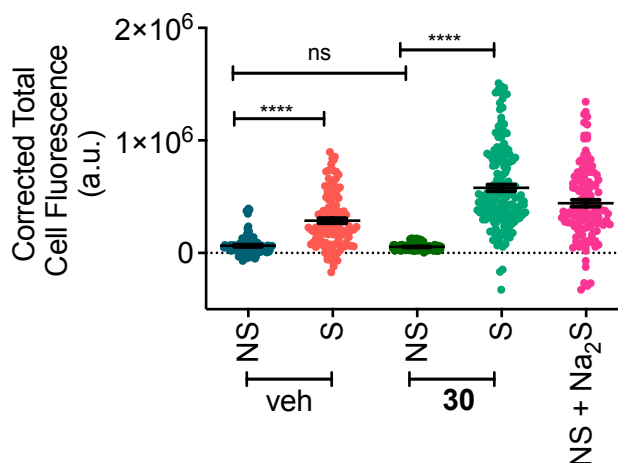


Figure 29. Quantification of the fluorescence signal induced by **30** and Na_2S in A549 senescent and non-senescent cell lines using the tag-switch technique. All data are presented as mean \pm SD (n

=3/group). Significance was determined with respect to control in each cell line by Student's two-tailed unpaired parametric t test: ****p < 0.0001 versus ctrl group while ns = non-significant.

Senescent cells treated with **30** produced a significantly enhanced signal compared to a similar treatment on non-senescent cells (Figure 29). This data implies that **30** is selectively activated and is able to induce persulfidation in senescent cells, possibly due to an overexpression of β -galactosidase.

References:

- (1) Mustafa, A. K.; Gadalla, M. M.; Sen, N.; Kim, S.; Mu, W.; Gazi, S. K.; Barrow, R. K.; Yang, G.; Wang, R.; Snyder, S. H., H₂S Signals Through Protein S-Sulfhydration. *Sci. Signal.* **2009**, *2* (96), ra72 LP-ra72.
- (2) Yang, G.; Wu, L.; Jiang, B.; Yang, W.; Qi, J.; Cao, K.; Meng, Q.; Mustafa, A. K.; Mu, W.; Zhang, S.; Snyder, S. H.; Wang, R., H₂S as a Physiologic Vasorelaxant: Hypertension in Mice with Deletion of Cystathionine γ -Lyase. *Science*, **2008**, *322* (5901), 587–590.
- (3) Mustafa, A. K.; Sikka, G.; Gazi, S. K.; Steppan, J.; Jung, S. M.; Bhunia, A. K.; Barodka, V. M.; Gazi, F. K.; Barrow, R. K.; Wang, R.; Amzel, L. M.; Berkowitz, D. E.; Snyder, S. H., Hydrogen Sulfide as Endothelial Derived Hyperpolarizing Factor Sulfhydrates Potassium Channels. *Circ. Res.* **2011**, *109* (11), 1259–1268.
- (4) Abe, K.; Kimura, H., The possible role of hydrogen sulfide as an endogenous neuromodulator. *J. Neurosci.* **1996**, *16* (3), 1066 LP – 1071.
- (5) Papapetropoulos, A.; Pyriochou, A.; Altaany, Z.; Yang, G.; Marazioti, A.; Zhou, Z.; Jeschke, M. G.; Branski, L. K.; Herndon, D. N.; Wang, R.; Szabo, C., Hydrogen sulfide is an endogenous stimulator of angiogenesis. *Proc. Natl. Acad. Sci.* **2009**, *106* (51), 21972–21977.
- (6) Szabó, C.; Papapetropoulos, A., Hydrogen sulphide and angiogenesis: mechanisms and applications. *Br. J. Pharmacol.* **2011**, *164* (3), 853–865.
- (7) Whiteman, M.; Winyard, P. G., Hydrogen sulfide and inflammation: the good, the bad, the ugly and the promising. *Expert Rev. Clin. Pharmacol.* **2011**, *4* (1), 13–32.
- (8) Li, L.; Bhatia, M.; Zhu, Y. Z.; Zhu, Y. C.; Ramnath, R. D.; Wang, Z. J.; Anuar, F. B. M.; Whiteman, M.; Salto-Tellez, M.; Moore, P. K., Hydrogen sulfide is a novel mediator of lipopolysaccharide-induced inflammation in the mouse. *FASEB J.* **2005**, *19* (9), 1196–1198.
- (9) Olson, K. R.; Healy, M. J.; Qin, Z.; Skovgaard, N.; Vulesevic, B.; Duff, D. W.; Whitfield, N. L.; Yang, G.; Wang, R.; Perry, S. F., Hydrogen sulfide as an oxygen sensor in trout gill chemoreceptors. *Am. J. Physiol. Integr. Comp. Physiol.* **2008**, *295* (2), R669–R680.
- (10) Zhao, Y.; Bhushan, S.; Yang, C.; Otsuka, H.; Stein, J. D.; Pacheco, A.; Peng, B.; Devarie-Baez, N. O.; Aguilar, H. C.; Lefer, D. J.; Xian, M., Controllable Hydrogen Sulfide Donors and Their Activity against Myocardial Ischemia-Reperfusion Injury.

- ACS Chem. Biol.* **2013**, *8* (6), 1283–1290.
- (11) Mills, G.; Schmidt, K. H.; Matheson, M. S.; Meisel, D., Thermal and photochemical reactions of sulfhydryl radicals. Implications for colloid photocorrosion. *J. Phys. Chem.* **1987**, *91* (6), 1590–1596.
- (12) Nagy, P.; Winterbourn, C. C., Rapid Reaction of Hydrogen Sulfide with the Neutrophil Oxidant Hypochlorous Acid to Generate Polysulfides. *Chem. Res. Toxicol.* **2010**, *23* (10), 1541–1543.
- (13) Filipovic, M. R.; Miljkovic, J.; Allgäuer, A.; Chaurio, R.; Shubina, T.; Herrmann, M.; Ivanovic-Burmazovic, I., Chemical Characterization of the Smallest S -Nitrosothiol, HSNO; Cellular Cross-talk of H₂S and S -Nitrosothiols. *Biochem. J.* **2012**, *441* (2), 609–621.
- (14) Finkel, T., From Sulfenylation to Sulfhydration: What a Thiolate Needs to Tolerate. *Sci. Signal.* **2012**, *5* (215).
- (15) Kabil, O.; Banerjee, R., Redox Biochemistry of Hydrogen Sulfide. *J. Biol. Chem.* **2010**, *285* (29), 21903–21907.
- (16) Franconeri, N. E.; Carrington, S. J.; Fukuto, J. M., The reaction of H₂S with oxidized thiols: Generation of persulfides and implications to H₂S biology. *Arch. Biochem. Biophys.* **2011**, *516* (2), 146–153.
- (17) Ida, T.; Sawa, T.; Ihara, H.; Tsuchiya, Y.; Watanabe, Y.; Kumagai, Y.; Suematsu, M.; Motohashi, H.; Fujii, S.; Matsunaga, T.; Yamamoto, M.; Ono, K.; Devarie-Baez, N. O.; Xian, M.; Fukuto, J. M.; Akaike, T., Reactive cysteine persulfides and S-polythiolation regulate oxidative stress and redox signaling. *Proc. Natl. Acad. Sci. U.S.A* **2014**, *111* (21), 7606–7611.
- (18) Toohey, J. I., Sulfur signaling: Is the agent sulfide or sulfane? *Anal. Biochem.* **2011**, *413* (1), 1–7.
- (19) Kimura, Y.; Mikami, Y.; Osumi, K.; Tsugane, M.; Oka, J.; Kimura, H., Polysulfides are possible H₂S-derived signaling molecules in rat brain. *FASEB J.* **2013**, *27* (6), 2451–2457.
- (20) Kimura, H., Signaling of Hydrogen Sulfide and Polysulfides. *Antioxid. Redox Signal.* **2014**, *22* (5), 347–349.
- (21) Ono, K.; Akaike, T.; Sawa, T.; Kumagai, Y.; Wink, D. A.; Tantillo, D. J.; Hobbs, A. J.; Nagy, P.; Xian, M.; Lin, J.; Fukuto, J. M., Redox chemistry and chemical biology of H₂S, hydropersulfides, and derived species: Implications of their possible biological activity and utility. *Free. Radic. Biol. Med.* **2014**, *77*, 82–94.

- (22) Du, J.; Huang, Y.; Yan, H.; Zhang, Q.; Zhao, M.; Zhu, M.; Liu, J.; Chen, S. X.; Bu, D.; Tang, C.; Jin, H., Hydrogen Sulfide Suppresses Oxidized Low-density Lipoprotein (Ox-LDL)-stimulated Monocyte Chemoattractant Protein 1 generation from Macrophages via the Nuclear Factor κ B (NF- κ B) Pathway. *J. Biol. Chem.* **2014**, *289* (14), 9741–9753.
- (23) Yang, G.; Zhao, K.; Ju, Y.; Mani, S.; Cao, Q.; Puukila, S.; Khaper, N.; Wu, L.; Wang, R., Hydrogen Sulfide Protects Against Cellular Senescence via S-Sulfhydration of Keap1 and Activation of Nrf2. *Antioxid. Redox Signal.* **2013**, *18* (15), 1906–1919.
- (24) Vandiver, M. S.; Paul, B. D.; Xu, R.; Karuppagounder, S.; Rao, F.; Snowman, A. M.; Seok Ko, H.; Il Lee, Y.; Dawson, V. L.; Dawson, T. M.; Sen, N.; Snyder, S. H., Sulfhydration mediates neuroprotective actions of parkin. *Nat. Commun.* **2013**, *4*, 1626.
- (25) Giovinazzo, D.; Bursac, B.; Sbodio, J. I.; Nalluru, S.; Vignane, T.; Snowman, A. M.; Albacarys, L. M.; Sedlak, T. W.; Torregrossa, R.; Whiteman, M.; Filipovic, M. R.; Snyder, S. H.; Paul, B. D., Hydrogen sulfide is neuroprotective in Alzheimer's disease by sulfhydrating GSK3 β and inhibiting Tau hyperphosphorylation. *Proc. Natl. Acad. Sci.* **2021**, *118* (4), e2017225118.
- (26) Paul, B. D.; Sbodio, J. I.; Xu, R.; Vandiver, M. S.; Cha, J. Y.; Snowman, A. M.; Snyder, S. H., Cystathionine γ -lyase deficiency mediates neurodegeneration in Huntington's disease. *Nature* **2014**, *509* (7498), 96–100.
- (27) Paulsen, C. E.; Carroll, K. S., Cysteine-Mediated Redox Signaling: Chemistry, Biology, and Tools for Discovery. *Chem. Rev.* **2013**, *113* (7), 4633–4679.
- (28) Woo, H. A.; Chae, H. Z.; Hwang, S. C.; Yang, K.-S.; Kang, S. W.; Kim, K.; Rhee, S. G., Reversing the Inactivation of Peroxiredoxins Caused by Cysteine Sulfenic Acid Formation. *Science (80-.)*. **2003**, *300* (5619), 653–656.
- (29) Wood, Z. A.; Poole, L. B.; Karplus, P. A., Peroxiredoxin Evolution and the Regulation of Hydrogen Peroxide Signaling. *Science (80-.)*. **2003**, *300* (5619), 650–653.
- (30) Cuevasanta, E.; Lange, M.; Bonanata, J.; Coitiño, E. L.; Ferrer-Sueta, G.; Filipovic, M. R.; Alvarez, B., Reaction of Hydrogen Sulfide with Disulfide and Sulfenic Acid to Form the Strongly Nucleophilic Persulfide. *J. Biol. Chem.* **2015**, *290* (45), 26866–26880.
- (31) Zhang, D.; Macinkovic, I.; Devarie-Baez, N. O.; Pan, J.; Park, C.-M.; Carroll, K. S.; Filipovic, M. R.; Xian, M., Detection of Protein S-Sulfhydration by a Tag-Switch Technique. *Angew. Chemie Int. Ed.* **2014**, *53* (2), 575–581.
- (32) Filipovic, M. R. 2015; pp 29–59.
- (33) Wedmann, R.; Onderka, C.; Wei, S.; Szijártó, I. A.; Miljkovic, J. L.; Mitrovic, A.; Lange, M.; Savitsky, S.; Yadav, P. K.; Torregrossa, R.; Harrer, E. G.; Harrer, T.; Ishii,

- I.; Gollasch, M.; Wood, M. E.; Galardon, E.; Xian, M.; Whiteman, M.; Banerjee, R.; Filipovic, M. R., Improved tag-switch method reveals that thioredoxin acts as depersulfidase and controls the intracellular levels of protein persulfidation. *Chem. Sci.* **2016**, *7* (5), 3414–3426.
- (34) Numakura, T.; Sugiura, H.; Akaike, T.; Ida, T.; Fujii, S.; Koarai, A.; Yamada, M.; Onodera, K.; Hashimoto, Y.; Tanaka, R.; Sato, K.; Shishikura, Y.; Hirano, T.; Yanagisawa, S.; Fujino, N.; Okazaki, T.; Tamada, T.; Hoshikawa, Y.; Okada, Y.; Ichinose, M., Production of reactive persulfide species in chronic obstructive pulmonary disease. *Thorax* **2017**, *72* (12), 1074–1083.
- (35) Zhang, T.; Ono, K.; Tsutsuki, H.; Ihara, H.; Islam, W.; Akaike, T.; Sawa, T., Enhanced Cellular Polysulfides Negatively Regulate TLR4 Signaling and Mitigate Lethal Endotoxin Shock. *Cell Chem. Biol.* **2019**, *26* (5), 686-698.e4.
- (36) Libiad, M.; Yadav, P. K.; Vitvitsky, V.; Martinov, M.; Banerjee, R., Organization of the Human Mitochondrial Hydrogen Sulfide Oxidation Pathway. *J. Biol. Chem.* **2014**, *289* (45), 30901–30910.
- (37) Yadav, P. K.; Yamada, K.; Chiku, T.; Koutmos, M.; Banerjee, R., Structure and kinetic analysis of H₂S production by human mercaptopyruvate sulfurtransferase. *J. Biol. Chem.* **2013**, *288* (27), 20002–20013.
- (38) Nagahara, N.; Yoshii, T.; Abe, Y.; Matsumura, T., Thioredoxin-dependent Enzymatic Activation of Mercaptopyruvate Sulfurtransferase: an intersubunit disulfide bond serves as a redox switch for activation. *J. Biol. Chem.* **2007**, *282* (3), 1561–1569.
- (39) Melideo, S. L.; Jackson, M. R.; Jorns, M. S., Biosynthesis of a Central Intermediate in Hydrogen Sulfide Metabolism by a Novel Human Sulfurtransferase and Its Yeast Ortholog. *Biochemistry* **2014**, *53* (28), 4739–4753.
- (40) Yamanishi, T.; Tuboi, S., The mechanism of the L-cystine cleavage reaction catalyzed by rat liver gamma-cystathionase. *J. Biochem.* **1981**, *89* (6), 1913–1921.
- (41) Akaike, T.; Ida, T.; Wei, F.-Y.; Nishida, M.; Kumagai, Y.; Alam, M. M.; Ihara, H.; Sawa, T.; Matsunaga, T.; Kasamatsu, S.; Nishimura, A.; Morita, M.; Tomizawa, K.; Nishimura, A.; Watanabe, S.; Inaba, K.; Shima, H.; Tanuma, N.; Jung, M.; Fujii, S.; Watanabe, Y.; Ohmuraya, M.; Nagy, P.; Feelisch, M.; Fukuto, J. M.; Motohashi, H., Cysteinyl-tRNA synthetase governs cysteine polysulfidation and mitochondrial bioenergetics. *Nat. Commun.* **2017**, *8* (1), 1177.
- (42) Sawa, T.; Motohashi, H.; Ihara, H.; Akaike, T., Enzymatic Regulation and Biological Functions of Reactive Cysteine Persulfides and Polysulfides. *Biomolecules* **2020**, *10* (9),

- 1245.
- (43) Bianco, C. L.; Akaike, T.; Ida, T.; Nagy, P.; Bogdandi, V.; Toscano, J. P.; Kumagai, Y.; Henderson, C. F.; Goddu, R. N.; Lin, J.; Fukuto, J. M., The reaction of hydrogen sulfide with disulfides: formation of a stable trisulfide and implications for biological systems. *Br. J. Pharmacol.* **2019**, *176* (4), 671–683.
- (44) Abiko, Y.; Shinkai, Y.; Unoki, T.; Hirose, R.; Uehara, T.; Kumagai, Y., Polysulfide Na₂S₄ regulates the activation of PTEN/Akt/CREB signaling and cytotoxicity mediated by 1,4-naphthoquinone through formation of sulfur adducts. *Sci. Rep.* **2017**, *7* (1), 4814.
- (45) Kawamura, S.; Kitao, T.; Nakabayashi, T.; Horii, T.; Tsurugi, J., Aralkyl hydrodisulfides. VIII. Alkaline decomposition and its competition with nucleophiles. *J. Org. Chem.* **1968**, *33* (3), 1179–1181.
- (46) Powell, C. R.; Dillon, K. M.; Wang, Y.; Carrazzone, R. J.; Matson, J. B., A Persulfide Donor Responsive to Reactive Oxygen Species: Insights into Reactivity and Therapeutic Potential. *Angew. Chem. Int. Ed.* **2018**, *57* (21), 6324–6328..
- (47) Mustafa, A. K.; Gadalla, M. M.; Sen, N.; Kim, S.; Mu, W.; Gazi, S. K.; Barrow, R. K.; Yang, G.; Wang, R.; Snyder, S. H., H₂S Signals Through Protein S-Sulfhydration. *Sci. Signal.* **2009**, *2* (96), ra72 LP-ra72.
- (48) Zhao, W.; Zhang, J.; Lu, Y.; Wang, R., The vasorelaxant effect of H₂S as a novel endogenous gaseous K(ATP) channel opener. *EMBO J.* **2001**, *20* (21), 6008–6016.
- (49) Friend, D. R.; Chang, G. W., A colon-specific drug-delivery system based on drug glycosides and the glycosidases of colonic bacteria. *J. Med. Chem.* **1984**, *27* (3), 261–266.
- (50) Englyst, H., Polysaccharide breakdown by mixed populations of human faecal bacteria. *FEMS Microbiol. Lett.* **1987**, *45* (3), 163–171.
- (51) Zhu, H.; Li, Y. R., Oxidative stress and redox signaling mechanisms of inflammatory bowel disease: updated experimental and clinical evidence. *Exp. Biol. Med.* **2012**, *237* (5), 474–480.
- (52) Tocmo, R.; Parkin, K., S-1-propenylmercaptocysteine protects murine hepatocytes against oxidative stress via persulfidation of Keap1 and activation of Nrf2. *Free Radic. Biol. Med.* **2019**, *143*, 164–175.
- (53) Hamid, H. A.; Tanaka, A.; Ida, T.; Nishimura, A.; Matsunaga, T.; Fujii, S.; Morita, M.; Sawa, T.; Fukuto, J. M.; Nagy, P.; Tsutsumi, R.; Motohashi, H.; Ihara, H.; Akaike, T., Polysulfide stabilization by tyrosine and hydroxyphenyl-containing derivatives that is important for a reactive sulfur metabolomics analysis. *Redox Biol.* **2019**, *21*, 101096.

- (54) Khodade, V. S.; Pharoah, B. M.; Paolocci, N.; Toscano, J. P., Alkylamine-Substituted Perthiocarbamates: Dual Precursors to Hydropersulfide and Carbonyl Sulfide with Cardioprotective Actions. *J. Am. Chem. Soc.* **2020**, *142* (9), 4309–4316.
- (55) Chengelis, C. P.; Neal, R. A., Studies of carbonyl sulfide toxicity: Metabolism by carbonic anhydrase. *Toxicol. Appl. Pharmacol.* **1980**, *55* (1), 198–202.
- (56) Chen, W.; Liu, C.; Peng, B.; Zhao, Y.; Pacheco, A.; Xian, M., New fluorescent probes for sulfane sulfurs and the application in bioimaging. *Chem. Sci.* **2013**, *4* (7), 2892.
- (57) Coletta, C.; Módis, K.; Szczesny, B.; Brunyánszki, A.; Oláh, G.; Rios, E. C. S.; Yanagi, K.; Ahmad, A.; Papapetropoulos, A.; Szabo, C., Regulation of Vascular Tone, Angiogenesis and Cellular Bioenergetics by the 3-Mercaptopyruvate Sulfurtransferase/H₂S Pathway: Functional Impairment by Hyperglycemia and Restoration by dl- α -Lipoic Acid. *Mol. Med.* **2015**, *21* (1), 1–14.
- (58) Wei, C.; Zhu, Q.; Liu, W.; Chen, W.; Xi, Z.; Yi, L., NBD-based colorimetric and fluorescent turn-on probes for hydrogen sulfide. *Org. Biomol. Chem.* **2014**, *12* (3), 479–485.
- (59) Kelkar, D. S.; Ravikumar, G.; Mehendale, N.; Singh, S.; Joshi, A.; Sharma, A. K.; Mhetre, A.; Rajendran, A.; Chakrapani, H.; Kamat, S. S., A chemical–genetic screen identifies ABHD12 as an oxidized-phosphatidylserine lipase. *Nat. Chem. Biol.* **2019**, *15* (2), 169–178.
- (60) Xu, F.; Tang, W.; Kang, S.; Song, J.; Duan, X., A highly sensitive and photo-stable fluorescent probe for endogenous intracellular H₂O₂ imaging in live cancer cells. *Dye. Pigment.* **2018**, *153*, 61–66.
- (61) Harman, D., Aging: A Theory Based on Free Radical and Radiation Chemistry. *J. Gerontol.* **1956**, *11* (3), 298–300.
- (62) Fusco, D.; Colloca, G.; Lo Monaco, M. R.; Cesari, M., Effects of antioxidant supplementation on the aging process. *Clin. Interv. Aging* **2007**, *2* (3), 377–387.
- (63) Bonnefoy, M.; Draï, J.; Kostka, T., Antioxidants to slow aging, facts and perspectives. *Presse Med.* **2002**, *31* (25), 1174–1184.
- (64) Chauhan, P.; Bora, P.; Ravikumar, G.; Jos, S.; Chakrapani, H., Esterase Activated Carbonyl Sulfide/Hydrogen Sulfide (H₂S) Donors. *Org. Lett.* **2017**, *19* (1), 62–65.

List of Figures

Figure 1.1	Sulfur can exist in different oxidation states. Some of the biologically relevant reactive sulfur species are shown. Red and blue are used to designate negative and positive oxidation states respectively	1
Figure 1.2	a) Persulfidation of proteins by reaction of H ₂ S with oxidized cysteine residues. b) Protein persulfidation induced by persulfides and polysulfides	2
Figure 1.3	Resonance structures of S-nitrosothiol. Nucleophilic attack is favoured on structure II, leading to the formation of a protein persulfide and HNO	3
Figure 1.4	Nucleophilic attack of thiol on persulfides, leading to either transpersulfidation or release of H ₂ S	4
Figure 1.5	Persulfidation regulating the KEAP1-Nrf2 pathway	5
Figure 1.6	Persulfidation protects protein from overoxidation under conditions of oxidative stress	6
Figure 1.7	Persulfidation of the p65 subunit of NFκB leads to an inhibition in phosphorylation, nuclear translocation and DNA binding activity of NFκB, resulting in the downregulation of pro-inflammatory cytokines. Persulfidation of NFκB elicits an anti-inflammatory effect	7
Figure 1.8	Regulatory role of persulfidation on the activity of parkin	7
Figure 1.9	Catalytic cycle of sulfurtransferase. First step of the catalytic cycle involves the active site cysteine forming a persulfide intermediate by accepting a sulfur from the sulfur donor. The second step of the catalytic cycle involves sulfur transfer from the persulfidated enzyme to a sulfur acceptor, reinstating the sulfurtransferase to its original state	9

Figure 1.10	CBS and CSE catalyzing the synthesis of CysS-SH using cystine as the substrate	10
Figure 1.11	CARS catalyzing the synthesis of CysS-SH from cysteine and tRNA of CysS-SH that can ultimately form a persulfidated protein via translation of the mRNA	11
Figure 1.12	Disproportionation of persulfides	12
Figure 1.13	a) Synthesis of persulfides from sulfenyl chlorides and thiols, followed by acid mediated hydrolysis of the acyl disulfide intermediate. b) Synthesis of persulfides by reacting alkyl disulfides with H ₂ S	14
Figure 1.14	Structures of few a) unhindered persulfides b) hindered persulfides	14
Figure 1.15	Prodrug strategy for intracellular generation of persulfides	15
Figure 1.16	9-Fluorenylmethyl disulfides as biomimetic precursors for persulfides	16
Figure 1.17	Fluoride sensitive prodrugs of persulfides	16
Figure 1.18	pH sensitive persulfide precursors based on -S to -N methoxycarbonyl transfer	17
Figure 1.19	pH sensitive thioisothiourea based persulfide precursors	17
Figure 1.20	Perthiocarbamate based pH sensitive persulfide precursors	18
Figure 1.21	Alkylsulfenyl thiocarbonate based pH sensitive persulfide precursors	18
Figure 1.22	Diacyl disulfide based pH sensitive persulfide precursors	19
Figure 1.23	a) Reaction of DATS with GSH, generating allyl persulfide, polysulfides and H ₂ S. b) Reaction of DADS with GSH. Pathway A indicates disulfide exchange with GSH and pathway B indicates α -carbon nucleophilic substitution of GSH	20
Figure 1.24	Cyclic acyl disulfides as precursors for persulfides	20

Figure 1.25	UV light activated persulfide donor	21
Figure 1.26	Esterase sensitive persulfide prodrugs	21
Figure 1.27	a) Esterase sensitive glutathione persulfide prodrug. b) Trimethyl lock based H ₂ S ₂ donor activated by esterase and phosphatase	22
Figure 1.28	Esterase sensitive EDP-NAC and poly(EDP-NAC) based persulfide donors	22
Figure 1.29	Nitroreductase activated persulfide donors	23
Figure 1.30	Esterase activated perthiocarbonate based persulfide donors	23
Figure 1.31	General strategy for prodrug activation to generate persulfides	24
Figure 2.1	HPLC traces for the decomposition of 5 in the presence of H ₂ O ₂ (10 eq) in pH 7.4 buffer	43
Figure 2.2	Decomposition of the boronic acid of compound 5 as monitored by HPLC. Curve fitting to first order gave a pseudo first order rate constant k_1 $5.3 \times 10^{-2} \text{ min}^{-1}$	43
Figure 2.3	HPLC analysis to monitor the formation of adduct 7 upon reaction of 5 with H ₂ O ₂ in the presence of FDNB in pH 7.4 buffer (containing 20% ACN) (Absorbance at 250 nm)	45
Figure 2.4	Reaction of 5 without H ₂ O ₂ in the presence of FDNB after 30 min	45
Figure 2.5	HPLC analysis to monitor the formation of adduct 8 upon reaction of 5 with H ₂ O ₂ in the presence of mBBr in pH 7.4 buffer (containing 20% ACN) (Absorbance at 250 nm)	46
Figure 2.6	Formation of cinnamaldehyde from 5 upon treatment with H ₂ O ₂ in the presence of mBBr, as monitored by HPLC. Curve fitting to first order gave a pseudo first order rate constant k_{cinn} $12.8 \times 10^{-2} \text{ min}^{-1}$	46
Figure 2.7	MALDI-TOF of the peak eluted at RT 6.5 min which is attributable to 8 [M+Na] ⁺ Calculated: 369.0707, Found: 369.2551	47

Figure 2.8	a) HPLC traces showing the formation of cinnamaldehyde from 6 upon treatment with H ₂ O ₂ . b) Area under the curve for the peak corresponding to cinnamaldehyde	48
Figure 2.9	TLC analysis to monitor the formation of 7 upon reaction of 5 with various analytes. (A) authentic 7 (R _f 0.37) (B) 5 alone (R _f 0.66) (C) 5 + H ₂ O ₂ (D) 5 + HOCl (E) 5 + TBHP (F) 5 + GSH	48
Figure 2.10	a) Formation of cinnamaldehyde from 6 was monitored using TLC. (A) authentic cinnamaldehyde (R _f 0.4) (B) 6 alone (C) 6 + H ₂ O ₂ (D) 6 + HOCl (E) 6 + TBHP (F) 6 + GSH. b) Formation of cinnamaldehyde from 6 in the presence of various reactive oxygen and sulfur species (Abs = 290 nm)	49
Figure 2.11	Cell viability assay with compound 5 and 6 on colon carcinoma cell line (DLD-1) for 2 h	51
Figure 2.12	(a) Generation of ROS from menadione. (b) Generation of ROS from JCHD	51
Figure 2.13	Induction of cell death in colon carcinoma cell line (DLD-1) upon incubation with menadione and JCHD for 2 h	52
Figure 2.14	a) Cytoprotective effects of compound 5 against menadione (50 μM). (b) Cytoprotective effects of compound 5 against JCHD (50 μM). A similar assay was conducted with 6 , and no significant effect was observed	52
Figure 3.1	β-glycosidase activated prodrugs	71
Figure 3.2	Design of β-glycosidase activated persulfide donor	72
Figure 3.3	a) Extracted ion chromatograms for 10b (m/z = 468.1146; expected m/z = 468.1151) at different time points. Decomposition of 10b over 60 min in the presence of β-galactosidase was observed. b) Curve fitting to first order gave a rate constant of 0.0684 min ⁻¹ (R ² = 0.9929)	74
Figure 3.4	a) Extracted ion chromatograms for the formation of byproduct (12) (m/z = 150.0545; expected m/z = 150.0555) at given time	74

	points. Formation of 12 from 10b over 60 min in the presence of β -galactosidase was observed. b) Curve fitting to first order gave a rate constant of 0.0858 min^{-1} ($R^2 = 0.999$)	
Figure 3.5	a) Extracted ion chromatogram of benzyl persulfides and polysulfides generated from compound 10b , detected as their HPE-AM adducts using LC-MS. b) Extracted ion chromatogram of hydrogen sulfide and hydrogen polysulfides detected as their bis-HPE-AM adducts.	76
Figure 3.6	Cell viability assay carried out with the compound 10b for 24 h on a) DLD-1 cells b) HepG2 cells. All data are presented as mean \pm SD (n =3/group)	76
Figure 3.7	a) Extracted ion chromatograms for 11a ($m/z = 521.1250$; expected $m/z = 521.1264$) at different time points (5, 30, 60, 120, 210, 300, 600 min). Decomposition of 11a over 10 h in the presence of β -glucosidase was observed, as monitored by LC/MS. b) Curve fitting to first order gave a rate constant of $5.4 \times 10^{-3} \text{ min}^{-1}$	78
Figure 3.8	a) Extracted ion chromatograms for the formation of byproduct (12) ($m/z = 150.0551$; expected $m/z = 150.0555$) at given time points (5, 30, 60, 120, 210, 300, 600 min). Formation of 12 over 10 h in the presence of β -glucosidase was observed. b) Curve fitting to first order gave a rate constant of $7.1 \times 10^{-3} \text{ min}^{-1}$	78
Figure 3.9	a) Extracted ion chromatograms for 11b ($m/z = 468.1153$; expected $m/z = 468.1151$) at different time points (5, 30, 60, 120, 210, 300, 600 min). Decomposition of 11b over 10 h in the presence of β -glucosidase was observed. b) Curve fitting to first order gave a rate constant of $4.4 \times 10^{-3} \text{ min}^{-1}$, ($R^2 = 0.958$)	79
Figure 3.10	a) Extracted ion chromatograms for the formation of byproduct (12) ($m/z = 150.0545$; expected $m/z = 150.0555$) at given time points (5, 30, 60, 120, 210, 300, 600 min). Formation of 12 from 11b over 10 h in the presence of β -glucosidase was observed. b)	79

	Curve fitting to first order gave a rate constant of $7.4 \times 10^{-3} \text{ min}^{-1}$ ($R^2 = 0.9936$)	
Figure 3.11	Extracted ion chromatograms for the formation of the persulfide adduct of HPE-IAM (NACMeS-SH) ($m/z = 387.1042$; expected $m/z = 387.1048$) at the given time points (5, 30, 60, 120, 210, 300, 600 min). Formation of NACMeS-SH over 10 h in the presence of β -glucosidase was observed	80
Figure 3.12	a) Extracted ion chromatogram of persulfides and polysulfides of <i>N</i> -acetylcysteine methyl ester (NACMe-S(S) _n H) generated from compound 11a , detected as their HPE-AM adducts using LC/MS (R = <i>N</i> -acetylcysteine methyl ester, NACMe). b) Extracted ion chromatogram of hydrogen sulfide and hydrogen polysulfides detected as their bis-HPE-AM adducts.	81
Figure 3.13	Disulfide and trisulfide (R = <i>N</i> -acetylcysteine methylester, NACMe) formed upon incubation of 11a in the presence of β -glucosidase.	81
Figure 3.14	Extracted ion chromatograms for the formation of the benzyl persulfide adduct of HPE-IAM (BnSS-HPE-AM) ($m/z = 334.0922$; expected $m/z = 334.0935$) from 11b upon incubation with β -glucosidase at the given time points (5, 30, 60, 120, 210, 300, 600 min). Formation of BnSSH over 10 h in the presence of β -glucosidase was observed	82
Figure 3.15	a) Extracted ion chromatogram of benzyl persulfides and polysulfides generated from compound 11b , detected as their HPE-AM adducts using LC-MS. b) Extracted ion chromatogram of hydrogen sulfide and hydrogen polysulfides detected as their bis-HPE-AM adducts.	82
Figure 3.16	a) Cell viability assay carried out with the compound 11a for 24 h on a) DLD-1 cells b) HepG2 cells.	83

Figure 3.17	Cell viability assay carried out with the compound 11b for 24 h on a) DLD-1 cells b) HepG2 cells.	83
Figure 3.18	a) Extracted ion chromatograms for the formation of byproduct (12) ($m/z = 150.0545$; expected $m/z = 150.0555$) upon incubation of 10b with β -galactosidase in the presence or absence of NAC. b) Quantification of the area under the curve (AUC) for the peak corresponding to 12 . 25% reduction in the yield of 12 was observed upon incubation with NAC	85
Figure 3.19	a) Extracted ion chromatograms for the formation of mixed disulfide NAC-SS-Bn ($m/z = 150.0545$; expected $m/z = 286.0572$) upon incubation of 10b with β -galactosidase in the presence of NAC. b) Extracted ion chromatograms for the formation of mixed trisulfide NAC-SSS-Bn ($m/z = 318.0309$; expected $m/z = 318.0292$) upon incubation of 10b with β -galactosidase in the presence of NAC	85
Figure 3.20	a) Extracted ion chromatograms for the formation of byproduct (12) ($m/z = 150.0558$; expected $m/z = 150.0555$) upon incubation of 10b with β -galactosidase in the presence or absence of GSH. b) Quantification of the area under the curve (AUC) for the peak corresponding to 12 . 65% reduction in the yield of 12 was observed upon incubation with GSH	86
Figure 3.21	Detection of persulfide/polysulfide generated by compound 11a in DLD-1 cells, using the dye SSP2. The cells were imaged in the 20x GFP filter. Scale bar is 200 μ m	87
Figure 3.22	a) Cell viability assay carried out with the MGR-1 for 4 h on DLD-1 cells to determine its IC_{50} . IC_{50} was calculated to be 27 μ M. All data are presented as mean \pm SD (n =3/group). b) Cell viability assay carried out with the MGR-1 for 4 h on HepG2 cells. IC_{50} was calculated to be 12 μ M	88
Figure 3.23	a) Cytoprotective effects of 11a against ROS induced cell death. DLD-1 cells were pre-treated with varying doses of 11a for 12 h	89

	followed by treatment with the cell permeable ROS generator MGR-1 (20 mM) for 4h. b) A similar experiment carried out on the liver cell line (HepG2). A dose dependant increment in cell viability was observed upon pre-treatment with 11a , against cell death induced by MGR-1.	
Figure 4.1.1	a) Reaction mechanism for turnover of 3-mercaptopyruvate (3-MP) by 3-mercaptopyruvate sulfurtransferase (3-MST) to form a transient 3-MST persulfide intermediate and pyruvate as the byproduct. b) The 3-MST persulfide can undergo reduction to generate H ₂ S or transfer the sulfur to other acceptor proteins leading to total cellular persulfidation.	107
Figure 4.1.2	An artificial substrate having a similar enolizable ketone and a sulfur donor was designed, which upon turnover by 3-MST feeds into the biosynthetic machinery of the cell to induce persulfidation and generate H ₂ S. Acetophenone would be generated as a byproduct.	108
Figure 4.1.3	Structures of reagents used in the tag-switch technique	110
Figure 4.1.4	Tag-switch technique for detection of protein persulfides.	110
Figure 4.1.5	(a) Persulfidation of 3-MST by the ethyl ester of 3-MP (24) and the artificial substrate (25) in presence of ES, detected using the modified tag-switch technique. (b) Relative quantification of the bands using ImageJ	111
Figure 4.1.6	(a) Persulfidation of wt 3-MST and 3-MST C238A mutant by compounds 24 and 25 in the presence of esterase (ES) were studied using the modified tag-switch technique (b) Relative quantification of the bands was done using ImageJ.	112
Figure 4.1.7	(a) Extracted ion chromatograms from an LC/MS analysis of GSS-bimane ([M+H] ⁺ expected = 530.1379; observed = 530.1357) showing the formation of GSSH upon reacting 25 with 3-MST in the presence of esterase followed by treatment	113

	with GSH. b) Area under the curve (AUC) for the peak corresponding to GSS-bimane.	
Figure 4.1.8	a) Extracted ion chromatograms from an LC/MS analysis of bis-S-bimane ($[M+H]^+$ expected = 415.144; observed = 415.1433) indicating the formation of H ₂ S upon reacting 25 with 3-MST in the presence of esterase followed by treatment with GSH. b) Area under the curve (AUC) for the peak corresponding to bis-S-bimane.	113
Figure 4.1.9	a) Extracted ion chromatograms from an LC/MS analysis of GSSSG ($[M+H]^+$ expected = 645.1319; observed = 645.1315) indicating the formation of GSSSG upon reacting 25 with 3-MST in the presence of ES followed by treatment with GSH. b) Area under the curve (AUC) for the peak corresponding to GSSSG.	114
Figure 4.1.10	Validation of the probe SSP2 using varying concentrations of GS-S _n H. (λ_{ex} = 482 nm; λ_{em} = 518 nm)	116
Figure 4.1.11	a) Persulfide/polysulfide detection using probe SSP2. Fluorescence emission spectra of SSP2 (λ_{ex} = 482 nm) upon treatment with 3-MST and 25 in the presence of esterase. b) Fluorescence quenching of SSP2 upon addition of DTT to the reaction sample containing 3-MST, 25 and esterase	117
Figure 4.1.12	Persulfide/polysulfide detection using SSP2	118
Figure 4.1.13	Activity of GAPDH was measured by monitoring the formation of NADH, real-time at 340 nm.	119
Figure 4.1.14	Each group was treated with 2 mM DTT following which the GAPDH activity was measured after 1 h.	119
Figure 4.1.15	Compound 25 was tested for its cytotoxicity in A549 cell line using the MTT assay.	120

Figure 4.1.16	a) Structures of the reagents used. b) H ₂ S detection using the NDB-Fluorescein dye in A549 cells. The cells were imaged in the 20× GFP filter. Scale bar is 200 μm.	121
Figure 4.1.17	a) Detection of H ₂ S in 3-MST KD A549 cell line and the corresponding scrambled cell line using NBD fluorescein. Ctrl refers to untreated cells. Scale bar represents 200 μm. b) Representative bright field images.	122
Figure 4.1.18	a) Structures of reagents used in the assay. b) (TOP) A549 cells were treated with veh control (DMSO), 25 (50 μM) and MGR-1 (25 μM).	123
Figure 4.1.19	Biomarkers for oxidative stress: Three cell lines (A549, mouse embryonic fibroblasts (MEF) and N2a) were pre-treated with vehicle, 25 or 28 and exposed to MGR-1 following which NAD ⁺ /NADH ratio and GSSG/GSH ratio were determined using an ELISA assay.	124
Figure 4.1.20	Cell viability assay conducted on mouse embryonic fibroblast (MEF) cells.	125
Figure 4.1.21	MEF cells were first treated with 25 or 28 followed by treatment with MGR-1, a known inducer of oxidative stress in cells. Dose-dependent protection of cells from MGR-1-induced cell death by 25 was observed.	125
Figure 4.1.22	Cell viability assay carried out with substrate 25 as well as negative control 28 on N2a cells for 12 h.	126
Figure 4.1.23	Cell viability assay conducted on N2a cells. A dose-dependent protection of cells from MGR-1 induced cell death by 25 was observed.	126
Figure 4.1.24	Cell viability assay conducted on N2a cells. Dose-dependent protection of cells from menadione-induced cell death by 25 was observed.	127

Figure 4.1.25	(A) Pro-inflammatory cytokines, TNF- α and IL-6 using a standard ELISA assay. (B) Prostaglandins PGE ₂ /D ₂ using LC/MS.	128
Figure 4.1.26	Mechanistic insights into pro-inflammatory prostaglandins formation.	129
Figure 4.2.1	Probes for β -galactosidase for imaging senescence	142
Figure 4.2.2	a) Design of β -galactosidase activated prodrug (30) of the artificial substrate (26). b) Catalytic turnover of 26 by 3-MST to generate H ₂ S and persulfides/polysulfides.	142
Figure 4.2.3	HPLC decomposition profile of 30 in the presence of β -galactosidase	144
Figure 4.2.4	HPLC profile for catalytic turnover of 26 , generated from 30 upon treatment with β -galactosidase (2 U/mL), by <i>b3</i> -MST.	145
Figure 4.2.5	a) Methylene blue absorbance profile obtained for catalytic turnover of 30 in the presence of β -galactosidase (2 U/mL), <i>b3</i> -MST and DTT. 25 was used as the positive control. b) 30 in the absence of β -galactosidase (2 U/mL) and <i>b3</i> -MST does not produce H ₂ S. 38 was used as the negative control.	146
Figure 4.2.6	Absorbance of methylene blue recorded at 676 nm as a function of H ₂ S formation. Significant generation of H ₂ S was observed from 30 upon incubation with β -galactosidase, <i>b3</i> -MST and DTT.	147
Figure 4.2.7	a) Methylene blue absorbance profile obtained for catalytic turnover of 30 in the presence of β -galactosidase (2 U/mL), <i>h3</i> -MST and DTT. b) 30 in the absence of β -galactosidase (2 U/mL) and <i>h3</i> -MST does not produce H ₂ S.	148
Figure 4.2.8	Absorbance of methylene blue recorded at 676 nm as a function of H ₂ S formation. Significant generation of H ₂ S was observed	148

	from 30 upon incubation with β -galactosidase, <i>h3</i> -MST and DTT.	
Figure 4.2.9	Quantification of the fluorescence signal induced by 30 and Na ₂ S in A549 senescent and non-senescent cell lines using the tag-switch technique.	149

List of Schemes

Scheme 1.1	Oxidation of persulfides.	1
Scheme 2.1	Classes of persulfide prodrugs based on the self-immolation strategy.	39
Scheme 2.2	Retro-Michael reaction of thiol-succinimide adducts.	40
Scheme 2.3	Design of persulfide prodrugs based on 1,4-O,S relay mechanism or retro-Michael reaction.	40
Scheme 2.4	Mechanism of boronate ester cleavage by H ₂ O ₂ .	40
Scheme 2.5	Boronate ester based fluorescent probes for detection of H ₂ O ₂ .	41
Scheme 2.6	Design of ROS sensitive persulfide donor.	41
Scheme 2.7	Synthesis of H ₂ O ₂ responsive persulfide prodrug 5 .	42
Scheme 2.8	Synthesis of negative control 6 .	42
Scheme 2.9	Detection of persulfide by trapping it with an electrophile.	44
Scheme 2.10	Detection of benzyl persulfide by trapping it with FDNB.	44
Scheme 2.11	Synthesis of FDNB-persulfide adduct 7 .	44
Scheme 2.12	Detection of benzyl persulfide by trapping it with mBBr.	45
Scheme 2.13	Decomposition of 6 in the presence of H ₂ O ₂ to generate cinnamaldehyde.	47
Scheme 2.14	Mechanism of persulfide generation from 5 in the presence of H ₂ O ₂ .	50
Scheme 2.15	Boronate ester based persulfide donors responsive to H ₂ O ₂	53
Scheme 2.16	Persulfide donors responsive to superoxide.	53
Scheme 2.17	Boronate ester based persulfide donors responsive to H ₂ O ₂ .	54
Scheme 3.1	Synthesis of β-galactopyranosyl derivatives (10).	73
Scheme 3.2	a) Reaction scheme showing detection of persulfides/polysulfides as their HPE-AM adducts. b) Hydrogen sulfide/ polysulfides as their bis-S-HPE-AM adducts.	75

Scheme 3.3	Synthesis of β -glucopyranosyl derivatives (11).	77
Scheme 3.4	a) Proposed mechanism for the generation of persulfides and polysulfides from compounds 10-11 . b) Probable pathways for decomposition in the presence of a thiol.	84
Scheme 3.5	Release of fluorescein from SSP2 upon reaction with persulfides/polysulfides.	86
Scheme 3.6	ROS generation from MGR-1	88
Scheme 4.1.1	3-MP ethyl ester exists as a dimer which rapidly dissociates in buffer to give the monomer.	109
Scheme 4.1.2	Synthesis of the dimer of 3-MP ethyl ester, 24 .	109
Scheme 4.1.3	Synthesis of phenacyl thiol 25 .	109
Scheme 4.1.4	Synthesis of negative control 28 .	110
Scheme 4.1.5	Synthesis of negative control 29 .	110
Scheme 4.1.6	A schematic diagram of the various reactive sulfur species formed when 3-MST-SS ⁻ , generated by reacting 3-MST and 25 is treated with GSH.	115
Scheme 4.1.7	A schematic for the generation of 3-MST polysulfide and its degradation products.	115
Scheme 4.1.8	Release of fluorescein from SSP2 upon reaction with persulfides/polysulfides.	116
Scheme 4.1.9	Reaction catalyzed by GAPDH.	118
Scheme 4.2.1	Synthesis of β -galactosidase activated prodrug of 3-MST artificial substrate 30 .	143
Scheme 4.2.2	Synthesis of negative control 38 .	144
Scheme 4.2.3	Formation of methylene blue dye by H ₂ S.	146

Copyright permit from Royal Society of Chemistry for reusing data in Chapter 3 and 4.1:

Acknowledgement:

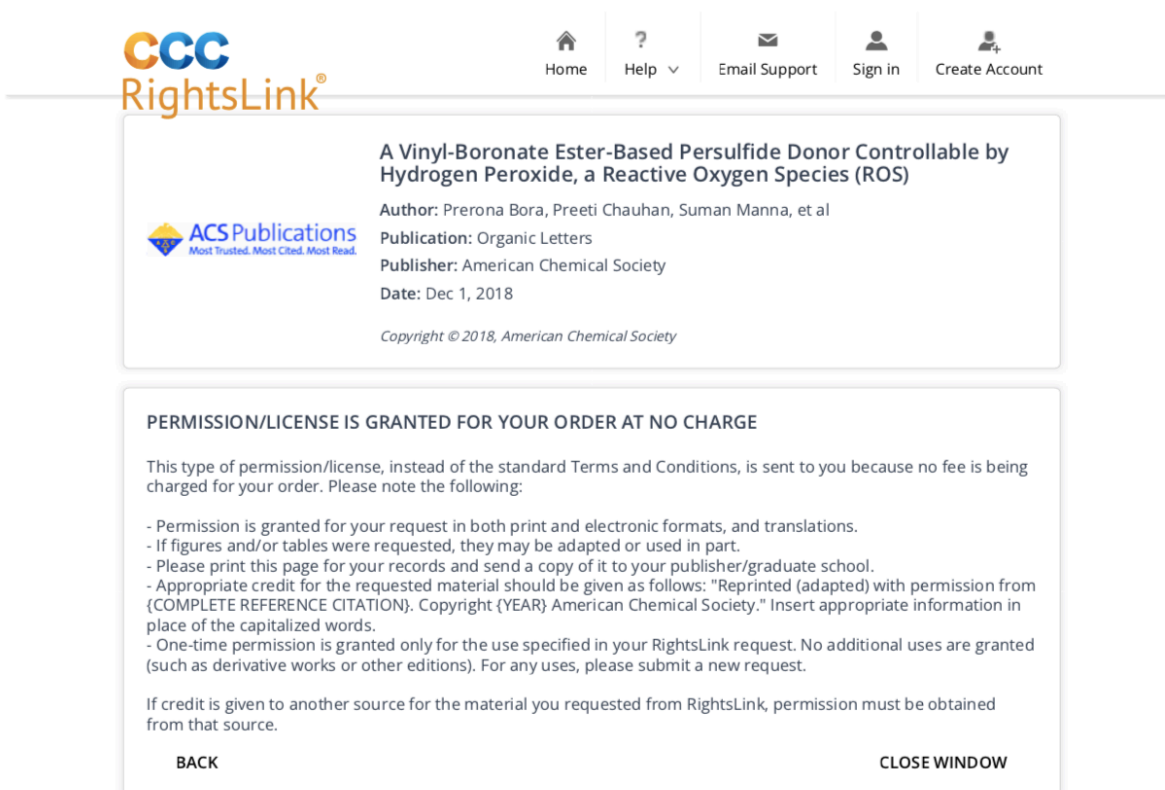
Data in Chapter 3 is reproduced from Ref [10.1039/D1CC07162A](https://doi.org/10.1039/D1CC07162A) with permission from the Royal Society of Chemistry

Data in Chapter 4.1 is reproduced from Ref *Chem. Sci.*, 2021, **12**, 12939-12949 with permission from the Royal Society of Chemistry

Author reusing their own work published by the RSC

You do not need to request permission to reuse your own figures, diagrams, tables, or images that were originally published in an RSC publication. However, permission should be requested for use of the whole article or chapter except if reusing it in a thesis. If you are including an article or book chapter published by the RSC in your thesis please ensure that your co-authors are aware of this.

Copyright permit from American Chemical Society for reusing data in Chapter 2:



CCC RightsLink

Home ? Help Email Support Sign in Create Account

A Vinyl-Boronate Ester-Based Persulfide Donor Controllable by Hydrogen Peroxide, a Reactive Oxygen Species (ROS)

Author: Prerona Bora, Preeti Chauhan, Suman Manna, et al
 Publication: Organic Letters
 Publisher: American Chemical Society
 Date: Dec 1, 2018
 Copyright © 2018, American Chemical Society

PERMISSION/LICENSE IS GRANTED FOR YOUR ORDER AT NO CHARGE

This type of permission/license, instead of the standard Terms and Conditions, is sent to you because no fee is being charged for your order. Please note the following:

- Permission is granted for your request in both print and electronic formats, and translations.
- If figures and/or tables were requested, they may be adapted or used in part.
- Please print this page for your records and send a copy of it to your publisher/graduate school.
- Appropriate credit for the requested material should be given as follows: "Reprinted (adapted) with permission from {COMPLETE REFERENCE CITATION}. Copyright {YEAR} American Chemical Society." Insert appropriate information in place of the capitalized words.
- One-time permission is granted only for the use specified in your RightsLink request. No additional uses are granted (such as derivative works or other editions). For any uses, please submit a new request.

If credit is given to another source for the material you requested from RightsLink, permission must be obtained from that source.

BACK **CLOSE WINDOW**

List of Publications

- 1) Chauhan, P.; **Bora, P.**; Ravikumar, G.; Jos, S.; and Chakrapani, H. Esterase Activated Carbonyl Sulfide/Hydrogen Sulfide (H₂S) Donors. *Org. Lett.*, **2017**, *19*, 62-65.
- 2) **Bora, P.**; Chauhan, P.; Pardeshi, K.; and Chakrapani, H. Small molecule generators of biologically reactive sulfur species. *RSC Adv.*, **2018**, *8*, 27359-27374.
- 3) **Bora, P.**; Chauhan, P.; Manna, S.; and Chakrapani, H. A Vinyl Boronate Ester Based Persulfide Donor Controllable by Hydrogen Peroxide, a Reactive Oxygen Sulfur Species. *Org. Lett.*, **2018**, *20*, 7916–7920.
- 4) **Bora, P.**; Manna, S.; Nair, M. A.; Sathe, R. R. M.; Singh, S.; Sreyas, V. S. A.; Gupta, K.; Mukherjee, A.; Saini, D. K.; Kamat, S. S.; Hazra, A. B.; Chakrapani, H. Leveraging an enzyme/artificial substrate system to enhance cellular persulfides and mitigate neuroinflammation. *Chem. Sci.*, **2021**, *12*, 12939-12949.
- 5) **Bora, P.**; Sathian, M. B.; Chakrapani, H. Enhancing cellular sulfane sulfur through β -glycosidase-activated persulfide donors: mechanistic insights and oxidative stress mitigation. *Chem. Commun.*, **2022**, *58*, 2987-2990.

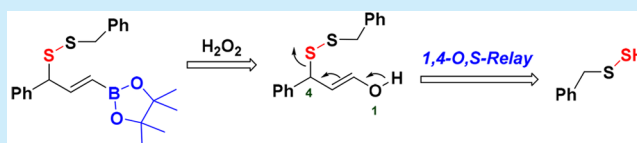
A Vinyl-Boronate Ester-Based Persulfide Donor Controllable by Hydrogen Peroxide, a Reactive Oxygen Species (ROS)

Prerona Bora, Preeti Chauhan, Suman Manna, and Harinath Chakrapani*¹

Department of Chemistry, Indian Institute of Science Education and Research Pune, Pune 411 008, Maharashtra, India

S Supporting Information

ABSTRACT: A vinyl boronate ester-based persulfidating agent that is selectively activated by hydrogen peroxide, which is a reactive oxygen species (ROS), and efficiently generated a persulfide by a hitherto unexplored 1,4-O,S-relay mechanism is reported. This donor was found to protect cells from cytotoxicity induced by oxidants, and the major byproduct is cinnamaldehyde, which is widely used in the food industry as an additive.



Hydrogen sulfide (H_2S) has emerged as an important mediator of redox cellular processes, especially in the context of cellular responses associated with oxidative stress.^{1–3} During several disease-like conditions, cells are exposed to increased reactive oxygen species (ROS), which contribute to neurodegenerative disorders, inflammation, diabetes, tumor progression, and aging.^{4–8} A mechanism by which H_2S exerts its effects is protein persulfidation (or S-sulfhydration),³ which is an oxidative post-translational modification where a cysteine (Cys-SH) residue is modified to Cys-SSH group.¹ Ambient protein persulfidation in cells is symptomatic of normal functioning in certain cells;⁴ a corollary to this observation is that diminished persulfidation is associated with stressed or diseased states. For example, diminished persulfidation of parkin, an E3 ubiquitin ligase that contains a reactive cysteine residue, is correlated with decreased rescue of damaged neurons. Increasing parkin persulfidation appears to protect neurons by removing damaged proteins. This finding has tremendous implications in the treatment of neurodegenerative diseases such as Parkinson's disease.⁹ However, this correlation does not hold for other proteins, underscoring the importance of developing new tools to interrogate the chemical biology of persulfidation under disease-relevant conditions.¹ Furthermore, since persulfides (RSS^-) are superior reductants, compared with RS^- , these species have gained traction as important intermediates in countering oxidative stress.^{10,11} However, since persulfides are unstable in biological milieu, it is challenging to generate these reactive sulfur species in a controllable manner,^{10,11} hence the growing interest in small-molecule persulfidating agents as tools to interrogate redox chemical biology of this reactive sulfur species.

An ideal donor would respond to elevated ROS to produce a protein persulfidating agent. The general strategy to generate a persulfide in situ involves stimuli responsive deprotection, followed by electronic rearrangement or a relay mechanism to release a persulfide.^{12,13} Subsequent exchange of the sulfhydryl group between the persulfidating agent and a protein occurs to induce protein persulfidation (Figure 1a). To closely mimic

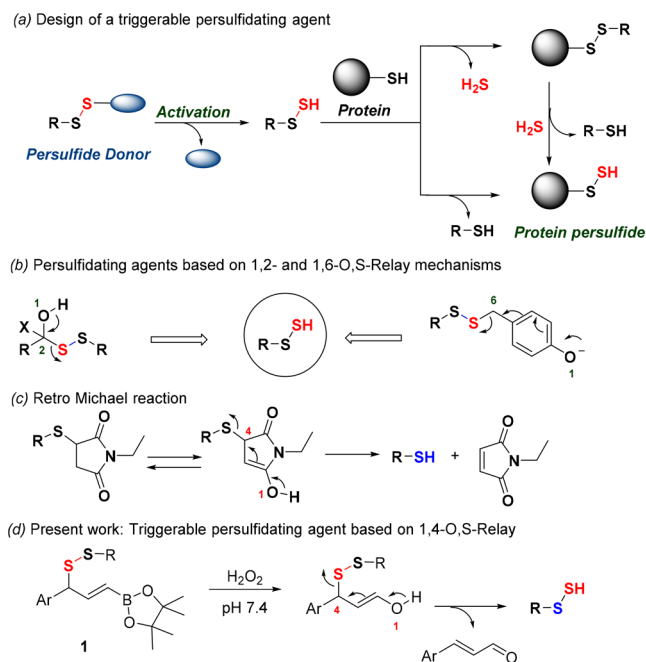


Figure 1. (a) Design of a triggerable protein S-sulfhydrating agent. (b) Key intermediates of some reported triggerable persulfide donors that operate via a 1,2- or a 1,6-O,S-relay mechanism. (c) An example of a retro Michael reaction: the first step is presumably the generation of an enol(ate), which generates a thiol by a 1,4-O,S-relay mechanism. (d) Design of a ROS-triggered persulfide donor that is expected to operate by a 1,4-O,S-relay mechanism.

inflammatory conditions, the donor would ideally need to be triggered by hydrogen peroxide, which is a stable ROS.¹⁴ The first major class of persulfidating agents are based on a 1,2-O,S-relay mechanism, where the oxygen and sulfur are placed adjacent to each other (Figure 1b).¹⁵ These donors respond to

Received: October 31, 2018

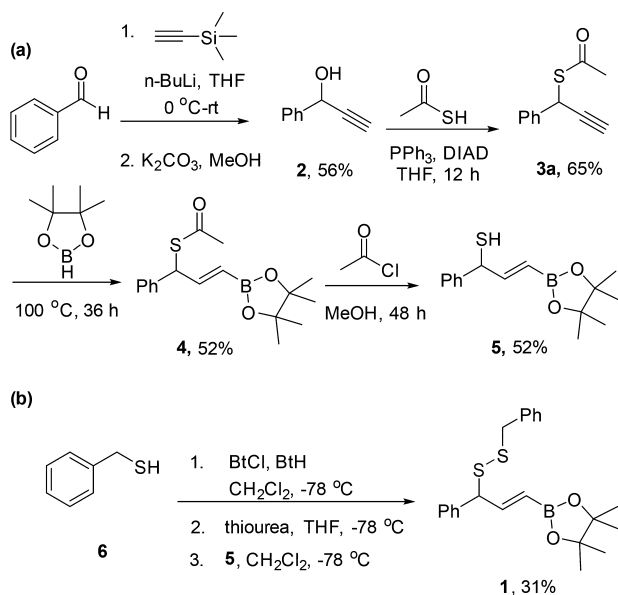
Published: December 7, 2018

a nucleophile,^{15,16} enzyme,^{17–19} or fluoride.²⁰ These donors, while useful, have limited selectivity toward oxidative stress conditions. The next class of persulfidating agents involves a 1,6-O,S-relay mechanism, where the oxygen is masked in the form of a boronate ester, which is a substrate for oxidation by ROS such as hydrogen peroxide.²¹ As a testament to its therapeutic utility, this donor was shown to protect cells from oxidative stress. The formation of a quinone-methide²² during persulfide delivery is possibly a limitation of this method.

To address these major gaps, we considered an alternate design for a ROS-triggerable persulfide donor, which was based on a hitherto unexplored 1,4-O,S-relay mechanism.¹² Formally, this type of rearrangement is a retro Michael reaction involving a thiol as a leaving group (Figure 1c).^{23,24} Here, the enol undergoes a 1,4-O,S-relay mechanism to generate a thiol and an α,β -unsaturated carbonyl compound. Since the pK_a of RSSH (6.2) is somewhat lower than a thiol (7–9), it was envisaged that this group might depart under these conditions.¹¹ The carbonyl was masked as a vinyl boronate ester **1**, which is known to undergo oxidation in the presence of hydrogen peroxide to generate an aldehyde (Figure 1d).^{25,26} The byproduct of decomposition of **1** is cinnamaldehyde, which is a constituent of cinnamon oil, and has been classified as Generally Recognized As Safe (GRAS). Together, **1** should respond to oxidative stress to generate a persulfide and relatively innocuous byproducts.

To synthesize **1** (Scheme 1a), benzaldehyde and TMS-acetylene were reacted in the presence of *n*-butyllithium to

Scheme 1. (a) Synthesis of Thiol **5**; (b) Reaction of Benzylthiol (**6**) with **5** Affords the Desired Compound **1**^a



^aBtCl = 1-chlorobenzotriazole and BtH = benzotriazole.

produce the secondary alcohol **2**.²⁷ Under Mitsunobu reaction conditions, **2** was converted to the thioacetate **3a** in 65% yield.²⁸ Hydroboration of **3a** gave **4** as the *trans* isomer (vicinal olefinic, $J = 17.2$ Hz). Deprotection of the thioacetate in the presence of acetyl chloride afforded the thiol **5** in 52% crude yield. Next, using a reported protocol, the reaction of benzyl thiol **6** with **5** afforded the desired product **1** in 31% yield.²⁹

First, to ascertain the reactivity of **1** toward ROS, **1** was incubated with H₂O₂ (10 equiv) in pH 7.4 buffer at 37 °C. HPLC analysis of the reaction mixture revealed the complete disappearance of this compound in 90 min (Figure S1a in the Supporting Information). A time course of this decomposition was obtained, and curve fitting to a first-order equation gave a rate constant k_1 of $5.3 \times 10^{-2} \text{ min}^{-1}$ (Figure 2a). The

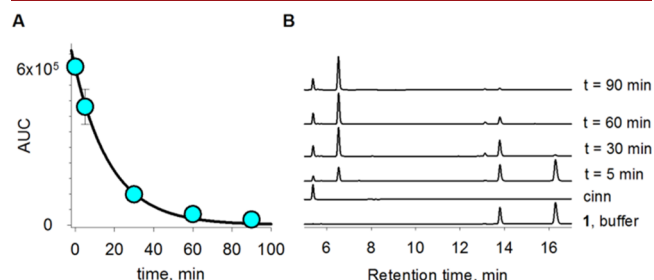


Figure 2. (a) Decomposition of **1**, as monitored by HPLC analysis. Curve fitting to first-order decomposition gave a rate constant (k_1) of $5.3 \times 10^{-2} \text{ min}^{-1}$. (b) HPLC analysis of the reaction of **1** with hydrogen peroxide in the presence of monobromobimane (mBBr) at 37 °C in pH 7.4 buffer (containing 20% CH₃CN).

estimated half-life of **1** under these conditions is 13 min. This value is comparable with arylboronate ester decomposition (0.09 min^{-1}), suggesting no significant difference in the mechanism of hydrogen peroxide-mediated oxidation. To study the potential for **1** to generate a persulfide, we used a method developed by Binghe Wang and co-workers, where they used 1-fluoro-2,4-dinitrobenzene (**7**, FDNB) to trap the persulfide.¹⁷ The resulting compound **8** (Figure 3) can be detected by HPLC analysis.

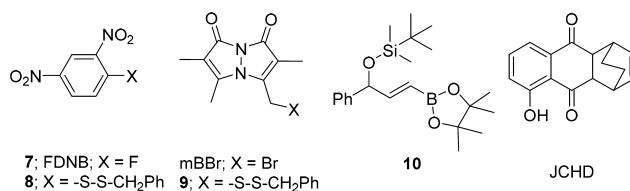
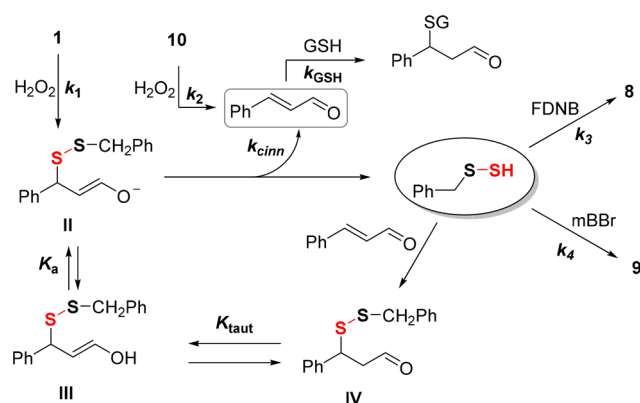


Figure 3. Structures of key tools and compounds used in this study.

Compound **8** was synthesized using a reported procedure and HPLC analysis showed a distinct peak at 11.3 min (Figure S3a in the Supporting Information). When **1** (retention time (RT) = 16.3 min) was coincubated with FDNB in the presence of H₂O₂, we found nearly complete decomposition in 90 min with a concomitant formation of **8** (Figure S3b in the Supporting Information). Because of the susceptibility of persulfides to decompose, this experiment was performed at room temperature. In the absence of hydrogen peroxide, we did not observe the formation of **8** (Figure S3d in the Supporting Information). These data support the generation of a persulfide when **1** was reacted with H₂O₂. The rate constant for the formation of **8** (k_3) was 0.15 min^{-1} and is a proxy to the persulfide formation rate (Scheme 2).

An independent assay based on monobromobimane (mBBr) was next used for detecting persulfides (Figure 2b). Reaction of mBBr with a persulfide is expected to produce the disulfide **9** (Figure 3). When **1** was reacted with hydrogen peroxide at 37 °C in the presence of mBBr, we find a distinct peak that is attributable to the formation of **9** ($m/z = 369.07$; observed,

Scheme 2. Mechanism of Persulfide Formation during the Oxidation of **1**^a

^aThe rate constant for decomposition of **1** was $k_1 = 5.3 \times 10^{-2} \text{ min}^{-1}$, whereas that for the decomposition of **10** was $k_2 = 4.8 \times 10^{-2} \text{ min}^{-1}$. The rate constant for the formation of cinnamaldehyde during the decomposition of **1** in the presence of FDNB was $k_{\text{cinn}} = 12.8 \times 10^{-2} \text{ min}^{-1}$. The rate constants for the formation of **8** ($k_3 = 0.15 \text{ min}^{-1}$) and **9** ($k_4 = 0.12 \text{ min}^{-1}$) were comparable.

369.25; see Figure S4 in the Supporting Information). The time course for formation of this compound was monitored, and a rate constant of k_4 of 0.12 min^{-1} was obtained. This rate constant is comparable with k_1 . Furthermore, the value of k_3 was determined at 25°C , and considering rate effects on temperature, we suggest that the values of k_1 , k_3 , and k_4 are similar.

Next, the silylated derivative **10** was synthesized in two steps from the propargyl alcohol **2** (Scheme S1 in the Supporting Information). Compound **10** should undergo decomposition in the presence of hydrogen peroxide but does not generate a persulfide. When **10** was incubated in the presence of H_2O_2 , indeed, we find evidence for the formation of cinnamaldehyde (Figure S2 in the Supporting Information).

Curve fitting yielded a rate constant (k_2) of $4.8 \times 10^{-2} \text{ min}^{-1}$ that was comparable in value with the rate of decomposition of **1** (Scheme 2). The yield of cinnamaldehyde under these conditions was 73%, which is comparable with the yield of **8** during incubation of **1** with hydrogen peroxide and FDNB (Figure S3b in the Supporting Information). Phillips and co-workers have previously demonstrated the use of vinyl boronate esters in the deprotection of alcohols with $\text{p}K_{\text{a}}$ values of >11 .²⁶ Since the estimated $\text{p}K_{\text{a}}$ value of *tert*-butyldimethylsilanol is 15, this result supports the use of such vinylboronate esters for the release of poorly acidic alcohols as well.

When **1** was incubated in the presence of hydrogen peroxide, we similarly observed the formation of cinnamaldehyde, but with diminished yield (Figure S1a in the Supporting Information). This diminished yield could be due to the collateral consumption of cinnamaldehyde by the persulfide. To test this possibility, we incubated **1** in the presence of H_2O_2 and mBBR, and we found that the yield of cinnamaldehyde was significantly better ($\sim 70\%$; Figure 2b). The rate constant for the formation of cinnamaldehyde (k_{cinn}) was $12.8 \times 10^{-2} \text{ min}^{-1}$ (Scheme 2). Persulfides, being good one-electron reductants, have a high propensity to undergo oxidation to form tetrasulfides (RSSSR) and polysulfides (RS_nR).³⁰ Although all assays were performed in the presence of diethylenetriaminepentaacetic acid (DTPA) as a chelating

agent, to prevent the decomposition of H_2O_2 and the subsequent radical-based oxidation of persulfides, the possibility of polysulfide formation cannot be ruled out. Furthermore, in cells, we would expect cinnamaldehyde to react with other thiols such as glutathione, which typically occurs in millimolar concentrations. When cinnamaldehyde was reacted with glutathione, the pseudo-first-order rate constant for this reaction was found as $2.3 \times 10^{-2} \text{ min}^{-1}$, which translates to a half-life of $\sim 30 \text{ min}$ (Figure S5 in the Supporting Information). Previously, cinnamaldehyde was found to react with thiols as well as bovine serum albumin;³¹ the half-life of the latter reaction was in the range of 3–8 min. These data suggested the possibility of cellular thiols competitively reacting with cinnamaldehyde and possibly sparing the persulfide to conduct protein persulfidation.

We next estimated the selectivity of **1** toward activation by H_2O_2 . We tested **1** against a variety of oxidants in the presence of FDNB and tested if the persulfide adduct **8** was produced. We find no evidence for decomposition of **1** or the formation of **8** under these conditions (Figure S6a in the Supporting Information). In a separate assay with **10**, we found no evidence for the formation of cinnamaldehyde, except when **10** was treated with H_2O_2 (Figure S6c in the Supporting Information). Together, these data support the excellent selectivity of the vinyl boronate ester functional group toward oxidation by hydrogen peroxide.

The proposed mechanism for the reaction of **1** with hydrogen peroxide involves the oxidation of the vinyl boronate ester (likely the boronic acid in pH 7.4 buffer) to produce an enolate intermediate, which decomposes to produce the persulfide and cinnamaldehyde. Since the value of k_{cinn} was comparable in magnitude with that of k_3 and k_4 , it is likely that the formation of the persulfide and cinnamaldehyde is concerted. Previously, retro Michael reactions involving thioethers of *N*-ethylmaleimide have been reported.^{23,24} These reactions are extremely slow (half-lives ranging from ~ 1 –7 days). Hence, the present method appears to be distinct from the previous reports due to the direct generation of an enolate **II** that rapidly rearranges to produce a persulfide. The equilibrium constant for tautomerism (K_{taut}), which is defined as $[\text{keto}]/[\text{enol}]$ for aliphatic aldehydes, is in the range of 10^{-3} – 10^{-4} .³²

These data suggest that, once formed, **III** would likely equilibrate to the aldehyde **IV** (Scheme 2). If the aldehyde (keto form) is indeed produced, it is likely that the generation of the persulfide might be extremely slow. Our attempts to detect this aldehyde **IV** were unsuccessful. Since the yields of products are in excess of 70%, we reasoned that tautomerism may not be a major competitive process. Thus, it is likely that the enolate **II**, once formed, would rapidly rearrange to generate the persulfide. The estimated $\text{p}K_{\text{a}}$ for the enol is 9–10, likely to be deprotonated in pH 7.4.³³ Previously, in basic solution, the enolate was found to be the dominant form for certain aldehydes.³³ Although the operating pH is 7.4, it appears to stabilize the enolate sufficiently to promote the 1,4-O,S-relay.

Lastly, since persulfides are reported to mitigate oxidative stress, we tested the ability of **1** to protect colon carcinoma DLD-1 cells from cytotoxicity induced by elevated ROS. Colon cells are constantly exposed to xenobiotics and stress induced by pathogens. It has been reported that hydrogen sulfide is an important mediator of stress response in the gut.^{34–36} Using DLD-1 colon carcinoma cells, a cell viability assay was first

conducted with increasing doses of **1**, and no significant inhibition up to 100 μM was observed (Figure S7a in the Supporting Information). Next, using menadione, which is a known redox cycling agent and inducer of oxidative stress, we evaluated the protective effects of **1**.^{37,38} DLD-1 cells were treated with menadione and viable cells were measured (Figure S7b in the Supporting Information). We found significant cell killing at 50 μM (30% viable cells); this concentration was chosen to study possible cytoprotective effects of **1**. When **1** was cotreated with menadione, a dose-dependent cytoprotection was observed (Figure 4a). A cell viability assay conducted

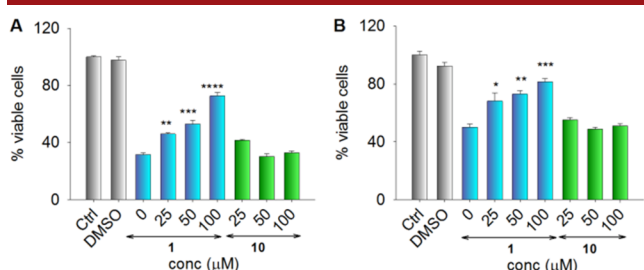


Figure 4. (a) Cytoprotective effects of compound **1** against menadione (50 μM). Results are expressed as mean \pm SEM ($n = 3$). [Legend: (**) $p < 0.01$, (***) $p < 0.001$, (****) $p < 0.0001$ vs menadione.] A similar assay was conducted with **10**. No significant effect on the percentage of viable cells during incubation of **10** with menadione was observed. (b) Cytoprotective effects of compound **1** against JCHD (50 μM). Results are expressed as mean \pm SEM ($n = 3$). [Legend: (*) $p < 0.05$, (**) $p < 0.01$, (***) $p < 0.001$, vs JCHD.] A similar assay was conducted with **10**, and no significant effect was observed.

with **10** revealed that this compound was not significantly cytotoxic (Figure S7a). However, **10** was unable to protect cells from menadione-induced cytotoxicity, supporting the importance of the persulfide in cytoprotective effects (Figure 4a). Next, JCHD, which is a derivative of juglone, was used to simulate increased ROS within cells. This compound has been previously characterized to generate ROS in pH 7.4 buffer under ambient aerobic conditions and increase ROS levels in cells (Figure S8 in the Supporting Information). Again, we find significant cytotoxicity induced at 50 μM by JCHD (Figure S7b).^{39–41} The persulfide donor **1** protected cells from JCHD-induced toxicity, while **10** showed no effect (Figure 4b). Thus, the results of these cell studies demonstrate the potential for this new donor to protect cells from xenobiotics and oxidative stress.

In summary, we report a new class of 1,4-O,S-relay mechanism-based persulfide donors with a unique retro Michael reaction as the key step. Generation of persulfide from this donor was independently validated by two assays, and the mechanism is consistent with experimental data. The major byproducts that are produced appear well tolerated by cells and this observation is encouraging for further development of this donor. We found that **1** was able to protect cells from oxidative stress induced by exogenous ROS generators. Taken together, this compound is a valuable addition to the growing redox toolbox to understand the chemical biology of reactive sulfur species better while progressing toward new classes of sulfur-based therapeutic agents.

■ ASSOCIATED CONTENT

Supporting Information

The Supporting Information is available free of charge on the ACS Publications website at DOI: 10.1021/acs.orglett.8b03471.

Synthesis and characterization data, analytical data, and protocols (PDF)

■ AUTHOR INFORMATION

Corresponding Author

*E-mail: harinath@iiserpune.ac.in.

ORCID

Harinath Chakrapani: 0000-0002-7267-0906

Notes

The authors declare no competing financial interest.

■ ACKNOWLEDGMENTS

The authors thank the Department of Science and Technology (DST, Grant No. EMR/2015/000668), Department of Biotechnology, India (No. BT/PR15848/MED/29/1025/2016) for financial support for our research. Council for Scientific and Industrial Research (CSIR) and the Department of Science and Technology–Innovation in Science Pursuit for Inspired Research (DST-INSPIRE) for fellowships.

■ REFERENCES

- Filipovic, M. R.; Zivanovic, J.; Alvarez, B.; Banerjee, R. *Chem. Rev.* **2018**, *118* (3), 1253.
- Kabil, O.; Vitvitsky, V.; Banerjee, R. *Annu. Rev. Nutr.* **2014**, *34* (1), 171.
- Mishanina, T. V.; Libiad, M.; Banerjee, R. *Nat. Chem. Biol.* **2015**, *11*, 457.
- Mustafa, A. K.; Gadalla, M. M.; Sen, N.; Kim, S.; Mu, W.; Gazi, S. K.; Barrow, R. K.; Yang, G.; Wang, R.; Snyder, S. H. *Sci. Signaling* **2009**, *2* (96), ra72.
- Yang, G.; Zhao, K.; Ju, Y.; Mani, S.; Cao, Q.; Puukila, S.; Khaper, N.; Wu, L.; Wang, R. *Antioxid. Redox Signaling* **2013**, *18* (15), 1906.
- Zhao, W.; Zhang, J.; Lu, Y.; Wang, R. *EMBO J.* **2001**, *20* (21), 6008.
- Mustafa, A. K.; Sikka, G.; Gazi, S. K.; Steppan, J.; Jung, S. M.; Bhunia, A. K.; Barodka, V. M.; Gazi, F. K.; Barrow, R. K.; Wang, R.; Amzel, L. M.; Berkowitz, D. E.; Snyder, S. H. *Circ. Res.* **2011**, *109* (11), 1259.
- Wallace, J. L.; Wang, R. *Nat. Rev. Drug Discovery* **2015**, *14*, 329.
- Vandiver, M. S.; Paul, B. D.; Xu, R.; Karuppagounder, S.; Rao, F.; Snowman, A. M.; Seok Ko, H.; Il Lee, Y.; Dawson, V. L.; Dawson, T. M.; Sen, N.; Snyder, S. H. *Nat. Commun.* **2013**, *4*, 1626.
- Ono, K.; Akaike, T.; Sawa, T.; Kumagai, Y.; Wink, D. A.; Tantillo, D. J.; Hobbs, A. J.; Nagy, P.; Xian, M.; Lin, J.; Fukuto, J. M. *Free Radical Biol. Med.* **2014**, *77*, 82.
- Park, C.-M.; Weerasinghe, L.; Day, J. J.; Fukuto, J. M.; Xian, M. *Mol. Biosyst.* **2015**, *11* (7), 1775.
- Alouane, A.; Labruere, R.; Le Saux, T.; Schmidt, F.; Jullien, L. *Angew. Chem., Int. Ed.* **2015**, *54* (26), 7492.
- Artaud, I.; Galardon, E. *ChemBioChem* **2014**, *15* (16), 2361.
- Li, L.; Rose, P.; Moore, P. K. *Annu. Rev. Pharmacol. Toxicol.* **2011**, *51* (1), 169.
- Park, C.-M.; Johnson, B. A.; Duan, J.; Park, J.-J.; Day, J. J.; Gang, D.; Qian, W.-J.; Xian, M. *Org. Lett.* **2016**, *18* (5), 904.
- Kang, J.; Ferrell, A. J.; Chen, W.; Wang, D.; Xian, M. *Org. Lett.* **2018**, *20* (3), 852.
- Zheng, Y.; Yu, B.; Li, Z.; Yuan, Z.; Organ, C. L.; Trivedi, R. K.; Wang, S.; Lefer, D. J.; Wang, B. *Angew. Chem., Int. Ed.* **2017**, *56* (39), 11749.

- (18) Yu, B.; Zheng, Y.; Yuan, Z.; Li, S.; Zhu, H.; De La Cruz, L. K.; Zhang, J.; Ji, K.; Wang, S.; Wang, B. *J. Am. Chem. Soc.* **2018**, *140* (1), 30.
- (19) Yuan, Z.; Zheng, Y.; Yu, B.; Wang, S.; Yang, X.; Wang, B. *Org. Lett.* **2018**, *20* (20), 6364.
- (20) Kang, J.; Xu, S.; Radford, M. N.; Zhang, W.; Kelly, S. S.; Day, J. J.; Xian, M. *Angew. Chem.* **2018**, *130* (20), 5995.
- (21) Powell, C. R.; Dillon, M. K.; Wang, Y.; Carrazzone, R. J.; Matson, J. B. *Angew. Chem., Int. Ed.* **2018**, *57* (21), 6324.
- (22) Monks, T. J.; Jones, D. C. *Curr. Drug Metab.* **2002**, *3*, 425–438.
- (23) Baldwin, A. D.; Kiick, K. L. *Bioconjugate Chem.* **2011**, *22* (10), 1946.
- (24) Weissman, M. R.; Winger, K. T.; Ghiassian, S.; Gobbo, P.; Workentin, M. S. *Bioconjugate Chem.* **2016**, *27* (3), 586.
- (25) Brooks, A. D.; Mohapatra, H.; Phillips, S. T. *J. Org. Chem.* **2015**, *80* (21), 10437.
- (26) Brooks, A. D.; Yeung, K.; Lewis, G. G.; Phillips, S. T. *Anal. Methods* **2015**, *7* (17), 7186.
- (27) Zheng, M.; Wu, F.; Chen, K.; Zhu, S. *Org. Lett.* **2016**, *18* (15), 3554.
- (28) Yang, F.; Jin, T.; Bao, M.; Yamamoto, Y. *Tetrahedron Lett.* **2011**, *52* (8), 936.
- (29) Hunter, R.; Caira, M.; Stellenboom, N. *J. Org. Chem.* **2006**, *71* (21), 8268.
- (30) Bianco, C. L.; Chavez, T. A.; Sosa, V.; Saund, S. S.; Nguyen, Q. N. N.; Tantillo, D. J.; Ichimura, A. S.; Toscano, J. P.; Fukuto, J. M. *Free Radical Biol. Med.* **2016**, *101*, 20.
- (31) Weibel, H.; Hansen, J. *Contact Dermatitis* **1989**, *20* (3), 161.
- (32) Keeffe, J. R.; Kresge, A. J.; Schepp, N. P. *J. Am. Chem. Soc.* **1990**, *112* (12), 4862.
- (33) Chiang, Y.; Kresge, A. J.; Krogh, E. T. *J. Am. Chem. Soc.* **1988**, *110* (8), 2600.
- (34) Motta, J.-P.; Flannigan, K. L.; Agbor, T. A.; Beatty, J. K.; Blackler, R. W.; Workentine, M. L.; Da Silva, G. J.; Wang, R.; Buret, A. G.; Wallace, J. L. *Inflamm. Bowel Dis.* **2015**, *21* (5), 1006.
- (35) Fiorucci, S.; Antonelli, E.; Distrutti, E.; Rizzo, G.; Mencarelli, A.; Orlandi, S.; Zanardo, R.; Renga, B.; Di Sante, M.; Morelli, A.; Cirino, G.; Wallace, J. L. *Gastroenterology* **2005**, *129* (4), 1210.
- (36) Fiorucci, S.; Orlandi, S.; Mencarelli, A.; Caliendo, G.; Santagada, V.; Distrutti, E.; Santucci, L.; Cirino, G.; Wallace, J. L. *Br. J. Pharmacol.* **2007**, *150* (8), 996.
- (37) Criddle, D. N.; Gillies, S.; Baumgartner-Wilson, H. K.; Jaffar, M.; Chinje, E. C.; Passmore, S.; Chvanov, M.; Barrow, S.; Gerasimenko, O. V.; Tepikin, A. V.; Sutton, R.; Petersen, O. H. *J. Biol. Chem.* **2006**, *281* (52), 40485.
- (38) Loor, G.; Kondapalli, J.; Schriewer, J. M.; Chandel, N. S.; Vanden Hoek, T. L.; Schumacker, P. T. *Free Radical Biol. Med.* **2010**, *49* (12), 1925.
- (39) Dharmaraja, A. T.; Chakrapani, H. *Org. Lett.* **2014**, *16* (2), 398.
- (40) Dharmaraja, A. T.; Alvala, M.; Sriram, D.; Yogeewari, P.; Chakrapani, H. *Chem. Commun.* **2012**, *48* (83), 10325.
- (41) Tyagi, P.; Dharmaraja, A. T.; Bhaskar, A.; Chakrapani, H.; Singh, A. *Free Radical Biol. Med.* **2015**, *84*, 344.



Cite this: DOI: 10.1039/d1cc07162a

 Received 21st December 2021,
Accepted 4th February 2022

DOI: 10.1039/d1cc07162a

rsc.li/chemcomm

Enhancing cellular sulfane sulfur through β -glycosidase-activated persulfide donors: mechanistic insights and oxidative stress mitigation†

 Prerona Bora,  Manjima B. Sathian  and Harinath Chakrapani *

Sulfane sulfur species such as persulfides and polysulfides along with hydrogen sulfide protect cells from oxidative stress and are key members of the cellular antioxidant pool. Here, we report perthiocarbamate-based prodrugs that are cleaved by β -glycosidases to produce persulfide and relatively innocuous byproducts. The β -glucosidase-activated persulfide donor enhances cellular sulfane sulfur and protects cells against lethality induced by elevated reactive oxygen species (ROS).

Redox-active species derived from sulfur play a central role in cellular signalling and metabolism, stress response and homeostasis.¹ Persulfides (RS-SH) and polysulfides (RS-(S)_n-H), which are members of the sulfane sulfur pool, have emerged as important mediators in stress response.^{2,3} Collectively, the sulfane sulfur pool together with hydrogen sulfide (H₂S) is now considered a reservoir of antioxidant species that responds to oxidative stress and protects key cellular components from oxidative damage.⁴ Hence, in addition to thiols such as glutathione and H₂S, persulfides are summoned to counter stress caused by elevated reactive oxygen species (ROS). RS-SH is more nucleophilic than RSH as evidenced by a higher HOMO (51 kJ mol⁻¹ for CysS-SH vs. CysSH) leading to superior reactivity with electrophilic species.⁵ Persulfides and polysulfides are also better at sequestering reactive oxygen species (ROS) and countering oxidative stress.⁶ Protein persulfidation, which is an oxidative post translational modification of cysteine residues, not only contributes to redox signalling but also protects cysteines from irreversible oxidation.⁷ Persulfides and polysulfides are excellent persulfidating agents compared to H₂S and hence new strategies to enhance cellular persulfides responsive to fluoride,⁸ esterase,⁹ pH,¹⁰ light,¹¹ H₂O₂,^{12,13} and nitroreductase¹⁴ have been developed. Recently, artificial substrates for 3-mercaptopyruvate sulfurtransferase (3-MST) as enhancers of cellular persulfides was reported.¹⁵ Several of the aforementioned strategies have shown promise in

mitigating oxidative stress in cellular and animal models (Fig. 1a). However, several of them produce byproducts that are electrophilic, some have poor selectivity across cell types, many have diminished aqueous solubility, and in a few cases, no therapeutic relevance was demonstrated. Here, we report the design and development of a cell permeable β -glycosidase-activated persulfide donor that protects cells from oxidative stress.

β -Glycosidases are a class of enzymes that cleave glycosidic bonds in oligo/polysaccharides. These enzymes are over-expressed in the gastrointestinal (GI) tract, especially the colon. Elevated levels of β -glycosidases are associated with certain pathophysiologies of the GI tract including inflammatory bowel disorder (IBD), Crohn's disease and ulcerative colitis and cancer.^{16,17} Increased reactive oxygen species (ROS) leading to collateral damage of the tissue is common in these conditions.¹⁸ Thus, enhancing antioxidants is a possible therapeutic approach for such conditions. Several colon-specific prodrug strategies that involve cleavage by β -D-glucosidase, β -D-galactosidase, β -D-xylosidase produced by the intestinal microflora are known.^{16,19} Hence, taking the aforementioned aspects into consideration, we designed β -glycosidase-activated

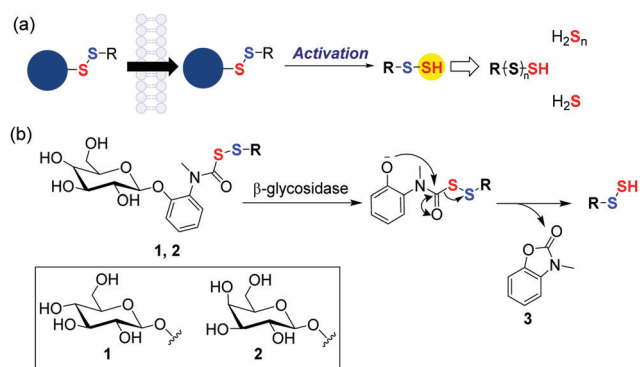


Fig. 1 (a) Prodrug strategies to generate sulfane sulfur in cells. (b) Present work; prodrugs of persulfides/polysulfides cleavable by β -glycosidase (1: β -glucosidase, 2: β -galactosidase).

Department of Chemistry, Indian Institute of Science Education and Research Pune, Pune 411 008, Maharashtra, India. E-mail: harinath@iiserpune.ac.in

† Electronic supplementary information (ESI) available: Preparative methods, assay protocols and spectral data. See DOI: 10.1039/d1cc07162a

persulfide prodrugs (Fig. 1b); two series of compounds were considered: one cleavable by β -glucosidase (**1**) and the other by β -galactosidase (**2**). Being sugars, these compounds are expected to have enhanced aqueous solubility and would therefore have better applicability. Lastly, unlike certain other donors, once a persulfide is generated, no electrophilic and potentially toxic byproduct is formed.²⁰

Compound **1a** (R = *N*-acetylcysteine methylester, Scheme 1) was synthesized in 5 steps (Scheme 1). First, the reaction of 2-nitrophenol with 2,3,4,6-tetra-*O*-acetyl- β -D-glucopyranosyl bromide **4**, using a reported protocol²¹ gave compound **5**. This was followed by reduction of the nitro group in **5** to its corresponding aniline **6** by using zinc in HCl. Formylation of the aniline followed by its reduction using borane dimethylsulfide²² gave the *N*-methylaniline derivative **7**. In a separate reaction, *N*-acetylcysteine methylester (NACMe) was treated with chlorocarbonylsulfonyl chloride to obtain the *S*-perthiocarbonyl chloride **8a**, which was immediately reacted with compound **7** to obtain compound **9**.¹⁰ Finally, deprotection of acetyl groups of **9** using sodium methoxide in methanol afforded **1a**.

To ascertain the reactivity of the compound towards β -glucosidase, **1a** was incubated with β -glucosidase in pH 7.4 phosphate buffer at 37 °C. LC/MS analysis of the reaction mixture revealed a complete decomposition of the compound within 10 h (Fig. 2a). A time course for this decomposition was obtained and curve fitting to a first order equation gave a rate constant of $5.4 \times 10^{-3} \text{ min}^{-1}$ with a half-life of 128 min (Fig. 2a and Fig. S1, ESI[†]).

Under these conditions, as expected, the formation of *N*-methyl benzoxazolone byproduct (**3**) was observed with $m/z = 150.0551 [M + H]^+$ (expected $m/z = 150.0555$) (Fig. S2, ESI[†]). Curve fitting gave a rate constant of $7.1 \times 10^{-3} \text{ min}^{-1}$, which is comparable to the rate of decomposition of **1a** (Fig. 2b). Together, these data suggest that the cleavage step is the rate determining and once the sugar is cleaved, the release of the persulfide is fast. The ability of **1a** to generate persulfides under these conditions was next evaluated. A standard method for the characterization of persulfide species is to trap them with an electrophile to form a covalent adduct, which can be detected using HPLC or LC/MS.

N-(4-Hydroxyphenethyl)-2-iodoacetamide (HPE-IAM) has been previously reported^{23,24} to be a potent and efficient persulfide/polysulfide alkylating agent (Scheme 2).²⁵ When **1a** was co-incubated in the presence of β -glucosidase and

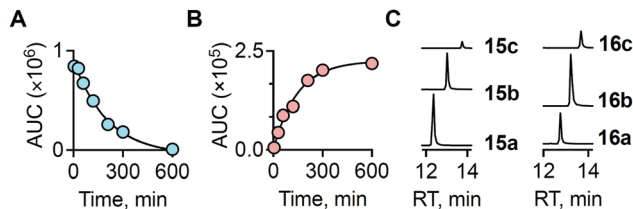
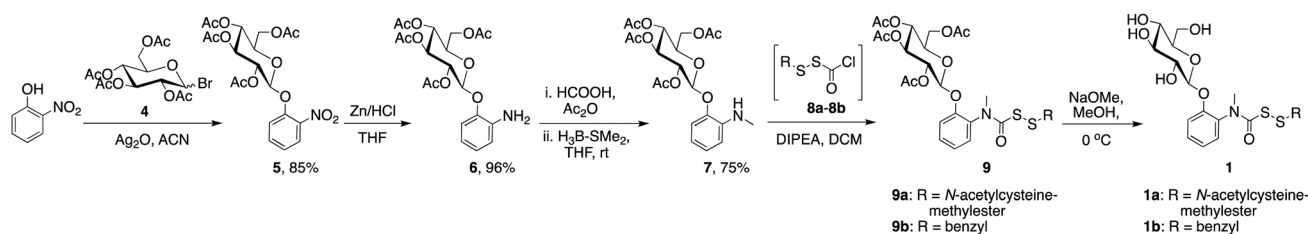


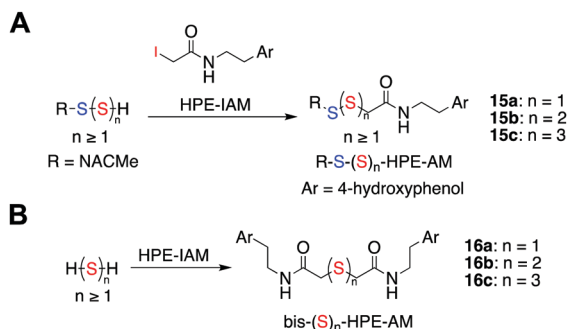
Fig. 2 (a) Decomposition of **1a** upon incubation with β -glucosidase (10 U mL^{-1}) as monitored by LC/MS ($m/z = 521.1250 [M + H]^+$; expected, 521.1264). Curve fitting to first order gave a rate constant of $5.4 \times 10^{-3} \text{ min}^{-1}$. (b) Formation of by-product **3** under the same conditions ($m/z = 150.0551 [M + H]^+$; expected, 150.0555). Curve fitting to first order gave a rate constant of $7.1 \times 10^{-3} \text{ min}^{-1}$. (c) Extracted ion chromatogram of persulfides and polysulfides of *N*-acetylcysteine methylester (NACMe- $S(S)_n$ H) generated from compound **1a**, detected as their HPE-AM adducts using LC/MS. **15a** ($m/z = 387.1042 [M + H]^+$; expected, 387.1048); **15b** ($m/z = 419.0781 [M + H]^+$; expected, 419.0769); **15c** ($m/z = 451.0500 [M + H]^+$; expected, 451.0490). (d) Extracted ion chromatogram of hydrogen sulfide and hydrogen polysulfides detected as their bis-HPE-AM adducts. **16a** ($m/z = 389.1545 [M + H]^+$; expected, 389.1535); **16b** ($m/z = 421.1272 [M + H]^+$; expected, 421.1256); **16c** ($m/z = 453.0991 [M + H]^+$; expected, 453.0976).

HPE-IAM, the appearance of a new peak at 12.36 min with $m/z = 387.1042 [M + H]^+$ was observed that gradually increased over time (Fig. S3, ESI[†]). It was attributed as the NACMe persulfide adduct, **15a** (expected $m/z = 387.1048$), thus confirming the generation of a persulfide under these conditions (Fig. 2c). We also found evidence for the formation of polysulfide adducts, **15b** and **15c** under these conditions (Fig. 2c). Additionally, appreciable amounts of H_2S as the bis-*S*-HPE-AM adduct (**16a**) with $m/z = 389.1545 [M + H]^+$ (expected $m/z = 389.1535$) was detected along with hydrogen polysulfides (H_2S_n , $n = 2$ and 3) (Fig. 2c). Furthermore, disulfide and trisulfide of NACMe were also detected (Fig. S4, ESI[†]). Together, these data demonstrate the ability of **1a** to produce a gamut of reactive sulfur species, hydrogen sulfide, persulfide and polysulfide.

Having confirmed the *in vitro* generation of persulfides/polysulfides from **1a**, we attempted to study its cell permeability and intracellular generation of sulfane sulfur. Human cytosolic β -glucosidase is present in significant concentrations in the liver, kidney, spleen and colon.^{26,27} Human colon carcinoma (DLD-1) and hepatocarcinoma (HepG2) cell line were therefore used as model systems. A standard cell viability assay was conducted to assess the cytotoxicity of **1a** on DLD-1 and HepG2 cells. No significant toxicity was observed up to a concentration of $100 \mu\text{M}$ (Fig. S5, ESI[†]). To detect intracellular sulfane sulfur,



Scheme 1 Synthesis of glucopyranosyl derivatives, **1**.



Scheme 2 (a) Reaction scheme showing detection of persulfides/polysulfides as their HPE-IAM adducts. Ar = 4-hydroxyphenol (b) hydrogen sulfide/polysulfides as their bis-S-HPE-IAM adducts.

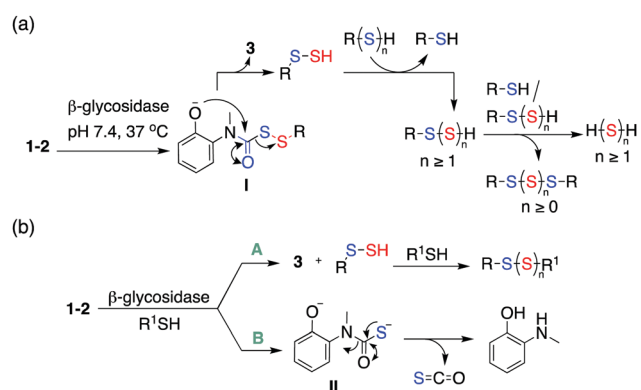
the persulfide probe SSP2 was used.²⁸ DLD-1 cells were pre-treated with SSP2 (50 μM) in the presence of CTAB (500 μM) followed by treatment with **1a**. A significant increment in the fluorescence signal corresponding to generation of sulfane sulfur was observed upon treatment with **1a** (Fig. S6, ESI[†]). The elevated concentration needed for enhancement of cellular persulfides is likely due to the diminished stability of persulfides in the reducing environment of the cells. Nevertheless, our data suggests that **1a** is cell permeable and is able to enhance the levels of intracellular sulfane sulfur pool.

Persulfides/polysulfides have previously been reported to have potent antioxidant effects and are efficient scavengers of ROS. Previously, H₂S-NSAID hybrids have been reported to have potent anti-inflammatory effects on models of colitis, attributable to H₂S.²⁹ In addition, COS/H₂S donors have shown to display cytoprotective effects against xenobiotic induced stress in colon cells.³⁰ To test the protective effects of persulfides/polysulfides in the colon against oxidative stress induced lethality, MGR-1, a cell permeable ROS generator was used to induce oxidative stress (Fig. S7, ESI[†]).³¹ DLD-1 cells that were pre-treated with **1a** for 12 h were next exposed to MGR-1 for 4 h, following which cell viability was determined using a standard MTT assay. The assay indicates that **1a** was able to rescue cells from ROS induced lethality in a dose dependant manner. Under similar conditions, NAC failed to exhibit protective effects (Fig. S8a, ESI[†]). Next, to further corroborate our results, we used another cell line with an elevated expression of β -glucosidase, HepG2 cell line. When tested on HepG2 cells, similar results were obtained supporting the cytoprotective effects of the cell permeable persulfide donor **1a** (Fig. S8b, ESI[†]).

The next series of compounds (**2**) were designed to be cleaved by β -galactosidase. Our attempts to synthesize the galactopyranosyl derivative with NACMe persulfide **2a** (Fig. 1b; R = *N*-acetylcysteine methyl ester) were unsuccessful. The benzyl persulfide derivative **2b** was however synthesized (Fig. 1b, R = Bn; Scheme S1, ESI[†]). The rate of cleavage of **2b** by β -galactosidase significantly faster than that of the β -glucosidase by β -glucosidase (Fig. S9a; rate constant, $6.8 \times 10^{-2} \text{ min}^{-1}$ and $t_{1/2} = 10 \text{ min}$, Fig. S9b, ESI[†]). The observed differences in the rates of cleavage by these enzymes is similar to previous

reports.^{32,33} The byproduct **3** was observed under these conditions and its rate of formation was calculated to be $8.6 \times 10^{-2} \text{ min}^{-1}$ (Fig. S10, ESI[†]). Upon co-incubation with β -galactosidase and HPE-IAM, as expected benzyl persulfide/polysulfide Bn(S)_{*n*}SH ($n = 1-3$) along with the H₂S_{*n*} ($n = 1-3$) adducts were detected (Fig. S11, ESI[†]). The compound **2b** was however found to be moderately cytotoxic when compared with **1a** (Fig. S12, ESI[†]). To verify if the benzyl persulfide contributed to cytotoxicity, the analogue **1b** was next synthesized by reacting **7** with the *S*-perthiocarbonyl chloride generated from benzyl mercaptan (**8b**) (Scheme 1). The decomposition profile of **1b** and persulfide/polysulfide generation profile of **1b** was comparable with that of **1a** (Fig. S13–S16, ESI[†]). The analogue **1b** was also found to be moderately cytotoxic in cells suggesting the importance of the functional group that is bound to the persulfide (Fig. S17, ESI[†]).

The following mechanism for the formation of persulfides/polysulfides from the glycopersulfide donors is proposed (Scheme 3a). The persulfide generators undergo decomposition in the presence of β -glycosidases to generate the intermediate phenolate **I**. Intramolecular cyclization of **I** produces a persulfide species along with the benzoxazolone byproduct **3**. The persulfide species once formed can further react with itself or reduced thiols to generate hydropolysulfide (RSS_{*n*}H) species. Hydropolysulfides (RSS_{*n*}H) upon reduction by thiols/persulfides would result in the generation of hydrogen polysulfide (H₂S_{*n*}, $n \geq 1$). A similar perthiocarbamate scaffold has been reported by Khodade *et al.* as precursors to persulfides that reacts with thiols to generate carbonyl sulfide (COS) as well.¹⁰ COS undergoes hydrolysis to produce H₂S and this reaction is accelerated by carbonic anhydrase, an enzyme that is widely prevalent in cells.³⁴ Hence, in the presence of β -glycosidase and thiols, two possible parallel pathways **A** and **B** are possible (Scheme 3b). Pathway **A** indicates cleavage by β -glycosidase that forms the carbamate byproduct **3** with concomitant formation of persulfides/polysulfides. Pathway **B** indicates the cleavage of



Scheme 3 (a) Proposed mechanism for the generation of persulfides and polysulfides from compounds **1-2** in the presence of β -glycosidases. (b) Major pathways for decomposition of **1** or **2** in the presence of a thiol and β -glycosidase. Pathway **A** involves decomposition by the enzyme while pathway **B** indicates disulfide bond cleavage by thiols to generate COS/H₂S.

the disulfide bond by thiols resulting in the generation of COS, which generates H₂S.³⁴ The donor **2b** was examined for its reactivity towards biologically relevant thiols like *N*-acetyl cysteine (NAC) and glutathione (GSH) in the absence of an electrophile. When **2b** was co-incubated with β-galactosidase and NAC (5 equiv.) at 37 °C, if pathway **B** is significant, a reduction in the yield of **3** is expected. Indeed, when this reaction was conducted, a 25% reduction in the yield of the byproduct **3** was observed within 30 min (Fig. S18, ESI†). Mixed disulfides/polysulfides of NAC and benzyl (NAC-SS-Bn and NAC-(S)₃-Bn) were also observed, which is indicative of pathway **A** (Scheme 3b and Fig. S19, ESI†). Whereas with GSH (10 equiv.), a 65% reduction in the formation of **3** was observed (Fig. S20, ESI†). The persulfide produced upon cleavage can also react with the prodrug *via* pathway **B**, forming COS. The derivative **1a** has a slower rate of cleavage by β-glucosidase derived from almonds with a half-life of 128 mins. Given the propensity of the compounds to react with thiols, it was envisaged that an important pathway for intracellular decomposition of **1a** would be pathway **B**. Previous reports show that human cytosolic β-glucosidases (hCBG) are more efficient at cleavage of β-glucosidic bonds compared to the enzyme derived from plants supporting the relevance of pathway **A** in mammalian cells.³⁵ Hence, our overall analysis suggests that the use of prodrugs developed herein results in the enhancement of cellular sulfur species, which have a protective effect against elevated ROS.

Financial support was from the Science and Engineering Research Board (CRG/2019/002900), Department of Science and Technology (PB, DST, INSPIRE Scheme), Department of Biotechnology (HC, BH/HRD/NBM-NWB/39/2020-21) and IISER Pune. DST Fund for Improvement of S&T Infrastructure (SR/FST/LSII-043/2016) to the IISER Pune Biology Department for setting up the Biological Mass Spectrometry Facility. The manuscript was written with inputs from all authors. PB and MBS carried out all experiments.

Conflicts of interest

There are no conflicts to declare.

Notes and references

- 1 T. V. Mishanina, M. Libiad and R. Banerjee, *Nat. Chem. Biol.*, 2015, **11**, 457.
- 2 M. R. Filipovic, J. Zivanovic, B. Alvarez and R. Banerjee, *Chem. Rev.*, 2018, **118**, 1253–1337.
- 3 C. Yang, N. O. Devarie-Baez, A. Hamsath, X. Fu and M. Xian, *Antioxid. Redox Signaling*, 2020, **33**, 1092–1114.
- 4 T. Zhang, H. Tsutsuki, K. Ono, T. Akaike and T. Sawa, *J. Clin. Biochem. Nutr.*, 2021, **68**, 5–8.
- 5 E. Cuevasanta, M. Lange, J. Bonanata, E. L. Coitiño, G. Ferrer-Sueta, M. R. Filipovic and B. Alvarez, *J. Biol. Chem.*, 2015, **290**, 26866–26880.
- 6 T. Ida, T. Sawa, H. Ihara, Y. Tsuchiya, Y. Watanabe, Y. Kumagai, M. Suematsu, H. Motohashi, S. Fujii, T. Matsunaga, M. Yamamoto, K. Ono, N. O. Devarie-Baez, M. Xian, J. M. Fukuto and T. Akaike, *Proc. Natl. Acad. Sci. U. S. A.*, 2014, **111**, 7606–7611.
- 7 J. Zivanovic, E. Kouroussis, J. B. Kohl, B. Adhikari, B. Bursac, S. Schott-Roux, D. Petrovic, J. L. Miljkovic, D. Thomas-Lopez, Y. Jung, M. Miler, S. Mitchell, V. Milosevic, J. E. Gomes, M. Benhar, B. Gonzalez-Zorn, I. Ivanovic-Burmazovic, R. Torregrossa, J. R. Mitchell, M. Whiteman, G. Schwarz, S. H. Snyder, B. D. Paul, K. S. Carroll and M. R. Filipovic, *Cell Metab.*, 2019, **30**, 1152–1170.
- 8 J. Kang, S. Xu, M. N. Radford, W. Zhang, S. S. Kelly, J. J. Day and M. Xian, *Angew. Chem., Int. Ed.*, 2018, **57**, 5893–5897.
- 9 Y. Zheng, B. Yu, Z. Li, Z. Yuan, C. L. Organ, R. K. Trivedi, S. Wang, D. J. Lefer and B. Wang, *Angew. Chem., Int. Ed.*, 2017, **56**, 11749–11753.
- 10 V. S. Khodade, B. M. Pharoah, N. Paolucci and J. P. Toscano, *J. Am. Chem. Soc.*, 2020, **142**, 4309–4316.
- 11 A. Chaudhuri, Y. Venkatesh, J. Das, M. Gangopadhyay, T. K. Maiti and N. D. P. Singh, *J. Org. Chem.*, 2019, **84**, 11441–11449.
- 12 P. Bora, P. Chauhan, S. Manna and H. Chakrapani, *Org. Lett.*, 2018, **20**, 7916–7920.
- 13 C. R. Powell, K. M. Dillon, Y. Wang, R. J. Carrazzone and J. B. Matson, *Angew. Chem., Int. Ed.*, 2018, **57**, 6324.
- 14 Y. Wang, K. M. Dillon, Z. Li, E. W. Winckler and J. B. Matson, *Angew. Chem., Int. Ed.*, 2020, **59**, 16698–16704.
- 15 P. Bora, S. Manna, M. A. Nair, R. R. M. Sathe, S. Singh, V. S. Sreyas Adury, K. Gupta, A. Mukherjee, D. K. Saini, S. S. Kamat, A. B. Hazra and H. Chakrapani, *Chem. Sci.*, 2021, **12**, 12939–12949.
- 16 D. R. Friend and G. W. Chang, *J. Med. Chem.*, 1984, **27**, 261–266.
- 17 H. Englyst, *FEMS Microbiol. Lett.*, 1987, **45**, 163–171.
- 18 H. Zhu and Y. R. Li, *Exp. Biol. Med.*, 2012, **237**, 474–480.
- 19 V. R. Sinha and R. Kumria, *Pharm. Res.*, 2001, **18**, 557–564.
- 20 The LD₅₀ of **3** has been found as 890 mg kg⁻¹ with no reported toxicity in mice, in *Registry of Toxic Effects of Chemical Substances*, ed. D. V. Sweet, US Department of Health and Human Services CDC, 1987.
- 21 X. Chen, X. Ma, Y. Zhang, G. Gao, J. Liu, X. Zhang, M. Wang and S. Hou, *Anal. Chim. Acta*, 2018, **1033**, 193–198.
- 22 I. Okamoto, M. Terashima, H. Masu, M. Nabeta, K. Ono, N. Morita, K. Katagiri, I. Azumaya and O. Tamura, *Tetrahedron*, 2011, **67**, 8536–8543.
- 23 H. A. Hamid, A. Tanaka, T. Ida, A. Nishimura, T. Matsunaga, S. Fujii, M. Morita, T. Sawa, J. M. Fukuto, P. Nagy, R. Tsutsumi, H. Motohashi, H. Ihara and T. Akaike, *Redox Biol.*, 2019, **21**, 101096.
- 24 T. Numakura, H. Sugiura, T. Akaike, T. Ida, S. Fujii, A. Koarai, M. Yamada, K. Onodera, Y. Hashimoto, R. Tanaka, K. Sato, Y. Shishikura, T. Hirano, S. Yanagisawa, N. Fujino, T. Okazaki, T. Tamada, Y. Hoshikawa, Y. Okada and M. Ichinose, *Thorax*, 2017, **72**, 1074–1083.
- 25 T. Akaike, T. Ida, F.-Y. Wei, M. Nishida, Y. Kumagai, M. M. Alam, H. Ihara, T. Sawa, T. Matsunaga, S. Kasamatsu, A. Nishimura, M. Morita, K. Tomizawa, A. Nishimura, S. Watanabe, K. Inaba, H. Shima, N. Tanuma, M. Jung, S. Fujii, Y. Watanabe, M. Ohmuraya, P. Nagy, M. Feelsch, J. M. Fukuto and H. Motohashi, *Nat. Commun.*, 2017, **8**, 1177.
- 26 B. Hultberg and P. A. Öckerman, *Clin. Chim. Acta*, 1970, **28**, 169–174.
- 27 H. M. M. Arafa, *Eur. J. Pharmacol.*, 2009, **616**, 58–63.
- 28 W. Chen, C. Liu, B. Peng, Y. Zhao, A. Pacheco and M. Xian, *Chem. Sci.*, 2013, **4**, 2892.
- 29 S. Fiorucci, S. Orlandi, A. Mencarelli, G. Caliendo, V. Santagada, E. Distrutti, L. Santucci, G. Cirino and J. L. Wallace, *Br. J. Pharmacol.*, 2009, **150**, 996–1002.
- 30 P. Chauhan, K. Gupta, G. Ravikumar, D. K. Saini and H. Chakrapani, *Chem. – Asian J.*, 2019, **14**, 4717–4724.
- 31 D. S. Kelkar, G. Ravikumar, N. Mehendale, S. Singh, A. Joshi, A. K. Sharma, A. Mhetre, A. Rajendran, H. Chakrapani and S. S. Kamat, *Nat. Chem. Biol.*, 2019, **15**, 169–178.
- 32 T. B. Cai, D. Lu, X. Tang, Y. Zhang, M. Landerholm and P. G. Wang, *J. Org. Chem.*, 2005, **70**, 3518–3524.
- 33 E. Calatrava-Pérez, S. A. Bright, S. Achermann, C. Moylan, M. O. Senge, E. B. Veale, D. C. Williams, T. Gunnlaugsson and E. M. Scanlan, *Chem. Commun.*, 2016, **52**, 13086–13089.
- 34 C. P. Chengelis and R. A. Neal, *Toxicol. Appl. Pharmacol.*, 1980, **55**, 198–202.
- 35 S. Tribolo, J.-G. Berrin, P. A. Kroon, M. Czjzek and N. Juge, *J. Mol. Biol.*, 2007, **370**, 964–975.

Cite this: *Chem. Sci.*, 2021, 12, 12939

All publication charges for this article have been paid for by the Royal Society of Chemistry

Leveraging an enzyme/artificial substrate system to enhance cellular persulfides and mitigate neuroinflammation†

Prerona Bora,^{‡a} Suman Manna,^{‡a} Mrutyunjay A. Nair,^{‡§a} Rupali R. M. Sathe,^{‡b} Shubham Singh,^b Venkata Sai Sreyas Adury,^a Kavya Gupta,^c Arnab Mukherjee,^a Deepak K. Saini,^c Siddhesh S. Kamat,^b Amrita B. Hazra^{‡*ab} and Harinath Chakrapani^{‡*a}

Persulfides and polysulfides, collectively known as the sulfane sulfur pool along with hydrogen sulfide (H₂S), play a central role in cellular physiology and disease. Exogenously enhancing these species in cells is an emerging therapeutic paradigm for mitigating oxidative stress and inflammation that are associated with several diseases. In this study, we present a unique approach of using the cell's own enzyme machinery coupled with an array of artificial substrates to enhance the cellular sulfane sulfur pool. We report the synthesis and validation of artificial/unnatural substrates specific for 3-mercaptopyruvate sulfurtransferase (3-MST), an important enzyme that contributes to sulfur trafficking in cells. We demonstrate that these artificial substrates generate persulfides *in vitro* as well as mediate sulfur transfer to low molecular weight thiols and to cysteine-containing proteins. A nearly 100-fold difference in the rates of H₂S production for the various substrates is observed supporting the tunability of persulfide generation by the 3-MST enzyme/artificial substrate system. Next, we show that the substrate **1a** permeates cells and is selectively turned over by 3-MST to generate 3-MST-persulfide, which protects against reactive oxygen species-induced lethality. Lastly, in a mouse model, **1a** is found to significantly mitigate neuroinflammation in the brain tissue. Together, the approach that we have developed allows for the on-demand generation of persulfides *in vitro* and *in vivo* using a range of shelf-stable, artificial substrates of 3-MST, while opening up possibilities of harnessing these molecules for therapeutic applications.

Received 13th July 2021
Accepted 24th August 2021

DOI: 10.1039/d1sc03828a

rsc.li/chemical-science

Introduction

Hydrogen sulfide (H₂S) and its redox congeners, persulfides (HSSH) and polysulfides (H₂S)_n act as mediators of several intracellular signaling processes.^{1,2} Persulfides and polysulfides, collectively known as the sulfane sulfur pool, along with H₂S are summoned in response to oxidative stress in cells, and dysfunctional sulfur metabolism is implicated in neurodegeneration,^{3,4} cardiovascular disease^{5,6} and antibiotic resistance.^{7,8} To regulate the sulfane sulfur pool, one of the strategies

used by cells is to employ protein persulfidation, a post-translational modification where the thiol group of a reactive cysteine (Cys-SH) is modified to a persulfide (Cys-SSH).⁹ The persulfidated protein mediates S-transfer to appropriate biomolecular targets, and not only provides protection against irreversible oxidation of cysteine residues but also regulates cellular signaling and sulfur homeostasis.^{10,11} Persulfidation has been linked to modulation of the catalytic activity of key proteins such as parkin and GSK-3β that are involved in neurodegenerative diseases, underscoring the therapeutic relevance of exogenously controlling this post-translational modification by administering persulfide/H₂S.^{4,9} Here, we report a novel approach of developing artificial/unnatural substrates for persulfide-generating enzymes *in vivo* as a tool to study and tune sulfur metabolism in cells with applications in mitigating neuroinflammation.

In this study, we leverage natural biochemical mechanisms for generating persulfides by the development of a new class of substrates for 3-mercaptopyruvate sulfurtransferase (3-MST), a central persulfide/polysulfide generating enzyme that has been implicated in the mitigation of oxidative stress.^{12–14} 3-MST

^aDepartment of Chemistry, Indian Institute of Science Education and Research Pune, Dr. Homi Bhabha Road, Pashan, Pune 411 008, Maharashtra, India. E-mail: amrita@iiserpune.ac.in; harinath@iiserpune.ac.in

^bDepartment of Biology, Indian Institute of Science Education and Research Pune, Dr. Homi Bhabha Road, Pashan, Pune 411 008, Maharashtra, India

^cDepartment of Molecular Reproduction, Development and Genetics, Indian Institute of Science, Bangalore 560012, Karnataka, India

† Electronic supplementary information (ESI) available. See DOI: 10.1039/d1sc03828a

‡ These authors contributed equally.

§ Presently at Department of Chemistry, The Pennsylvania State University, USA.



operates by generating its own persulfide by the activation of a hyper-reactive active site cysteine with the sulfur atom of 3-mercaptopyruvate (3-MP) and produces pyruvate as the byproduct (Fig. 1A).¹⁵ The persulfidated 3-MST (3-MST-SS⁻) can transfer the sulfur to low molecular weight thiols such as glutathione (GSH) to produce a persulfide (GSSH), which in turn persulfidates proteins (Fig. 1B).¹⁶ Alternately, 3-MST-SS⁻ can produce a polysulfide species (3-MST-S_nS⁻) which subsequently persulfidates low molecular weight thiols and other proteins in the cell.² 3-MST-SS⁻ has been found to be involved in

mitochondrial respiration and fatty acid metabolism,^{17,18} synthesis of thiouridine in tRNA,¹⁹ iron-sulfur cluster formation,²⁰ and in cyanide detoxification.²¹ Also, 3-MST is among the major H₂S-generating enzymes in the brain and is thus implicated in regulation of the sulfane sulfur pool and sulfur trafficking in neuronal cells.¹⁴ Therefore, a methodology that generates 3-MST-SS⁻ in a specific, controlled and catalytic manner would be advantageous for understanding the mechanisms of sulfur metabolism, and its role in signaling and disease.

The natural substrate 3-MP can, in principle, be used for this purpose. However, previous reports suggest that 3-MP produces H₂S even in the absence of 3-MST in the cell, thus, using it may have limitations.²² Hence, our strategy of developing a suite of artificial substrates specific for 3-MST as a methodology for the controlled generation of its persulfide is unique with diverse implications. Since cellular signaling is highly dependent on the concentration and rate of generation of the signaling species, it is important that the new methodology developed contains in-built characteristics for tuning these parameters. We expect that the systematic functionalization of the artificial substrates will alter their binding to the enzyme, as well as the rate of persulfide generation (Fig. 1C). Together, these factors will consequently allow for tuning the sulfur transfer reaction. Finally, since thiols are prone to oxidation, it was envisaged that the unnatural substrate could be generated *in situ* from the corresponding thioesters through ester hydrolysis that is catalyzed by a widely prevalent esterase enzyme (Fig. 1C).

Results and discussions

Docking studies, synthesis, enzymology, detection of persulfide and H₂S

Molecular docking studies of the crystal structure of the human homolog of 3-MST (*h3-MST*, PDB ID: 4JGT) with the natural substrate 3-MP were conducted (Fig. 2A). The most energetically favorable conformation (-4.2 kcal mol⁻¹) revealed interactions with arginine residues R188 and R197 that are consistent with previous accounts of these residues aiding in anchoring the substrate carboxylate and carbonyl groups.^{23,24} The cysteine C248 residue was proximal to the reactive sulfhydryl group of 3-MP at a distance of 4.4 Å.

When a similar study was conducted with the proposed aryl substrate, this compound **2a** (R¹ = Ph, R² = H in Fig. 1C) was well accommodated in the active site and key interactions of **2a** with R188 and R197 were preserved (Fig. 2B). The distance between the C248 and the sulfur of **2a** was 5.2 Å, which was comparable with the lowest energy conformation of 3-MP in the active site of 3-MST. The binding energy of **2a** was nearly identical with 3-MP, -4.2 kcal mol⁻¹.

We cloned and purified *h3-MST* and a bacterial 3-MST (*b3-MST*) from *Escherichia coli* (Table S3, Fig. S1†) for subsequent *in vitro* assays.^{23,25} Compound **1a** (Fig. 1C) was synthesized by the treatment of 2-bromoacetophenone with potassium thioacetate using a reported protocol.²⁶ This compound should produce the thiol **2a** upon reaction with an esterase enzyme (ES). Compound **1a** was incubated in the presence of ES and *h3-MST* enzymes.

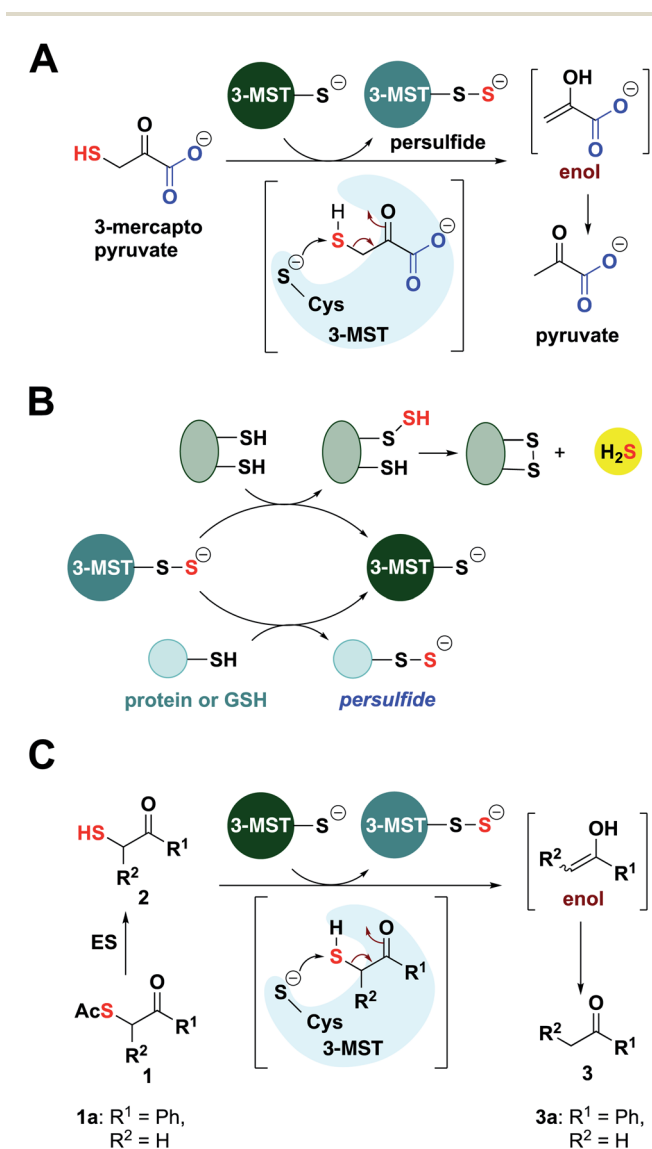


Fig. 1 (A) Catalytic cycle of 3-MST: the sulfur of 3-MP is transferred to 3-MST to produce 3-MST-SS⁻ and pyruvate. (B) 3-MST-SS⁻ reacts with reducing agents containing two cysteine residues such as thioredoxin (Trx) to generate H₂S. 3-MST-SS⁻ can also generate a protein persulfide through protein-protein interaction or transfer sulfur to low molecular weight thiols such as GSH to produce glutathione persulfide (GSSH). (C) Thioacetate **1** is expected to be cleaved by esterase (ES) to produce the designed 3-MST substrate **2**. This thiol is positioned to undergo a sulfur transfer reaction to produce 3-MST-SS⁻ and a ketone **3** as the byproduct.



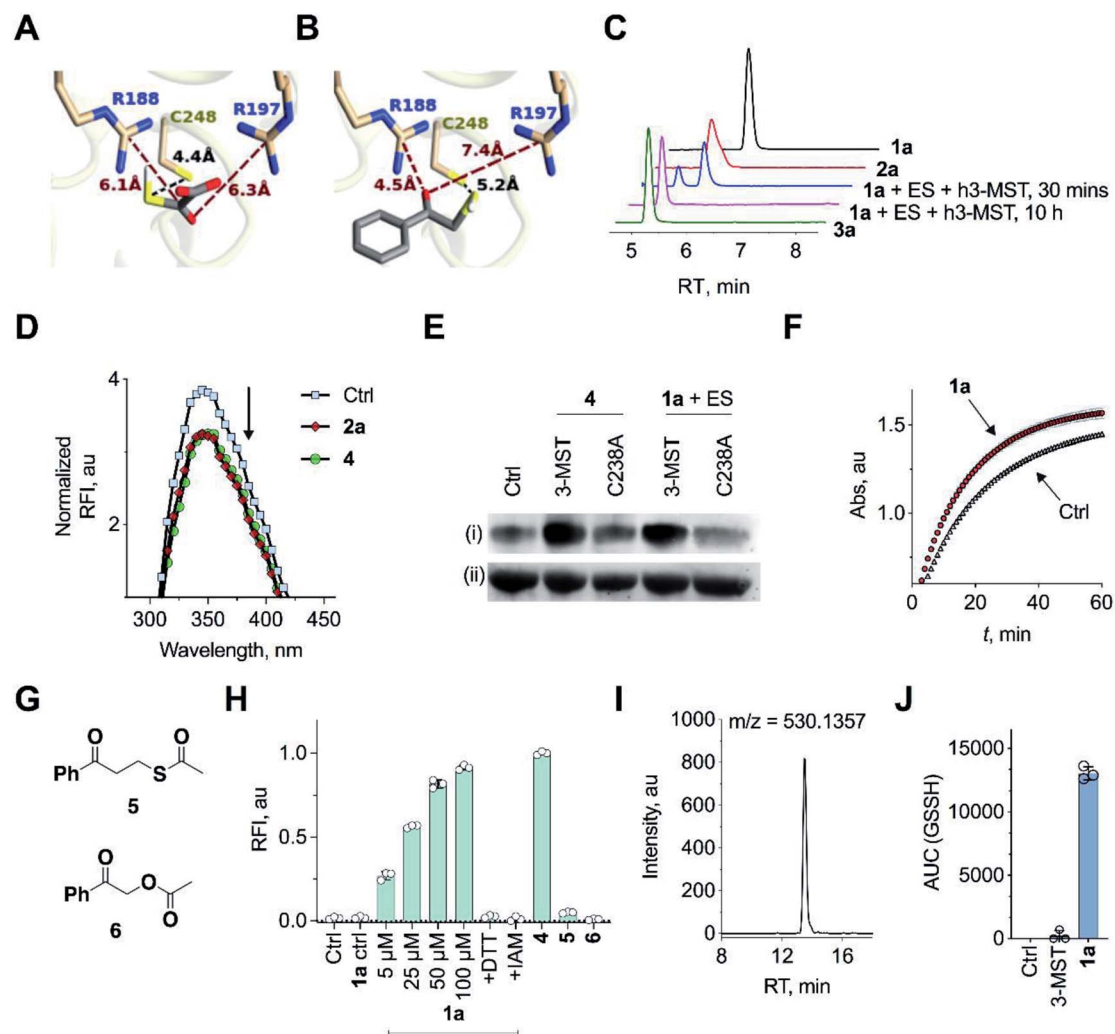


Fig. 2 (A) Docking analysis of the active site of *h3*-MST with 3-MP shows a favorable conformation with the S–S bond distance as 4.4 Å. The R188 residue is 6.1 Å from the carboxyl group whereas the R197 residue is at a distance of 6.3 Å from the carbonyl group. (B) Docking analysis of the designed substrate 2a ($R^1 = \text{Ph}$, $R^2 = \text{H}$ in Fig. 1C) reveals a similar anchoring of the substrate by the two arginine residues and the S–S bond distance was found as 5.2 Å. (C) HPLC analysis of 1a + ES in the presence of *h3*-MST shows the formation of the thiol 2a which is then subsequently converted to acetophenone 3a during 10 h. (D) Intrinsic fluorescence assay on 3-MST with dimer of ethyl 3-mercaptopyruvate (E3-MP) 4 shows a decrease in fluorescence intensity which is consistent with the generation of 3-MST-SS⁻. A similar result was observed with the unnatural substrate 2a. Ctrl refers to 3-MST alone. (E) Detection of 3-MST-SS⁻ using the modified tag-switch technique (Fig. S7a†), conducted with 4 and 1a + ES; the C238A 3-MST mutant treated under similar conditions showed a diminished band corresponding to the formation of 3-MST-SS⁻: (i) detection of 3-MST persulfide (ii) loading control. (F) Effect of persulfidation on the activity of GAPDH: GAPDH upon treatment with 1a + ES + 3-MST enhances its activity compared to GAPDH alone presumably due to the formation of the persulfide of GAPDH. Ctrl refers GAPDH + ES + 3-MST; 1a refers to co-incubation of 1a + ES + 3-MST followed by addition of GAPDH (absorbance 340 nm). (G) Structures of compounds 5 and 6. (H) Persulfide/polysulfide detection using SSP-2: Ctrl refers to 3-MST alone and 1a ctrl refers to 1a + ES only (100 μM); 1a refers to co-incubation of varying concentrations of 1a, ES and 3-MST; +DTT: addition of DTT; +IAM: addition of iodoacetamide, an electrophile that reacts with thiols; 4 refers to incubation of the compound with 3-MST; 5 and 6 refers to the incubation of the compounds with ES followed by treatment with 3-MST. (I) Extracted ion chromatogram from a mass spectrometry-based analysis of reaction products formed upon incubation of 1a and 3-MST in the presence of ES followed by addition of GSH as the thiol acceptor. Reaction of the reactive sulfur species (GSSH) with an electrophile monobromobimane (mBBr) was employed. LC/MS analysis revealed the formation of the GSS-bimane adduct (expected $m/z = 530.1379$; observed $m/z = 530.1357$) when 1a was incubated with ES and 3-MST. (J) Area under the curve (AUC) for the peak corresponding to GSS-bimane (Fig. 2I); Ctrl refers to 1a alone while 3-MST refers to 3-MST alone and 1a refers to 1a + ES + 3-MST.

Gradual disappearance of 1a and concomitant formation of the thiol 2a was observed (Fig. 2C and S2†). After 10 hours, complete disappearance of 2a along with the formation of acetophenone 3a was recorded. These observations suggest that after 1a produces 2a upon ester hydrolysis, it is utilized by 3-MST to

produce 3a. Under the same conditions, *b3*-MST also shows complete conversion to 3a in 2 h (Fig. S3†).

The next series of experiments were designed to probe the intermediates during this transformation. The first intermediate that is expected to be formed in this reaction is 3-MST-SS⁻.



The formation of 3-MST-SS⁻ was monitored by measurement of the intrinsic fluorescence of this enzyme using a reported protocol.²⁷ Upon incubation of 3-MST with **2a**, a significant quenching of intrinsic fluorescence of the enzyme as compared to the apo-protein was observed suggesting the formation of 3-MST-SS⁻ (Fig. 2D and S4†).

Compound **4**, which exists as a dimer and dissociates in buffer to produce the ethyl 3-mercaptopyruvate, E3-MP, was synthesized and used as a substrate for 3-MST (Scheme 1).²¹ Molecular docking analysis gave a binding energy for this ester as $-4.2 \text{ kcal mol}^{-1}$ (Table S4†), identical to that of 3-MP. When 3-MST was incubated with **4**, quenching of fluorescence was observed as before supporting the generation of the protein persulfide (Fig. 2D and S4†). A similar set of results was also recorded for *h3*-MST (Fig. S5†). The compounds themselves did not show significant fluorescence under these conditions (Fig. S6†).

A reported tag-switch assay (Fig. S7†) was used for detecting persulfidated proteins (Fig. 2E).²⁸ When 3-MST was reacted with **4** or with **1a** and ES, as expected, this assay confirmed the formation of 3-MST-SS⁻ (Fig. 2E). In contrast, under similar conditions, the mutant of 3-MST where the catalytic cysteine was replaced with alanine (3-MST C238A) showed no significant increase in the signal corresponding to the 3-MST-SS⁻ (Fig. 2E and S7†). This result is consistent with a previous report of a similar lack of activity of the *h3*-MST cysteine mutant.²⁹

Next, we assayed the ability of the 3-MST-SS⁻ to transfer the sulfide to another protein. GAPDH is a redox-sensitive protein involved in the glycolytic cycle whose active site cysteine residue is susceptible to redox fluctuations and its function is influenced by this modification.³⁰ Accordingly, 3-MST-SS⁻ was prepared by treating 3-MST with **1a** in presence of ES, following which GAPDH was added and incubated for 30 min. The activity of the enzyme was then estimated using a previously reported protocol.⁹ Under these conditions, the GAPDH activity was found to be significantly enhanced as compared to a GAPDH only control (Fig. 2F, S8a). Treatment with dithiothreitol (DTT), which is expected to cleave the persulfide and produce the native enzyme, resulted in an activity profile that was comparable with the control GAPDH (Fig. S8b†). Thus, 3-MST-SS⁻, through sulfur trafficking, regulates the activity of key enzymes such as GAPDH.

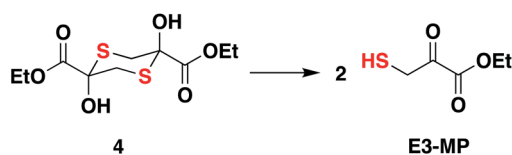
The formation of persulfide/polysulfide was then assessed using SSP-2, a fluorescence turn-on probe that is sensitive to these species.³¹ The probe was validated using GS_nSH (prepared using a reported protocol) (Fig. S9†).¹⁰ When exposed to **1a** + ES, a distinct increase in fluorescence was recorded (Fig. 2H and

S10a†). When the standard reaction mixture was treated with the reducing agent DTT, a decrease in signal, likely due to the cleavage of persulfide by DTT, was observed (Fig. 2H and S10b†). Pre-treatment with iodoacetamide (IAM), a thiol alkylating agent, is expected to inactivate the enzyme. When IAM-pre-treated 3-MST was reacted with **1a** + ES, nearly complete abrogation of signal attributable to persulfide/polysulfide generation was observed (Fig. 2H). This result is consistent with the previous observation in the tag-switch persulfide assay where we found no evidence for persulfide generation in the catalytically dead 3-MST C238A mutant. Notably, compound **4** generated persulfide at levels comparable with **1a** (Fig. S11†). Next, two control compounds – **5**, the thioacetate with an additional methylene group and **6**, the analogous ester where sulfur was replaced with oxygen – were prepared (Fig. 2G). Both these analogues should not produce persulfide under the standard assay conditions. Generation of persulfide was assessed by the tag-switch assay (Fig. S12†) as well as by the fluorescence turn-on assay and no evidence for generation of persulfide from **5** or **6** was found (Fig. 2H).

The formation of persulfide/polysulfide was next studied by leveraging the ability of 3-MST-SS⁻ to transfer its sulfane sulfur to an acceptor thiol. GSH, a thiol found abundantly in biological systems, was reacted with the 3-MST-SS⁻ formed from the reaction of **1a** + ES with 3-MST. The formation of various reactive sulfur species was analysed using LC/MS, where monobromobimane was used as an alkylating agent (Scheme S4†).¹⁰ LC/MS analysis showed the formation of the GSS-bimane adduct only in the presence of **1a** + ES and 3-MST (Fig. 2I, J and S13†). In addition, we found evidence for the formation of GSSSG and H₂S as its bis-S-bimane adduct (Fig. S14 and S15†). Together, these data support the ability of our unnatural substrate-enzyme system to transfer S to low molecular weight thiols.

A standard methylene blue colorimetric assay for the detection of H₂S was conducted in the presence of DTT (Fig. 1B).^{23,32} This assay revealed the formation of H₂S during incubation of **1a** with 3-MST in the presence of DTT (Fig. 3A). H₂S release from compound **4** when treated with 3-MST was also observed (Fig. S16†). Based on our observation that the thioacetate **1a** could be cleaved by DTT even in the absence of the esterase to produce **2a**, the remaining experiments were conducted with **1a** + 3-MST + DTT (Fig. S17†). The rate constant k_h for H₂S generation from **1a** when treated with *h3*-MST in the presence of DTT was 1.48 h^{-1} (Table 1). A similar rate constant k_b was observed with *h3*-MST (Table 1).

Having established that the substrates we designed could be used to generate persulfides as well as H₂S *in vitro*, their ability to permeate cells to function as substrates for cellular 3-MST was studied. A human lung carcinoma A549 cell line with 3-MST knocked down (3-MST KD) was first generated (Fig. S18†). This cell line was used in conjunction with the corresponding scrambled cell line where 3-MST levels are not perturbed (Fig. S18†). When treated with an esterase-activated H₂S donor³² (Fig. S19†), significant enhancement in H₂S levels in both these cell lines was observed as measured by the H₂S-sensitive dye NBD-fluorescein (Fig. 3B).³³ However, in the presence of **1a**,



Scheme 1 Compound **4** is the dimer of E3-MP and in pH 7.4 buffer, dissociates to produce the E3-MP.



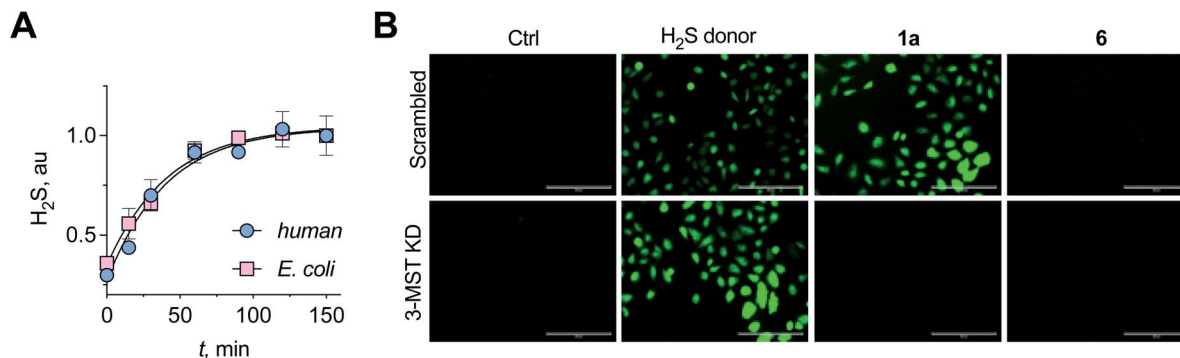


Fig. 3 (A) A methylene blue assay was used to measure the rate of H₂S generation with **1a** in the presence of *h3*-MST or *b3*-MST and DTT as the reducing agent. Nearly identical rates of H₂S generation were observed. (B) 3-MST KD refers to knock-down of expression of 3-MST in A549 cells while scrambled refers to A549 cells containing non-targeting scrambled shRNA. The H₂S donor used is an esterase-sensitive COS/H₂S donor that has been previously characterized. H₂S levels were assessed using a previously reported dye NBD-fluorescein (see ESI, Fig. S20†). Ctrl refers to untreated cells. Scale bar represents 200 μm.

Table 1 Kinetics of H₂S generation^a

Compd	X	Y	<i>h3</i> -MST		<i>b3</i> -MST	
			<i>k_h</i> (h ⁻¹)	Rel. rate ^b	<i>k_b</i> (h ⁻¹)	<i>k_b/k_h</i>
1a	H	H	1.48	30	1.45	1.0
1b	NO ₂	H	11.13	223	9.27	0.8
1c	CN	H	2.5	50	4.9	2.0
1d	CF ₃	H	7.51	150	5.83	0.8
1e	OCF ₃	H	4.48	90	2.29	0.5
1f	F	H	1.11	22	1.54	1.4
1g	Me	H	1.02	20	0.97	1.0
1h	OMe	H	0.39	8	0.37	0.9
1i	H	F	1.68	34	3.85	2.5
1j	H	OMe	0.08	2	0.99	12.5
1k	H	Me	0.05	1	1.22	25.0
1l	R ¹ = Ph; R ² = Me		Slow	—	0.19	—
1m	R ¹ = 1-naphthyl; R ² = H		0.23	5	2.87	12.5
1n	R ¹ = 2-naphthyl; R ² = H		0.50	10	1.98	4.0

^a Reaction conditions: compound + 3-MST + DTT. H₂S was monitored using a methylene blue assay. ^b Calculated based on normalizing the rate constant with respect to **1k**.

when the 3-MST KD cells were imaged, a significantly diminished signal for intracellular H₂S levels was observed (Fig. 3B). In the scrambled cell line, however, where endogenous 3-MST levels are not perturbed, an enhanced signal corresponding to intracellular H₂S was seen (Fig. 3B). Compound **6**, which lacks a sulfur, failed to enhance H₂S in both cell lines (Fig. 3B, S20 and S21†). Together, these data suggest that **1a** is a cell-permeable persulfidating agent that is activated by 3-MST

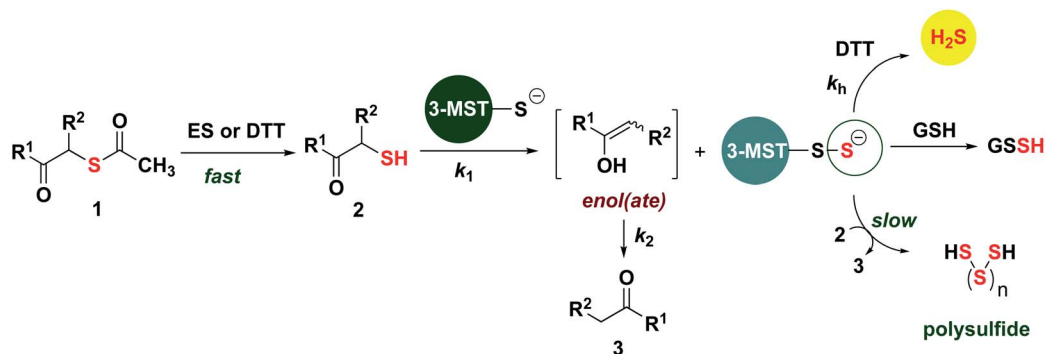
within cells to produce H₂S, putatively *via* an intracellular persulfidation mechanism, as confirmed by a separate tag-switch fluorescence reporter technique³⁴ (Fig. S22†).

Based on the above observations, we put forth the following mechanism for persulfide generation from this unnatural substrate – 3-MST system (Scheme 2). Cleavage of **1a** by esterase produces the thiol **2a**, which then reacts with 3-MST to produce the 3-MST-SS⁻ and an enol(ate), which is expected to tautomerize to the ketone **3a**. In the absence of a reducing agent, 3-MST-SS⁻ appears to catalyze the turnover of **2a** to produce **3a** and produces polysulfide during this transformation (Schemes 2 and S5; Fig. S15†). Under reducing conditions (DTT), 3-MST-SS⁻ is cleaved to produce H₂S (Scheme 2, Fig. 3A). HPLC analysis of the reaction mixture containing **2a**, 3-MST and DTT showed gradual disappearance of **2a** and the rate constant *k₁* was found to be 0.99 h⁻¹. The formation of **3a** was observed and a rate constant *k₂* of 0.75 h⁻¹ was obtained (Fig. 4A and S23†). The rate of disappearance of **2a** and formation of **3a** was nearly identical and both parameters are comparable with the rate of H₂S generation under these conditions (Table 1, see *h3*-MST data). In the absence of 3-MST, compound **2a** is prone to oxidation to its disulfide PhCOCH₂S-SCH₂COPh under ambient aerobic conditions (Fig. S24†). The conversion of **1a** to **2a** (and its disulfide) occurs in a nearly quantitative yield. Hence, our overall analysis demonstrates that compound **1a** is an excellent substrate for 3-MST and produces a persulfide intermediate, which is cleaved under reducing conditions to produce H₂S. In the absence of esterase, **1a** is gradually consumed in the presence of 3-MST and the formation of **3a** is observed after several hours (Fig. S25 and S26†). Also, persulfide/polysulfide were detected using the probe SSP-2 under similar conditions (Fig. S27†). We find no evidence for the formation of the thiol **2a**. This may be explained by the formation of 3-MST thioacetate as a possible intermediate during the transformation of **1a** to **3a** (Scheme S5†).

Substrate scope

In order to assess the unnatural substrate scope and the possibility of tuning sulfur transfer using this newly developed





Scheme 2 Proposed mechanism: thioacetate **1** is cleaved by esterase or DTT (HPLC in Fig. S23, ESI[†]) to produce the thiol **2**, which is then turned over by 3-MST to produce 3-MST-S-S⁻ and an enol(ate). The enol(ate) in aqueous buffer is rapidly converted to the ketone **3**. 3-MST-S-S⁻ in the presence of a reducing agent produces H₂S. 3-MST-S-S⁻ can react with low molecular weight thiols such as GSH to produce GSSH. Under non-reducing conditions, 3-MST-S-S⁻ can further turn over **2**, generating the ketone **3**; the likely byproduct of this reaction is polysulfide.

protocol, we synthesized a series of analogues. Arginine residues in the active site interact with the carbonyl group of 3-MP and are implicated in stabilizing the pyruvate enolate.^{23,24,27} In order to test if the stability of the incipient enolate played a role in the rates of H₂S production, compounds **1b–1h** with electron-withdrawing or electron-donating groups were synthesized. Molecular docking analysis with the corresponding thiols **2b–2h** showed nearly identical conformations (Table S5[†]). The rate constants of H₂S release ranged from 0.39 to 7.51 h⁻¹ (Table 1, Fig. S28[†]). Hammett analysis of rate constants gave a positive ρ value of +1.11, that is consistent with a partial negative charge developing in the transition state in the rate limiting step of the reaction (Fig. 4B).

Due to the proximity of a substituent at the *ortho* position of the aryl ring, enolate formation is likely to be affected by stereoelectronic effects. In order to investigate these effects, compounds **1i–1k** were prepared and their H₂S release was recorded (Table 1, Fig. S29[†]). While the rate of H₂S release from **1i** was comparable with **1a**, compounds **1j** and **1k** were substantially slower in generating H₂S when compared with **1a**. Molecular docking studies with the 2-fluorophenyl derivative **2i** showed a conformation and S–S distance comparable with that of **2a** bound to the active site (Table S6[†]). However, the lowest energy conformation of the thiol **2k** was significantly removed from the active site with the S–S bond distance of 10.7 Å (Fig. 4C). Unlike **2a**, the interaction of **2k** with the active site cysteine is restricted by steric clashes of A185 and R188 with its *ortho*-Me group, as illustrated in a higher energy conformation (Fig. 4D). A similar result was recorded for the 2-methoxy derivative **2j** (Tables S6 and S7[†]). These studies provide a molecular basis for the diminished H₂S release rates from these analogues.

In addition to electronics, enolate stability and reactivity can also be affected by sterics. In order to study the effects of an added substituent, compound **1l** which has an α -methyl substituent was synthesized. Docking analysis of **2l** with 3-MST revealed a docking score as well as a conformation that was comparable with **2a** (Table S6[†]). H₂S release from **1l** was, however, found to be extremely slow (Table 1, Fig. S30[†]). The

formation of the enolate appears to be more sensitive to steric effects than electronic effects. Recently, inhibitors for 3-MST were developed and one of these inhibitors had a naphthyl ring.³⁵ Taking this cue, compounds **1m** and **1n** were synthesized (Table S2[†]). Our assays confirmed that these compounds were substrates for 3-MST, and H₂S generation rates were moderately higher when compared with **1a** (Table 1, Fig. S30[†]) suggesting that a combination of binding and turnover is essential for tuning 3-MST-mediated sulfur transfer reactions.

Normalizing the rate constants with respect to **1k** revealed more than a 100-fold difference in relative rates for H₂S release (Table 1). This observation suggests that this series of substrates can be used to tune rates of persulfide/polysulfide generation. Next, bacterial 3-MST was used to study the rates of H₂S generation from the analogues and first-order rate constants were calculated (Table 1). Linear free energy relationship study of H₂S generation rates of **1a–1h** with *b*3-MST gave a slope of +1.13 (Fig. S31[†]), comparable with the data from *h*3-MST. Control compounds **5** and **6** do not produce H₂S under these conditions, as expected (Fig. S32[†]). Under the standard reaction conditions with 3-MST homologs, we found no major difference in rates of H₂S release from **4** (Fig. S16[†]). While a majority of the substrates tested showed similar rates, compounds **1j**, **1k** and **1m** whose $k_b/k_h > 10$, were notable exceptions. These results indicate that our approach differentiates between human and bacterial 3-MST homologs, and is capable of achieving selective H₂S generation between species. To the best of our knowledge, this is the first example of tuning persulfide/polysulfide generation, with the added advantage of species selectivity.

Antioxidant activity

Persulfides are widely prevalent in cells as protein persulfides as well as other low molecular weight persulfide species. For example, glutathione persulfide/polysulfide has excellent *in vitro* ROS-scavenging activity when compared with glutathione or H₂S alone.¹⁰ These species have been previously shown to have potent antioxidant activity likely through the Nrf2-KEAP1 pathway, imparting protection from ROS-induced injury.^{36,37} Selected analogues with varying relative rates of H₂S generation



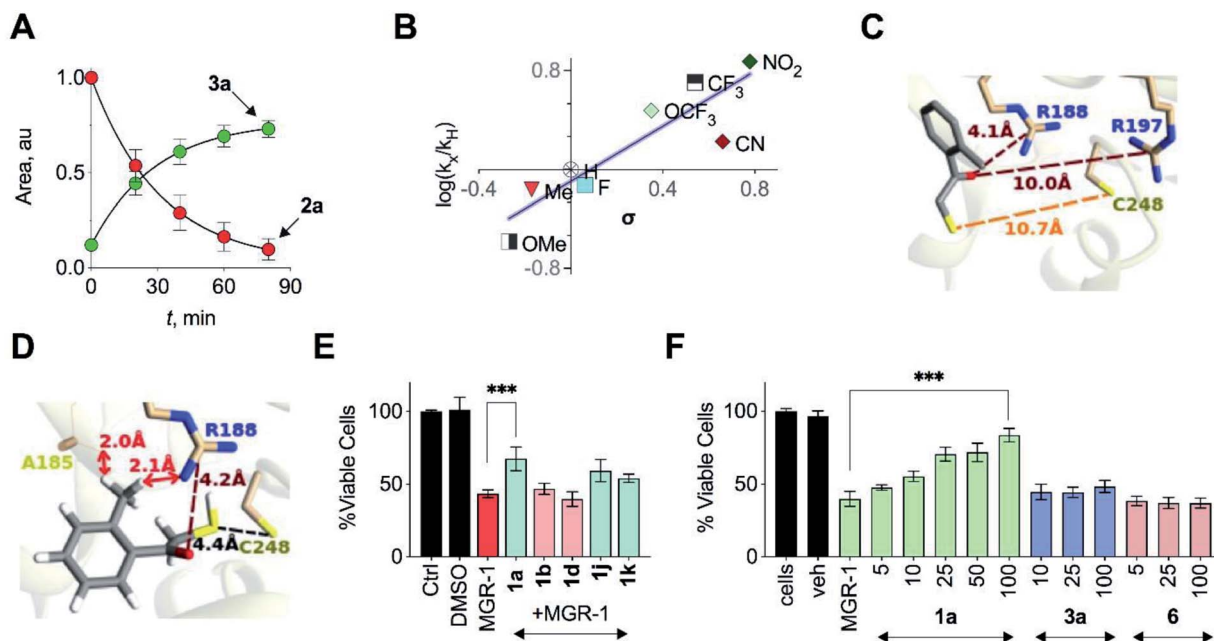


Fig. 4 (A) HPLC analysis of a reaction mixture containing **2a** and 3-MST in the presence of DTT showed the gradual disappearance of **2a** and concomitant formation of **3a**. Curve fitting to first order kinetics gave rate constants of 0.99 h^{-1} and 0.75 h^{-1} for the disappearance of **2a** and the formation of **3a**, respectively. (B) Hammett analysis of rate constants of H_2S generation from unnatural substrates (see Table 1) with wt *h3*-MST. Linear regression analysis yielded a slope of $+1.11$ ($R^2 = 0.8$). (C) Docking of **2k** in the active site of *h3*-MST shows S–S bond distance of 10.7 \AA which is substantially larger when compared with the low energy conformation of **2a** (5.2 \AA). (D) Docking of **2k** in the active site of *h3*-MST shows steric clashes of ortho-Me group of **2k** with A185 and R188 residues in a higher energy conformation. (E) Cell viability assay conducted on N2a cells: Cells were pre-treated with $25 \mu\text{M}$ of compounds **1a**, **1b**, **1d**, **1j** and **1k** for 12 h and then exposed to MGR-1 ($25 \mu\text{M}$) for 4 h. Ctrl refers to untreated cells. Cell viability was determined using a standard MTT assay. Results are expressed as mean \pm SD ($n = 3$). *** $p < 0.001$ vs. MGR-1. (F) Cell viability assay conducted on N2a cells: cells that were pre-treated with **1a**, **3a** or **6** were then treated with a cell permeable ROS generator MGR-1. A dose-dependent protection of cells from MGR-1 induced cell death by **1a** was observed. The byproduct ketone **3a** or the negative control **6** did not show any protection against the cytotoxic effects of MGR-1. All data are presented as mean \pm SD ($n = 3$ per group). *** $p < 0.001$ vs. MGR-1.

(in the range of 1 to 223) were next tested to study their protective ability against oxidative stress-induced cell death. A mouse neuroblastoma cell line N2a was used in this experiment. MGR-1, a known cell-permeable ROS generator, was used to induce oxidative stress and cell viability was determined.³⁸ N2a cells were first independently treated with fast H_2S generators **1b** and **1d** (relative rate > 50), **1a** (relative rate = 30) as well as slow generators **1j** and **1k** (relative rate < 2). At $25 \mu\text{M}$, these compounds showed no significant effect on the growth of cells as determined by a cell viability assay (Fig. S33[†]). Cells that were independently pre-incubated with these compounds ($25 \mu\text{M}$) for 12 h were next exposed to MGR-1. Viable cells were determined using a standard cell viability assay. The results of this assay indicate that the fast generators did not significantly protect cells from oxidative stress-induced cell death while the other analogues **1a**, **1j** and **1k** showed remarkable protective effects (Fig. 4E). From this initial screen, we identified compound **1a** for further evaluation. The compound **1a** itself was well tolerated by cells (Fig. S34[†]) and the byproduct of turnover of **1a** is **3a**, which is classified as Generally Recognized as Safe (GRAS) by the Food and Drug Administration.

The lead compound **1a** was next tested against N2a cells using MGR-1, and a dose-dependent protection from lethality

was recorded (Fig. 4F). The control compound **6** and the acetophenone **3a** tested under similar conditions failed to show any protective effects (Fig. 4F). To further corroborate our results, menadione, another known ROS generator was used to induce lethality. Again, a dose-dependent protection was recorded when cells were pre-treated with **1a** (Fig. S35[†]). In a separate experiment with mouse embryonic fibroblasts (MEF), **1a** was similarly found to have significant protective effects (Fig. S36[†]). Together, these data illustrate the cytoprotective effect of the cell-permeable persulfide generator **1a**.

To validate the molecular basis of this result, the effect of **1a** in reducing hydrogen peroxide (H_2O_2) levels in cells was studied. Again, MGR-1 was used to increase H_2O_2 as determined by the TCF-B fluorescent dye in A549 cells (Fig. 5A).³⁹ When cells pre-treated with **1a** were exposed to MGR-1, a significant decrease in H_2O_2 levels was observed (Fig. 5A). Under similar conditions, control compound **6** did not affect H_2O_2 levels in cells, suggesting that the ROS-quenching effects were directly mediated by persulfide/ H_2S generated by **1a** (Fig. S37[†]).

Elevation of ROS in cells leads to perturbation of redox homeostasis and alteration of levels of various components of cellular antioxidant response. NAD^+/NADH and GSSG/GSH ratio serve as reliable markers of oxidative stress.⁴⁰ Three cell lines



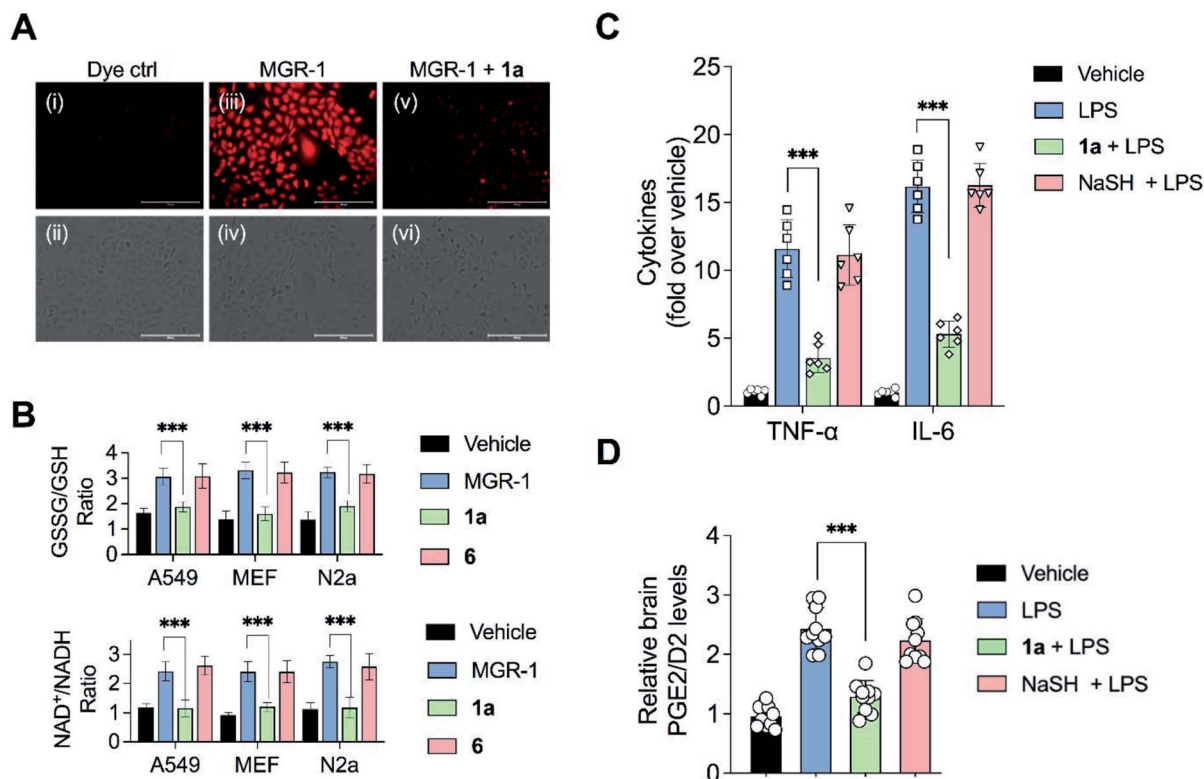


Fig. 5 (A) Effects of **1a** on quenching hydrogen peroxide (H_2O_2) generated by MGR1:A549 cells treated with: (i and ii) dye control; (iii and iv) $25 \mu\text{M}$ MGR-1; (v and vi) $25 \mu\text{M}$ of **1a** for 12 h followed by addition of the $25 \mu\text{M}$ MGR-1 for 1 h. Intracellular H_2O_2 was detected using a reported H_2O_2 -sensor TCF-B ($25 \mu\text{M}$). Scale bar represents $200 \mu\text{m}$. (B) Biomarkers for oxidative stress: Three cell lines (A549, mouse embryonic fibroblasts (MEF) and N2a) were pre-treated with vehicle, **1a** or **6** and exposed to MGR-1 following which NAD^+/NADH ratio and GSSG/GSH ratio were determined using an ELISA assay. All data are presented as mean \pm SD ($n = 5$ per group). *** $p < 0.001$ vs. MGR-1. (C and D) Mouse endotoxin shock model: animals were treated with **1a** (20 mg kg^{-1}) or NaSH (20 mg kg^{-1}) 4 h prior to treatment with lipopolysaccharide (LPS, 5 mg kg^{-1}). 30 min post-administration of LPS, another dose of **1a** or NaSH was given. The brain tissue samples were harvested followed by measurement of: (C) Pro-inflammatory cytokines, $\text{TNF-}\alpha$ and IL-6 using a standard ELISA assay. All data are presented as mean \pm SD ($n = 6$ per group). *** $p < 0.001$ vs. LPS; and (D) prostaglandins PGE2/D2 using LC/MS. All data are presented as mean \pm SD ($n = 10$ per group). *** $p < 0.001$ vs. LPS.

(A549, MEF and N2a) were exposed to MGR-1 and enhanced NAD^+/NADH as well as GSSG/GSH ratios were recorded (Fig. 5B). Pre-treatment of cells with **1a** followed by incubation with MGR-1 showed restoration of nearly normal ratios, and the control compound **6** was found to be ineffective in doing so. Taken together, these studies conclusively establish the efficacy of the artificial substrate **1a** that we designed to mitigate oxidative stress in both human as well as mouse-derived cell lines (Fig. 5B).³⁵

Mitigation of neuroinflammation

Recently, a polysulfide donor was used to study the effect of enhanced endogenous polysulfide levels on innate immune response using a mouse endotoxin shock model.⁴¹ Lipopolysaccharides (LPS), a common constituent of bacterial cell walls, are recognized by toll-like receptor 4 (TLR4) and trigger the innate immune response leading to the activation of macrophages to generate pro-inflammatory cytokines that contribute to clearance of bacteria (Fig. S38[†]). The major finding of this study was that elevated polysulfides can negatively regulate TLR4-mediated pro-inflammatory signaling and the polysulfide

donor protects against this endotoxin shock. Taking this cue, we evaluated the ability of **1a** to mitigate neuroinflammation in a similar mouse model system. First, C57BL/6J mice were intraperitoneally injected once daily with compound **1a** over a period of seven days, and it was found to be well tolerated. Next, mice were treated with LPS alone and increased levels of pro-inflammatory cytokines $\text{TNF-}\alpha$ and IL-6 in the brain were observed as compared with vehicle-treated mice (Fig. 5C).

In a separate experiment, mice which were treated with LPS and **1a** were found to have significantly lower levels of $\text{TNF-}\alpha$ and IL-6 in the brain, suggesting that **1a** suppressed the inflammatory response triggered by LPS. No evidence for reduction of pro-inflammatory cytokines in mice treated with LPS and NaHS was observed, consistent with the previous report that NaHS had little or no effect on the reduction of cytokines.⁴¹ LPS is also known to induce the formation of pro-inflammatory prostaglandins in the brain. Prostaglandin E2 (PGE2) has a variety of functions in the nervous system. Interaction of PGE2 with prostaglandin EP3 receptors leads to an increase in body temperature and inflammation (Fig. S39[†]). The use of nonsteroidal anti-inflammatory drugs (NSAIDs) blocks the activity of cyclooxygenase-2 (COX-2) which decreases PGE2 production,



resulting in remediation of fever and inflammation.⁴² Hence, measurement of PGE₂/D₂ levels is a reliable inflammation biomarker. LC/MS analysis of brain homogenates was carried out to measure PGE₂/D₂ levels. LPS-treated mice were found to have significantly higher levels of PGE₂/D₂ when compared with vehicle-treated mice. Animals which were exposed to both LPS and **1a** were found to have significantly lower levels of PGE₂/D₂, reiterating the ability of **1a** to reduce neuro-inflammation (Fig. 5D). Again, NaSH-treated mice that were exposed to LPS did not show any effect on PGE₂/D₂ levels. Taken together, these assays conclusively demonstrate the ability of **1a** to act as an antioxidant as well as an anti-inflammatory agent.

Our data shows that the unnatural substrate is able to transfer sulfur to low molecular weight thiols *via* 3-MST, and induce protein persulfidation in cells. Other strategies for generating persulfides in cells have relied on installing the persulfide/polysulfide functional group in the donor.^{5,6,41,43–53} These strategies work very well but have limitations in the ease of synthesis, poor shelf-life due to susceptibility towards decomposition, and heterogeneity of the persulfide source due to the ambiguity in the number of sulfurs in the donor. The protocol developed here involves the synthesis of a thioacetate, which is easy to prepare with high reproducibility and is stable for extended periods. For *in vitro* experiments to generate persulfide, the addition of enzymes that are readily available (esterase and 3-MST) is necessary while for cellular experiments to enhance persulfide, addition of the compound is sufficient. The substrates we have developed allow for systematic study of cellular sulfur transfer, and can be used to investigate the persulfide proteome which has been elusive till date.¹¹

Conclusions

The study of reactive sulfur species is often complicated by poor detection techniques, artefacts and uncharacterized cellular interactions. Thus, several facets of sulfur metabolism remain to be studied in molecular-level detail. The use of selective tools developed herein allow for systematic study of redox biology through the lens of an important enzyme, 3-MST. Our data underscores the potential of this approach as a novel therapeutic paradigm in mitigating inflammation. The importance of persulfides in ameliorating symptoms associated with neurodegenerative disorders as well as favourably impacting behavior in animals are some of the possible applications of the strategy developed here.⁴ The tunability of rates of persulfide generation using the class of compounds that we have developed adds a new dimension to persulfide donors that has hitherto not been studied. Projecting forward, further structural optimization of the substrate would be necessary to fully exploit the translational potential of this approach. The deficits associated with diminished expression of 3-MST will likely need mapping out the 3-MST-SS⁻ proteome and identification of proteins that depend on this enzyme for persulfidation. Given the selectivity of the substrate towards 3-MST in cells, the use of our compounds as probes for studying sulfur trafficking will provide insights into molecular mechanisms associated with

the dysfunction or deficiency of 3-MST in neuronal diseases, such as intellectual disability and Down's syndrome.^{54,55}

Data availability

Experimental protocols, characterization and all data pertaining to the manuscript have been uploaded in the ESI.†

Author contributions

ABH and HC wrote the manuscript with inputs from all authors. PB, SM, MN, RRMS, SS, VSSA and KG carried out the experiments and computation under the supervision of AM, DKS, SSK, ABH and HC.

Conflicts of interest

There are no conflicts to declare.

Acknowledgements

Financial support from the SERB, DST (CRG/2019/002900) and IISER Pune is acknowledged. This work was supported by the DBT-Ramalingaswami Re-entry Fellowship (grant number BT/RLF/Re-entry/12/2014) awarded to ABH. DBT/Wellcome Trust India Alliance Fellowship (grant number IA/I/15/2/502058) awarded to SSK. DST Fund for Improvement of S&T Infrastructure (SR/FST/LSII-043/2016) to the IISER Pune Biology Department for setting up the Biological Mass Spectrometry Facility. The National Facility for Gene Function in Health and Disease at IISER Pune is thanked for maintaining and providing mice for this study (DBT: BT/INF/22/SP17358/2016). Research fellowship for PB (DST-INSPIRE), SM (UGC) and RRMS (CSIR) are acknowledged. The authors thank Dr Rajesh Viswanathan, IISER Tirupati and Dr Sridhar Rajaram, JNCASR Bengaluru for their critical reading of the manuscript.

Notes and references

- M. R. Filipovic, J. Zivanovic, B. Alvarez and R. Banerjee, *Chem. Rev.*, 2018, **118**, 1253–1337.
- T. V. Mishanina, M. Libiad and R. Banerjee, *Nat. Chem. Biol.*, 2015, **11**, 457.
- M. S. Vandiver, B. D. Paul, R. Xu, S. Karuppagounder, F. Rao, A. M. Snowman, H. Seok Ko, Y. Il Lee, V. L. Dawson, T. M. Dawson, N. Sen and S. H. Snyder, *Nat. Commun.*, 2013, **4**, 1626.
- D. Giovino, B. Bursac, J. I. Sbodio, S. Nalluru, T. Vignane, A. M. Snowman, L. M. Albaricarys, T. W. Sedlak, R. Torregrossa, M. Whiteman, M. R. Filipovic, S. H. Snyder and B. D. Paul, *Proc. Natl. Acad. Sci. U. S. A.*, 2021, **118**, e2017225118.
- Y. Zheng, B. Yu, Z. Li, Z. Yuan, C. L. Organ, R. K. Trivedi, S. Wang, D. J. Lefer and B. Wang, *Angew. Chem., Int. Ed.*, 2017, **56**, 11749–11753.
- V. S. Khodade, B. M. Pharoah, N. Paolocci and J. P. Toscano, *J. Am. Chem. Soc.*, 2020, **142**, 4309–4316.



- 7 K. Shatalin, E. Shatalina, A. Mironov and E. Nudler, *Science*, 2011, **334**, 986–990.
- 8 P. Shukla, V. S. Khodade, M. SharathChandra, P. Chauhan, S. Mishra, S. Siddaramappa, B. E. Pradeep, A. Singh and H. Chakrapani, *Chem. Sci.*, 2017, **8**, 4967–4972.
- 9 A. K. Mustafa, M. M. Gadalla, N. Sen, S. Kim, W. Mu, S. K. Gazi, R. K. Barrow, G. Yang, R. Wang and S. H. Snyder, *Sci. Signaling*, 2009, **2**, ra72.
- 10 T. Ida, T. Sawa, H. Ihara, Y. Tsuchiya, Y. Watanabe, Y. Kumagai, M. Suematsu, H. Motohashi, S. Fujii, T. Matsunaga, M. Yamamoto, K. Ono, N. O. Devarie-Baez, M. Xian, J. M. Fukuto and T. Akaike, *Proc. Natl. Acad. Sci. U. S. A.*, 2014, **111**, 7606–7611.
- 11 J. Zivanovic, E. Kouroussis, J. B. Kohl, B. Adhikari, B. Bursac, S. Schott-Roux, D. Petrovic, J. L. Miljkovic, D. Thomas-Lopez, Y. Jung, M. Miler, S. Mitchell, V. Milosevic, J. E. Gomes, M. Benhar, B. Gonzales-Zorn, I. Ivanovic-Burmazovic, R. Torregrossa, J. R. Mitchell, M. Whiteman, G. Schwarz, S. H. Snyder, B. D. Paul, K. S. Carroll and M. R. Filipovic, *Cell Metab.*, 2019, **30**, 1152–1170.
- 12 N. Nagahara and A. Katayama, *J. Biol. Chem.*, 2005, **280**, 34569–34576.
- 13 N. Nagahara, *Br. J. Pharmacol.*, 2018, **175**, 577–589.
- 14 Y. Kimura, S. Koike, N. Shibuya, D. Lefer, Y. Ogasawara and H. Kimura, *Sci. Rep.*, 2017, **7**, 10459.
- 15 N. Nagahara and T. Nishino, *J. Biol. Chem.*, 1996, **271**, 27395–27401.
- 16 M. Libiad, P. K. Yadav, V. Vitvitsky, M. Martinov and R. Banerjee, *J. Biol. Chem.*, 2014, **289**, 30901–30910.
- 17 K. Módis, C. Coletta, K. Erdélyi, A. Papapetropoulos and C. Szabo, *FASEB J.*, 2013, **27**, 601–611.
- 18 M. Li, C. Xu, J. Shi, J. Ding, X. Wan, D. Chen, J. Gao, C. Li, J. Zhang, Y. Lin, Z. Tu, X. Kong, Y. Li and C. Yu, *Gut*, 2018, **67**, 2169–2180.
- 19 P. M. Palenchar, C. J. Buck, H. Cheng, T. J. Larson and E. G. Mueller, *J. Biol. Chem.*, 2000, **275**, 8283–8286.
- 20 E. G. Mueller, *Nat. Chem. Biol.*, 2006, **2**, 185.
- 21 H. T. Nagasawa, D. J. W. Goon, D. L. Crankshaw, R. Vince and S. E. Patterson, *J. Med. Chem.*, 2007, **50**, 6462–6464.
- 22 C. Coletta, K. Módis, B. Szczesny, A. Brunyánszki, G. Oláh, E. C. S. Rios, K. Yanagi, A. Ahmad, A. Papapetropoulos and C. Szabo, *Mol. Med.*, 2015, **21**, 1–14.
- 23 P. K. Yadav, K. Yamada, T. Chiku, M. Koutmos and R. Banerjee, *J. Biol. Chem.*, 2013, **288**, 20002–20013.
- 24 G.-T. Huang and J.-S. K. Yu, *J. Phys. Chem. B*, 2016, **120**, 4608–4615.
- 25 F. van den Ent and J. Löwe, *J. Biochem. Biophys. Methods*, 2006, **67**, 67–74.
- 26 A. A. Heredia, S. M. Soria-Castro, L. M. Bouchet, G. Oksdath-Mansilla, C. A. Barrionuevo, D. A. Caminos, F. R. Bisogno, J. E. Argüello and A. B. Peñeñory, *Org. Biomol. Chem.*, 2014, **12**, 6516–6526.
- 27 J.-C. Lec, S. Boutserin, H. Mazon, G. Mulliert, S. Boschi-Muller and F. Talfournier, *ACS Catal.*, 2018, **8**, 2049–2059.
- 28 D. Zhang, I. Macinkovic, N. O. Devarie-Baez, J. Pan, C.-M. Park, K. S. Carroll, M. R. Filipovic and M. Xian, *Angew. Chem., Int. Ed.*, 2014, **53**, 575–581.
- 29 N. Shibuya, M. Tanaka, M. Yoshida, Y. Ogasawara, T. Togawa, K. Ishii and H. Kimura, *Antioxid. Redox Signaling*, 2009, **11**, 703–714.
- 30 C. Tristan, N. Shahani, T. W. Sedlak and A. Sawa, *Cell. Signalling*, 2011, **23**, 317–323.
- 31 W. Chen, C. Liu, B. Peng, Y. Zhao, A. Pacheco and M. Xian, *Chem. Sci.*, 2013, **4**, 2892.
- 32 P. Chauhan, P. Bora, G. Ravikumar, S. Jos and H. Chakrapani, *Org. Lett.*, 2017, **19**, 62–65.
- 33 C. Wei, Q. Zhu, W. Liu, W. Chen, Z. Xi and L. Yi, *Org. Biomol. Chem.*, 2014, **12**, 479–485.
- 34 R. Wedmann, C. Onderka, S. Wei, I. A. Szijártó, J. L. Miljkovic, A. Mitrovic, M. Lange, S. Savitsky, P. K. Yadav, R. Torregrossa, E. G. Harrer, T. Harrer, I. Ishii, M. Gollasch, M. E. Wood, E. Galardon, M. Xian, M. Whiteman, R. Banerjee and M. R. Filipovic, *Chem. Sci.*, 2016, **7**, 3414–3426.
- 35 K. Hanaoka, K. Sasakura, Y. Suwanai, S. Toma-Fukai, K. Shimamoto, Y. Takano, N. Shibuya, T. Terai, T. Komatsu, T. Ueno, Y. Ogasawara, Y. Tsuchiya, Y. Watanabe, H. Kimura, C. Wang, M. Uchiyama, H. Kojima, T. Okabe, Y. Urano, T. Shimizu and T. Nagano, *Sci. Rep.*, 2017, **7**, 40227.
- 36 G. Yang, K. Zhao, Y. Ju, S. Mani, Q. Cao, S. Puukila, N. Khaper, L. Wu and R. Wang, *Antioxid. Redox Signaling*, 2012, **18**, 1906–1919.
- 37 S. Koike, Y. Ogasawara, N. Shibuya, H. Kimura and K. Ishii, *FEBS Lett.*, 2013, **587**, 3548–3555.
- 38 D. S. Kelkar, G. Ravikumar, N. Mehendale, S. Singh, A. Joshi, A. K. Sharma, A. Mhetre, A. Rajendran, H. Chakrapani and S. S. Kamat, *Nat. Chem. Biol.*, 2019, **15**, 169–178.
- 39 A. C. Sedgwick, H.-H. Han, J. E. Gardiner, S. D. Bull, X.-P. He and T. D. James, *Chem. Commun.*, 2017, **53**, 12822–12825.
- 40 F. Q. Schafer and G. R. Buettner, *Free Radical Biol. Med.*, 2001, **30**, 1191–1212.
- 41 T. Zhang, K. Ono, H. Tsutsuki, H. Ihara, W. Islam, T. Akaike and T. Sawa, *Cell Chem. Biol.*, 2019, **26**, 686–698.
- 42 J. R. Vane, *Nat. New Biol.*, 1971, **231**, 232–235.
- 43 P. Bora, P. Chauhan, S. Manna and H. Chakrapani, *Org. Lett.*, 2018, **20**, 7916–7920.
- 44 A. Chaudhuri, Y. Venkatesh, J. Das, M. Gangopadhyay, T. K. Maiti and N. D. P. Singh, *J. Org. Chem.*, 2019, **84**, 11441–11449.
- 45 R. A. Hankins, S. I. Suarez, M. A. Kalk, N. M. Green, M. N. Harty and J. C. Lukesh, *Angew. Chem.*, 2020, **132**, 22422–22429.
- 46 V. S. Khodade, S. C. Aggarwal, B. M. Pharoah, N. Paolucci and J. P. Toscano, *Chem. Sci.*, 2021, **12**, 8252–8259.
- 47 B. Yu, Y. Zheng, Z. Yuan, S. Li, H. Zhu, L. K. De La Cruz, J. Zhang, K. Ji, S. Wang and B. Wang, *J. Am. Chem. Soc.*, 2018, **140**, 30–33.
- 48 Z. Yuan, Y. Zheng, B. Yu, S. Wang, X. Yang and B. Wang, *Org. Lett.*, 2018, **20**, 6364–6367.
- 49 J. Kang, S. Xu, M. N. Radford, W. Zhang, S. S. Kelly, J. J. Day and M. Xian, *Angew. Chem., Int. Ed.*, 2018, **57**, 5893–5897.
- 50 C. R. Powell, M. K. Dillon, Y. Wang, R. J. Carrazzone and J. B. Matson, *Angew. Chem., Int. Ed.*, 2018, **57**, 6324–6328.



- 51 K. M. Dillon, R. J. Carrazzone, Y. Wang, C. R. Powell and J. B. Matson, *ACS Macro Lett.*, 2020, **9**, 606–612.
- 52 Y. Wang, K. M. Dillon, Z. Li, E. W. Winckler and J. B. Matson, *Angew. Chem., Int. Ed.*, 2020, **59**, 16698–16704.
- 53 V. S. Khodade and J. P. Toscano, *J. Am. Chem. Soc.*, 2018, **140**, 17333–17337.
- 54 Y. Suwanai, N. Nagahara, Z. Naito and H. Orimo, *Adv. Tech. Biol. Med.*, 2016, **4**, 167.
- 55 T. Panagaki, E. B. Randi and C. Szabo, *Biomolecules*, 2020, **10**, 653.

